THE PHYSICAL REVIEW

VOLUME 89 Second Series NUMBER 5

MARCH 1, 1953

Published for the

AMERICAN PHYSICAL SOCIETY

by the

AMERICAN INSTITUTE OF PHYSICS

LANCASTER, PA., AND NEW YORK, N. Y.

THE PHYSICAL REVIEW

A journal of experimental and theoretical physics established by E. L. Nichols in 1893

Published by the American Institute of Physics
for the
AMERICAN PHYSICAL SOCIETY

Officers

President

ENRICO FERMI
Institute for Nuclear Studies
University of Chicago
Chicago 37, Illinois

Vice-President

H. A. BETHE
Cornell University
Ithaca, New York

Secretary

K. K. DARROW
Bell Telephone Laboratories
Office
Columbia University
New York 27, New York

Treasurer

G. B. PEGRAM
Columbia University
New York 27, New York

Local Secretary
for the Pacific Coast

J. KAPLAN
University of California at Los Angeles
Los Angeles, California

Managing Editor

S. A. GOUDSMIT
Brookhaven National Laboratory
Upton, Long Island
New York

BOARD OF EDITORS

Editor

S. A. Goudsmit

Assistant Editor

S. Pasternack

Associate Editors

1953–1957

E. L. Chaffee
[illegible]
[illegible]
[illegible]
[illegible]
L. J. Tassie

1953–1954

W. P. Allis
P. G. Bergmann
W. B. Fretter
Conyers Herring
H. W. Lewis
Arnold Nordsieck

1953–1955

W. A. Fowler
Kameshwar Gaisser
Charles Kittel
R. E. Marshak
W. K. H. Panofsky
V. F. Weisskopf

Manuscripts for publication should be submitted to S. A. Goudsmit, Brookhaven National Laboratory, Upton, Long Island, New York. The authors' institutions are requested to pay a publication charge of $15 per printed page. If requested, reprints to 100 free reprints. Instructions will be sent with galley proofs.

Orders and all correspondence concerning papers in the process of publication should be addressed to the Publication Manager, American Institute of Physics, 57 East 55 Street, New York 22, New York.

Subscription Price

United States and Canada.....$20.00
Elsewhere.....$22.00

Back Numbers[1]

Yearly back number rate when complete year is available:
Prior to 1940: $25.00
Twenties: $22.00
Single copies: $2.00 each, prior to July, 1929;
$1.50 each, July, 1929–December, 1941;
$2.00 each, January, 1942–December, 1946;
$1.00 each, thereafter.
Foreign postage, $0.50–$0.80.

Subscriptions, renewals, and orders for back numbers should be addressed to the American Institute of Physics, 57 East 55 Street, New York 22, New York.

Changes of address in the case of members of the American Physical Society should be addressed to the Treasurer; in the case of other subscribers to the American Institute of Physics.

[1] Address: Miss Claire Phillips, Serials Department, Cornell University Library, Ithaca, New York.

The Physical Review is published monthly by the American Institute of Physics at Lancaster, Pennsylvania.

Entered as second-class matter March 1, 1929, at the Post Office at Lancaster, Pennsylvania, under the Act of March 3, 1879.

Acceptance for mailing at special rate of postage provided for in paragraph (d-2), section 34.40, P. L. & R. of 1948, authorized January 27, 1925.

THE
PHYSICAL REVIEW

A journal of experimental and theoretical physics established by E. L. Nichols in 1893

SECOND SERIES, VOL. 89, NO. 5 MARCH 1, 1953

The Decay of Resonance Radiation by Spontaneous Emission

E. J. HELLUND
Argonne National Laboratory, Lemont, Illinois
(Received April 3, 1952)

A critical examination of the theory of resonance radiation has been carried through, employing the mathematical technique of Laplace and Stieltjes transforms. Particular attention has been devoted to the question of the temporal behavior of the excited state. With no restrictions on the interaction between atom and radiation field other than that it be real, and that processes of sufficiently high frequency contribute only negligible effects, one can prove that the probability amplitude of the excited state cannot decay according to the general law

$$\Sigma_{\mu,\nu} C_{\mu\nu} t^{\lambda_\mu} e^{-\beta_\nu t},$$

where the λ_μ and β_ν are complex constants lying in the right half-plane and the $C_{\mu\nu}$ are arbitrary complex coefficients. The deviation from the law just cited can be termed a straggling phenomenon since exact analysis shows that the probability amplitude, for sufficiently long times, is greater than that defined according to the radioactive decay law.

Rigorous analysis of the source of this apparently anomalous behavior reveals the following explanation. Although the probability amplitude of the excited state is, strictly speaking, a functional of the interaction between the transition current in the atom and the photon states of the electromagnetic field, the essential features are determined principally by those states lying near the resonance frequency. Three elementary observations are immediately apparent. First, a particularly tractable analytical approximation for the interaction can be made such that the value of the actual interaction is reproduced at the resonance frequency and such that the behavior for high and low frequency photon states is at least qualitatively correct. Exact solutions in closed form can be obtained for this interaction. Second, in terms of the preceding representation it is possible to show that, associated with the transition between two atomic states, one is presented with a concomitant picture of a damped oscillation of charge describable in purely classical terms. Third, this classical motion can be interpreted as forming a source function for a continuous stochastic process in terms of which one finally derives the representation of the probability amplitude of the excited state. The straggling phenomenon previously cited is therefore that associated with all diffusion processes. The consideration of the exact interaction leads to more involved diffusion phenomena but does not in any case permit a radioactive decay law.

INTRODUCTION

A CLASSIC investigation on the theory of natural line breadth[1] is that of Weisskopf and Wigner. Their analysis is concerned with the reaction of the emitted radiation on the atomic electrons.

The quantum-mechanical description of the behavior of an atom in the presence of the ambient electromagnetic field, according to Dirac, is contained in the following equation of motion:[2]

$$\frac{h}{i}\frac{\partial\psi}{\partial t} = (E_Q + 2\pi h \textstyle\sum_\rho \nu_\rho N_\rho)\psi(Q; N_1, N_2, \cdots)$$
$$+ \textstyle\sum \omega_{QU}{}^\rho [(N_\rho+1)^{\frac{1}{2}}\psi(U; N_1, N_2, \cdots N_\rho+1, \cdots)$$
$$+ N_\rho{}^{\frac{1}{2}}\psi(U; N_1, N_2, \cdots N_\rho-1, \cdots)], \quad (1)$$

where Ψ is the Schrödinger probability amplitude for the system of atom plus photons; Q, U the designation of atom states; N_1, N_2, $\cdots$ the occupation numbers of the photon states; and, where $\omega_{UQ}{}^\rho$ denotes the matrix element of the interaction between the electromagnetic field and the atomic electric current associated with the transition between the two states Q and U. The symbol ρ serves to label the direction of emission of the photon, its polarization, and, finally, its energy.

Weisskopf and Wigner have applied Eq. (1) to the case of resonance radiation, assuming that in the notation of the preceding section the physical system could be described completely in the Hilbert space having for basis vectors

$$\Psi(A, 0), \quad \Psi(B, 1_\rho), \quad (2)$$

where A denotes the excited atomic state and 0 the absence of any photons in the field. B then denotes the ground state of the atom, and 1_ρ a photon in the state labeled by ρ.

[1] V. Weisskopf and E. Wigner, Z. Physik **63**, 54 (1930); **65**, 19 (1930).
[2] W. Heitler, *Quantum Theory of Radiation* (Clarendon Press, Oxford, 1936), first edition, Chap. III.

PRELIMINARY ANALYSIS

The objective confronting us is the specialization of Eq. (1) to the problem at hand. We shall begin by working with the theory reduced to its simplest basis; that is, we shall at first make no specific assumption about the form of the matrix elements ω_{QU^ρ}, avoiding in this way reference to a particular atomic model. The excited state, further, is assumed to be "oriented at random." The probability of emission is then isotropic with respect to direction and polarization. We shall also assume that the "hohlraum" is large enough to go from the sums employed in Eq. (1) to integrals by using the Jeans formula

$$\sum_\rho \cdots \equiv \int_0^\infty \cdots \frac{8\pi\nu^2 V}{c^3} d\nu, \tag{3}$$

where V designates the volume of configuration space and c the velocity of light. We shall introduce the notation that

$$\omega_{A B^\rho} \equiv \hbar W(\nu). \tag{4}$$

The replacement of ρ as a label by ν accords with the picture of isotropic emission. The dropping of A, B is permissible because no other states participate in the emission. Finally, we adopt the following symbols for the various probability amplitudes

$$\Psi(A, 0) \equiv a(t), \quad \Psi(B, 1_\rho) \equiv b(\nu, t). \tag{5}$$

Selecting our energy scale so that $E_A = 0$, we find that Eqs. (1) become

$$\begin{aligned} -i\frac{\partial a}{\partial t} &= \int_0^\infty W(\nu) b(\nu, t) S(\nu) d\nu, \\ -i\frac{\partial b}{\partial t} &= 2\pi(\nu - \nu_B{}^A) b + W^* a, \end{aligned} \tag{6}$$

where $S(\nu)$ represents

$$S(\nu) \equiv 8\pi\nu^2 V/c^3. \tag{7}$$

One can readily verify that

$$aa^* + \int_0^\infty bb^* S(\nu) d\nu = 1 \tag{8}$$

for all t, if the relation is satisfied at $t = 0$.

The implication that processes involving frequencies much greater than $\nu_B{}^A$ do not contribute appreciably to the decay of the excited state is expressed mathematically by the assignment of the property of uniform convergence to the integral occurring in the first of Eqs. (6). It is not difficult to establish that $W(\nu)$ does actually have the requisite behavior when calculated for an actual atomic model. For sufficiently large values of ν, the Fourier components of the vector potential oscillate rapidly over the atomic domain, thus forcing $\omega_{A B^\rho}$ to cut off sharply in this limit.

Equations (6) are now to be solved subject to the following boundary conditions:

$$a(0) = 1, \quad b(\nu, 0) = 0. \tag{9}$$

Taking the Laplace transforms[3] of Eqs. (6), with z as the transform parameter, and solving them, we obtain

$$\begin{aligned} \bar{a}(z) &= 1 \Big/ \left[z + g\left(\frac{zi}{2\pi} - \nu_B{}^A \right) \right], \\ \bar{b}(\nu, z) &= -W^*(\nu) \bar{a}(z) / [zi + 2\pi(\nu - \nu_B{}^A)], \end{aligned} \tag{10}$$

where

$$g(z) = \frac{i}{2\pi} \int_0^\infty \frac{f(\nu)}{z + \nu} d\nu \tag{11}$$

and

$$f(\nu) = |W(\nu)|^2 S(\nu). \tag{12}$$

The bar above a or b denotes the transform in all subsequent analysis.

INTRODUCTION OF ELECTROSTATIC ANALOG

Clearly, if one is to ascertain the properties of $\bar{a}(z)$ and hence $a(t)$, it is necessary to determine first the properties of the function g. The latter represents the Stieltjes transform[4] of $f(\nu)$, and one could simply draw upon the available store of representation theorems to establish the functional properties of g. However, the content of these theorems can be obtained directly by noting that g can be taken as representing a conformal representation of potential[5] and field lines of a double layer of electric charge placed along the imaginary axis in the z plane from $-2\pi i \nu_B{}^A$ to $+i\infty$. This is made clearer by writing

$$g\left(\frac{zi}{2\pi} - \nu_B{}^A \right) = \frac{1}{2\pi} \int_{-2\pi\nu_B{}^A}^{+\infty} \frac{f(\eta/2\pi + \nu_B{}^A)}{z - i\eta} d\eta, \tag{13}$$

where

$$\eta = 2\pi(\nu - \nu_B{}^A).$$

The "moment density" is evidently to be taken as $(1/2\pi) f(\eta/2\pi + \nu_B{}^A)$ and directed so that the "potential" is positive in the right half-plane and negative in the left half-plane. The field lines are clearly symmetrical with respect to the imaginary axis. Using the terminology of the electrostatic analog, we can rewrite the first of Eqs. (10) in the more useful form

$$\bar{a}(z) = [z + V(x, y) + iU(x, y)]^{-1}, \tag{14}$$

where V and U now denote the "potential" and "field."

[3] This method is particularly advantageous. Compare the treatment of internal conversion by N. Tralli and G. Goertzel, Phys. Rev. **83**, 399 (1951).

[4] D. V. Widder, *The Laplace Transform* (Princeton University Press, Princeton, 1946), first edition, Chap. VIII.

[5] For example the so-called complex inversion theorem for the Stieltjes transform becomes the well-known theorem of electrostatics that the potential is discontinuous at a double layer by an amount equal to 2π times the moment density.

An immediate consequence of the properties of V and U is that the $\bar{a}(z)$ can have no singularities in the entire z plane[6] with the possible exception of the imaginary axis. It is, therefore, impossible to expand $a(t)$ in a finite series of the form[7]

$$a(t)=\sum_{\mu,\nu} C_{\mu\nu} t^{\lambda_\mu} e^{-\beta_\nu t}, \tag{15}$$

where

$$\mathrm{Re}(\lambda_\mu)\geq 0, \quad \mathrm{Re}(\beta_\nu)>0, \tag{16}$$

with $C_{\mu\nu}$ arbitrary. It will be noted that the conclusion is valid with no other restrictions on $W(\nu)$ than that it be of such a form as to make the integral in Eqs. (6) converge uniformly. The Hermitean nature of the interaction has, of course, already been exploited in writing $\omega_{AB^\rho}=\omega_{BA^\rho}{}^*$ and in effect forces the moment density to be real.

Reverting to the second of Eqs. (10), one can prove by elementary means that the spectrum of emitted radiation is given by[2]

$$\lim_{t\to\infty}|b(\nu,t)| = \left|\frac{W^*(\nu)}{\{2\pi(\nu-\nu_B{}^A)+U[0,2\pi(\nu-\nu_B{}^A)]+iV[0,2\pi(\nu-\nu_B{}^A)]\}}\right|. \tag{17}$$

One sees that the line shape is necessarily asymmetric

INTRODUCTION OF PARTICLE OSCILLATOR

While the rejection of Eq. (15) is somewhat disturbing, no "model" has been presented in terms of which this result could have been foreseen.

It is perhaps of some interest to point out that such a model can be derived on the basis of elementary concepts. One simply retains the picture that the emission of radiation is associated with an actual oscillation of charge. This oscillation must be damped, in accordance with energy conservation. The reaction force, representing this damping action, should, of course, be derivable from Eqs. (10) as a functional of the interaction matrix. The precise form of the reaction force clearly cannot be assumed *a priori*. However, one point of primary importance emerges from this picturization. The reaction force represents the *integrated* effect of all modes of oscillation of the radiation field in retarding the charge vibration. In terms of the *electrostatic analog* one must therefore anticipate the replacement of the "moment density" along the imaginary axis by an "equivalent dipole," in the simplest possible case. This "dipole" is, schematically, the origin of the reaction force causing the decay of the classical vibration. The preceding discussion, it will be shown, provides a framework adequate to define the mathematical procedure which must now be followed.

We note first that the z plane is not sufficient to map $\bar{a}(z)$ completely. One must employ the concept of a multisheeted Riemannian surface of which one sheet is the z plane. The remaining sheets are entered through the cut in the z plane along the imaginary axis from $-2\pi i\nu_B{}^A$ to $+i\infty$. The simplest space of this type would be one of two sheets. For an arbitrary assumption as to the matrix elements $W(\nu)$ one would require an infinite number of sheets to map $\bar{a}(z)$ uniquely.

From the appearance of the spectrum of emitted photons, as given by Eq. (17), we see, however, that only frequencies near the resonance frequency $\nu_B{}^A$ are important in causing the excited state to decay. In seeking to replace the actual interaction matrix ω_{AB^ρ} by an equivalent form more amenable to calculation, one must, therefore, match the magnitude of ω_{AB^ρ} for $\nu\sim\nu_B{}^A$ and merely achieve a qualitative fit in the regions $\nu\ll\nu_B{}^A$ and $\nu\gg\nu_B{}^A$. By way of comparison, it may be mentioned that Weisskopf and Wigner considered that ω_{AB^ρ} could be replaced in the final formulas by its value at $\nu=\nu_B{}^A$. The approximation is good because of the smallness of the natural widths.

It will now be demonstrated that the equivalent form can be selected in such a way that $\bar{a}(z)$ will then be mapped on a two-sheeted Riemannian surface. The dipole previously described as replacing the continuous "moment density" will appear on the second sheet. If one then maps the points of this surface upon a ζ-plane, with ζ taken to mean the transform parameter for the classical damped oscillations, the prescription is complete.

The "model" interaction permitting a solution for $a(t)$ in terms of elementary functions is

$$f(\nu)=\frac{A\nu^{\frac{1}{2}}}{\pi(\nu+B^2)}, \tag{18}$$

where A and B are constants to be determined by comparison with the actual matrix ω_{AB^ρ}.

With $f(\nu)$ defined according to Eq. (18), g can be evaluated by elementary methods and is found to be[9]

$$g\left(\frac{zi}{2\pi}-\nu_B{}^A\right)=\frac{Ai}{2\pi[(zi/2\pi-\nu_B{}^A)^{\frac{1}{2}}+B]}. \tag{19}$$

The ζ-plane (representation) is obtained by pulling this dipole through the cut along the imaginary axis by means of the transformation

$$\zeta^2=2\pi i\nu_B{}^A(z+2\pi i\nu_B{}^A). \tag{20}$$

The meaning of the various terms of Eq. (20) follows. The factor $z+2\pi i\nu_B{}^A$ merely expresses the fact that the

[6] Derivation of an exponential decay results from an approximation which creates a singularity in the left half z plane [M. F. Ripelle, Compt. rend. **232**, 2403 (1951)].

[7] The class of functions excluded is broader than that indicated by Eq. (15).

[8] G. Doetsch, *Laplace Transformation* (Dover Publications, New York, 1943), first edition, Part III.

[9] The insertion of this result into Eq. (10) can be shown to lead to the expression of $a(t)$ in terms of three error functions of complex argument. Owing to the lack of complete tables, the result is not of practical interest.

cut in the z plane extends to $-2\pi i\nu_B{}^A$. The factor "i" outside guarantees that the axis of imaginaries in the ζ plane corresponds to the cut in the z plane. The factor $2\pi\nu_B{}^A$ insures that the classical vibration "keeps correct time."

By transformation (20), g becomes

$$g=\frac{iA(\nu_B{}^A)^{\frac{1}{2}}}{\zeta+2\pi B(\nu_B{}^A)^{\frac{1}{2}}}. \tag{21}$$

The "dipole" accordingly is found in the ζ-plane at $\zeta=-2\pi(\nu_B{}^A)^{\frac{1}{2}}B$ and has a "moment" equal to $A(\nu_B{}^A)^{\frac{1}{2}}$. The transform derived by the insertion of the value of g given by Eq. (21) into the first of Eqs. (10) must be understood as the Laplace transform image, not of $a(t)$ but of a motion, say $R(t)$.[10]

Using the same symbolism for this function, we have

$$\bar{R}(\zeta)=\frac{2\pi i\nu_B{}^A}{\zeta^2+(2\pi\nu_B{}^A)^2-2\pi(\nu_B{}^A)^{\frac{1}{2}}A/[\zeta+2\pi(\nu_B{}^A)^{\frac{1}{2}}B]}. \tag{22}$$

The last term in the denominator represents the damping of the harmonic oscillation $\zeta^2+2\pi(\nu_B{}^A)^2$. Actually all three poles of $\bar{R}(\zeta)$ lie in the left half-plane. $R(t)$ therefore contains only retarded effects.[11] In fact, the damping force is a memory term of the form

$$2\pi m(\nu_B{}^A)^{\frac{1}{2}}A\int_0^t \exp[-2\pi(\nu_B{}^A)^{\frac{1}{2}}B(t-\tau)]R(\tau)d\tau. \tag{23}$$

The equation of motion of such a particle oscillator is thus

$$m\frac{d^2R}{dt^2}+4\pi^2m(\nu_B{}^A)^2R-2\pi m(\nu_B{}^A)^{\frac{1}{2}}A\times\int_0^t \exp[-2\pi(\nu_B{}^A)^{\frac{1}{2}}B(t-\tau)]R(\tau)d\tau=0. \tag{24}$$

Generally,[12]

$$m\frac{d^2R}{dt^2}+4\pi^2m(\nu_B{}^A)^2R-4\pi m\nu_B{}^A\times\int_0^t\int_0^\infty f(\nu^2/\nu_B{}^A)e^{-2\pi\nu(t-\tau)}d\nu R(\tau)d\tau=0. \tag{25}$$

[10] The transformation of $R(t)$ into $a(t)$ can be considered as representing a perturbation in the equation of motion governing $R(t)$. One may consider the stochastic perturbation of a harmonic oscillator as illustrative of this point of view [W. R. van Wijk, Physica **3**, 1111 (1936)].

[11] Compare F. Bopp, Naturforsch. **1**, 53 (1946).

[12] Assuming that $f(\nu)$ is single values and that $f(\nu)\nu^{-\frac{1}{2}}$ is expressible as a Stieltjes transform.

One can easily show that $R(t)$ defined by Eq. (24) has two decay periods. The "fast" decay, which is non-oscillatory, is important only for very short times.

Finally, we note that $a(t)$ can be expressed directly in terms of $R(t)$.[13]

$$|a(t)|=\left|\frac{1}{4\pi D^{\frac{1}{2}}t^{\frac{1}{2}}}\int_0^\infty R'(\tau)\tau\exp(-\tau^2/4Dt)d\tau\right|, \tag{26}$$

where

$$D=(2\pi i\nu_B{}^A)^{-1} \tag{27}$$

and

$$R'=2\pi^{\frac{1}{2}}DR. \tag{28}$$

This relation between $R(t)$ and $a(t)$ can be expressed most conveniently in terms of an auxiliary function $\varphi(t,\tau)$ satisfying the following equation,

$$\frac{\hbar}{i}\frac{\partial\varphi}{\partial t}=\frac{1}{2M_B{}^A}\left[\left(i\hbar\frac{\partial}{\partial c\tau_1}\right)^2+\left(i\hbar\frac{\partial}{\partial c\tau_2}\right)^2+\left(i\hbar\frac{\partial}{\partial c\tau_3}\right)^2\right]\varphi, \tag{29}$$

where

$$\tau^2=\tau_1{}^2+\tau_2{}^2+\tau_3{}^2, \tag{30}$$

$$M_B{}^A=\tfrac{1}{2}h\nu_B{}^A/c^2, \tag{31}$$

with the "initial" condition,

$$4\pi\tau^2|\varphi(0,\tau)|^2=|R'|^2. \tag{32}$$

One finds then that Eq. (26) reduces to

$$|a(t)|^2=|\varphi(t,0)|^2. \tag{33}$$

The straggling phenomenon previously discussed is thus identified with a characteristic behavior of wave packets.

It has been frequently suggested that the results may be altered on considering the scattering problem. This point will be dealt with in a subsequent paper.

[13] The Laplace transform of $a(t)$ is

$$\bar{a}(z)=\bar{R}(\zeta)=\int_0^\infty R(\tau)\exp\left[-\tau\left\{\frac{1}{D}\left(z+\frac{1}{D}\right)\right\}^{\frac{1}{2}}\right]d\tau,$$

using Eqs. (20) and (27). If we then find the inverse Laplace transform of the integrand as a function of z (reference 8, pages 402 and 148) and take absolute values, Eq. (26) follows.

Magnetic Moments of Si^{29}, S^{33}, Zn^{67}, As^{75}, Se^{77}, Te^{123}, and Te^{125}*†

H. E. Weaver, Jr.
Stanford University, Stanford, California
(Received October 14, 1952)

An improved nuclear induction spectrometer has been employed for the detection and measurement of the resonances of several stable nuclei. The sign and value of the magnetic moments are listed in Table I. No diamagnetic correction has been applied. The sensitivity of the apparatus is indicated by the photographs of the output signal of H^2 and O^{17} which occur in water with a natural abundance of 0.02 and 0.04 percent, respectively.

I. INTRODUCTION

A SPECTROMETER which employs the well-known principles of nuclear induction[1,2] has been used for the detection and measurement of unknown nuclear moments. Several of these measurements have been carried out with an apparatus described by Proctor[3] which has continued to be useful.

There are, however, instances wherein it is desirable to have greater sensitivity and stability than those available with the above-mentioned apparatus. Such instances occur particularly in the case of isotopes of relatively low abundance and large natural line widths. In order to have signal amplitudes sufficient for observation, it is not only necessary to use considerable rf amplification, but also to apply a relatively large driving rf field. Optimum conditions require, in fact, that the broadening of the lines, resulting from the rf field, is comparable to the natural line width. The combination of these two features introduces characteristic practical difficulties which must be minimized through careful design and construction of the nuclear induction head in particular and the transmitter, receiver, and power supplies in general. In the use of a spectrometer with crossed receiver and transmitter coils, it is desirable to decouple the two coils to such an extent that the voltage induced in the resonated receiver coil is of the order of a few millivolts; this voltage is referred to below as the "leakage voltage." Resulting from the thermal and mechanical instabilities, this decoupling is the more difficult to attain the larger the driving rf field, thus limiting in practice the useful range of operation of the apparatus.

A nuclear induction head has been constructed which achieves sufficient long-time mechanical stability in the presence of rf field amplitudes up to one gauss; at the same time it provides a simple and reproducible method of balancing to a minimum the induced leakage voltage. The design details of the apparatus, as well as examples of nuclear induction signals which serve to test the behavior of the spectrometer, are given in the following section.

II. APPARATUS

The essential principles of the present spectrometer have already been described by Proctor.[3] However, the design of new elements and certain other modifications merit discussion here. The new water-cooled electromagnet which supplies the electronically stabilized dc magnet field has pole faces of $7\frac{13}{16}$ inches in diameter and a gap of $1\frac{3}{4}$ inches and is of the double-yoke type. One particularly useful feature of this magnet lies in the fact that the poles may be tilted with respect to one another. It is thus possible to correct for any original lack of parallelism of the pole faces as well as for the distortion of the field produced by asymmetrical movement of the steel yoke under the application of the magnetic field in the gap. With this arrangement, it is quite simple to adjust the field homogeneity while observing the transients of the nuclear induction signal.[4] Thus fields with a homogeneity of the order of one part in hundred thousand over the sample volume of three cubic centimeters may be obtained by simple adjustment of the relative position of the pole pieces while the field is on. Since this uniformity of the dc field over the sample volume is sufficient for most purposes and relatively insensitive to field changes, no attempt has been made to shim the field.

The transmitter which supplies the rf driving field for the nuclear induction head, the head itself, and the rf receiver are illustrated schematically in the accompanying circuit diagram of Fig. 1. These units will be described in some detail in the following passages.

The variable frequency oscillator consists of a push-pull Hartley circuit employing a 6SN7 double triode which generates sufficient rf power to provide adequate grid driving current for the 832A amplifier over the entire frequency range of four to ten megacycles. The power amplifier serves both to isolate the master oscillator from load variations and to provide variable rf power to the head. The output inductance for the power amplifier is remotely located in the nuclear induction head. The air core twin-lead coaxial line serves not only

* This paper is based on a thesis submitted to the Department of Physics and the Committee on Graduate Study of Stanford University in partial fulfillment of the requirements for the degree of Doctor of Philosophy.

† Assisted by the joint program of the U. S. Atomic Energy Commission and U. S. Office of Naval Research.

[1] F. Bloch, Phys. Rev. **70**, 460 (1946), and Bloch, Hansen, and Packard, Phys. Rev. **70**, 474 (1946).

[2] Bloembergen, Purcell, and Pound, Phys. Rev. **73**, 679, 712 (1948).

[3] W. G. Proctor, Phys. Rev. **79**, 35 (1950).

[4] B. A. Jacobsohn and R. K. Wangsness, Phys. Rev. **73**, 942 (1948).

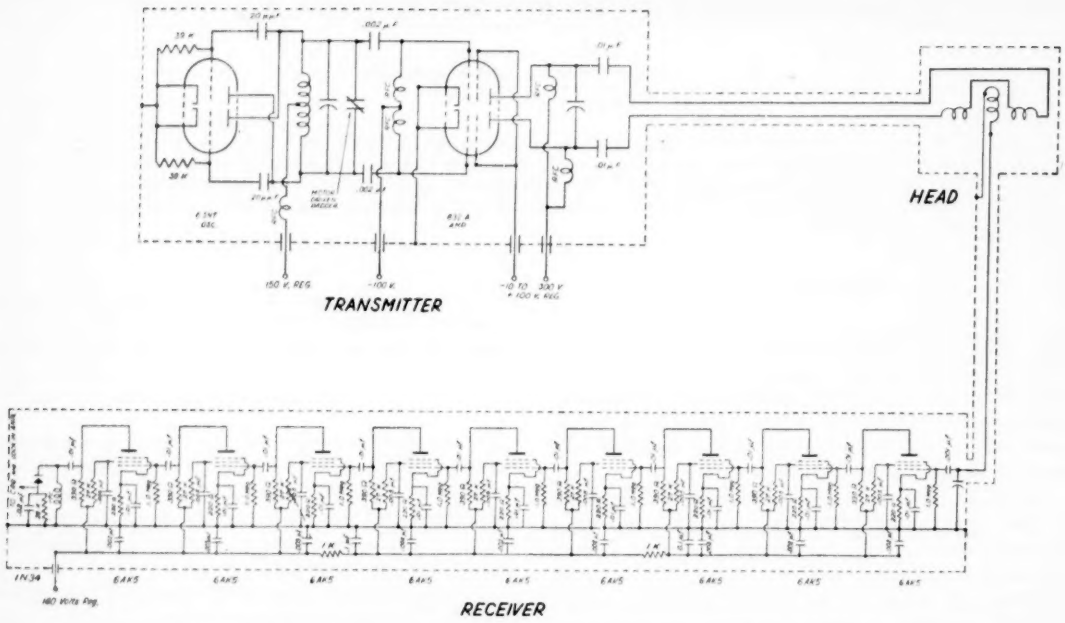

FIG. 1. Schematic diagram illustrating the transmitter, the nuclear induction head, and the rf receiver.

for the transmission of rf power, but also for the mechanical support of the head.

The intensity of the rf driving field is controlled by means of the screen voltage of the 832A amplifier tube. The rf half-amplitude H_1 increases in such a way that, with approximately 300 and 150 volts on the plates of the 832A and 6SN7, respectively, and with two milliamperes driving current on the control grid of the 832A, intensities from 0.1 to 1.0 gauss are included in a range of zero to one hundred volts on the screen grid of the amplifier tube. Somewhat lower rf fields may be obtained by using negative bias on the screen grid. Owing to the fact that the receiver amplifier and the transmitter are located next to each other, care must be exercised to provide shielding such that unwanted direct coupling between these two components does not cause an excessive leakage voltage on the final diode detector. For this reason the entire transmitter is mounted in a brass cylinder about $5\frac{1}{4}$ inches in diameter and 12 inches long. The two end plates which support the nuclear induction head and the power feed-through condensers, respectively, are machined to fit the cylinder snugly in order to minimize the leakage (see Fig. 2). In order to reduce undesirable coupling of the rf units through the regulated power supplies, all the power for the transmitter is brought in through standard 0.01 μf "Hypass" condensers.

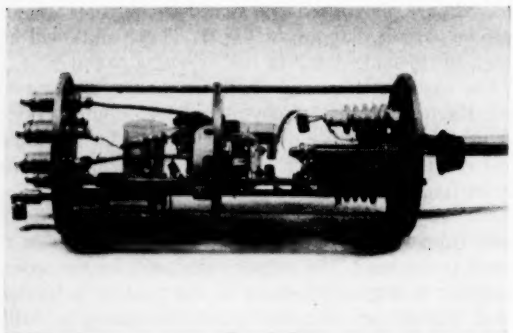

FIG. 2. The photograph illustrates the arrangement of the components of the transmitter. The external shield has been removed.

The construction of the nuclear induction head is shown in the external view of Fig. 3 and in the drawing of Fig. 4. The head is of the crossed coil type as mentioned by previous authors[5,6] with certain alterations in design which will be mentioned below.

For an rf field intensity H_1 of the order of $\frac{1}{3}$ gauss, there exist voltages in excess of 100 volts across the transmitter coil. However, the maximum allowable induced voltage across the resonated receiver coil at the input of the amplifier is of the order of 10 millivolts, and is in fact generally less than 2 millivolts. Voltages larger than two millivolts cause, after amplification, unduly large leakage voltages at the final diode and are undesirable from the standpoint of optimum over-all signal-to-noise ratio of the apparatus. The reduction is obtained by the balancing schemes inherent in the "crossed-coil" technique. Gross decoupling between the

[5] M. E. Packard, Rev. Sci. Instr. **19**, 435 (1948).
[6] F. Bloch and D. H. Garber, Phys. Rev. **76**, 585 (1949).

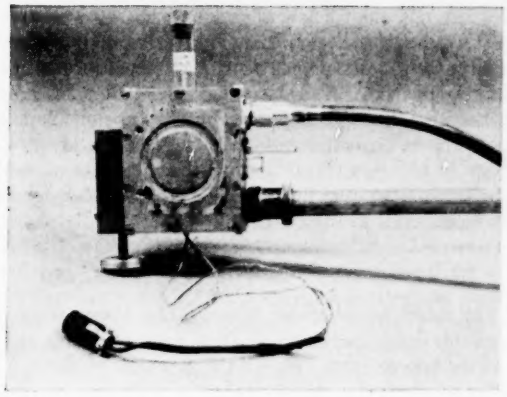

FIG. 3. External view of the nuclear induction head showing the relative position of the various leakage voltage controls. A sample test tube is shown in place.

transmitter and receiver coils is accomplished by having the axes of the coils perpendicular. Additional compensation is achieved by "tilting" the rf field with respect to the axis of the receiver coil. This is accomplished with a high degree of facility and stability by means of a differential screw drive moving a Lucite form on which half of the transmitter coil is wound. The relative movement of the two halves of the coil tilts the rf field and thereby produces complete balancing of the quadrature voltage of the rf leakage induced in the resonated receiver coil. This particular phase of the driving rf field is associated with the absorption mode, or v mode,[7] of the nuclear induction signals. As may be noted from Fig. 4, the transmitter and receiver coaxial lines are located at the lower and upper extremities of the head. Between these leads as well as between the receiver and transmitter coils proper are internal ground planes which further minimize any coupling to the receiver coil. With this arrangement at an rf field of about $\frac{1}{3}$ gauss half-amplitude, the residual leakage after complete "v mode" balance amounts to somewhat less than one-tenth of a volt. This residual leakage is due to the in-phase voltage induced in the receiver coil and is associated with the dispersion mode, or u mode,[7] of the nuclear induction signals. Although this remaining voltage is quite small in comparison with the voltage across the transmitter coil, it is still too large to permit realization of the maximum sensitivity of the rf amplifier. The final cancelling of the remaining leakage is accomplished by a u mode control[8] consisting of an inductance loop and a series resistance of such a magnitude that the total series impedance is predominantly resistive. The design of the control is simple and is schematically indicated in Fig. 5. Since the field resulting from the transmitter coil is predominantly in the y direction, the voltage induced in the circular loop, located in the xz plane, does not change upon rotation around the y axis. With the axis of the receiver coil fixed and perpendicular to the y axis, its coupling with the rectangular loop and, thereby, with the transmitter coil changes upon rotation around the y axis. The control is mounted in a threaded Lucite rod which is machined to fit very accurately the corresponding threaded hole in the main body of the nuclear induction head. An additional control provides a fine adjustment of the v mode leakage and is located just above the u mode control as shown in Figs. 3 and 4. This control consists of a small copper disk about 2 mm thick and approximately 5 mm in diameter mounted on the end of a threaded Lucite rod. The combined effect of these two controls is to affect the magnitude and phase of the "homodyning leakage" voltage applied to the input of the rf receiver. This leakage voltage is important for providing sufficient voltage for the proper operation of the crystal detector and for determining the mode of the observed resonance line.

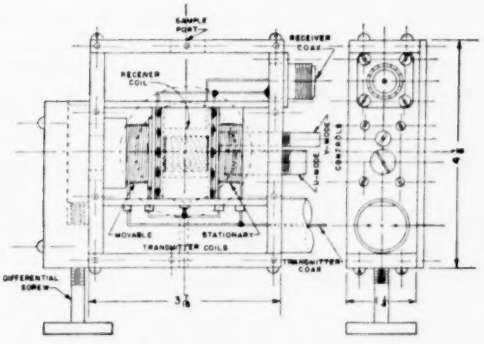

FIG. 4. View of nuclear induction head with the left cover plate removed showing the arrangement of the component parts.

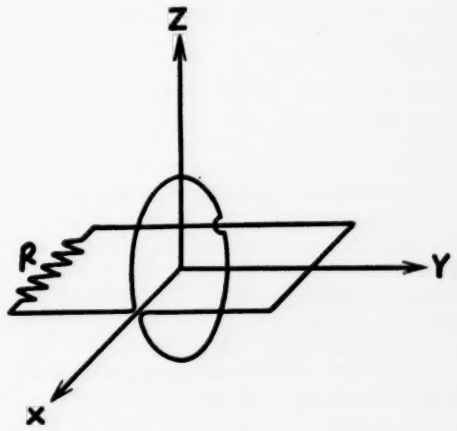

FIG. 5. Schematic diagram of the u mode control.

[7] F. Bloch, Phys. Rev. **70**, 460 (1946).

[8] This method of balance is that of F. Western at Varian Associates. The author wishes to thank Mr. Western for pointing it out to him.

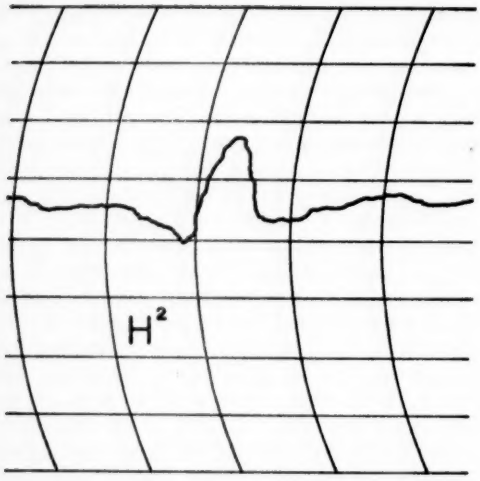

FIG. 6. Deuterium signal, *u* mode, in natural water with 8 molar $MnCl_2$ added. Rf half amplitude of $\frac{1}{2}$ gauss and sweep amplitude of $\frac{1}{2}$ gauss were used.

It is the stability of the balancing which limits the magnitude of the rf intensity H_1, for thermal heating and sensitivity to microphonics increase rapidly with the intensity of the rf field. In the case of overnight searching when the apparatus runs unattended for many hours, the rf field, H_1, is generally held below one-half gauss. At fields of the order of one-third gauss or less, and after having warmed up, the apparatus is sufficiently stable to run without rebalance for as much as twenty hours.

The rf receiver, the circuit of which is also shown in Fig. 1, has a pass-band frequency range of four to ten megacycles. When used in conjunction with the rest of the spectrometer, it has a noise figure of 3.0 ± 0.6 at an rf level in the head of 0.3 gauss. With the exception of the input coil, the receiver is untuned and the gain-bandwidth design parameters were determined according to the principles outlined in the book *Electronics* by Elmore and Sands.[9] There are nine stages of amplification with a gain per stage of 1.67 resulting in a total gain of 100 over a usable frequency range of 4.0 to 9.4 Mc. The maximum frequency is determined by the minimum capacitance of the tuning condenser, the capacitance of the copper coaxial line, and the distributed capacitance of the receiver coil in the head. The detected output from the 1N34 is then fed into the "lock-in" amplifier in exactly the same manner as has been described earlier by Proctor.[3]

There are two examples of nuclei which are readily available and whose induction signals serve as excellent tests of the sensitivity and performance of the spectrometer. They are H^2 and O^{17}, both occurring naturally in water. These two nuclei have been chosen because they are not only of low abundance, but also because they require little preparation. Both H^2 and O^{17} possess small quadrupole moments which, when interacting with the molecular fields, provide a means for attaining thermal equilibrium. However, in the case of H^2 it is necessary in general to add paramagnetic catalysts in order to obtain natural line widths in excess of field inhomogeneities over the sample volumes. These signals are reproduced in Figs. 6 and 7.

[9] W. C. Elmore and M. Sands, *Electronics* (McGraw-Hill Book Company, Inc., New York, 1949), first edition.

III. APPLICATION OF THE SPECTROMETER

For many nuclei under investigation information is available from spectroscopic data concerning the spin and the approximate value of the magnetic moment. In order to search for the resonance of a nucleus, the frequency is fixed at some convenient value and the magnetic field is slowly varied so as to cover a range of values on both sides of the expected gyromagnetic ratio. For a given frequency setting, the total search time as determined by the clock drive of the magnet current control amounts to about thirty hours. Once the resonance has been detected on the recording tape, the field is held fixed at the point of resonance and the signal is again traced out by slowly varying the frequency on either side of the resonance. This slowly changing frequency is constantly monitored by a General Radio Model LR-1 Heterodyne Frequency Meter and in this way the frequency at which the resonance occurs can be measured to within fifty cycles. The resonance of the unknown nucleus is then compared, at the same field,

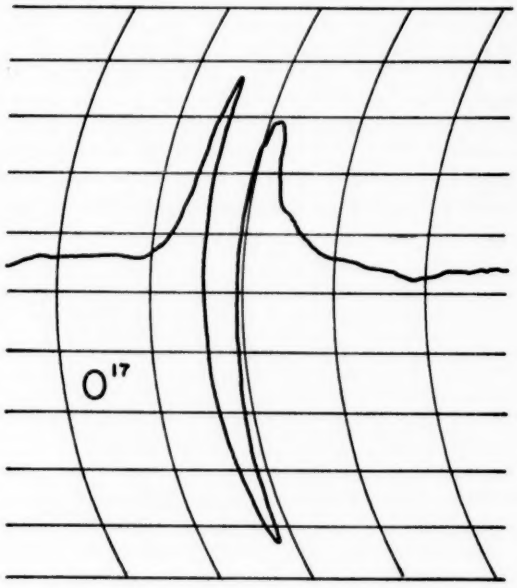

FIG. 7. O^{17} signal, *u* mode, in natural water without any catalyst added. Rf half-amplitude of 2/10 gauss and sweep amplitude of 3/10 gauss were used. The audio gain for this trace was reduced to 7/10 of that used in the trace of Fig. 6.

with that of a known nucleus. Typical examples of standard nuclei are H^2 in heavy water, Na^{23} in NaCl, and N^{14} in HNO_3.

In order to insure that a systematic error arising from the drift of the dc field does not occur while measurements are being made, the measured values of the frequency are plotted as a function of time, and by interpolation these values can be obtained as if they were measured at the same time and hence at the same field.

In this manner the magnetic moments of seven new isotopes have been determined with high precision and are listed in Table I.[10] Only the frequency ratios, known spins, and the known magnetic moments of standard nuclei have been used in the computation of these values and no diamagnetic corrections have been applied.

Due to the fact that the resonance frequency is sometimes dependent upon the compound used in a sample,[11] the compounds employed for the actual frequency measurement have been included in the tabulation. The compounds used for the standard nuclei have been mentioned above. For the purpose of computation the value of the magnetic moment of Na^{23} was determined by taking $\mu(H^1)=2.79268\pm0.00006$ nm[12] and $\nu(Na^{23})/\nu(H^1)=0.26450\pm0.00003$.[13] The value of the magnetic moment of deuterium used in these comparisons is $\mu(H^2)=0.857606$.[14]

The sign[3] of the magnetic moment was ascertained in all cases, while the spin determinations were not carried out except as noted. In the instances where the spin of the nucleus has been measured, the phenomenological equations[7] for the description of nuclear induction have been applied under suitable conditions.[7,15]

TABLE I. Magnetic moments and magnetic moment ratios.

Nuclei	Spin	Compound used	Magnetic moment in nuclear magnetons
Si^{29}	(1/2?)	Cobalt glass	(-0.55492 ± 0.00004)
S^{33}	3/2	Cs_2	$+0.64292\pm0.00014$
Zn^{67}	5/2	$ZnSO_4$	$+0.87378\pm0.00013$
As^{75}	3/2	Na_2AsO_4	$+1.4347\ \pm0.0003$
Se^{77}	1/2	H_2SeO_3	$+0.53326\pm0.00005$
Te^{123}	1/2	$TeCl_2$	-0.73188 ± 0.00004
Te^{125}	1/2	$TeCl_2$	-0.88235 ± 0.00004
$\mu(Te^{125})/\mu(Te^{123})=1.20560\pm0.00007$			

A. Silicon

A tentative assignment of the value of the spin[16] and the magnetic moment[17] of the Si^{29} nucleus has been reported to be $\frac{1}{2}$ and 0.55 nm, respectively. These experimental results are consistent with the model of the nucleus proposed by Mayer[18] and with the value of the magnetic moment of the Si^{29} nucleus predicted by the scheme of Schawlow and Townes.[19]

The first nuclear induction signals of silicon were reported by Hatton *et al.*[17] as having been observed in beryl and also in two types of glass. Accordingly, a Pyrex rod was inserted into the receiver coil of the induction head and the spectrometer set to search over a small region on either side of the reported value of 0.55 nm. Resonances were subsequently detected not only in samples containing Pyrex glass, but also in cobalt-, lead-, uranium-, vicor-, and soft glass.

A comparison of the resonant frequency of the Si^{29} signal in cobalt glass with that of deuterium in D_2O gave

$$\nu(Si^{29})/\nu(H^2)=1.29410\pm0.00007.$$

Assuming the spin of Si^{29} to be $\frac{1}{2}$, the value of the magnetic moment is

$$\mu(Si^{29})=-0.55492\pm0.00004.$$

The sign of the magnetic moment was observed to be negative. It should be pointed out that according to the shell model this observation further supports the assumption of a spin of $\frac{1}{2}$ for Si^{29}. In fact this isotope belongs to the third shell of odd-neutron nuclei, so that only $S_{\frac{1}{2}}$, $D_{\frac{3}{2}}$, and $D_{\frac{5}{2}}$ states are available for the odd nucleon. Since a $D_{\frac{5}{2}}$ state would lead to a positive moment, the spin value of $\frac{5}{2}$ can safely be excluded. The only other possibility for a negative moment would be the $D_{\frac{3}{2}}$ state which, however, would lead to the implausibly small value of -0.111 for the magnetic moment. Although no conclusive proof has been given yet that the spin of Si^{29} is $\frac{1}{2}$, this value must be considered by far the most probable one.

Nuclear induction resonances with a signal-to-noise ratio of about ten have also been observed in a three molar solution of SiO_2 in NaOH and in a three molar solution of silicon metal in KOH, without the addition of paramagnetic catalyst. The aspects of these signals as registered by the recording dc milliammeter indicate that in these samples the experimental conditions are not those of slow passage. Measurement of the transverse relaxation times of the protons in these same solutions[20] yielded values of the order of thirty milliseconds, while the normal relaxation times of the protons in the cp reagents, NaOH and HOH, are considerably longer. This suggests that the commercially prepared samples of SiO_2 and silicon metal contain small amounts of paramagnetic catalysts as con-

[10] As the measurements mentioned in this section progressed, the results were published in a preliminary form: S. S. Dharmatti and H. E. Weaver, Phys. Rev. **83**, 845 (1951); **84**, 367 (1951); **84**, 843 (1951); **85**, 927 (1952); **86**, 259 (1952).

[11] W. G. Proctor and F. C. Yu, Phys. Rev. **77**, 717 (1950); W. C. Dickenson, Phys. Rev. **77**, 736 (1950).

[12] Hipple, Sommer, and Thomas, Phys. Rev. **80**, 487 (1950).

[13] F. Bitter, Phys. Rev. **75**, 1326 (1949).

[14] Supplement 1 to *Nuclear Data*, National Bureau of Standards Circular No. 499 (1951), p. 1.

[15] F. Alder and F. C. Yu, Phys. Rev. **81**, 1067 (1951).

[16] Townes, Mays, and Dailey, Phys. Rev. **76**, 700 (1949).

[17] Hatton, Rollin, and Seymour, Phys. Rev. **83**, 672 (1951).

[18] M. G. Mayer, Phys. Rev. **78**, 16 (1950); Haxel, Jensen, and Suess, Phys. Rev. **75**, 1766 (1949).

[19] A. L. Schawlow and C. H. Townes, Phys. Rev. **82**, 268 (1951).

[20] The author wishes to thank D. E. Maxwell of the Physics Laboratory of Stanford University for the measurement of the proton relaxation times by means of the spin-echo method.

taminants and that it is these contaminants which cause relaxation of the protons and, to a much smaller degree, also of the Si^{29} nuclei.

Attempts have been made to achieve the proper slow passage conditions which would allow a spin determination from the magnitude of the signal by adding several paramagnetic catalysts to the solutions of SiO_2. With none of the catalysts exhibiting the desired effects, these attempts of a conclusive spin determination for Si^{29} have been temporarily abandoned.

Resonances have also been observed in samples of powdered silicon metal, and these signals exhibited a slight chemical shift of about 1/5500 toward lower fields. By far the best signals with a signal-to-noise ratio of about one hundred are obtained in cobalt and lead glass. However, these samples of glass are not suitable for spin determination because of the uncertainty in the number of nuclei which actually contribute to the nuclear induction signal and because of the fact that the measured longitudinal and transverse relaxation times were considerably different.

B. Sulfur

Eshbach, Hillger, and Jen,[21,22] by observing the Zeeman effect on the microwave rotational spectrum of OCS enriched in S^{33}, determined the magnetic moment of the stable odd sulfur isotope to be $\mu(S^{33}) = 0.632 \pm 0.010$ nm. The nuclear induction resonance of S^{33} in a sample of CS_2 was first observed near 3.05 Mc and in the neighborhood of 9.4 kilogauss. A comparison of the resonant frequency of N^{14} in 3.2 normal HNO_3 with that of S^{33} in CS_2 yielded the result

$$\nu(S^{33})/\nu(N^{14}) = 1.06174 \pm 0.00013.$$

Taking for the spin the value $\frac{3}{2}$,[23] the magnetic moment was calculated to be

$$\mu(S^{33}) = +0.64292 \pm 0.00014.$$

The positive sign of the moment was verified by a comparison of the sign of the S^{33} signal with that of N^{14} at the same frequency and different magnetic fields.

C. Zinc

The isotope Zn^{67} with an abundance of 4.11 percent is the only odd nucleon nucleus of the five naturally occurring isotopes of zinc. Lyshede and Rasmussen[24] by means of spectroscopic analysis tentatively assigned a value of 5/2 for the spin of the nucleus and also reported a value of +0.9 nm for the magnetic moment. Later Arroe[25] from a study of the hfs of an enriched sample confirmed the above value of the nuclear spin.

Nuclear induction signals in $Zn(NH_3)^{++}$ were observed at about 2.35 Mc and 8.84 kilogauss, with a signal-to-noise ratio of about six. A comparison of the resonant frequency of N^{14} with that of Zn^{67} and $ZnSO_4$ yielded the result

$$\nu(Zn^{67})/\nu(N^{14}) = 0.86580 \pm 0.00001.$$

Taking for the spin the value of 5/2, the following magnetic moment results:

$$\mu(Zn^{67}) = +0.87378 \pm 0.00013.$$

The sign of the magnetic moment was determined to be positive and the nuclear spin of 5/2 was verified by careful comparison of the signal amplitudes and line widths of Zn^{67} in $ZnSO_4$ and of H^2 in 0.5 percent solution of D_2O in 8 molar $MnCl_2$.

D. Arsenic

Arsenic has only one naturally occurring isotope and a spin of $\frac{3}{2}$.[26] Spectroscopically, Schuler and Marketu[27] measured the magnetic moment as 1.5 ± 0.3 nm and also reported a nuclear quadrupole moment of $+0.3 \times 10^{-24}$ cm^2. This value of the magnetic moment would seem to be an exception to the average distribution of nuclear moments as represented by Bloch.[28] It was therefore advisable to attempt a more precise determination of the magnetic moment by means of nuclear induction. Owing to the rather large quadrupole moment, it was necessary to choose a compound which when dissociated would place the arsenic nucleus in a symmetrical configuration. The solution of 2 molar Na_2HAsO_4 in 3 molar NaOH was employed on the assumption that AsO_4^{-3} ions of tetrahedral symmetry are formed. As a result, the gradient of the electric fields to which the arsenic nucleus is subjected would be minimized for the reason of symmetry and an excess quadrupole broadening of the line would be avoided. The nuclear resonance obtained in the above solution was compared to the sodium resonance resulting from a solution of NaCl to which 0.5 molar $MnCl_2$ had been added as a catalyst. This comparison yielded the result

$$\nu(As^{75})/\nu(Na^{23}) = 0.64745 \pm 0.00015. \quad (1)$$

Taking the spin of $\frac{3}{2}$, the sign and value of the magnetic moment were found to be

$$\mu(As^{75}) = +1.4347 \pm 0.0003. \quad (2)$$

Since the publication of the above result, Staub and collaborators[29] have also independently measured the magnetic moment of arsenic in both AsO_4^{-3} and AsS_4^{-3} ions. The value reported by Staub *et al.* agrees within the experimental error with the value given in Eq. (2).

[21] Eshbach, Hillger, and Jen, Phys. Rev. **80**, 1106 (1950).
[22] Eshbach, Hillger, and Strandberg, Phys. Rev. **85**, 532 (1952).
[23] C. H. Townes and S. Geschwind, Phys. Rev. **74**, 626 (1948).
[24] J. M. Lyshede and E. Rasmussen, Z. Physik **104**, 375 (1937).
[25] O. H. Arroe, Phys. Rev. **74**, 1263 (1948).
[26] Dailey, Rusinow, Shulman, and Townes, Phys. Rev. **74**, 1245 (1948).
[27] H. Schuler and M. Marketu, Z. Physik **102**, 703 (1936).
[28] F. Bloch, Phys. Rev. **83**, 839 (1951).
[29] Staub, Jeffries, and Loeliger, Helv. Phys. Acta **24**, 643 (1951) and Phys. Rev. **85**, 478 (1952).

E. Selenium

Of the six naturally occurring isotopes, selenium has only one odd isotope Se^{77}, with an abundance of about 7.5 percent. The spin of this nucleus has recently been determined to be $\frac{1}{2}$,[30] which is the value predicted by the shell model of the nucleus. According to this model, the odd nucleon would be in the $P_{\frac{1}{2}}$ level and hence would exhibit a positive magnetic moment. Taking the Schmidt value of 0.64 nm as the upper limit for the magnetic moment of Se^{77}, the spectrometer was set to search over a range of values extending as far below this limit as possible. Since the spin of the selenium isotope is known to be $\frac{1}{2}$, the question arises concerning the addition of a paramagnetic catalyst. Normally for nuclei with spin $\frac{1}{2}$, it is necessary to add a catalyst in order to enhance the establishment of thermal equilibrium. However, in this case, the catalyst was not only unnecessary but acutally deleterious in the sense that the effect of the catalyst was to cause a less favorable ratio of the relaxation times T_1 and T_2.

The fact that relatively narrow lines were observed in a solution of H_2SeO_3 in water, not containing any catalyst, can possibly be attributed to the slight action of the paramagnetic monatomic selenium in acid solutions. The presence of a paramagnetic catalyst was supported by the observed fact that it not only affected the relaxation times of the selenium nuclei, but also shortened significantly the relaxation times of the sodium nuclei which were added to the selenous acid for the purpose of comparing the resonant frequencies.

A comparison of the resonant frequency of Se^{77} with that of Na^{23} gave the result:

$$\nu(Se^{77})/\nu(Na^{23})=0.72193\pm0.00002.$$

With the known magnetic moment of Na^{23} and the fact that the spin of Se^{77} is $\frac{1}{2}$, the sign and value of the magnetic moment were found to be

$$\mu(Se^{77})=+0.53326\pm0.00005.$$

F. Tellurium

Tellurium has two odd isotopes Te^{123} and Te^{125}, which occur naturally with an abundance of 0.85 percent and 7.0 percent, respectively. The spins of these isotopes have been measured as $\frac{1}{2}$.[31,32] Mack and Arroe[32] from their studies of hfs reported that the ratio of the magnetic moments of the isotopes is 1.208 with a maximum deviation of 5 percent. Recently Ross and Murakawa[33] have reported the magnetic moments to be

$$\mu(Te^{125})=-0.7\pm0.2 \text{ nm}$$

and

$$\mu(Te^{123})=-0.6\pm0.2 \text{ nm}.$$

Using a 3.1 molar solution of TeO_2 in HCl and also one of cp tellurium metal in aqua regia, signals of Te^{125} and Te^{123} were observed in both the above solutions without the addition of paramagnetic catalyst.

The resonant frequencies of $Te^{125,123}$ were compared with that of Na^{23} in NaCl, with the result

$$\nu(Te^{125})/\nu(Na^{23})=1.19457\pm0.00004$$

and

$$\nu(Te^{123})/\nu(Na^{23})=0.99085\pm0.00003.$$

Taking the value of the spin of the two isotopes to be $\frac{1}{2}$, the signs and values of the magnetic moments of $Te^{125,123}$ are, respectively,

$$\mu(Te^{125})=-0.88235\pm0.00004$$

and

$$\mu(Te^{123})=-0.73188\pm0.00004.$$

The ratio of the magnetic moments of the two isotopes is therefore calculated to be

$$\mu(Te^{125})/\mu(Te^{123})=1.20560\pm0.00007,$$

which is in good agreement with the original value obtained by Mack and Arroe.[32]

If the leakage voltage of the spectrometer is adjusted for the observation of the absorption mode of the nuclear resonance, the tellurium signals in solutions of $TeCl_2$ are found to saturate at a half-amplitude of the rf field of about 0.06 gauss. The application of the phenomenological equations to this case and the measurement of the line widths (for the most part determined by the field inhomogeneity over the sample) yielded for the ratio of T_1/T_2 the approximate value of 12. The fact that slow passage conditions were achieved in these solutions with nuclei of spin $\frac{1}{2}$ suggests that there are paramagnetic contaminants in the chemical reagents. It is known that there are small traces of iron in every stock solution of cp HCl which might possibly account for the relatively short relaxation time. However, it is also known that there exists monatomic tellurium[34] in acid solutions and further that these atoms are likely to be paramagnetic in analogy with oxygen. This situation is similar to that encountered in the case of Se^{77} (see Part E of this section), which belongs to the same group of the periodic table. The nuclei of both elements had sufficiently short relaxation times to exhibit good signals in spite of the fact that different solvents were used in the two cases. This result indicated, therefore, that the relaxation in this case is probably due to the action of paramagnetic atoms rather than of possible contaminants. Another similarity of tellurium with selenium lies in the observed fact that the addition of manganese ions with a few tenths molar concentration was sufficient to diminish the signal amplitudes to a point where they could no longer be detected.

The first tellurium signals were detected in a sample

[30] S. P. Davis and F. A. Jenkins, Phys. Rev. **83**, 1269 (1951).
[31] F. Bitter, Phys. Rev. **75**, 1326 (1949).
[32] C. R. Fowles, Phys. Rev. **76**, 571 (1949); **78**, 744 (1950); J. E. Mack and O. H. Arroe, Phys. Rev. **76**, 1002 (1949).
[33] J. S. Ross and K. Murakawa, Phys. Rev. **85**, 559 (1952).
[34] *Textbook of Inorganic Chemistry*, edited by J. Newton Friend (Charles Griffin and Company, Ltd., London, 1931), Vol. VII, Part 2, p. 365.

of powdered tellurium metal. Under the conditions of slow passage and with sweep amplitudes small compared to the natural line width of the nuclear induction signals, the output voltage of the spectrometer as registered by the dc milliammeter is the derivative of the slow passage signal. Under these conditions the area under the trace is zero. The aspect of the signals in metallic tellurium indicated that the experimental conditions of the metal were not those of slow passage; in addition, it was not possible to detect an absorption mode with the lowest available half-amplitude of the rf field of about 0.01 gauss. Both facts indicate that the longitudinal relaxation time in the metal is comparatively long. No observable chemical shift was detected between the resonant frequency of Te^{125} in the pulverized metal and in the solutions.

The author wishes to express his profound gratitude to Professor Felix Bloch for his active interest and stimulating guidance throughout the course of this research. He would also like to express his appreciation to Dr. S. S. Dharmatti who assisted him in the measurements of the nuclear moments discussed in this paper. Thanks are also due Dr. H. S. Johnston and other members of the Department of Chemistry of Stanford University for their aid in the preparations of several of the compounds used.

PHYSICAL REVIEW VOLUME 89, NUMBER 5 MARCH 1, 1953

Atomic Excitation and Ionization Accompanying Orbital Electron Capture by Nuclei*

H. PRIMAKOFF AND F. T. PORTER
Department of Physics, Washington University, St. Louis, Missouri
(Received October 10, 1952)

The process of atomic excitation and ionization accompanying orbital electron capture by nuclei is treated on the basis of the general theory of β-decay using a configuration space representation for both nucleons and leptons. Quantitative expressions are obtained (a) for the total number of double holes produced in the K-shell due to K-capture accompanied by excitation or ejection of the other K-electron [Eq. (15)], and (b) for the total probability of electron ejection in orbital electron capture together with the ejected electron momentum spectrum [Eqs. (17)–(18)]. A discussion is given of the possibilities of experimental verification of the theory developed.

I. INTRODUCTION

IN the customary physical description of orbital electron capture, one views the process as involving the transformation of one of the atomic orbital electrons (most probably from the K-shell) into an emitted neutrino with the simultaneous transformation of one of the nuclear protons into a neutron. In this description, no other particles are considered to be emitted, and the other electrons in the atom are presumed to remain in their original orbits, adjusted from the charge of the parent nucleus Z_i to that of the daughter $Z_f=Z_i-1$. Actually, however, a certain nonvanishing probability exists (a) for photon emission as a result of the charge acceleration involved in the orbital electron capture[1] and (b) for the excitation of one (or more) of the noncaptured orbital electrons into unoccupied atomic bound[2] states and into unbound states as a consequence of the nuclear charge alteration as conditioned by the electron-electron Coulomb interaction. In a certain proportion of the orbital electron captures then, the emitted neutrino is accompanied by another particle, *viz.*, a photon or a previously bound electron with which the neutrino must share the available energy. The energy release in orbital electron capture, which is otherwise not directly obtainable, may then be found by measuring the maximum energy carried off by the photon or by the ejected electron. Such a measurement has indeed been carried out recently for the case of photons associated with orbital electron capture in $_{26}Fe^{55}$,[3,4] and the energy release in the transition accurately determined.

In the present paper we shall calculate (a) the total number of double holes produced in the K-shell due to the transformation of one of the K-electrons into the emitted neutrino and the excitation of the other K-electron into an unoccupied bound[2] or into an unbound (ejected) state, and (b) the total probability of (other) electron ejection in orbital electron capture together with the ejected electron momentum distribution. Our work is closely related to the work of Migdal[5] and of Feinberg[6] on the ejection of atomic orbital electrons during nuclear negatron decay.[7]

* Assisted by the joint program of the U. S. Office of Naval Research and the U. S. Atomic Energy Commission.

[1] P. Morrisson and L. Schiff [Phys. Rev. **58**, 24 (1940)] give the theory.

[2] The binding is virtual in all cases of interest (see reference 11).

[3] Bell, Jauch, and Cassidy, Science **115**, 12 (1952).

[4] D. Maeder and P. Preiswerk, Phys. Rev. **84**, 595 (1951); see also the work on $_{18}A^{37}$ by Anderson, Wheeler, and Watson, Phys. Rev. **87**, 668 (1952).

[5] A. Migdal, J. Phys. (U.S.S.R.) **IV**, 449 (1941).

[6] E. L. Feinberg, J. Phys. (U.S.S.R.) **IV**, 423 (1941).

[7] See also the careful discussion of atomic electron excitation and ejection in the negatron transition $_2He^6 \rightarrow {}_3Li^6$, by A. Winther,

II. CALCULATIONS

Specification of Ψ_{initial}, Ψ_{final}; $H^{(0)}$, $H^{(1)}$

We consider for the time being only orbital electron capture from the K-shell and the possibility of excitation of the other K-electron. Neglecting the influence of the L, M, $\cdots$ electrons on the K-electrons, we have for the (effectively two-electron) wave function of the parent atom in the initial state

$$\Psi_{\text{ini}}=\Phi_{E_i,Z_i}(\cdots,\mathbf{x}_n,s_n,q_n,\cdots)\left(\frac{1-P_{12}}{\sqrt{2}}\right)\times[u_{\text{ini}}(\mathbf{r}_1,\mathbf{r}_2)v_+(s_1)v_-(s_2)w_e(q_1)w_e(q_2)], \quad (1)$$

and for the (effectively one-electron) wave function of the daughter atom plus emitted neutrino

$$\Psi_{\text{fin}}=\Phi_{E_f,Z_f}(\cdots,\mathbf{x}_n,s_n,q_n,\cdots)\left(\frac{1-P_{12}}{\sqrt{2}}\right)\times[u_{\text{fin}}(\mathbf{r}_1,\mathbf{r}_2)v_{\sigma_\nu}(s_1)v_{\sigma_e}(s_2)w_\nu(q_1)w_e(q_2)]. \quad (2)$$

In Eqs. (1) and (2), the Φ's are wave functions of the parent and daughter nuclei, the $\mathbf{x}_n$, s_n, q_n, being nucleon space, spin and charge coordinates; P_{12} is the lepton coordinate permutation operator; $v_{\sigma_\nu}(s_l)=v_+(s_l)$ or $v_-(s_l)$, $v_{\sigma_e}(s_l)=v_+(s_l)$ or $v_-(s_l)$, are the lepton spin wave functions; $w_e(q_l)$, $w_\nu(q_l)$ are lepton charge wave functions ($w_e(1)=1$; $w_e(0)=0$; $w_\nu(1)=0$, $w_\nu(0)=1$); $u_{\text{ini}}(\mathbf{r}_1,\mathbf{r}_2)$ and $u_{\text{fin}}(\mathbf{r}_1,\mathbf{r}_2)$ are the lepton space wave functions. Explicitly we have

$$u_{\text{fin}}(\mathbf{r}_1,\mathbf{r}_2)=V^{-\frac{1}{2}}\exp(i\mathbf{k}_\nu\cdot\mathbf{r}_1)\chi_f(\mathbf{r}_2), \quad (3)$$

where $u_{\text{fin}}(\mathbf{r}_1,\mathbf{r}_2)$ can be written as a product of single lepton space wave functions since the two leptons have no electromagnetic interaction with each other in the final state (one of the two leptons is a neutrino, the other an electron); $\chi_f(\mathbf{r}_2)$ is the space wave function of the other (noncaptured) electron after the K-capture. Thus, for example, if we are calculating the probability that the other electron is still in the K-shell (about the daughter nucleus) after the capture, we would put (since $Z_f=Z_i-1$)

$$\chi_f(\mathbf{r}_2)=(\pi a^3)^{-\frac{1}{2}}(Z_i-1)^{\frac{3}{2}}\exp[-r_2(Z_i-1)/a], \quad (4)$$

whereas, if we are calculating the probability that the other electron is ejected from the atom as a consequence of the capture, we would write

$$\chi_f(\mathbf{r}_2)=V^{-\frac{1}{2}}\exp(i\mathbf{k}_e\cdot\mathbf{r}_2)F_{\mathbf{k}_e,Z_i-1}(\mathbf{r}_2), \quad (5)$$

$F_{\mathbf{k}_e,Z_i-1}(\mathbf{r}_2)$ being the (properly normalized) Coulomb field confluent hypergeometric function. Further,

$$u_{\text{ini}}(\mathbf{r}_1,\mathbf{r}_2)=N(\pi a^3)^{-1}Z_i^3\exp[-Z_i(r_1+r_2)/a]\times\exp[\gamma_2(r_1+r_2)/a]\exp(\gamma_1 r_{12}/a), \quad (6)$$

with $N^2\cong 1-(35/8)(\gamma_1/Z_i)-6\gamma_2/Z_i$. In Eq. (6) we use a space wave function for the two leptons in the initial state (both are electrons) which describes the effect of their mutual Coulomb interaction (a) on the electrostatic shielding of the Coulomb attraction of the parent nucleus (factor $\exp[\gamma_2(r_1+r_2)/a]$), and (b) on their spatial correlation (factor $\exp[\gamma_1 r_{12}/a]$). The analytic forms chosen for these shielding and correlation factors make u_{ini} a reasonably good fit to Hylleraas' variational nonrelativistic wave function for the problem of two electrons in the ground state about a nucleus of charge Z_i,[8] providing that the numerical values for γ_1 and γ_2 are chosen as 0.38 and 0.12, respectively. In spite of the smallness of γ_1 and γ_2 compared to Z_i, it is essential to keep the factors containing these quantities since the approximate orthogonality of u_{fin} and u_{ini} makes the transition matrix element, $M_{i\to f}$, depend sensitively on γ_1 and γ_2 (see Eqs. (14)–(16) below—according to Eq. (16), $M_{i\to f}\sim[(Z_i-\gamma_1-\gamma_2)-(Z_i-1)]=1-\gamma_1-\gamma_2$; the here neglected largely shielding effect of the L, M, $\cdots$ electrons on the K electrons is expected, at least in first order, to affect (Z_i-1) and $(Z_i-\gamma_1-\gamma_2)$ equally and so to cancel out in their difference).

The initial and final state wave functions Ψ_{ini} and Ψ_{fin} are eigenfunctions of the "zero order" Hamiltonian $H^{(0)}$,

$$H^{(0)}=H_{\text{nucleons}}(\cdots,\mathbf{x}_n,s_n,q_n,\cdots)+\sum_{l=1}^{2}H_{\text{leptons};l}(\mathbf{x}_l,s_l,q_l)+\frac{e^2q_1q_2}{r_{12}}+\sum_{n=1}^{A}\sum_{l=1}^{2}\left[\frac{(-e^2)q_nq_l}{|\mathbf{x}_n-\mathbf{r}_l|}\right], \quad (7)$$

to within the errors made in using the approximate form for u_{ini} in Eq. (6), instead of the rigorous solution of

$$\left\{\sum_{l=1}^{2}(H_{\text{leptons};l})+\frac{e^2}{r_{12}}-\sum_{n=1}^{A}\frac{e^2q_n}{|\mathbf{x}_n-\mathbf{r}_1|}-\sum_{n=1}^{A}\frac{e^2q_n}{|\mathbf{x}_n-\mathbf{r}_2|}\right\}u_{\text{ini}}=\epsilon_{\text{ini}}u_{\text{ini}}.$$

Kgl. Danske Videnskab. Selskab, Mat.-fys. Medd. **27**, No. 2 (1952). Very recently also, a thorough discussion of the "Effects of radioactive disintegrations on the inner electrons of the atom" has been given by J. S. Levinger (Bull. Am. Phys. Soc. **27**, No. 5, 23 (1952)). We wish to thank Dr. Levinger for a helpful discussion and letter and for the communication of a copy of his paper before publication. In general, agreement exists between his results and ours on the probability of excitation and ejection of atomic orbital electrons in $\beta^\pm$ decay and in K-capture.

[8] See, for example, H. Bethe, *Handbuch der Physik* (J. Springer, Berlin, 1933), Vol. XXIV/1, p. 362

The wave functions Ψ_{ini} and Ψ_{fin} are also eigenfunctions of all operators commuting with $H^{(0)}$ such as the total nuclear charge operator

$$Z_{\text{op}}=\sum_{n=1}^{A} q_n$$

(with eigenvalues Z_i, $Z_f=Z_i-1$). We note that the last term in $H^{(0)}$ [Eq. (7)] (nucleon-lepton Coulomb interaction) is very well approximated by

$$(-e^2)Z_{\text{op}}\sum_{l=1}^{2}\frac{q_l}{|\mathbf{r}_l|},$$

and that the nonrelativistic (Schrödinger) approximation to the free particle Dirac H_{lepton} is used when the leptons are in the electron state; also the relatively small effect of daughter atom recoil on Ψ_{fin} is neglected.

Finally, in calculating the transition probability for K-orbital electron capture with excitation of the other K-electron, we need to specify the nucleon-lepton β-decay interaction Hamiltonian, $H^{(1)}$. This takes the form, in our configuration space representation for both nucleons and leptons,

$$H^{(1)}=g\sum_{n=1}^{A}\sum_{l=1}^{2} Q_n\Omega_n{}^{(\mu)}Q_l\Omega_l{}^{(\mu)}\delta(\mathbf{x}_n-\mathbf{r}_l)$$
$$+(\text{Hermitian conjugate}). \quad (8)$$

The Q_l are lepton charge transformation operators [$Q_l w_\nu(q_1)=w_\nu(q_1)$; $Q_l w_\nu(q_1)=0$; etc.]. The Q_n are the analogous and usual nucleon charge transformation operators. The $\Omega_n{}^{(\mu)}$ and $\Omega_l{}^{(\mu)}$ are the customary Dirac covariant operators appropriate to the form of β-decay coupling employed (e.g., $\Omega_l{}^{(\mu)}=\sigma_l{}^{(1)}$, $\sigma_l{}^{(2)}$, $\sigma_l{}^{(3)}$, $\beta_l\alpha_l{}^{(1)}$, $\beta_l\alpha_l{}^{(2)}$, $\beta_l\alpha_l{}^{(3)}$ for tensor coupling), a summation being implied over the repeated superscript (μ).

The transition probability per unit time, $P_{i\to f}$, from the initial to the final state is then given by the standard formula involving the square of the matrix element of $H^{(1)}$ taken between Ψ_{ini} and Ψ_{fin}:

$$P_{i\to f}=\frac{2\pi}{\hbar}\left|\int\Psi^*_{\text{fin}}H^{(1)}\Psi_{\text{ini}}\right|^2\rho_{\text{fin}}. \quad (9)$$

III. CALCULATION

Evaluation of Matrix Element and $P_{i\to f}$

In order to calculate the total probability of the noncaptured K electron *not* remaining in the K-shell as a result of the K-capture, we calculate the complementary probability of its remaining in the K-shell. We have then, from Eqs. (1), (2), (4), (8),

$$\begin{aligned}M_{i\to f}&=\int\Psi^*_{\text{fin}}H^{(1)}\Psi_{\text{ini}}\\
&=\int\Phi^*_{E_f,Z_i-1}\left\{\left[\frac{1-P_{12}}{\sqrt{2}}\right][V^{-\frac{1}{2}}\exp(i\mathbf{k}_\nu\cdot\mathbf{r}_1)\right.\\
&\times(\pi a^3)^{-\frac{1}{2}}(Z_i-1)^{\frac{3}{2}}\exp[-(r_2/a)(Z_i-1)]\\
&\left.\times v_{\sigma_\nu}(s_1)v_{\sigma_e}(s_2)w_\nu(q_1)w_e(q_2)]\right\}^*\\
&\cdot\left\{g\sum_{n=1}^{A}\sum_{l=1}^{2}Q_n\Omega_n{}^{(\mu)}Q_l\Omega_l{}^{(\mu)}\delta(\mathbf{x}_n-\mathbf{r}_l)\right\}\\
&\cdot\Phi_{E_i,Z_i}\left\{\left[\frac{1-P_{12}}{\sqrt{2}}\right][N(\pi a^3)^{-\frac{1}{2}}Z_i{}^{\frac{3}{2}}\exp(-Z_i r_1/a)\right.\\
&\times\exp(-Z_i r_2/a)\exp[(\gamma_2/a)(r_1+r_2)]\\
&\left.\times\exp(\gamma_1 r_{12}/a)v_+(s_1)v_-(s_2)w_e(q_1)w_e(q_2)]\right\}. \quad (10)\end{aligned}$$

Neglecting, x_n compared to r_2 in $\exp[(\gamma_1/a)|\mathbf{x}_n-\mathbf{r}_2|]$ (x_n nuclear, r_2 atomic dimensions, respectively), we can write

$$\begin{aligned}M_{i\to f}&=\int\{(\pi a^3)^{-\frac{1}{2}}(Z_i-1)^{\frac{3}{2}}\exp[-(r_2/a)(Z_i-1)]\}\\
&\times\{N(\pi a^3)^{-\frac{1}{2}}Z_i{}^{\frac{3}{2}}\exp[-(r_2/a)(Z_i-\gamma_1-\gamma_2)]\}d\mathbf{r}_2\\
&\cdot\int v_{\sigma_\nu}{}^*(s_1)v_{\sigma_e}{}^*(s_2)\Omega_1{}^{(\mu)}(1-P_{12})v_+(s_1)v_-(s_2)\\
&\cdot g\int\Phi^*_{E_f,Z_i-1}\sum_{n=1}^{A}Q_n\Omega_n{}^{(\mu)}V^{-\frac{1}{2}}\\
&\times\exp(-i\mathbf{k}_\nu\cdot\mathbf{x}_n)(\pi a^3)^{-\frac{1}{2}}Z_i{}^{\frac{3}{2}}\\
&\times\exp[-(x_n/a)(Z_i-\gamma_2)]\Phi_{E_i,Z_i}\\
&=N(Z_i-1)^{\frac{3}{2}}Z_i{}^{\frac{3}{2}}[Z_i-\tfrac{1}{2}(1+\gamma)]^{-3}\\
&\cdot S^{(\mu)}\cdot[\text{M.E.}^{\text{nucl. }(\mu)}]_{if}, \quad (11)\end{aligned}$$

where $\gamma\equiv\gamma_1+\gamma_2\approx 0.5$; $S^{(\mu)}$, the lepton spin term, involves the integral over s_1, s_2; and $[\text{M.E.}^{\text{nucl. }(\mu)}]_{if}$ involves the integral over $\mathbf{x}_n$, s_n, q_n $[\text{M.E.}^{\text{nucl. }(\mu)}]_{if}$ is just the nuclear matrix element of the usual theory of K-capture where, in effect, the system considered to represent the parent atom is the nucleus plus one K-shell electron which is subsequently transformed into a neutrino.

The total probability per unit time for K capture is

similarly

$$1/\tau_K = 2\pi\hbar^{-1}\sum_f |M_{i\to f}|^2\rho_f$$
$$= 2\pi\hbar^{-1}\sum_f \left| \int \chi_f^*(\mathbf{r}_2)\{N(\pi a^3)^{-\frac{1}{2}}Z_i^{\frac{3}{2}} \times \exp[-(r_2/a)(Z_i-\gamma)]\}d\mathbf{r}_2 \right|^2 \cdot \sum_{\sigma_\nu,\sigma_e,M_f} |S^{(\mu)}|^2 |\text{M.E.}^{\text{nucl. }(\mu)}]_{if}|^2 \times 4\pi[p_\nu]_f^2 V(8\pi^3\hbar^3 c)^{-1}$$
$$= \sum_f \{[p_\nu]_f^2/(p_\nu^{(0)})^2\} \left| \int \cdots d\mathbf{r}_2 \right|^2 \times \{2\pi\hbar^{-1}2 \sum_{\sigma_\nu,M_f} |(\sigma_\nu|\Omega^{(\mu)}|+)|^2 |[\text{M.E.}^{\text{nucl. }(\mu)}]_{if}|^2 \cdot 4\pi(p_\nu^{(0)})^2 V(8\pi^3\hbar^3 c)^{-1}\}, \quad (12)$$

where

$$c[p_\nu]_f = [(\mathfrak{M}_i - \mathfrak{M}_f)c^2 - B_{(Z_i-1)}] - B_{(Z_i-1)} - \epsilon_f \equiv cp_\nu^{(0)} - (B_{(Z_i-1)} + \epsilon_f),$$

and the sum over f runs over every energetically possible final state for the noncaptured electron. Here $\mathfrak{M}_i$ and $\mathfrak{M}_f$ are atomic masses in ground-state electronic configurations, $B_{(Z_i-1)}$ is the K-shell electron binding energy about a nucleus of charge Z_i-1, and ϵ_f is the energy (not inclusive of the rest energy) of the noncaptured K-shell electron in its final state.[9] Thus $cp_\nu^{(0)}$ is the neutrino energy in the conventional "one-electron" type calculation; in this type of calculation, the total K-capture probability per unit time $(1/\tau_K)_{\text{one-elec.}}$ is just the expression in the curly brackets in the third form of Eq. (12).

In order to perform the sum over f, we introduce the definition

$$K_{\text{op}} \equiv 1 - (cp_\nu^{(0)})^{-1}\left[B_{(Z_i-1)} + \left\{\frac{-\hbar^2}{2m}\nabla_{\mathbf{r}_2}^2 - \frac{(Z_i-1)e^2}{r_2}\right\}\right],$$

and note that

$$\tfrac{1}{2}(K_{\text{op}} + |K_{\text{op}}|)\chi_f(\mathbf{r}_2) = ([p_\nu]_f/p_\nu^{(0)})\chi_f(\mathbf{r}_2) \quad \text{or} \quad = 0,$$

depending on whether $[p_\nu]_f > 0$ or < 0, i.e. depending on whether the final state f is energetically possible or not. Equation (12) now becomes

$$\frac{1}{\tau_K} = \sum_{\text{all } f} \left| \int [\tfrac{1}{2}(K_{\text{op}} + |K_{\text{op}}|)\chi_f(\mathbf{r}_2)]^* \{N(\pi a^3)^{-\frac{1}{2}}Z_i^{\frac{3}{2}} \times \exp[-(Z_i-\gamma)r_2/a]\}d\mathbf{r}_2 \right|^2 (1/\tau_K)_{\text{one-elec.}}$$
$$= \int |\tfrac{1}{2}(K_{\text{op}} + |K_{\text{op}}|)\{N(\pi a^3)^{-\frac{1}{2}}Z_i^{\frac{3}{2}} \times \exp[-(Z_i-\gamma)r_2/a]\}|^2 d\mathbf{r}_2 (1/\tau_K)_{\text{one-elec.}}, \quad (13a)$$

the second equality following from the completeness of the χ_f since the sum over f now runs over all final states without exception. Neglecting $1-\gamma$ compared to Z_i-1 in $\exp\{-(r_2/a)[(Z_i-1)+(1-\gamma)]\}$ and remembering that $\exp[-(r_2/a)(Z_i-1)]$ is an eigenfunction of K_{op} with eigenvalue 1, we obtain from Eq. (13a)

$$1/\tau_K \cong N^2 Z_i^3 (Z_i-\gamma)^{-3}(1/\tau_K)_{\text{one-elec.}}, \quad (13b)$$

with a relative error of order $[(1-\gamma)/(Z_i-1)] \cdot [B_{(Z_i-1)}/cp_\nu^{(0)}]$ if $B_{(Z_i-1)}/cp_\nu^{(0)} \ll 1$ and of order $(1-\gamma)/(Z_i-1)$ if $B_{(Z_i-1)}/cp_\nu^{(0)} \gtrsim 1$. The ratio of $1/\tau_K$ to $(1/\tau_K)_{\text{one-elec.}}$ in Eq. (13b) is just the ratio of the electronic charge densities at the nucleus, calculated in the present, and, in the "one-electron type," formulations.

Thus, the probability, per K-capture, P_{remain}, for the noncaptured electron to remain in the K-shell is, from Eqs. (11), (12), (13b),

$$P_{\text{remain}} = \frac{N^2(Z_i-1)^3 Z_i^3}{[Z_i - \tfrac{1}{2}(1+\gamma)]^6}\left(\frac{1}{\tau_K}\right)_{\text{one-elec.}} \div \frac{N^2 Z_i^3}{(Z_i-\gamma)^3}\left(\frac{1}{\tau_K}\right)_{\text{one-elec.}}$$
$$\cong 1 - (3/4)(1-\gamma)^2/Z_i^2, \quad (14)$$

neglecting higher order terms in $1/Z_i$.[10] The probability per K-capture for the production of a double hole in the K-shell is, then,

$$1 - P_{\text{remain}} \cong (3/4Z_i^2)(1-\gamma)^2 \cong 3/16Z_i^2. \quad (15)$$

The sensitivity of this result [as well as of others below, e.g., Eq. (17)] to the somewhat uncertain value of γ should be especially noted. *Note added in proof:*— In addition, in the actual many-electron atom, the probability per K-capture for the production of a double hole in the K-shell is equal to $1 -$ {probability per K-

[9] The present formulation makes it obvious that in the analogous case of negatron (or positron) emission from β-unstable nuclei, the available transition energy arising both from the difference in nuclear mass and from the difference in atomic binding (as between parent and daughter atoms) is shared statistically between the emitted negatron, the emitted neutrino, and any excited or ejected orbital electron. The necessity of inclusion of this difference of atomic binding energy into the transition energy so that it is shared statistically between the emitted negatron and the emitted neutrino, has recently been emphasized by H. M. Schwartz [Phys. Rev. **86**, 195 (1952)]. See also R. Serber and H. S. Snyder, Phys. Rev. **87**, 152 (1952); and, Freedman, Wagner, and Engelkemeir, Phys. Rev. **88**, 1155 (1952).

[10] The quantitative validity of the deviations of P_{remain} from 1 as given in Eq. (14) holds only when Eq. (13b) for $1/\tau_K$ is quantitatively valid, i.e., in the usual case: $B_{(Z_i-1)}/cp_\nu^{(0)} \ll 1$. If $B_{(Z_i-1)}/cp_\nu^{(0)} \gg 1$, the only possible value for ϵ_f is $-B_{(Z_i-1)}$, and $1/\tau_K = N^2(Z_i-1)^3 Z_i^3[Z_i - \tfrac{1}{2}(1+\gamma)]^{-6}(1/\tau_K)_{\text{one-elec.}}$, yielding, as required, $P_{\text{remain}} = 1$.

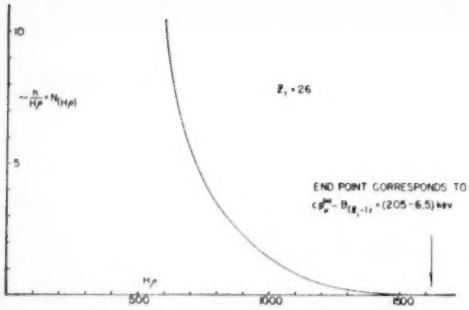

FIG. 1. Predicted shape of the momentum distribution of ejected orbital electrons [Eq. (18a, b)] with energies above 30 kev, accompanying K-capture for $Z_i=26$ and with $cp_\nu^{(0)}=205$ kev. Note that the end point would be difficult to determine from any experimental data unless this data is treated as suggested in the text.

capture for the production of a single hole in the K-shell$\}-\{$probability per K-capture for the production of zero holes in the K-shell$\}\equiv 1-p^{(1)}-p^{(0)}\equiv p^{(2)}$; a treatment entirely analogous to the above, but using atomic many-electron wave functions built up out of an appropriately antisymmetrized superposition of products of hydrogenic one-electron orbital wave functions, indicates that $1-p^{(1)}\cong 1-P_{\text{remain}}$ of Eqs. (14), (15), while

$$p^{(0)}\cong\sum_{n=2}^{\infty}[(\Delta Z)_n/Z_i]^2 C_n\eta_n.$$

In the expression for $p^{(0)}$, the successive terms in the series give the contributions of the L, M, $\cdots$ shells, the η_n being 1, $\frac{1}{2}$, or 0 depending on whether the ns orbit in the corresponding shell is filled, half-filled, or unfilled; the C_n are given by $C_2=0.31$, $C_3=0.06$, $\cdots$, while $(\Delta Z)_n$ is the difference between the effective nuclear charges associated with an hydrogenic ns orbit in the parent atom and an hydrogenic ls orbit in the daughter atom (in fact, the nth term in the series for $p^{(0)}$ is just the square of an integral analogous to the integral over $\mathbf{r}_2$ in Eq. (11) with the first factor there replaced by a daughter atom hydrogenic ls orbital wave function and the second factor by a parent atom hydrogenic ns orbital wave function). The value of $p^{(0)}$ can be roughly estimated as about one-third of $1-p^{(1)}$, so that $p^{(2)}\cong[(3/4Z_i^2)(1-\gamma)^2](2/3)$; the importance of this correction has been emphasized to us by Levinger (reference 7) who, however, estimates the correction factor to $p^{(2)}$ as $\frac{1}{2}$ instead of our 2/3. In light of the uncertainty regarding the exact numerical value of this correction factor, we have generally omitted it in the text below.

We now calculate the total probability in K-orbital electron capture that the other K-electron is ejected, and we also obtain the momentum distribution of the ejected K-electrons. In a manner wholly analogous to the above, the matrix element $M_{i\to f}$ for K-capture with the other K-electron ejected with a wave number $\mathbf{k}_e$ is [see Eqs. (5), (10), (11)],

$$\begin{aligned}M_{i\to f}=&\int[V^{-\frac{1}{2}}\exp(i\mathbf{k}_e\cdot\mathbf{r}_2)F_{\mathbf{k}_e,Z_i-1}(\mathbf{r}_2)]^*\\&\times\{N(\pi a^3)^{-\frac{1}{2}}Z_i^{\frac{3}{2}}\exp[-(r_2/a)(Z_i-\gamma)]\}d\mathbf{r}_2\\&\cdot S^{(\mu)}\cdot[\text{M.E.}^{\text{nucl. }(\mu)}]_{if}\\=&NV^{-\frac{1}{2}}(\pi a^3)^{-\frac{1}{2}}Z_i^{\frac{3}{2}}\{[2\pi(Z_i-1)/(137\beta_e)]\\&\times[1-\exp(-2\pi(Z_i-1)/137\beta_e)]^{-1}\}^{\frac{1}{2}}\\&\cdot\{8\pi/a[(Z_i-\gamma)^2/a^2+k_e^2]^2\}\\&\cdot\left[\frac{Z_i-\gamma-ik_ea}{Z_i-\gamma+ik_ea}\right]^{(Z_i-1)/i137\beta_e}{}^{[(Z_i-\gamma)-(Z_i-1)]}\\&\cdot S^{(\mu)}\cdot[\text{M.E.}^{\text{nucl. }(\mu)}]_{if},\end{aligned}\quad(16)$$

the integral over $\mathbf{r}_2$ being evaluated from formulas given in A. Sommerfeld's *Wellenmechanik* (this integral with $\gamma=0$ has also been previously evaluated by Migdal[5] and by Feinberg[6] in their problem of orbital electron ejection associated with nuclear negatron decay). The total probability per K-capture, P_{ejec}, for ejection of the other K-electron with any (energetically possible) wave number $k_e=(mc/\hbar)p_e$ is then from Eqs. (16), (12), (13b),

$$\begin{aligned}P_{\text{ejec}}=&\left[\frac{N^2Z_i^3}{(Z_i-\gamma)^3}\right]^{-1}\int_0^{(p_e)_{\max}}\frac{N^2}{\pi}\frac{Z_i^3(137)^3}{(Z_i-\gamma)^8}64\pi^2(1-\gamma)^2\\&\times\left\{\frac{2\pi(Z_i-1)}{137\beta_e}\left(1-\exp\left[\frac{-2\pi(Z_i-1)}{137\beta_e}\right]\right)^{-1}\right\}\\&\cdot\exp\left[-4\tan^{-1}\left(\frac{137p_e}{Z_i-\gamma}\right)\frac{(Z_i-1)}{137\beta_e}\right]\\&\times\{1+[137/(Z_i-\gamma)]^2p_e^2\}^{-4}\\&\cdot[1-(cp_\nu^{(0)})^{-1}(B_{(Z_i-1)}+mc^2p_e^2/2)]^2\\&\times(2\pi^2)^{-1}p_e^2dp_e\end{aligned}\quad(17a)$$

or remembering that

$$(p_e)_{\max}=[(Z_i-1)/137][(cp_\nu^{(0)}/B_{(Z_i-1)})-1]^{\frac{1}{2}},$$

and neglecting the difference between $Z_i-\gamma$ and Z_i-1 and between β_e and p_e,

$$P_{\text{ejec}}\cong[(1-\gamma)^2/(Z_i-\gamma)^2]0.3\cong 0.08/Z_i^2.\quad(17b)^{11}$$

The approximate equalities in Eq. (17b) are valid for the usual case: $cp_\nu^{(0)}/B_{(Z_i-1)}\gg 1$. On the other hand, near the energetic threshhold for other K-electron ejection: $[cp_\nu^{(0)}/B_{(Z_i-1)}]-1\ll 1$, the integral in Eq.

[11] From Eqs. (15), (17b) one sees that the probability per K-capture, of excitation of the other K electron into a previously unoccupied orbit of the actual many electron atom is $\cong(0.75-0.30)(1-\gamma)^2/Z_i^2$. The corresponding excited state of the daughter atom then possesses two holes in the K-shell (as indeed it also does after other-K-electron ejection), and, in all cases of interest is energetically capable of spontaneous ionization. In the readjustment of this atomic excited state to the ground state one will thus in general have even more Auger electrons emitted (with kinetic energy $\lesssim B_{(Z_i-1)}$) than in the readjustment of the atomic excited state following a K-capture with the other K-electron remaining in the K-shell.

(17a) gives

$$P_{\text{ejec}} \cong [(1-\gamma)^2/(Z_i-\gamma)^2](32/3) \times e^{-4(cp_\nu^{(0)}/B_{(Z_i-1)}-1)^3}. \quad (17c)$$

Equation 17(a) shows that the ejected electron momentum distribution $D_{\text{ejec}}(p_e)dp_e$ is of the form (see Fig. 1)

$$D_{\text{ejec}}(p_e) = D_{\beta^-}(p_e) \exp\left\{\frac{-4(Z_i-1)}{137\beta_e}\tan^{-1}\left(\frac{137p_e}{Z_i-\gamma}\right)\right\} \times\left[1+\left(\frac{137}{Z_i-\gamma}\right)^2 p_e^2\right]^{-4}, \quad (18a)$$

where

$$D_{\beta^-}(p_e) = \text{const}\times p_e^2\left[\frac{cp_\nu^{(0)}}{mc^2}-\frac{B_{(Z_i-1)}}{mc^2}-\frac{p_e^2}{2}\right]^2 \times\left[\frac{2\pi(Z_i-1)}{137\beta_e}\left(1-\exp\left[\frac{-2\pi(Z_i-1)}{137\beta_e}\right]\right)^{-1}\right] \quad (18b)$$

is the type of momentum distribution found in an allowed negatron transition of a beta-unstable nucleus with available kinetic energy $cp_\nu^{(0)}-B_{(Z_i-1)}$. It is, therefore, seen that the momentum distribution of the ejected K-electrons is very different from the momentum distribution of negatrons from beta-unstable nuclei, since $\exp\{-4[(Z_i-1)/137\beta_e]\ \tan^{-1}[137p_e/(Z_i-\gamma)]\} \times\{1+[137/(Z_i-\gamma)]^2 p_e^2\}^{-4}$ is a very rapidly varying function of p_e—in fact for $(2cp_\nu^{(0)}/mc^2)^{\frac{1}{2}} \gg p_e \gg Z_i/137$, we have

$$D_{\text{ejec}}(p_e) \cong [(1-\gamma)^2/Z_i^2]64(Z_i/137p_e)^7\ (137/Z_i) \times[\exp(2\pi Z_i/137\beta_e)-1]^{-1}. \quad (18c)$$

It is also apparent from the form of Eqs. (18a), (18b) that the data in any future observation of ejected electrons associated with K-capture may be treated in a manner analogous to the treatment of nuclear β-momentum distributions via the F-K plot. Thus, one can graph

$$\{N(p_e)\}^{\frac{1}{4}} \div \left\{\exp\left[-\frac{4(Z_i-1)}{137\beta_e}\right]\tan^{-1}\left(\frac{137p_e}{Z_i-\gamma}\right)\right\} \times\left[1+\left(\frac{137p_e}{Z_i-\gamma}\right)^2\right]^{-4}\left\{\frac{2\pi(Z_i-1)}{137\beta_e} \times\left[1-\exp\left(-\frac{2\pi(Z_i-1)}{137\beta_e}\right)\right]^{-1} p_e^2\right\}^{\frac{1}{4}}$$

vs $1+p_e^2/2$ and a straight line should result. The extrapolated end point of the plot

$$1+cp_\nu^{(0)}/mc^2-\tfrac{1}{2}(Z_i-1)^2/(137)^2 = 1+(\mathfrak{M}_i-\mathfrak{M}_f)/m-\tfrac{1}{2}(Z_i-1)^2/(137)^2 -\tfrac{1}{2}(Z_i-1)^2/(137)^2$$

will then give the K-capture transition energy

$$[(\mathfrak{M}_i-\mathfrak{M}_f)/m-\tfrac{1}{2}(Z_i-1)^2/(137)^2]mc^2.$$

IV. DISCUSSION

It is to be noted that our Eq. (15) for the total number of double holes per K-capture and Eq. (17) for the number of K-electrons ejected per K-capture involve the shielding and correlation parameters γ_1 and γ_2 (through their sum $\gamma=\gamma_1+\gamma_2$) in the initial wave function of the two K-electrons, bearing out the remark made earlier regarding the importance for our problem of a reasonably accurate choice of $u_{\text{ini}}(\mathbf{r}_1, \mathbf{r}_2)$. Physically, our process involves the effect, on one of the two Coulomb interacting electrons, arising from the transformation of the other into a neutrino (with simultaneous passage of a nuclear proton into a neutron); it is then obvious that a proper theory of the process necessitates a reasonably accurate description of the electron-electron interaction. The present point of view also indicates that, if one considers the possibility of L-electron ejection accompanying K-capture, the appropriate (effectively two-atomic electron) initial lepton space wave function is

$$u_{\text{ini}} \sim \exp[-Z_i r_1/a]\exp[-(Z_i-2)r_2/a] \times[1-(r_2/2a)(Z_i-2)],$$

while the appropriate (effectively one-ejected atomic electron) final lepton space wave function becomes

$$u_{\text{fin}} \sim \exp(i\mathbf{k}_\nu\cdot\mathbf{r}_1)\exp(i\mathbf{k}_e\cdot\mathbf{r}_2)F_{\mathbf{k}_e;Z_i-2}(\mathbf{r}_2).$$

Here, it is to be noted that the shielding parameters for the K and L electrons in u_{ini} are taken as 0 and 2, respectively, and that the correlation factor is neglected. This is roughly justified by examination of variational calculations in He and Li.[12] It is also to be noted that in u_{fin} the effective nuclear charge seen by the ejected (originally L) electron after the K-capture is taken as Z_i-2. The justification of this last choice involves the idea that, at values of $\mathbf{r}_2$ where the ejected L-electron wave function in u_{fin} makes the most important contribution to $M_{i\to f}$, the electrostatic potential which is due to the daughter nuclear charge of Z_i-1 plus the electrostatic potential due to the uncaptured K-electron very roughly look like the electrostatic potential of a point charge of Z_i-2. Hence, it is not too inaccurate to use, as a first approximation for the Coulomb field correction factor to the plane wave describing the ejected electron, a confluent hypergeometric function appropriate to an effective nuclear charge of Z_i-2, $[F_{\mathbf{k}_e;Z_i-2}(\mathbf{r}_2)]$. It then follows that the probability of L-electron ejection accompanying K-capture is relatively small, in our approximation zero, because of the orthogonality of the factors depending on $\mathbf{r}_2$ in u_{ini} and u_{fin}; these factors will enter into the expression for $M_{i\to f}$ in a manner analogous to that in Eq. (16). Physically, the L-electron is shielded from the Coulomb force of the nucleus by the two K-electrons in such a way that, in the simultaneous transformation of one of the nuclear protons into a neutron together with that of one of the K-shell electrons into a neutrino, the L-electron experiences comparatively little change in its electrostatic environment and so has small incentive to leave its original orbit. On the other hand it is obvious that this conclusion is extremely sensitive

[12] See reference 8, p. 365.

to any departures from orthogonality of u_{ini} and u_{fin}, so that its quantitative validation will require a rather accurate (and at present unavailable) calculation of the form of the ejected L-electron wave function.

In any case, one can show that the momentum spectrum, of whatever ejected L, M, etc., electrons may be associated with K-capture, must have approximately the same dependence on p_e, for $(mcp_e)^2/2m \gg B_{(Z_i-1)}$, as the momentum spectrum of the ejected K-electrons [Eqs. (17), (18)]. This can be seen by evaluating integrals analogous to that in Eq. (16) with $(u_{\text{ini}})_{K,\ L \text{ or } M \text{ or } \cdots}$ replacing $(u_{\text{ini}})_{K,\ K}$.

The possibility of electron ejection (from the K, L, $\cdots$ shells) accompanying orbital L-capture should also be mentioned. Discussing for simplicity the case of allowed transitions, one sees, first of all, that only capture from the $2s$ orbits need be considered, since the nuclear matrix element involves u_{ini} at points within the nucleus where the (nonrelativistic) $2p$ orbital wave functions effectively vanish. On the other hand, the normalizing factor in the ns orbital wave functions is proportional to $n^{-\frac{3}{2}}(Z_i-\gamma_{Z_i;ns})^{\frac{3}{2}}$, so that, for example, the contribution of L-capture relative to K-capture, to the K-electron ejection, is smaller approximately in the ratio

$$\frac{2(Z_i-\gamma_{Z_i;2s})^3}{2^3(Z_i-\gamma_{Z_i;1s})^3}\left(\frac{1-(1/2^2)B_{(Z_i-1)}/(\mathfrak{M}_i-\mathfrak{M}_f)c^2}{1-B_{(Z_i-1)}/(\mathfrak{M}_i-\mathfrak{M}_f)c^2}\right)^2.$$

The momentum distribution is again essentially given by Eqs. (17), (18). Analogous arguments can be given for the various forbidden transitions.

It now remains to discuss the related problem, previously treated by Migdal[5] and by Feinberg,[6] of orbital electron ejection associated with negatron (or positron) emission from a beta-unstable nucleus. In the perturbation scheme used in the present paper, we would have, for example, in the case of negatron emission with K-shell electron ejection

$$u_{\text{ini}} = V^{-\frac{1}{2}}\exp(-i\mathbf{k}_\nu\cdot\mathbf{r}_1)(\pi a^3)^{-\frac{1}{2}}Z_i^{\frac{3}{2}}\exp(-Z_i r_2/a),$$

$$u_{\text{fin}} = V^{-\frac{1}{2}}\exp(i\mathbf{k}_\beta\cdot\mathbf{r}_1)F_{\mathbf{k}_\beta,Z_i+1}(\mathbf{r}_1)V^{-\frac{1}{2}} \times\exp(i\mathbf{k}_e\cdot\mathbf{r}_2)F_{\mathbf{k}_e,Z_i+1}(\mathbf{r}_2),$$

as the appropriate forms of the (effectively one-atomic electron) lepton space wave functions. The shielding and correlation factors analogous to the γ_1, γ_2 above are quite negligible in this u_{fin} because of the relatively large velocity of the negatron (shielding and relativistic corrections in the electron part of u_{ini} are also neglected). The ejected electron spectrum for a given $\beta^\mp$ momentum is then given by Eqs. (18) with γ replaced by 0, (Z_i-1) replaced by $(Z_i\pm1)$, and $cp_\nu^{(0)}/mc^2$ redefined as $(\mathfrak{M}_i-\mathfrak{M}_f)/m-[(1+p_\beta^2)^{\frac{1}{2}}-1]-(1\mp1)$. This result has already been obtained by Migdal[5] and by Feinberg[6] using an argument in which the Coulomb interaction between the β^- and the ejected K-shell electron, as well as the β-decay nucleon-lepton interaction, are treated as perturbations in the sense of the time-dependent perturbation theory. We may also add that we have calculated the probability for orbital electron ejection associated with K-capture by this last method, with the further refinements of (a) use of the Möller rather than the Coulomb interaction between the two electrons, and (b) consideration of virtual intermediate states of negative as well as positive energy for them. The results obtained agree with our work above, in the nonrelativistic approximation, i.e., to within errors $\approx(mcp_e)^2/2m(mc^2)$.

An interesting difference between L, $M\cdots$ orbital electron ejection associated with K-capture (as treated above) and L, $M\cdots$ orbital electron ejection associated with $\beta^\mp$ emission must now be emphasized. We have seen that in the K-capture case relatively little L, $M\cdots$ orbital ejection occurs as a consequence of the near orthogonality of the bound and unbound wave functions of the electron which is to be ejected (effective charge $\approx Z_i-2$ for an L electron, see above). In the $\beta^\mp$ case, however, the unbound wave function of any ejected L-electron must be taken as approximately appropriate to an effective nuclear charge $\approx[(Z_i\pm1)-2]$ so that nothing like near orthogonality obtains. It even follows, as pointed out by Migdal,[5,7] that the total probability of electron ejection from the L or the M shell in $\beta^\mp$ emission is actually larger than that from the K-shell. We may add the remark that, as in the second paragraph of this section, the momentum distribution of electrons ejected from the L, $M\cdots$ shells and from the K-shell should be roughly the same for $(mcp_e)^2/2m \gg B_{(Z_i\pm1)}$.

Certain comments must be made in conclusion. It will be seen from Eqs. (11)–(18) above that in the nonrelativistic approximation for the leptons in the electron state, the probability, per nuclear disintegration, of electron excitation or ejection accompanying K-capture (and also $\beta^\mp$ emission) is independent of the form of the nucleon-lepton beta-interaction and of the degree of forbiddenness of the K or $\beta^\mp$-transition. In addition, the calculated mean life for K-capture results in a slightly different expression when one takes into account all possible "other" K-electron excitation and ejection processes than if one considers the "one-electron" model. Thus Eq. (13b) shows that

$$(1/\tau_K)\div(1/\tau_K)_{\text{one-elec.}} = N^2Z_i^3/(Z_i-\gamma)^3 \approx 1-1/Z_i.$$

This necessitates a small adjustment, compared to the conventional procedure, in estimating nuclear matrix elements for K-capture from the observed values of τ_K and $\mathfrak{M}_i-\mathfrak{M}_f$. On the other hand, the conventionally calculated mean lives for $\beta^\mp$ emission are unaffected (in our approximation) by the possibility of orbital electron excitation and ejection, since, in this case, the electrostatic shielding of the nuclear charge by the $\beta^\mp$, and the $\beta^\mp$-orbital electron correlation effects are negligible.

V. SUGGESTED EXPERIMENTAL VERIFICATION OF THE THEORY

In our opinion no certain experimental observation of orbital electron ejection associated with orbital

electron capture by nuclei has been reported up to the present. However, Bruner's[13] magnetic spectrometer work on negative electrons accompanying β^+ emission in $_{21}Sc^{44}$ should be briefly discussed. Bruner's value of 0.04 for the total number of electrons with energy greater than 30 kev, per β^+ disintegration, is much higher than the value[14] $2\times(2\times10^{-5})$ predicted by Migdal,[5] by Feinberg,[6] and by Eqs. (17)–(18) above with $\gamma=0$ and $(137/Z_i)p_e>(137/21)(2\times30/511)^{\frac{1}{2}}=2.3$. The shape of Bruner's electron momentum distribution is also quite different from that predicted above, he having observed relatively many more high energy electrons than would be expected from Eq. (18). Altogether, no satisfactory theoretical explanation of Bruner's results seems available. Admitting the experimental difficulties, magnetic spectrometer work still appears to offer the best means of checking the shape of the ejected electron momentum spectrum, at least in the case of K-capture or of β^+ emission where there is no superimposed spectrum of β^- electrons. For example, for reasonably successful detection (4 times background) of ejected electrons with energies, say, $\gtrsim$30 kev, working with a typical spectrometer-counter arrangement (effective solid angle $\cong10^{-3}\times4\pi$ steradians: effective resolution $\cong10^{-2}$, counter background $\cong$0.1 count/sec), one would need a source strength of [see Eq. (18)]

$$4\times0.1\times10^3\times10^2\times\left\{(1-\gamma)^2\times2\times10^{-5}\left[\left(\frac{Z_i}{21}\right)^4\times\exp\left[-\left(\frac{2\pi}{2.3}\right)\left(\frac{Z_i}{21}-1\right)\right]\right]\right\}^{-1}\text{ disintegrations/sec,}$$

or

$$50(1-\gamma)^{-2}(21/Z_i)^4\exp[(2\pi/2.3)(Z_i/21-1)]$$

millicuries of K-capturing material.[15] In addition, to avoid excessive "thick source" difficulties, this quantity of radioactive material on a spectrometer source should have a surface density of less than 10^{-1} mg/cm^2 (i.e., a specific activity$\approx$curie/mg). The above expression for the necessary amount of K-capture material indicates that for every K-capture there must be less than

$$(1/100)\{(Z_i/21)^4\exp[(-2\pi/2.3)(Z_i/21-1)](1-\gamma)^2\times2\times10^{-5}\}$$

extraneous β^- disintegrations if no more than 1 percent impurity contribution to the electron counting rate is to be tolerated. Such requirements on the specific activity and radiochemical purity are obviously severe but perhaps may be attained.

One method of detection of the ejected electrons accompanying K-capture which does not require as strong sources as the spectrometer method (but requires comparable purity criteria) is the magnetic cloud-chamber technique. An experiment of this type has recently been performed[16] in which an upper limit, consistent with Eqs. (17), (18), is set on the number of ejected electrons with energies $\geqq$30 kev accompanying K-capture in $_{26}Fe^{55}$. On the other hand, magnetic spectrometer observation of the ejected electrons accompanying K-capture, in coincidence with the immediately afterward emitted K x-ray photons or the corresponding Auger electrons, while clearly not subject to stringent purity requirements nevertheless poses other difficult problems.

Another prediction of the theory here developed which may become accessible to experimental verification involves the expected number of double holes in the K-shell per K-capture: $3/16Z_i^2$ [Eq. (15)]. This quantity might be observed by comparison of the relative numbers, of K x-ray photon proportional counter pulses of the normal energy, and, of pulses of twice this energy, since, the filling of any double hole will result in the emission of two photons practically coincident in time. Thus, with a 4π solid angle proportional counter, the ratio r of the total number of double energy pulses per sec to the number of single energy pulses per sec, N_{single}, is expected to be

$$r=(3/16Z_i^2)+N_{\text{single}}\tau,$$

where τ is the effective resolving time of the proportional counter and the second term represents the contribution of accidental double energy pulses (arising from x-ray photons emitted by different atoms). For example, considering $_{26}Fe^{55}$ and taking $\tau\cong10^{-6}$ sec, N_{single} must be $\leqq30$ sec^{-1}, if the accidental double energy counting rate is to be $\leqq10$ percent of the real rate. Such a low value for N_{single} places stringent requirements on the allowable background rate.

A final possibility for verification of the ideas of electron ejection accompanying β^- emission involves the detection of the number of single K-shell holes due to K-electron excitation and ejection; this number is $2\times(3/4Z_i^2)$ per β^- emission [see Migdal,[5] Feinberg[6] and our Eqs. (14) and (15) with $\gamma=0$]. These single holes in the K-shell may be observed by the detection of the subsequent x-ray photons. Such photons have been reported by Novey[17] in RaE, where $2\times(3/4Z_i^2)\cong2\times10^{-4}$. Novey finds roughly one K x-ray photon per 10^4 β^- decays, which seems of the correct order of magnitude. *Note added in proof:*—Similarly, J. J. Howland, Jr., and W. Rubinson at Brookhaven have recently observed 5×10^{-4} x-ray per β^- emission in $_{16}S^{35}$ (private communication from J. Levinger, reference 7) and this is again in order of magnitude agreement with the theoretical expectation of (see Eq. (15), et seq.) $2\times(\frac{3}{4}Z_i^2)\times(2/3)\times$fluorescence yield$=2\times[\frac{3}{4}\cdot(16)^2]\times2/3\times10^{-1}=4\times10^{-4}$.

[13] J. A. Bruner, Phys. Rev. **84**, 282 (1951).

[14] The additional factor of 2 outside the parenthesis is inserted since there are in this case two K-electrons to be ejected. Inclusion of the contribution of L, M, and N shell ejection with energy greater than 30 kev will raise the theoretically expected number from $2\times(2\times10^{-5})$ to a value some twenty percent larger ($\approx2\times(2\times10^{-5})\{1^{-3}+2^{-3}+3^{-3}+4^{-3}\}$). Moreover, as pointed out above, the ejected electron momentum distribution for $(mcp_e)^2/2m\gg B(Z_i-1)$ is roughly the same from all shells.

[15] Note that this expression has its minimum at $Z_i=33$.

[16] F. T. Porter and H. P. Hotz, following paper [Phys. Rev. **89**, 938 (1953)]

[17] T. B. Novey, Phys. Rev. **86**, 619 (1952).

An Upper Limit for Atomic Orbital Electron Ejection Accompanying *K*-Capture in Fe^{55}†

F. T. PORTER AND H. P. HOTZ
Physics Department, Washington University, St. Louis, Missouri
(Received October 10, 1952)

An upper limit has been determined for the number of atomic orbital electrons ejected during the decay of Fe^{55} by orbital capture. From cloud-chamber observations it is concluded that less than 0.6×10^{-6} electron are ejected per disintegration with energies in the range 30 kev to 205 kev. The theoretical prediction gives the order of 10^{-6} electron per disintegration for the frequency of the process in the energy range studied.

I. INTRODUCTION

THE fact that a continuous photon spectrum accompanies nuclear beta-decay and orbital electron capture has been verified[1–5] and is in good agreement with the theory.[6–8] In addition, Bruner[9] has observed electrons in a magnetic spectrometer accompanying the decay of Sc^{44}, a positron emitter. Novey[10] has observed weak x-radiation associated with the decay of the supposedly pure negatron emitter RaE. These last two observations suggest the possibility that atomic orbital electrons may be excited and even ejected from an atom during the processes of nuclear beta-decay and orbital electron capture. A theoretical treatment of the problem of atomic electron excitation and ejection accompanying orbital electron capture appears in this issue of *The Physical Review*.[11] In the present paper experiments will be described which place an upper limit on the number of atomic orbital electrons ejected with energies greater than 30 kev accompanying orbital electron capture in $_{26}Fe^{55}$.

II. SOURCE MATERIAL

It is well established[12] that Fe^{55} decays only by orbital electron capture. The source material used in the present investigations was produced by deuteron bombardment of 100 percent abundant Mn^{55} as the oxide. The target material of high chemical purity was obtained through the courtesy of the Mallinckrodt Chemical Company. In particular, it was specified that iron was present in less than one part in 10^5 by weight. Our own chemical analyses verified this figure. The cyclotron target backing was aluminum. Iron content of the backing was barely detectable chemically and was much lower than other copper and brass backings available. The aluminum backing was washed repeatedly in HCl after machining to remove all traces of iron. These precautions were taken to assure a minimum of Fe^{59} (a negatron emitter) from an $Fe^{58}(d,p)Fe^{59}$ reaction. If only Mn^{55} were present in the target, the reactions $Mn^{55}(d,p)Mn^{56}$ and $Mn^{55}(d,2n)Fe^{55}$ would be the only reactions to be considered.

The Mn^{55} was bombarded for 10 hours at 180 microamperes with the 10-Mev deuterons from the Washington University Cyclotron. The target was aged for three weeks to allow the Mn^{56} (2.6 hr) to decay. The MnO_2 target material was dissolved in warm 8*N* HCl; a few milligrams of cobalt hold-back carrier were added, and an extraction in di-isopropal ether carried out. The ether fraction was washed twice with warm 8*N* HCl and finally the iron fraction was back-extracted into H_2O.

Aluminum absorption curves of this carrier free iron fraction were obtained using a 3.5 mg/cm²-mica end-window counter. A straight line was obtained on the usual semilog plot out to 50 mg/cm² of Al; the slope or half-thickness in Al corresponded to the characteristic K_α x-ray of Mn following the *K*-capture in Fe. In order to have still a better verification of the activity, a small fraction of the material was studied in a proportional counter and compared to a known low specific activity source of Fe^{55}. With a resolution of 19 percent for the 5.9-kev Mn x-ray, the identification was established without doubt that the radiation from the sample was that of the Mn K_α x-ray.

Most of the sample was deposited on a source for the magnetic spectrometer[13] in order to observe any gross number of charged particle radiations. The spectrometer source strength was (measured in a way similar to that described below) approximately 10^7 disintegrations/sec. The spectrometer counter window had a 10-kev low energy cutoff for beta-particles. No negatrons or positrons could be detected above background.

III. CLOUD-CHAMBER OBSERVATIONS

A more sensitive means of determining the upper limit for orbital electron ejection was sought in the cloud chamber. A portion of the Fe^{55} source solution was deposited on a 2 mg/cm² mica backing, supported

† Assisted by the joint program of the U. S. Office of Naval Research and the U. S. Atomic Energy Commission.
[1] C. S. Wu, Phys. Rev. **59**, 481 (1951).
[2] L. Madansky and F. Rasetti, Phys. Rev. **83**, 187 (1951).
[3] Bell, Jauch, and Cassidy, Science **115**, 12 (1952).
[4] D. Maeder and P. Preiswerk, Phys. Rev. **84**, 595 (1951).
[5] Anderson, Wheeler, and Watson, Phys. Rev. **87**, 668 (1952).
[6] J. K. Knipp and G. E. Uhlenbeck, Physica **3**, 425 (1936).
[7] F. Bloch, Phys. Rev. **50**, 472 (1936).
[8] P. Morrison and L. I. Schiff, Phys. Rev. **58**, 24 (1940).
[9] J. A. Bruner, Phys. Rev. **84**, 282 (1951).
[10] T. B. Novey, Phys. Rev. **86**, 619 (1952).
[11] H. Primakoff and F. T. Porter, Phys. Rev. **89**, 930 (1953). This article also gives reference to and discussion of the related problem in β^+ decay.
[12] National Bureau of Standards Circular No. 499 (1950) and supplements.
[13] F. T. Porter and C. S. Cook [Phys. Rev. **87**, 464 (1952)] mention recent modifications of the spectrometer.

by a thin brass frame, and inserted in a 25 cm diameter, automatically cycled, cloud chamber[14] of conventional design. With a field of 200 gauss, 1400 frames were taken and scanned by reprojection. The criteria for an acceptable event were that the track appear to originate in the source and that it have the curvature appropriate to an electron in the field. The apparent radii of curvature of all tracks were measured in addition to counting them. In the first 1400 pictures 15 electron tracks were observed. A second sequence of 1500 pictures produced 28 acceptable tracks. Of the 43 tracks, only 4 had curvatures indicating energies greater than 205 kev (the transition energy[3,4] of $Fe^{55} \rightarrow Mn^{55}$). No positrons were observed to originate in the source in all 2900 pictures.

In establishing the lower limit on the electron energy which could be successfully detected, it was noted that the two lowest energy tracks which were observed were apparently between 15–20 kev, but these were badly scattered. In addition, the range of a 30-kev electron in the gas of the chamber (hydrogen at 1.7 atmospheres saturated with ethanol) is calculated to be 5–6 cm. This would seem to give a good chance for detection even though the track would most probably be scattered.

The combination sensitive time solid angle factor for the cloud chamber has been determined by counting the number of electron tracks per picture from a bare source of Co^{60} in the source position of the chamber and with no magnetic field applied. An upper limit for the number of electrons emitted per second by this source has be endetermined by β-counting in known geometries, and the disintegration rate has been checked by comparison γ-counting with a standard Co^{60} source. The solid angle sensitive time factor is not less than 4.9×10^{-3} sec (the most probable value is 5.5×10^{-3} sec).

IV. DISINTEGRATION RATE OF THE SOURCE; RESULTS

The disintegration rate of the Fe^{55} cloud-chamber source was determined by obtaining absorption curves in aluminum of the Mn K_α radiation in a fixed geometry. The straight line semilog plots were extrapolated to zero absorber thickness, considering the 10 mg/cm^2 of air and 3.5 mg/cm^2 mica window of the counter to contribute roughly the same absorption as an equivalent thickness of aluminum. Two experimental arrangements were used. The first involved no collimation of the x-rays. The aluminum absorber foils were placed just in front of the counter window, a circular aperture 1.06 inches in diameter. The inside diameter of the counter is 1.12 inches with a sensitive length of approximately 4 cm. This arrangement is the usual one for weak sources of photons.[15]

Extrapolating to zero absorber and applying a solid angle correction involving simply the window diameter and the distance from the source to window (the area of the source is 0.25 cm^2), the value 2.5×10^5 disintegrations/sec was obtained, uncorrected for counter efficiency and fluorescence yield. The second arrangement was the same except that a lead sheet $\frac{1}{8}$ inch thick with a $\frac{3}{8}$ inch hole was placed just below the absorbers to act as a collimator. The slopes of the absorption curves in both arrangements were identical (both giving a half-thickness in Al corresponding to the Mn K_α x-ray), but with collimation an extrapolation to zero absorber and correction for solid angle defined by the collimator gave 9.7×10^5 disintegrations/sec uncorrected for counter efficiency and fluorescence yield. The reason for the difference is apparently that in the first case the efficiency is a function of the region in which the x-rays enter the counter. With no collimation it seems probable that x-rays entering near the edge of the counter have less path length in the gas and less probability of causing an ionizing event which can trigger the Geiger tube. In the second case the x-rays all enter the counter relatively close to the central wire and have a chance to traverse the entire sensitive length of the counter. There appears to be no reason to reject the higher figure and some reason to question the lower one, so we take as the disintegration rate of the source 9.7×10^5 disintegrations/sec uncorrected for counter efficiency and fluorescence yield.

TABLE I. Number of electron tracks originating in the Fe^{55} source in the indicated energy range as determined from cloud-chamber observations. The four tracks with energies greater than the available energy ($Fe^{55} \rightarrow Mn^{55}$) are also included.

Electron energy kev	Number of tracks
15–30	6
30–60	13
60–90	8
90–120	6
120–150	4
150–180	3
180–210	3
320	2
500	1
575	1

The counter efficiency is probably the most uncertain of all the data. The counter gas is predominantly argon; the gas pressure approximately 10 cm of Hg. A consideration of the mass absorption coefficient for 6-kev x-rays in argon at this pressure and of the sensitive length of the counter gives a figure of 25 percent efficiency for detection of these photons. Since we are seeking an upper limit for the number of electrons ejected per disintegration, it seems prudent to double this value in the light of its tenuous basis, so that we may be sure we do not overestimate the disintegration rate of the Fe^{55} source. Further, less than a third[16] of the K-capture events are followed by a K_α x-ray of

[14] K. H. Morganstern and K. P. Wolf, Phys. Rev. **76**, 1261 (1949).

[15] See, for example, L. E. Glendenin, Nucleonics **2**, No. 1, 29 (1947).

[16] Steffen, Huber, and Humbel, Helv. Phys. Acta **22**, 167 (1949).

Mn; the others result in Auger electrons of energies well below the low energy cutoff of the counter window. Consequently, the observed decay rate is increased by a factor 3 to correct for fluorescence yield. Corrections for L capture and for the small "dead space" between the window and the sensitive region of the end-window counter are not made. This also is consistent with the setting of an upper limit for the process. The disintegration rate of the Fe^{55} source is, then, corrected for 50 percent efficiency and for fluorescence yield, 5.8×10^{6} disintegrations/sec.

Finally, taking into account the statistical error in the small number of tracks observed, we conclude there are less than 0.6×10^{-6} ejected electron per disintegration with energies greater than 30 kev.

V. DISCUSSION

The origin of the electrons observed may well be questioned. No doubt some of them are nuclear beta-particles from the decay of impurities in the source. The most likely impurity is Fe^{59}. The currently available information indicates that Fe^{59} has two negatron groups of approximately the same abundance with end points at 260 kev and 460 kev. If a majority of the tracks observed here were to be attributed to an Fe^{59} impurity, the absence of more tracks with energies greater than 210 kev would be difficult to explain. The fact that only 4 tracks corresponded to electrons with energies greater than 210 kev is at least suggestive that a major portion of the observed tracks actually are due to atomic electrons ejected during the decay of Fe^{55} by orbital capture.[17] In any case all tracks below 210 kev are included in setting the upper limit on the frequency of the process.

The theoretical expression[11] for the number of ejected noncaptured K electrons per K-capture was numerically integrated, with $Z_i=26$, from 30 kev to (205–6.5 kev). The result is 3.6×10^{-6} electron/disintegration. The numerical factor (3.6) is sensitive to the value of the lower limit of the integration; thus, if a lower limit of 50 kev is used, the theoretical prediction is reduced to 1.0×10^{-6} electrons/disintegration. We have therefore considered the question as to whether we have actually observed most of the electrons emerging from the source with energies between, say, 30 kev and 50 kev. To what extent multiple scattering and self-absorption in the source may discriminate against observation of the lower energy electrons is a question which does not have a clear quantitative answer. Certainly there is no sharply defined energy below which one cannot observe a track and above which one can observe all the tracks. We seek a lower energy limit above which there is a reasonable chance to observe, say, 90 percent of the tracks in the given solid angle. As was mentioned before, calculations indicate that a 30-kev electron has a mean range of approximately 5 to 6 cm in the cloud chamber and, with a field of 200 gauss, a radius of curvature of approximately 3 cm. Further, it can be said that a majority of the tracks in the 40–60 kev range did not appear to be badly scattered and that the apparent curvature measurements were made with errors of the order of 20 percent. If, on the other hand, one believes that most of the observed events are the result of orbital electron ejection and also believes that the theoretical predictions concerning the momentum distribution are essentially correct, then it would appear that there is considerable discrimination against the observation of the lower energy events.

Actually the point to be emphasized is that the experimental upper limit for the process does not exceed the theoretical prediction. That the upper limit given here could be increased by a factor of 2 seems doubtful; that the theory is refined enough to predict the total number of ejected electrons in the energy range studied within a factor of 2 or 3 is not claimed. Unfortunately, the cloud chamber is not a reliable instrument with which to investigate the momentum distribution of electrons in this energy range even if it had been feasible to obtain enough events to make such a study statistically acceptable, so that nothing can really be said about the the question of the momentum distribution of the ejected electrons from the above observations.

Finally, it is interesting to note that apparently in the case of orbital electron capture in Fe^{55} the number of ejected electrons per disintegration with energies greater than 30 kev is considerably smaller than in the case of positron decay of Sc^{44} (0.04 electron/disintegration).[9] It has been pointed out[11] that even taking into account certain differences in the treatment of K-capture and $\beta^{\mp}$ decay, it is difficult to account theoretically for the large number of electrons observed[9] accompanying the decay of Sc^{44}.

The authors wish to thank Mr. R. Light for performing the proportional counter investigations, Dr. J. Hudis for suggestions about the chemical procedures, Dr. C. S. Cook for discussions concerning the measurements of the disintegration rates, and Dr. H. Primakoff for his interest and comments.

[17] Other possibilities for the origin of the observed electrons may be considered. First of all there is no evidence available that any orbital electron capture transitions in Fe^{55} go to excited states in Mn^{55}; no nuclear gamma-rays or conversion electrons have been reported. If the electrons detected in the present observations result from Compton or photoelectric interaction in the source and surrounding material of a nuclear gamma-ray, the intensity of this gamma-ray would have to be of such a magnitude as to make its prior detection most likely. On the other hand, if the detected electrons arise from a weak highly converted transition, the branching ratio of this transition cannot be greater than $\approx10^{-6}$, and, of course, the electron spectrum is monoenergetic. Further, since the continuous inner bremsstrahlung photon spectrum has an intensity of the order of 10^{-5} photon/disintegration and since the effective source thickness is certainly less than 5 mg/cm², the observed electrons are most probably not the result of Compton or photoelectric interaction of the inner bremsstrahlung photons. *Note added in proof:*—Hausman *et al.*, Phys. Rev. **88**, 1297 (1952) report the existence of 15 excited states in Mn^{55}. Only the lowest of these, 130 kev above the ground state, is energetically attainable by the K-capture of Fe^{55}.

Theory of the Magnetoresistive Effect in Semiconductors*

V. A. JOHNSON AND W. J. WHITESELL
Department of Physics, Purdue University, Lafayette, Indiana
(Received October 16, 1952)

Experiments show that the application of a magnetic field increases the resistivity of a semiconductor and produces a decrease in the magnitude of the Hall coefficient. Existing theoretical treatments predict much smaller effects than are actually observed in semiconductors. The present calculation has been carried out to see if theory is brought closer to experiment by considering (1) scattering of conduction electrons by impurity ions as well as by the lattice, and (2) conduction by both holes and electrons at high temperatures. The calculation shows that the presence of impurity scattering decreases the magnitude of the effects produced by a magnetic field and thus increases the gap between theoretical and experimental values. It is noted that the discrepancy decreases with falling temperatures and is no longer present for data measured on a Ge sample at 20°K. The calculated magnetic field effects are very much greater for an intrinsic semiconductor than for an impurity semiconductor. The fractional changes in resistivity and Hall coefficient are given, for several different values of the electron-hole mobility ratio, as functions of a parameter containing magnetic field strength and temperature. The absence of experimental values of the magnetic field effects at high temperatures prevents comparison of theory and experiment for the intrinsic semiconductor.

I. INTRODUCTION

THE magnetoresistive effect is studied by measuring the resistance of a sample in the presence of a magnetic field which is perpendicular to the electric current density. Just as for metals, it is observed that the application of the magnetic field increases the resistivity of a semiconductor[1–7] and produces a decrease in the magnitude of the Hall coefficient.[2–5] The first theoretical treatment of this effect is that of Gans;[8] this early work has been extended by Harding,[9] Sangupta,[10] and Davis.[11] More recently, theories have been developed by Seitz[12] and by Pearson and Suhl[7] to apply to cubic crystals in various orientations relative to the electric and magnetic fields. It is generally found that theory predicts a much smaller magnetoresistive effect than is actually observed in semiconductors. The present calculation has been carried out to find the changes produced in theoretical values by considering (1) scattering of conduction electrons by impurity ions as well as by the lattice, and (2) conduction by both holes and electrons in high temperature semiconductors.

The effect of magnetic field upon the resistivity and Hall coefficient is calculated from the electric current density equations.[8] Assume that no temperature gradients exist, electric current flows in the X direction (j_x), a magnetic field is applied in the Z direction (H), and that there is no current flow in the Y direction. The sample is assumed to be ohmic, homogeneous, and isotropic. The electric current densities j_x and j_y are related to the electric field intensities E_x and E_y by the equation[13]

$$j_x = AE_x - BE_y, \tag{1.1}$$

$$j_y = BE_x + AE_y = 0, \tag{1.2}$$

where, if current is carried by electrons only,

$$A = -\frac{4\pi e^2}{3}\int_0^\infty lv^3(1+s^2)^{-1}\frac{\partial f}{\partial \epsilon}dv, \tag{1.3}$$

$$B = -\frac{4\pi e^2}{3}\int_0^\infty slv^3(1+s^2)^{-1}\frac{\partial f}{\partial \epsilon}dv, \tag{1.4}$$

in which

$$s = elH/mv, \tag{1.5}$$

and e denotes the magnitude of electronic charge, l the mean free path, m the effective mass of conduction electrons, f the classical distribution function

$$f = n\{m/(2\pi kT)\}^{\frac{3}{2}}\exp(-\epsilon/kT), \tag{1.6}$$

n the number of conduction electrons per unit volume, and ϵ the kinetic energy $mv^2/2$.

Equations (1.1) and (1.2) yield for the conductivity σ and Hall coefficient R

$$\sigma = j_x/E_x = A + (B^2/A), \tag{1.7}$$

$$R = E_y/(j_x H) = -B/\{H(A^2+B^2)\}. \tag{1.8}$$

If the current is carried only by holes, Eq. (1.7) is unchanged and the negative sign in Eq. (1.8) becomes positive.

* Work assisted by contract between the U. S. Signal Corps and the Purdue Research Foundation.

[1] P. Kapitza, Proc. Roy. Soc. (London) **A123**, 292 (1929).
[2] W. C. Dunlap, Phys. Rev. **71**, 471 (1947); **79**, 286 (1950).
[3] W. W. Scanlon, Ph.D. thesis, Purdue University, 1948, unpublished.
[4] J. W. Cleland, M.S. thesis, Purdue University, 1949, unpublished.
[5] R. Bray, private communication (1949).
[6] I. Estermann and A. Foner, Phys. Rev. **79**, 365 (1950).
[7] G. L. Pearson and H. Suhl, Phys. Rev. **83**, 768 (1951).
[8] R. Gans, Ann. Physik **20**, 293 (1906).
[9] J. W. Harding, Proc. Roy. Soc. (London) **A140**, 205 (1933).
[10] M. Sangupta, Indian J. Phys. **11**, 319 (1937).
[11] L. Davis, Phys. Rev. **56**, 93 (1939).
[12] F. Seitz, Phys. Rev. **79**, 372 (1950).

[13] All derivations in this paper are carried out in electromagnetic units.

TABLE I. Values of $J_1(\beta,\gamma)$,[a] and $F(\beta)$.[b]

γ[c] = \ β =	0	2/3	3/2	4	9	24
0.00	1.00000	0.71609	0.59156	0.42182	0.28701	0.15698
0.01	0.99041	0.71391	0.59024	0.42129	0.28680	0.15693
0.04	0.95649	0.70723	0.58642	0.41970	0.28620	0.15680
0.10	0.88828	0.69437	0.57889	0.41658	0.28500	0.15652
0.20	0.78806	0.67401	0.56678	0.41147	0.28303	0.15608
0.50	0.66884	0.61982	0.53345	0.39698	0.27731	0.15476
1.00	0.59639	0.54727	0.48618	0.37513	0.26836	0.15262
2.00	0.44530	0.44470	0.41374	0.33848	0.25239	0.14860
4.00	0.25949	0.32516	0.32010	0.28438	0.22631	0.14137
$F(\beta)$	1.0000	0.7957	0.7395	0.7030	0.7175	0.7849

[a] $J_1(\beta,\gamma)$ is the integral defined by Eq. (2.5).
[b] $F(\beta)$ is defined as the ratio of the sum of resistivity owing to lattice scattering only and the resistivity owing to impurity scattering only to the total resistivity when both types of scattering are present; the parameter β is defined as 6 times the ratio of resistivity owing to impurity scattering to resistivity owing to lattice scattering.
[c] γ is defined as $(9\pi/16)(\mu_L{}^0)^2H^2$, where H is the magnetic field strength in gauss and $\mu_L{}^0$ is the mobility associated with lattice scattering only if $H=0$, measured in cm²/abvolt-sec.

II. RESISTIVITY OF AN IMPURITY SEMICONDUCTOR

A sample may be termed an impurity semiconductor if conduction is practically due only to electrons excited to the conduction band from impurity donor levels (or to holes formed in the filled band by excitation of electrons to impurity acceptor levels); conduction owing to intrinsic electrons and holes is negligible in an impurity semiconductor. It is assumed that the conduction electron density does not exceed the limit of applicability of classical statistics.

Analysis[14,15] of measured resistivity data for impurity semiconducting samples, especially silicon and germanium, has shown that the temperature behavior can be explained only by the existence of another scattering process in addition to the scattering of conduction electrons by the lattice. Such an additional process, which has the appropriate temperature behavior to account for the experimental results, is scattering of conduction electrons by the impurity ions. A satisfactory model[16] for describing impurity ion scattering is based upon Rutherford scattering; the mean free path associated with this process is approximately proportional to ϵ^2. If an electron experiences collisions with both the lattice atoms and the impurity ions independently, the mean free path l is related to l_L, the mean free path if only lattice scattering exists, and l_I, the mean free path if only impurity scattering exists, by the relation:[17]

$$1/l=1/l_L+1/l_I. \tag{2.1}$$

This expression for l is now used to evaluate the quantities A and B.

The quantity l_L is approximately independent[18] of ϵ; it is also independent of the magnetic field strength. Equations (1.3) and (1.7) may be used to relate l_L to $\rho_L{}^0$, the resistivity for $H=0$ when only lattice scattering exists

$$l_L=3(2\pi mkT)^{\frac{1}{2}}(4ne^2\rho_L{}^0)^{-1}. \tag{2.2}$$

Let $l_I=\alpha_I\epsilon^2$; then Eqs. (1.3) and (1.7) relate α_I to $\rho_I{}^0$, the resistivity for $H=0$ when only impurity scattering exists

$$\alpha_I=(\pi m)^{1/2}(2^{5/2}ne^2\rho_I{}^0)^{-1}(kT)^{-3/2}. \tag{2.3}$$

A combination of Eqs. (2.1), (2.2), and (2.3) leads to the mean free path

$$l=l_Ll_I(l_L+l_I)^{-1}=l_L\epsilon^2(\epsilon^2+l_L/\alpha_I)^{-1}$$
$$=l_L\epsilon^2\{\epsilon^2+6\rho_I{}^0(kT)^2/\rho_L{}^0\}^{-1}. \tag{2.4}$$

Use Eq. (2.4) for l, replace ϵ/kT by x, and express l_L by Eq. (2.2) to convert the quantity A of Eq. (1.3) into

$$A=\frac{1}{\rho_L{}^0}\int_0^\infty\frac{x^3e^{-x}(x^2+\beta)dx}{(x^2+\beta)^2+\gamma x^3}, \tag{2.5}$$

where

$$\beta=6\rho_I{}^0/\rho_L{}^0, \tag{2.6}$$

and

$$\gamma=(9\pi/16)(\mu_L{}^0)^2H^2, \tag{2.7}$$

in which $\mu_L{}^0$, the mobility associated with lattice scattering only, if $H=0$, is given by

$$\mu_L{}^0=4el_L(18\pi mkT)^{-\frac{1}{2}}. \tag{2.8}$$

Denote the integral on the right side of Eq. (2.5) by $J_1(\beta,\gamma)$ so that

$$J_1(\beta,\gamma)=\rho_L{}^0A. \tag{2.9}$$

In a similar manner, one obtains

$$B=\frac{\gamma^{\frac{1}{2}}}{\rho_L{}^0}\int_0^\infty\frac{x^{9/2}e^{-x}dx}{(x^2+\beta)^2+\gamma x^3}\equiv\frac{\gamma^{\frac{1}{2}}}{\rho_L{}^0}J_2(\beta,\gamma). \tag{2.10}$$

Algebraic combination of Eqs. (1.7), (2.9), and (2.10) yields the result

$$\frac{\rho(H)}{\rho_T{}^0}=\frac{J_1}{J_1{}^2+\gamma J_2{}^2}\cdot\frac{\rho_L{}^0}{\rho_T{}^0}, \tag{2.11}$$

TABLE II. Values of $J_2(\beta,\gamma)$, the integral defined by Eq. (2.10).

γ = \ β =	0	2/3	3/2	4	9	24
0.00	0.88623	0.39704	0.27416	0.14674	0.07334	0.02484
0.01	0.87132	0.39569	0.27348	0.14649	0.07323	0.02481
0.04	0.82537	0.39190	0.27164	0.14591	0.07306	0.02479
0.10	0.74423	0.38454	0.26804	0.14475	0.07272	0.02473
0.20	0.63769	0.37289	0.26225	0.14286	0.07215	0.02464
0.50	0.52255	0.34197	0.24633	0.13751	0.07051	0.02438
1.00	0.45711	0.30076	0.22382	0.12946	0.06796	0.02396
2.00	0.32871	0.24289	0.18947	0.11602	0.06342	0.02318
4.00	0.18613	0.17606	0.14537	0.09633	0.05608	0.02178

[14] K. Lark-Horovitz and V. A. Johnson, Phys. Rev. **69**, 258 (1946); K. Lark-Horovitz, Elec. Eng. **68**, 1047 (1949).
[15] G. L. Pearson and J. Bardeen, Phys. Rev. **75**, 865 (1949).
[16] E. Conwell and V. F. Weisskopf, Phys. Rev. **69**, 258 (1946); **77**, 388 (1950).
[17] V. A. Johnson and K. Lark-Horovitz, Phys. Rev. **82**, 977 (1951).
[18] A. Sommerfeld and H. Bethe, *Handbuch der Physik* (J. Springer, Berlin, 1933), **24**, No. 2, p. 560.

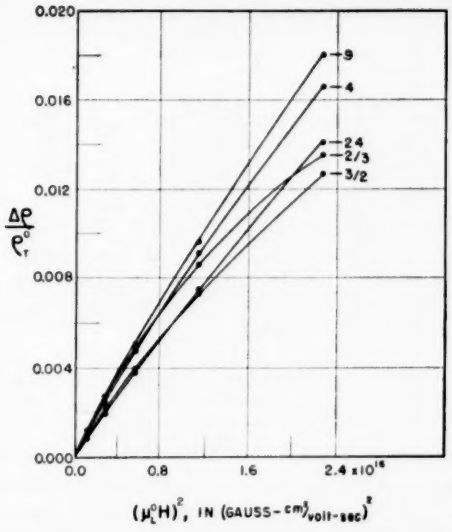

FIG. 1. Fractional increase in resistivity with rising magnetic field for an impurity semiconductor. The numbers at the ends of the curves are the values of the parameter β, defined as six times the ratio of resistivity resulting from impurity scattering to resistivity owing to lattice scattering. The abscissae, given as squares of the product of magnetic field strength and carrier mobility in the absence of magnetic field and scattering by impurities, may be converted into H^2T^{-3} values by taking $\mu_L{}^0=1.7\times10^7T^{-\frac{3}{2}}$ for germanium, or $5\times10^8T^{-\frac{3}{2}}$ for silicion, or $2.6\times10^6T^{-\frac{3}{2}}$ for tellurium, where T is the temperature in °K.

where $\rho_T{}^0$ is the total resistivity at zero magnetic field. The ratio $\rho_L{}^0/\rho_T{}^0$ can be replaced by $F(\beta)(1+\beta/6)^{-1}$, where the quantity $F(\beta)$, defined as $(\rho_L{}^0+\rho_I{}^0)/\rho_T{}^0$, has been previously evaluated[17] as a function of the ratio of impurity scattering to lattice scattering. Finally, the magnetoresistive effect is calculable from the relation

$$\frac{\Delta\rho}{\rho_T{}^0}=\frac{\rho(H)-\rho_T{}^0}{\rho_T{}^0}=\frac{J_1}{J_1{}^2+\gamma J_2{}^2}\cdot\frac{F}{1+\beta/6}-1. \quad (2.12)$$

Tables I and II give the values, as found by numerical integration, of the integrals J_1 and J_2 for selected values β and γ. The β values are chosen to correspond to $\rho_I{}^0/(\rho_I{}^0+\rho_L{}^0)$ values of 0.0, 0.1, 0.2, 0.4, 0.6, and 0.8. Table I also includes the values of $F(\beta)$ corresponding to the chosen β values. Figure 1 shows the behavior of the ratio $\Delta\rho/\rho_T{}^0$ as a function of the quantity $(\mu_L{}^0)^2H^2$. The quantity γ, or $(\mu_L{}^0H)^2$, is used because the theoretical plot of $\Delta\rho/\rho_T{}^0$ against γ, for a given value of β, is the same for all materials. From Fig. 1 one can get a plot of $\Delta\rho/\rho_T{}^0$ against H^2 for a given material at a chosen temperature T by using the appropriate value of $\mu_L{}^0$. One can also consider Fig. 1 to be a plot of magnetoresistive change against H^2T^{-3} if $\mu_L{}^0$ is proportional to $T^{-\frac{3}{2}}$, as is expected[18] for a classical semiconductor.

It is observable that (a) the change in resistivity is directly proportional to the square of the magnetic flux density at weak magnetic fields, (b) the predicted magnetoresistive effects are quite small, under 2 percent for the mobility-field combinations likely to be encountered except at very low temperatures, and (c) the effect of impurity scattering is to decrease the calculated resistivity change, thus increasing the gap between measured and calculated values.

Figure 2 gives a comparison between theory and experiment for germanium sample 33E, an n-type polycrystalline sample of rather low resistivity, prepared by doping with antimony. This sample was chosen because its magnetoresistive effect had been measured[6] at liquid nitrogen and liquid hydrogen temperatures as well as at room temperature, and also because a previous study[19] of resistivity and Hall coefficient for this sample gave information about the ratio of impurity to lattice scattering at various temperatures. As may be seen from Fig. 2, there is a great discrepancy between theory and experiment at 295°K, a much smaller discrepancy at 77°K, and relatively little discrepancy at 20°K.

III. HALL COEFFICIENT OF AN IMPURITY SEMICONDUCTOR

The dependence of the Hall coefficient of an impurity semiconductor upon magnetic field strength is computed from Eq. (1.8) with the use of the mean free path

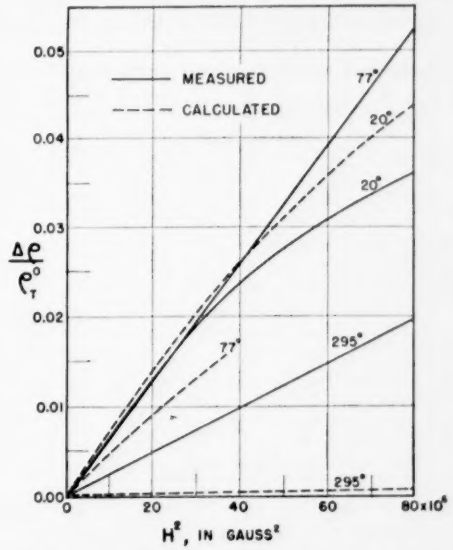

FIG. 2. Comparison between measured and calculated values of the fractional increase in resistivity with magnetic field for germanium sample 33E, an n-type polycrystalline sample, prepared by doping with antimony, having a room temperature resistivity of 0.05 ohm-cm, and found to be quite homogeneous. The measured curves are from Estermann and Foner.[6]

[19] K. Lark-Horovitz, National Defense Research Committee Report NDRC 14-585, 1945, unpublished, Fig. 7.

defined by Eq. (2.4). Simplification with the use of Eqs. (2.7), (2.9), and (2.10) yields

$$R=-\frac{\gamma^{\frac{1}{2}}J_2}{\rho_L{}^0H}\left\{\frac{J_1{}^2}{(\rho_L{}^0)^2}+\frac{\gamma J_2{}^2}{(\rho_L{}^0)^2}\right\}^{-1}=-\frac{3\pi^{\frac{1}{2}}}{4}\frac{\mu_L{}^0\rho_L{}^0J_2}{J_1{}^2+\gamma J_2{}^2}. \quad (3.1)$$

Since $\mu_L{}^0=(ne\rho_L{}^0)^{-1}$, one can write

$$R=-\frac{3\pi^{\frac{1}{2}}}{4ne}\frac{J_2}{J_1{}^2+\gamma J_2{}^2}. \quad (3.2)$$

If one defines a ratio r by

$$|R|=r/(ne), \quad (3.3)$$

one can also write

$$r(\beta,\gamma)=\frac{3\pi^{\frac{1}{2}}}{4}\frac{J_2}{J_1{}^2+\gamma J_2{}^2}. \quad (3.4)$$

If β is taken equal to zero, corresponding to the absence of impurity scattering, Eq. (3.2) yields the magnetic field dependence of Hall coefficient calculated by Harding.[9] If β is set equal to infinity, one finds the magnetic field dependence of Hall coefficient for a sample in which impurity scattering completely dominates; this case was worked out earlier by Johnson and Lark-Horovitz.[20] The values of the ratio $r(\beta,\gamma)$ for these limiting cases and for β values corresponding to $\rho_I{}^0/(\rho_I{}^0+\rho_L{}^0)=0.1$, 0.2, 0.4, 0.6, and 0.8 are given in Table III. Because $\mu_L{}^0$ no longer has significance when only impurity scattering exists ($\beta\to\infty$), the r values for this limiting case are given as a function of a new parameter γ^*, defined by

$$\gamma^*=(\pi/64)(\mu_I{}^0)^2H^2. \quad (3.5)$$

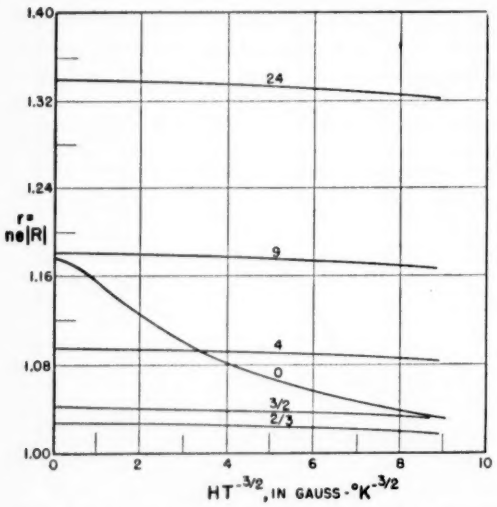

FIG. 3. Dependence of Hall effect upon magnetic field strength for germanium. The ordinate r is defined as the dimensionless product of the Hall coefficient, electronic charge, and carrier density. The numbers on the various curves are the values of β, defined as six times the ratio of resistivity owing to impurity scattering to resistivity owing to lattice scattering.

[20] V. A. Johnson and K. Lark-Horovitz, Phys. Rev. **79**, 176 (1950).

TABLE III. Values of the Hall ratio $r=ne|R|$ as a function of β and γ.

γ \ β =	0	2/3	3/2	4	9	24	γ^* [a]	$\beta=\infty$
0.00	1.1781	1.0289	1.0411	1.0962	1.1833	1.3399	0.0000	1.9328
0.01	1.1718	1.0289	1.0411	1.0959	1.1828	1.3390	0.0005	1.8616
0.04	1.1591	1.0289	1.0411	1.0958	1.1826	1.3389	0.002	1.7561
0.10	1.1441	1.0286	1.0410	1.0956	1.1824	1.3386	0.005	1.6558
0.20	1.1264	1.0282	1.0407	1.0953	1.1820	1.3381	0.025	1.4565
0.50	1.0996	1.0270	1.0399	1.0942	1.1808	1.3369	0.050	1.3750
1.00	1.0762	1.0253	1.0386	1.0928	1.1788	1.3346	0.250	1.2183
2.00	1.0545	1.0226	1.0366	1.0900	1.1751	1.3306	1.000	1.1251
4.00	1.0356	1.0188	1.0334	1.0853	1.1685	1.3230		

[a] The parameter $\gamma=(9\pi/16)(\mu_L{}^0)^2H^2$, where $\mu_L{}^0$ is the mobility when only lattice scattering is present, becomes meaningless for $\beta=\infty$, which corresponds to the absence of lattice scattering. Hence r for $\beta=\infty$ is given in terms of a parameter γ^*, defined as $(\pi/64)(\mu_I{}^0)^2H^2$, where $\mu_I{}^0$ is the mobility when only impurity scattering is present.

Figure 3 shows a plot of r *vs* $HT^{-\frac{3}{2}}$ for six different β values. The γ-parameter has been converted into terms of $HT^{-\frac{3}{2}}$, by assuming that $\mu_L{}^0$ is proportional to $T^{-\frac{3}{2}}$, the behavior expected[18] for lattice scattering in any classical semiconductor; the constant of proportionality is found by setting $\mu_L{}^0$ at 300°K equal to 3300 cm²/volt-sec, a value characteristic of germanium.[21] It is apparent that the introduction of impurity scattering lessens the variation of r with magnetic field strength. Scanlon[3] and Cleland[4] have observed that pure germanium samples show more variation in Hall coefficient with changing magnetic field than do relatively impure samples. However, a quantitative comparison between the behavior of Hall coefficients in a magnetic field as predicted by Eq. (3.2) and as measured[2–5] shows that the theoretical values are almost always too low, usually by a factor between 2 and 10.

IV. RESISTIVITY OF AN INTRINSIC SEMICONDUCTOR

At high temperatures, thermal energy is sufficient to excite appreciable numbers of electrons from the filled band to the conduction band of a semiconductor; for each electron excited to the conduction band, there exists a conducting hole in the filled band. Conduction by such electron-hole pairs is termed intrinsic.

Since both holes and electrons act as current carriers, the electrical current density equations must include terms characteristic of each carrier. Thus one replaces Eqs. (1.1) and (1.2) by

$$j_x=(A_1+A_2)E_x-(B_1-B_2)E_y, \quad (4.1)$$

$$j_y=(B_1-B_2)E_x+(A_1+A_2)E_y, \quad (4.2)$$

where subscript 1 applies to electrons and subscript 2 to holes. The coefficients A_1 and A_2 are defined by Eq. (1.3) with the electron mean free path l_1, the effective electron mass m_1, and the electron distribution function f_1 used in A_1 and the corresponding quantities for holes,

[21] Pearson, Haynes, and Shockley, Phys. Rev. **78**, 295 (1950).

TABLE IV. Values of $K_1(\gamma)$,[a] and $K_2(\gamma)$.[b]

γ	$K_1(\gamma)$	$K_2(\gamma)$
0.0000	1.00000	0.88623
0.0025	0.99760	0.88217
0.01	0.99041	0.87132
0.05	0.95649	0.82537
0.15	0.88828	0.74423
0.35	0.78806	0.63769
0.70	0.66884	0.52255
1.00	0.59639	0.45711
2.00	0.44530	0.32871
5.00	0.25945	0.18613

[a] $K_1(\gamma)=\int_0^\infty x^2e^{-x}(x+\gamma)^{-1}dx$.
[b] $K_2(\gamma)=\int_0^\infty x^{\frac{1}{2}}e^{-x}(x+\gamma)^{-1}dx$.

l_2, m_2, and f_2, used in A_2. The symbol e represents the magnitude of the electron charge; the proper signs for electrons and holes have been considered in writing Eqs. (4.1) and (4.2). The terms B_1 and B_2 are found from Eq. (1.4) by the appropriate insertions of l_1, m_1, and f_1, for B_1 and of l_2, m_2, and f_2 for B_2.

Equations (4.1) and (4.2) lead to the relations

$$\sigma=\frac{j_x}{E_x}=\frac{(A_1+A_2)^2+(B_1-B_2)^2}{A_1+A_2} \tag{4.3}$$

and

$$R=\frac{E_y}{j_xH}=\frac{-(B_1-B_2)}{H\{(A_1+A_2)^2+(B_1-B_2)^2\}}. \tag{4.4}$$

Resistivity due to scattering by impurity ions decreases rapidly as temperature rises,[16] whereas resistivity because of scattering by the lattice rises as the $\frac{3}{2}$ power of the temperature;[18] hence impurity scattering is treated as negligible in an intrinsic semiconductor. Further simplification comes from assuming that the temperature of the sample is high enough that the concentration of impurity electrons or holes is negligible in comparison to the concentration of intrinsic electrons and holes; in this case, one takes n_1, the electron concentration, equal to n_2, the hole concentration.

Since l_1 and l_2 are independent of the velocity v the terms A_1 and A_2 reduce to

$$A_1=n_1e\mu_1{}^0\int_0^\infty x^2e^{-x}(x+\gamma_1)^{-1}dx \tag{4.5}$$

and

$$A_2=n_2e\mu_2{}^0\int_0^\infty x^2e^{-x}(x+\gamma_2)^{-1}dx, \tag{4.6}$$

where $\mu_1{}^0$ and $\mu_2{}^0$ represent the electron and hole mobilities, respectively, in zero magnetic field, and

$$\gamma_{1,2}=(9\pi/16)(\mu_{1,2}{}^0H)^2. \tag{4.7}$$

Define

$$K_1(\gamma)\equiv\int_0^\infty x^2e^{-x}(x+\gamma)^{-1}dx$$
$$=1-\gamma+\gamma^2e^\gamma\{-\mathrm{Ei}(-\gamma)\}. \tag{4.8}$$

The terms B_1 and B_2 reduce to

$$B_{1,2}=n_{1,2}e\mu_{1,2}{}^0\gamma_{1,2}{}^{\frac{1}{2}}\int_0^\infty x^{\frac{1}{2}}e^{-x}(x+\gamma_{1,2})^{-1}dx. \tag{4.9}$$

Define

$$K_2(\gamma)\equiv\int_0^\infty x^{\frac{1}{2}}e^{-x}(x+\gamma)^{-1}dx$$
$$=\pi^{\frac{1}{2}}/2-\gamma\int_0^\infty x^{\frac{1}{2}}e^{-x}(x+\gamma)^{-1}dx. \tag{4.10}$$

The integral in $K_2(\gamma)$ has been evaluated numerically for a series of γ-values; the results are presented in Table IV along with the corresponding values of $K_1(\gamma)$.

Let c denote the ratio of electron to hole mobility, $\mu_1{}^0/\mu_2{}^0$, and, in addition, take $n_1=n_2=n$. Then it follows that

$$\gamma_1=c^2\gamma_2. \tag{4.11}$$

The resistivity at zero magnetic field is

$$\rho^0=(ne\mu_1{}^0+ne\mu_2{}^0)^{-1}. \tag{4.12}$$

The algebraic combination of Eqs. (4.3), (4.5), through (4.12) yields an expression for the magnetoresistive effect

$$\frac{\Delta\rho}{\rho^0}=\frac{\rho(H)-\rho^0}{\rho^0}=(c+1)\left[cK_1(\gamma_1)+K_1(\gamma_2)+\frac{\gamma_2\{c^2K_2(\gamma_1)-K_2(\gamma_2)\}^2}{cK_1(\gamma_1)+K_1(\gamma_2)}\right]^{-1}-1. \tag{4.13}$$

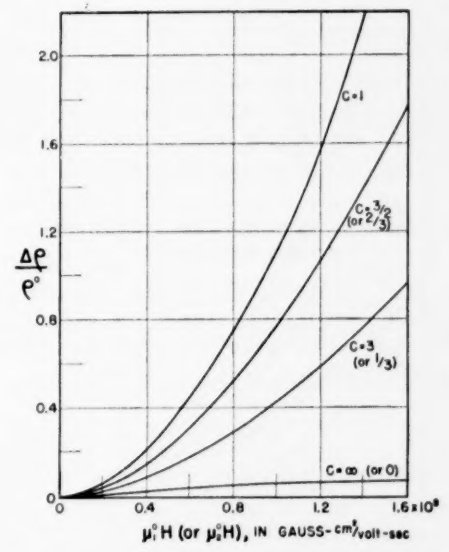

FIG. 4. Fractional increase in resistivity with magnetic field strength for an intrinsic semiconductor. The ratio of electron mobility to hole mobility is denoted by c. The abscissa is the product of magnetic field strength and electron mobility when $c=1$, $\frac{1}{3}$, 3, or ∞, or the product of magnetic field strength and hole mobility when $c=1$, $\frac{1}{3}$, $\frac{1}{3}$, or 0.

TABLE V. Relation between γ_1 and H for intrinsic germanium.[a]

γ_1	$\mu_1{}^0H$ gauss-cm²/volt-sec	H (gauss) at 295°K	H (gauss) at 625°K
0.01	0.07522×10^8	2250	6900
0.05	0.16821×10^8	5030	15 420
0.15	0.29135×10^8	8710	26 700
0.35	0.44504×10^8	13 300	40 800
0.70	0.62938×10^8	18 800	57 700
1.00	0.75225×10^8	22 500	69 000
2.00	1.06385×10^8	31 800	97 500
5.00	1.68209×10^8	50 300	154 300

[a] Values based upon taking $\mu_1{}^0=1.7\times10^8T^{-\frac{1}{2}}$ cm²/volt-sec, corresponding to $\mu_1{}^0=3300$ cm²/volt-sec at 300°K.

Inspection of Eq. (4.13) shows that $\Delta\rho/\rho^0$ depends upon the ratio c as well as upon the quantity γ_1 or $\mu_1{}^0H$. For this reason, the dependence of $\Delta\rho/\rho^0$ upon $\mu_1{}^0H$ is shown for four c values in Fig. 4. Because of the symmetry of terms arising from electron conduction and from hole conduction, one finds that $\Delta\rho/\rho^0$ for given c and $\mu_1{}^0H$ values is equal to $\Delta\rho/\rho^0$ for $1/c$ and $\mu_2{}^0H$. The curve in Fig. 4 for $c=\infty$ or 0 corresponds to the curve of Fig. 1 with $\beta=0$ (i.e., to Harding's curve). Thus, Fig. 4 indicates that the introduction of a second type of carrier causes an increase in the magnetoresistive effect, which becomes greatest when the two carriers have the same mobility.

Table V indicates the magnetic field intensities corresponding to various γ_1 values for intrinsic germanium at temperatures of 295°K and 625°K. Thus, relatively large magnetoresistive effects should be observed in pure samples which become intrinsic at comparatively low temperatures, whereas magnetic field strengths several times stronger would be required to produce the same $\Delta\rho/\rho^0$ value in an impure sample that becomes intrinsic only at very high temperatures.

V. HALL COEFFICIENT OF AN INTRINSIC SEMICONDUCTOR

The Hall coefficient of an intrinsic semiconductor is given by Eq. (4.4). By employing Eqs. (4.5) through (4.10) and taking $n_1=n_2=n$, one obtains an expression for the Hall coefficient

$$R=-\frac{3\pi^{\frac{1}{2}}}{4ne}\frac{c^2K_2(\gamma_1)-K_2(\gamma_2)}{\{cK_1(\gamma_1)+K_1(\gamma_2)\}^2+\gamma_2\{c^2K_2(\gamma_1)-K_2(\gamma_2)\}^2}. \tag{5.1}$$

For very weak magnetic fields, this equation reduces to

$$R_0=-\frac{3\pi}{8ne}\frac{c-1}{c+1}. \tag{5.2}$$

Thus the ratio R/R_0 becomes

$$\frac{R}{R_0}=\frac{2}{\pi^{\frac{1}{2}}}\frac{(c+1)}{(c-1)}\times\frac{c^2K_2(\gamma_1)-K_2(\gamma_2)}{\{cK_1(\gamma_1)+K_1(\gamma_2)\}^2+\gamma_2\{c^2K_2(\gamma_1)-K_2(\gamma_2)\}^2}. \tag{5.3}$$

The change in Hall coefficient with magnetic field may be described by

$$\Delta R/R_0=(R/R_0)-1. \tag{5.4}$$

This quantity depends upon the mobility ratio c as well as upon $\mu_1{}^0H$; in fact, $\Delta R/R_0$ for given c and $\mu_1{}^0H$ equals $\Delta R/R_0$ for $1/c$ and $\mu_2{}^0H$, in analog to the resistivity behavior. Figure 5 shows the dependence of $\Delta R/R_0$ upon $\mu_1{}^0H$ for several mobility ratios. As $\mu_1{}^0H$ increases, R decreases to a value about 85 percent of R_0. When $c=\infty$ (or 0), R approaches $0.85R_0$ asymptotically, as was found by Harding.[9] For other c values, the $\Delta R/R_0$ curve shows a minimum at about -0.15 with the position of the minimum moving to smaller $\mu_1{}^0H$ values as c goes toward unity. Although R_0 becomes zero as c approaches unity, the ratio $\Delta R/R_0$ has a determinate limit;

$$\lim_{c\to1}\left(\frac{\Delta R}{R_0}\right)=\frac{2}{\pi^{\frac{1}{2}}}\frac{K_2(\gamma_1)}{\{K_1(\gamma_1)\}^2}, \tag{5.5}$$

a positive value, which is indicated on Fig. 5.

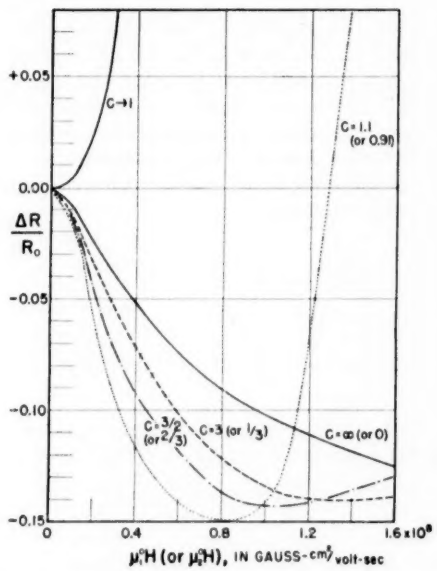

FIG. 5. Fractional change in Hall coefficient with magnetic field strength for an intrinsic semiconductor, given for several values of the ratio of electron mobility to hole mobility.

Thus, it is found that the calculated variation of resistivity and Hall coefficient with magnetic field intensity is very much greater for an intrinsic semiconductor than for an impurity semiconductor. At the present time experimental investigations of the magnetic field dependence of resistivity and Hall coefficient have not been published, and hence theory and experiment cannot be compared for such conditions.

The authors wish to thank Dr. K. Lark-Horovitz for his advice and encouragement during the progress of this work, and R. Bray, J. W. Cleland, and W. W. Scanlon for discussions of their experimental studies of magnetic field effects.

PHYSICAL REVIEW VOLUME 89, NUMBER 5 MARCH 1, 1953

Tables for Second Born Approximation Scattering from Various Potential Fields

LYMAN MOWER
Department of Physics, Massachusetts Institute of Technology, Cambridge, Massachusetts
(Received October 22, 1952)

By means of a variational approach, the scattering amplitude for electron scattering from various potentials is calculated. Numerical values for the functions involved are tabulated as a function of energy and scattering angle.

RECENTLY variational methods have been applied to scattering problems in nuclear physics; it was of interest to see with what success these methods would meet in problems on the atomic scale. At the same time it was felt that it was important to make available in tabular form the various functions involved. Here, scattering of a particle from various static potentials is considered. The variational principle used is essentially that as introduced by Schwinger and is in the form suited for determining scattering amplitudes as presented by Lax[1] and by Morse and Feshbach.[2] It is as follows:

$$J(\theta)=\frac{-\int e^{i\mathbf{k}_i\cdot\mathbf{r}}U(r)\psi_s^*(r)dv\cdot\int e^{-i\mathbf{k}_s\cdot\mathbf{r}_1}U(r_1)\psi_i(r_1)dv_1}{4\pi\int\psi_s^*(r)U(r)\psi_i(r)dv+\int\int\psi_s^*(r)U(r)(e^{ik|r-r_1|}/|r-r_1|)U(r_1)\psi_i(r_1)dv,\,dv_1}.$$

This quantity $J(\theta)$, the scattering amplitude which we wish to minimize, was calculated for various potentials $U(r)$; namely, an exponential, Yukawa, and a potential of the form $-2(U_0/a_0)(1/r+\lambda/2)\exp(-r/\lambda)$. The trial wave function which was used in the above expression for $J(\theta)$ was $\psi_i=\exp(i\mathbf{k}_i\cdot\mathbf{r})$ and $\psi_s^*=\exp(-i\mathbf{k}_s\cdot\mathbf{r})$, where $\mathbf{k}_i$ is the momentum vector in the direction of the incident wave, $\mathbf{k}_s$ is the momentum vector in the direction of the scattered wave, $|\mathbf{k}_s|^2=|\mathbf{k}_i|^2$, and θ is the angle between the two vectors.

Many of the integrals involved have been calculated previously; the evaluation of those integrals not readily

TABLE I. Algebraic values for $S_i(\theta)$, where $S_i(\theta)$ is essentially the ratio of the second to the first Born approximation for the indicated potentials.

Potential	$S_i(\theta)$
Yukawa $U(r)=U_0(\lambda/r)\exp(-\lambda r)$	$S_y=-U_0(1+x^2c^2)I_y$ [a]
Exponential $U(r)=U_0\lambda^2\exp(-\lambda r)$	$S_e=U_0(1+x^2c^2)^2I_e$
Mixed $U(r)=-U_0(2/a_0)(1/r+\lambda/2)\times\exp(-\lambda r)$	$S_m=U_0(2/\lambda a_0)(1+x^2c^2)^2I_m/(2+x^2c^2)$

where

$$I_y=(2/xcA)\left[\arctan\left(\frac{xc}{A}\right)+\frac{i}{2}\ln\left(\frac{A+x^2c}{A-x^2c}\right)\right],$$

$$I_e=a+ib+dI_y,$$

$$a=4/[c^2A^2(A^2+x^2c^2)]-(2+x^2)^2(4-8x^2-2x^4c^2)/A^4(A^2+x^2c^2)-2/(x^2c^2+4)^2,$$

$$b=x/A^2c^2(1+x^2)-3x(2+x^2)^2/A^4(1+x^2),$$

$$d=-2/A^2c^2+4/A^2-6(2+x^2)^2/A^4,$$

$$I_m=[1+2(x^2+2)/A^2]I_y+(4-x^4c^2)/A^2(A^2+x^2c^2)+ix(2+x^2)/A^2(1+x^2)-I_e/2,$$

and where we have also used the notation:

$$x=2k/\lambda,\qquad A^2=4+4x^2+x^4c^2,$$
$$c=\sin\theta/2,\qquad \cos\theta=\mathbf{k}_i\cdot\mathbf{k}_s/k^2,$$
$$k=|\mathbf{k}_i|=|\mathbf{k}_s|=(mc/\hbar)(2E/mc^2)^{\frac{1}{2}}.$$

E denotes the energy of the incident electrons, m their mass, and $\hbar$ Planck's constant.

[a] See reference 3.

TABLE II. Algebraic values for $S_i(\theta)$ for $\theta=0$ and for the potentials indicated.

Potential	$S_i(\theta)_{\theta=0}$
Yukawa	$S_y=-U_0(1+ix)/2(1+x^2)$
Exponential	$S_e=-2U_0[(15+10x^2+3x^4)/24(1+x^2)^3+ix(3+3x^2+x^4)/3(1+x^2)^3]$
Mixed	$S_m=(U_0/2a_0\lambda)[(75+106x^2+39x^4)/24(1+x^2)^3+ix(12+18x^2+7x^4)/3(1+x^2)^3]$

[1] M. Lax, Phys. Rev. **78**, 306 (1950).
[2] P. M. Morse and H. Feshbach, *Methods of Theoretical Physics*, to be published.

TABLE III. Numerical values of S_y and S_e as functions of θ and x.

(a) $S_y/-U_0=(1+x^2c^2)I_y$.

x \ θ	0° Re	0° Im	30° Re	30° Im	60° Re	60° Im	90° Re	90° Im	120° Re	120° Im	150° Re	150° Im	180° Re	180° Im
0.8	0.3049	0.2439	0.3159	0.2537	0.3455	0.2800	0.3843	0.3154	0.4214	0.3501	0.4476	0.3751	0.4570	0.3841
1.0	0.2500	0.2500	0.2638	0.2652	0.3000	0.3061	0.3463	0.3597	0.3891	0.4120	0.4186	0.4489	0.4290	0.4621
1.2	0.2049	0.2459	0.2208	0.2671	0.2616	0.3230	0.3118	0.3953	0.3566	0.4632	0.3864	0.5105	0.3968	0.5273
1.6	0.1404	0.2247	0.1590	0.2680	0.2039	0.3426	0.2543	0.4459	0.2953	0.5374	0.3208	0.5984	0.3293	0.6196
2.0	0.1000	0.2000	0.1198	0.2449	0.1644	0.3540	0.2094	0.4782	0.2426	0.5819	0.2619	0.6481	0.2681	0.6706
2.4	0.0740	0.1775	0.0943	0.2334	0.1363	0.3618	0.1741	0.4981	0.1995	0.6055	0.2134	0.6715	0.2177	0.6936
2.8	0.0566	0.1584	0.0769	0.2244	0.1152	0.3675	0.1460	0.5090	0.1650	0.6150	0.1749	0.6783	0.1779	0.6992
3.0	0.0500	0.1500	0.0703	0.2208	0.1066	0.3696	0.1342	0.5120	0.1505	0.6161	0.1588	0.6776	0.1614	0.6978
3.2	0.0445	0.1423	0.0646	0.2178	0.0989	0.3713	0.1235	0.5135	0.1376	0.6154	0.1447	0.6749	0.1468	0.6943
3.6	0.0358	0.1289	0.0555	0.2130	0.0857	0.3735	0.1055	0.5133	0.1159	0.6099	0.1209	0.6653	0.1224	0.6833
4.0	0.0294	0.1176	0.0485	0.2096	0.0750	0.3743	0.0906	0.5099	0.0985	0.6008	0.1022	0.6523	0.1033	0.6690
4.4	0.0246	0.1081	0.0429	0.2071	0.0661	0.3738	0.0785	0.5042	0.0845	0.5896	0.0872	0.6375	0.0880	0.6528
4.8	0.0208	0.0998	0.0385	0.2054	0.0586	0.3723	0.0685	0.4970	0.0731	0.5772	0.0752	0.6217	0.0758	0.6360
5.2	0.0178	0.0927	0.0348	0.2041	0.0522	0.3698	0.0602	0.4889	0.0638	0.5642	0.0654	0.6057	0.0658	0.6193
5.6	0.0155	0.0865	0.0316	0.2032	0.0468	0.3668	0.0533	0.4806	0.0561	0.5510	0.0573	0.5898	0.0576	0.6023
6.0	0.0135	0.0811	0.0290	0.2024	0.0421	0.3631	0.0474	0.4712	0.0496	0.5379	0.0506	0.5745	0.0508	0.5860

(b) $S_e/U_0=(1+x^2c^2)^2I_e$.

0.8	−0.214	−0.322	−0.226	−0.347	−0.259	−0.416	−0.302	−0.517	−0.342	−0.625	−0.371	−0.707	−0.379	−0.738
1.0	−0.146	−0.291	−0.158	−0.325	−0.187	−0.420	−0.219	−0.559	−0.243	−0.705	−0.254	−0.815	−0.257	−0.855
1.2	−0.102	−0.256	−0.112	−0.300	−0.135	−0.418	−0.152	−0.588	−0.152	−0.760	−0.141	−0.884	−0.136	−0.930
1.6	−0.056	−0.203	−0.063	−0.259	−0.070	−0.414	−0.050	−0.613	−0.003	−0.809	+0.043	−0.931	+0.062	−0.972
2.0	−0.034	−0.165	−0.039	−0.233	−0.031	−0.417	−0.018	−0.634	+0.094	−0.802	+0.157	−0.898	+0.180	−0.928
2.4	−0.023	−0.138	−0.026	−0.218	−0.005	−0.422	+0.065	−0.629	+0.151	−0.764	+0.214	−0.831	+0.238	−0.858
2.8	−0.017	−0.119	−0.018	−0.210	+0.015	−0.426	+0.095	−0.611	+0.178	−0.712	+0.233	−0.755	+0.251	−0.767
3.0	−0.015	−0.111	−0.015	−0.208	+0.023	−0.426	+0.105	−0.598	+0.185	−0.684	+0.234	−0.718	+0.251	−0.727
3.2	−0.013	−0.104	−0.012	−0.207	+0.030	−0.426	+0.112	−0.584	+0.186	−0.656	+0.231	−0.682	+0.247	−0.688
3.6	−0.010	−0.092	−0.007	−0.206	+0.041	−0.422	+0.120	−0.553	+0.183	−0.602	+0.219	−0.617	+0.231	−0.619
4.0	−0.008	−0.083	−0.004	−0.206	+0.049	−0.416	+0.121	−0.520	+0.175	−0.522	+0.203	−0.559	+0.212	−0.560
4.4	−0.007	−0.076	−0.001	−0.208	+0.054	−0.405	+0.120	−0.487	+0.163	−0.507	+0.186	−0.509	+0.193	−0.509
4.8	−0.006	−0.069	+0.002	−0.210	+0.058	−0.393	+0.116	−0.456	+0.151	−0.467	+0.169	−0.467	+0.174	−0.466
5.2	−0.005	−0.064	+0.004	−0.211	+0.059	−0.379	+0.110	−0.427	+0.139	−0.432	+0.153	−0.429	+0.157	−0.428
5.6	−0.004	−0.059	+0.006	−0.212	+0.060	−0.364	+0.104	−0.400	+0.127	−0.401	+0.138	−0.397	+0.142	−0.395
6.0	−0.003	−0.056	+0.008	−0.213	+0.059	−0.350	+0.098	−0.375	+0.117	−0.374	+0.126	−0.369	+0.128	−0.367

available is that used by Dalitz.[3] The results are tabulated below and are compared with their corresponding first Born approximation. Using the above trial wave functions, the results are of the form $J(\theta)=f(\theta)/[1-S(\theta)]$, where $f(\theta)$ is the first Born approximation and the function $S(\theta)=U_0I(\theta)/f(\theta)$ represents essentially the ratio of the second Born approximation to the first. In order to obtain the total cross section for elastic scattering, use was made of the relationship existing between the scattering amplitude and the total cross section; namely,[1,2]

$$Q=(4/k)\times\text{imaginary part of } J(\theta)_{\theta=0}.$$

The algebraic results are summarized in Table I. In order to facilitate the numerical calculation of the total cross section for elastic scattering we list the algebraic value of $S_i(\theta)_{\theta=0}$ in Table II. Numerical values for the functions $S_i(\theta)$ as a function of θ are found in Tables III and IV for different values of the variables $x=2k/\lambda$.

For the case of the elastic scattering of electrons from monatomic hydrogen assuming no exchange or polarization, we may set $2U_0/\lambda a_0=1$; $\lambda=2/a_0$; thus $x=2k/\lambda=ka_0=(1/\alpha)(2E/mc^2)^{\frac{1}{2}}$ (as in Mott and Massey[4]), where α is the fine structure constant. We tabulate the numerical values of the function $|1/[1-S_m(\theta)]|^2$ in

TABLE IV. $S_m/(2U_0/\lambda a_0)=(1+x^2c^2)^2I_m/(2+x^2c^2)$.

x	0° Re	0° Im	30° Re	30° Im	60° Re	60° Im	90° Re	90° Im	120° Re	120° Im	150° Re	150° Im	180° Re	180° Im
0.8	0.375	0.399	0.394	0.422	0.446	0.486	0.514	0.574	0.578	0.661	0.624	0.724	0.640	0.747
1.0	0.286	0.385	0.309	0.420	0.366	0.513	0.439	0.639	0.505	0.761	0.549	0.847	0.564	0.878
1.2	0.221	0.361	0.245	0.406	0.305	0.528	0.377	0.688	0.436	0.836	0.474	0.938	0.486	0.974
1.6	0.139	0.307	0.164	0.373	0.222	0.545	0.280	0.751	0.320	0.927	0.342	1.039	0.348	1.076
2.0	0.094	0.261	0.118	0.347	0.170	0.557	0.211	0.785	0.235	0.960	0.245	1.066	0.248	1.100
2.4	0.067	0.225	0.091	0.329	0.134	0.566	0.162	0.796	0.174	0.960	0.179	1.054	0.182	1.084
2.8	0.050	0.197	0.073	0.317	0.109	0.572	0.126	0.793	0.132	0.942	0.133	1.024	0.134	1.050
3.0	0.044	0.185	0.066	0.314	0.098	0.572	0.112	0.788	0.116	0.929	0.117	1.006	0.117	1.031
3.2	0.038	0.175	0.061	0.311	0.089	0.572	0.099	0.782	0.102	0.914	0.103	0.987	0.103	1.010
3.6	0.031	0.157	0.052	0.306	0.073	0.570	0.080	0.764	0.081	0.883	0.081	0.948	0.081	0.968
4.0	0.025	0.142	0.045	0.304	0.061	0.565	0.065	0.744	0.066	0.852	0.066	0.909	0.066	0.927
4.4	0.021	0.130	0.039	0.303	0.052	0.558	0.054	0.723	0.054	0.820	0.054	0.872	0.054	0.889
4.8	0.017	0.119	0.035	0.302	0.044	0.549	0.045	0.701	0.045	0.790	0.045	0.838	0.045	0.853
5.2	0.015	0.110	0.031	0.302	0.038	0.539	0.039	0.680	0.039	0.762	0.038	0.805	0.038	0.819
5.6	0.013	0.103	0.028	0.301	0.033	0.529	0.033	0.660	0.033	0.735	0.033	0.775	0.033	0.788
6.0	0.011	0.096	0.025	0.300	0.029	0.518	0.029	0.639	0.029	0.708	0.029	0.748	0 029	0.759

[3] R. H. Dalitz, Proc. Roy. Soc. (London) **A206**, 509 (1951).
[4] N. F. Mott and H. S. W. Massey, *The Theory of Atomic Collisions* (Oxford University Press, London, 1949), p. 184.

TABLE V. $|1/(1-S_m)|^2=1/[(1-\mathrm{Re}S_m)^2+(\mathrm{Im}S_m)^2]$.[a]

x \ θ	0°	30°	60°	90°	120°	150°	180°
0.8	1.819	1.834	1.840	1.767	1.626	1.501	1.452
1.0	1.521	1.528	1.504	1.385	1.213	1.085	1.040
1.2	1.357	1.360	1.313	1.161	0.983	0.364	0.825
1.6	1.196	1.193	1.108	0.923	0.757	0.661	0.632
2.0	1.124	1.114	1 001	0.808	0.663	0.586	0.563
2.4	1.085	1.070	0.935	0.748	0.624	0.560	0.542
2.8	1.062	1.042	0.892	0.718	0.610	0.556	0.540
3.0	1.054	1.031	0.876	0.709	0.608	0.558	0.543
3.2	1.047	1.022	0.863	0.703	0.609	0.562	0.548
3.6	1.037	1.007	0.844	0.699	0.616	0.574	0.561
4.0	1.030	0.995	0.833	0.701	0.626	0.588	0.577
4.4	1.025	0.985	0.826	0.706	0.638	0.604	0.594
4.8	1.021	0.977	0.823	0.713	0.651	0.620	0.610
5.2	1.018	0.970	0.822	0.721	0.665	0.636	0.627
5.6	1.015	0.965	0.823	0.730	0.678	0.651	0.643
6.0	1.013	0.960	0.826	0.740	0.692	0.666	0.658

[a] Where $\mathrm{Re}S_m$ and $\mathrm{Im}S_m$ denote the real and imaginary part of $S_m(\theta)$, respectively.

Table V. In Table VI we tabulate

$$Q=\frac{(4/x)\ \mathrm{Im}S_m(\theta)_{\theta=0}}{|1-S_m(\theta)_{\theta=0}|^2}=\pi a_0{}^2\frac{(12+18x^2+7x^4)}{3(1+x^2)^3}\left|\frac{1}{1-S_m(0)}\right|^2,$$

which represents the numerical values for the total cross section for elastic scattering as a function of the energy parameter x. In Table VII we tabulate

$$I(\theta)/a_0{}^2=[f(\theta)]^2|1/[1-S_m(\theta)]|^2$$
$$=\tfrac{1}{4}[(2+x^2c^2)/(1+x^2c^2)^2]^2|1/[1-S_m(\theta)]|^2,$$

which represents the square of the scattering amplitude as a function of θ for various values of x.

In Fig. 1 the total cross section for elastic scattering as derived from the first Born approximation and that as derived from the above variational principle are compared as a function of the energy parameter x.

TABLE VI. $Q=4\ \mathrm{Im}S_m/x|1-S_m|^2$.[a]

x	Q
0.8	3.627
1.0	2.345
1.2	1.633
1.6	0.919
2.0	0.587
2.4	0.407
2.8	0.299
3.0	0.260
3.2	0.229
3.6	0.181
4.0	0.146
4.4	0.121
4.8	0.102
5.2	0.0865
5.6	0.0745
6.0	0.0649

[a] $\mathrm{Im}S_m$ denotes the imaginary part of $S_m(\theta)_{\theta=0}$, and $|1-S_m|^2$ is also evaluated at $\theta=0$.

TABLE VII. $I(\theta)/a_0{}^2=(1/4)[(2+x^2c^2)/(1+x^2c^2)^2]^2|1/[1-S_m(\theta)]|^2$.

x \ θ	0°	30°	60°	90°	120°	150°	120°
0.8	1.819	1.618	1.185	0.783	0.521	0.389	0.350
1.0	1.521	1.259	0.800	0.477	0.245	0.167	0.146
1.2	1.357	1.034	0.535	0.256	0.125	0.080	0.069
1.6	1.196	0.747	0.267	0.092	0.040	0.024	0.020
2.0	1.124	0.554	0.141	0.0399	0.016	0.0096	0.008
2.4	1.085	0.413	0.078	0.0196	0.0078	4.61(−3)	3.90(−3)
2.8	1.062	0.307	0.045	0.0107	4.23(−3)	2.52(−3)	2.14(−3)
3.0	1.054	0.265	0.035	8.2(−3)[a]	3.23(−3)	1.64(−3)	1.65(−3)
3.2	1.047	0.228	0.028	6.35(−3)	2.51(−3)	1.51(−3)	1.29(−3)
3.6	1.037	0.170	0.018	4.01(−3)	1.60(−3)	0.97(−3)	0.83(−3)
4.0	1.030	0.127	0.012	2.67(−3)	1.07(−3)	0.65(−3)	0.56(−3)
4.4	1.025	0.096	8.30(−3)	1.85(−3)	0.75(−3)	0.46(−3)	0.39(−3)
4.8	1.021	0.073	5.05(−3)	1.33(−3)	0.54(−3)	0.33(−3)	0.287(−3)
5.2	1.018	0.056	4.35(−3)	0.97(−3)	0.40(−3)	0.249(−3)	0.21(−3)
5.6	1.015	0.439	3.26(−3)	0.72(−3)	0.30(−3)	0.189(−3)	0.16(−3)
6.0	1.013	0.034	2.50(−3)	0.57(−3)	0.24(−3)	0.147(−3)	0.126(−3)

[a] (−3) denotes that the entry should be multiplied by 10^{-3}.

Here we have denoted the cross section derived from the first Born approximation as

$$Q(\mathrm{Born})=\pi a_0{}^2(12+18x^2+7x^4)/3(1+x^2)^3,$$

and the cross section derived from the variational principle as

$$Q(\mathrm{Variational})=\text{the above } Q.$$

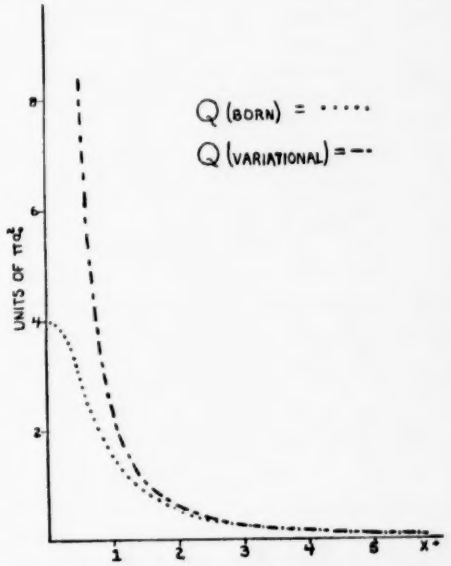

FIG. 1 A comparison of the total cross section of the elastic scattering of electrons from atomic hydrogen not including exchange or polarization using the first Born approximation and the above variational principle

I wish to thank Professor P. M. Morse for suggesting the need for the above tabulations and for aid in their development, and also to thank Elgie Ginsburgh for her painstaking calculations.

Electron-Electron Scattering at 6.1 Mev*

W. C. Barber, G. E. Becker,† and E. L. Chu
Microwave Laboratory, Department of Physics, Stanford University, Stanford, California
(Received June 17, 1952)

The absolute differential cross section for the scattering of 6.1-Mev electrons by the electrons in a beryllium foil has been measured at 90 degrees and 109 degrees in the center-of-mass system. Electrons from a linear accelerator were first magnetically analyzed and then collimated to form the incident beam. Electron-electron scattering events were detected by end-window Geiger counters connected in coincidence. The counter with the defining aperture was connected in coincidence (1) with a counter at the conjugate scattering-angle, lying in the plane determined by the incident beam and the scattering direction to the defining counter; and (2), with another counter at the conjugate angle, but lying outside this plane, thus counting only accidental coincidences. The number of e-e coincidences was then given by the difference between (1) and (2), with appreciable corrections arising from asymmetry in the background and from dead-time losses. These corrections required measurements of single and coincidence count rates with the scatterer in and out of the beam.

The result at 109 degrees was 4.4 percent lower than that predicted by the Møller theory, with a standard deviation based on the number of counts recorded of ±6 percent. At 90 degrees the expected standard deviation was ±2 percent, and here the experimental result was 8 percent below the theoretical. The latter result suggests the possibility that the Møller theory overestimates the cross section. However, consideration of the effects produced by radiative collisions, and of possible systematic errors in the experiment, leads to the conclusion that the experimental result is not incompatible with the Møller theory.

I. INTRODUCTION

A CALCULATION of the differential cross section for electron-electron scattering was made by Møller,[1] using the Dirac theory. His result may be written as follows:

$$\sigma(\theta)=2\left(\frac{e^2}{m_0v^2}\right)^2\frac{\gamma+1}{\gamma^2}\frac{(\gamma^*)^2\cos\theta}{[\cos^2\theta+(\gamma^*)^2\sin^2\theta]^2}\times\left\{\csc^4\frac{\theta^*}{2}+\sec^4\frac{\theta^*}{2}-\csc^2\frac{\theta^*}{2}\sec^2\frac{\theta^*}{2}+\left(\frac{\gamma-1}{\gamma}\right)^2[1+4\csc^2\theta^*]\right\},\quad(1)$$

where θ is the scattering angle in the laboratory system, θ^* the corresponding angle in the center-of-mass system, e, m_0, and v the electron charge, rest mass, and velocity, respectively, $\gamma=1/[1-v^2/c^2]^{\frac{1}{2}}=m/m_0$, and $\gamma^*=[(\gamma+1)/2]^{\frac{1}{2}}$. The relationship of $\sigma(\theta)$ to experimentally observable quantities is given by

$$\sigma(\theta)=V/nN\Omega,\quad(2)$$

where V is the number of scattered electrons reaching a detector at the angle θ which subtends a small solid angle Ω at the scatterer, N is the number of incident electrons, and n is the number of electrons per cm^2 in the scatterer. A theory based on the Schrödinger equation yields the Mott[2] formula, which differs from (1) only in that the fourth term in the bracket is missing. The relativistic classical expression results when both the third and the fourth terms in the bracket of (1) are dropped.

Until very recently, the only experimental checks were made by studying cloud-chamber tracks.[3,4] All these results taken together discriminated against the classical expression, but were not sufficiently precise to show that the Møller formula was more accurate than the Mott formula. Within the last two years, experiments have been done in which counting techniques were used to obtain more precise results.[5,6] These experiments gave results which agreed with the Møller formula within the experimental uncertainty, and which, together with the earlier results, showed the inadequacy of all other published formulas not based on the Dirac theory.

This paper describes an experiment using electrons from a linear accelerator, with a kinetic energy of 6.1 Mev. The corresponding energy in the center-of-mass system is 0.85 Mev, assuming that the target electron is at rest in the laboratory. This energy is very suitable for a study of e-e scattering since the collisions are quite relativistic, the differential cross section is large (about 10^{-25} cm^2/steradian), and the laboratory scattering angles of chief interest are of a convenient magnitude.

II. COINCIDENCE METHOD

A coincidence method may be used to distinguish electron-electron scattering from other types of scattering which occur in the foil. If an electron of momentum $\mathbf{p}_0$ makes an elastic collision with a second electron initially at rest, the two electrons emerge with momenta $\mathbf{p}_1$ and $\mathbf{p}_2$, at angles θ and ϕ, respectively (see Fig. 1). The laws of conservation of energy and momentum permit the calculation of ϕ, $\mathbf{p}_1$, and $\mathbf{p}_2$, if $\mathbf{p}_0$ and θ are given. The relationship between the labo-

* Assisted in part by the joint program of the U. S. Office of Naval Research and the U. S. Atomic Energy Commission.
† Now at Hudson Laboratories, Columbia University, Dobbs Ferry, New York.
[1] C. Møller, Ann. Physik **14**, 531 (1932).
[2] N. F. Mott, Proc. Roy. Soc. (London) **A126**, 259 (1930).
[3] F. C. Champion, Proc. Roy. Soc. (London) **A137**, 688 (1932).
[4] Groetzinger, Leder, Ribe, and Berger, Phys. Rev. **79**, 454 (1950). This reference contains a review of earlier cloud-chamber work.
[5] L. A. Page, Phys. Rev. **81**, 1062 (1951).
[6] Scott, Hanson, and Lyman, Phys. Rev. **84**, 638 (1951).

ratory angles θ and ϕ is given by $\tan\theta=[2/(1+\gamma)]\cot\phi$, where $\gamma=[1-(v^2/c^2)]^{-\frac{1}{2}}$, v is the velocity of the incident electron in the laboratory, and c is the velocity of light. $\mathbf{p}_2$ must lie in the plane determined by the vectors $\mathbf{p}_0$ and $\mathbf{p}_1$. An electron detector with a defining aperture at the angle θ connected in coincidence with another detector with a conjugate aperture at the conjugate angle ϕ should count the *e-e* events at the angle θ. In practice, because of the finite resolving time of the coincidence circuit, there will be chance coincidences, resulting, for example, from two distinct nuclear scattering events in the foil. These chance coincidences may be measured and subtracted from the total by connecting in coincidence with the detector at θ a third detector at the angle ϕ, but lying outside the plane determined by the vectors $\mathbf{p}_0$ and $\mathbf{p}_1$. It is assumed that the number of chance coincidences arising from events occurring in the scattering foil is the same for each coincidence pair. The same may not be assumed for the number of chance coincidences arising from the general background, with no scattering foil, and it is necessary to make a separate measurement of these.

Of course, it is possible to write down an expression for the expected number of accidental coincidences if the single count rates for the two counters of a coincidence pair are known. This procedure of calculating the number of accidental coincidences is less accurate than actually measuring them with a second coincidence pair, for reasons which can be better discussed below, after the apparatus has been described.

While it is true that the incident electron beam may be contaminated with x-rays which can give rise to Compton scattering or pair production in the foil, such events will not lead to a false result for the number of *e-e* coincidences. The two photons and the electron involved in a Compton scattering process do have co-planar paths, but the conjugate angles after scattering are not the same as for the *e-e* case. As for the pair production process, the probability that the angle between the positron-photon and electron-photon planes have a given value between 0 degrees and 180 degrees is almost constant as a function of angle. The slightly greater probability for angles near 180 degrees would not lead to any measureable effects in this experiment.

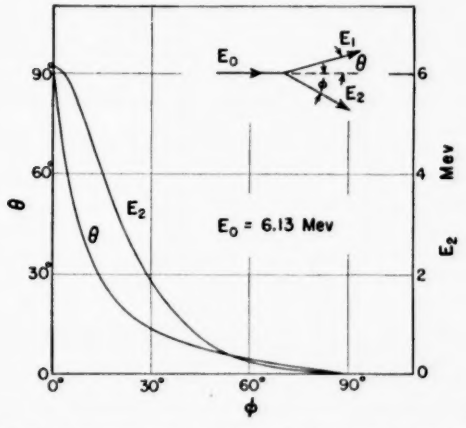

FIG. 1. One curve gives the relationship between the conjugate laboratory angles θ and ϕ for the case of an electron-electron collision, with incident electron energy=6.1 Mev. The other curve gives the energy of the electron scattered at the angle θ for the same case.

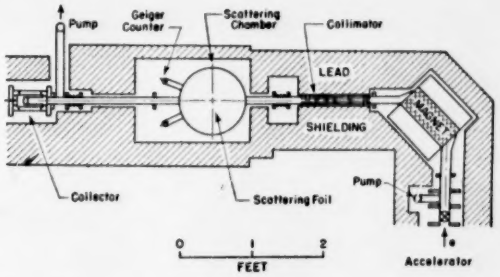

FIG. 2. Schematic diagram of the arrangement of the apparatus.

In order that no coincidences be missed, the conjugate aperture must be larger than the defining aperture. The reasons for this have been thoroughly presented previously,[7] and need not be repeated in detail here. The effects of the finite beam size and the fact that $(d\phi/d\theta)\neq 1$ are easily taken into account. Other factors which are important in determining the required conjugate aperture size are (1) multiple scattering, (2) possible small misalignments, and (3) the initial motions of the target electrons in the foil. A first approximation to the required aperture size may be based on numerical estimates for each of these factors. But in order that one may be certain that the conjugate aperture has been made large enough, a series of measurements must be made with increasing conjugate aperture size, until the point is reached where the observed result no longer increases with conjugate aperture size.

Counting corrections which arise because of the dead time of the electron detectors will be discussed in a separate section below.

III. APPARATUS

A. Beam Formation

A schematic diagram of the arrangement of the apparatus is given in Fig. 2. The electron beam from the accelerator was first passed through a $\frac{1}{32}$-in. cylindrical hole in a 1-in. thickness of polystyrene, and was then magnetically analyzed and collimated. The range of energies of the electrons transmitted by the magnet and collimator system was ± 0.13 Mev at an energy of 6.1 Mev. The 14-in. length of collimator consisted of $\frac{1}{16}$-in. cylindrical holes in aluminum and

[7] See, for example, Karr, Bondelid, and Mather, Phys. Rev. **81**, 37 (1951).

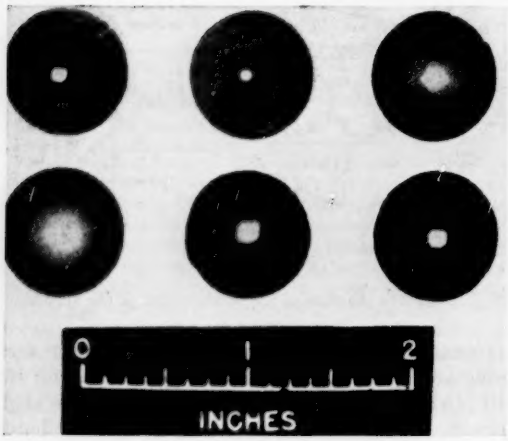

FIG. 3. Cross sections of the electron beam at various points along its path. Upper row from right to left: (1) At the entrance to the collimator tube. The horizontal spread results from the spread in energy of the electrons from the accelerator. (2) At the exit of the collimator tube. (3) At the position of the scattering foil. Lower row from right to left: (1) At the end of the exit tube of the scattering chamber. (2) At a point 4 inches in front of the collection cup. (3) Same position as for (2), but with a $\frac{1}{4}$-mil nylon foil scatterer.

polystyrene, separated by lead spacers with larger holes. Electrons could strike only the low Z materials, which were used to minimize bremsstrahlung.

The apparatus was first lined-up approximately with various mechanical devices. Final adjustment was made with the aid of films inserted at various points, which revealed the shape of the beam and its location with respect to the axis of the apparatus. The beam was made to coincide with this axis to within $\pm\frac{1}{32}$ inch. Figure 3 shows the cross section of the beam at various points along its path. After collimation, the total angle of spread was 0.2 degree.

B. Scattering Chamber

The cylindrical scattering chamber was made of brass, 12 inches in diameter, 8 inches in height, with $\frac{1}{8}$-in. walls. The chamber was lined with polystyrene $\frac{3}{16}$ in. in thickness, coated with Aquadag. This was done to minimize backscattering of electrons from the walls. Thin windows in the wall at a few fixed angles served as exit ports for the scattered electrons. Figure 4 shows a view of the scattering chamber from the exit tube, giving the projection of each window on a plane perpendicular to the beam. The pairs of windows for counters lying in a plane with the incident beam are indicated by the dotted lines. On the assumption that the electron beam was correctly aligned, knowledge of the scattering angle θ depended on the precision of the machine work in locating the holes for the windows. The various angles should be correct to within ± 0.1 degree, but no other means were devised to check this.

C. Detectors

End-window type Geiger-Müller counters were used as detectors. Those used in the earlier stages of the experiment were made by bolting the counter cathode shells directly onto the scattering chamber. A single 0.001-inch aluminum window separated the vacuum of the scattering chamber from the counter gas, which was a mixture of argon and alcohol at a total pressure of 8 cm of mercury. The plateaus of these counters were very poor, rising 30 to 50 percent in 100 volts. However, the counter characteristics remained stable over a period of several months. The excessive rise of the plateaus was chiefly caused by multiple pulses, which would not affect the coincidence count rates appreciably. The multiple pulses produced errors in the single count rates until gating circuits were introduced to limit the sensitive time to the period when the accelerator was on. Even without the gating circuits, the errors in the single count rates produced only second-order errors in the final result.

While there was no specific reason to doubt the results obtained with these counters, it was decided to repeat the experiment, at angle $\theta^*=90$ degrees, using commercial (Tracerlab) mica-window counters, with good plateaus. This necessitated the use of two windows, but the separation of the windows was only $\frac{3}{16}$ inch, and the combined window thickness did not exceed 12 mg/cm^2, so that the transmission for electrons of energy greater than 1 Mev was still essentially 100 percent. These counters were filled with helium and a quenching gas to a total pressure near one atmosphere. The *e-e* scattered electrons had energies in excess of 2 Mev at the angles studied in this experiment. Calculations show that, with the given geometry and window thickness, any such electron should have had a path

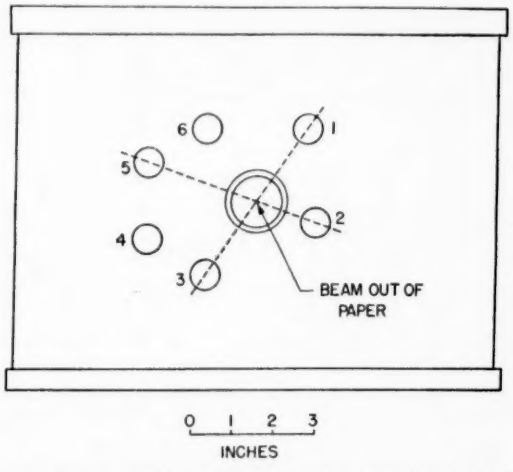

FIG. 4. A view of the scattering chamber from the exit tube, giving the approximate location of the Geiger counters. The numbered circles give the distorted projection of each counter window on a plane perpendicular to the incident beam.

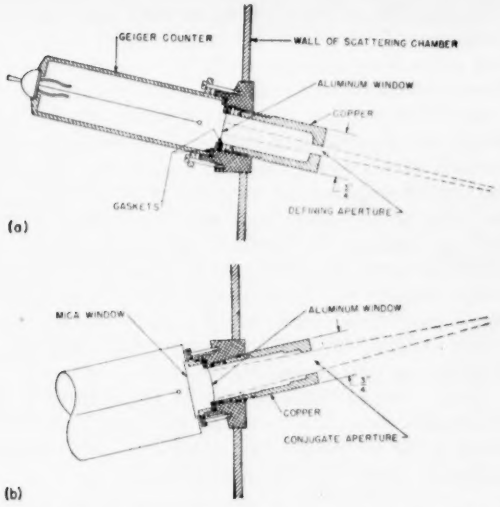

FIG. 5. Scale drawing showing the aperture determining the solid angle subtended at the scatterer. (a) A defining aperture with tapered walls is shown in front of an argon-alcohol counter with a single aluminum window. (b) A conjugate aperture is shown in front of a helium-filled (Tracerlab) counter with a mica window.

length of at least one cm within the active volume of the Geiger counter. The gas pressures in the Geiger counters were great enough to make the probability of producing one or more ions negligibly less than 100 percent under these circumstances.

At the conclusion of the experiment, a standard coincidence method[8] employing the sea-level cosmic radiation was used to check the efficiency of one of the Tracerlab counters. The result indicated that the efficiency is in the range of 0.975 to 1.00, but the possibility of wide angle scattering and the uncertainty of the correction for showers restricted the precision of the determination to the above limits. The result of this measurement is not inconsistent with the theoretically estimated efficiency of essentially 100 percent. This theoretical estimate has been used in calculating cross sections, but since there is no experimental proof of this point, we must allow the possibility of a systematic error.

The solid angle subtended at the foil by a detector was determined by a tapered cylindrical hole in a copper solid cylinder screwed into position in front of the Geiger counter, as shown in Fig. 5. In order to vary the aperture size, it was necessary to remove the lid of the scattering chamber and insert a new copper cylinder. The knowledge of the solid angle subtended by an aperture depended on mechanical measurements which were accurate to within $\pm\frac{1}{2}$ percent. The fact that the axis of each copper cylinder intersected the path of the electron beam at the center of the chamber was checked by mechanical means. Any errors in the position of this point of intersection were found to be less than $\frac{1}{32}$-in.

[8] J. C. Street and R. H. Woodward, Phys. Rev. **46**, 1029 (1934).

D. Electronic Circuits

A block diagram of the electronic circuits is shown in Fig. 6. The gates insured that counts were registered only when the accelerator was turned on. In the early stages of the experiment, these gates were not used, and it was necessary to measure and subtract counts arising from cosmic rays and other background with the accelerator off. The resolving time of the coincidence circuits was 2 μsec, a convenient number somewhat larger than the 0.8-μsec pulse of electrons from the accelerator. Thus, the effective resolving time was just the length of this electron pulse.

E. Scattering Foil

Some preliminary tests were made with nylon and polystyrene foils, but careful measurements were made only with a beryllium scatterer. A scatterer of low Z was chosen for three reasons: (1) to minimize the ratio of electron-nuclear scattering to e-e scattering; (2) to minimize any effects arising from the binding of the target electron in the atom; and (3) to minimize multiple scattering in the foil.

Dr. H. Bradner of the Radiation Laboratory at Berkeley kindly supplied beryllium foils, each about 0.4 mg/cm^2 in thickness. The actual scattering foil was made by mounting several of these on top of each other on a circular brass ring with inside diameter equal to one inch. The area and the mass of each foil could be determined within ± 1 percent. The uniformity of the final scattering foil was tested by measuring the transmission of polonium alpha-particles, which were near the end of their range, through various regions of the foil. The beam of alpha-particles was collimated to a cross-sectional area about equal to that of the electron beam used in the scattering experiment. The transmission of the alpha-beam was measured at 12 different places on the foil. The root mean square variation in thickness of the measured places from their mean value was 1.7 percent. The region near the center of the foil, where the electron beam passed, was more

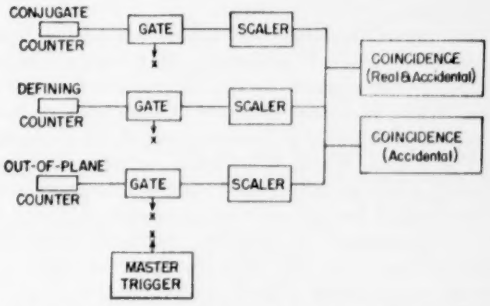

FIG. 6. Block diagram of the electronic circuits employed.

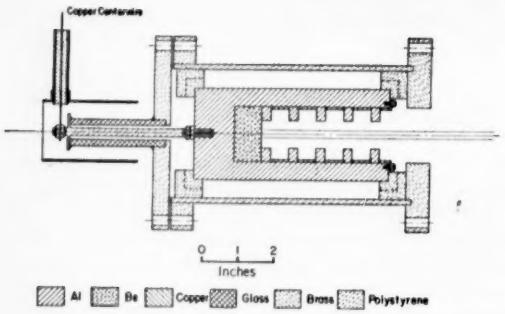

FIG. 7. Scale drawing of the current collection cup.

uniform than the foil as a whole and of thickness not appreciably different from the mean value.

After extensive measurements were made with one scatterer, it was accidentally destroyed. The measurements were repeated with an entirely new scatterer, and the observed results were unchanged. The purity of the evaporated beryllium foils was high, but was not critical in this experiment. In the light of the foregoing, we think it very unlikely that the computed number of target electrons per cm^2 is in error by more than 2 percent.

IV. CURRENT MEASUREMENT

The average current carried by the incident electron beam was of the order of 10^{-13} amp. The electrons in the beam were collected in the insulated cup shown in Fig. 7. Beryllium was used at the base of the cup to minimize bremsstrahlung and backscattering. On the basis of recently published measurements on backscattering,[9] and the small solid angle subtended at the base by the mouth of the cup (0.5 percent of 2π), it is estimated that less than 0.1 percent of the electrons could escape from the cup.

As is shown in Fig. 8, the electron current was integrated by measuring the potential across the polystyrene-insulated capacitor. The quadrant electrometer served simply as a null indicator. The electrometer deflection was held at zero by continuously adjusting the potentiometer setting during each run, so that the collector cup and associated leads were maintained at ground potential.

This procedure minimized any errors arising from ionization currents. It was shown that the application of a positive or negative bias to the collector cup could, respectively, increase or decrease the measured current by a saturation value of 3 percent from the value found with zero bias. A bias curve taken by using a Geiger counter, which measured the bremsstrahlung produced at the base of the cup, as a beam monitor is shown in Fig. 9. Because of the observed symmetry about the point of zero bias, we conclude that the ionization current is very small if the bias on the cup is zero.

[9] W. Bothe, Z. Naturforsch. **4a**, 542 (1949).

Observations of the electrometer drift rate with the accelerator off were made before and after each run, so that corrections could be made for leakage currents. These corrections were of the order of 1 percent or less.

Once it was established that spurious effects were absent, the integration of the current depended on the potential measurement, made with an L and N potentiometer and standard cell to within ± 0.1 percent, and the value of the capacitor. This was measured at the National Bureau of Standards under dc conditions similar to those used during the experiment. The value of the capacity was found to be 0.001017 microfarad, with a stated limit of error of 0.5 percent. This determination checks with bridge measurements made at a frequency of 1000 cycles/sec.

For an over-all limit of error in the integration of the current we assign the value ± 2 percent, most of which is due to the possibility that our interpretation of the bias curve is not entirely correct.

V. COLLECTION OF DATA

Measurements with the foil in and out were made alternately, while every effort was made to keep all other conditions constant. In order to minimize the statistical error of the difference, approximately twice as much running time was devoted to measurements with the foil in. During a given run (typically of two hours' duration), the current was monitored and was held constant within ± 10 percent by making small adjustments in the accelerator operating conditions.

With a given set of apertures, several series of runs were taken, at different current levels. The requirement of reasonable values for the count rates limited the range of current values to a variation by a factor of 3. No systematic differences in the results at different current levels were observed.

For the case where the defining aperture was at $\theta = 28$ degrees 4 minutes, the scattering foil was rotated 20 degrees about a vertical axis, in such a way as to reduce the path of the low energy scattered electrons in the foil. This was done to minimize multiple scattering.

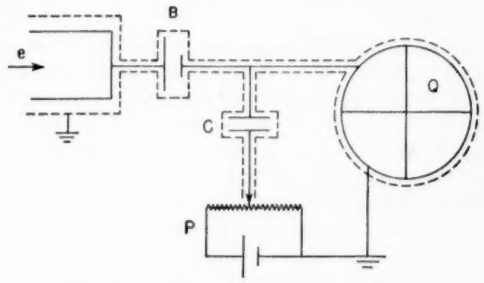

FIG. 8. Diagram for the current-integrating circuit. C is a polystyrene-insulated capacitor of high leakage resistance. B is a hearing-aid type battery used only in preliminary tests. Q is a quadrant electrometer, used as a null indicator.

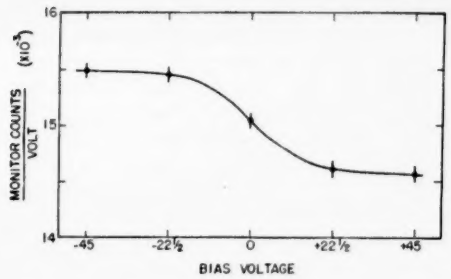

FIG. 9. The ratio (total monitor counts)/(total volts on capacitor) as a function of the bias voltage on the current collection cup. The monitor counts should be independent of the bias voltage, while the volts on the capacitor depend on the different ionization currents at different bias voltages.

VI. ANALYSIS OF DATA

The recorded data consisted of measurements of the average single and coincidence count rates with the foil in and out of position. Because there are two coincidence pairs for each foil position, there are four sets of data which can be used to determine four desired unknown quantities. The important unknown quantity is the real *e-e* coincidence rate due to the scattering foil which gives directly the quantity Y of Eq. (2). Other unknowns which affect the coincidence measurements are the in and out-of-plane real coincidences, which may be produced by scattering processes in the collimator, and the accidental coincidences. The latter could be predicted from the measured single count average rates were it not for the fact that the accelerator operation is not uniform in time. If the accelerator operation is nearly uniform, it can be shown that the accidental coincidences are determined to close approximation by the average count rates and the average value of $s^2(t)$, where $s(t)$ is the fractional deviation of the beam current at time t from the average value. The average value, $\langle s^2\rangle_{Av}$, of $s^2(t)$ is the fourth parameter determined by the data, and with this it becomes possible to make a good approximate solution for Y of Eq. (2). The necessary approximations involve only these assumptions: (1) the probability of two or more real *e-e* or background coincidences per burst of the accelerator is negligible; (2) the average values of powers higher than the second of $s(t)$ are negligible; and (3) that in many runs the average value of $s^2(t)$ is the same with the foil in as out. From the data it was determined that these approximations would make errors considerably less than one percent.

Considerable data was evaluated using no other approximations than the three listed above. In practice it was found useful to combine the four equations predicting observed coincidences as a sum of real and accidental coincidences into the following result, which can be used to illustrate the magnitudes of the count rates and a good approximate method of solution.

$$\begin{aligned}(n_{13}-n_{36})-(n_{13}^{\circ}-n_{36}^{\circ})&=\epsilon_{13}'[1-(1+\langle s^2\rangle_{Av})(n_1+n_3)]\\&\quad+(1+\langle s^2\rangle_{Av})[n_3(n_1-n_6)-n_3^{\circ}(n_1^{\circ}-n_6^{\circ})]\\&\quad+(1+\langle s^2\rangle_{Av})\epsilon_{13}^{\circ}(n_1^{\circ}+n_3^{\circ}-n_1-n_3)\\&\quad-(1+\langle s^2\rangle_{Av})\epsilon_{36}^{\circ}(n_6^{\circ}+n_3^{\circ}-n_3-n_6).\end{aligned}\quad(3)$$

Equation (3) is written for the case of a measurement at $\theta^*=90°$, where counters 1 and 3 (Fig. 4) are coplanar with the incident beam so as to detect *e-e* coincidences. The defining aperture is in front of counter 3, while counters 1 and 6 have larger equal apertures. In Eq. (3) the quantities n_1, n_3, n_6 represent the measured average count rates in counters 1, 3, and 6 per pulse of the accelerator, with foil in place. The measured average coincidence rates per pulse with foil in are given by n_{13} and n_{36}. The corresponding rates with foil out are given by the same symbols with superscript zero. The quantity ϵ_{13}' is the unknown to be evaluated which represents the true *e-e* coincidence probability per burst of the accelerator, while ϵ_{13}° and ϵ_{36}° represent the true coincidence probabilities produced by the background. In forming Eq. (3), large terms containing $\langle s^2\rangle_{Av}$ have cancelled out. The most important term on the right-hand side is ϵ_{13}' alone. Because of the near equality of n_1 and n_6, only a small error (less than one percent) is introduced by neglecting $\langle s^2\rangle_{Av}$. The ϵ° quantities can be determined from the data with the foil out of the beam, and then Eq. (3) can be solved to yield ϵ'_{13} in terms of experimental quantities.

Table I gives some typical values of the count rates and results observed in the experiment.

It may be noted here that the quantities $(n_1-n_1^{\circ})$ and $(n_6-n_6^{\circ})$ have the physical significance of being the count rates arising from the foil alone. Ideally, they should be equal, since, in this example, counters 1 and 6 have equal apertures. This was found to be true experimentally, with a standard deviation of about 5 percent, which can be attributed to variations in the accelerator operating conditions. The experimental equality of these rates constitutes an important check on the line-up of the apparatus.

VII. RESULTS

The results are summarized in Table II. Each line in the table corresponds to some one set of operating

TABLE I. Typical average count rates. (The notation is the same as in the text.)

n_1	n_3	n_6	n_{13}	n_{36}	n_1°	n_3°	n_6°	n_{13}°	n_{36}°	ϵ_{13}°	ϵ_{36}°	ϵ_{13}'
1.043 $\times10^{-1}$	3.86 $\times10^{-3}$	8.34 $\times10^{-2}$	8.19 $\times10^{-4}$	3.26 $\times10^{-4}$	7.65 $\times10^{-2}$	1.80 $\times10^{-3}$	5.48 $\times10^{-2}$	1.88 $\times10^{-4}$	1.30 $\times10^{-4}$	5.05 $\times10^{-5}$	3.15 $\times10^{-5}$	4.43 $\times10^{-}$

TABLE II. Summary of results.

Positions and types of counters used	Position and solid angle of defining aperture	Solid angle of conjugate aperture (sterad.)	Thickness of Be foil mg/cm²	Møller theory $\sigma\times10^{25}$ cm²/(sterad.)	Exp. σ and percent diff.	Remarks
(1,3,6) Argon-alcohol	(3)($\theta^*=90°$) 7.15×10^{-4}	5.21×10^{-3}	0.790	2.32	2.12 ± 0.08 -8.6%	
(1,3,6) Argon-alcohol	(3)($\theta^*=90°$) 7.15×10^{-4}	5.21×10^{-3}	0.790	2.32	2.07 ± 0.24 -10.8%	Large current-integrating capacitor.
(1,3,6) Argon-alcohol	(3)($\theta^*=90°$) 7.15×10^{-4}	3.31×10^{-3}	0.790	2.32	1.82 ± 0.10 -21.6%	Conjugate aperture made too small intentionally.
(1,3,6) Argon-alcohol	(3)($\theta^*=90°$) 3.68×10^{-4}	5.21×10^{-3}	0.790	2.32	1.87 ± 0.18 -19.4%	
(1,3,6) (3)Argon-alcohol (1,6)Tracerlab	(3)($\theta^*=90°$) 7.15×10^{-4}	8.95×10^{-3}	1.473	2.32	2.05 ± 0.11 -11.6%	
(1,3,6) (3)Argon-alcohol (1,6)Tracerlab	(3)($\theta^*=90°$) 7.15×10^{-4}	7.25×10^{-3}	1.473	2.32	2.16 ± 0.10 -7.1%	
(1,3,6) Tracerlab	(1)($\theta^*=90°$) 7.15×10^{-4}	8.95×10^{-3}	1.473	2.32	2.15 ± 0.11 -7.3%	
(1,3,6) Tracerlab	(1)($\theta^*=90°$) 14.6×10^{-4}	8.95×10^{-3}	1.473	2.32	2.24 ± 0.11 -3.5%	
(2,4,5) Argon-alcohol	(4)($\theta^*=109°\,19'$) 7.98×10^{-4}	5.67×10^{-3}	$\frac{0.790}{\cos20°}$	1.71	1.63 ± 0.10 -4.4%	

conditions, which are indicated in the first four columns and in the column headed "Remarks."

The probable errors indicated in column 6 are the expected standard deviations computed solely on the basis of the number of counts recorded. Possible systematic errors will be discussed below.

Line 2 in the table gives the result obtained when two 0.001-microfarad condensers were used in parallel, in place of the usual one, in the current integrating circuit. This was done to check for the possibility of gross errors in the current measurement.

For the case given in line 3, the conjugate aperture was deliberately made smaller than the minimum size demanded by calculations. As was expected, the result was lower in this case, by an amount which agreed with estimates of the effects of plural scattering in the foil.

The points obtained under various conditions at $\theta^*=90$ degrees are plotted in Fig. 10 as a function of the difference between the conjugate aperture diameter and the defining aperture diameter. The expected influence of plural scattering is shown by the dashed curve which was computed numerically using the multiple scattering theory of Snyder and Scott,[10] and taking into account the finite size and divergence of the incident beam. The dashed curve was normalized to yield the Møller cross section at large values of the conjugate aperture. Within the statistical accuracy of the data, the experimental points would fit a curve lying parallel to the dashed curve. The numerical calculations are thus supported by the data in indicating that the loss due to plural scattering is very small for those experiments where the larger conjugate apertures were used.

The expected standard deviation in the result at $\theta^*=109$ degrees (line 9) was not made less than ±6 percent because the time required for this would have been excessive.

The quantity σ is the cross section (per electron) per unit solid angle. Theoretical values were calculated from Eq. (1).

VIII. DISCUSSION

The weighted average of the results at $\theta^*=90$ degrees (excluding lines 2 and 3 of Table II) is 2.13 ± 0.043. This is about 8 percent lower than the Møller value, with an expected standard deviation from statistics alone of ±2 percent. At $\theta^*=109$ degrees 19 minutes, the experimental result is 4.4 percent too low, with an expected standard deviation of ±6 percent. A similar comparison with the Mott formula[2] shows the experimental results to be about 90 percent higher at 90 degrees and 65 percent higher at 109 degrees than the Mott formula predicts. Our result is thus in agreement with other experiments,[5,6] conducted with different energy electrons, in supporting the Møller formula.

Most of the points at which systematic errors may have been introduced have been discussed above. Our estimate of the expected maximum values of the chief possible errors, together with the direction in which they would be expected to affect the experimental result, may be summarized as follows: (1) Geiger counter efficiency, $+0$, -3 percent; (2) foil thickness, ±2 percent; (3) integration of electron current, ±2 percent; (4) inadequate conjugate aperture size (excluding radiative effects), $+0$, -1 percent; (5) error in

[10] H. S. Snyder and W. T. Scott, Phys. Rev. **76**, 220 (1949).

incident electron energy, ±2 percent; (6) uncertainty in defining aperture size because of leakage effects, +1, −0 percent; (7) approximations in calculations, ±1 percent. It may be seen that an unfortunate combination of these errors could make the experimental result as much as 8 percent too low. However, we believe that these estimates are conservative, and that a systematic error greater than 5 percent is unlikely. With the view, the experiment leaves room for a discrepancy between theory and experiment.

The Møller theory did not take into account the radiative effects accompanying an *e-e* event. Heitler[11] has shown that the order of magnitude of the real radiation is given by the Bethe-Heitler bremsstrahlung formula. Lanzl and Hanson[12] find experimental support for this conclusion. Therefore it is to be expected that in some of the *e-e* events an appreciable fraction of the energy will be carried off by a photon, and the angular correlation, essential for the coincidence technique, will be destroyed. However, some allowance can be made for such de-correlation by increasing the size of the conjugate aperture. The larger conjugate apertures used in the present experiment were large enough to catch both electrons, even though a photon carried off an energy of approximately 100 kev. Numerical calculations of the probability that photons of this energy or greater be radiated in a 6-Mev *e-e* collision are not available as yet. In the corresponding case of an *e-p* collision the probability is the order of several percent for those collisions where the electron suffers large deflections. The purely quantum electrodynamical radiative correction for *e-e* scattering has been calculated by Lomanitz,[13] and its magnitude is probably considerably less than one percent.[14] The radiative effects are thus due to the emission of real quanta. They are in the correct direction to account for the difference between the Møller theory and experiment, and it is not improbable that they are of sufficient magnitude.

[11] W. Heitler, *Quantum Theory of Radiation* (Oxford University Press, London, 1947), second edition, Appendix.
[12] L. H. Lanzl and A. O. Hanson, Phys. Rev. **83**, 959 (1951).
[13] R. Lomanitz, thesis, Dept. of Physics, Cornell University (unpublished).
[14] H. A. Bethe (private communication).

In addition to radiation there are other effects which might produce a discrepancy between Møller theory and experiment. For example, the Møller theory applies to free electrons, whereas in any experiment some of the target electrons are near the nucleus. Small effects due to interference with nuclear scattering should therefore be expected.

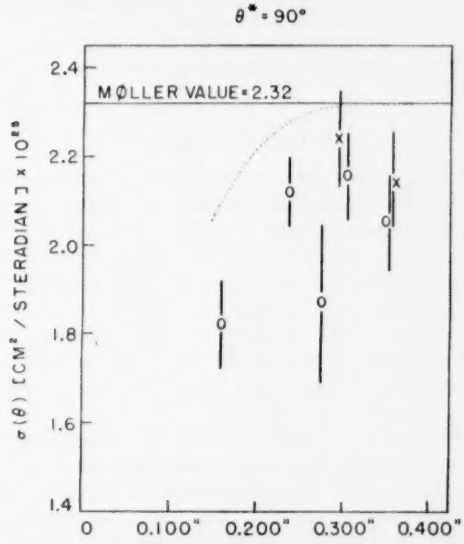

FIG. 10. Observed values of the absolute differential cross section as a function of the difference between the conjugate aperture diameter and the defining aperture diameter. This difference is a measure of the allowance made for the effects of multiple scattering and possible misalignment. The dashed curve gives a theoretical result for the expected loss due to multiple scattering. The theoretical curve has been normalized to give the Møller cross section at large aperture differences.

In closing, we should like to point out that recent results obtained elsewhere[5,6] on *e-e* scattering are also a few percent lower than the Møller theory predicts. In one of these cases,[6] the authors mention the possibility that systematic errors could account for the difference.

We are indebted to Mr. R. Torres, who built and tested some of the electronic components and to Mr. D. A. Caswell, who assisted in some of the early design work.

Pair Creation in Intermediate Coupling Theory

R. G. MOORHOUSE
Natural Philosophy Department, Glasgow University, Glasgow, Scotland
(Received October 29, 1952)

The approximations of the intermediate coupling method are applied to a model of the self-field of a single nucleon (interacting with a pseudoscalar meson field) in which only processes involving pair creation and annihilation are allowed. In order to do this a method of subtracting the vacuum before these approximations are made, is suggested. The magnetic moment of the self-field on this model is investigated, and a comparison is made with the antithetic model of the self-field in which only processes not involving pair creation or annihilation are allowed.

I. INTRODUCTION

IN his original paper on the intermediate coupling method, Tomonaga[1] treated the example of a nucleon interacting with a self-field of charged scalar mesons with scalar coupling. The recoil of the nucleon on emission and absorption of mesons was neglected. The matrix elements for pair creation (and annihilation) involve "small components" of the Dirac spinors and this, together with the fact that pair creation is unlikely for energetic reasons, made it safe to neglect pairs in the self-field for this example.

But if we try the more realistic case of pseudoscalar mesons with pseudoscalar coupling, the neglect of pairs is no longer safe.[2] The matrix elements for pair creation and annihilation are now the large ones, while the matrix elements for meson emission and absorption without pair creation involve small components of the Dirac spinors. It is true that transition probabilities are gained by dividing these matrix elements by an energy factor, and that this energy denominator is of order $2hc\kappa$ in the pair creation case and $hc\mu$ in the meson emission case, κ and μ being the inverse Compton wavelengths for nucleon and meson, respectively. But the energy denominator only serves to make about equal the probabilities for pair creation (or annihilation) and for meson emission (or absorption) without pair creation. For this reason it is difficult to conjecture which, if either, of these processes gives the more important contribution to the self-field of the nucleon. The approximation of no pairs has been treated by Matthews and Salam,[2] and in the next section is considered the antithetic approximation in which nonpair creation or annihilation events are left out.

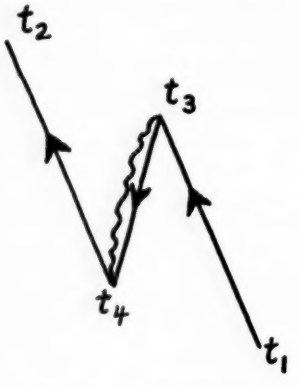

FIG. 1. A Feynman graph with an intermediate state with just one pair present.

II. THE SELF-FIELD OF PAIRS

Though in a pseudoscalar theory with pseudoscalar coupling it must be possible to eliminate consistently all high frequency divergences, their elimination in the intermediate coupling method becomes practically difficult. As in the paper of Tomonaga,[1] the difficulty is avoided by taking a cutoff in momentum space.

Creation and annihilation of pairs takes place in the vacuum, as well as when one nucleon is present originally. The observable nucleon consists of the difference of the nucleon and its self-field from the vacuum self-field. In order to avoid the difficulties of, and the approximations involved in, using the intermediate coupling method for the vacuum self-field, it becomes necessary to eliminate the vacuum before proceeding to the intermediate coupling method. In order to do this we consider the perturbation or S-matrix expansion in the form given by Feynman[3] in his paper on the theory of positrons. In the appendix to this paper Feynman shows that the matrix element, $M(T)$, given by second quantization for a transition in a time $t=0$ to $t=T$ is given by $M(T)=C_v(T)F(T)$. Here $C_v(T)$ is the probability that if there is a vacuum at $t=0$ there remains a vacuum at $t=T$, while $F(T)$ is the quantity corresponding to the sum of Feynman graphs for the process in question. The physically observable transition probability (that is, the transition probability after elimination of vacuum effects) is given by $F(T)$. It is to this, or a corresponding quantity, that it is proposed to apply the intermediate coupling method. In order to do so we now analyze a Feynman graph containing pairs. The

[1] S. Tomonaga, Prog. Theoret. Phys. **2**, 6 (1947).
[2] P. T. Matthews and A. Salam, Phys. Rev. **62**, 85 (1952).
[3] R. P. Feynman, Phys. Rev. **76**, 749 (1949).

example taken is shown in Fig. 1 and gives the quantity.

$$-\int \bar{g}(x_2)\beta K_+(2,4)A(4)K_+(4,3) \times A(3)K_+(3,1)\beta f(x_1)d^3x_1d^3x_2d\tau_3d\tau_4. \quad (1)$$

Here $t_4<t_3$, $t_1=0$, $t_2=T$. The notation of Feynman[3] is used in (1); the fact that Feynman's notation is given for an electron-photon theory while we are thinking of a nucleon-meson theory only requires that a trivial change be made in the meaning of the symbols. (For example, A, instead of being $\gamma_\mu A_\mu$ becomes $\gamma_5\phi$ or $\gamma_5\phi^*$, where ϕ is the usual meson field quantity.)

From the definition of the K_+ [reference 3, Eq. (17)] it follows that (1) is equal to

$$\left\{\int \bar{g}(x_4)A(4)\phi_n(x_4)\bar{\phi}_n(x_3)A(3)f(x_3)d^3x_3d^3x_4\right\} \times\int_{t_1}^{t_2}dt_3\int_{t_1}^{t_3}dt_4\exp(-iE_2t_2)\exp[(-it_4)(E_2-E_n)] \times\exp[-it_3(E_n-E_2)]\exp(iE_1t_1). \quad (2)$$

The ϕ_n are fermion wave functions as given by Feynman.

Here E_1, E_2 is the free particle energy of the system at time t_1, t_2, and E_n is the free particle energy of the particles in the intermediate state n. By free particle energy is meant the energy the particles would have moving freely without interaction. Equation (2) is just the usual matrix element to give a transition probability in time dependent perturbation theory[4] except for a change in sign, with a pair of nucleons and a meson being created at t_4 and a pair of nucleons and a meson annihilated at t_3. On performing the time integrations we obtain

$$-\sum_n \frac{H_{2n}'H_{n1}'}{E_1-E_n}\left[\frac{\exp[-i(E_1-E_2)T]-1}{E_1-E_2} - \frac{\exp[-i(E_n-E_2)T]-1}{E_n-E_2}\right]\exp(-iE_2T). \quad (3)$$

Here H_{n1}', H_{2n}' are the matrix elements for the interaction part of the Hamiltonian. In the limit $T\to\infty$, this just gives rise to the usual expression for the self-energy to second order in the coupling constant,

$$-\sum_n \frac{H_{2n}'H_{n1}'}{E_1-E_n}. \quad (4)$$

Now consider the Feynman graph shown in Fig. 2(a). Here t_6, $t_4<t_5$, t_3. Consider here that the pair produced at t_6 has the same free energy as the pair produced at t_4. Let the free energy of the state along the middle dotted line be E_i and on the top dotted line be E_j. Then it can be shown, in just the same way as before, that the self-energy corresponding to this diagram is

$$4\frac{H_{2i}'H_{ij}'H_{j1}'H_{i1}'}{(E_1-E_i)(E_1-E_j)(E_1-E_i)}+I. \quad (5)$$

The factor 4 comes from the fact that t_4 may occur before or after t_6 and t_3 may occur before or after t_5. I is an infinite term occuring because two of the intermediate states have the same energy.

These two examples serve to illustrate the following points. (*a*) The Pauli principle does not operate in intermediate states of the Feynman graphs. For ex-

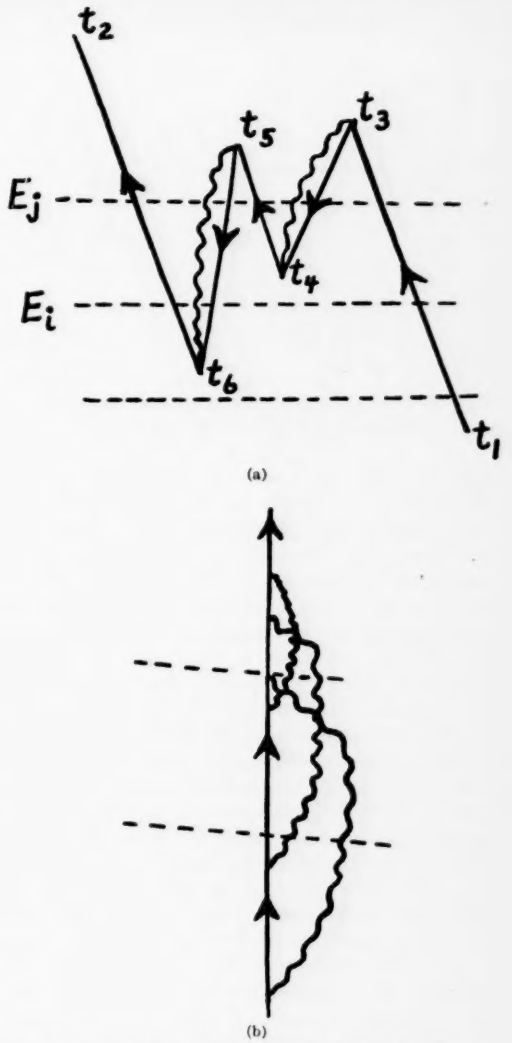

FIG. 2. (a) A graph with two pairs present simultaneously in an intermediate state. (b) A graph with no pair creation occurring but many mesons present in intermediate states.

[4] W. Heitler, *Quantum Theory of Radiation* (Oxford University Press, London, 1944), second edition, p. 87.

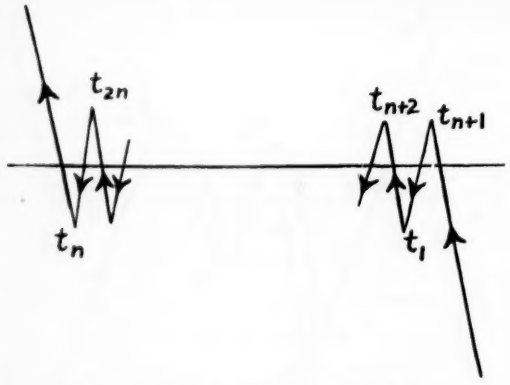

FIG. 3. A process with many pair creations, but all the creations occurring before any annihilation.

ample, in Figs. 1 and 2(a) the crossed lines represent nucleons in the same state—and these exist at the same time in intermediate "Feynman graph" states. This does not, of course, mean that the Pauli principle does not operate in the physical intermediate states: it is the elimination of the vacuum effects which leads to the Feynman graphs and the apparent contradiction to the Pauli principle. (*b*) With each nucleon line directed backward in time in a Feynman graph there is associated a factor (-1) in the corresponding analytic expression. This comes from the definition of K_+, and is a direct result of the operation of the Pauli principle on the elimination of the vacuum. (*c*) Except for the factors (-1) of (*b*), the analytic expression corresponding to the Feynman diagram can be calculated by the ordinary mechanism of time dependent perturbation theory; the pairs shown in the Feynman graph are created and annihilated in the chronological order shown in the Feynman graph. The factors (-1) give rise to a total factor $(-1)^{m/2}$, where m is the total number of pair creations and annihilations. (*d*) Even where we have a succession of creations (annihilations) where the particles created (annihilated) at one vertex are entirely similar to those at the next, the time ordering of the creations (annihilations) gives rise to a multiplying factor. This is the factor 4 in (5), and for the n creations and n annihilations shown in Fig. 3 it would be $(n!)$.[2]

The intermediate coupling method of Tomonaga deals with a stationary state theory. To transform from the time dependent fluctuations we have considered so far, to a stationary theory, we take the following equations, which, it will be seen, are analogous to the Fock equations for no pairs present. (That is to say, from analogy with the Fock equations for no pairs present, we write down the "Fock equations after subtraction of the vacuum" (6) for pairs present. Only these Eqs. (6) are in accord with the Feynman outlook for intermediate states; thus the exclusion principle is neglected—except for the change in sign indicated by (*b*) above. The speculation (6) is then partly justified below by examining the solution of (6) in a perturbation series.)

$$\begin{aligned}
&(E-E^0)c^0=\textstyle\sum_k H_k{}^{0,1}c_k{}^1,\\
&(E-E_k{}^1)c_k{}^1=-H_k{}^{1,0}c^0-\textstyle\sum_i H_{k,i}{}^{1,2}c_i{}^2,\\
&(E-E_i{}^2)c_i{}^2=\textstyle\sum_k H_{i,k}{}^{2,1}c_k{}^1+\sum_l H_{i,l}{}^{2,3}c_l{}^3,\\
&(E-E_l{}^3)c_l{}^3=-\textstyle\sum H_{l,i}{}^{3,2}c_i{}^2-\sum_j H_{l,j}{}^{3,4}c_j{}^4,\\
&\qquad\qquad\cdots
\end{aligned}\tag{6}$$

The c's are defined by these equations. However, they can be thought of in a semi-intuitive manner as follows. The "state" of the system of the nucleon and self-field, after elimination of vacuum effects, is thought of as a sum of spacelike sections of Feynman diagrams. Typical sections are those along each of the dotted lines in Fig. 2. Then c^0 represents the amplitude for the occurence of one nucleon in the "state" [section along the bottom dotted line in Fig. 2(a)]. $c_k{}^1$ represents the amplitude for the occurence of one nucleon and one pair in the "state," k signifying the number of mesons and also the momenta of the particles present in the section. A typical such section is the one along the middle dotted line in Fig. 2(a). And so on for $c_l{}^3$, $c_j{}^4$, etc.

The c's, though having this intuitive interpretation, are defined by (6), but the E^0, $E_k{}^1$, etc., and the H's are now to be defined. $E_p{}^n$ is the free particle energy of the particles in the section corresponding to $c_p{}^n$. $H_{k,i}{}^{1,2}$, for example, is the ordinary matrix element of the interaction Hamiltonian for the transition from the section $c_k{}^1$ to the section $c_i{}^2$. Thus $H^{m,m'}$ is just the ordinary transition matrix element for a pair creation or annihilation with the exception of the following part of its definition. This is that, if a nucleon is created (annihilated) and n similar nucleons of the same spin and momentum have already been created and are present in the section, then $\mathrm{H}^{m,m'}$ is $(n+1)^{\frac{1}{2}}[(n^{\frac{1}{2}})]$ times the ordinary matrix element. Equations (6) are eigenvalue equations for E.

Equation (6) can be solved in a perturbation series and gives, to the second order in the coupling constant,

$$E-E^0=-\sum_n \frac{H_k{}^{01}H_k{}^{10}}{E^0-E_k{}^1};\tag{7}$$

and this, allowing for the difference in notation, is just the same as (4). The fourth order self-energy given by (6) is

$$\sum_{k,i,l}\frac{H_k{}^{01}H_{ki}{}^{12}H_{il}{}^{21}H_l{}^{10}}{(E^0-E_k{}^1)(E^0-E_i{}^2)(E^0-E_l{}^1)}-\sum_k\frac{H_k{}^{01}H_k{}^{10}}{(E^0-E_k{}^1)^2}\sum_l\frac{H_l{}^{01}H_l{}^{10}}{(E^0-E_l{}^1)}.\tag{8}$$

In the case where the first created pair is just the same as the second created pair, each of $H_{ki}{}^{12}$, $H_{il}{}^{21}$ in (8)

contain a factor 2, by definition. This just gives the requisite factor 4 to make this part of the first term of (8) equal to (5). The negative signs occuring on the right-hand side of alternate equations in (6) compensate for the negative signs from each line going backward in time in a Feynman graph.

The second term of (8) indicates the breakdown of a formal correspondence between time dependent and stationary state perturbation theory. The second part of (8) probably corresponds to a Feynman diagram of the form shown in Fig. 4(a) (where $t_3<t_6$), but no formal correspondence can be set up between the last part of (8), and the part of $F(T)$ resulting from Fig. 4(a). The situation is exactly analogous to the relation between time dependent (Feynman) perturbation theory and stationary state perturbation theory in the case where pairs are not allowed. In this case the stationary states can be defined perfectly well as sums of states corresponding to various numbers of mesons in company with one nucleon. These correspond to sections such as those along the dotted lines in Fig. 2(b) and the Fock equations in a nonpair theory [reference 1, Eq. (3.4)] in a similar notation to that used in paragraph (6) are

$$(E-E^0)\gamma^0=\sum \mathfrak{C}_k{}^{01}\gamma_k{}^1,$$
$$(E-E_k{}^1)\gamma_k{}^1=\mathfrak{C}_k{}^{10}\gamma^0+\sum_i \mathfrak{C}_{ki}{}^{12}\gamma_i{}^2,$$
$$\cdot\quad\cdot\quad\cdot$$

$\gamma_i{}^n$ is the amplitude for the presence of n mesons, the i denoting momentum and change variables; the $E_i{}^n$ are the corresponding energies. The $\mathfrak{C}_{k,i}{}^{1,2\cdots}$, etc., are transition matrix elements for meson emission without pair creation or annihilation. The negative signs in (6) arise because of the factors (-1) referred to in (*b*) above.

In the nonpair theory there is a manifest equality between certain terms in the self-energy from the stationary and certain terms in the self-energy from the time-dependent, perturbation theory, but this equality and correspondence breaks down too for graphs like Fig. 4(b).

The cases in which equality holds are now propounded. Consider a self-energy Feynman graph, with initial state 1, energy E_1 and intermediate states 3, 4, $5\cdots$ in chronological order with energies E_3, E_4, $E_5\cdots E_n$. We suppose that none of these intermediate energies is equal to E_1. Then from this Feynman graph, in the Feynman-S-matrix perturbation theory, there arises the following term in the self-energy:

$$\frac{H_{1,3}H_{3,4}H_{4,5}\cdots H_{n-1,n}}{(E_1-E_3)(E_1-E_4)\cdots(E_1-E_n)}\times(\text{factor}).$$

In the nonpair theory a term equal to this can be got from the perturbation solution of the Fock equations. In the pair theory a term equal to this can be got from the perturbation solution of (6). The breakdown of the

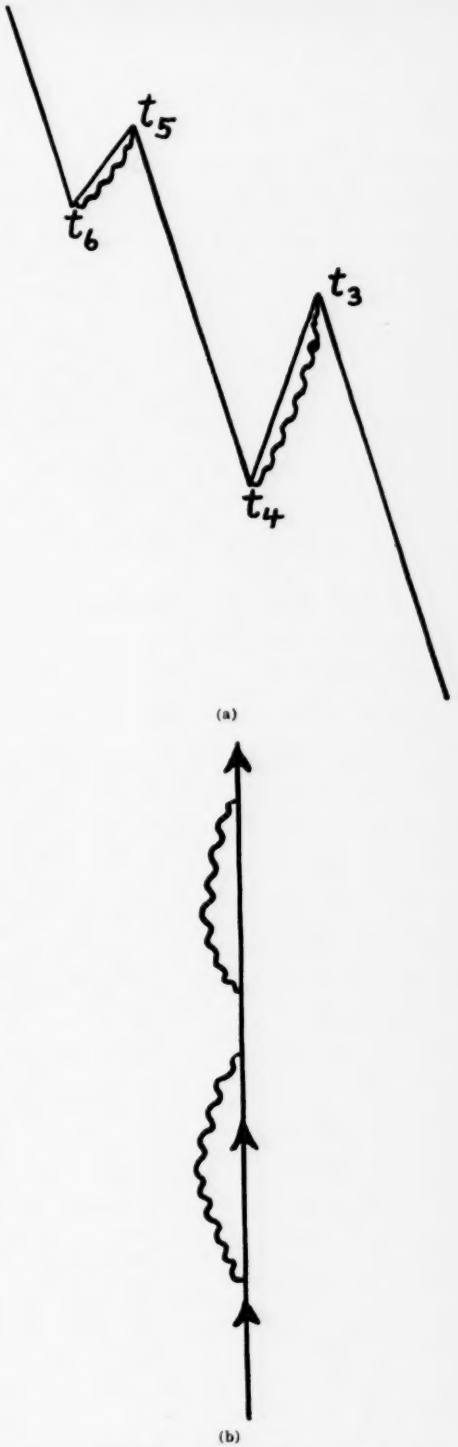

FIG. 4. (a), (b) Graphs with an intermediate state the same as the initial state.

equality and correspondence comes when the energy of one of the intermediate states is equal to E_1. In ensuring that time and stationary perturbation theory bear the same relation to each other in pair and nonpair theory, it is evident that the negative signs on the r.h.s. of (6) exactly correspond to the factors (-1) in the Feynman diagrams from particles going backwards in time. It can be checked, by examining various Feynman graphs in detail that the statistical factors $\sqrt{n}$ defined before in $H_{k,l}^{m,m'}$ on creation or annihilation of nucleons give just the right factors resulting from the time ordering of creations (annihilation) in the Feynman graphs.

To sum up, Eqs. (6) are proposed as equations in a pair theory (after elimination of vacuum effects) corresponding to the Fock equations in a nonpair theory. To demonstrate the plausibility of equations (6) an analogy is set up between (1) the relation of the Feynman results to the results of the perturbation solution of the Fock equations in no pair theory and (2) the relation of the Feynman results to the results of the perturbation solution of (6) in pair theory.

III. THE TOMONAGA APPROXIMATION

Having set up equations for a "stationary state" after elimination of the vacuum in pair theory, we can now proceed to solve them by the intermediate coupling, or Tomonaga, approximation method. The steps of the approximation used in solving (6) could be defined entirely without reference to the semi-intuitive meaning of the c's as sections of Feynman graphs. But, though unnecessary, it is much shorter to write in the language of Feynman graphs, and it makes the meanings and results of the approximations used very perspicuous.

The first approximation is the neglect of recoil. Thus if the original nucleon represented by the line t_1t_2 in Fig. 2(a) has zero momentum, we neglect the reaction of the absorbed meson at t_3 on the nucleon t_4t_3, and thus consider the nucleon t_4t_3 to have effectively zero momentum. Similarly at t_4, t_5, and t_6; thus all the nucleons in a section (along any of the dotted lines) of Fig. 2(a) have effectively zero momentum. The effect of the nonrecoil approximation is that all the nucleons in any section (c_k^n) are taken to have zero momentum if the original nucleon has zero momentum. In general, if a nucleon has momentum $\boldsymbol{p}$ the neglect of the meson momentum means that the nucleon with which it annihilates, or is created, has momentum $-\boldsymbol{p}$. Thus if the incoming nucleon has momentum $\boldsymbol{p}$ the nonrecoil approximation implies that all nucleons in a section have momenta $\boldsymbol{p}$, all antinucleons momenta $-\boldsymbol{p}$.

Now let us suppose that the original nucleon (moving with nonrelativistic velocity) has spin $\frac{1}{2}$. Then it can easily annihilate at t_3 [see Fig. 2(a)] with a nucleon of spin $-\frac{1}{2}$. On the other hand, the matrix element for annihilation at t_3 with a nucleon of spin $\frac{1}{2}$ is small (and on a strict application of the nonrecoil approximation would be zero). So the nucleon t_4t_3 is taken to have spin $-\frac{1}{2}$. But at t_4 the probability for the creation of nucleons with opposite spins is large, while that for the creation of nucleons of the same spin is small. Thus t_4t_5 is taken to have spin $\frac{1}{2}$. Thus if the original nucleon is a proton of spin $\frac{1}{2}$, in general we can say that the protons in any section have spin $\frac{1}{2}$, while the neutrons have spin $-\frac{1}{2}$. Conservation of angular momentum then implies that the emitted and absorbed mesons are in s-states with respect to the nucleons. The approximation of this paragraph (which follows from the neglect of recoil) is strictly comparable with that of Tomonaga for the scalar case, when he assumes that all the mesons are in s-states, and that the original nucleon does not change its spin state.

We now take the original nucleon to be a proton of spin $\frac{1}{2}$. We take all the nucleons to be in the same space (or momentum space) wave function. (As will be seen below, this can be done consistently with the approximation of nonrecoil). The mesons are taken to be all in the same s-state wave function, to be chosen later. This limitation of the number of meson wave functions is the essential feature of the intermediate coupling approximation.

The limitation on the number of admissible wave functions immediately limits the number of c's. More precisely the solution of Eqs. (6) is approximated to by replacing certain sets of c's in (6) by a single c. We can now denote the c's as $c(n, x)$. Here n is the number of pairs in the section for which c is the amplitude and x is the number of negative mesons. Then by charge conservation $x-n$ is the number of positive mesons.

Let $\hbar c\kappa_1$ be the free particle energy of the nucleons, and $\hbar c\mu_1$ be the free particle energy of the mesons. Then the free particle energy of the section n, x is given by $E_x^n=\hbar c[(2n+1)\kappa_1+(2x-n)\mu_1]$. Let the matrix element for the creation or annihilation of a pair, with the creation or annihilation of a positive or negative meson, be T. Then Eqs. (6) reduce to

$$(E-\hbar c\kappa_1)c(0,0)=Tc(1,1),$$

$$[E-\hbar c(3\kappa_1+\mu_1)]c(1,1)=Tc(0,0)-2Tc(2,2)-Tc(0,1),$$

$$\cdots$$

$$\begin{aligned}[E-\hbar c\{(2n+1)\kappa_1+(2x-n)\mu_1\}]c(n,x) \qquad (9)\\ =[(n+1)(x+1)^{\frac{1}{2}}Tc(n+1,x+1)\\ +(n+1)(x-n)^{\frac{1}{2}}Tc(n+1,x)+nx^{\frac{1}{2}}Tc(n-1,x-1)\\ +n(x-n+1)^{\frac{1}{2}}Tc(n-1,x)](-1)^n.\end{aligned}$$

With suitable choice of phase of the wave functions, T is a real quantity. The factors $(x+1)^{\frac{1}{2}}$, $(x-n)^{\frac{1}{2}}$, $x^{\frac{1}{2}}$, $(x-n+1)^{\frac{1}{2}}$ on the r.h.s. are the usual meson statistical factors due to all the mesons being in the same state. The factors n, $n+1$ on the r.h.s. are statistical factors for the nucleons, due to their being in the same state, and coming from the definition of the $H^{m,m'}$.

Multiplying the equation containing $c(n, x)$ on the l.h.s. by $(-1)^n c(n, x)$ and adding all the equations, we

get the following expression for the energy analogous to that obtained in nonpair theory:

$$E(\textstyle\sum_{n,x}(-1)^n c^2(n,x)) = \sum_{n,x}[(-1)^n hc((2n+1)\kappa_1+(2x-n)\mu_1)c^2(n,x) + 2Tc(n,x)c(n+1,x)(n+1)(x-n)^{\frac{1}{2}} + 2Tc(n,x)c(n+1,x+1)(n+1)(x+1)^{\frac{1}{2}}]. \quad (10)$$

Equations (9) must be solved numerically, and in order to do this we need values for κ_1, μ_1 and T. We take the momentum space wave function of the "original" proton to be

$$N_1\begin{pmatrix} 1 \\ 0 \\ \dfrac{p_z}{\kappa+(\kappa^2+p^2)^{\frac{1}{2}}} \\ \dfrac{p_x+ip_y}{\kappa+(\kappa^2+p^2)^{\frac{1}{2}}} \end{pmatrix}\left[1+\frac{p^2}{[\kappa+(\kappa^2+p^2)^{\frac{1}{2}}]^2}\right]^{-1} \quad (11)$$

for $|p|<\kappa$ and zero for $|p|>\kappa$. Then the nonrecoil approximation means that all the protons are in this state and all the neutrons in the state given by

$$N_1\begin{pmatrix} \dfrac{-p_z}{\kappa+(\kappa^2+p^2)^{\frac{1}{2}}} \\ -\dfrac{p_x+ip_y}{\kappa+(\kappa^2+p^2)^{\frac{1}{2}}} \\ 1 \\ 0 \end{pmatrix}\left[1+\frac{p^2}{[\kappa+(\kappa^2+p^2)^{\frac{1}{2}}]^2}\right]^{-1}$$

for $|p|<\kappa$ and zero for $|p|>\kappa$.

This is a "wave packet" of extension of order $1/\kappa$ in configuration space. The meson wave function is taken to be that given by first-order perturbation theory[5] $N_2(\mu^2+p^2)^{-1}$. Here the N's are normalization factors. With these assumptions—and always a cutoff of divergent momentum integrations at κ—

$$\kappa_1=(5/4)\kappa, \quad \mu_1=\tfrac{2}{3}\kappa, \quad T=hc\kappa l/(2\pi)^{\frac{1}{2}}, \quad l=f/(4\pi hc)^{\frac{1}{2}}.$$

To simplify the solution of (9) we assume there are no positive mesons present. That is $x=n$. Since positive mesons only contribute to fourth and higher orders in the coupling constant, there is probably not too much error for not too large a coupling constant. Putting $c(n,n)=c_n$ the equations reduce to

$$[E-hc(n(2\kappa_1+\mu_1)+\kappa_1)]c_n(-1)^n = T[(n+1)^{\frac{1}{2}}c_{n+1}+n^{\frac{1}{2}}c_{n-1}]. \quad (12)$$

For $l^2=10$ this reduces to

$$(n+1)^{\frac{1}{2}}c_{n+1}+(-1)^n(2n-W)c_n+n^{\frac{1}{2}}c_{n-1}=0, \quad (13)$$

where

$$W=(E-hc\kappa_1)/\tfrac{3}{2}hc\kappa.$$

This can easily be solved numerically to give

$$W=0.342.$$

Also, if $c_0=1$,

$$c_1=0.342, \quad c_2=-(0.153), \quad c_3=-(0.078), \quad c_4=(0.044), \quad c_5=(0.026), \quad c_6=-(0.016), \quad \cdots.$$

It should be noted that in the course of this section terms corresponding to Feynman graphs containing closed loops have been tacitly dropped.

IV. NUCLEON MAGNETIC MOMENT

Besides the relation of the mass of the bare nucleon to that of the real nucleon (given by the self-energy) the solution of the self-field should also elucidate the proton and neutron magnetic moments. To do this in the picture of the self-field given here, we consider a proton of spin $\frac{1}{2}$ in the direction of a small uniform magnetic field, and find the increase in the energy of the proton due to the presence of the magnetic field. As the mesons in our picture of the self-field are in s-states, the only contribution to the magnetic moment of the nucleon should come from the Dirac magnetic moments of the protons.

The magnetic field M will modify Eqs. (9). As it is a uniform magnetic field we should expect that the only modification is that the free particle energy corresponding to $c(n,x)$ (that is with $n+1$ protons of spin $\frac{1}{2}$ present) would be changed from

$$hc[(2n+1)\kappa_1+(2x-n)\mu_1]$$

to

$$hc[(2n+1)\kappa_1+(2x-n)\mu_1]+(n+1)\gamma M.$$

γ is the magnetic moment of the bare particle wave packet and is thus approximately one nuclear magneton. Thus Eqs. (9) are changed to

$$[\bar{E}-hc\{(2n+1)\kappa_1+(2x-n)\mu_1\}-(n+1)\gamma M]\bar{c}(n,x) = [(n+1)(x+1)^{\frac{1}{2}}T\bar{c}(n+1,x+1) + (n+1)(x-n)^{\frac{1}{2}}T\bar{c}(n+1,x)+nx^{\frac{1}{2}}T\bar{c}(n-1,x-1) + n(x-n+1)^{\frac{1}{2}}T\bar{c}(n-1,x)](-1)^n. \quad (14)$$

By treating both the magnetic field and the nucleon-meson interaction as perturbations, it can be shown by solving these equations, or rather Eqs. (6) correspondingly modified, for $\bar{E}$ that the perturbation expansion bears the same relation as before to the Feynman S-matrix series.

To find the magnetic moment from (14), we find the increase in energy due to the presence of M. For this let E and $c(n,x)$ be the solutions of (9). Put

$$E'+E\approx\bar{E}, \quad c'(n,x)+c(n,x)\approx\bar{c}(n,x), \quad (15)$$

[5] K. M. Watson and E. W. Hart, Phys. Rev. **79**, 918 (1950).

where $\approx$ denotes that equality is to first order in M only, E' and c' being of first order in M. The expansion of (14) into two equations, one of zero and one of first order in M, is

$$[E-hc\{(2n+1)\kappa_1+(2x-n)\mu_1\}]c(n,x)$$
$$=[(n+1)(x+1)^{\frac{1}{2}}Tc(n+1,x+1)$$
$$+(n+1)(x-n)^{\frac{1}{2}}Tc(n+1,x)+nx^{\frac{1}{2}}Tc(n-1,x-1)$$
$$+n(x-n+1)^{\frac{1}{2}}Tc(n-1,x)](-1)^n; \quad (16)$$

$$[E-hc\{(2n+1)\kappa_1+(2x-n)\mu_1\}]c'(n,x)$$
$$+[E'-(n+1)\gamma M]c(n,x)$$
$$=[(n+1)(x+1)^{\frac{1}{2}}Tc'(n+1,x+1)$$
$$+(n+1)(x-n)^{\frac{1}{2}}Tc'(n+1,x)$$
$$+nx^{\frac{1}{2}}Tc'(n-1,x-1)+n(x-n+1)^{\frac{1}{2}}$$
$$\times Tc'(n-1,x)](-1)^n. \quad (17)$$

Equation (16) is identically satisfied. Multiply (17) by $(-1)^n c(n,x)$ and add all equations of the form (17) to get

$$\sum_{n,x}[E'-(n+1)\gamma M](-1)^n c^2(n,x)$$
$$+\sum_{n,x}c'(n,x)\{[E-hc\{(2n+1)\kappa_1+(2x-n)\mu_1\}]$$
$$\times c(n,x)(-1)^n-[nx^{\frac{1}{2}}Tc(n-1,x-1)$$
$$+n(x-n+1)^{\frac{1}{2}}Tc(n-1,x)+(n+1)(x+1)^{\frac{1}{2}}$$
$$\times Tc(n+1,x+1)+(n+1)(x-n)^{\frac{1}{2}}Tc(n+1,x)]=0.$$

The coefficient of $c'(n,x)$ is zero by definition of E and the $c(n,x)$. Thus

$$E'=\gamma M\sum_{n,x}(-1)^n(n+1)c^2(n,x)/\sum_{n,x}(-1)^n c^2(n,x). \quad (18)$$

This is the energy due to the presence of the magnetic field M and is what would be expected intuitively, $c^2(n,x)$ being the amplitude squared for $n+1$ protons and x positive mesons, and the negative sign occuring when there are an odd number of particles going backward in time. From (18) the magnetic moment is

$$\mu_P=\gamma\sum_{n,x}(-1)^n(n+1)c^2(n,x)/\sum_{n,x}(-1)^n c^2(n,x). \quad (19)$$

Consider now a neutron of spin $\frac{1}{2}$. The self-field will include charged nucleons and, if the original neutron is taken to be going forward in time, these charged nucleons are going backward in time (though actually like, as Feynman shows, a negative proton of spin $-\frac{1}{2}$ going forward in time). But the fact that they are going backward in time introduces an extra negative sign when one of these charged nucleons interacts with the electromagnetic field. Thus the addition to the energy must be taken as $-n\gamma M$ instead of $+(n+1)\gamma M$. As before, this result can be checked by a perturbation expansion. Thus the magnetic moment is

$$\mu_N=\gamma\frac{\sum_{n,x}(-1)^{n-1}nc^2(n,x)}{\sum_{n,x}(-1)^n c^2(n,x)}. \quad (20)$$

Therefore,

$$\mu_P+\mu_N=\gamma \quad (>\gamma_B).$$

Thus this picture gives the sum of the proton and neutron moments as the magnetic moment belonging to the wave packet of the "original" bare particle. From the sign of the self-energy (see the expression for W) in the last section it follows that this is greater than the nuclear magneton of a corresponding real particle, γ_B, say.

For $f^2/4\pi hc=10$, the result of Sec. III on the self-energy gives

$$\gamma=\tfrac{3}{2}\gamma_B,$$

and

$$\mu_P=\frac{3}{2}\gamma_B\frac{(c_0^2-2c_1^2+3c_2^2-\cdots)}{(c_0^2-c_1^2+c_2^2-\cdots)}=\frac{4}{3}\gamma_B,$$

$$\mu_N=\tfrac{1}{6}\gamma_B.$$

Apart from the neglect of positive mesons and of meson emission without pair creation no reliance can be placed on the quantitative aspects of this result for μ_P due to the neglect of recoil and the uncertainty in the high momentum cutoff. However, it is interesting that in this "pairs only" picture the sum of the proton and neutron moments is more than a Bohr nucleon magneton, however strong the coupling. (In a strong coupling theory with no pairs the sum of the proton and neutron moments tends to be zero.[6] This result, however, might perhaps be modified if recoil, with its accompanying currents were taken properly into account.

V. DISCUSSION

The crucial point of this paper is the speculation of Sec. II on the equation for the stationary state, with pairs after the elimination of the vacuum. Matthews and Salam[2] have also made a suggestion for the elimination of the vacuum in stationary state theory. This, however, is made in the context of one-pair theory, and their model also differs from the present one in allowing (unlimited) meson creation and annihilation with no pairs present. The vacuum subtraction prescription of the present paper can easily be amended to apply to the model of Matthews and Salam and, in that model, is equivalent to their prescription. (This is apart from the fact that the intermediate coupling approximation used by the latter authors involves all the mesons being in p-states; while here those occuring in pair creation or annihilation are in s-states.)

Given the speculation of Sec. II, the approximations of nonrecoil and high frequency cutoff are equivalent to those made by Tomonaga. Thus the theory suffers from the same kind of quantitative fault that the pseudoscalar theory without pair creation does. This unreliability arises largely from the uncertainty about the

[6] W. Pauli and S. M. Dancoff, Phys. Rev. **62**, 85 (1942).

high frequency cutoff, for upon the accuracy of this depends the accuracy of a nonrecoil or first-order recoil approximation. Both pair and nonpair theory miss out one important type of process (and, even in the pair theory, no attempt is made to deal with closed loop Feynman graphs).

As the method suffers from these faults, the comparatively unrefined calculations made in this paper were made to see if the results suggested any qualitative rather than quantitative ideas. One such idea perhaps suggested is that the result of the equality of proton and neutron magnetic moments in a strong coupling nonpair nonrecoil theory[6] may be adequately compensated when pairs are taken into account. For the "pairs only" theory presented here seems to err in the opposite direction.

The author would like to acknowledge the award of a Nuffield Foundation Fellowship at Glasgow University, during the tenure of which this work was performed.

PHYSICAL REVIEW VOLUME 89, NUMBER 5 MARCH 1, 1953

First-Order Meson Wave Equations

H. S. GREEN
University of Adelaide, Adelaide, Australia
(Received August 26, 1952)

A method is developed for the simple representation of the symbols introduced in the generalization of Dirac's first-order wave equation for the electron. This enables one to obtain an explicit general solution of the generalized equations. The sign of the energy is discussed in order to determine which of the various possible representations are physically admissible.

1. INTRODUCTION

THE success of Dirac's theory of the electron has stimulated a widespread investigation of first-order differential wave equations of a type differing from the equation for the electron only in the properties of the matrices involved. The best known of these equations is the equation of Kemmer[1] for scalar and vector mesons of given mass. Some of the more recent investigations are due to Pétiau,[2] Bhabha,[3] and the author,[4] and contain references to earlier work. So far, little application has been found for this work, since no particles in nature could be said definitely to correspond to those described by the equations. Recently discovered mesons of various masses may, however, supply the missing data. The fact that the ζ-meson has a mass almost exactly twice that of the π-meson[5] is in significant correspondence with the prediction of one of the simplest generalizations of Kemmer's theory for particles with integral spin. It has seemed worth while to the author to make a further investigation of this theory, which is given in the following paper.

One of the difficulties of the theories previously advanced has been the complicated nature of the algebra and representation of the matrices involved. The irreducible representations of these matrices can be obtained by simple group-theoretical considerations,[6] but not in a very explicit form; so the explicit solution of the general particle wave equation has not yet been given. A practical method of solution is, however, explained in the following: it is hoped that this method will facilitate further investigations. The method is applicable, in its simplest form, only to the theory of particles with integral spin; though a generalization to particles with half-odd integral spin is possible.

The conventions of general relativity theory will be observed, with a Galilean metric tensor g_{kl} whose diagonal components are $(-1, -1, -1, 1)$.

2. THEORY FOR SPIN 0 OR 1

For purposes of illustration, the method will first be applied to Kemmer's equation,

$$(i\beta^k\partial_k-\mu)\Psi=0, \tag{1}$$

for the meson of spin 0 or 1. It is well known[7] that the β_k may be represented in terms of two commuting sets of Dirac matrices:

$$\gamma_1{}^k\gamma_1{}^l+\gamma_1{}^l\gamma_1{}^k=2g^{kl}, \quad \gamma_2{}^k\gamma_2{}^l+\gamma_2{}^l\gamma_1{}^k=2g^{kl}, \quad \gamma_1{}^k\gamma_2{}^l=\gamma_2{}^l\gamma_2{}^k. \tag{2}$$

Instead of writing $\beta^k=\frac{1}{2}(\gamma_1{}^k+\gamma_2{}^k)$ in the usual way, however, it is convenient to set

$$\beta^k=\tfrac{1}{2}(\gamma_1{}^k-\tilde{\gamma}_2{}^k), \tag{3}$$

where $\tilde{\gamma}_2{}^k$ is the transpose of the matrix $\gamma_2{}^k$. Since the

[1] N. Kemmer, Proc. Roy. Soc. (London) **A173**, 91 (1939); Proc. Cambridge Phil. Soc. **39**, 189 (1943).
[2] G. Pétiau, J. phys. et radium **10**, 215 (1949).
[3] H. J. Bhabha, Proc. Indian Acad. Sci. **A21**, 241 (1945); Revs. Modern Phys. **21**, 451 (1949).
[4] H. S. Green, Proc. Cambridge Phil. Soc. **45**, 263 (1949).
[5] Danysz, Lock, and Yekutieli, Nature, **169**, 364 (1952); R. B. Leighton and S. D. Wanlass, Phys. Rev. **86**, 426 (1952).
[6] B. S. Madhava Rao, Proc. Indian Acad. Sci. **A26**, 221 (1947).
[7] See W. Pauli, Revs. Modern Phys. **13**, 203 (1941).

algebra of the matrices $-\tilde{\gamma}_2{}^k$ is isomorphic with that of the $\gamma_2{}^k$, this departure is obviously only of formal significance. But if $\Psi_1{}^\alpha$ and $\Psi_2{}^\alpha$ ($\alpha=1, 2, 3, 4$) are two sets of independent 4-spinors, on which $\gamma_1{}^k$ and $\gamma_2{}^k$ may operate, respectively, the wave vector Ψ in (1) can be expressed in the form

$$\Psi=\sum_{\alpha,\beta} c_{\alpha\beta}\Psi_1{}^\alpha\bar{\Psi}_2{}^\beta, \tag{4}$$

where the $c_{\alpha\beta}$ are numbers, and $\bar{\Psi}_2{}^\beta$ is conjugate to $\Psi_2{}^\beta$; and since $\tilde{\gamma}_2{}^k\Psi=\Psi\gamma_2{}^k$, one will have

$$\beta^k\Psi=\tfrac{1}{2}(\gamma_1{}^k\Psi-\Psi\gamma_2{}^k). \tag{5}$$

Since $\gamma_1{}^k$ and $\gamma_2{}^k$ will always appear only before and after their operands, respectively, no confusion can arise through dropping the suffixes 1 and 2, and writing simply[8]

$$\beta^k\Psi=\tfrac{1}{2}(\gamma^k\Psi-\Psi\gamma^k)=\tfrac{1}{2}[\gamma^k, \Psi]. \tag{6}$$

The operand Ψ may now be regarded as an ordinary Dirac matrix.

Thus, by a simple change in representation, Kemmer's is expressed in a form which involves only one set of Dirac matrices. The appropriate Lagrangian density is

$$L=-\tfrac{1}{2}\,\mathrm{qs.}\{\Psi(i\gamma^k\partial_k-\mu)\Psi\}, \tag{7}$$

where qs. is the quarter spur operator; the normal variational procedure applied to L yields the field equation:

$$\tfrac{1}{2}i\partial_k[\gamma^k, \Psi]-\mu\Psi=0, \tag{8}$$

as required, and the canonical energy-momentum tensor density:

$$T_l{}^k=-\tfrac{1}{2}\,\mathrm{qs.}(\Psi_i\gamma^k\partial_l\Psi)-L\delta_l{}^k. \tag{9}$$

There are some advantages to be derived from the introduction of[9]

$$\gamma_5=-\gamma^5=(1/24)\epsilon_{klmn}\gamma^k\gamma^l\gamma^m\gamma^n, \tag{10}$$

which is a scalar, identical with the pseudo-scalar $\gamma^1\gamma^2\gamma^3\gamma^4$ only so long as no reflections of the coordinate system are contemplated. Then Ψ, like every other Dirac matrix, may be expressed in the form

$$\Psi=a+a_k\gamma^k+\tfrac{1}{4}ia_{kl}[\gamma^k, \gamma^l], \tag{11}$$

where the repeated affixes are now summed over the values 1 to 5 instead of 1 to 4. The above expression will be regarded as real if $\gamma_4\Psi$ is Hermitean, i.e., if a, a_k, and $a_{kl}=-a_{lk}$ are all real numbers.

The affixes k in (8) may be regarded as running from 1 to 5, so long as it is admitted that Ψ does not depend on x_5. It follows from (11) that

$$\tfrac{1}{2}[\gamma^j, \Psi]=\tfrac{1}{2}a_k[\gamma^j, \gamma^k]+ig^{jk}a_{kl}\gamma^l. \tag{12}$$

Hence (8) reduces to the set of equations:

$$\begin{aligned} -\mu a&=0,\\ (\partial_j a_k-\partial_k a_j)-\mu a_{jk}&=0,\\ -\partial^k a_{kl}-\mu a_l&=0. \end{aligned} \tag{13}$$

The last two of these yield Proca's equations for the vector meson field, and also

$$\partial^k\partial_k a_5+\mu^2 a_5=0, \tag{14}$$

which is the wave equation for the scalar meson. The reduction of the 16-dimensional representation to a 10+5+1-dimensional representation is obvious.

The Lagrangian density L vanishes by virtue of the field equations, as one sees most simply on multiplying (8) by Ψ and taking the spur. On substitution from (11), the energy density therefore reduces to

$$\begin{aligned} T_4{}^4&=-\tfrac{1}{2}i\,\mathrm{qs.}(\Psi\gamma^4\partial_4\Psi)\\ &=\tfrac{1}{2}(a_k\partial_4 a^{4k}+a^{k4}\partial_4 a_k). \end{aligned} \tag{15}$$

This differs from $a^{k4}\partial_4 a_k$ by the time derivative of $\frac{1}{2}a^{k4}a_k$, whose average value must vanish; and since $a_5=-a^5$, the energy of both the scalar and the vector field is positive definite.

3. THEORY FOR TWO REST-MASSES

The simplest generalization of the theory just described is obtained on replacing the Dirac matrices by Kemmer matrices in the Lagrangian density (7), and regarding Ψ as an element of the ring generated by the Kemmer matrices β^k. Then Ψ is of the form

$$\begin{aligned} \Psi=b+b_k\beta^k+\tfrac{1}{4}ib_{kl}[\beta^k, \beta^l]+B_{kl}\beta^k\beta^l\\ +iB_{kl,\,m}[\beta^m, \beta^k\beta^l]-B_{kl,\,mn}[\beta^m, \beta^k][\beta^n, \beta^l], \end{aligned} \tag{16}$$

where B_{kl}, $B_{kl,\,m}$, and $B_{kl,\,mn}$ may be considered to be symmetric in the affixes k and l, and $B_{kl,\,mn}$ symmetric in the affixes m and n also. Now, since

$$[\beta^k, [\beta^l, \beta^m]]=g^{kl}\beta^m-g^{km}\beta^l, \tag{17}$$

one has

$$\begin{aligned} \partial_j[\beta^j, \Psi]=\partial_k b_l[\beta^k, \beta^l]+\tfrac{1}{2}i\partial^l b_{lk}\beta^k+\partial_m B_{kl}[\beta^m, \beta^k\beta^l]\\ +i(2\partial^m B_{kl,\,m}-\partial^m B_{ml,\,k}-\partial^m B_{km,\,l})\beta^k\beta^l\\ +i(\partial_n B_{kl,\,m}+\partial_m B_{kl,\,n})[\beta^m, \beta^k][\beta^n, \beta^l]\\ +(\partial^n B_{kn,\,ml}-\partial^n B_{kl,\,mn})[\beta^m, \beta^k\beta^l]. \end{aligned} \tag{18}$$

It is convenient to impose the auxiliary condition,

$$\partial^m B_{ml,\,k}=0, \tag{19}$$

which is analogous to the Lorentz condition on a vector potential. Then the field equations are

$$\partial_k b_l-\partial_l b_k=\mu b_{kl}, \quad \partial^l b_{kl}=4\mu b_k, \tag{20}$$

and

$$\begin{aligned} -\partial^m B_{kl,\,m}&=\mu B_{kl},\\ \tfrac{1}{2}\partial_m B_{kl}-\tfrac{1}{2}(\partial^n B_{kl,\,mn}-\partial^n B_{kn,\,ml})&=\mu B_{kl,\,m},\\ \tfrac{1}{2}(\partial_n B_{kl,\,m}+\partial_m B_{kl,\,n})&=\mu B_{kl,\,mn}. \end{aligned} \tag{21}$$

[8] See L. de Broglie, *Théorie générale des particules à spin* (Gauthier Villars, Paris, 1943).

[9] This definition secures the invariance of the theory under improper, as well as proper, Lorentz transformations.

Equations (20) are similar in form to those of (13), except that they characterize particles of mass $2\mu\hbar$ instead of $\mu\hbar$. Equations (21), on the other hand, imply

$$\partial^m\partial_m B_{kl}+\mu^2 B_{kl}=0,$$
$$\partial^m\partial_m B_{kl,n}+4\mu^2 B_{kl,n}=3\mu\partial_n B_{kl}, \quad (22)$$

so that if

$$B'_{kl,n}=B_{kl,n}+\mu^{-1}\partial_n B_{kl} \quad (23)$$

one has

$$\partial^m\partial_m B'_{kl,n}+4\mu^2 B'_{kl,n}=0, \quad (\partial^n B'_{kl,n}=0). \quad (24)$$

By giving k and l the value 5, one has, therefore, a scalar field for particles of mass $\mu\hbar$ and a vector field for particles of mass $2\mu\hbar$; by allowing only one of them to assume the value 5, one has a vector field for particles of mass $\mu\hbar$. There are also other tensor fields for both mass values.

The wave vector Ψ is considered as real if $(2\beta_4^2-1)\Psi$ is Hermitean. This condition is satisfied if all the b's and B's are real.

The energy density is

$$T_4{}^4=-\tfrac{1}{2}i\,\mathrm{spur}(\Psi\beta^4\partial_4\Psi), \quad (25)$$

apart from a normalizing factor. The evaluation of the spur is rather tedious, however, and is most easily effected indirectly by writing down the Lagrangian density corresponding to the field equations (21), namely

$$L=\tfrac{1}{2}\{B^{kl}\partial^m B_{kl,m}-B^{kl,mn}\partial_n B_{kl,m}$$
$$-B^{kl,m}(\partial_m B_{kl}-\partial^n B_{kl,mn})$$
$$+\mu(B^{kl}B_{kl}+2B^{kl,m}B_{kl,m}+B^{kl,mn}B_{kl,mn})\}. \quad (26)$$

(The term $\partial^n B_{kn,ml}$ in the second of the equations (21) is not essential: it vanishes, on account of (19) and the last of the field equations. The terms coming from the b's are omitted, since they are amenable to the same treatment as those arising from the a's of the previous section.) The energy density therefore differs from

$$-(B^{kl,m4}\partial_4 B_{kl,m}+B^{kl,4}\partial_4 B_{kl}) \quad (27)$$

by a perfect time derivative, whose average value must vanish. This, again, differs by a perfect divergence from

$$-(\tfrac{1}{2}\mu^{-1}\partial_4 B'^{kl,m}\partial_4 B'_{kl,m}+2\mu^{-1}\partial_4 B^{kl}\partial_4 B_{kl}). \quad (28)$$

Since $\partial^k B_{kl}=0$ and $\partial^k B'_{kl,m}=\partial^k B'_{ml,k}=0$, the energy of the fields represented by $B'_{kl,m}$ is positive definite, but that of the fields represented by B_{kl} is negative definite.

One way out of this difficulty would be to abandon the restriction which makes Ψ, and hence B_{kl}, real. Another would be to impose the auxiliary condition $B_{kl}=0$, or some condition which allows the appearance of particles of negative energy only in "virtual" intermediate states. However, no particles in the lower mass state could then be observed.

4. GENERALIZATIONS OF THE THEORY

The only property of the Kemmer matrices which was required for the derivation of Eqs. (21) was that the commutation relation,

$$[\sigma^i,[\sigma_k,\sigma_l]]=\delta_k{}^i\sigma_l-\delta_l{}^i\sigma_k, \quad (29)$$

is satisfied by $\sigma^i=\beta^i$. It is well known, however, that this commutation relation is satisfied also by

$$2\sigma^i=\gamma_1{}^i+\gamma_2{}^i+\gamma_3{}^i+\cdots+\gamma_n{}^i, \quad (30)$$

where the $\gamma_1{}^i$, $\gamma_2{}^i$, etc. are mutually commuting sets of Dirac matrices, whose number (n) is arbitrary. The equations so far considered are particular instances of the general equation

$$in^{-1}\partial_j[\sigma^j,\Psi]-\mu\Psi=0. \quad (31)$$

Particular representations of Ψ may be obtained as a linear combination of the elements

$$\sum\mathrm{perm}\,\sigma^i\sigma^k\cdots\sigma^s \quad (32)$$

(where $\sum$perm represents the sum of all permutations of the affixes) and the other independent elements obtained by forming commutators of (32) with the σ^j. Since (31) may be written

$$i(\sigma^j-\bar{\sigma}^j)\partial_j\Psi-n\mu\Psi=0, \quad (33)$$

it is obvious from earlier work (e.g., reference 4) that possible mass values represented are $n\mu/n_1$, where $n_1=1, 2, \cdots n$. By restricting attention to the representation

$$\Psi=f\sigma_5{}^n+if_k[\sigma^k,\sigma_5{}^n]+\cdots, \quad (34)$$

one can examine the structure of the field equations,

$$-\partial^k f_k=\mu f, \quad n^{-1}(\partial_j f-\partial^k f_{jk})=\mu f_j, \quad \text{etc.}, \quad (35)$$

and convince oneself that the sign of the energy of the fields described alternates with decreasing mass values. Thus the admixture of different spin values does not, in this instance, change essentially, the features noted by Pais and Uhlenbeck[10] in connection with an admixture of fields with the same spin. Also, about one-half of the possible masses have to be rejected as inadmissible. In the simplest theory with two admissible mass values, the larger is three times the smaller. In the next generalization $(n=4)$, there are again two masses, one of which is either twice or three times the other. For higher values of n, fractional mass ratios appear.

The question arises whether the theory can be adapted to half-odd-integral spins. This is indeed possible: for example, the Dirac equation for the electron can be written entirely in terms of one set of Pauli spin matrices, thus:

$$i(\partial_4\Psi\sigma_1-\boldsymbol{\sigma}\cdot\boldsymbol{\partial}\Psi\sigma_2)=\mu\Psi.$$

Here Ψ is itself regarded as a Pauli matrix. However, one loses the four-dimensional symmetry which is apparent in the theories for particles of integral spin.

[10] A. Pais and G. E. Uhlenbeck, Phys. Rev. **79**, 145 (1950).

Eleven-Mev Thick Target Bremsstrahlung

J. W. Motz, William Miller, and H. O. Wyckoff
National Bureau of Standards, Washington, D. C.
(Received September 29, 1952)

The intensity distribution of the photons in the forward direction from the 60-mil tungsten wire target of the U. S. Naval Ordnance Laboratory 11-Mev betatron was determined in an energy range of 0.3 to 12 Mev from measurements made with a magnetic Compton spectrometer. The experimental results showed good agreement with the Bethe-Heitler bremsstrahlung theory after corrections were made for target thickness effects and the absorption produced by materials in the path of the photon beam.

The photon energy flux density for the measured spectrum was converted to an equivalent roentgen rate value, which agreed within 10 percent with the value obtained from measurements made with a Victoreen thimble chamber.

I. INTRODUCTION

RECENT measurements[1] of the bremsstrahlung from 300-Mev electrons in a thin target have shown good agreement with the predictions of the Bethe-Heitler theory.[2] However, for measurements[3] involving electron energies below 50 Mev, an accurate comparison of the experimental results with theory is difficult to make, because the electron scattering and energy loss produced by the target cannot be neglected in the theory.

The present investigation is concerned with the bremsstrahlung from the 60-mil tungsten wire target of the U. S. Naval Ordnance Laboratory 11-Mev betatron. The energy distribution of the photons in the forward direction from the target was determined from measurements made with a magnetic Compton spectrometer.[4] The results of these spectrometer measurements were compared with the Bethe-Heitler theory after a theoretical estimate was made of the distortion produced in the shape of the photon spectrum by electron energy loss in the target and by photon absorption in the target and in the surrounding materials.

Other methods[1,3] by which the bremsstrahlung from 11-Mev electrons can be experimentally determined, depend on processes associated with photon-nucleon interactions, such as pair production and nuclear photodisintegration, and are limited to photon energies above approximately 4 Mev. The present method involves the Compton process primarily and covers a range of photon energies from 0.3 to 12 Mev. In these measurements, the spectrometer determines the momentum distribution of the Compton electrons ejected from a thin beryllium foil into a small prescribed solid angle.[5] The conversion to photon intensities is based on the Klein-Nishina differential cross section which, in comparison with the theoretical cross sections for the processes mentioned above, can be considered to be well established.

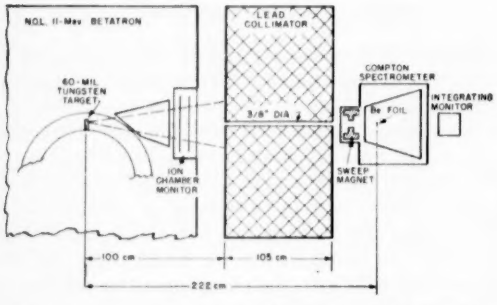

FIG. 1. Schematic diagram of the experimental arrangement. The photon beam in the forward direction from the 60-mil tungsten wire target passes through 1.43 cm glass, 1.59 cm Bakelite, 0.48 cm aluminum, 0.32 cm tin, and 3 cm G.E. 10-C transformer oil, before reaching the $\frac{3}{8}$ inch diameter collimator placed in front of the spectrometer.

II. METHOD AND EXPERIMENTAL RESULTS

The experimental arrangement for these measurements is shown in Fig. 1. The photon beam passed through various materials in the betatron as described in Fig. 1. On emergence from the window of the betatron monitor, the beam had a spread such that the total angle of the half-intensity cone was approximately 14 degrees. Only the photons in the forward direction passed through the $\frac{3}{8}$-in. diameter lead collimator and impinged on a Be foil situated between the pole faces of an electromagnet. A sweep magnet removed stray electrons at the entrance of the spectrometer vacuum chamber.

Electrons were ejected from the Be foil with a certain energy and angular distribution. The spectrometer accepted only those electrons confined to a small angle in the direction of the incident photon beam so that the variation of the Compton electron energy with angle could be neglected.

[1] Powell, Hartsough, and Hill, Phys. Rev. **81**, 213 (1951); J. W. DeWire and L. A. Beach, Phys. Rev. **83**, 476 (1951).
[2] H. A. Bethe and W. Heitler, Proc. Roy. Soc. (London) **146**, 83 (1934).
[3] Bosley, Craggs, Nash, and Payne, Nature **161**, 1022 (1948); H. W. Koch and R. E. Carter, Phys. Rev. **77**, 165 (1950); K. Phillips, Proc. Phys. Soc. (London) **65, A385**, 57 (1952).
[4] Motz, Miller, and Wyckoff, Phys. Rev. **86**, 584 (1952). A detailed description of this spectrometer has been submitted for publication in *The Review of Scientific Instruments*.
[5] This method has been used for the analysis of gamma rays from radioactive sources by G. D. Latyschev *et al.*, J. Phys. (U.S.S.R.) **3**, 251 (1940).

The momentum distribution of the electrons accepted by the spectrometer was found by a magnetic analysis. Measurements were made of the counting rate of the spectrometer detector as a function of the magnetic field in the pole face gap. For a given magnetic field, the contribution of pair production electrons was determined by reversing the field and measuring the positron counting rate on the assumption that the cross section is symmetrical with respect to positron and electron.[2] During the measurments, the variation of the photon beam intensity was less than 2 percent, as indicated by the current output from an ionization chamber and from an integrating monitor.

The results of these measurements are shown in Fig. 2, where the electron counting rate N^- and the positron counting rate N^+ are indicated by open and closed circles, respectively. It will be observed that for this particular photon spectrum, the number of pair production electrons is less than 10 percent of the number of Compton electrons accepted by the spectrometer detector in each momentum interval. These data were obtained with a spectrometer resolution of approximately 20 percent. In addition, the high energy cut-off point of the electron counting rate was determined with a resolution of 3 percent, with the result that the energy of the electrons in the betatron was found to be 11.3 $\pm$0.2 Mev. This value is in good agreement with the result of a previous measurement made with deuterium-loaded emulsions.[6]

The spectrometer measurements shown in Fig. 2 were converted to a corresponding photon spectrum in the following manner. For a continuous input photon spectrum, the spectrometer counting rate, $N(H)$, at a given magnetic field, H, can be expressed as

$$N(H)=\int_0^\infty P(k)S(k,H)dk, \tag{1}$$

where k is the photon energy, $P(k)$ is the photon flux density per unit energy interval at the position of the beryllium foil of the spectrometer, and $S(k,H)$ is the energy response of the spectrometer.

The spectrometer response was determined indirectly from line shape measurements of the electron counting rate *versus* magnetic field with monoenergetic photons from sources of Cs^{137} (0.661 Mev) and Na^{24} (1.37 Mev, 2.76 Mev) incident on the Be foil. The measured line shape was represented by the function $R(\rho)$, where ρ is effectively the radius of curvature corresponding to H. $R(\rho)$ was normalized so that the peak value was equal to one. Then, the response $S(k,H)$ is given as

$$S(k,H)dk=\left[nT(k)\int_0^{\frac{1}{2}\pi} f(\theta)\sigma(k,\theta)d\theta\right]\times\left[\frac{H}{3650}\frac{dk}{dE_e}\right]R(\rho)d\rho. \tag{2}$$

[6] P. K. S. Wang and M. Wiener, Phys. Rev. **76**, 1724 (1949).

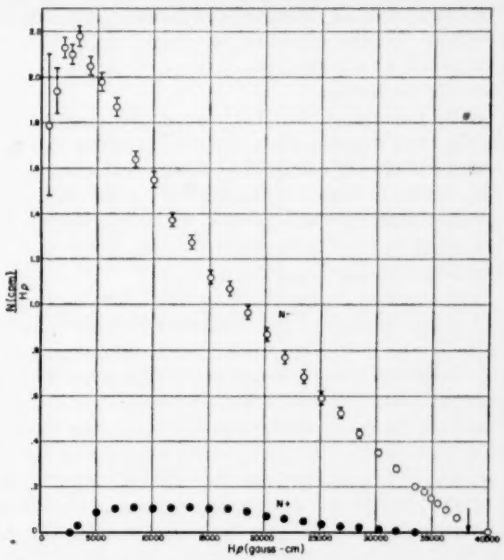

FIG. 2. Momentum distribution of electrons (open circles) and positrons (closed circles) which are ejected from the Be foil of the spectrometer by the incident photon beam and which are contained in a small solid angle determined by the spectrometer baffles.

In this equation, $\sigma(k,\theta)d\theta$ is the Klein-Nishina differential cross section, $f(\theta)$ depends on the geometry of the spectrometer defining baffle, $T(k)$ is the correction which accounts for electron scattering in the beryllium foil, and n is the number of foil electrons in the photon beam. Accordingly, the expression in first square brackets[7] represents an *effective* cross section that applies to those processes in which a Compton electron with an initial recoil angle θ is accepted by the spectrometer after emergence from the foil. The expression in the second square brackets, where E_e is the Compton electron energy in the forward direction ($\theta=0$), arises from a change of variables from photon energy to Compton electron momentum in gauss-cm. Because the function $R(\rho)$ is sharply peaked in a small interval, all other terms can be removed from the integral in Eq. (1). The remaining integral, $\int_0^\infty R(\rho)d\rho$, represents the area under the line shape.[8] The photon spectrum may be computed finally from the following equation (energies in Mev):

$$P(k)=\frac{3650}{nH}\times\frac{\{N^-(H)-N^+(H)\}}{\left\{T(k)\int_0^{\frac{1}{2}\pi} f(\theta)\sigma(k,\theta)d\theta\right\}M(H)\int_0^\infty R(\rho)d\rho}\frac{dE_e}{dk}. \tag{3}$$

[7] This quantity is evaluated by J. W. Motz in Phys. Rev. **86**, 753 (1952).

[8] Although the line shape depends on the electron energy loss in the foil, the area under the line shape depends only on the electron backscattering in the foil, and accordingly, has a negligible variation over this energy range.

The function $M(H)$ is introduced here as the correction necessary for the experimental points near the high energy end of the spectrum because of the finite spectrometer resolution.

With the aid of Eq. (3), the photon energy flux density was determined in units of ergs/cm² sec as a function of photon energy. The results are shown by the open circles in Fig. 3. The errors given for each point include the errors which arose in evaluating the various quantities in Eq. (3) as well as the statistical error of the measured counting rate.

As a check on the use of cavity ionization chambers in this energy range,[9] a 25-r Victoreen thimble chamber covered with a 1.95-cm thick Lucite cap was placed at the position of the spectrometer foil with the collimator removed. For the same incident energy flux per unit area as in the spectrometer measurements (the betatron monitor indicated 30 roentgens per minute at a meter), the dose rate measured by the thimble chamber and corrected for photon absorption in the Lucite wall was found to be 3.14±0.10 roentgens per minute. In comparison, the values of the energy flux density as a function of the photon energy (Fig. 3), which were determined from the spectrometer measurements, were converted to corresponding values of roentgens produced in an air cavity in Lucite, by the use of true absorption coefficients in air with the proper correction made for the difference in stopping power of Lucite relative to air. The value of the area under this roentgen curve was 3.24±0.30 roentgens per minute, which is in good agreement with the total number of roentgens measured by the thimble chamber for this particular spectrum.

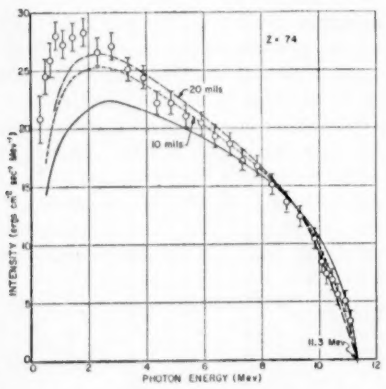

FIG. 3. Photon intensity spectrum in the forward direction. The experimental points are given by the open circles. The Bethe-Heitler thin target spectrum, modified by the photon absorption in the materials surrounding the target (Fig. 1), is shown by the solid line. The spectra to be expected from a 10-mil and a 20-mil target and also corrected for absorption in the materials, are shown by the dashed curves.

[9] W. V. Mayneord, British J. Radio., Supplement No. 2, 133 (1950); T. J. Wang, Nucleonics 7, 68 (1950).

III. COMPARISON WITH THEORY

The bremsstrahlung spectrum for 11.3-Mev electrons incident on a thin tungsten target was computed using the Bethe-Heitler formula in the form given by Schiff.[10] Under the present experimental conditions, it is expected that the shape of this thin target spectrum will be modified by the following processes: (a) energy loss and scattering of the electrons in the target, (b) photon absorption in the target, and (c) photon absorption in the materials surrounding the target (see Fig. 1). The effect of (c) is accounted for by the use of total absorption coefficients.[11] The calculated thin target spectrum modified only by (c) is given by the solid line in Fig. 3, where the curve has been arbitrarily normalized to agree with the experimental data at 9 Mev.

The additional distortion produced in the shape of the spectrum by processes (a) and (b) was estimated in the following manner. For a target of thickness t, the photon intensity spectrum $I_{tE_B}(k)$ was expressed as

$$I_{tE_B}(k) \propto \int_0^t e^{-\mu(k)[t-x]} S(x) I\left(k, E_B + \frac{\partial E}{\partial x} x\right) dx, \quad (4)$$

where $\mu(k)$ is the total absorption coefficient for tungsten, E_B is the energy of the betatron electrons before they enter the target, and the quantity $[E_B+(\partial E/\partial x)x]$ is the energy of the electrons at a depth x in the target (neglecting straggling). The function $I(k, E)$ is the photon intensity spectrum for electrons of energy E as given by reference 10, and for the sake of this calculation, it was represented as a linear function of E. The function $S(x)$ is the *relative* probability that the radiation produced by electrons at depth x reaches the detector.

$S(x)$ is estimated from information on the angular distribution of the electron velocities *versus* depth in the target, and on the angular distribution of the bremsstrahlung. The radiation from the electrons is largely confined to a cone of half angle mc^2/E, which is centered about the electron velocity direction just before radiation. For this reason, the radiation from an electron will not be detected if its velocity direction makes an angle greater than mc^2/E with the initial direction of the electron beam (i.e., the forward direction). It then follows that $S(x)$ is to a good approximation equal to the probability that the velocity vector of an electron at depth x will make an angle smaller than mc^2/E with the forward direction. (This approximation is tantamount to replacing the angular distribution of the bremsstrahlung by a rectangular function which goes to zero at mc^2/E.) The angular distribution of electron velocities was represented as Gaussian, and the

[10] L. I. Schiff, Phys. Rev. 83, 252 (1951), Eq. (3). R. Sagane, Phys. Rev. 85, 1065 (1952) has discussed reasons for the use of Schiff's Eq. (3), which gives the spectrum averaged over angles of photon emission, rather than the spectrum in the forward direction.

[11] Gladys R. White, National Bureau of Standards Report NBS 1003 (1952) (unpublished).

dependence of the mean square angle on x was calculated from the results of Lewis.[12] Accordingly, the function $S(x)$ was found to be of the form

$$1-\exp\left\{-\frac{mc^2}{51(E_B-E)}\left(\frac{E_B}{E}\right)^2\right\},$$

where mc^2 is the rest energy of the electron, E_B the initial energy (including rest energy), and E_B-E the energy loss.

Although the diameter of the tungsten wire target is 60 mils, the radiation comes from a region near the tip of the target (see Fig. 1), where the thickness is not well defined. However, an estimate of the effective target thickness can be made from information about the angular distribution of the radiation. It has been shown[13] that for a given target thickness and incident electron energy, the angular distribution of the bremsstrahlung can be accurately predicted. In the present experiment, Eastman type M x-ray film, for which the dose-density relationship had been experimentally determined, was exposed to the betatron radiation at a distance of 150 cm from the target. The film was developed in Kodak Liquid x-ray developer under standard conditions, and the film densities were measured with a Model 273 Ansco color densitometer. A plot of the film densities *versus* angle, with the peak density normalized to unity, is shown by the open circles in Fig. 4. For comparison, the angular distributions that are expected[14] for tungsten target thicknesses of 40, 20, 10, 5, and zero mils are shown by the solid lines. It is seen that the experimental measurements show the closest agreement with the theoretical angular distribution for a 10-mil target. The rise of the experimental values above the theoretical curve at the larger angles suggests the possibility that some of the radiation is coming from portions of the target that are thicker than 10 mils.

With the above information on the target thickness, the intensity spectrum $I_{tE_B}(k)$ was evaluated by the relation given in Eq. (4) for target thicknesses of 10 and 20 mils. The results, modified to account for the photon absorption in the materials surrounding the target, are shown in Fig. 3 by the dashed lines, which are normalized (as was the thin target curve) at 9 Mev.

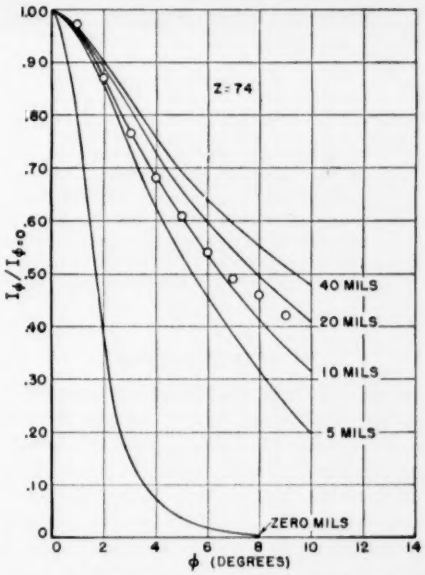

FIG. 4. Angular distribution of the x-ray intensity from 11.3-Mev electrons incident on a tungsten target. The solid lines are the theoretical distributions expected [Eq. (6), reference 13] for target thicknesses of 40, 20, 10, 5, and zero mils. The open circles represent the distribution determined by film measurements.

The theoretical curve for the 10-mil target shows good agreement with the experimental measurements over the major part of the spectrum. The excess number of photons measured in the low energy region may possibly be explained as the contribution from thicker portions of the target, in view of the poor target geometry and the consequent uncertainty in the target thickness.

The authors wish to thank Dr. U. Fano and Dr. H. W. Koch for helpful discussions. Also, they wish to express their appreciation to Dr. D. T. O'Connor of the Naval Ordnance Laboratory for his kind cooperation, and to Mr. Donald Case for his help and time spent in the operation of the betatron.

[12] H. W. Lewis, Phys. Rev. **78**, 526 (1950).
[13] L. H. Lanzl and A. O. Hanson, Phys. Rev. **83**, 959 (1951).
[14] The theoretical distribution was calculated from Eq. (6) in reference 13.

Second-Order Acoustic Fields: Relations between Energy and Intensity*

JORDAN J. MARKHAM
Applied Physics Laboratory, Johns Hopkins University, Silver Spring, Maryland
(Received October 24, 1952)

In this paper, the effects of the recent change in the expression for the average acoustic energy are considered. In particular, its relation to the modified expression for the acoustic intensity is explored. Use is made of Airy's second-order solution of the field equations. The accepted average energy-intensity relation has to be reinterpreted in that only part of the energy travels with the velocity of sound. When a wave is propagated down a tube, it is headed by a region of higher density, while behind this region the average density is decreased. The calculation seems to explain the origin of the new term in the average energy density and to relate it to the radiation pressure.

I. INTRODUCTION

IT has recently been found that the accepted expression for the average energy density is in error.[1,2] As far as the author knows, the needed correction was originally discovered by Andrejew. It applies to average quantities, since the correct instantaneous energy expression appears in the literature.[3] In view of this energy modification, one would suspect that the accepted expression for the intensity needs revision.[4,5] Schoch[6] has recently shown that one may separate the equation relating the instantaneous intensity to the instantaneous energy into two parts. One is the accepted energy-intensity relation, and the other connects the additional terms. Schoch's calculations are very general, not being limited to infinitesimal disturbances. Being general, however, they do not follow the disturbance in detail.

In this paper, explicit calculations will be made for the average energy density and for the average intensity of an acoustic wave. The calculations are based on Airy's general solution for the propagation of an elastic disturbance in a one-dimensional gas. Three types of disturbances will be considered, i.e., the infinite plane wave, the slowly rising wave train (an infinite wave whose amplitude varies from zero to a fixed value), and a rapidly rising wave train. It will be shown that the front of the wave is a region of high density, and that it is followed by a region of lower density. This is true, regardless of the magnitude of the disturbance, and seems to be an essential feature of acoustic propagation in gases. The details of the calculation will be given in the next sections.

II. BASIC EQUATIONS FOR THE PROBLEM

We shall first state the basic equations governing the propagation of sound in a one-dimensional gas and follow this by a discussion. The equations of interest are: the equation of motion

$$\xi_{tt} = -v_0 p_x; \tag{1}$$

the equation of continuity

$$v_e = v_0 \xi_x; \tag{2}$$

the equation of state,

$$p/p_0 = (v_0/v)^\gamma; \tag{3}$$

Airy's equation for the displacement

$$\xi = f(\tau) + [(\gamma+1)/4c^2]x[f_\tau(\tau)]^2 \text{ (to second-order terms)}; \tag{4}$$

the equation for the instantaneous energy per unit mass

$$Ev_0 = -p_0 v_e + \tfrac{1}{2}(c^2/v_0^2)v_e^2 + \tfrac{1}{2}\xi_t^2 \text{ (to second-order terms)}; \tag{5}$$

and the equation for the instantaneous intensity

$$I = p\xi_t = p_0\xi_t - (c^2/v_0^2)v_e\xi_t \text{ (to second-order terms)}. \tag{6}$$

The following notations have been used: p = pressure; v = specific volume;[7] x = initial or rest position of the particle; ξ = displacement of the particle whose initial position is at x; t = time; c = sound velocity at pressure p_0; γ = ratio of the specific heats; f = an arbitrary function which is twice differentiable; $\tau = t - x/c$; I = instantaneous intensity; and E = instantaneous excess energy per unit initial volume.[8] We are using a type of Lagrangian coordinate system.[9] The subscript zero refers to the initial (or equilibrium) state, while the subscripts x, t, and τ refer to differentiation with respect to these quantities.

* This article is based on a paper given at the Brown University Symposium on Ultrasonic Absorption in Fluids, October, 1952. The research was supported by the Bureau of Ordnance, U. S. Navy.

[1] N. Andrejew, J. Phys. (U.S.S.R.) **2**, 305 (1940).

[2] J. J. Markham, Phys. Rev. **86**, 712 (1952). The following typographical errors have been noted: In Eq. (14), ϵ should be replaced by E_M; 7 lines after this equation, 0.175d should read 0.0175d.

[3] H. Lamb, *Hydrodynamics* (Dover Publications, New York, 1945), pp. 8–10.

[4] G. W. Stewart and R. B. Lindsay, *Acoustics* (D. Van Nostrand Company, Inc., New York, 1930), p. 30.

[5] P. M. Morse, *Vibration and Sound* (McGraw-Hill Book Company, Inc., New York, 1936), p. 188.

[6] A. Schoch, unpublished.

[7] In this coordinate system it is simpler to use the excess specific volume instead of the excess density. This simplifies the continuity equation.

[8] E is the difference between the energy contained in a space whose initial volume is unity and the energy contained initially (rest) in this same volume.

[9] This coordinate system is not the same as the Lagrangian system developed by Lamb, reference 3, p. 12.

Equations (1), (2), and (3) are found in Lamb.[10] A combination of Eqs. (1), (2), and (3) leads to a differential equation identical to the one obtained for the propagation of a disturbance in a channel. In 1845 Airy solved this problem[11] in a manner which is appropriate for small disturbances. Many years later Lamb[10] applied the solution to sound propagation. A generalization of this has been given by Fubini-Ghiron.[12] Our equation (4) is actually a special solution of a more general one. It is useful since the vibration at $x=0$ is given by $f(t)$. This leads to the following graphic picture (Fig. 1). Assume that the propagation is along a tube parallel to the x axis. Further, let a piston be located at $x=0$, and its displacement described by $f(t)$. The problems which arise owing to reflection from the other end of the tube will not be considered here. Either no reflection takes place, or one may imagine that at the time of interest the wave train has not yet arrived at the other end of the tube.

One should note that a completely different approach to this problem has been made by Poisson, Earnshaw, Riemann, and many others.[13] This method obtains an exact solution of the equations and has to be applied to shock waves. Without further study it is impossible to tell how this approach will modify our problem.

The explicit form of Eq. (5) has been given previously;[2] it is an expansion of an equation found in Lamb.[3] The last term is the contribution to the kinetic energy. One may refer to the first term of (5) as Andrejew's part. Perhaps a more descriptive name is the stored part; we shall see the reason for this presently. The two last terms may be called the Rayleigh or oscillatory terms. Equation (6) is almost a definition, and this form has been considered by Andrejew and by Schoch. The names of Andrejew and Rayleigh (first and second terms) can also be applied to this equation.

In the analysis, two types of integrals will be used, one with respect to time and the other with respect to space. Select t and x in a way which satisfies the relation

$$\omega\tau=2\pi n, \tag{7a}$$

where n is any integer and ω is the angular frequency; then the time average of any quantity $Q(x, t)$ can be defined as

$$\langle Q(x;t)\rangle_t=\frac{\omega}{2\pi}\int_t^{t+2\pi/\omega} Q(x,t)dt. \tag{7b}$$

For some considerations it will be useful to define a space integral as follows:

$$(x_0+L|Q(t)|x_0)=\int_{x_0}^{x_0+L} Q(t,x)dx. \tag{7c}$$

The symbolism $\langle x_0+L|Q(t)|x_0\rangle_t$ is a combination of (7b) and (7c)—i.e., the time average of $(x_0+L|Q(t)|x_0)$. Of course it is assumed the L has been so chosen that (7a) can be satisfied at x_0 and x_0+L.

We shall now consider special forms of the function f and calculate various physical quantities which might be of interest.

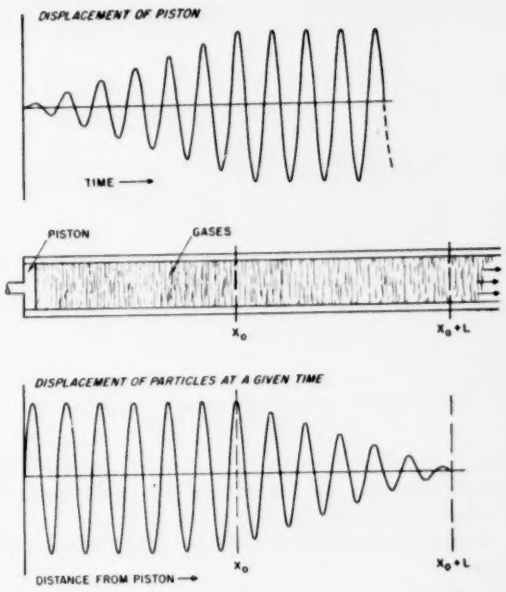

FIG. 1. An illustration of the slowly rising wave train. The top plot shows the displacement of the piston as a function of time. The bottom graph is the particle displacement as a function of the distance from the piston for a fixed time. The middle figure shows the actual physical set-up. The distance between x_0+L and x_0 is the head of the wave at instant $t=(x_0+L)/c$.

III. SPECIAL SOLUTIONS

The Constant Amplitude Plane Wave

In this case, the following function for f will be assumed:

$$f(t)=A\sin\omega t, \tag{8}$$

where A is the displacement amplitude of the piston. Substituting into (4) one obtains:

$$\xi=A\sin\omega\tau+\tfrac{1}{8}(\gamma+1)A^2k^2x(1+\cos2\omega\tau), \tag{9}$$

[10] H. Lamb, *The Dynamical Theory of Sound* (E. Arnold and Company, London, 1931), second edition, pp. 177–186. The use of (3) for second-order fields has recently been justified. See J. J. Markham, Phys. Rev. **86**, 710 (1952). Since some of the excess pressure and some of the excess specific volume do not average to zero, one cannot be sure that they are related adiabatically. Further work on the use of Eq. (3) is needed.

[11] G. B. Airy, *Encyclopaedia Metropolitana* (1845), "Tides and Waves," Sec. VI, p. 297.

[12] E. Fubini-Ghiron, Alta Frequenza **4**, 530 (1935), particularly p. 543 ff. This section is sufficiently mathematical that it can be followed without a background in Italian.

[13] Some references are: A. Sommerfeld, *Mechanics of Deformable Bodies* (Academic Press, Inc., New York, 1950), pp. 262–271; Lord Rayleigh, Proc. Roy. Soc. (London) **A84**, 247 (1910) and the many papers given in the listed treatments.

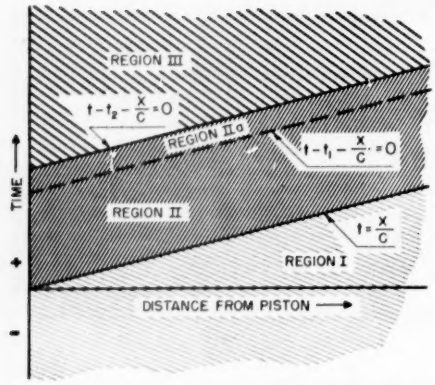

FIG. 2. Illustration of the way one obtains solutions for the slowly rising wave train.

k is $2\pi/\lambda$, where λ is the wavelength of the first-order sound pulse—i.e., the first term of (9). In this case, the average displacement of the piston is zero.

Using the definitions of averages, Eq. (5) and Eq. (6) result in

$$\langle E\rangle_t=[-\tfrac{1}{8}(\gamma+1)p_0+\tfrac{1}{4}\gamma p_0+\tfrac{1}{4}\gamma p_0]A^2k^2 \quad (10a)$$

$$=\tfrac{1}{8}(3\gamma-1)p_0A^2k^2, \quad (10b)[14]$$

and

$$\langle I\rangle_t=\tfrac{1}{2}\gamma p_0cA^2k^2. \quad (11)$$

Traditionally,[4,5] one compares Eq. (11) with the last two terms (vibrational and kinetic) of (10a). One concludes that the disturbance formed in a region simply travels along x with the velocity c. This is in complete agreement with the propagation of electromagnetic waves in a vacuum, where one may arrive at this conclusion without making any mathematical approximation except the physical idealization of the medium.[15] This corresponds to the use of Eq. (3). We note that the Andrejew term is a sizeable fraction of the total energy. What does the additional term mean, and how does it get into the field? We shall attempt to answer this question by examining a disturbance which is initially zero and rises with time.

The Slowly Rising Wave

To understand the nature of the new energy term, one might study a sinusoidal function modulated by a Gaussian error function. Unfortunately, such a function leads to lengthy expansions, and the evaluation of Eqs. (7b) and (7c) is difficult.

We shall, therefore, express ξ in terms of four functions. Consider the x, t plane for $x>0$ which can be divided into four parts by the three straight lines

$$t-x/c=0,\ t_1,\ t_2$$

(see Fig. 2). We may define f in regions I, II, and III as follows:

$$f^{\mathrm{I}}(t)=0, \quad \text{for } t<0;$$
$$f^{\mathrm{II}}(t)=A_1t\sin\omega t, \quad 0<t<t_1; \quad (12)$$
$$f^{\mathrm{III}}(t)=A\sin\omega t, \quad t_2<t.$$

In region I there is no disturbance. This corresponds to the time before the pulse has started. In region II the piston slowly starts to vibrate, reaching its full amplitude after t_2 seconds. The piston cannot change suddenly from f^{II} to f^{III}, so that in the time interval t_1 and t_2 one must assume that the motion of the piston is described by another function. If t_2-t_1 is made small, this region (IIa) will not be of great interest; indeed, f^{IIa} will not be given analytically. The above conditions suggest that A_1t_1 is slightly less than A. The general form of the wave is given in Fig. 1. We see that the wave train rises slowly from zero to a fixed amplitude. Region II, corresponding to the space between x_0+L and x_0, will be called the head of the wave train.

Along the boundary between regions I and II, f, f_x, and f_t are continuous; indeed, they are equal to zero. From Eqs. (2) and (4) one sees that this assures a continuity in the specific volume, pressure, particle displacement, and particle velocity between the regions. The discontinuity occurs in the force. This follows because ξ_{xx} (i.e., p_x) is discontinuous. For future reference we calculate the average displacement of the piston directly from (12), namely

$$\langle\xi\rangle_t=-A_1/\omega. \quad (12a)$$

Equations (9), (10), and (11) hold for region III. The corresponding expressions for region II are

$$\xi^{\mathrm{II}}(t,x)=A_1\tau\sin\omega\tau+(1/8c^2)(\gamma+1)xA_1^2[(\tau^2\omega^2+1)+2\omega\tau\sin2\omega\tau+(\tau^2\omega^2-1)\cos2\omega\tau]; \quad (13)$$

$$\langle E^{\mathrm{II}}\rangle_t=(-p_0/8c^2)(\gamma+1)A_1^2\{(\omega^2\tau_0^2+2\pi\tau_0\omega+4\pi^2/3+\tfrac{1}{2})-(4x/c)(\omega^2\tau_0+\omega\pi)\}+(1/2v_0)A_1^2(\omega^2\tau_0^2+2\pi\omega\tau_0+4\pi^2/3+\tfrac{1}{2})+\text{terms of order } A_1^3; \quad (14)$$

and

$$\langle I^{\mathrm{II}}\rangle_t=p_0(\omega/2c^2)(\gamma+1)A_1^2x(\omega\tau_0+\pi)+(c/2v_0)A_1^2\{\omega^2\tau_0^2+2\pi\omega\tau_0+4\pi^2/3+\tfrac{1}{2}\}+\text{term of order of } A^3. \quad (15)$$

The τ_0 are values of τ which satisfy Eq. (7a). These expressions are exact to the order of A^3. Terms of order A do not appear. This is due to the definitions (7) and Eq. (12). If (7a) were replaced by

$$\omega\tau=2\pi n+\tfrac{1}{2}\pi,$$

these terms would appear. Some simplification is obtained by considering the domain (Fig. 2) near the upper boundary of region II (below IIa, however) where x is small—i.e., x_0 is not too far from the piston.

[14] Andrejew's calculation of $\langle E\rangle_t$ seems to be in error. The discrepancy is traceable to his Eq. (L43) which the author believes is incorrect.

[15] See, for example, M. Abraham and R. Becker, *Electricity and Magnetism* (Blackie and Company, London, 1937), pp. 182–187.

Under these conditions,

$$\tau_0 \gg 2\pi/\omega \quad \text{or} \quad 4x/c=(2\pi/\omega)(4x/\lambda),$$

and it follows that

$$\langle E^{II}\rangle_t \approx [-\tfrac{1}{8}(\gamma+1)p_0+\tfrac{1}{2}p_0\gamma]A_1^2k^2\tau_0^2 \qquad (14a)$$

and

$$\langle I^{II}\rangle_t \approx \tfrac{1}{2}(\gamma+1)p_0xA_1^2k^2\tau_0+\tfrac{1}{2}p_0\gamma A_1^2k^2\tau_0^2c. \qquad (15a)$$

The following comments can be made: (a) Eq. (14a) is identical to Eq. (10a) if we set $A=A_1\tau_0$. The value of $\langle E\rangle_t$ in region II approaches the value in region III. (b) An additional term appears in the intensity which feeds out energy, accounting for Andrejew's term. Before we analyze this case more fully, let us develop a third solution of Eq. (4).

The Rapidly Rising Wave

Fubini-Ghiron has suggested a solution for the problem which eliminates region II. All the necessary conditions are fulfilled for $x=0$, if one sets

$$f^{I}=0 \text{ for } t<0 \qquad (16)$$

and

$$f^{III}=A(1-\cos\omega t) \text{ for } t>0.$$

This assures that ξ, ξ_t, and ξ_x are continuous, and that there is only a discontinuity in the force at $\tau=0$. This solution achieves the required continuity condition by shifting the average position of the piston from zero to

$$\langle \xi(0,t)\rangle_t = A \text{ for } t>0. \qquad (16a)$$

Here regions II, IIa, and III of the previous solution blend into one. For simplicity, however, we shall call the domain where $0<\tau<2\pi/\omega$ region II. The concept of the head is rather vague and arbitrary. At an instant $t=x_0/c$, there is no disturbance beyond x_0. One period later, however, the disturbance has passed on to $x_0+\lambda$. We shall shortly see that energetically the region between x_0 and $x_0+\lambda$ plays a very important role for the time interval x_0/c and $x_0/c+2\pi/\omega$. It, therefore, seems appropriate to define the head as the region between x_0 and $x_0+\lambda$ for the time interval $t=x_0/c$ to $t=x_0/c+2\pi/\omega$.

Using (4) and (16), it follows that

$$\xi=A(1-\cos\omega\tau)+\tfrac{1}{8}(\gamma+1)xA^2k^2(1-\cos2\omega\tau) \text{ for } \tau>0. \qquad (17)$$

Equation (17) does not change the time average values of the intensity and the energy given by Eqs. (10b) and (11). The apparent contradiction—i.e., the extra term of (10a) remains. Evidently, during the first cycle the stored energy is injected into the medium and remains there. The way this is achieved will be discussed next.

IV. THE TRANSFER OF THE STORED ENERGY

We start with a statement of the conservation of energy. Consider two planes in the tube at x_0 and x_0+L; L can be an arbitrary distance or the length of the head. At instant t it follows that:[16]

$$I(x_0+L;t)-I(x_0;t)=-\frac{\partial}{\partial t}\int_{x_0}^{x_0+L}E(x;t)dx. \qquad (18)$$

By integrating between t and some fixed time t_0, one obtains

$$\int_{t_0}^{t}[I(x_0+L;t)-I(x_0;t)]dt = -\int_{x_0}^{x_0+L}[E(x;t)-E(x;t_0)]dx. \qquad (19)$$

The expression for the total excess energy in a period between x_0 and x_0+L is obtained by integrating (19) with respect to time between T and $T+2\pi/\omega$. This results in

$$\int_{T}^{T+2\pi/\omega}dt\int_{t_0}^{t}I(x_0+L;t)-I(x_0;t)dt = -\int_{T}^{T+2\pi/\omega}dt\int_{x_0}^{x_0+L}[E(x;t)-E(x;t_0)]dx. \qquad (20)$$

It has been shown that (18) holds[3,6,16] for any order of A. By direct substitution from Eq. (4), one may show that Eq. (19) holds for the stored terms and for the vibrational terms of Eqs. (5) and (6) independently, in

[16] We may obtain Eq. (18) directly from Eqs. (1) through (6). Multiplying the partial derivative of Eq. (2) with respect to t by p/v_0 and subtracting it from $(1/v_0)\xi_t$ times Eq. (1), results in

$$\frac{1}{v_0}\left[\frac{1}{2}\frac{\partial}{\partial t}\xi_t^2-p\frac{\partial v}{\partial t}\right]=-\xi_t\frac{\partial}{\partial x}p-p\frac{\partial}{\partial x}\xi_t,$$

where the order of differentiation has been interchanged. This can be written in the form

$$\frac{\partial}{\partial t}E=-\frac{\partial}{\partial x}(p\xi_t)=-\frac{\partial I}{\partial x}.$$

Equation (18) follows by integrating with respect to x. Equation (2) can be written in the form

$$-\frac{\partial}{\partial t}\left(\frac{p_0}{v_0}v_e\right)=-\frac{\partial}{\partial x}p_0\xi_t,$$

from which it follows that the stored energy is related to the stored intensity. By subtracting the third equation of this footnote from the second, it follows that

$$\frac{1}{v_0}\frac{\partial}{\partial t}\left\{\frac{1}{2}\xi_t^2-\int_{v_0}^{v_0+v_e}(p-p_0)dv_e\right\}=-\frac{\partial}{\partial x}[(p-p_0)\xi_t],$$

which relates the Rayleigh energy term, the kinetic term, and the Rayleigh intensity term. No approximations have been made. This footnote follows Schoch's derivation, except that a different coordinate system has been used. It indicates the way the energy should be related to the intensity. In our coordinate system v_0 appears, while v appears in Schoch's.

Since there are several ways to define the energy, one must know which one is related to the intensity. This can be done by the use of the field equations. The developments owing to Andrejew (reference 1) and B. P. Konstantinow and I. M. Bronstein [Physik. Z. Sowjetunion **9**, 630 (1936)] seem to be ambiguous with respect to this problem. The object of this footnote was to determine just which energy comes into the energy-intensity relations.

agreement with Schoch's general theorem. Equation (19) gives a relation between the time integral of the intensities at x_0+L and x_0 and the energy at instant t and t_0 between these limits. Equation (20) states the relation between the net energy (or the average energy) between these limits and the intensity. No direct relation between $\langle I\rangle_t$ and $\langle E\rangle_t$ appears.

It is convenient at this point to consider the stored and the oscillatory energy expressions separately. Consider first the slowly rising pulse. We would like to calculate the time average energy in the head of the wave train. Select points in the tube such that when the pulse has just reached x_0+L, it is almost fully developed at x_0 (Fig. 1). This means that at the time T, the point x_0+L is just below the boundary of regions I and II, while the point x_0 is just below the boundary of regions II and IIa. In other words, we may let

$$ct_0=x_0,$$

$$T+2\pi/\omega-x_0/c \text{ almost equal to } t_1\ (2\pi/\omega \text{ in case 3}), \quad (21)$$

$$T+2\pi/\omega-(x_0+L)/c\lesssim 0.$$

From the left-hand side of Eq. (20), one obtains for the total stored energy in the head during the time interval T to $T+2\pi/\omega$,

$$p_0\int_T^{T+2\pi/\omega}\xi(x_0;t)dt.$$

If T satisfies (9a), $(\tau_h=T-x_0/c)$, the time average of this energy is

$$\langle x_0+L|E_s(T)|x_0\rangle_t=-p_0\frac{A_1}{\omega}+\frac{p_0}{8x^2}(\gamma+1)$$

$$\times x_0A_1{}^2(\omega^2\tau_h{}^2+2\pi\omega\tau_h+4\pi^2/3+\tfrac{1}{2}). \quad (22)$$

Using the same approximation as was used before, it follows that

$$\langle x_0+L|E_s(T)|x_0\rangle_t \qquad \text{(a)} \qquad \text{(b)}$$

$$\approx -p_0A/\omega+\tfrac{1}{8}p_0(\gamma+1)x_0k^2A_1{}^2\tau_0{}^2. \quad (22a)$$

Consider next the rapidly rising pulse (case 3). The pulse is established in one wavelength; therefore, $L=\lambda$ and $t_0=T$. Using Eqs. (20) and (17), one obtains

$$\langle x_0+\lambda|E_s(T)|x_0\rangle_t=p_0A+\tfrac{1}{8}p_0(\gamma+1)x_0A^2k^2 \quad (23)$$

(a) (b)

where no approximations have been made. Let us compare Eqs. (22a) and (23) with Eq. (10a), which holds in region III for both cases. At time $T+2\pi/\omega$, the boundary between regions II and III is near x_0. The equations inform us that the stored energy is made of two terms. Term (a) seems to be an accidental term arising from the fact that our expressions—i.e., Eqs. (12) and (16)—shift the mean position of the piston, as shown by Eqs. (12a) and (16a). It would seem that one is justified in ignoring this term on the assumption that it would not arise if the average position of the piston had not shifted. Term (b) seems to be the important term, for it equals the negative of the average of the stored energy between 0 and x_0, since $A_1\tau\approx A$.

Something seems to reduce the average density in this region but increases the average density in the head of the pulse. Let us now calculate the radiation pressure. The instantaneous pressure is given by

$$p_s=\gamma p[\tfrac{1}{2}(\gamma+1)\xi_x{}^2-\xi_x],$$

while the average value is

$$\langle p_s\rangle_t=\tfrac{1}{8}\gamma(\gamma+1)p_0A^2k^2. \quad (24)$$

One may obtain a graphic illustration of what happens by imagining that the pressure in the region $x<x_0$ is composed of two parts, the sum of which equals the outside pressure. One of these is the radiation pressure, while the other is the residual pressure. If one further assumes that the density is determined only by the residual pressure, one obtains an explanation of the phenomenon. The division of pressure is similar to the situation of two gases in a vessel where the concentrations are determined by the partial pressures, not the total pressure. Thus, after the wave has progressed to x_0, the density is determined by the residual pressure —i.e., $p_0-\langle p_s\rangle_t$. This change in pressure causes an expansion which in turn decreases the internal energy. The amount is given by the first term of Eq. (10a). Beyond x_0 there is a region of higher density followed by a region with a normal density—(i.e., region I in Fig. 1).

One would strongly suspect that form of f in region II will not affect this conclusion nor would definitions (7a) and (7b). It is not known, however, if Airy's form of the solution affects this conclusion—i.e., if similar results are obtained from a Poisson-Earnshaw-Riemann type of equation. It should be stressed that the idea of a pressure division is based on these calculations. The author does not know of any fundamental reason for this division.

One should next consider the oscillatory terms. There is actually no problem here, since the vibrational energy-intensity relations are satisfactory even for an infinite plane wave. The calculations using Eqs. (19) and (20) lead to nothing new and will not be given. The general conclusions will be stated in the next section.

V. CONCLUSIONS

The following conclusions seem justified:

1. The additional term in the energy arises from a decrease in the density of the gas. The amount depends on the intensity of the wave.

2. For an infinite plane wave of constant intensity the usual energy-intensity relation holds, although the average density has decreased.

3. The shift from an infinite wave of one amplitude to another is accompanied by an inflow or an outflow

of energy in excess of the accepted value. This accounts for the additional energy term.

4. When a wave train travels down a tube, there is a region of higher density (where the wave forms) followed by a region of lower density. The density variation seems to be a basic feature of a traveling wave and does not depend on the amplitude.

Two additional conclusions, first given by Schoch, should be mentioned:

5. One may separate the relation between the energy and the intensity into two parts. One is related to the stored energy, while the other is related to the oscillatory energy.

6. As long as the total volume is held fixed, the net stored energy is zero. This does not mean that the energy may not have a space distribution.

One would expect the effect described in this paper to be unimportant in liquids. Equation (4) is for an ideal gas; however, corresponding forms exist in liquids.[17] Combining the expression for water[2] with Eqs. (10a) and (15a), one may see that Andrejew's terms are not important. One might expect similar results for other liquids. These calculations, however, have not been made.

The author would like to thank Dr. Schoch for an advance copy of his important paper, Miss A. Fogelgren for assistance with the manuscript, and Miss D. Rubenfeld for the illustrations. Finally, the author would like to thank his wife for her encouragement.

[17] See, for example, P. J. Westervelt, J. Acoust. Soc. Am. **22**, 319 (1950).

PHYSICAL REVIEW VOLUME 89, NUMBER 5 MARCH 1, 1953

Transport Phenomena in a Completely Ionized Gas*

LYMAN SPITZER, JR., AND RICHARD HÄRM
Princeton University Observatory, Princeton, New Jersey

(Received November 10, 1952)

The coefficients of electrical and thermal conductivity have been computed for completely ionized gases with a wide variety of mean ionic charges. The effect of mutual electron encounters is considered as a problem of diffusion in velocity space, taking into account a term which previously had been neglected. The appropriate integro-differential equations are then solved numerically. The resultant conductivities are very close to the less extensive results obtained with the higher approximations on the Chapman-Cowling method, provided the Debye shielding distance is used as the cutoff in summing the effects of two-body encounters.

I. INTRODUCTION

A PREVIOUS paper by Cohen, Spitzer, and Routly,[1] referred to hereafter as CSR, presented a new approach to the problem of transport phenomena in a completely ionized gas. In effect, the influence of mutual electron encounters on the velocity distribution function for electrons was considered as a problem of diffusion in velocity space. In particular, the electrical conductivity of an electron-proton gas was computed in this way. However, the results were not exact, since one term in the diffusion equation was neglected. In the present paper, a solution of the complete diffusion equation is obtained, and the results are extended to completely ionized gases with different mean nuclear charges. Computations are carried out for the thermal as well as the electrical conductivity.

In the first section below the general principles are explained and justified. Subsequent sections outline the derivation of the equations, the method of solution, and the results obtained.

* This work has been supported in part by the U. S. Atomic Energy Commision.

[1] Cohen, Spitzer, and Routly, Phys. Rev. **80**, 230 (1950).

II. GENERAL PRINCIPLES

The velocity distribution function $f_r(v)$ for particles of type r is determined by the familiar Boltzmann equation, basic in all studies of this sort,

$$\frac{\partial f_r}{\partial t}+\sum_i v_{ri}\frac{\partial f_r}{\partial x_i}+\sum_i F_{ri}\frac{\partial f_r}{\partial v_{ri}}=\sum_s\left(\frac{\partial_e f_r}{\partial t}\right)_s, \qquad (1)$$

where the notation in CSR has been followed. The complexity of the problem arises entirely from the term $(\partial_e f_r/\partial t)_s$, which gives the change in f_r produced by encounters of r particles with particles of type s.

To visualize the physical situation more accurately, let us follow a single electron as it moves through the gas. The random electrical fields encountered by the electron will produce deflections and changes in velocity. To some extent these fields can be described in terms of separate two-body encounters; let b be the impact parameter for such an encounter—the distance of closest approach between the two particles in the absence of any mutual force. The situation is characterized by the values of the following four distances: d, the mean distance from an electron to its nearest neighbor; b_0, the value of the collision parameter for

TABLE I. Values of the velocity distribution function $D(x)$ when an electrical field is present.

	$ZD(x)/A$				
x	$Z=1$	$Z=2$	$Z=4$	$Z=16$	$Z=\infty$
0.10	0.0008093	0.0001340	···	···	0.0001000
0.11	0.001300	0.0002262	···	···	0.0001464
0.12	0.001970	0.0003630	···	···	0.0002074
0.13	0.002847	0.0005582	···	···	0.0002856
0.14	0.003955	0.0008262	···	···	0.0003842
0.15	0.005317	0.001183	···	···	0.0005062
0.16	0.006955	0.001645	···	···	0.0006554
0.17	0.008886	0.002228	···	···	0.0008352
0.18	0.01113	0.002952	···	···	0.001050
0.19	0.01370	0.003832	···	···	0.001303
0.20	0.01660	0.004884	0.002163	0.001645	0.001600
0.22	0.02347	0.007576	0.003373	0.002432	0.002343
0.24	0.03180	0.01116	0.005044	0.003477	0.003318
0.26	0.04165	0.01575	0.007280	0.004833	0.004570
0.28	0.05304	0.02146	0.01018	0.006560	0.006147
0.30	0.06601	0.02840	0.01386	0.008721	0.008100
0.32	0.08057	0.03666	0.01842	0.01139	0.01049
0.34	0.09672	0.04632	0.02398	0.01463	0.01336
0.36	0.1145	0.05746	0.03063	0.01853	0.01680
0.38	0.1338	0.07012	0.03849	0.02317	0.02085
0.40	0.1548	0.08440	0.04764	0.02866	0.02560
0.44	0.2015	0.1180	0.07028	0.04249	0.03748
0.48	0.2545	0.1586	0.09924	0.06082	0.05308
0.52	0.3137	0.2066	0.1352	0.08443	0.07312
0.56	0.3792	0.2620	0.1789	0.1142	0.09834
0.60	0.4508	0.3254	0.2309	0.1511	0.1296
0.64	0.5285	0.3968	0.2917	0.1958	0.1678
0.68	0.6123	0.4764	0.3618	0.2494	0.2138
0.72	0.7023	0.5646	0.4416	0.3127	0.2687
0.76	0.7983	0.6612	0.5324	0.3868	0.3336
0.80	0.9005	0.7668	0.6336	0.4722	0.4096
0.88	1.123	1.005	0.8704	0.6819	0.5997
0.96	1.371	1.281	1.156	0.9499	0.8493
1.04	1.645	1.596	1.494	1.287	1.170
1.12	1.945	1.952	1.889	1.702	1.574
1.20	2.273	2.352	2.344	2.204	2.074
1.28	2.630	2.796	2.864	2.804	2.684
1.36	3.017	3.290	3.455	3.510	3.421
1.44	3.435	3.836	4.120	4.331	4.300
1.52	3.887	4.440	4.868	5.281	5.338
1.60	4.375	5.096	5.700	6.366	6.554
1.76	5.465	6.604	7.660	8.996	9.595
1.92	6.728	8.406	10.06	12.34	13.59
2.08	8.190	10.54	12.96	16.54	18.72
2.24	9.880	13.05	16.46	21.74	25.18
2.40	11.83	16.00	20.64	28.10	33.18
2.56	14.06	19.40	25.60	35.80	42.95
2.72	16.62	23.3	31.4	45.0	54.74
2.88	19.53	27.7	38.2	56.0	68.80
3.04	22.74	32.7	46.0	68.8	85.41
3.20	26.00	38.5	54.6	83.9	104.9

which an electron is deflected 90° in an encounter with a stationary positive ion; h, the Debye shielding distance; and λ, the mean free path for a net deflection of 90°. It is readily verified that for virtually all situations of interest,

$$b_0 \ll d \ll h \ll \lambda. \tag{2}$$

It is clear that encounters for which $b \ll d$ can be described adequately in terms of successive two-body encounters, since usually an encounter with one particle will be effectively over before another particle approaches to a distance less than d. These successive encounters may be divided into two classes. Those with $b \leqslant b_0$ produce large deflections, and will be termed "close" encounters. Those with $b_0 < b < d$ produce relatively small deflections, and will be called "distant" encounters. As shown in CSR and elsewhere, the cumulative effect of many distant encounters outweighs the effect of the less frequent close encounters, in the special case of inverse-square forces between the particles.

Encounters for which $d \leqslant b < h$ cannot be regarded as independent, since several such encounters will be taking place at the same time. More correctly, the deflection of a particular electron caused by such "encounters" must be attributed to statistical fluctuations of the electron density in a sphere of radius b. As shown in CSR, however, the mean square change of electron velocity produced by such fluctuations is correctly given if the formulas derived for successive two-body encounters are applied for $b > d$.

Particles passing at a distance large compared to h produce a negligible effect. From the standpoint of the Debye shielding theory, the effective field of a charge in a plasma varies as $e^{-h r}/r$, where h is given by

$$h^2 = \frac{kT}{4\pi n_e e^2 (1+Z)}. \tag{3}$$

If one considers rather the statistical fluctuations in electron density, Pines and Bohm[2] have shown that collective phenomena in a plasma reduce markedly the statistical fluctuations in electron density with wavelengths large compared to h, thus justifying the neglect of encounters such that $b > h$. There is some interaction between a single electron and the organized oscillations of the plasma—see Eq. (59a) of Pines and Bohm. However, comparison of their Eqs. (59a) and (59b) shows that for thermal electrons, with mean kinetic energies of the order kT, the rate of energy loss due to this process is less by a factor $1/\ln(h/b_0)$ than the energy loss due to random encounters such that $b < h$. The generation of plasma oscillations by a single thermal electron may therefore be neglected, together with a number of other terms of the same order.[3] Hence, we may neglect all interactions between electrons for which the distance of closest approach exceeds h.

Since λ is much greater than h, it is evident that many small deflections will be experienced by a particle traversing its mean free path. It is also clear that these deflections are essentially independent of each other. Inasmuch as collective phenomena (oscillations) have been neglected, the random electrical fields encountered by an electron in one region will be completely independent from the fields in a similar region separated by a distance appreciably greater than h. Hence, the successive changes in velocity represent a Markoff process, and the change of the velocity distribution function may be found from the Fokker-Planck equation.[4] This equation neglects the close encounters; the relative error introduced is again of the order $1/\ln(h/b_0)$.

III. DERIVATION OF EQUATIONS

Equations (10), (23), and (24) of CSR give the basic equations of the problem on the following assumptions: (a) the Fokker-Planck equation may be used to give $\partial f_e/\partial t$; (b) a steady state is established; (c) the velocity

[2] D. Pines and D. Bohm, Phys. Rev. **85**, 338 (1952).

[3] The various terms of relative magnitude $1/\ln(d/b_0)$ have been called "nondominant" by Chandrasekhar, and are usually neglected in the computation of diffusion coefficients—see S. Chandrasekhar, *Principles of Stellar Dynamics* (University of Chicago Press, Chicago, 1939).

[4] See S. Chandrasekhar, Revs. Modern Phys. **15**, 1 (1943).

distribution function may be expressed as the sum of a Maxwellian function $f^{(0)}$ plus a small term $f^{(1)}$ whose square may be neglected. The values of the diffusion coefficients have now been recomputed, using a straightforward and conceptually very simple method. A new integro-differential equation has then been obtained for $D(lv)$, the function which gives the dependence of the ratio $f^{(1)}/f^{(0)}$ on the velocity v; $1.5/l^2$ is the mean square electron velocity.

The electron-ion interaction is relatively simple to consider. Equation (28) of CSR must be modified to include a factor Z, the mean ionic charge, defined by

$$Z \equiv \sum_i n_i Z_i^2 / n_e, \tag{4}$$

summed over all positive ions, each of charge $Z_i e$ and of particle density n_i. We find

$$K(ff_i) = [3ZLf^{(0)} D(lv)\cos\theta]/2v^3, \tag{5}$$

where all the symbols have the same meaning as in CSR, except that to avoid confusion with the current density, j has been replaced by l.

The quantity $K(ff)$, giving the contribution of electron-electron interactions to $\partial_e f/\partial t$, is much more complicated. To evaluate the diffusion coefficients needed, the values of Δ_ξ, Δ_η, and Δ_ζ, the changes of velocity in a single collision, along coordinates parallel and perpendicular, respectively, to the original velocity, were first determined. In this computation, the velocity changes were first taken in a frame of reference moving with the center of gravity of the two particles. If the orbit lies in the xy plane, and the x axis is taken to be in the direction in which the original particle is moving, the velocity changes become very simple. The components of the vector change in velocity along the ξ, η, and ζ axes may then be found by successive rotations of the coordinate axes.

Next the values of the velocity changes, together with their products and squares, are averaged over all collisions, in accordance with Eq. (8) of CSR. The final values for $\langle\Delta_\xi\rangle$, $\langle\Delta_\xi^2\rangle$, and $\langle\Delta_\eta^2\rangle$ are the same as given in Eqs. (31) through (35) of CSR. For the two remaining coefficients we find

$$\langle\Delta_\eta\rangle = -\frac{4L^2}{\pi^{\frac{1}{2}}} \sin\theta\{I_0(\infty) - I_0(x) + I_3(x)/x^2\}, \tag{6}$$

$$\langle\Delta_\xi\Delta_\eta\rangle = -\frac{2Ll}{\pi^{\frac{1}{2}}} \sin\theta\{0.4x(I_0(\infty) - I_0(x)) + I_3(x)/x^2 - 0.6I_5(x)/x^4\}, \tag{7}$$

where L and $I_n(x)$ are defined in Eqs. (29) and (37) of CSR.

If these values of the diffusion coefficients are substituted into $K(ff)$, Eq. (1) yields, after considerable algebra, the equation

$$D''(x) + P(x)D'(x) + Q(x)D(x) = R(x) + S(x), \tag{8}$$

exactly as in Eq. (41) of CSR; x is defined as lv. While $P(x)$ is unchanged from the form given in Eq. (42) of CSR, $Q(x)$ and $S(x)$ become

$$Q(x) = \frac{1}{x^2} - 2\frac{Z + \Phi(x) - 2x^3\Phi'(x)}{\Lambda}, \tag{9}$$

$$S(x) = \frac{16}{3\pi^{\frac{1}{2}}\Lambda}\{xI_3(x) - 1.2xI_5(x) - x^4 I_0(x)(1 - 1.2x^2)\}, \tag{10}$$

where $\Phi(x)$ is the error function, while $\Lambda(x)$ is defined in Eq. (46) of CSR. If an electrical field is present,

$$R(x) = -(2x^4 A/Z\Lambda)\{Z - 1 + 1.2x^2\}, \tag{11}$$

where A is again given by Eq. (40) of CSR. If a temperature gradient is present, we have

$$R(x) = -(x^4 B/\Lambda)\{2.5 - x^2\}, \tag{12}$$

where

$$B = \frac{2k^2 T|\nabla T|}{\pi n_e e^4 \ln(qC^2)}; \tag{13}$$

qC^2 is given in Eq. (65), CSR.

TABLE II. Values of the velocity distribution function $D(x)$ when a temperature gradient is present.

	$ZD(x)/B$				
x	$Z=1$	$Z=2$	$Z=4$	$Z=16$	$Z=\infty$
0.10	0.0005906	0.0002306	···	···	0.0001245
0.11	0.0009023	0.0003630	···	···	0.0001821
0.12	0.001309	0.0005460	···	···	0.0002577
0.13	0.001821	0.0007914	···	···	0.0003546
0.14	0.002448	0.001110	···	···	0.0004764
0.15	0.003197	0.001515	···	···	0.0006271
0.16	0.004074	0.002016	···	···	0.0008108
0.17	0.005082	0.002624	···	···	0.001032
0.18	0.006225	0.003348	···	···	0.001295
0.19	0.007504	0.004200	···	···	0.001605
0.20	0.008922	0.005188	0.003095	0.002146	0.001968
0.22	0.01217	0.007601	0.004668	0.003156	0.002872
0.24	0.01596	0.01064	0.006744	0.004487	0.004052
0.26	0.02027	0.01434	0.009400	0.006199	0.005558
0.28	0.02508	0.01874	0.01270	0.008356	0.007442
0.30	0.03035	0.02384	0.01673	0.01103	0.009760
0.32	0.03607	0.02966	0.02152	0.01428	0.01257
0.34	0.04218	0.03616	0.02713	0.01818	0.01593
0.36	0.04865	0.04338	0.03360	0.02281	0.01991
0.38	0.05545	0.05126	0.04092	0.02824	0.02456
0.40	0.06254	0.05978	0.04916	0.03453	0.02995
0.44	0.07746	0.07866	0.06840	0.04995	0.04322
0.48	0.09302	0.09966	0.09116	0.06955	0.06024
0.52	0.1090	0.1224	0.1174	0.09370	0.08151
0.56	0.1250	0.1466	0.1468	0.1226	0.1075
0.60	0.1407	0.1717	0.1790	0.1565	0.1387
0.64	0.1558	0.1973	0.2134	0.1952	0.1754
0.68	0.1700	0.2228	0.2497	0.2386	0.2178
0.72	0.1829	0.2476	0.2871	0.2864	0.2663
0.76	0.1944	0.2714	0.3249	0.3384	0.3207
0.80	0.2036	0.2934	0.3624	0.3940	0.3809
0.88	0.2151	0.3296	0.4324	0.5135	0.5174
0.96	0.2139	0.3506	0.4896	0.6384	0.6703
1.04	0.1965	0.3502	0.5244	0.7584	0.8297
1.12	0.1587	0.3210	0.5252	0.8565	0.9800
1.20	0.0957	0.2546	0.4796	0.9096	1.099
1.28	+0.0021	+0.1414	0.3717	0.8858	1.156
1.36	−0.1289	−0.0302	+0.1834	0.7474	1.113
1.44	−0.3041	−0.2734	−0.1067	+0.4525	0.9167
1.52	−0.5339	−0.6040	−0.5240	−0.1736	+0.5060
1.60	−0.8268	−1.040	−1.098	−0.7999	−0.1966
1.76	−1.657	−2.320	−2.861	−3.313	−2.867
1.92	−2.921	−4.330	−5.752	−7.691	−8.061
2.08	−4.774	−7.366	−10.25	−14.79	−17.09
2.24	−7.448	−11.81	−16.98	−25.78	−31.69
2.40	−11.23	−18.18	−26.78	−42.20	−54.08
2.56	−16.5	−27.1	−40.6	−66.0	−87.05
2.72	−23.5	−39.3	−59.9	−99.4	−134.1
2.88	−33.2	−55.9	−86.0	−145.	−199.3
3.04	−46.0	−77.8	−121.	−207.	−287.9
3.20	−62.0	−106.	−166.	−290.	−405.8

From the principle of conservation of momentum the integral $I_0(\infty)$ can be evaluated in simple form. In the case of an electrical field, Eq. (39) of CSR becomes modified if Z differs from unity, and we have

$$I_0(\infty)=3\pi^{\frac{1}{2}}A/8Z. \tag{14}$$

If a temperature gradient is considered, then we have instead

$$I_0(\infty)=0. \tag{15}$$

IV. SOLUTION OF THE EQUATIONS

The method of numerical solution followed is, in principle, identical with that employed in CSR. For values of Z different from unity the functions $Q_{01}(x)$ and $Q_{02}(x)$ differed from those used previously, with somewhat different forms for the solutions $U(x)$ and $V(x)$. No changes in $P_{01}(x)$ or $P_{02}(x)$ were required. In each specific range the substitutions given below were the same for both electrical and thermal conductivity.

In the range $x\leqslant 0.80$, we have

$$Q_{01}(x)=(-3Z\pi^{\frac{1}{2}}/2x^3)-2/x^2, \tag{16}$$

$$U_1=(Z/x)^{\frac{1}{2}}I_3(Z^{\frac{1}{2}}\alpha/x^{\frac{1}{2}}), \tag{17}$$

$$V_1=(Z/x)^{\frac{1}{2}}K_3(Z^{\frac{1}{2}}\alpha/x^{\frac{1}{2}}), \tag{18}$$

where α^2 is again equal to $6\pi^{\frac{1}{2}}$. For the range $0.80\leqslant x<3.20$, we have

$$Q_{02}=-2(Z+1), \tag{19}$$

$$U_2=D_Z(i2^{\frac{1}{2}}x)\exp(x^2/2), \tag{20}$$

$$V_2=D_{-1-Z}(2^{\frac{1}{2}}x)\exp(x^2/2). \tag{21}$$

In Eqs. (20) and (21) $D_n(y)$ is the parabolic cylinder function, which, for any integral value of n, may be expressed in terms of the error function $\Phi(x)$ by means of the recursion formula.[5]

As before, two independent numerical solutions were computed, each satisfying the boundary condition for small x. A linear combination of these was taken to satisfy the boundary condition at $x=3.2$. The resulting values of the velocity distribution function are given in Table I for electrical conductivity and in Table II for thermal conductivity. For $Z=4$ the integration was started at $x=0.20$, and no values were computed for smaller x.

As Z becomes very large, the mutual electron interactions become unimportant, and the following simple formulas for a so-called Lorentz gas are applicable.

$$D(x)=x^4A/Z \text{ for electrical conductivity,} \tag{22}$$

$$D(x)=x^4B(2.5-x^2)/2Z \text{ for thermal conductivity.} \tag{23}$$

Hence, for ready comparison with the Lorentz gas, Table I gives values of $ZD(x)/A$, and Table II gives $ZD(x)/B$.

Also listed in Tables I and II are values of the velocity distribution function for Z equal to 16 and ∞. The latter values were found directly from Eqs. (22) and (23). Those for $Z=16$ were determined from an asymptotic series for $D(x)$ in increasing powers of $1/Z$, which we may write

$$D(x)=\sum_{n=1}^{\infty}\frac{d_n(x)}{Z^n}. \tag{24}$$

If Eq. (24) is substituted into Eq. (8) and coefficients of each power of Z are separately set equal to zero, each d_n is given as a function of d_{n-1}, the first and second derivatives of d_{n-1}, and certain integrals over d_{n-1}. The quantity d_1 is simply the value of $D(x)$ for a Lorentz gas, given by Eqs. (22) or (23); successive functions d_n were found by straightforward computation up to $n=4$.

V. RESULTS

In the presence of a weak electrical field $\mathbf{E}$ and a small temperature gradient ∇T, the current density $\mathbf{j}$ and the rate of flow of heat $\mathbf{Q}$ per unit area are given by

$$\mathbf{j}=\sigma\mathbf{E}+\alpha\nabla T, \tag{25}$$

$$\mathbf{Q}=-\beta\mathbf{E}-K\nabla T. \tag{26}$$

In terms of the velocity distribution function $D(x)$, j, summed over all electrons—see Eq. (61) of CSR—is given by

$$j=-2\pi^{-\frac{1}{2}}en_eC(2/3)^{\frac{1}{2}}I_3(\infty), \tag{27}$$

while for the heat flow Q we have

$$Q=\pi^{-\frac{1}{2}}mn_eC^3(2/3)^{5/2}I_5(\infty), \tag{28}$$

where e and m are the electron charge and mass, and C is the root mean square electron velocity. From the numerical values found for the integrals $I_3(\infty)$ and $I_5(\infty)$, values of the coefficients σ, α, β, and K may be determined.

It is convenient to express these transport coefficients in terms of their values in a Lorentz gas. In the case of an electrical field, we define

$$\gamma_E=ZI_3(\infty)/3A, \tag{29}$$

$$\delta_E=ZI_5(\infty)/12A. \tag{30}$$

When $Z=1$, γ_E is identical with the quantity γ introduced in CSR. In the corresponding case where a

TABLE III. Values of transport coefficients.

	$Z=1$	$Z=2$	$Z=4$	$Z=16$	$Z=\infty$
γ_E	0.5816	0.6833	0.7849	0.9225	1.000
γ_T	0.2727	0.4137	0.5714	0.8279	1.000
δ_E	0.4652	0.5787	0.7043	0.8870	1.000
δ_T	0.2252	0.3563	0.5133	0.7907	1.000
ϵ	0.4189	0.4100	0.4007	0.3959	0.4000

[5] See section 16.7, E. T. Whittaker and G. N. Watson, *Modern Analysis* (Cambridge University Press, Cambridge, 1950).

temperature gradient is present, we write

$$\gamma_T = -4ZI_3(\infty)/9B, \tag{31}$$

$$\delta_T = -ZI_5(\infty)/15B. \tag{32}$$

From Eqs. (22) and (23) above the definition of $I_n(\infty)$—see Eq. (37) of CSR—it is readily verified that for a Lorentz gas all four of these coefficients are unity. On elimination of A and B by means of Eq. (40) of CSR and Eq. (13) above, we obtain, after some substitutions,

$$\sigma = \frac{2mC^3}{e^2Z\ln(qC^2)}\left(\frac{2}{3\pi}\right)^{\frac{1}{2}}\gamma_E, \tag{33}$$

$$\alpha = \frac{3mkC^3}{e^3Z\ln(qC^2)}\left(\frac{2}{3\pi}\right)^{\frac{1}{2}}\gamma_T, \tag{34}$$

$$\beta = \frac{8m^2C^5}{3e^3Z\ln(qC^2)}\left(\frac{2}{3\pi}\right)^{\frac{1}{2}}\delta_E, \tag{35}$$

$$K = \frac{20m^2kC^5}{3e^4Z\ln(qC^2)}\left(\frac{2}{3\pi}\right)^{\frac{1}{2}}\delta_T. \tag{36}$$

Values of the four transport coefficients are given in Table III for various values of Z.

The quantity qC^2, which is essentially h/b_0, is given in Eq. (65) of CSR, while values of $\ln(qC^2)$ are tabulated in Table IV of the same paper. The electron charge e has here been taken in electrostatic units throughout. To obtain the conductivity in practical units (mho) the value found from Eq. (33) must be divided by 9×10^{11}.

It should be noted that if a temperature gradient is present in a steady state, but no steady current is flowing, the electrostatic field E will build up to such a value that j vanishes. This field then reduces the flow of heat, and K', the effective coefficient of heat conductivity is readily shown to be

$$K' = \epsilon K, \tag{37}$$

where

$$\epsilon = 1 - 3\delta_E\gamma_T/(5\delta_T\gamma_E). \tag{38}$$

Values of ϵ are also given in Table III.

It remains to compare these results with those of previous workers. When this work was undertaken, the best available results for the electrical conductivity of a completely ionized gas were those of Chapman and Cowling[6] and of Cowling,[7] who had obtained first and second approximations, respectively, for the conductivity. In terms of the present notation, the Chapman-Cowling method utilizes the expansion

$$D(x) = \frac{3\pi^{\frac{1}{2}}x}{4}\sum_{j=0}^{n-1}(-1)^j\frac{\Delta_{0j}^{(n)}}{\Delta^{(n)}}L_j^{(3/2)}(x^2), \tag{39}$$

where $L_j^{(3/2)}$ is a Laguerre polynomial, and the ratios $\Delta_{0j}^{(n)}/\Delta^{(n)}$ are determined from encounter theory and the Boltzmann equation; n is the order of the approximation used. Since the value of σ found by Cowling[7] with $n=2$ was about twice the value obtained by Chapman and Cowling[6] with $n=1$, it appeared that the present treatment, equivalent to letting $n=\infty$ in Eq. (39), might give a markedly different value.

TABLE IV. Comparison with results obtained by Landshoff for $Z=1$.

n	1	2	3	4	∞
γ_E	0.2945	0.5693	0.5743	0.5777	0.5816

More recently, this same problem has been considered by Landshoff,[8] using the Chapman-Cowling method, but with values of n up to 4. From the values of $\Delta_{0j}^{(n)}/\Delta^{(n)}$ which he gives for $Z=1$, the constant γ_E has been computed, and is given in Table IV, together with the value found in the present work ($n=\infty$).

In view of the large difference between the first and second approximation, it is rather remarkable how close to the truth is the second approximation for γ_E. For thermal conductivity the convergence is somewhat less rapid, with the fourth approximation in close agreement with the value for $n=\infty$. Evidently the present results agree with Cowling's[7] second approximation for the electrical conductivity, provided that for the cutoff in the integration over the impact parameter b, we take the Debye shielding distance h rather than the electronic separation d taken by Cowling. The value 0.490 obtained for γ_E in CSR, in disagreement with Cowling's value 0.578, was the consequence of the neglect of the $\langle\Delta_i\Delta_j\rangle$ term in $K(ff)$; inclusion of this term removes virtually all the disagreement in γ_E.

It should be emphasized that the present theory considers only those terms in $\partial f_e/\partial t$ which are of order $\ln(h/b_0)$, and a variety of terms of order unity have been neglected, including, for example, the interaction between a high speed electron and its wake of plasma oscillation, an effect explored by Pines and Bohm.[2] Thus, the relative accuracy of the present theory does not exceed $1/\ln(h/b_0)$, or some 5 to 10 percent for most conditions of astrophysical interest. In view of the lack of observational data in this field, development of a more refined theory does not seem worth the very considerable effort required.

[6] S. Chapman and T. G. Cowling, *The Mathematical Theory of Non-Uniform Gases* (Cambridge University Press, Cambridge, 1939).

[7] T. G. Cowling, Proc. Roy. Soc. (London) **A183**, 453 (1945).

[8] R. Landshoff, Phys. Rev. **82**, 442 (1951).

An Enhanced Reactor

F. E. O'MEARA
Bendix Aviation Research Laboratories, Detroit, Michigan
(Received September 8, 1952)

The possibility of using a thermal uranium reactor to induce secondary fusion reactions is examined. Deuterons and tritons are accelerated by collisions with neutrons and fission fragments and the resulting $D-T$ reactions are calculated to yield 10^{-3} neutron per fission.

IN order to produce useful particles or energy from light element fusion, it is necessary to accelerate the nuclei in some fashion so that the reaction probability reaches some reasonable value. Two methods of doing this are (1) the ordinary laboratory procedure of electrically accelerating particles to high energies, and (2) the use of some high temperature trigger reaction, such as an atomic bomb, to raise the macroscopic temperature of the light nuclei to the point where their mutual reaction cross section becomes appreciable.

A third possibility, not previously mentioned, is the use of a thermal uranium reactor to induce secondary light element reactions on a controlled basis. If the kinetic energy of the recoiling fission fragments and fast neutrons can be used to accelerate some light nuclei, then a secondary reaction is possible which would release additional energy and neutrons.

The preliminary scheme studied consists of a thermal uranium reactor with enriched U^{235} as a fuel and a mixture of deuterium and tritium as a moderator. The actual composition of the moderator is not specified; however, the hydrogen density has been assumed to be the same as in water. In such a reactor the optimum hydrogen-uranium ratio is about 600:1, so that in a homogeneous reactor each uranium atom is effectively surrounded by hydrogen atoms. To a first approximation such a chain reaction will proceed in a normal manner, with the hydrogen (H^2 and H^3) merely slowing down the fission neutrons by elastic collisions and the only energy release being from the direct uranium fissions.

If the reactions are examined in greater detail, it is seen that deuterons and tritons will be accelerated by collisions with the fission fragments and fast neutrons and, as accelerated particles, can react in a $D-T$ reaction releasing energy and neutrons. These possible reactions have been examined in order to obtain some quantitative estimate of their importance.

Fission fragments slow down by two distinct processes. The first is by electronic excitation and ionization of the moderator atoms and the second is by nuclear collisions. According to Bohr's theory of fission fragment energy loss,[1] the first process is the dominant one until the fragments have slowed down to a velocity equal to the electronic velocity of the most loosely bound electron in the atomic shell. This is approximately 2.2×10^8 cm/sec and corresponds to an energy of 2.4 Mev for the light fission fragment of mass 95 and initial energy 97 Mev. After this energy is reached the fission fragment reactions with the electronic cloud are primarily adiabatic and the energy loss mechanism becomes the elastic nuclear collision process. For the light fragment colliding with tritons, the average energy loss per collision is 0.059. By calculating this series of collisions, multiplying by the appropriate cross section[2] and integrating, the total yield of secondary neutrons is found to be 0.97×10^{-4} neutrons/fission fragment.

The slowing down of the fission neutrons takes place only by elastic collisions (ignoring possible inelastic collisions) and there is no electronic collision term to be calculated. The elastic collisions result in an average loss per collision with tritons of 0.375. Assuming an average fission neutron energy of 2.3 Mev at birth, this series of collisions is calculated and operated upon in the same fashion as the fission fragment collisions. The net result is a total yield of 3.25×10^{-4} neutron/fission neutron. Summing these yields for the two fission fragments and the 2.5 neutrons per fission gives a total yield of 1×10^{-3} neutron/fission.

Although this is a rather small increment to the uranium chain reaction, it is not an impossible line of development. The calculations are admittedly rough and might be in error by an order of magnitude. There may be some method of developing a very high localized temperature which would increase the reaction cross section. There may be some alternative accelerator-induced reaction which would yield high energy fragments or neutrons by fission or spallation, thus giving higher yields. Finally, there may be other reactions than the $D-T$ one with more favorable yields at the energies considered.

[1] N. Bohr, Phys. Rev. **58**, 654 (1940).
[2] Hanson, Taschek, and Williams, Revs. Modern Phys. **21**, 635 (1949).

The Gamma-Rays from Negative μ-Meson Capture in Lead*†

GERARD G. HARRIS‡ AND T. J. B. SHANLEY§
Palmer Physical Laboratory, Princeton University, Princeton, New Jersey
(Received November 6, 1952)

The gamma-rays produced when a negative μ-meson stops in lead have been studied by means of a cloud chamber in a magnetic field. The presence of these gamma-rays is confirmed. It is concluded that both nuclear gamma-rays and Bohr orbit gamma-rays are necessary to explain the experimental data.

INTRODUCTION

IT is known that when a negative μ-meson is captured by a nucleus only a small fraction of the meson-rest mass appears as nuclear excitation.[1,2] It is also known that the meson-rest-mass energy is not emitted in the form of energetic gamma-rays.[3–5] There is nuclear plate evidence[6] that sometimes low energy protons are emitted, indicating a nuclear excitation of about 15 Mev and that on the average 1.9±0.7 low energy neutrons are emitted per meson capture in lead.[7–9] These experimental meson results are consistent with the charge exchange reaction for capture as proposed by Tiomno and Wheeler,[10] which has the form $\mu^-+P\rightarrow\mu^0+N$ where μ^0 is probably a neutrino. According to this hypothesis, most of the rest energy of the meson would be taken by the neutral particle, leaving the nucleus with about 15 Mev of excitation. The nucleus would then have lost its excitation by emitting one or two neutrons and rarely a proton. When the nuclear excitation is too low for neutron emission, low energy gamma-rays would be emitted. Tiomno and Wheeler have also shown that the excitation energy is roughly the same if the meson interacts with the whole nucleus rather than with a single proton.

Chang[2] has obtained evidence for the emission of low energy gamma-rays when a negative meson stops in lead. These may be due to Bohr orbit transitions of the meson around the nucleus. Hincks[11] has estimated the total energy of the gamma-rays emitted between 1 and 10 Mev to be near 9 Mev.

The present paper gives the results of a cloud-chamber experiment performed to investigate the nature of the low energy gamma-rays emitted when a negative meson stops in lead.

APPARATUS

The experimental apparatus, a general view of which is shown in Fig. 1 consists essentially of a cloud chamber in a magnetic field. A 1-cm lead plate is placed inside of the cloud chamber to stop and capture cosmic-ray mesons. Foils of lead are also placed in the cloud chamber so that gamma-rays from meson capture will occasionally produce pairs of Compton electrons. Thus, we would like to obtain cloud-chamber pictures which show a track stopping in the Pb plate and an electron track of the same age coming from one of the foils and tending to point back toward the meson stopping point. The cloud chamber is placed in a magnetic field so that the momentum and energy of the electrons may be determined. The energy spectrum of these electrons yields information about the gamma-rays which produce them.

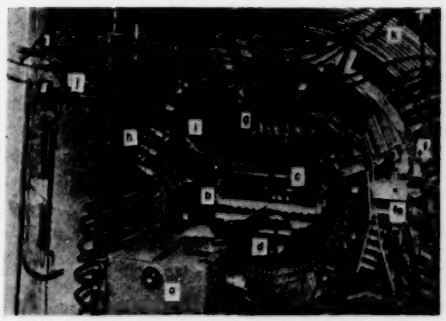

FIG. 1. Front view of the apparatus. (a) Camera; (b) mirror; (c) cloud chamber; (d) anticoincidence counters; (e) anticoincidence preamplifier; (f) tray 3 preamplifier; (g) tray 2 preamplifier; (h) water pipes for cooling coils; (i) coils; (j) compressed air valves; (k) lead shield.

* Assisted by the joint program of the U. S. Office of Naval Research and the U. S. Atomic Energy Commission.

† The experiment described in this paper was started by T. J. B. Shanley and preliminary results were obtained by him and submitted to the Department of Physics, Princeton University, in partial fulfillment of the requirements for the Doctor of Philosophy degree. G. G. Harris modified and improved the experimental arrangement and obtained the results reported in this paper. He submitted part of this material to the Department of Physics, Princeton University, in partial fulfillment of the requirements for the Doctor of Philosophy degree. It seemed advisable because of the continuity of the experiment to submit a single paper for publication.

‡ Now at the University of Bristol, Bristol, England.

§ Lieutenant Colonel now returned to duty with the United States Army and stationed at Fort Monroe, Virginia.

[1] Lattes, Muirhead, Occhialini, and Powell, Nature **159**, 694 (1947); Lattes, Occhialini, and Powell, Nature **160**, 453, 486 (1947).

[2] W. Y. Chang, Revs. Modern Phys. **21**, 166 (1949).

[3] R. D. Sard and E. J. Althaus, Phys. Rev. **73**, 1251 (1948).

[4] O. Piccioni, Phys. Rev. **74**, 1754 (1948).

[5] B. Pontecorvo, Phys. Rev. **73**, 257 (1948).

[6] E. P. George and J. Evans, Proc. Phys. Soc. (London) **A64**, 193 (1951).

[7] A. M. Conforto and R. D. Sard, Phys. Rev. **82**, 335 (1951).

[8] M. F. Crouch, Phys. Rev. **81**, 164 (1951).

[9] Groetzinger, Berger, and McClure, Phys. Rev. **81**, 969 (1951).

[10] J. Tiomno and J. A. Wheeler, Revs. Modern Phys. **21**, 153 (1949).

[11] E. P. Hincks, Phys. Rev. **81**, 313 (1951).

TABLE I. Summary of statistics from cloud-chamber photographs.

Number of pictures with particles stopping		9040
Number of pictures examined for meson curvature		2483
No curvature identified	1964	
Positive curvature	290	
Negative curvature	229	
Proportion of electrons and positrons stopping in the counter box		0.10±0.01
Positive decays from the counter box		
in an upward direction	450±20	
in a downward direction	120±30	
Positive decays in a foil	40	
Positive decay in the gas	3	
Negative mesons stopping in a foil	35	
Negative meson stopping in the gas	1	

A telescope of Geiger counters is used to control the expansion of the chamber. Two trays of Geiger counters above the cloud chamber and a third tray just above the lead plate which is inside the cloud chamber are connected in coincidence. These trays are placed so that an ionizing particle entering the cloud chamber from above will be counted by all of the trays. A fourth set of Geiger counters is placed around the bottom and sides of the cloud chamber to detect the ionizing particles which pass through the first three trays but do not stop in the chamber. The chamber is expanded when the first three trays of counters register simultaneously, but the fourth tray does not register. Six inches of lead or its equivalent in copper is placed above the cloud chamber so that most of the particles which stop in the cloud chamber will be μ-mesons.

The cloud chamber has a sensitive volume of 10 in. $\times$10 in.$\times$5 in. and is illuminated from the rear. It was originally designed for random expansions at high altitude[12] and has been modified for counter control by decreasing the expansion time. The third tray of Geiger counters, which is made from 14 counters each $\frac{1}{4}$ in. diameter$\times$7 in. sensitive length, is placed on top of the 1-cm plate and incased in a gas-tight box to provide adequate electrical shielding and to avoid turbulence. The 1-cm lead plate is a compromise in thickness. A thicker plate would stop more mesons, but the resulting gamma-ray spectrum would be altered more before leaving the plate. The lead foils are 0.0085 in. thick and are spaced 3 cm apart—two below the lead plate and one above. There is a 6-cm space above the top foil so that in favorable cases the sign of the stopping particle may be determined.

The cloud chamber was photographed by a camera which had its lens' optical axis $\frac{1}{2}$ in. to the left of the camera's horizontal front-rear axis of symmetry. This effect makes it possible both to photograph a mirror image for stereoptic purposes and to keep the optical axis of the lens parallel to the magnetic field at the chamber, thus minimizing errors on the photographed track curvature.

A magnetic field of 2000 gauss is produced by a current of approximately 180 amperes flowing through four coils. The coils act like a set of Helmholtz coils 28 in. in diameter and separated 14 in. With the cloud chamber placed in the center of this system, the magnetic field over the sensitive volume is uniform to within two percent. The coils are water-cooled with the rate of water flow controlled by a motorized valve which is regulated by a temperature sensitive element placed near the cloud chamber. All of the equipment with the exception of the electronic control circuits and the dc generator was in a temperature controlled room.

[12] R. R. Rau, Rev. Sci. Instr. **23**, 443 (1952).

MEASUREMENT, CALCULATION, AND ERRORS

All photographs of cloud-chamber expansions triggered by the coincidence-anticoincidence circuit were examined for interesting pictures. An event was selected for measurement if (1) the direct and stereo pictures showed the tracks clearly, (2) the electron track was in a favorable part of the chamber, and (3) both tracks appeared to be of the same age.

To find the curvature of an electron track, two points on the track were selected and the chord and sagitta defined by the points were measured. To compute the angle of the track with respect to the magnetic field, the depths of the two points were determined by measuring the parallax of each point from a mark on the front of the foil system. A Bausch and Lomb contour measuring projector, which enabled distances on the film to be accurately determined, was used for all measurements. The calculations of the electron energy from the curvature are made in the usual manner. However, some corrections might be mentioned. The path of a charged particle in a magnetic field being a helix, it is necessary to measure both the radius of the helix and its pitch in order to find the momentum of the particle. If a helix is photographed, the image will be in the form of a spiral with an apparent curvature different from the real curvature. Moreover, in most cases the helix is photographed inclined to its axis, thus further affecting the apparent curvature. Corrections for both effects have been applied to the curvature measurements.

One angle is also found, i.e., the angle that the electron makes with the normal to a foil as it emerges from the foil.

The main error in the determination of the electron energy is due to multiple scattering in the gas. There is an unknown energy loss in the foil in which the electron originated. Since the path length in the foil is unknown, it is assumed that each electron track was produced in the middle of the foil. Thus, the energy loss of an electron, traversing a distance equal to half a foil thickness divided by the cosine of the angle the electron makes with the foil, is added to the measured energy and to the error in energy. The errors incurred in the film measurement and in the magnetic field measurement are not large and total to about 5 percent for all tracks.

The most important error in angle determination is

caused by the multiple scattering of the electron in the foil. When the equation given in Rossi and Greisen[13] is used, it is found that the root mean square angle of multiple scattering is larger than 35° for an electron of 5 Mev traversing half of a foil thickness. This large angle of multiple scattering prohibits firm conclusions which depend upon the angular distribution of the electron tracks.

DATA

During operation of the apparatus, over 16 000 counter controlled pictures and over 6000 randomly operated pictures were taken. All of these pictures were examined once and most of them twice. Fifty-five percent of the counter controlled pictures showed a track stopping in the counter box. The remaining pictures were either blank or had tracks going through the counter box and out of the chamber. Most of the blank pictures are attributed to small showers in which a gamma-ray triggers the counters inside the cloud chamber. About 20 percent of the through tracks are due to the inefficiency of the anticoincidence counters, while the remaining through tracks are attributed to particles which stop in the matter (about 4 g cm^{-2}) between the lead plate and the anticoincidence counters. In a portion of the pictures the radius of curvature of the stopping track was recorded. The curvature of most tracks, however, cannot be judged because of distortions which were appreciable for radii of curvature of about one meter. By virtue of large curvature and minimum ionization, a portion of the stopping tracks were classified as positrons or electrons. A picture is counted as a positive meson decay if there is a positron associated with the stopping track. The statistics on curvature, etc., are given in Table I.

From Table I the positive to negative meson ratio is found to be

$$\mu^+/\mu^- = 1.27 \pm 0.11. \quad (1)$$

This ratio, together with the proportion of stopped particles which are electrons or positrons and the total number of stopped tracks, yields the number of stopped mesons of each charge. It is found that there are $4530 \pm 300 \mu^+$ tracks and $3580 \pm 300 \mu^-$ tracks. Two of the the negative mesons which stopped in a foil showed a low energy electron coming from the stopping point. The electrons are probably from Compton collisions by the gamma-rays from negative meson capture and are included in the events.

None of the pictures showed heavily ionizing tracks coming from the meson stopping point. George and Evans[14] find that 8.7 percent of the negative mesons which stop in photographic plates have low energy protons (1–10 Mev) associated with them. However, our data are not inconsistent with theirs since the foil thickness is equal to the range of a 6-Mev proton.

The positive to negative meson ratio [Eq. (1)] is for particles stopping in the 1-cm lead plate after they have passed through 15-cm lead equivalent above the chamber and so includes a momentum range of about 200–220 Mev/c. This ratio is lower than the positive meson excess in the atmosphere because energetic decay positrons from stopped positive mesons may trigger the anticoincidence circuit and thus some positive mesons will be missed. As a lower estimate of the number of missed positive mesons we note from Table I that 450 ± 20 mesons decayed in the upward direction and 120 ± 30 decayed in the downward direction. So 330 ± 35 decayed in the downward direction and were missed. If this is added onto the number of positive mesons, the positive to negative ratio becomes

$$\mu^+/\mu^- = 1.36 \pm 0.12. \quad (2)$$

This result is insensitive to the percentage of protons which stopped in the counter box, since a stopping proton has too small a curvature and too large an ionization to be counted as a positive meson. The above μ^+/μ^- ratio is consistent with the results of others,[15–17] although it is not accurate enough to distinguish between a constant μ^+/μ^- ratio from 200 Mev/c to 10

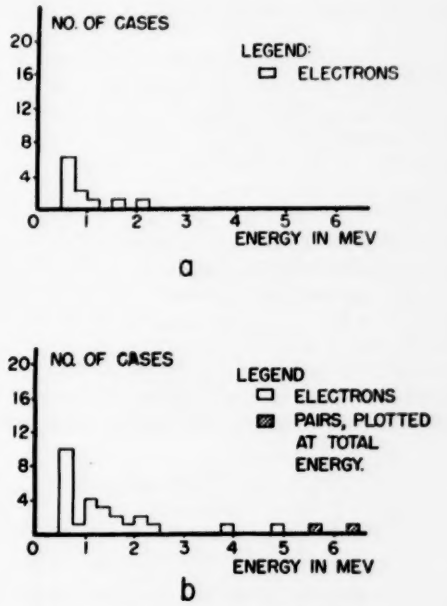

FIG. 2. (a) Histogram of events having single electrons with energy >0.5 Mev, associated with 950 ± 100 stopped positive mesons, plotted in 0.25-Mev intervals. (b) Histogram of events having single electrons and pairs of electrons with energy >0.5 Mev, associated with 750 ± 80 stopped negative mesons, plotted in 0.25-Mev intervals.

[13] B. Rossi and K. Greisen, Revs. Modern Phys. **13**, 240 (1941).
[14] E. P. George and J. Evans, Proc. Phys. Soc. (London) **A64**, 193 (1951).
[15] R. B. Brode, Phys. Rev. **78**, 92 (1950).
[16] Glaser, Hamermesch, and Safanov, Phys. Rev. **80**, 625 (1950).
[17] B. G. Owen and J. Wilson, Proc. Phys. Soc. (London) **A62**, 601 (1949).

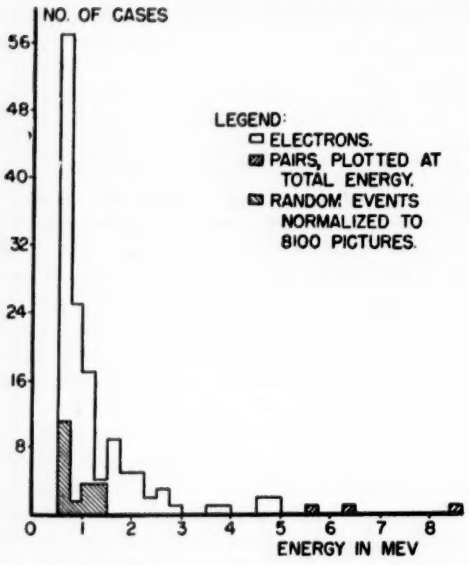

FIG. 3. Histogram of all events having single electrons and pairs of electrons with energy >0.5 Mev associated with stopped mesons, plotted in 0.25-Mev intervals.

Bev/c and a ratio which increases with decreasing momentum.

Figure 2 shows histograms of electron tracks with energy greater than 0.5 Mev associated with stopping meson tracks of different sign. A careful survey of all events was made to determine the charge of the stopping particle. Only cases which showed a clear curvature were identified with a sign. From the information in Table I we can estimate the total number of identifiable positive mesons. The events associated with a positive stopping track are attributed to this number of mesons. A similar number was estimated for the electrons associated with a negative stopping track. Figure 3 shows the histogram of the electron tracks of the correct age found in the random expansions normalized to the number of stopped mesons together with a histogram of all electron tracks associated with stopping mesons.

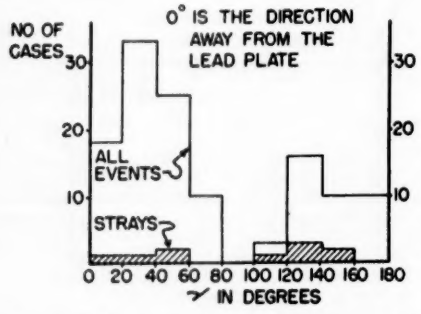

FIG. 4. Histogram showing the distribution of γ, the angle between the vertical and the electron track.

A histogram of the angular distribution with respect to the vertical direction is shown in Fig. 4. In spite of the multiple scattering, it is evident that there is a rough angular correlation. In Fig. 4 the zero angle is taken as away from the lead plate, i.e., upwards above the plate and downwards below the plate. The greater number of events have $\gamma<90°$, which supports the hypothesis that the parent photons come from the lead plate.

Three cases of pairs associated with a stopping meson were found and are listed in Table II. In Fig. 5 a meson stops in the first foil and a pair comes from the foil. The electron track could be caused by a positron from the lead plate which scatters in the first foil and then in the lead plate, but the picture is taken as a pair because of the small chance of a meson stopping in a foil with a scattered positron which is space and time coincident. The other two pictures attributed to pairs show two tracks of different energy coming from the same point. The more energetic track tends to point back at the stopping meson. These two pictures were selected as pairs because of this angular correlation and because, if one particle is assumed to produce the event by scattering, the particle would suffer an improbable energy loss.

There are too few pairs to draw any conclusions. Event A is consistent with a 4.5-Mev Bohr orbit transition but may also be due to a nuclear gamma-ray. The same may be said for event C. Event B has higher energy than might be expected from negative meson capture, and, since the charge of the stopping meson is unknown, it could be attributed to bremsstrahlung from a decay positron.

ANALYSIS OF THE DATA

Given an electron spectrum, our problem is to find the spectrum of parent gamma-rays which produce the electrons by the Compton and photoelectric effects. Now, for a particular gamma-ray energy the photoelectric effect gives a unique electron energy. However, monoenergetic gamma-rays produce a continuous spectrum of Compton electron energies. It is difficult, therefore, to determine a unique gamma-ray spectrum from an electron spectrum in a direct manner. Rather, our approach will be to assume a gamma-ray spectrum, calculate the resulting electron distribution, and see if it is consistent with the data.

We wish to test the hypothesis that when a negative meson is captured by a lead nucleus, gamma-rays are emitted both from Bohr orbit transitions of the meson around the nucleus and from the nucleus after meson capture. We, therefore, calculate the expected electron spectra from Bohr orbit and nuclear gamma-rays. Since the gamma-rays originate in the lead plate, some will be absorbed. A portion of these will give secondary gamma-rays of lower energy which will be added to the original spectrum. Of the number that leave the lead

plate, only a small fraction will produce electrons in the foils.

Our data show that there are a number of electron tracks associated with stopping positive mesons. These electrons are attributed to bremsstrahlung gamma-rays from decay positrons (about 80 percent of these positrons do not get out of the lead plate) and to radiation from positrons which are annihilated in flight. The annihilation spectrum, however, is similar in shape to the electron spectrum due to bremsstrahlung, but about one-tenth the magnitude, so only bremsstrahlung is considered. A spectrum due to stray gamma-rays is also estimated.

The photoelectric effect, Compton effect, and pair production are important in the energy range from 1–10 Mev. In particular, gamma-rays produced in the lead plate will be absorbed by all three processes. However, we assume that only gamma-rays which are absorbed by the Compton process will produce additional gamma-rays.

The differential radiation probability for electrons of 1 to 50 Mev is difficult to estimate accurately. Rossi and Greisen[13] have calculated the differential radiation

TABLE II. Energy of observed pairs.

	Energy in Mev	Sign of stopping track	γ-ray energy in Mev
A	$e^+=3.8\pm0.8$ $e^-=0.8\pm0.5$	negative	5.6 ± 1.2
B	$e^+=0.4\pm0.3$ $e^-=7.0\pm1.1$	unknown	8.4 ± 1.4
C[a]	$e^+=2.4\pm0.5$ $e^-=2.9\pm0.7$	negative	6.4 ± 1

[a] In event *C* a negative meson stops in a foil and the pair starts from the same point.

probability per radiation length $\rho(v)dv$ for an electron of 10 Mev and found it to be approximated by the formula

$$\rho(v)dv=(4/3)(1-v)dv/v, \tag{3}$$

where v is defined as the ratio W/E of the energy of the secondary photon to the total energy of the electron. The energy loss by collisions from 1 to 50 Mev is well approximated by

$$(dE/dx)_{\text{coll}}=-1.5 \text{ Mev/g cm}^2. \tag{4}$$

From these assumptions the expected electron spectrum ejected from the foils by bremsstrahlung gamma-rays is calculated and is shown in Fig. 6. This is the number expected per Mev per positron, which loses all its energy in the lead, and has to be multiplied by the number of positive mesons stopping in the lead plate and by the fraction of absorbed positrons per stopped positive meson. We can check this spectrum by comparing it with the data due to stopped positive mesons, which represent the electrons from 950 ± 100 mesons. The total number of electrons from 0.75–10 Mev expected for 950 mesons is found to be 10.8 electrons.

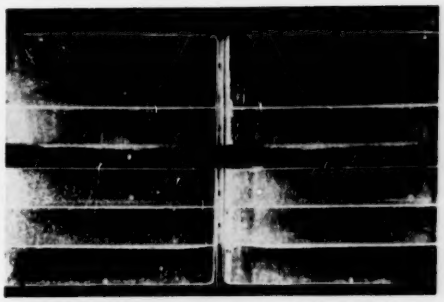

FIG. 5. A heavily ionizing negative particle stops in the first lead foil. An electron-positron pair emerge from the stopping point and enter the counter box. The energy of the photon which produced the pair is calculated to be 6.4 ± 1 Mev (event *C* in Table II).

The actual number of electrons observed was 5 ± 2. In order to apply a correction for the positive mesons, we assume that the shape of the spectrum is correct and that only its absolute magnitude is in error. If η is a normalization factor and σ is the efficiency for detecting electrons, then $\eta\sigma=0.46$. Since the efficiency as determined by the spectrum from negative mesons is close to 1, η must be close to 0.46. There are two factors which help to explain the small η. (1) High energy decay positrons tend to escape from the plate so that the spectrum absorbed in the plate has a low average energy. (2) If a decay positron is traveling in a direction such that a bremsstrahlung gamma-ray would pass through a foil, it has a larger than average chance of escaping from the plate and so would not be as likely to produce bremsstrahlung gamma-rays.

It is necessary to know three things about an excited nucleus in order to calculate the gamma-ray spectrum. None of these factors is known precisely. The first is the nuclear excitation energy. After a lead nucleus captures a negative meson, it will have about 15 Mev of excitation. According to Bethe,[18] in heavy elements neutron emission predominates over photon emission when the nuclear excitation is greater than the neutron dissociation energy by only a few kev. Since the disso-

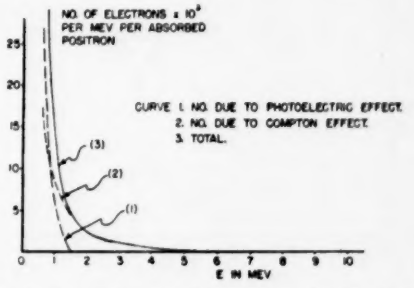

FIG. 6. Number of electrons of energy *E* produced in the foils by bremsstrahlung from a 37-Mev positron absorbed in the lead plate.

[18] H. Bethe, Revs. Modern Phys. **9**, 160 (1937).

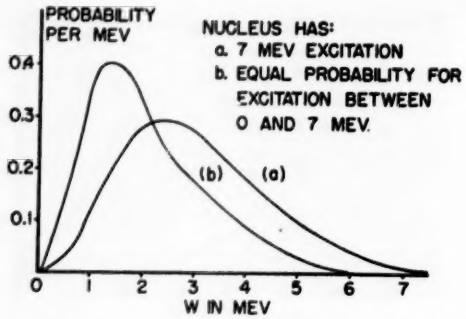

FIG. 7. First photon spectra from a heavy nucleus. Dipole radiation and energy level density $\sim\exp(1.2E)$ are assumed.

ciation energy for a lead nucleus is around 7 Mev, the nucleus will have an excitation ranging from 0 to 7 Mev after particle emission. The probability that it will have a particular energy is unknown. The second unknown factor is the type of radiation, i.e., dipole or quadrupole. The third is the energy level density $D(E)$ of the excited lead nucleus.

For simplicity in calculation, the following two sets of assumptions are made:[19] I dipole radiation with $D(E)\sim e^{1.2E}$ and all nuclei start with 7-Mev excitation; II dipole radiation with $D(E)\sim e^{1.2E}$ and the nuclei have any energy between 0 and 7 Mev with equal probability. The spectra for these models are calculated, assuming that each nucleus emits two photons. The first photon spectrum for each of these models is shown in Fig. 7.

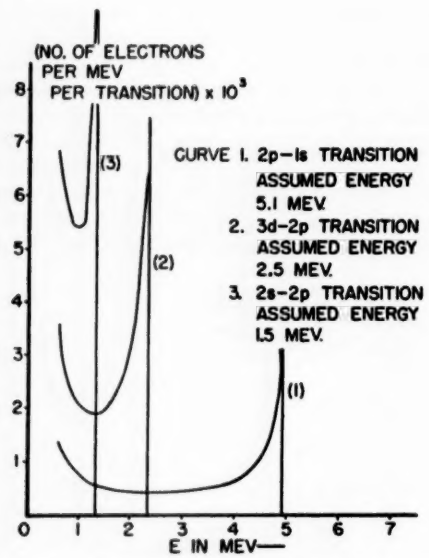
(NO. OF ELECTRONS PER MEV PER TRANSITION) x 10³
CURVE I. 2p–1s TRANSITION ASSUMED ENERGY 5.1 MEV.
2. 3d–2p TRANSITION ASSUMED ENERGY 2.5 MEV.
3. 2s–2p TRANSITION ASSUMED ENERGY 1.5 MEV.
(1)
(2)
(3)
8 7 6 5 4 3 2 1
0 1 2 3 4 5 6 7
E IN MEV

FIG. 8. Expected electron spectra from Bohr orbit transitions.

[19] There is some evidence for a level density $D(E)\sim e^{1.2E}$ for lead for the energy range 6–10 Mev from neutron emission experiments [see P. C. Gugelot, Phys. Rev. **81**, 51 (1951)].

Theory[10] predicts that when a negative meson is captured by a nucleus, there should be energetic Bohr orbit transitions. For lead there should be a $2p-1s$ transition of about 4.5 Mev for nearly every meson capture and a high probability of a $3d-2p$ transition of around 2.5 Mev or a $2s-2p$ transition of around 1.5 Mev. Because of the number of electrons between 4.5 and 5 Mev, a $2p-1s$ transition of 5.1 Mev is assumed and spectra calculated. However, because all the events between 3.5 Mev and 5.5 Mev are grouped together, the data is insensitive to the exact energy of the $2p-1s$ transition. Electron spectra are also calculated for 2.5 and 1.5 Mev gamma-rays. One of the calculated curves is shown in Fig. 8.

Our data indicates that the stray background electrons are not negligible. So we have assumed a spectrum of gamma-rays proportional to $1/W$, where W is the gamma-ray energy. This spectrum seems reasonable in view of the $1/W$ dependence of bremsstrahlung and also the fact that any Compton collisions will tend to build up the low energy portion of the spectrum rather than the high energy region. The calculated electron spectrum is normalized to the observed number of background events.

Only electrons with energy greater than 0.75 Mev are considered in the statistical analysis because both the errors in measurement and in calculation increase rapidly for lower energies. In order to test the consistency of various assumed photon spectra, the data is divided into groups. The various expected electron spectra are summed up over the same groups and the sums are listed in Table III. The bremsstrahlung spectrum has been multiplied by $\eta=0.46$. The background spectrum has been normalized to 9.6 electrons. Since in 5860 pictures there were 7 random events, in 8100 pictures, therefore, there should be 9.6 ± 3 events.

For the most general type of fit, suppose (1) that the $2p-1s$ transition occurs with every negative meson capture, (2) that the $2s-2p$ transition occurs a fraction f_1 of the time, (3) that the $3d-2p$ transition occurs a fraction f_2 of the time, and (4) that the nuclear photon spectra have a multiplying factor m. Let the efficiency for detecting an electron be σ.

If we assume that the meson reaches the $2p$ state either from the $2s$ or $3d$ state ($f_1+f_2=1$), then the condition that the total number of expected electrons should equal the observed number of electrons yields $m+0.084f_2=(1.92/\sigma)-1.01$ for nuclear model I. The most important variables are m and σ. If the efficiency is low, then m is large, which means a lot of energy in nuclear gamma-rays. Since we would expect $m<1.5$, we shall assume that the efficiency is unity.

Another condition is imposed by finding a weighted least square fit to the data which determines f_1, f_2, and m. The values found for both nuclear model I and model II are listed in Table IV.

The chi-square test is used as a statistical test of consistency. The quantity $\chi^2=\sum_i(x_i-n_i)^2/n_i$ is com-

TABLE III. Number of electrons expected and observed.

Assumed spectra		Group 1	2	3	4	5	6	7	8	Total
		Energy range in Mev								
		0.75–1	1–1.25	1.25–1.5	1.5–2	2–2.5	2.5–3.5	3.5–4.5	4.5–5.5	0.75–10.0
Bremsstrahlung	a_i[a]	9.00	4.63	2.60	2.73	1.57	1.97	0.84	0.31	23.8
Stray background	b_i	2.41	1.41	0.93	1.14	0.75	1.06	0.58	0.38	9.65
$2p-1s$ (5.1)[b]	c_i	0.81	0.58	0.46	0.79	0.75	1.62	2.57	2.31	9.89
$2s-2p$ (1.5)	d_i	5.19	6.65	1.29						13.10
$3d-2p$ (2.5)	g_i	2.20	1.76	1.74	4.72	4.62				15.0
Nuclear mod. I	j_i	4.86	3.72	2.79	3.65	2.72	3.54	1.14	0.28	22.7
Nuclear mod. II	j_i'	7.15	4.58	2.72	2.07	0.93	1.00	0.32	0.07	18.8
Data[c]	x_i	25	17	4	14	7	4	2	4	77

[a] a_i, b_i, etc., are the number of electrons expected in this experiment in each group i.
[b] The number in parentheses refer to the assumed transition energy in Mev.
[c] The actual number of electrons observed in each group.

puted, where x_i is the observed number of electrons in a group, n_i is the predicted number of electrons, and the sum is over all the groups. The function $F(\chi^2)$ gives the probability of finding in another set of data a χ^2 which is larger than the given χ^2, providing that the data is really from the assumed parent distribution. For a given χ^2 the values of $F(\chi^2)$ depend on the number of degrees of freedom in the data. In order that the values of $F(\chi^2)$ will be comparable, the same grouping is used for each assumed spectra. The results of these tests are listed in Table IV.

For the chi-square test to be reliable, the number of degrees of freedom N^1 and the expected value n_i of any group should not be too small. One criterion is that N^1 should be 4 or greater and that all n_i should be 5 or greater. In the tests listed in Table IV all N^1 are 4 or greater, but sometimes the n_i are less than 5. However, in all cases where an n_i is less than 5, a regrouping does not lead to substantially different results, so the original groupings are listed.

The total energy per μ^- capture emitted in gamma-rays from 0.75 to 7 Mev has been computed for the different spectra and is listed in Table IV. For this purpose the $2p-1s$ transition was assumed to be 5.1 Mev.

DISCUSSION AND CONCLUSIONS

By studying the energies and directions of the electrons associated with μ-mesons which stop in the lead plate of the cloud chamber, we conclude that these electrons are produced by photons with energy between 0.75 and 7 Mev which are also associated with the stopping mesons. By noting the sign of some of the stopping μ-mesons, we are able to confirm the existence of photons associated with the capture of negative μ-mesons in lead. More direct evidence for the existence of photons is given by two cloud-chamber pictures which show a negative meson stopping in an 0.0085-in. lead foil and an electron emerging from the same spot. Another picture shows a negative meson which stops in a foil with a pair coming from the stopping point.

Of the two spectra which were fitted to the data by the method of least squares, the spectrum using nuclear model II is the more consistent. The total energy emitted for this spectrum is 10.6 Mev which is consistent with the estimate of Hincks.[11] The fact that the nuclear gamma-ray spectrum which has more low energy gamma-rays fits the data best is a justification for the use of dipole radiation in the calculations, since quadrupole radiation would give a higher average energy.

When only nuclear photons are assumed, $F(\chi^2)\sim 0.08$ for both nuclear models. Not only are these distributions unlikely, but to account for the data the nucleus has to emit a total energy of 10.4 Mev for nuclear model I, where the nucleus has 7 Mev excitations, or a total energy of 7.2 Mev for nuclear model II, where the nucleus has an average energy of 3.5 Mev. These total energies are inconsistent with the assumed spectra. Again, when only Bohr orbit transitions are considered, $F(\chi^2)\sim 0.10$ which not only indicates a poor fit, but also means that the total energy emitted (13.2 Mev) is inconsistent with theory. From these two types of assumed spectra, we conclude that neither nuclear

TABLE IV. Summary of fits to the data.[a]

Assumed spectra	$\Sigma n_i=\Sigma x_i$	E_t	χ^2	N^1	$F(\chi^2)$
Bohr orbit transition and					
Nuc. mod. I	($m=0.87$, $f_3=0.45$)	11.7	7.59	4	0.10
Nuc. mod. II	($m=1.03$, $f_3=0.75$)	10.6	4.89	4	0.30
Nuclear gamma-rays alone:					
Nuc. Mod. I	$m=1.92$	10.4	9.37	5	0.10
Nuc. Mod. II	$m=2.32$	7.2	11.37	5	0.05
Bohr orbit transitons alone:	($M=1.84$, $f_3=0.56$)	13.2	7.99	4	0.10
No $2p-1s$ transition					
Nuc. mod. I	($m=1.30$, $f_3=0.46$)	9.0	7.01	4	0.13
Nuc. mod. II	($m=1.53$, $f_3=0.91$)	7.1	5.91	4	0.20
All stray background	$M=7.98$	···	11.57	5	0.04
All bremsstrahlung	$M=3.24$	10.0	9.20	5	0.10
		($2p-1s=5.1$ Mev)			

[a] $\Sigma n_i=\Sigma x_i$ is the condition that the total number of predicted electrons should equal the total number of observed electrons. To make this equation hold the following multiplying factors are used: f_3 is the coefficient for the $3d-2p$ transition spectra. f_1 is the coefficient for the $2s-2p$ transition spectra, which is found from the equation $f_1+f_3=1$. m is the multiplicity coefficient for the nuclear spectra. M is the normalizing factor when applied to the whole spectrum. The values of m and f_3 listed for the first two spectra are determined with the additional condition that the assumed spectra make a weighted least square fit to the data. E_t is the total energy in Mev per μ^- meson capture in lead emitted by photons between 0.75 and 7 Mev. χ^2 is defined by the sum $\chi^2=\Sigma(n_i-x_i)^2/n_i$. N^1 is the number of degrees of freedom of the statistical sample for purposes of the chi-square test. $F(\chi^2)$ is a statistical measure of consistency. It gives the probability of finding another χ^2 which is larger than the given χ^2 if the experimental data really comes from the assumed source.

gamma-rays alone nor Bohr orbit transitions alone will explain the observed spectra. This conclusion is based on the assumption that the residual thallium nuclei are not unstable with a lifetime short enough to be within the resolving time of the cloud chamber ($\sim$0.05 second). It is unlikely that there are such short lifetimes among the residual nuclei. If we take the experimental evidence on the emission of neutrons and protons from meson capture, then from a Segrè chart the most unfavorable lifetime is about three minutes.

Nothing definite can be said about the existence of a $2p-1s$ Bohr orbit transition. For if the $2p-1s$ transition is emitted from the assumed spectra the spectra which remain are consistent with the data. The data is consistent with the assumed spectra being totally due to bremsstrahlung photons from positrons and stray background photons. It is extremely unlikely, however, that the data could be accounted for by stray background photons alone, and the data could not be accounted for by bremsstrahlung photons alone because of the large numbers of electrons associated with negative mesons.

We wish to thank Professor R. Ronald Rau for encouragement and helpful discussions. We are grateful to Professor George T. Reynolds and Dr. J. W. Keuffel and Dr. Georgio Salvini for assistance.

PHYSICAL REVIEW VOLUME 89, NUMBER 5 MARCH 1, 1953

The Acousto-Electric Effect*

R. H. PARMENTER
Massachusetts Institute of Technology, Cambridge, Massachusetts
(Received November 25, 1952)

A new effect, the acousto-electric effect, is predicted on the basis of theoretical calculations. This effect deals with the generation of an electric current by a traveling longitudinal acoustic wave. The time-average of the generated current is found to depend on the sound power but not on the frequency of the acoustic wave. Illustrative calculations on a metal (sodium) and a semiconductor (n-type germanium) indicate that the effect should be experimentally measurable. An interesting analogy with the thermoelectric effect is pointed out.

I. INTRODUCTION

IN this paper we discuss the effect on the conduction electrons of a crystal resulting from a single traveling longitudinal acoustic wave in the crystal. It is not difficult to see qualitatively how the electrons will be affected when the amplitude of the acoustic wave is small. The presence of a sinusoidal traveling acoustic wave gives rise to a sinusoidal electric field, this field traveling through the crystal with the same velocity as that of the acoustic wave. Consider the component of velocity of a conduction electron parallel to the velocity of the acoustic wave. For most of the conduction electrons, this component of velocity will be much larger in magnitude than the speed of the acoustic wave, so that these electrons are "out of phase" with respect to the traveling electric field. Thus, the time average of this field over their trajectories is zero, and these electrons are essentially unaffected by the presence of the acoustic wave. There are a few electrons, however, having components of velocity parallel to the wave which are comparable to the speed of the wave. These electrons are capable of being trapped by the moving electric field so that their time-averaged velocity in the direction of the field is exactly that of the field. Among these electrons, those having a maximum energy will be found to give rise to a net electric current. In a metal, these electrons are at the Fermi level. In an n-type semiconductor, these electrons are in the conduction band. Such a generation of an electric current by a traveling acoustic wave may be called the acousto-electric effect. It is interesting that the qualitative explanation of this effect which has just been given is analogous to the qualitative explanation of the operation of a linear accelerator.[1]

Let us consider a single traveling longitudinal acoustic wave moving along a long uniform rod of material, the ends of the rod being electrically insulated. The traveling acoustic wave could be induced by driving one end of the rod with a vibrator while matching the other end to the proper acoustic impedance to insure no reflection of the wave at the termination. The ends of the rod being electrically insulated, the acoustic wave would drag conduction electrons to one end of the rod, creating a deficiency of electrons at the other end. The resultant electric field along the rod will generate a conventional electric current which exactly cancels the current associated with the acousto-electric effect. The acousto-electric effect, therefore, may be measured by determining the electric potential difference between the two ends of the rod. An interesting comparison pointed out to the writer[2] is the striking analogy between this

* This work was supported by the U. S. Office of Naval Research.

[1] J. C. Slater, Revs Modern Phys. **20**, 473 (1948). See especially p. 483.
[2] H. Brooks, private communication.

potential difference and that occurring in the thermoelectric effect when the two ends of a metal rod are maintained at different temperatures. The net flow of phonons along a temperature gradient may be considered as a net flow of traveling acoustic waves along the gradient.

II. THE PERTURBATIVE POTENTIAL

In order to discuss the acousto-electric effect quantitatively, wave mechanics is necessary. We will use the one-electron approximation in solving Schrödinger's equation. Thus, a conduction electron of the crystal is assumed to move in an effective potential resulting from the nuclei plus all the other electrons of the crystal. We will assume that this potential $V(\mathbf{r}, t)$ may be written

$$V(\mathbf{r}, t)=V_0(\mathbf{r})+V_1(\mathbf{r}, t), \tag{1}$$

where $V_0(\mathbf{r})$ is the correct potential in the absence of the traveling acoustic wave and $V_1(\mathbf{r}, t)$, the perturbative potential, is an additional term resulting from the presence of the acoustic wave. We will make the approximation that V_1 is a slowly varying function of position (on the atomic scale).

The perturbative potential can be broken into two parts,

$$V_1=V_{1a}+V_{1b}, \tag{2}$$

where V_{1a} results from the charge unbalances set up by the acoustic wave, while V_{1b} results from the changes in interatomic spacing set up by the acoustic wave. We shall first determine V_{1a}.

Consider a simple longitudinal traveling acoustic wave

$$\mathbf{s}=\mathbf{S}\sin\boldsymbol{\sigma}\cdot(\mathbf{r}-\mathbf{C}t), \tag{3}$$

where the displacement $\mathbf{s}$, the amplitude $\mathbf{S}$, the acoustic wave vector $\boldsymbol{\sigma}$, and the wave velocity $\mathbf{C}$ all have the same direction. Let $\rho_+(\mathbf{r}, t)$ be the macroscopic charge density resulting from the ion cores of the crystal, an ion core being an atom of the crystal without its conduction electrons. If ρ_0 is the average value of ρ_+, then

$$(\rho_+-\rho_0)/\rho_0=-\nabla\cdot\mathbf{s}, \tag{4}$$

i.e., the fractional variation of the ion-core charge density equals the negative of the dilation $\nabla\cdot\mathbf{s}$. This variation of the ion-core charge density from its average value will be partially, but not completely, cancelled by a corresponding variation of the conduction-electronic macroscopic charge density $\rho_-(\mathbf{r}, t)$ from its mean value $-\rho_0$. This question has been discussed by Bardeen,[3] who points out that for decreasing acoustic wavelength (increasing σ) the cancellation becomes less complete. We will assume that this effect may be expressed as

$$(-\rho_--\rho_0)/(\rho_+-\rho_0)=g(\boldsymbol{\sigma}). \tag{5}$$

We know that for infinite wavelength ($\sigma=0$) cancellation will be complete so that $g(0)=1$. For finite wavelength cancellation will be incomplete so that $g<1$. Since g should be independent of the orientation of $\boldsymbol{\sigma}$, it may be expanded as a power series in σ^2.

$$g(\boldsymbol{\sigma})=1-\beta\sigma^2+\cdots. \tag{6}$$

Having determined the macroscopic charge density $(\rho_++\rho_-)$ resulting from the acoustic wave, we may now obtain V_{1a} from Poisson's equation[4]

$$(\rho_++\rho_-)=(\epsilon/8\pi)\nabla^2V_{1a}, \tag{7}$$

where ϵ is the dielectric constant. Equations (4), (5), (6), and (7) give

$$\mathbf{s}=-(\epsilon/8\pi\rho_0\beta\sigma^2)\nabla V_{1a}. \tag{8}$$

Substituting (3) into (8) gives

$$V_{1a}(\mathbf{r}, t)=\mathcal{U}_a\cos\boldsymbol{\sigma}\cdot(\mathbf{r}-\mathbf{C}t), \tag{9}$$

where

$$\mathcal{U}_a=(8\pi\beta\rho_0/\epsilon)(\boldsymbol{\sigma}\cdot\mathbf{S}). \tag{10}$$

In order to determine V_{1b}, we make use of the idea of a deformation potential as suggested by Bardeen and Shockley.[5] A uniform dilation or compression of a crystal will cause the bottom (or top) of some energy band of the crystal to shift its energy. For sufficiently small dilations the shift in energy of a given portion of the band will be directly proportional to the dilation. Starting with the potential acting on an electron in the undilated crystal, we can correctly express the effect of the dilation on a given portion of the band by adding to the original potential a constant perturbative potential equal to the shift in energy of that portion of the band. This perturbative potential is called a deformation potential. The assumption is now made that such a procedure is also valid for non-uniform dilations of the crystal, whereupon a non-uniform deformation potential is required. This assumption seems plausible provided that the dilation varies very slowly with position (on the atomic scale); i.e., the dilation results from a long wavelength acoustic wave. Taking V_{1b} proportional to the dilation, we have[6]

$$V_{1b}=A'\nabla\cdot\mathbf{s}. \tag{11}$$

Substituting (3) into (11), we obtain

$$V_{1b}(\mathbf{r}, t)=\mathcal{U}_b\cos\boldsymbol{\sigma}\cdot(\mathbf{r}-\mathbf{C}t), \tag{12}$$

where

$$\mathcal{U}_b=A'(\boldsymbol{\sigma}\cdot\mathbf{S}). \tag{13}$$

[3] J. Bardeen, Phys. Rev. **52**, 688 (1937).

[4] Throughout this paper we will use atomic units; i.e. mass and charge are measured in units of the electronic mass and charge, respectively, energy is measured in Rydbergs (13.6 ev), distance in units of the Bohr radius, velocity in units of αc (the fine-structure constant multiplied by the velocity of light), time in units of $\hbar^3/me^4$, wave number in units of $me^4/2\pi\hbar^3$.

[5] J. Bardeen and W. Shockley, Phys. Rev. **80**, 72 (1950).

[6] We may disregard the fact that the constant of proportionality A' is a function of position in the band. It will later be shown that the acousto-electric effect results from conduction electrons lying in a very small energy range. Over such a small energy range A' may be assumed constant.

Equation (2) now gives

$$V_1(\mathbf{r}, t)=\mathcal{U}\cos\boldsymbol{\sigma}\cdot(\mathbf{r}-\mathbf{C}t), \tag{14}$$

and

$$\mathcal{U}=A(\boldsymbol{\sigma}\cdot\mathbf{S}), \tag{15}$$

where

$$A=A'+(8\pi\beta\rho_0/\epsilon). \tag{16}$$

III. THE WANNIER-SLATER THEOREM

Having determined $V(\mathbf{r}, t)$, we are in a position to write down Schrödinger's equation for the problem, namely

$$[-\nabla^2+V(\mathbf{r}, t)]\psi(\mathbf{r}, t)=2i\partial/\partial t\psi(\mathbf{r}, t). \tag{17}$$

The method we shall use in solving this equation was first used by Wannier[7] in studying excitons in crystals. The importance and generality of the method was first pointed out by Slater,[8] who showed that the motion of an electron in a periodic potential plus a slowly varying perturbative potential can be derived from the energy of the electron in the periodic potential alone. Slater restricted himself to time-independent perturbative potentials, but we can easily remove this restriction. In the absence of the traveling acoustic wave Schrödinger's equation is

$$[-\nabla^2+V_0(\mathbf{r})]\psi_0(\mathbf{k}, \mathbf{r}, t)=2i\partial/\partial t\psi_0(\mathbf{k}, \mathbf{r}, t), \tag{18}$$

where the wave vector $\mathbf{k}$ is a parameter determining the translational properties of the wave function; i.e.,

$$\psi_0(\mathbf{k}, \mathbf{r}+\mathbf{r}_n, t)=e^{i\mathbf{k}\cdot\mathbf{r}_n}\psi_0(\mathbf{k}, \mathbf{r}, t), \tag{19}$$

$\mathbf{r}_n$ being the position vector to the nth unit cell of the undeformed crystal. The wave function may be written in the form

$$\psi_0(\mathbf{k}, \mathbf{r}, t)=\textstyle\sum_n \Psi_0(\mathbf{k}, \mathbf{r}_n, t)a(\mathbf{r}-\mathbf{r}_n), \tag{20}$$

where

$$\Psi_0(\mathbf{k}, \mathbf{r}, t)=e^{i(\mathbf{k}\cdot\mathbf{r}-\frac{1}{2}E_0t)}. \tag{21}$$

$a(\mathbf{r})$ is the Wannier function,[7] while $E_0(\mathbf{k})$ (a function of $\mathbf{k}$) is the energy of the electron. Following Slater, we assume that in the presence of the traveling acoustic wave, the wave function can be expanded in terms of the Wannier function, i.e.,

$$\psi(\mathbf{k}, \mathbf{r}, t)=\textstyle\sum_n \Psi(\mathbf{k}, \mathbf{r}_n, t)a(\mathbf{r}-\mathbf{r}_n), \tag{22}$$

ψ being the solution to Eq. (17). The Wannier-Slater theorem states that

$$[E_0(-i\nabla)+V_1(\mathbf{r}-\mathbf{C}t)]\Psi(\mathbf{r}, t)=2i\partial/\partial t\Psi(\mathbf{r}, t). \tag{23}$$

This form of the theorem, including time explicitly, can be derived straightforwardly by the methods used in the appendix of reference 8. It is possible to determine the expectation values of the energy and the velocity of an electron in the deformed lattice from a knowledge of $\Psi(\mathbf{r}, t)$. In the appendix to this article it is shown that

$$E(\mathbf{k})=2i\int_\infty \Psi^*\frac{\partial}{\partial t}\Psi d\tau \Big/ \int_\infty \Psi^*\Psi d\tau, \tag{24}$$

$$\mathbf{v}(\mathbf{k})=\int_\infty \Psi^*\mathbf{v}_0(-i\nabla)\Psi d\tau \Big/ \int_\infty \Psi^*\Psi d\tau. \tag{25}$$

($\int_\infty d\tau$ denotes an integral over the entire crystal.) $\mathbf{v}_0(\mathbf{k})$, the velocity of an electron in the undeformed lattice, is given by

$$\mathbf{v}_0(\mathbf{k})=\tfrac{1}{2}\nabla_k E_0(\mathbf{k}). \tag{26}$$

At this point we will introduce the effective-mass approximation, i.e., over the filled portion of the conduction band $E_0(\mathbf{k})$ will be approximated by

$$E_0(\mathbf{k})=\alpha k^2. \tag{27}$$

Here the zero of energy is taken at the bottom of the band. Substituting (27) into (26), we get

$$\mathbf{v}_0(\mathbf{k})=\alpha\mathbf{k}, \tag{28}$$

whereupon (25) becomes

$$\mathbf{v}(\mathbf{k})=-i\alpha\int_\infty \Psi^*\nabla\Psi d\tau \Big/ \int_\infty \Psi^*\Psi d\tau. \tag{29}$$

Substituting (27) into (23), we get

$$[-\alpha\nabla^2+V_1(\mathbf{r}-\mathbf{C}t)]\Psi(\mathbf{r}, t)=2i\partial/\partial t\Psi(\mathbf{r}, t). \tag{30}$$

The power of the Wannier-Slater method lies in the interpretation we may attach to Eq. (30). It is clear that (30) may be interpreted as Schrödinger's equation for a particle of mass m/α moving in the potential $V_1(\mathbf{r}-\mathbf{C}t)$. ($m$ is the mass of the electron.) $\Psi(\mathbf{r}, t)$ is thus the wave function determining the motion of the particle. A comparison of Eqs. (24) and (29) with Eqs. (39) and (34), respectively, of Sec. IV shows that this particle of mass m/α moving in the potential V_1 has the same energy and velocity as an electron moving in the potential V_0+V_1. Henceforth we need concern ourselves only with the determination of Ψ rather than the true wave function ψ, since Ψ may be interpreted as a wave function for the purpose of determining expectation values of physical quantities.

IV. TRANSFORMATION OF SCHRÖDINGER'S EQUATION

In attempting to solve Eq. (30), we are faced with the problem that the equation is not separable since the Hamiltonian contains the time explicitly. The key to the method of attack is given by the observation that the time dependence of $V_1(\mathbf{r}-\mathbf{C}t)$ can be removed by the Galilean transformation

$$\mathbf{r}'=\mathbf{r}-\mathbf{C}t, \quad t'=t. \tag{31}$$

Let us therefore study the general properties of the

[7] G. H. Wannier, Phys. Rev. **52**, 191 (1937).
[8] J. C. Slater, Phys. Rev. **76**, 1592 (1949).

wave function Ψ under such a transformation, this wave function being associated with a particle of mass m/α moving in the potential $V_1(\mathbf{r}-\mathbf{C}t)$. Equation (30), the Schrödinger's equation for such a particle, will transform into

$$[-\alpha\nabla'^2+V_1(\mathbf{r}')]\Psi'(\mathbf{r}',t')=2i\partial/\partial t'\Psi'(\mathbf{r}',t') \quad (32)$$

with the aid of (31). We now ask ourselves for the relation between $\Psi(\mathbf{r},t)$ and $\Psi'(\mathbf{r}',t')$. This relationship is determined by the following three conditions:

(1) Equations (30) and (32) must be equivalent.

(2) The velocity of the particle of mass m/α as measured in one coordinate system must be related to its velocity in the other system by the equation

$$\mathbf{v}'=\mathbf{v}-\mathbf{C}, \quad (33)$$

where the velocity of the particle is given by

$$\mathbf{v}=-i\alpha\int_\infty \Psi^*\nabla\Psi d\tau \Big/ \int_\infty \Psi^*\Psi d\tau, \quad (34)$$

and similarly for $\mathbf{v}'$.

(3) Probability density must be invariant to coordinate transformations, i.e.,

$$\Psi'^*(\mathbf{r}',t')\Psi'(\mathbf{r}',t')=\Psi^*(\mathbf{r},t)\Psi(\mathbf{r},t). \quad (35)$$

These three conditions can be satisfied,[9] provided

$$\Psi'(\mathbf{r}',t')=\Psi(\mathbf{r},t)\exp[-i(\mathbf{C}\cdot\mathbf{r}-\tfrac{1}{2}C^2t)/\alpha]. \quad (36)$$

Condition (3) is obviously satisfied by Eq. (36). Condition (2) follows from (36) since

$$\begin{aligned}\mathbf{v}'&=-i\alpha\int_\infty \Psi'^*\nabla'\Psi' d\tau' \Big/ \int_\infty \Psi'^*\Psi' d\tau'\\ &=-i\alpha(-i\mathbf{C}/\alpha)-i\alpha\int_\infty \Psi^*\nabla\Psi d\tau \Big/ \int_\infty \Psi^*\Psi d\tau\\ &=\mathbf{v}-\mathbf{C}.\end{aligned}$$

Making use of the equations

$$\nabla'=\nabla, \quad (37)$$

$$\partial/\partial t'=\partial/\partial t+\mathbf{C}\cdot\nabla, \quad (38)$$

we have

$$\begin{aligned}&[-\alpha\nabla'^2+V_1(\mathbf{r}')-2i\partial/\partial t']\Psi'(\mathbf{r}',t')\\ &\quad=[-\alpha\nabla^2+V_1(\mathbf{r}-\mathbf{C}t)-2i\mathbf{C}\cdot\nabla-2i\partial/\partial t]\\ &\qquad\times\Psi(\mathbf{r},t)\exp[-i(\mathbf{C}\cdot\mathbf{r}-\tfrac{1}{2}C^2t)/\alpha]\\ &\quad=\exp[-i(\mathbf{C}\cdot\mathbf{r}-\tfrac{1}{2}C^2t)/\alpha][C^2/\alpha+2i\mathbf{C}\cdot\nabla\\ &\qquad-\alpha\nabla^2+V_1(\mathbf{r}-\mathbf{C}t)-2i\mathbf{C}\cdot\nabla-2C^2/\alpha\\ &\qquad+C^2/\alpha-2i\partial/\partial t]\Psi(\mathbf{r},t)\\ &\quad=\exp[-i(\mathbf{C}\cdot\mathbf{r}-\tfrac{1}{2}C^2t)/\alpha][-\alpha\nabla^2+V_1(\mathbf{r}-\mathbf{C}t)\\ &\qquad-2i\partial/\partial t]\Psi(\mathbf{r},t),\end{aligned}$$

so that condition (1) is satisfied by Eq. (36). The energy of a particle of mass m/α is given by

$$E=2i\int_\infty \Psi^*\frac{\partial}{\partial t}\Psi d\tau \Big/ \int_\infty \Psi^*\Psi d\tau. \quad (39)$$

We can now determine the transformation properties of E under a Galilean transformation. Thus,

$$\begin{aligned}E'&=2i\int_\infty \Psi'^*\frac{\partial}{\partial t'}\Psi' d\tau' \Big/ \int_\infty \Psi'^*\Psi' d\tau'\\ &=2i\int_\infty \Psi^*\frac{\partial}{\partial t}\Psi d\tau \Big/ \int_\infty \Psi^*\Psi d\tau\\ &\qquad+2i\mathbf{C}\cdot\int_\infty \Psi^*\nabla\Psi d\tau \Big/ \int_\infty \Psi^*\Psi d\tau+C^2/\alpha\\ &=E-2\mathbf{C}\cdot\mathbf{v}/\alpha+C^2/\alpha. \end{aligned} \quad (40)$$

In analogy with Eq. (19), we may define the wave vector $\mathbf{k}'$ in the transformed system by

$$\psi_0'(\mathbf{k}',\mathbf{r}'+\mathbf{r}_n,t')=e^{i\mathbf{k}'\cdot\mathbf{r}_n}\psi_0'(\mathbf{k}',\mathbf{r}',t'). \quad (41)$$

We may now apply Eqs. (19) and (41) to the case of a particle of mass m/α. Making use of Eq. (36), we get

$$\mathbf{k}'=\mathbf{k}-\mathbf{C}/\alpha, \quad (42)$$

so that $\mathbf{k}$ has the transformation properties of momentum.

V. SOLUTION OF SCHRÖDINGER'S EQUATION

Having transformed Eq. (30) into (32), we may separate variables in the wave function Ψ',

$$\Psi'(\mathbf{k}',\mathbf{r}',t')=e^{-\frac{1}{2}iE't'}\Phi'(\mathbf{k}',\mathbf{r}'). \quad (43)$$

Φ' satisfies the time-independent Schrödinger equation

$$[-\alpha\nabla'^2+V_1(\mathbf{r}')]\Phi'=E'\Phi'. \quad (44)$$

Let us orient our coordinate system such that the acoustic wave is moving along the x axis. Then we may write

$$\Phi'(\mathbf{r}')=\varphi_x'(x')\varphi_y'(y')\varphi_z'(z'), \quad (45)$$

$$E'=E_x'+E_y'+E_z', \quad (46)$$

where

$$[-\alpha\partial^2/\partial x'^2+V_1(x')]\varphi_x'=E_x'\varphi_x', \quad (47)$$

$$-\alpha\partial^2\varphi_y'/\partial y'^2=E_y'\varphi_y', \quad (48)$$

$$-\alpha\partial^2\varphi_z'/\partial z'^2=E_z'\varphi_z'. \quad (49)$$

Equations (48) and (49) give

$$\varphi_y'=\exp(ik_y'y'), \quad (50)$$

$$\varphi_z'=\exp(ik_z'z'), \quad (51)$$

$$E_y'=\alpha k_y'^2, \quad (52)$$

$$E_z'=\alpha k_z'^2. \quad (53)$$

[9] W. Pauli, *Handbuch der Physik* (Springer, Berlin, 1933), Vol. 24, Chap. 2, p. 100.

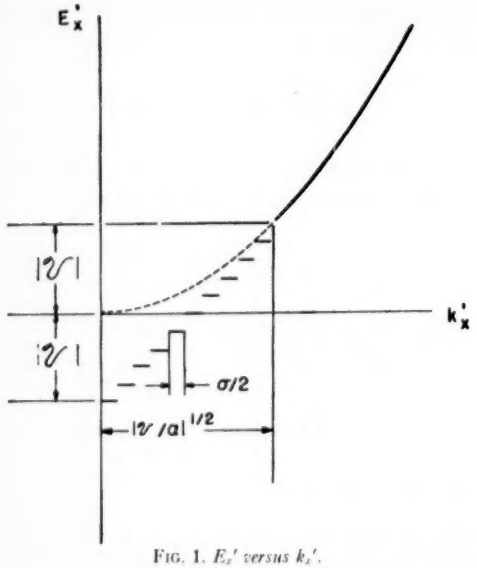

FIG. 1. E_x' *versus* k_x'.

Substituting Eq. (14) into (47), we get

$$[-\alpha\partial^2/\partial x'^2+\mathcal{U}\cos(\sigma x')]\varphi_x'=E_x'\varphi_x'. \tag{54}$$

Dividing Eq. (54) by α, we obtain an equation mathematically equivalent to Schrödinger's equation for an electron traveling in a one-dimensional sinusoidal potential (Mathieu's equation). This problem has recently been exhaustively studied by Slater,[10] whose results indicate that the following approximate conclusions may be drawn concerning the energy levels associated with Eq. (54). For energies larger (in absolute value) than the amplitude $|\mathcal{U}|$, the curve of E_x' *versus* k_x' is essentially unchanged from its form in the absence of the acoustic wave; i.e., $E_x'=\alpha k_x'^2$. For energies smaller (in absolute value) than the amplitude $|\mathcal{U}|$, the curve of E_x' *versus* k_x' resembles a staircase function, E_x' being independent of k_x' throughout a given Brillouin zone associated with the deformed lattice. These discrete allowed values of E_x' correspond to the energy levels of the harmonic oscillator formed by each trough of the perturbative potential. We will assume that the staircase function rises uniformly from the energy $-|\mathcal{U}|$ to the energy $+|\mathcal{U}|$. Each step will have a width $\sigma/2$. The curve of E_x' *versus* k_x' is shown in Fig. 1.

Equation (44), like (18), is Schrödinger's equation for a periodic potential, so that, like Eq. (26), we have

$$\mathbf{v}'(\mathbf{k}')=\tfrac{1}{2}\nabla_{k'}E'(\mathbf{k}'), \tag{55}$$

so that for $k_x'^2>|\mathcal{U}/\alpha|$,

$$v_x'=\alpha k_x', \tag{56}$$

while for $k_x'^2<|\mathcal{U}/\alpha|$,

$$v_x'=0. \tag{57}$$

[10] J. C. Slater, Phys. Rev. **87**, 807 (1952). See especially Fig. 3, p. 813.

Making use of the transformation properties of energy and velocity previously given, we can now determine these quantities in the unprimed coordinate system. For $(k_x-C/\alpha)^2>|\mathcal{U}/\alpha|$,

$$\begin{aligned}E&=E'+2\mathbf{C}\cdot\mathbf{v}'/\alpha+C^2/\alpha\\&=\alpha(\mathbf{k}'+\mathbf{C}/\alpha)^2\\&=\alpha k^2,\end{aligned} \tag{58}$$

$$\begin{aligned}v_x&=\alpha k_x'+C\\&=\alpha k_x.\end{aligned} \tag{59}$$

For $(k_x-C/\alpha)^2<|\mathcal{U}/\alpha|$,

$$\begin{aligned}E&=E'+C^2/\alpha\\&=E_x'+\alpha(k_y^2+k_z^2)+C^2/\alpha,\end{aligned} \tag{60}$$

$$v_x=C. \tag{61}$$

Because of Eq. (60), surfaces of constant E do not have inversion symmetry in k space, as can be seen from Fig. 2, showing the surface of $E=E_F$ (the Fermi level).

VI. APPLICATION TO A METAL

In this section we shall apply our previous results to the calculation of the electronic current density in a metal. The average value of velocity in the direction of the acoustic wave for the conduction electrons is given by

$$\langle v_x\rangle=\textstyle\sum_{\mathbf{k}}{}' v_x(\mathbf{k})/\sum_{\mathbf{k}}{}' 1, \tag{62}$$

the prime denoting a summation over the occupied states. We will assume that the energy levels below a certain energy E_F (the Fermi energy) are all filled, while those above this energy are all empty. Since the levels are very closely spaced, we can replace the sums in Eq. (62) by the equivalent integrals over k space, i.e.,

$$\langle v_x\rangle=\int' v_x(\mathbf{k})d\tau_k\Big/\int' d\tau_k. \tag{63}$$

Because of the reflection symmetry of $\mathbf{v}(\mathbf{k})$ and of the Fermi surface (surface in k space for which $E=E_F$) with respect to k_y and k_z, it follows that

$$\langle v_y\rangle=\langle v_z\rangle=0. \tag{64}$$

Thus the electronic current density J is

$$J=n\langle v_x\rangle, \tag{65}$$

where n, the number of conduction electrons per unit volume, is given by

$$n=2/(2\pi)^3\int' d\tau_k. \tag{66}$$

For metals, n can be expressed in the form

$$n=n_e n_a/\Omega, \tag{67}$$

where n_e is the number of conduction electrons per atom, n_a is the number of atoms per unit cell of the

crystal, and Ω is the volume of the unit cell. It will be necessary to compute $\langle v_z\rangle$ separately for the following three ranges of the variable $|\mathcal{U}/\alpha|^{\frac{1}{2}}$.

Range I $|\mathcal{U}/\alpha|^{\frac{1}{2}}<|E_F/\alpha|^{\frac{1}{2}}-C/\alpha$;
range II $|E_F/\alpha|^{\frac{1}{2}}+C/\alpha>|\mathcal{U}/\alpha|^{\frac{1}{2}}>|E_F/\alpha|^{\frac{1}{2}}-C/\alpha$;
range III $|\mathcal{U}/\alpha|^{\frac{1}{2}}>|E_F/\alpha|^{\frac{1}{2}}+C/\alpha$.

First we consider range I.

$$\int' d\tau_k=\frac{4}{3}\pi\left(\frac{E_F}{\alpha}\right)^{\frac{3}{2}}+\frac{\pi}{\alpha}\int_{C/\alpha-|v/\alpha|^{\frac{1}{2}}}^{C/\alpha+|v/\alpha|^{\frac{1}{2}}}\left\{\left[E_F-E_z'\left(k_z-\frac{C}{\alpha}\right)-\frac{C^2}{\alpha}\right]-[E_F-\alpha k_z^2]\right\}dk_z$$
$$=\frac{4\pi}{3}\left(\frac{E_F}{\alpha}\right)^{\frac{3}{2}}+\frac{2\pi}{3}\left|\frac{\mathcal{U}}{\alpha}\right|^{\frac{3}{2}}. \tag{68}$$

$$\int' v_z(\mathbf{k})d\tau_k=\frac{\pi}{\alpha}\int_{C/\alpha-|v/\alpha|^{\frac{1}{2}}}^{C/\alpha+|v/\alpha|^{\frac{1}{2}}}\left\{\left[E_F-E_z'\left(k_z-\frac{C}{\alpha}\right)-\frac{C^2}{\alpha}\right]C-[E_F-\alpha k_z^2]\alpha k_z\right\}dk_z$$
$$=2\pi C|\mathcal{U}/\alpha|^{\frac{3}{2}}. \tag{69}$$

In obtaining (68) and (69), we have made use of the fact that

$$\int_0^{\pm|v/\alpha|^{\frac{1}{2}}}E_z'(k_z')dk_z'=0. \tag{70}$$

Combining (63), (68), and (69), we get

$$\langle v_z\rangle=3C[1+2|E_F/\mathcal{U}|^{\frac{3}{2}}]^{-1}. \tag{71}$$

Combining (63), (65), (66), and (69), we get

$$J=(C/2\pi^2)|\mathcal{U}/\alpha|^{\frac{3}{2}}. \tag{72}$$

It should be pointed out that $\langle v_z\rangle$ fails to vanish in range I not because of the form of $v_z(\mathbf{k})$ but rather because of the shape of the Fermi surface (see Fig. 2). For example, if the Fermi surface were cylindrical in shape with the axis of the cylinder parallel to the k_z axis, then $\langle v_z\rangle$ would vanish in spite of Eqs. (59) and (61). The net average velocity results entirely from a thin ring of electrons in k space—this ring being those electrons lying near the Fermi surface which have $\mathbf{v}_z=\mathbf{C}$, the velocity of the acoustic wave.

In range III, however, all the electrons contribute equally to the net electronic current. This follows from the fact that all the occupied states are associated with a value of k_z such that $(k_z-C/\alpha)^2<|\mathcal{U}/\alpha|$, so that each electron moves with an average value of v_z equal to C. It immediately follows that in range III

$$\langle v_z\rangle=C. \tag{73}$$

Combining Eqs. (65), (67), and (73), we get

$$J=(n_e n_a/\Omega)C \tag{74}$$

for the current density in range III.

We shall not bother to determine $\langle v_z\rangle$ in range II since this intermediate range covers only a very small variation in the variable $|\mathcal{U}/\alpha|$. This can be seen from the fact that $|E_F/\alpha|^{\frac{1}{2}}$ is about 300 times the size of C/α in a typical metal. Henceforth we will assume

range I $|\mathcal{U}/\alpha|^{\frac{1}{2}}<|E_F/\alpha|^{\frac{1}{2}}$,
range II $|\mathcal{U}/\alpha|^{\frac{1}{2}}>|E_F/\alpha|^{\frac{1}{2}}$.

It can be seen that at the upper limit of range I, Eq. (71) goes into Eq. (73).

We wish to express the current density J in terms of the acoustic intensity Υ (the acoustic energy crossing unit area in unit time). Υ may be expressed in terms of U, the acoustic energy per atom, by

$$\Upsilon=(n_a C U/\Omega). \tag{75}$$

If M is the mass of the atom, then from Eq. (3) we get

$$U=M s_{\max}{}^2=M(\sigma SC)^2. \tag{76}$$

Combining Eqs. (15), (75), and (76), we get

$$|\mathcal{U}/\alpha|=|A/\alpha|(\Omega\Upsilon/n_a MC^3)^{\frac{1}{2}}. \tag{77}$$

Combining Eqs. (72), (74), and (77), we get

$$J=B\Upsilon^{\frac{1}{2}},\quad \Upsilon\leqslant\Upsilon_M; \tag{78}$$
$$J=J_M,\quad \Upsilon\geqslant\Upsilon_M; \tag{79}$$

where

$$B=\frac{2}{(2\pi C)^2}\left|\frac{A}{\alpha}\right|^{\frac{3}{2}}\left(\frac{\Omega C}{n_a M}\right)^{\frac{1}{2}}, \tag{80}$$

$$J_M=(n_e n_a C/\Omega), \tag{81}$$

$$\Upsilon_M=(J_M/B)^{4/3}. \tag{82}$$

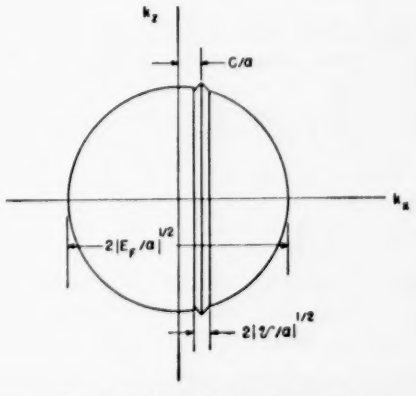

FIG. 2. The Fermi surface in k space.

As an example, let us compute the current density in sodium, where $\Omega=257.5$, $|A|=0.161$, $M=4.22\times10^4$, $n_e=1$, $n_a=1$, $C=1.75\times10^{-3}$, and $\alpha=1$. (As is noted in Appendix B of reference 5, $\frac{3}{2}|A|$ is equal to the "interaction constant" of Sommerfeld and Bethe, a constant which may be determined from high-temperature conductivity data. The value of the interaction constant for sodium quoted by Sommerfeld and Bethe[11] has been used to determine the above value of $|A|$.) Using the above values, we obtain $B=0.199$, $\Upsilon_M=1.11\times10^{-6}$, and $J_M=6.80\times10^{-6}$. If, in place of atomic units, we wish to express Υ in units of ergs/cm^2 sec and J in units of microamperes/cm^2, then $B=601$, $\Upsilon_M=3.60\times10^{16}$ ergs/cm^2 sec, and $J_M=1.60\times10^{15}$ μa/cm^2$=1600\times10^6$ amperes/cm^2. The above values of Υ_M and J_M show that it would be experimentally impossible to ever reach saturation, so that range I is the only range of interest. The above value of B indicates that it should be possible to detect the acousto-electric effect experimentally. For example, if $\Upsilon=10^{-4}$ ergs/cm^2 sec (equivalent to an intensity level of 50 db), then $J=0.601$ μa/cm^2.

VII. APPLICATION TO AN *N*-TYPE SEMICONDUCTOR

We wish to calculate the current density resulting from the electrons in the conduction band of an *n*-type semiconductor. It is assumed that, in the conduction band, the Fermi factor can be approximated by the Boltzmann factor

$$\exp-[E(\mathbf{k})-E_F]/\kappa T,$$

where E_F is the Fermi energy and κ is Boltzmann's constant. Thus

$$\langle v_x\rangle=\frac{\int_\infty v_x(\mathbf{k})e^{-[E(\mathbf{k})-E_F]/\kappa T}d\tau_k}{\int_\infty e^{-[E(\mathbf{k})-E_F]/\kappa T}d\tau_k}. \tag{83}$$

Since $E(\mathbf{k})$ differs from αk^2 only over a very small region of k space, we may make the approximation

$$\int_\infty e^{-E(\mathbf{k})/\kappa T}d\tau_k\cong\int_\infty e^{-(\alpha/\kappa T)k^2}d\tau_k$$
$$=\left(\frac{\pi\kappa T}{\alpha}\right)^{\frac{3}{2}}. \tag{84}$$

This approximation is not sufficient for the numerator of (83), however, since the total nonvanishing contribution to $\langle v_x\rangle$ comes from this small region where $E(\mathbf{k})\neq\alpha k^2$.

$$\int_\infty v_x(\mathbf{k})e^{-E(\mathbf{k})/\kappa T}d\tau_k=\frac{\pi\kappa T}{\alpha}\int_{C/\alpha-|v/\alpha|^{\frac{1}{2}}}^{C/\alpha+|v/\alpha|^{\frac{1}{2}}}$$
$$\times[C\exp\{-(1/\kappa T)[E_x'(k_x-C/\alpha)+C^2/\alpha]\}$$
$$-\alpha k_x\exp\{-(\alpha/\kappa T)k_x^2\}]dk_x. \tag{85}$$

For the purpose of evaluating the above integral, we may take

$$E_x'(k_x-C/\alpha)=2\alpha|\mathcal{U}/\alpha|^{\frac{1}{2}}(|k_x-C/\alpha|-\tfrac{1}{2}|\mathcal{U}/\alpha|^{\frac{1}{2}}). \tag{86}$$

We will also assume the temperature is large enough such that

$$C^2/\alpha\ll\kappa T, \tag{87}$$

$$|\mathcal{U}|\ll\kappa T. \tag{88}$$

It will later be shown that these two conditions are satisfied under almost all practical experimental conditions. After some manipulation (85) becomes

$$\int_\infty v_x(\mathbf{k})e^{-E(\mathbf{k})/\kappa T}d\tau_k=2\pi C|\mathcal{U}/\alpha|^{\frac{1}{2}}, \tag{89}$$

so that

$$\langle v_x\rangle=(2C/\sqrt{\pi})|\mathcal{U}/\kappa T|^{\frac{1}{2}}. \tag{90}$$

If the semiconductor is doped with impurity atoms having a valence one unit greater than that of the semiconducting atoms, then for sufficiently high temperatures the number of conduction electrons per unit volume is n_af/Ω, f being the fraction of atoms which are impurity atoms, while n_a and Ω have the same meaning as in Sec. VI. For low temperatures, however, most of the excess electrons will be trapped in donor levels lying below the bottom of the conduction band, so that there will be very few conduction electrons. We will assume that there are two donor levels (one for each spin) for each impurity atom, these levels lying below the bottom of the conduction band. The energy of these levels will be denoted by E_D. (Taking the zero of energy at the bottom of the conduction band will make E_D negative.) The number of conduction electrons per unit volume can now be written in two forms:

$$n=[2/(2\pi)^3]\int_\infty e^{-[E(\mathbf{k})-E_F]/\kappa T}d\tau_k, \tag{91}$$

$$n=(n_af/\Omega)[1-2\{e^{(E_D-E_F)/\kappa T}+1\}^{-1}]. \tag{92}$$

It should be noted that the Fermi factor *cannot* be approximated by the Boltzmann factor in Eq. (92), since the Fermi level may lie very close to the donor levels. Combining Eqs. (84), (91), and (92), we may

[11] A. Sommerfeld and H. Bethe, *Handbuch der Physik* (Springer, Berlin, 1933), Vol. 24, Chap. 2, p. 524.

solve for n in terms of E_D. Defining the quantity

$$\eta=(\Omega/4n_af)(\kappa T/\pi\alpha)^{\frac{1}{2}}e^{-|E_D|/\kappa T}, \tag{93}$$

we may consider the two limiting cases of $\eta\gg1$ (high temperature) and $\eta\ll1$ (low temperature). For $\eta\gg1$,

$$n=n_af/\Omega, \tag{94}$$

while for $\eta\ll1$,

$$n=\tfrac{1}{4}(\kappa T/\pi\alpha)^{\frac{1}{2}}e^{-|E_D|/\kappa T}. \tag{95}$$

Combining Eqs. (65), (77), (90), (94), and (95), we get, for $\eta\gg1$,

$$J=\mathfrak{B}f(\Upsilon/T^2)^{\frac{1}{2}}, \tag{96}$$

where

$$\mathfrak{B}=\frac{2}{(\pi)^{\frac{1}{2}}MC}\left(\frac{n_aM}{\Omega C}\right)^{\frac{1}{4}}\left(\frac{A}{\kappa}\right)^{\frac{3}{2}}, \tag{97}$$

while for $\eta\ll1$,

$$J=Be^{-|E_D|/\kappa T}\Upsilon^{\frac{1}{2}}, \tag{98}$$

B being given by Eq. (80). From (96) and (98), it can be seen that J vanishes both at very low and at very high temperatures.

As an example, we take germanium, where $\Omega=306.4$, $|A|=0.125$, $M=1.335\times10^5$, $n_a=2$, $C=2.46\times10^{-3}$, $\alpha=1$, and $|E_D|=2.94\times10^{-3}$. (The above value of $|A|$ was obtained from reference 5.) Expressing J in units of microamperes/cm², T in degrees Kelvin, and Υ in ergs/cm² sec, we have

$$\mathfrak{B}=7.10\times10^8,$$
$$Be^{-|E_D|/\kappa T}=78.4\times10^{-(202/T)},$$
$$\eta=1.10(T^{\frac{1}{2}}/f)\times10^{-(7+202/T)}.$$

Condition (87) for germanium is

$$T\gg0.955,$$

while condition (88) is

$$T\gg3.06\times10^{-5}\sqrt{\Upsilon},$$

so that these two conditions are completely satisfied under most experimental conditions. The above values of B and $\mathfrak{B}$ indicate that it should be possible to detect the acousto-electric effect in germanium. For example, if $f=10^{-5}$, $T=273$°K, and $\Upsilon=1$ erg/cm² sec (90 db), then $\eta=9.05$, and $J=1.57$ μa/cm². If $f=10^{-5}$, $T=100$°K, and $\Upsilon=1$ erg/cm² sec, then $\eta=0.105$, and $J=0.75$ μa/cm².

The writer is indebted to Professors J. C. Slater, J. Bardeen, and H. Brooks and to Dr. E. P. Gross for discussion and correspondence.

APPENDIX

In order to prove Eq. (24), we start with the definition of the expectation value of energy,

$$E(\mathbf{k})=2i\int_\infty\psi^*\frac{\partial}{\partial t}\psi d\tau\Big/\int_\infty\psi^*\psi d\tau. \tag{1a}$$

Making use of Eq. (22), we get

$$E(\mathbf{k})=2i\frac{\sum_{n,n'}\Psi^*(\mathbf{k},\mathbf{r}_{n'},t)(\partial/\partial t)\Psi(\mathbf{k},\mathbf{r}_n,t)\int_\infty a^*(\mathbf{r}-\mathbf{r}_{n'})a(\mathbf{r}-\mathbf{r}_n)d\tau}{\sum_{n,n'}\Psi^*(\mathbf{k},\mathbf{r}_{n'},t)\Psi(\mathbf{k},\mathbf{r}_n,t)\int_\infty a^*(\mathbf{r}-\mathbf{r}_{n'})a(\mathbf{r}-\mathbf{r}_n)d\tau}. \tag{2a}$$

In reference 7, it is shown that

$$\int_\infty a^*(\mathbf{r}-\mathbf{r}_{n'})a(\mathbf{r}-\mathbf{r}_n)d\tau=\delta_{n,n'}, \tag{3a}$$

so that

$$E(\mathbf{k})=2i\frac{\sum_n\Psi^*(\mathbf{k},\mathbf{r}_n,t)(\partial/\partial t)\Psi(\mathbf{k},\mathbf{r}_n,t)}{\sum_n\Psi^*(\mathbf{k},\mathbf{r}_n,t)\Psi(\mathbf{k},\mathbf{r}_n,t)}. \tag{4a}$$

Since the perturbative potential is slowly varying on the atomic scale, Ψ_k will also be slowly varying, and the crystal sums in (4a) may be replaced by the corresponding integrals, i.e.,

$$E(\mathbf{k})=2i\int_\infty\Psi^*\frac{\partial}{\partial t}\Psi d\tau\Big/\int_\infty\Psi^*\Psi d\tau. \tag{5a}$$

The proof of Eq. (25) is somewhat more involved. The method to be used is similar to that used by Slater in the appendix of reference 8. The Wannier function may be written

$$a(\mathbf{r}-\mathbf{r}_n)=N^{-1}\textstyle\sum_{\mathbf{k}'}e^{-i[\mathbf{k}'\cdot\mathbf{r}_n-\frac{1}{2}E_0(\mathbf{k}')t]}\psi_0(\mathbf{k}',\mathbf{r},t), \tag{6a}$$

where N is the number of unit cells in the crystal. The sum is over all the allowed values of $\mathbf{k}$ in the first Brillouin zone of reciprocal space. To check the correctness of (6a), we multiply both sides of the equation by $\exp i[\mathbf{k}\cdot\mathbf{r}_n-\frac{1}{2}E_0(\mathbf{k})t]$ and sum over n. Using the fact that

$$\begin{aligned}\textstyle\sum_n e^{i(\mathbf{k}-\mathbf{k}')\cdot\mathbf{r}_n}&=N \quad \text{if} \quad \mathbf{k}=\mathbf{k}'\\ &=0 \quad \text{if} \quad \mathbf{k}\neq\mathbf{k}',\end{aligned} \tag{7a}$$

we immediately obtain Eqs. (20) and (21). Applying (6a) to (22), we get

$$\psi(\mathbf{k},\mathbf{r},t)=N^{-1}\textstyle\sum_{n,\mathbf{k}'}e^{-i[\mathbf{k}'\cdot\mathbf{r}_n-\frac{1}{2}E_0(\mathbf{k}')t]}\times\Psi(\mathbf{k},\mathbf{r}_n,t)\psi_0(\mathbf{k}',\mathbf{r},t), \tag{8a}$$

so that the ψ's are expanded in terms of the ψ_0's. The proof of Eq. (25) starts with the definition of the expectation value of velocity,

$$\mathbf{v}(\mathbf{k}) = -i\frac{\int_{\infty}\psi^*(\mathbf{k},\mathbf{r},t)\nabla\psi(\mathbf{k},\mathbf{r},t)d\tau}{\int_{\infty}\psi^*(\mathbf{k},\mathbf{r},t)\psi(\mathbf{k},\mathbf{r},t)d\tau}. \quad (9a)$$

We will have occasion to use the orthogonality property of the ψ_0's,

$$\int_{\infty}\psi_0^*(\mathbf{k}',\mathbf{r},t)\psi_0(\mathbf{k},\mathbf{r},t)d\tau = I\delta(\mathbf{k},\mathbf{k}'), \quad (10a)$$

where $\delta(\mathbf{k},\mathbf{k}')$ is the Kronecker delta, and I is some normalization constant independent of $\mathbf{k}$. Another useful property is the fact that

$$-i\int_{\infty}\psi_0^*(\mathbf{k}',\mathbf{r},t)\nabla\psi_0(\mathbf{k},\mathbf{r},t)d\tau = I\mathbf{v}_0(\mathbf{k})\delta(\mathbf{k},\mathbf{k}'). \quad (11a)$$

(11a) follows from (9a) and (10a) when $\mathbf{k}=\mathbf{k}'$. The fact that the integral vanishes when $\mathbf{k}\neq\mathbf{k}'$ is mathematically equivalent to the well-known fact that optical transitions between two energy levels in the same band are forbidden. If we now substitute (8a) into (9a) and simplify with the help of (10a) and (11a), we obtain

$$\mathbf{v}(\mathbf{k}) = \frac{\sum_{n,n',\mathbf{k}'}\Psi^*(\mathbf{k},\mathbf{r}_n,t)\mathbf{v}_0(\mathbf{k}')e^{-i\mathbf{k}'\cdot(\mathbf{r}_{n'}-\mathbf{r}_n)}\Psi(\mathbf{k},\mathbf{r}_{n'},t)}{\sum_{n,n',\mathbf{k}'}\Psi^*(\mathbf{k},\mathbf{r}_n,t)e^{-i\mathbf{k}'\cdot(\mathbf{r}_{n'}-\mathbf{r}_n)}\Psi(\mathbf{k},\mathbf{r}_{n'},t)}. \quad (12a)$$

The denominator of the right-hand side of (12a) may be simplified by the relation

$$\delta_{n,n'} = N^{-1}\sum_{\mathbf{k}'}e^{-i\mathbf{k}'\cdot(\mathbf{r}_{n'}-\mathbf{r}_n)}. \quad (13a)$$

(13a) may be checked by multiplying both sides of the equation by $\exp[i\mathbf{k}\cdot(\mathbf{r}_{n'}-\mathbf{r}_n)]$ and summing over n'. Using (7a), we obtain the obviously correct relation

$$1 = \sum_{n'}\delta_{n,n'}e^{i\mathbf{k}\cdot(\mathbf{r}_{n'}-\mathbf{r}_n)}.$$

Since $\mathbf{v}_0(\mathbf{k})$, as a function of $\mathbf{k}$, has the periodicity of the reciprocal lattice, we may expand $\mathbf{v}_0$ as a Fourier series,

$$\mathbf{v}_0(\mathbf{k}) = \sum_{n'}\mathbf{A}_{n,n'}e^{i\mathbf{k}\cdot(\mathbf{r}_{n'}-\mathbf{r}_n)}, \quad (14a)$$

where

$$\mathbf{A}_{n,n'} = N^{-1}\sum_{\mathbf{k}'}\mathbf{v}_0(\mathbf{k}')e^{-i\mathbf{k}'\cdot(\mathbf{r}_{n'}-\mathbf{r}_n)}. \quad (15a)$$

(15a) may be checked by multiplying both sides of the equation by $\exp[i\mathbf{k}\cdot(\mathbf{r}_{n'}-\mathbf{r}_n)]$ and summing over n', whence, with the aid of (7a), Eq. (14a) is obtained. Combining (14a) and (15a), we may write the operator equation

$$\mathbf{v}_0(-i\nabla) = \sum_{n',\mathbf{k}'}\mathbf{v}_0(\mathbf{k}')e^{-i\mathbf{k}'\cdot(\mathbf{r}_{n'}-\mathbf{r}_n)}\exp[(\mathbf{r}_{n'}-\mathbf{r}_n)\cdot\nabla]. \quad (16a)$$

We have need of the relation

$$\Psi(\mathbf{k},\mathbf{r}_{n'},t) = \exp[(\mathbf{r}_{n'}-\mathbf{r}_n)\cdot\nabla]\Psi(\mathbf{k},\mathbf{r}_n,t), \quad (17a)$$

which is Taylor's expansion in a vector form. Combining (16a) and (17a) gives

$$N\mathbf{v}_0(-i\nabla)\Psi(\mathbf{k},\mathbf{r}_n,t) = \sum_{n',\mathbf{k}'}\mathbf{v}_0(\mathbf{k}')e^{-i\mathbf{k}'\cdot(\mathbf{r}_{n'}-\mathbf{r}_n)}\Psi(\mathbf{k},\mathbf{r}_{n'},t). \quad (18a)$$

The numerator of the right-hand side of (12a) may be simplified with the aid of (18a). Substituting (13a) and (18a) into (12a) gives

$$\mathbf{v}(\mathbf{k}) = \frac{\sum_n\Psi^*(\mathbf{k},\mathbf{r}_n,t)\mathbf{v}_0(-i\nabla)\Psi(\mathbf{k},\mathbf{r}_n,t)}{\sum_n\Psi^*(\mathbf{k},\mathbf{r}_n,t)\Psi(\mathbf{k},\mathbf{r}_n,t)}. \quad (19a)$$

Since Ψ is slowly varying on the atomic scale, the crystal sums in (19a) may be replaced by the corresponding integrals; i.e.,

$$\mathbf{v}(\mathbf{k}) = \int_{\infty}\Psi^*\mathbf{v}_0(-i\nabla)\Psi d\tau \Big/ \int_{\infty}\Psi^*\Psi d\tau. \quad (20a)$$

Multiple Compton Scattering of Low Energy Gamma-Radiation

R. C. O'ROURKE
Electricity Division, Naval Research Laboratory, Washington, D. C.
(Received October 29, 1952)

The exact problem of multiple Compton scattering in an infinite plane parallel medium is set up for a monochromatic primary spectral distribution normally incident upon a semi-infinite medium for isotropic scattering. It is treated by a different approach to that previously used by the author, the new approach being based in part on Marshak's method of spherical harmonics. Numerical results are presented for the P_1 approximation to this problem. This result is compared with the corresponding solution obtained previously. The present method shows that the broadening is not as severe as the previous method had indicated.

SECTION 1. BASIC EQUATIONS AND METHOD OF SOLUTION

IN a previous paper[1] the author found approximate solutions to several problems of multiple Compton scattering of low energy ($E \ll 0.5$ Mev) gamma-radiation. The present paper contains a different approach to the problem, based in part on Marshak's[2] method of spherical harmonics. None of the approximations of the first paper are made. The problem is to find accurate expressions for the broadening of a primary monochromatic spectral distribution as a function of the distance into the medium and the angle (measured from the direction of the primary beam).

Referring to (I), the appropriate transport equation which must be solved in the case of Compton scattering with no photoelectric absorption and for an infinite plane-parallel scattering medium (semi-infinite or of finite thickness) is the following

$$\mu\frac{\partial}{\partial\tau}I(\tau,\mu,\sigma)+I(\tau,\mu,\sigma)=\frac{3}{16\pi}\int_{-1}^{+1}d\mu'\int_0^{2\pi}d\varphi'(1+\cos^2\Theta)I(\tau,\mu',\sigma'), \quad (1.01)$$

where $\tau=(8/3)N\pi r_0^2\cdot Z$, Z=actual distance into medium in cm, r_0=classical electron radium in cm, N=number of electrons per cm^3, $\mu=\cos\vartheta$; $\mu'=\cos\vartheta'$, $\sigma=(mc/h)\lambda$, σ_0=primary "wavelength" $(mc/h)\lambda_0$, $\sigma'=\sigma-1+\cos\Theta$, and

$$\cos\Theta=\mu\mu'+(1-\mu^2)^{\frac{1}{2}}\cdot(1-\mu'^2)^{\frac{1}{2}}\cos\varphi'.$$

To begin with, we shall carry out, the problem of isotropic scattering in which $\frac{3}{4}(1+\cos^2\Theta)$ is set to unity. This is done because it is one of the purposes of this paper to check the results of (I), where isotropic scattering was also considered. An appendix shows the modifications necessary in order to solve the nonisotropic problem (1.01). The only limitation on the methods to be presented is the usual one; namely, the exact Klein-Nishina differential cross section, which is energy dependent, cannot be handled by the operational methods below.

$$\mu\frac{\partial}{\partial\tau}I(\tau,\mu,\sigma)+I(\tau,\mu,\sigma)=\frac{1}{4\pi}\int_{-1}^{+1}d\mu'\int_0^{2\pi}d\varphi'I(\tau,\mu',\sigma'). \quad (1.02)$$

This transport equation will now be solved for the case of a plane parallel semi-infinite scattering medium with a monochromatic beam of gammas incident normal to the face $z=0$. The unscattered component is singular in wavelength and direction, and one can therefore introduce the spectral density $J(\tau,\mu,\sigma)$ of all gammas scattered at least once as follows:

$$I(\tau,\mu,\sigma)=\pi Fe^{-\tau}\delta(1-\mu)\delta(\sigma-\sigma_0)+J(\tau,\mu,\sigma). \quad (1.03)$$

The delta function $\delta(1-\mu)$ is normalized to unity over the whole solid angle. The transport equation for $J(\tau,\mu,\sigma)$ then becomes

$$\mu\frac{\partial}{\partial\tau}J(\tau,\mu,\sigma)+J(\tau,\mu,\sigma)=\frac{F}{4}e^{-\tau}\delta(\sigma-\sigma_0-1+\mu)+\frac{1}{4\pi}\int_{-1}^{+1}d\mu'\int_0^{2\pi}d\varphi'J(\tau,\mu',\sigma'), \quad (1.04)$$

in which the singular factor $(1-\mu)\delta(1-\mu)$ occurred and was considered identically zero, operationally speaking, since it would drop out in what follows below. One now makes a Fourier integral decomposition in wavelength shift $(\sigma-\sigma_0\equiv y)$ where, again, σ_0 is the dimensionless primary wavelength $(mc/h)\lambda_0$.

$$J(\tau,\mu,\sigma)=\frac{1}{2\pi}\int_{-\infty}^{\infty}M(\tau,\mu,\alpha)e^{i\alpha y}d\alpha. \quad (1.05)$$

One must note the important fact that physically the scattered radiation consists only of wavelengths larger than $\lambda_0(\sigma-\sigma_0\geq 0)$. This indicates that one should perhaps use a one-sided Laplace transform in wavelength shift which is ideally suited for variables which range from zero to infinity. This is however not practicable since the inversion of such transforms leads to

[1] R. C. O'Rourke, Phys. Rev. **85**, 881 (1952) [referred to hereafter as (I)].
[2] R. Marshak, Phys. Rev. **71**, 443 (1947).

complex integrals which are very difficult to handle. The inversion of Eq. (1.05) is, of course,

$$M(\tau, \mu, \alpha)=\int_{-\infty}^{\infty} J(\tau, \mu, y)e^{-i\alpha y}dy,$$

which is formally an integral over negative values of $\sigma-\sigma_0$. By representing $J(\tau, \mu, \sigma)$ as a Fourier integral one must find the function $M(\tau, \mu, \alpha)$ to be such a function that there is no "violet shift" i.e., $J(\tau, \mu, \sigma)$ should turn out identically zero for $\sigma-\sigma_0\leqslant 0$. One however has no control over the function $M(\tau, \mu, \alpha)$, as will be seen since it is obtained by successive approximations in the spherical harmonic method. In any P_{l_0} approximation one must expect a small violet shift [see (I)]. As will become evident, the violet shift is quite small even in the P_1 approximation, and the amount of violet shift seems to be a critical method of evaluating the success of the spherical harmonic method in handling problems of the type under consideration here.

Proceeding then, one substitute Eqs. (1.05) into (1.04) and obtains

$$\mu\frac{\partial M}{\partial\tau}+M=\frac{F}{4}e^{-\tau}e^{-i\alpha(1-\mu)}+\frac{1}{4\pi}\int_{-1}^{+1}d\mu'\int_{0}^{2\pi}d\varphi' \times e^{-i\alpha(1-\cos\Theta)}M(\tau, \mu', \alpha). \quad (1.06)$$

One now represents the angular dependence of $M(\tau, \mu, \alpha)$ by the method of spherical harmonics as follows,

$$M(\tau, \mu, \alpha)=\sum_{l=0}^{l_0}\frac{2l+1}{2}K_l(\tau, \alpha)P_l(\mu), \quad (1.07)$$

where

$$K_l(\tau, \alpha)=\int_{-1}^{+1}d\mu P_l(\mu)M(\tau, \mu, \alpha).$$

Since only low energy gamma-scattering is being considered one expects that one will not need a large value of l_0 to represent the solution. As in the case of problems of diffusion with no wavelength shift this is fortunate since, here as well, only the P_1 and P_2 approximations can be carried out with limited numerical facilities. This statement is also made here because the transport equation for high energy gamma-scattering is mathematically equivalent to the problem being considered here, if one makes the same approximations that Foldy[3] does in his work. One could not, however, expect to represent the high energy angular dependence (which is predominantly forward) by only a small cut-off value of l_0.

To proceed, then one substitutes Eq. (1.07) into Eq. (1.06) multiplies by $P_m(\mu)$ and integrates over $-1\leqslant\mu\leqslant+1$. Using the recurrence relation

$$(2l+1)\mu P_l(\mu)=lP_{l-1}(\mu)+(l+1)P_{l+1}(\mu),$$

one is led to the result

$$lK'_{l-1}+(l+1)K'_{l+1}+(2l+1)K_l =\frac{F}{4}(2l+1)e^{-\tau}\int_{-1}^{+1}d\mu e^{-i\alpha(1-\mu)}P_l(\mu) +\sum_{m=0}^{l_0}\mathfrak{a}_{lm}(\alpha)K_m(\tau, \alpha), \quad (1.08)$$

where the prime means derivative with respect to τ, and where

$$\mathfrak{a}_{lm}(\alpha)=\frac{(2l+1)(2m+1)}{4}\frac{1}{2\pi}\int_{-1}^{+1}d\mu\int_{-1}^{+1}d\mu'\int_{0}^{2\pi}d\varphi' \times e^{-i\alpha(1-\cos\Theta)}P_l(\mu)P_m(\mu').$$

All of the integrals can be carried out in closed form and are actually quite simple. To see this, introduce the well-known expansion,[4]

$$e^{i\alpha\cos\Theta}=\sum_{n=0}^{\infty}i^n(2n+1)j_n(\alpha)P_n(\cos\Theta), \quad (1.09)$$

and the addition theorem for spherical harmonics,

$$P_n(\cos\Theta)=P_n(\mu)P_n(\mu') +2\sum_{K=1}^{n}\frac{(n-K)!}{(n+K)!}P_n^K(\mu)P_n^K(\mu')\cos K\varphi'; \quad (1.10)$$

the second term gives nothing since one integrates over φ' from 0 to 2π. One has then

$$\frac{4e^{i\alpha}\mathfrak{a}_{lm}}{(2l+1)(2m+1)} =\sum_{n=0}^{\infty}i^n(2n+1)j_n(\alpha)\int_{-1}^{+1}d\mu\int_{-1}^{+1}d\mu \times P_l(\mu)P_n(\mu)P_m(\mu')P_n(\mu') =\frac{4}{(2l+1)(2m+1)}\sum_{n=0}^{\infty}i^n(2n+1)j_n(\alpha)\delta_{ln}\delta_{mn}. \quad (1.11)$$

Therefore only diagonal elements survive,

$$\mathfrak{a}_{lm}(\alpha)=e^{-i\alpha}i^l(2l+1)j_l(\alpha)\delta_{lm}. \quad (1.12)$$

Similarly, for the other integral in Eqs. (1.08), one can use the same method,

$$\int_{-1}^{+1}e^{i\alpha\mu}P_l(\mu)d\mu=2i^lj_l(\alpha). \quad (1.13)$$

[3] L. Foldy, Phys. Rev. **81**, 395 (1951).

[4] J. Stratton, *Electromagnetic Theory* (McGraw-Hill Book Company, Inc., New York, 1941), p. 409.

Finally, the system of equations (1.08) reduces to

$$lK'_{l-1}+(l+1)K'_{l+1}+(2l+1)K_l = \tfrac{1}{2}Fi^l(2l+1)e^{-i\alpha}j_l(\alpha)e^{-\tau} + i^l(2l+1)e^{-i\alpha}j_l(\alpha)K_l, \quad (1.14)$$

and then the formal solution would be:

$$J(\tau,\mu,y)=\sum_{l=0}^{l_0}\frac{2l+1}{2}P_l(\mu)\cdot\frac{1}{2\pi}\int_{-\infty}^{\infty}K_l(\tau,\alpha)e^{i\alpha y}d\alpha.$$

SECTION 2. THE SEMI-INFINITE MEDIUM-P_1 APPROXIMATION

One could apply a Laplace transformation to the system (1.14) in the variable τ and reduce it to a system of algebraic equations for the transforms of the $K_l(\tau,\alpha)$. However, for the P_1 and P_2 approximations it is easier to solve the system directly. In the P_1 approximation (i.e., $l_0=1$) one cuts the system off by keeping only terms in $K_0(\tau,\alpha)$ and $K_1(\tau,\alpha)$. This method of cut-off can only be judged by its success in the numerical sense of doing both the P_1 and P_2 approximations (and higher if possible) and seeing how the successive solutions to $K_l(\tau,\alpha)$ compare with each other.[5]

In the P_1 approximation, then, the system (1.14) becomes simply

$$\begin{aligned}K_1'+K_0&=\mathfrak{a}_{00}(K_0+\tfrac{1}{2}Fe^{-\tau}),\\ K_0'+3K_1&=\mathfrak{a}_{11}(K_1+\tfrac{1}{2}Fe^{-\tau}),\end{aligned} \quad (2.01)$$

where

$$\mathfrak{a}_{00}(\alpha)=e^{-i\alpha}j_0(\alpha),\quad \mathfrak{a}_{11}(\alpha)=3ie^{-i\alpha}j_1(\alpha).$$

Uncoupling these equations leads one to the following equation:

$$K_0''-\Omega^2K_0=\tfrac{1}{2}F(\Omega^2-3)e^{-\tau}, \quad (2.02)$$

where

$$\Omega^2(\alpha)=(1-\mathfrak{a}_{00})(3-\mathfrak{a}_{11})\equiv\Lambda_1+i\Lambda_2,$$

$$\Lambda_1(\alpha)=3[1-\cos\alpha j_0(\alpha)-\sin\alpha j_1(\alpha)+\sin 2\alpha j_0(\alpha)j_1(\alpha)],$$

$$\Lambda_2(\alpha)=3[\sin\alpha j_0(\alpha)-\cos\alpha j_1(\alpha)+\cos 2\alpha j_0(\alpha)j_1(\alpha)].$$

The solution of Eq. (2.02) is simply

$$K_0(\tau,\alpha)=\tfrac{1}{2}F[A(\alpha)e^{-\Omega\tau}+B(\alpha)e^{\Omega\tau}+e^{-\tau}/(1-\Omega^2)]\cdot(\Omega^2-3), \quad (2.03)$$

where

$$\Omega(\alpha)\equiv\Theta_1(\alpha)+i\Theta_2(\alpha),$$

$$\Theta_1(\alpha)=2^{-\frac{1}{2}}[\Lambda_1+(\Lambda_1^2+\Lambda_2^2)^{\frac{1}{2}}]^{\frac{1}{2}},\quad \Theta_2(\alpha)=\Lambda_2[2\Theta_1(\alpha)]^{-1}.$$

The boundary conditions for the determination of $A(\alpha)$, $B(\alpha)$ are the following:

$$\int_0^1 J(0,\mu,\sigma)\mu d\mu=0, \text{ for all } \sigma; \quad (2.04)$$

$$\lim_{\tau\to\infty}\int_{-1}^{+1}J(\tau,\mu,\sigma)d\mu=0, \text{ for all } \sigma. \quad (2.05)$$

[5] M. Wang and E. Guth, Phys. Rev. **84**, 1092 (1951).

These are to be used for a semi-infinite plane parallel medium. The first condition simply states that the net flux of gammas scattered at least once "into" the medium must vanish at $\tau=0$. This is the exact boundary condition because the incident beam and the unscattered beam are equal at $\tau=0$, and the flux of the latter has been separated completely from the problem. The second boundary condition (2.05) simply assumes that the spectral distribution averaged over angles approaches zero properly as $\tau\to\infty$, for all finite σ. Since photoelectric absorption is being neglected, one of course cannot assign physical significance to wavelengths larger than those wavelengths at which photons would be lost by absorption. This is always a difficulty in treating a semi-infinite medium. As far as broadening is concerned, however, the results of (I) have indicated already that at a distance τ_1 into a semi-infinite medium one has a broadened spectral distribution which does not differ greatly from the corresponding solution for a finite medium of the same thickness τ_1. A quantitative answer to the above difficulty can of course only be obtained by solving the present problem for a finite scattering medium (see below). One would then replace Eq. (2.05) by the exact condition

$$\int_{-1}^{0}J(\tau_1,\mu,\sigma)\mu d\mu=0, \text{ for all } \sigma \text{ (vacuum for } \tau>\tau_1). \quad (2.06)$$

Proceedings with the semi-infinite medium one substitutes Eqs. (1.05) and (1.07) into the boundary conditions (2.04) and (2.05) and obtains $B(\alpha)\equiv 0$ and

$$A(\alpha)=\frac{1}{3+2\Omega-\mathfrak{a}_{11}}\left[\frac{2\mathfrak{a}_{11}}{3-\Omega^2}-\frac{5-\mathfrak{a}_{11}}{1-\Omega^2}\right]. \quad (2.07)$$

The results in the P_1 approximation are then (after some tedious but simple algebra)

$$K_0(\tau,\alpha)=\tfrac{1}{2}F\left[\frac{\Delta_1+i\Delta_2}{\Delta_7}e^{-\Omega\tau}+\frac{\Delta_3+i\Delta_4}{\Delta_7\Delta_8}e^{-\Omega\tau}+\frac{\Delta_5+i\Delta_6}{\Delta_7\Delta_8}e^{-\tau}\right], \quad (2.08)$$

where the Δ's are defined below;

$$\Delta_1=Q_1(5-3C_1)-3C_2Q_2,$$
$$\Delta_2=-3C_2Q_1-Q_2(5-3C_1),$$
$$\Delta_3=2(5-C_1)(Q_1Q_3+\Lambda_2Q_2)-2C_2(Q_2Q_3-\Lambda_2Q_1),$$
$$\Delta_4=2(5-C_1)(\Lambda_2Q_1-Q_2Q_3)-2C_2(Q_1Q_3+\Lambda_2Q_2),$$
$$\Delta_5=Q_3(\Lambda_1-3)-\Lambda_2^2,$$
$$\Delta_6=Q_3\Lambda_2+2(\Lambda_1-3),$$
$$\Delta_7=Q_1^2+Q_2^2,$$
$$\Delta_8=Q_3^2+\Lambda_2^2,$$
$$Q_1(\alpha)=3-C_1+2\Theta_1,$$
$$Q_2(\alpha)=2\Theta_2-C_2,$$
$$Q_3(\alpha)=1-\Lambda_1;$$

and, finally,

$$\mathfrak{a}_{11}(\alpha)\equiv C_1+iC_2,$$
$$C_1(\alpha)=(3\sin\alpha/\alpha)(\sin\alpha/\alpha-\cos\alpha),$$
$$C_2(\alpha)=\cot\alpha C_1(\alpha).$$

Finally, one needs $K_1(\tau,\alpha)$ since in this P_1 approximation the spectral density $J(\tau,\mu,\sigma)$ is given by

$$J(\tau,\mu,y)=\frac{1}{2\pi}\int_{-\infty}^{\infty}\{\tfrac{1}{2}K_0(\tau,\alpha)+\tfrac{3}{2}\mu K_1(\tau,\alpha)\}e^{i\alpha y}d\alpha. \tag{2.09}$$

From the original Eqs. (2.01) one finds

$$K_1(\tau,\alpha)=1/(3-\mathfrak{a}_{11})\{-K_0'+\tfrac{1}{2}F\mathfrak{a}_{11}e^{-\tau}\}, \tag{2.10}$$

or

$$K_1(\tau,\alpha)=\tfrac{1}{2}F[e^{-(\Theta_1+i\Theta_2)\tau}(\mathfrak{M}_1+i\mathfrak{M}_2)+e^{-\tau}(\mathfrak{M}_3+i\mathfrak{M}_4)], \tag{2.11}$$

where the $\mathfrak{M}$'s are defined below.

$$\mathfrak{M}_1(\alpha)=\Gamma(\alpha)\{(3-C_1)(\Theta_1\omega_1-\Theta_2\omega_2)-C_2(\Theta_2\omega_1+\Theta_1\omega_2)\},$$
$$\mathfrak{M}_2(\alpha)=\Gamma(\alpha)\{(3-C_1)(\Theta_2\omega_1+\Theta_1\omega_2)+C_2(\Theta_1\omega_1-\Theta_2\omega_2)\},$$
$$\mathfrak{M}_3(\alpha)=\Gamma(\alpha)\{(3-C_1)\omega_3-C_2\omega_2\},$$
$$\mathfrak{M}_4(\alpha)=\Gamma(\alpha)\{(3-C_1)\omega_4+C_2\omega_3\},$$

where,

$$\omega_1=\Delta_1\Delta_8+\Delta_3,\quad \omega_3=\Delta_5+C_1\Delta_8\Delta_7,$$
$$\omega_2=\Delta_2\Delta_8+\Delta_4,\quad \omega_4=\Delta_6+C_2\Delta_8\Delta_7,$$
$$\Gamma(\alpha)=[\Delta_7\Delta_8\{(3-C_1)^2+C_2^2\}]^{-1}.$$

Finally, for the solution one needs only the real parts of $K_0(\tau,\alpha)e^{i\alpha y}$ and $K_1(\tau,\alpha)e^{i\alpha y}$, which are: $(y\equiv\sigma-\sigma_0)$

$$\mathrm{Re}\{K_0e^{i\alpha y}\}=\tfrac{1}{2}F(e^{-\Theta_1\tau}/\Delta_7\Delta_8)[\omega_1\cos(\Theta_2\tau-\alpha y)+\omega_2\sin(\Theta_2\tau-\alpha y)]+\tfrac{1}{2}F(e^{-\tau}/\Delta_8)[\Delta_5\cos\alpha y-\Delta_6\sin\alpha y], \tag{2.12}$$

TABLE I. Values of the integrals $\mathcal{J}^{(0)}(\tau,y)$ and $\mathcal{J}^{(1)}(\tau,y)$ for $\tau=1$, $\tau=2$ as defined in Eq. (2.15).

y	$\mathcal{J}^{(0)}/2$	$\frac{3}{2}\mathcal{J}^{(0)}$	$\frac{\mathcal{J}^{(0)}}{2}+\frac{3}{2}\mathcal{J}^{(1)}$
		$\tau=1$	
−0.50	−0.01	0.23	0.22
0.00	+0.07	0.31	0.38
0.25	+0.14	0.26	0.40
0.5	+0.14	0.16	0.30
1.0	+0.13	−0.04	0.09
2.0	+0.12	−0.16	−0.04
3.0	+0.11	+0.07	+0.18
		$\tau=2$	
−0.50	0.00	0.08	0.08
0.00	0.04	0.14	0.18
0.25	0.08	0.15	0.23
0.50	0.09	0.12	0.21
1.0	0.08	0.04	0.12
3.0	0.08	0.05	0.13
5.0	0.07	0.01	0.08

and

$$\mathrm{Re}\{K_1e^{i\alpha y}\}=\tfrac{1}{2}Fe^{-\Theta_1\tau}[\mathfrak{M}_1\cos(\Theta_2\tau-\alpha y)+\mathfrak{M}_2\sin(\Theta_2\tau-\alpha y)]+\tfrac{1}{2}Fe^{-\tau}[\mathfrak{M}_3\cos\alpha y-\mathfrak{M}_4\sin\alpha y]. \tag{2.13}$$

The spectral distribution is finally given by the following Fourier integral, in the P_1 approximation,

$$J(\tau,\mu,y)=\frac{1}{\pi}\int_0^{\infty}\mathrm{Re}\{[\tfrac{1}{2}K_0+\tfrac{3}{2}\mu K_1]e^{i\alpha y}\}d\alpha \tag{2.14}$$

or the following

$$J(\tau,\mu,y)=\tfrac{1}{2}F[\tfrac{1}{2}\mathcal{J}^{(0)}(\tau,y)+\tfrac{3}{2}\mu\mathcal{J}^{(1)}(\tau,y)], \tag{2.15}$$

$$\mathcal{J}^{(0)}(\tau,y)=\frac{1}{\pi}\int_0^{\infty}d\alpha\left[\frac{e^{-\Theta_1\tau}}{\Delta_7\Delta_8}\{\omega_1\cos(\Theta_2\tau-\alpha y)+\omega_2\sin(\Theta_2\tau-\alpha y)\}+\frac{e^{-\tau}}{\Delta_8}\{\Delta_5\cos\alpha y-\Delta_6\sin\alpha y\}\right],$$

$$\mathcal{J}^{(1)}(\tau,y)=\frac{1}{\pi}\int_0^{\infty}d\alpha[e^{-\Theta_1\tau}\{\mathfrak{M}_1\cos(\Theta_2\tau-\alpha y)+\mathfrak{M}_2\sin(\Theta_2\tau-\alpha y)\}+e^{-\tau}\{\mathfrak{M}_3\cos\alpha y-\mathfrak{M}_4\sin\alpha y\}].$$

These Fourier integrals $\mathcal{J}^{(0)}(\tau,y)$ and $\mathcal{J}^{(1)}(\tau,y)$ have been evaluated for $\tau=1$, $\tau=2$. The results are presented in Table I. Then from Eq. (2.15) one can obtain $J(\tau,\mu,\sigma)$ for any angle ϑ where $(\mu=\cos\vartheta)$. Figure 1 shows the spectral distribution for $\mu=1$, $F=1$, for both $\tau=1$ and $\tau=2$ along with the corresponding results obtained in (I). One sees that the two methods agree quite well for $\tau=2$ in giving the magnitude of the maximum intensity but disagree as to the location of the maximum and the shape of the distribution. The present method yields a rather poor result in the P_1 approximation for small τ-values (say $\tau<2$) in the practical sense that the Fourier integrals are more difficult to handle, and the results indicate rather large oscillations in the tails of the spectral distributions, i.e., at wavelength shifts beyond the maximum (see Fig. 1). For $\tau=2$ these oscillations damp out and approximate a monotonic decreasing function as one expects. We will forego a detailed discussion of the numerical aspects of the problem at this time since they are not complete.

The net flux across a surface of unit area per unit σ interval is given by

$$\pi\mathfrak{F}(\tau,\sigma)=2\pi\int_{-1}^{+1}J(\tau,\mu,\sigma)\mu d\mu+\pi F\delta(y)e^{-\tau}=\pi F\mathcal{J}^{(1)}(\tau,y)+\pi F\delta(y)e^{-\tau}. \tag{2.16}$$

Thus, only $\mathcal{J}^{(1)}(\tau, y)$ survives in the calculation of net flux. This is true, of course, in all higher orders of approximation $l_0=1, 2, \cdots$ and is one of the attractive features of the spherical harmonic method. At the same time one may have to calculate all the $K_l(\tau, \alpha)$, $l=0, 1, \cdots l_0$ in order to determine $K_1(\tau, \alpha)$ from which $\mathcal{J}^{(1)}(\tau, y)$ follows.

The corresponding results for a finite medium of thickness τ_1 can be readily solved by using the boundary conditions (2.04) and (2.06) along with Eqs. (2.01) and (2.03). The results are not recorded here because of their length and a lack of numerical facilities which makes it impossible to evaluate the Fourier integral solutions at the present time.

APPENDIX

For the problem of anisotropic scattering one must solve Eq. (1.01) as it stands. Only a few modifications are introduced and these will be indicated here. One introduces Eqs. (1.03) and (1.01) and obtains

$$\mu\frac{\partial J}{\partial\tau}+J=\frac{3}{16\pi}Fe^{-\tau}\delta(\sigma-\sigma_0-1+\mu)$$

$$+\frac{3}{16\pi}\int_{-1}^{+1}d\mu'\int_0^{2\pi}d\varphi'(1+\cos^2\Theta)J(\tau,\mu',\sigma'). \quad \text{(A.01)}$$

One again makes a Fourier integral decomposition (1.05) which gives

$$\mu\frac{\partial}{\partial\tau}M(\tau,\mu,\alpha)+M$$

$$=\frac{3}{16}Fe^{-\tau}(1+\mu^2)e^{-i\alpha(1-\mu)}$$

$$+\frac{3}{16\pi}\int_{-1}^{+1}d\mu'\int_0^{2\pi}d\varphi'(1+\cos^2\Theta)$$

$$\times e^{-i\alpha(1-\cos\Theta)}M(\tau,\mu',\alpha). \quad \text{(A.02)}$$

Introducing the "spherical harmonic" expansion (1.07) for $M(\tau, \mu, \alpha)$ leads one to

$$lK'_{l-1}+(l+1)K'_{l+1}+(2l+1)K_l$$

$$=\frac{3}{16}Fe^{-\tau}(2l+1)\int_{-1}^{+1}d\mu(1+\mu^2)e^{-i\alpha(1-\mu)}P_l(\mu)$$

$$+\sum_{m=0}^{l_0}\mathfrak{a}_{lm}(\alpha)K_m(\tau,\alpha), \quad \text{(A.03)}$$

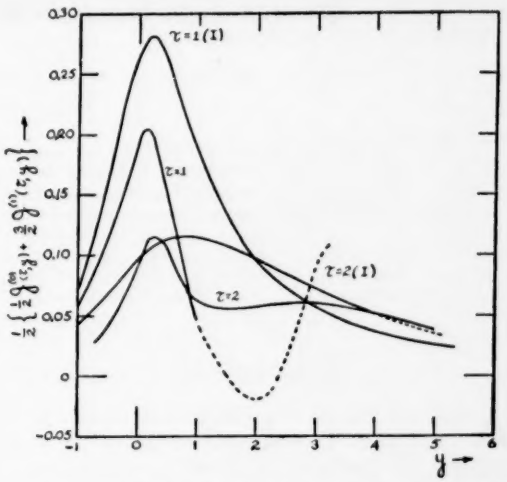

FIG. 1. Spectral distribution of all gammas scattered more than once are shown for distances $\tau=1$ and $\tau=2$. The unscattered spectral component would be a delta-function at $y=0$. The corresponding solutions obtained in an earlier paper are drawn for comparison. The primary intensity is unity. The solutions are for $\mu=1$ in both cases.

where

$$\frac{4}{(2l+1)(2m+1)}e^{i\alpha}\mathfrak{a}_{lm}(\alpha)$$

$$=\frac{3}{8\pi}\int_{-1}^{+1}d\mu\int_{-1}^{+1}d\mu'\int_0^{2\pi}d\varphi'(1+\cos^2\Theta)$$

$$\times e^{i\alpha\cos\Theta}P_l(\mu)P_m(\mu').$$

For the small values of l, m needed in the P_1 and P_2 approximations these integrals can be readily evaluated just as above. The only difference is that $\mathfrak{a}_{lm}(\alpha)$ is not diagonal and therefore the system of Eqs. (A.03) will differ slightly from (1.14). This case of anisotropic scattering has not been studied (numerically) and should not until the P_2 approximation to the above isotropic scattering problems is better understood (i.e., in the numerical sense of the convergence of the method which can be estimated by the decrease of the "violet shift" in passing from the P_1 to the P_2 approximation). In the P_2 approximation one can again uncouple the system of equations. One obtains again a second-order differential equation for $K_0(\tau, \alpha)$ just as above and $K_1(\tau, \alpha)$, $K_2(\tau, \alpha)$ can be expressed in terms of $K_0(\tau, \alpha)$ and the entire solution carried through in the same manner as in the P_1 approximation.

The author would like to thank the Computations Staff of the National Bureau of Standards for carrying out the laborious numerical work for this paper. He would also like to thank Mr. H. Hancock and Mr. B. Zimmerman of the Naval Research Computation staff for assistance in formulating the numerical program.

Quantum Field Theory in the Light of Distribution Analysis

WERNER GÜTTINGER
Department of Physics, University of Tübingen, Tübingen, Germany
(Received August 29, 1952)

It is shown that part of the divergences and ambiguities of the current quantum theory of fields can be overcome by the consistent use of distribution analysis. Representing the singular functions of field theory by distributions, nongauge invariant and nonequivalent terms will be eliminated from the S-matrix in renormalizable as well as in nonrenormalizable theories without any limiting process. Instead of divergent quantities, there appear arbitrary normalization and division constants. Feynman's cutoff as well as the renormalization are automatically contained in a theory which gives a correct meaning to delta-functions. Applications to closed loop processes are discussed in detail. It is not possible to attribute definite values to the parameters of bare particles; for that, some modifications of the theory seem to be necessary.

INTRODUCTION

AS is well known, the difficulties appearing in the application of covariant formalisms to meson problems are closely connected with the mathematical defects of quantum field theory. Neither formal limiting methods[1] nor realistic modifications[2] of the theory have given satisfactory results in a self-consistent way. In such a situation an examination of the mathematical foundations of field theoretical formalisms seems to us to be necessary. In our opinion the difficulties are partly due to our inability to handle the singular propagation functions correctly. In fact, it is impossible, in a strict sense, to treat delta-functions, which are not elements of classical analysis, by the methods of this analysis itself. Therefore, we are obliged to look for a generalization of classical analysis which contains Dirac functions as regular elements. In such a correct formalism, all inconsistencies due to mathematical defects of current field theory must vanish. An analysis of the required kind exists in the form of the so-called distribution analysis, introduced recently into mathematics by Schwartz.[3] Schwartz defines distributions as certain linear functionals which can be used to represent singular expressions. Such functionals are suitable for a strict foundation of the mathematical formalism of the field theory.

After a sketch of the conventional treatment of closed loop processes in Part I, we give a survey of distribution analysis in the following second part. In Secs. III and IV the new aspects of the field theory resulting from the introduction of distributions are discussed. Some formulas used extensively in the conventional formalism have to be modified. A so-called Pf symbol (pseudofunction) is introduced which enables one to consider singular functions at their singularities themselves. The Pf-symbol may be regarded as a generalization of the notion of principal value, taking account of the fact that we must define each singularity in a theory containing elements with point structure like Dirac functions. The field theory is shown to be convergent. In some cases the Pf symbol introduces an arbitrary finite "normalization constant" which is connected with a lack of invariance of certain quantities with respect to dilatation transformations of the "support" of distributions.

Feynman's cutoff and the renormalization factors are direct consequences of this constant, which appears in unobservable quantities only. The normalization constant is to be found only in processes of low order simultaneously with so-called division constants in distributions, the support of which is the origin, arising from the fact that delta-algebra contains divisors of zero. A determination of these constants is possible only for matrix elements which are subjected to general rules, for instance, to gauge invariance. By the help of the division constants, unphysical quantities will be eliminated from the S-matrix. Such elimination processes are due in a much more direct way to the normalization constants contained in one expression together with nongauge invariant or nonequivalent terms in the S-matrix. The lack of dilatation invariance named above is characteristic for particles with nonvanishing mass. According to the existence of the normalization constant there is no longer any distinction in principle between renormalizable and nonrenormalizable theories; in the latter the normalization constant yields an indirect renormalization effect.

The regulator of Pauli and Villars[1] is shown to be equivalent to the introduction of distributions with the origin as support, but such limiting processes are thoroughly superfluous. The discrepancy between the classical quadratic divergence of the photon self-energy

[1] W. Pauli and F. Villars, Revs. Modern Phys. **21**, 434 (1949); Y. Katayama, Prog. Theoret. Phys. **5**, 272 (1950); **6**, 309 (1951); H. Fukuda and T. Kinoshita, Prog. Theoret. Phys. **5**, 1024 (1950); Z. Koba *et al.*, Prog. Theoret. Phys. **6**, 322 (1951); J. McConnell, Nature **164**, 218 (1949); P. T. Matthews, Phys. Rev. **81**, 936 (1951); D. C. Peaslee, Phys. Rev. **81**, 107 (1951); J. Steinberger, Phys. Rev. **76**, 1180 (1949).

[2] D. Feldman, Phys. Rev. **76**, 1369 (1949); R. Jost and J. Rayski, Helv. Phys. Acta **22**, 458 (1950); W. Heisenberg, Z. Naturforsch. **5a**, 251 (1950); A. Pais and G. E. Uhlenbeck, Phys. Rev. **79**, 145 (1950).

[3] L. Schwartz, Ann. Univ. Grenoble **21**, 57 (1945); **23**, 7 (1948); *Théorie des distributions I/II* (Hermann et Cie, Paris, 1950); Lecture notes at the Canadian Mathematical Congress, second summer seminar, University of British Columbia, August, 1949 (unpublished).

and the finite result of Wentzel[4] originates from an inadmissible integration by parts which has to be modified. Self-energies and self-charges become finite and are in agreement with the results of Schwinger and Feynman[5] if we identify the normalization constant included with the cut-off factor of these authors. We discuss further some meson processes. For instance, the postulate of gauge invariance for the two-photon decay of neutral π-mesons and the equivalence theorem for the decay of a τ-meson into π-mesons will be fulfilled correctly, giving transition elements in a unique way also for nonrenormalizable models. The discrepancies connected with the transition from the S_F-functions to $\bar{S}$ and $S^{(1)}$ as well as the problem of normal dependent terms can also be clarified. Various problems, for instance, radiative corrections, may be treated by means of the theory of distributions in a self-consistent way. It should be pointed out that some results are affected by arbitrary functions whose physical meaning is uncertain. Finally, some remarks are made on the nature of normalization constants and the structure of nivariant propagation functions.

I. FORMALISM OF CLOSED LOOP PROCESSES

We start with an outline of the formalism of interaction of bosons through virtual fermions via closed loop graphs, adopting Schwinger's[5] notation with $\hbar=c=1$. The interaction energy of a system of $n+1$ bosons interacting via fermions is given in the interaction representation by

$$H=\sum_{i=0}^{n} g_i U_i \bar{\psi}\Gamma_i\tau_i\psi,$$

where U_i represents the potential of the ith boson field obeying the Proca equation (mass μ_i) and ψ means the fermion spinor (mass m). Γ_i and τ_i mean the spin and isotopic spin operators, respectively, Γ_i corresponding to scalar coupling, pseudoscalar coupling, etc.; the g_i are coupling constants. Neglecting radiative corrections, the S-matrix element describing the decay of a boson U_0 into n bosons via closed fermion loop reads

$$\mathfrak{M}_n=\int_{-\infty}^{+\infty} d^4x_0 U_0(x_0) M_n(x_0),$$

with

$$M_n(x_0)=G\prod_{i=1}^{n}\left(\int_{-\infty}^{+\infty} d^4x_i U_i(x_i)\right)\mathrm{Sp}\sum_{k=0}^{n}\bar{S}(0,1)$$

$$\times\Gamma_1\bar{S}(1,2)\cdots\Gamma_k S^{(1)}(k,k+1)\cdots\Gamma_n\bar{S}(n,0)\Gamma_0, \quad (1.1)$$

where $c=0$ or 1 in

$$G=c\prod_{i=0}^{n} g_i$$

reveals the selection rules and $S(i,k)=S(x_i-x_k)$. If there are photon fields among the U_i, the matrix element M_n is subjected to the postulate of gauge invariance. Further, the vector coupling of scalar mesons vanishes in some cases by the divergence theorem, and finally we often have equivalence between pseudoscalar and pseudovector couplings of pseudoscalar mesons. These theorems, assured in coordinate space, are generally destroyed in the results of the actual calculation of matrix elements, so we cannot decide which terms are physically significant. In order to evaluate (1.1) the Fourier representations of $\bar{S}$ and $S^{(1)}$ are substituted, using the relation[6]

$$\sum_{r=0}^{n}(k_r^2+m^2)\prod_{i\neq r}(k_i^2+m^2)^{-1}$$

$$=\prod_{r=1}^{n}\left(\int_{-1}^{+1} da_r\right)\alpha_n\delta^{(n)}\left(m^2+\sum_{i=0}^{n}\beta_i k_i^2\right), \quad (1.2)$$

with

$$2^{i+1}\beta_i=(1+a_{i+1})\prod_{k=0}^{i}(1-a_k), \quad \alpha_n=(-2)^n\prod_{i=0}^{n}\beta_i(1-a_i^2)^{-1},$$

$$a_0=0, \quad a_{n+1}=1, \quad \sum_{i=0}^{n}\beta_i=1, \quad \delta^{(n)}(x)=d^n\delta(x)/dx^n.$$

Then the transformation,

$$k_i\to k+\lambda_i(p_j), \quad \lambda_i(p_j)=\sum_{l\neq i} p_l\sum_{s=l}^{i-1}\beta_s,$$

is carried out, neglecting boundary values. Using the spherical symmetry in the momentum variable k we set $k_\mu k_\nu\to\frac{1}{4}\delta_{\mu\nu}k^2=D_1k^2, \cdots$. Finally we derive from

$$\int_{-\infty}^{+\infty} d^4k\exp(izk^2)=i\pi^2\epsilon(z)z^{-2},$$

with $\epsilon(z)=z/|z|$, the formula

$$\int_{-\infty}^{+\infty} d^4k(k^2)^n\exp(izk^2)=i^{1+n}\pi^2(n+1)!\epsilon(z)z^{-(n+2)}, \quad (1.3)$$

and find

$$M_n=\frac{G}{4(2\pi)^{4n+2}}\prod_{k=1}^{n}\left[\int_{-\infty}^{+\infty} d^4p_k\bar{U}_k(p_k)\int_{-1}^{+1} da_k\right]$$

$$\times\left(\sum_{j=0}^{n_0} A_j\right)\alpha_n i^{n+j+1}(j+1)!\int_{-\infty}^{+\infty} dz\epsilon(z)z^{n-j-2}$$

$$\times\exp\left[iz\left(m^2+\sum_{l=0}^{n}\beta_l\lambda_l^2\right)\right]\exp(-ip_0x), \quad (1.4)$$

[4] G. Wentzel, Phys. Rev. **74**, 1070 (1948).

[5] J. Schwinger, Phys. Rev. **74**, 1439 (1948); **75**, 651, 1912 (1949); R. P. Feynman, Phys. Rev. **76**, 749, 769 (1949); F. J. Dyson, Phys. Rev. **75**, 486, 1736 (1949).

[6] H. Fukuda *et al.*, Prog. Theoret. Phys. **5**, 283, 352 (1950).

where A_i is defined by

$$\mathrm{Sp}\left(\prod_{j=0}^{n}(i\gamma(k+\lambda_j)-m)\Gamma_{j+1}\right)=\sum_{i=0}^{n_0}A_i\cdot(k^2)^i;$$

$n_0=n/2$, $(n+1)/2$ if n even, odd. $\bar{U}_k(p_k)$ is the Fourier transform of $U_k(x_k)$. M_n is seen to be convergent if $n>3$. By evaluating the spur in A_i for respective sets of mesons and expanding the integrand in powers of μ_0/m, we obtain the transition probabilities of various processes. However, as is well known, the results are quite ambiguous.

II. PRINCIPLES OF DISTRIBUTION ANALYSIS

In order to generalize classical analysis in the sense of Schwartz[3] let us consider the space D of all continuous complex functions $\varphi(x)$, defined on a linear vector space which is represented by the real points x with coordinates $x_1, \cdots, x_n$. For simplicity we take one coordinate only, $x=x_1$. The functions $\varphi(x)$ shall be differentiable to any order and vanish with their derivatives $d^n\varphi/dx^n=\varphi^{(n)}(x)$ identically beyond a compact, for instance, finite, manifold in the space of the x: $\varphi^{(n)}(\pm\infty)\equiv 0$. We define the support of $\varphi(x)$ to be the closed manifold of those points x for which $\varphi(x)\neq 0$. On the space D of the functions φ we consider functionals $T(\varphi)$: To each φ of D a complex number $T(\varphi)$ is attached, and, if φ runs over D, the attached system of complex numbers represents the functional $T(\varphi)$. These functionals shall be linear [i.e., $T(c_1\varphi_1+c_2\varphi_2)=c_1T(\varphi_1)+c_2T(\varphi_2)$] and continuous [i.e., if $\varphi_i\to\varphi_0$ then $T(\varphi_i)\to T(\varphi_0)$]. Such functionals are called distributions. Now we attribute to each function $f(x)$, which is summable in the sense of Lebesgue, a special distribution $f(\varphi)$ defined by

$$f(x)[\varphi]\equiv f(\varphi)=\int_{-\infty}^{+\infty}dx\,f(x)\varphi(x). \tag{2.1}$$

This Lebesgue integral does not change its value if $f(x)$ is changed, for instance, in a finite number of points x. Then we identify $f(x)$ with $f(\varphi)$: instead of calculating with the function $f(x)$ we operate with the associated functional $f(\varphi)$. Hence ordinary functions appear as special distributions. The support of the distribution $T(\varphi)$ is defined as the smallest manifold of those points x beyond which T vanishes. Further, we *define* a special distribution $\delta(\varphi)$ by

$$\delta(\varphi)=\varphi(0),\quad \delta_a(\varphi)=\varphi(x). \tag{2.2}$$

This is not equal to $\int dx\delta(x)\varphi(x)$ with the usual delta function definition, since the Lebesgue integral allows a modification of the integrand $\delta(0)=0$, which gives the integral the value zero; $\delta(\varphi)$ is a distribution which is not attached to a function. In the space of distributions we define the "distribution-derivative" $D[T(\varphi)]$ by

$$D[T(\varphi)]=-T(\varphi'). \tag{2.3}$$

It is clear that every distribution is differentiable to any order:

$$D^n[T(\varphi)]=(-1)^nT(\varphi^{(n)}). \tag{2.4}$$

Instead of D^nT we write often $T^{(n)}$. $T(\varphi^{(n)})$ is a linear and continuous form in $\varphi^{(n)}$, and therefore a distribution in φ. Equation (2.3) will be established in Appendix I. In particular, we have from (2.4)

$$\delta^{(n)}(\varphi)=(-1)^n\delta(\varphi^{(n)})=(-1)^n\varphi^{(n)}(0). \tag{2.5}$$

Let us consider a distribution $f(\varphi)$ associated with a summable function $f(x)$ whose ordinary function-derivative $df(x)/dx\equiv[f'(x)]$ is summable. The distribution-derivative $Df(\varphi)$ of $f(\varphi)$ reads according to (2.3) and (2.1):

$$f^{(1)}(\varphi)\equiv Df(\varphi)=-f(\varphi')=-\int_{-\infty}^{+\infty}f(x)\varphi'(x)dx.$$

By partial integration we obtain, on account of $\varphi(\pm\infty)\equiv 0$,

$$Df(\varphi)=\int_{-\infty}^{+\infty}[f'(x)]\varphi(x)dx=[f'(x)](\varphi), \tag{2.6}$$

i.e.,

$$f^{(1)}(\varphi)\equiv Df(\varphi)=[f'(x)](\varphi).$$

This implies that, if $f(x)$ and $[f'(x)]$ are summable, the distribution-derivative $Df(\varphi)\equiv f^{(1)}(\varphi)$ of a distribution $f(\varphi)$ associated with $f(x)$ coincides with the distribution which is attributed to the function-derivative $[f'(x)]$ of $f(x)$, i.e., with $[f'(x)](\varphi)$. If $f(x)$ is summable, but $g(x)=[f^{(n)}(x)]\,(n\geqq 1)$ is not, the distribution-derivatives $D^nf(\varphi)$ of $f(\varphi)$ do exist according to (2.4). But $D^nf(\varphi)$ is not equal to $g(\varphi)=[f^{(n)}(x)](\varphi)$, since a functional

$$\int_{-\infty}^{+\infty}dx g(x)\varphi(x)$$

associated with a nonsummable function $g(x)$ is not a distribution.[7] For instance, we find for the distribution-derivative of the distribution $\epsilon(\varphi)$ which is associated with the (summable) function $\epsilon(x)$ [$\epsilon(x)=1$ if $x>0$, $=-1$ if $x<0$, not defined for $x=0$]:

$$\epsilon^{(1)}(\varphi)\equiv D\epsilon(\varphi)=-\epsilon(\varphi')=-\int_{-\infty}^{+\infty}dx\epsilon(x)\varphi'(x)$$

$$=[\varphi(x)]_{-\infty}^{0}-[\varphi(x)]_{0}^{\infty}=2\varphi(0)=2\delta(\varphi). \tag{2.7}$$

Hence we write, for short,

$$\epsilon^{(1)}(x)=2\delta(x), \tag{2.8}$$

the argument x noting only the fact that ϵ and δ are distributions "in x". On the other hand, the function-derivative $[\epsilon'(x)]$ is equal to zero if $x\neq 0$, but it does

[7] This follows from the theory of Lebesgue-integrals: If $\int|f(x)|dx$ is convergent, then $\int f(x)dx$ is convergent and conversely. Hence, since $\int|g(x)|dx$ is divergent, $\int g(x)dx$ and, therefore, $\int g(x)\varphi(x)dx$ do not exist.

not exist for $x=0$; $[\epsilon'(x)]$ is not a summable function. So we have, as stated above, $\epsilon^{(1)}(\varphi) \neq [\epsilon'(x)](\varphi)$, the right side of this inequality not being a distribution. We demonstrated that, if $f(x)$ is summable, the distribution $f(\varphi)$ defined by (2.1) exists, and also the distribution-derivatives $D^n f(\varphi)$ exist to any order [according to (2.4)], even if the function-derivatives $[f^{(n)}(x)]$ are nonsummable, i.e., even if the distributions $[f^{(n)}(x)](\varphi)$ do not exist. This case will be investigated in detail.

Let us define $f_\pm(x)$ by $f_\pm(x)=f(x)$ if $x>0$, $=0$ if $x<0$, $f_\pm(x)$ being not explained for $x=0$. Then we consider the summable function $f_+(x)=(1/\alpha x^\alpha)_+$ (i.e., $=0$ if $x<0$, $=1/\alpha x^\alpha$ if $x>0$, not defined for $x=0$) α being a number with $0<\alpha<1$. The distribution $f_+(\varphi)$ exists, according to (2.1), together with its distribution-derivatives $D^n f_+(\varphi)$, which are defined by $(-1)^n f_+(\varphi^{(n)})$ [Eq. (2.4)]. At first we treat $Df_+(\varphi)=-f_+(\varphi')$. This is a distribution associated with the function f_+ by means of φ', and, therefore, defined according to (2.1) by

$$f_+(\varphi')=\int_{-\infty}^{+\infty} dx f_+(x)\varphi'(x)=\int_0^{+\infty} dx f(x)\varphi'(x).$$

Since f_+ is not defined for $x=0$, the integral on the right hand of this equation has to be determined in the usual manner by

$$\lim_{\epsilon\to 0}\int_\epsilon^\infty dx f(x)\varphi'(x);$$

that is, $-f_+(\varphi')$ is defined by

$$-f_+(\varphi')=\lim_{\epsilon\to 0}\int_\epsilon^\infty dx(1/\alpha x^\alpha)\varphi'(x). \tag{2.9}$$

As is well known from the theory of Lebesgue-integrals, partial integration is allowed, which yields

$$-f_+(\varphi')=\lim_{\epsilon\to 0}\left\{\int_\epsilon^\infty dx[(1/\alpha x^\alpha)']\varphi(x)+(1/\alpha\epsilon^\alpha)\varphi(\epsilon)\right\},$$

$[(1/\alpha x^\alpha)']$ being the usual function-derivative $-1/x^{\alpha+1}$. Since $\varphi(\epsilon)=\varphi(0)+O(\epsilon)$, we may write

$$D\{f_+(\varphi)\}=D(1/\alpha x^\alpha)_+(\varphi)=-f_+(\varphi')$$

$$=-\lim_{\epsilon\to 0}\left\{\int_\epsilon^\infty dx(1/x^{\alpha+1})\varphi(x)-(1/\alpha\epsilon^\alpha)\varphi(0)\right\}. \tag{2.10}$$

This is by definition the explicit form of the distribution-derivative of $f_+(\varphi)=(1/\alpha x^\alpha)(\varphi)$, expressed in terms of φ. *For abbreviation* we write

$$\lim_{\epsilon\to 0}\left\{\int_\epsilon^\infty dx x^{-\alpha-1}\varphi(x)-(1/\alpha)\epsilon^{-\alpha}\varphi(0)\right\}$$

$$\equiv \mathrm{Pf}\int_0^\infty dx x^{-\alpha-1}\varphi(x)=\mathrm{Pf}\int_{-\infty}^{\infty} dx(x^{-\alpha-1})_+\varphi(x). \tag{2.11}$$

It is convenient to write symbolically

$$\mathrm{Pf}\int_{-\infty}^{+\infty} dx(x^{-\alpha-1})_+\varphi(x)\equiv \mathrm{Pf}\{(x^{-\alpha-1})_+(\varphi)\}$$
$$\equiv\{\mathrm{Pf}(x^{-\alpha-1})_+\}(\varphi). \tag{2.12}$$

Hence the distribution-derivative Df_+ of $f_+=(1/\alpha x^\alpha)$ is given by

$$(1/\alpha x^\alpha)_+{}^{(1)}(\varphi)\equiv D\{(1/\alpha x^\alpha)_+(\varphi)\}$$
$$=-\{\mathrm{Pf}(x^{-\alpha-1})_+\}(\varphi). \tag{2.13}$$

The definition (2.11, 12) is a very suggestive one since with the use of the Pf symbol the Eq. (2.13) is very similar to Eq. (2.6); the latter holds if f_+ and $[f_+']$ both are summable. It is seen that

$$f_+{}^{(1)}(\varphi)=(1/\alpha x^\alpha)_+{}^{(1)}(\varphi)\equiv D\{(1/\alpha x^\alpha)_+(\varphi)\}$$

is not equal to $[f_+{}'](\varphi)=-(x^{-\alpha-1})_+(\varphi)$ as one would expect by adopting (2.6) without any care, since $(x^{-\alpha-1})_+(\varphi)$ does not exist as a distribution.[7] Only distributions are allowed to be considered if we want to operate with singular quantities correctly. Hence the distribution associated with $(x^{-\alpha-1})_+$ is given by $\mathrm{Pf}(x^{-\alpha-1})_+(\varphi)$ but not by $(x^{-\alpha-1})_+(\varphi)$. It should be stated once more that the "Pf integral" is only an abbreviation for a well-defined quantity. An interesting remark about the notation Pf will be made in Appendix II.

Now we compute the distribution-derivatives $D^n f_+(\varphi)$, which exist according to (2.4) since $f_+(\varphi)$ does so. (Note that $[f_+{}^{(n)}](\varphi)$ does not exist!) For the second derivatives we obtain by legitimate integrations by parts,

$$D^2\{f_+(\varphi)\}=f_+(\varphi'')=\lim_{\epsilon\to 0}\int_\epsilon^\infty dx(1/\alpha x^\alpha)\varphi''(x)$$

$$=\lim_{\epsilon\to 0}\left\{(1+\alpha)\int_\epsilon^\infty dx x^{-\alpha-2}\varphi(x)\right.$$
$$\left.-\epsilon^{-\alpha-1}\varphi(\epsilon)-(1/\alpha)\epsilon^{-\alpha}\varphi'(\epsilon)\right\},$$

on account of $\varphi^{(n)}(\pm\infty)\equiv 0$. With $\varphi(\epsilon)=\varphi(0)+\epsilon\varphi'(0)+O(\epsilon)$, $\varphi'(\epsilon)=\varphi'(0)+O(\epsilon)$, we find easily

$$(1+\alpha)^{-1}D^2\{f_+(\varphi)\}=\lim_{\epsilon\to 0}\left\{\int_\epsilon^\infty dx x^{-\alpha-2}\varphi(x)\right.$$
$$\left.-\frac{\varphi(0)}{(1+\alpha)\epsilon^{\alpha+1}}-\frac{1}{\alpha\epsilon^\alpha}\varphi'(0)\right\}. \tag{2.14}$$

The right side of this equation will be abbreviated as

$$\mathrm{Pf}\int_{-\infty}^{+\infty} dx(x^{-\alpha-2})_+\varphi(x)\equiv\{\mathrm{Pf}(x^{-\alpha-2})_+\}(\varphi)$$
$$\equiv \mathrm{Pf}\{(x^{-\alpha-2})_+(\varphi)\}. \tag{2.15}$$

So we have

$$D^p\{(1/\alpha x^\alpha)_+(\varphi)\}=(1+\alpha)\ \mathrm{Pf}\{(1/x^{\alpha+2})_+\}(\varphi). \quad (2.16)$$

Taking into account (2.13), the left hand of (2.16) is equal to $-D\{\mathrm{Pf}(x^{-\alpha-1})_+(\varphi)\}$. Hence

$$D\{\mathrm{Pf}(x^{-\alpha-1})_+(\varphi)\}=-(1+\alpha)\ \mathrm{Pf}(x^{-\alpha-2})_+(\varphi). \quad (2.17)$$

The distribution $\mathrm{Pf}(x^{-\alpha-2})_+(\varphi)$ appears to be attributed to the nonsummable function $(x^{-\alpha-2})_+$. By continuing in this manner for the computation of $f_+^{(n)}(\varphi)$, i.e., by successively integrating by parts the distribution

$$(-1)^n \lim_{\epsilon\to 0}\int_\epsilon^\infty dx(1/\alpha x^\alpha)\varphi^{(n)}(x),$$

and using

$$\varphi(\epsilon)=\sum_{r=0}^{\infty}(\epsilon^r/r!)\varphi^{(r)}(0),$$

we come in a direct manner to the definition of the distribution $\mathrm{Pf}(x^{-m})_+(\varphi)$ associated with $(x^{-m})_+$, *viz.*,

$$\mathrm{Pf}(x^{-m})_+(\varphi)=\lim_{\epsilon\to 0}\left\{\int_\epsilon^\infty dx x^{-m}\varphi(x) + \sum_{\mu=0}^{[m-1]}\frac{\varphi^{(\mu)}(0)\epsilon^{\mu+1-m}}{\mu!(\mu+1-m)}\right\}, \quad (2.18)$$

where m is not an integer $\geqslant 1$ and $[m-1]$ is the highest integer which is $\leqslant m-1$. If m is an arbitrary number with $-\infty<m<1$, the sum in (2.18) must be omitted; i.e., the Pf symbol is superfluous, since in this case $(x^{-m})_+(\varphi)$ is a distribution associated with a summable function according to (2.1). Distributions of the form (2.18) will be called "pseudofunctions." We can see by generalizing Eq. (2.17) that, if m is an arbitrary number, but not an integer $\geqslant 1$, the following relation holds:

$$D\ \mathrm{Pf}(x^{-m})_\pm(\varphi)=-m\ \mathrm{Pf}(x^{-m-1})_\pm(\varphi), \quad (2.19)$$

and, since $\mathrm{Pf}(x^{-m})(\varphi)=\mathrm{Pf}(x^{-m})_+(\varphi)+\mathrm{Pf}(x^{-m})_-(\varphi)$,

$$D\ \mathrm{Pf}x^{-m}(\varphi)=-m\ \mathrm{Pf}x^{-(m+1)}(\varphi), \quad (2.20)$$

i.e., the distribution-derivative of the pseudofunction $\mathrm{Pf}x^{-m}(\varphi)$ (m not being an integer $\geqslant 1$) is obtained by the ordinary differentiation rule.

Now we study the case $(1/x^m)_+$ when m is an integer $\geqslant 1$, say $m=n$. For that purpose we consider the summable function $f_+(x)=(\log|x|)_+$, whose associated distribution is given according to (2.1) by

$$f_+(\varphi)=\lim_{\epsilon\to 0}\int_\epsilon^\infty dx\log|x|\cdot\varphi(x). \quad (2.21)$$

As is well known, the definition by a limiting process of the integral involving $\log|x|$ is necessary since $\log|x|$ is undetermined for $x=0$. Since the distribution-derivative $D\{f_+(\varphi)\}$ defined by $-f_+(\varphi')$ exists, we have

$$D\{f_+(\varphi)\}=-f_+(\varphi')=-\lim_{\epsilon\to 0}\int_\epsilon^\infty dx\log|x|\cdot\varphi'(x). \quad (2.22)$$

By performing a legitimate partial integration, taking account of $\varphi(\epsilon)=\varphi(0)+O(\epsilon)$, we find

$$D\{f_+(\varphi)\}=\lim_{\epsilon\to 0}\left\{\int_\epsilon^\infty dx x^{-1}\varphi(x)+\log\epsilon\cdot\varphi(0)\right\}. \quad (2.23)$$

If we define for abbreviation

$$\mathrm{Pf}\{(x^{-1})_+(\varphi)\}=\lim_{\epsilon\to 0}\left\{\int_\epsilon^\infty dx x^{-1}\varphi(x)+\log\epsilon\cdot\varphi(0)\right\}, \quad (2.24)$$

we have

$$D\{(\log|x|)_+(\varphi)\}=\mathrm{Pf}\{(x^{-1})_+(\varphi)\}. \quad (2.25)$$

The definition (2.24) is contained in (2.18) if we prescribe that, if m is an integer $\geqslant 1$, say $m=n$, the term $\mu=m-1$ in (2.18), i.e., $\epsilon^0/0$, is to be replaced by $\log\epsilon$. Hence, for n an integer, we define $\mathrm{Pf}(x^{-n})_+(\varphi)$ by

$$\mathrm{Pf}(x^{-n})_+(\varphi)=\mathrm{Pf}\int_{-\infty}^{+\infty}dx(x^{-n})_+\varphi(x)$$

$$=\lim_{\epsilon\to 0}\left\{\int_\epsilon^\infty dx x^{-n}\varphi(x)+\sum_{\mu=0}^{n-2}\frac{\varphi^{(\mu)}(0)}{\mu!}\times\frac{\epsilon^{\mu+1-n}}{\mu+1-n}+\frac{\varphi^{(n-1)}(0)}{(n-1)!}\log\epsilon\right\}. \quad (2.26)$$

In the case $n=1$, the first sum on the right hand has to be omitted according to (2.24). $\mathrm{Pf}(x^{-n})_+(\varphi)$ is the distribution associated with $(x^{-n})_+$. To get the distribution associated with the function $(x^{-n})_-$ we define the distribution $\bar{T}$ obtained from T by reflection in the origin as $\bar{T}(\varphi(x))=T(\varphi(-x))$. Then we easily find (for instance, by considering the integral representations) that $\mathrm{Pf}\{(x^{-n})_-(\varphi)\}=(-1)^n\,\mathrm{Pf}\{(x^{-n})_+(\varphi(-x))\}$. Hence $\mathrm{Pf}(x^{-n})_-(\varphi)$ follows from the definition of $\mathrm{Pf}(x^{-n})_+(\varphi)$ by substituting of $\varphi(x)\to(-1)^n\varphi(-x)$ and $\varphi^{(\mu)}(0)\to(-1)^{n+\mu}\varphi^{(\mu)}(0)$ on the right side of (2.26):

$$\mathrm{Pf}(x^{-n})_-(\varphi)=\mathrm{Pf}\int_{-\infty}^{+\infty}dx(x^{-n})_-\varphi(x)$$

$$=\lim_{\epsilon\to 0}\left\{\int_{-\infty}^{-\epsilon}dx x^{-n}\varphi(x)+\sum_{\mu=0}^{n-2}(-1)^{n+\mu}\times\frac{\varphi^{(\mu)}(0)\epsilon^{\mu+1-n}}{\mu!(\mu+1-n)}-\frac{\varphi^{(n-1)}(0)}{(n-1)!}\log\epsilon\right\}, \quad (2.27)$$

n being an integer $\geqslant 1$. Since $\mathrm{Pf}(x^{-n})(\varphi)=\mathrm{Pf}(x^{-n})_+(\varphi)+\mathrm{Pf}(x^{-n})_-(\varphi)$, we obtain from (2.26, 27)

$$\mathrm{Pf}(x^{-1})(\varphi)=\mathrm{p.v.}\int_{-\infty}^{+\infty}dx x^{-1}\varphi(x)=\mathrm{p.v.}(x^{-1})(\varphi),$$

p.v. being Cauchy's principal value which appears as a direct consequence of the Pf symbol. As we will see in Sec. III, the rule given by (2.19) breaks down if m is an integer $\geqslant 1$, $\mathrm{Pf}(x^{-m})_+(\varphi)$ being defined according to (2.26).

These results can be generalized to the case of more than one variable. For instance, a quantity $\mathrm{Pf}(r^{-1})(\varphi)$ can be obtained,[8] where $r=(x^2+y^2+z^2)^{\frac{1}{2}}$. This will not be explained here, but a result may be noted which demonstrates the efficacy of the pseudofunction. In order to satisfy the Poisson equation $\Delta\Phi=0$ by the function $\Phi=1/r$ the value $r=0$ has to be excluded—a case which is physically important. But distribution-analytically we have $\Delta\{\mathrm{Pf}(r^{-1})\}(\varphi)=-\delta(\varphi)$, a relation which shows that a singularity will correctly be defined by means of the Pf symbol.

Some further properties of the distributions will be reported. For each distribution whose support is the origin, an expansion of the form $T(\varphi)=\sum c_n\delta^{(n)}(\varphi)$ exists, from which we conclude $c_n=0$ if $T=0$. With distributions defined on subspaces we can form direct products, for instance, $\delta_x\cdot\delta_y$, and construct extensions to the entire space. For example, we have (in two dimensions) the general solution $T(x,y)$ of the equation $y^mT=0$ as

$$T=\sum_{\mu=0}^{m-1}T_\mu(x)\delta^{(\mu)}(y),$$

with arbitrary distributions $T_\mu(x)$. The product of an arbitrary distribution T with an indefinitely differentiable function $g(x)$ obeys the usual rules of multiplication and differentiation, and is defined as $(Tg)(\varphi)=T(g\varphi)$. We have $D\{(Tg)(\varphi)\}=(g'T)(\varphi)+g\{DT(\varphi)\}$. For instance, we get $x\delta(\varphi)=\delta(x\varphi)=(x\varphi)_{x=0}=0$ and $(g\delta')(\varphi)=\delta'(g\varphi)=-\delta((g\varphi)'g)=(g(0)\delta'-g'(0)\delta)(\varphi)$.

The problem of division is very important. Division is defined by the inversion of multiplication, as is usual in mathematics. But the division problem of distribution analysis is distinguished from that of classical analysis by the fact that δ-algebra contains divisors of zero. The following theorem holds: If S is an arbitrary distribution, there is an infinite set of distributions T satisfying the equation

$$x\cdot T=S, \tag{2.28}$$

and two distributions of the set are distinguished from each other by an arbitrary multiple of δ. In other words, the general solution T of (2.28) is given by

$$T=S/x+c\delta, \tag{2.29}$$

c being an arbitrary "division constant." The proof of this theorem is given by Schwartz.[9] We confine ourselves to its interpretation. It is seen that the general solution T of (2.28) is the sum of a special solution of this inhomogeneous equation, i.e., S/x, and of the general solution T_0 of the homogeneous equation $x\cdot T_0=0$, i.e., $T_0=c\delta$; the latter contains an arbitrary constant c. Since the division can be defined only by the inversion of the multiplication, even in classical analysis, it must be concluded from this theorem that arbitrary constants together with distributions whose support is the origin appear automatically whenever negative powers of x are introduced by division. At first sight this statement seems a little strange, but it is absolutely correct. It should be pointed out that the first term of the right hand of (2.29) is determined only by the adoption of the Pf symbol. For instance, with $S=x$, the solution of (2.28) is not $T=1$ but $T=1+c\delta$. The uncertainty in c of this solution originates from the indeterminacy at the point $x=0$ of T in (2.28). In the same way one obtains the general solution T of $x^nT=0$ as

$$T=S/x^n+\sum_{\mu=0}^{n-1}c_\mu\delta^{(\mu)}(x),$$

the c_μ being arbitrary complex division constants. These results may be generalized to more than one variable.

The "convolution" of two functions $f(x)$ and $g(x)$, defined by

$$h(x)=f(x)*g(x)=\int_{-\infty}^{+\infty}dt f(x-t)g(t)$$

yields

$$h(\varphi)=\int_{-\infty}^{+\infty}dx h(x)\varphi(x)=\int_{-\infty}^{+\infty}\int d\zeta d\eta f(\zeta)g(\eta)\varphi(\zeta+\eta)$$
$$\equiv f_\zeta\{g_\eta[\varphi(\zeta+\eta)]\}.$$

Hence we define the convolution of two distributions S,T by

$$(S*T)_x(\varphi(x))=S_\zeta\{T_\eta[\varphi(\zeta+\eta)]\}=T_\eta\{S_\zeta[\varphi(\zeta+\eta)]\}.$$

δ appears as the unit operator of the convolution:

$$(\delta*T)_x(\varphi)=T_\zeta\{\delta_\eta[\varphi(\zeta+\eta)]\}=T_\zeta[\varphi(\zeta)]=T(\varphi).$$

It is easily to be seen that $\delta'*T=DT$. So we are led to Dirac's original definition of δ. In the space of the so-called tempered distributions, Fourier transforms will be defined by starting with the Parseval relation,

$$\int dy V(y)v(y)=\int dx U(x)u(-x),$$

or, symbolically written,

$$V_y[v(y)]=U_x[u(-x)],$$

where $V(y)=FU(x)$, $v(y)=Fu(x)$ and F implies the ordinary Fourier transformation ($\bar{F}$ is its reciprocal).

[8] L. Schwartz, reference 3, distributions I, p. 46.

[9] L. Schwartz, reference 3, distributions I, p. 121.

With u and v playing the role of φ, the Parseval relation defines the Fourier transform V of a distribution U according to

$$(FU)(v)=V_y[v(y)]=U_x[u(-x)]=(1/2\pi)U_x[(Fv)]$$
$$=(1/2\pi)U_x[v_y(\exp(-ixy))].$$

For instance, we have

$$(F\delta_x')_y(v_y)=(1/2\pi)\delta_x'[Fv]=(1/2\pi)\delta_x'[v_y(\exp(-ixy))]$$
$$=(-1/2\pi)d[v_y(\exp(-ixy))/dx]_{x=0}=(1/2\pi)iy(v_y),$$
$$\text{i.e., } F\delta_x'=(1/2\pi)iy.$$

This outline of the theory of distributions will be sufficient to cover the applications in the following sections.

III. DISTRIBUTION-ANALYTICAL TREATMENT OF CLOSED LOOP PROCESSES

The formalism sketched in the preceding section will give the basis for the treatment of quantum-theoretical problems. Without any restriction we confine ourselves for simplicity to the discussion of processes of the closed loop type. It should be pointed out that most of the quantities appearing in the following have to be considered as distributions, for instance, the self-charge and the matrix element M, even if the symbol φ is not written explicitly.

We start with the proof of Eq. (1.2), which reads, for $n=1$,

$$\mathrm{Pf}[\delta(x)y^{-1}+\delta(y)x^{-1}]$$
$$=-\tfrac{1}{2}\int_{-1}^{+1}da\,\delta'(x(1+a)/2+y(1-a)/2). \quad (3.1)$$

This equation does not hold, e.g., for $x=y$ as is easily seen from the evaluation of the right-hand side. However, the case $x=y$ is physically important. In order to prove (3.1), the relation

$$[\delta(x)y^{-1}+\delta(y)x^{-1}]=[\delta(x)-\delta(y)](y-x)^{-1} \quad (3.2)$$

is used in the conventional formalism by representing the right-hand side of this equation by Fourier integrals in a well-known manner which yields the right-hand side of (3.1). The relation (3.2) is no identity, and it is necessary to verify it explicitly. Both sides of (3.2) exist as distributions only by adopting the Pf symbol. Since $(y-x)$ appears in the denominator of the right-hand side of (3.2), the left-hand side of this equation can only be explained as the solution of an equation like (2.28). The division of $[\delta(x)-\delta(y)]$ by $(y-x)$ is defined only by the inversion of the multiplication. Therefore, we must look for the general solution T of the equation

$$[(y-x)T(x,y)](\varphi(x,y))=[\delta(x)-\delta(y)](\varphi(x,y)). \quad (3.3)$$

A special solution is found to be

$$S(x,y)=\mathrm{Pf}[\delta(x)y^{-1}+\delta(y)x^{-1}],$$

since we have

$$[(y-x)S](\varphi)=S[(y-x)\varphi]$$
$$=\mathrm{Pf}\int\int dxdy[\delta(x)y^{-1}+\delta(y)x^{-1}](y-x)\varphi(x,y)$$
$$=\int dy\varphi(0,y)-\int dx(x,0)=[\delta(x)-\delta(y)](\varphi(x,y)).$$

But according to the theorem stated in Sec. II [see Eqs. (2.28, 29)], the general solution T is given by the sum of the special solution S of the inhomogeneous Eq. (3.3) and of the general solution $S_0(x,y)$ of the homogeneous equation $[(y-x)S_0](\varphi)=0$; the latter is $S_0(x,y)=f(x)\delta(x-y)$, $f(x)$ being an arbitrary function. So we have, instead of (3.2),

$$\mathrm{Pf}[\delta(x)y^{-1}+\delta(y)x^{-1}]$$
$$=[\delta(x)-\delta(y)]\,\mathrm{Pf}(y-x)^{-1}+f(x)\delta(y-x). \quad (3.4)$$

The uncertainty in $f(x)$ of the second term on the right-hand side of (3.4) originates from the indeterminacy in the point $x=y$ of the first term on the right-hand side. By multiplying Eq. (3.4) by $(y-x)$ its correctness may be verified directly. Equations of this kind, containing arbitrary constants or functions, are important, for example, for $\delta_\pm$-functions and scattering problems.[10] Hence Eq. (3.1) has to be supplied by $f(x)\delta(x-y)$. The same result is obtained by evaluating the left side of (3.1) by a transformation of the variables of the integrals represented [see Eqs. (42, 43) in the paper of Pauli-Villars[1]] and symmetrization; by the latter process an arbitrary function is induced again. By generalizing this result a term of the form

$$\sum_{i<k}T_i(x_0,\cdots,x_{k-1},x_{k+1},\cdots,x_n)\delta(x_i-x_k), \quad (3.5)$$

with $x_i=k_i^2+m^2$, has to be added to the right-hand side of (1.2), the T_i being arbitrary distributions with respect to the variables x_k $(k\neq i)$ and arbitrary functions with respect to x_i. Carrying out the transformations of Sec. II, we find that the matrix elements obtained contain arbitrary distributions which modify observable effects in a quite uncertain way.

For the further analysis of the matrix elements M_n, the derivatives of $\mathrm{Pf}(x^{-n})_\pm$ are needed. As we have shown in Sec. II, the distributions associated with the nonsummable functions $(x^{-n})_\pm$ are given by $\mathrm{Pf}(x^{-n})_\pm(\varphi)$, Eqs. (2.26, 27). There it was stated that their distribution-derivatives cannot be equal to distributions associated with the respective function-derivatives. According to (2.21) the distribution $f_+(\varphi)=(\log|x|)_+(\varphi)$ exists together with its distribution-derivatives, the first of which is given by (2.22). The nth derivative

[10] See P. A. M. Dirac, *Die Prinzipien der Quantenmechanik* (Teubner, Leipzig, 1930), first edition, Chap. 10.

$D^n f_+(\varphi)$ is defined according to (2.4) by

$$D^n(f_+(\varphi))=(-1)^n(\log|x|)_+(\varphi^{(n)}(x))$$
$$=(-1)^n\lim_{\epsilon\to 0}\int_\epsilon^\infty dx\log|x|\cdot\varphi^{(n)}(x). \quad (3.6)$$

To rewrite the right-hand side of this equation in a form which contains φ explicitly, we perform a legitimate successive integration by parts:

$$D^n(f_+(\varphi))$$
$$=(-1)^{n-1}\lim_{\epsilon\to 0}\left\{\int_\epsilon^\infty dx x^{-1}\varphi^{(n-1)}(x)+\log\epsilon\cdot\varphi^{(n-1)}(\epsilon)\right\}$$
$$=\cdots=(-1)^{n-1}\lim_{\epsilon\to 0}\left\{(n-1)!\int_\epsilon^\infty dx x^{-n}\varphi(x)\right.$$
$$\left.+\varphi^{(n-1)}(\epsilon)\log\epsilon-\sum_{\mu=1}^{n-1}(\mu-1)!\epsilon^{-\mu}\varphi^{(n-\mu-1)}(\epsilon)\right\},$$

since $\varphi^{(n)}(\pm\infty)\equiv 0$. Taking into account

$$\varphi(\epsilon)=\sum_{r=0}^{N}(\epsilon^r/r!)\varphi^{(r)}(0)+O(\epsilon),$$

and evaluating the resulting double sum, we obtain

$$D^n[f_+(\varphi)]$$
$$=(-1)^{n-1}(n-1)!\lim_{\epsilon\to 0}\left\{\int_\epsilon^\infty dx x^{-n}\varphi(x)\right.$$
$$\left.+\sum_{\mu=0}^{n-2}(\varphi^{(\mu)}(0)/\mu!)\frac{\epsilon^{\mu+1-n}}{\mu+1-n}+\frac{\varphi^{(n-1)}(0)}{(n-1)!}\log\epsilon\right\}$$
$$-\sum_{\mu=1}^{n-1}(1/\mu)\delta^{(n-1)}(\varphi). \quad (3.7)$$

According to (2.26), the first term of the right side of (3.7) is identical with $(-1)^{n-1}(n-1)!\ \mathrm{Pf}[(x^{-n})_+(\varphi)]$. Thus $(n\geqslant 2)$

$$D^n[f_+(\varphi)]=(-1)^{n-1}(n-1)!\ \mathrm{Pf}[(x^{-n})_+(\varphi)]$$
$$-\sum_{\mu=1}^{n-1}(1/\mu)\delta^{(n-1)}(\varphi). \quad (3.8)$$

This equation can also be proved by induction (see Appendix III). On the other hand, starting with

$$f_-(\varphi)=(\log|x|)_-(\varphi)=\lim_{\epsilon\to 0}\int_{-\infty}^{-\epsilon}dx\log|x|\,\varphi(x),$$

we find

$$D[f_-(\varphi)]=-f_-(\varphi')=-\lim_{\epsilon\to 0}\int_{-\infty}^{-\epsilon}dx\log|x|\,\varphi'(x)$$
$$=\lim_{\epsilon\to 0}\left\{\int_{-\infty}^{-\epsilon}dx x^{-1}\varphi(x)-\log\epsilon\cdot\varphi(0)\right\}=\mathrm{Pf}(x^{-1})_-(\varphi). \quad (3.9)$$

In the same manner as above, we obtain the formula $(n\geqslant 2)$

$$D^n[f_-(\varphi)]$$
$$=(-1)^{n-1}(n-1)!\lim_{\epsilon\to 0}\left\{\int_{-\infty}^{-\epsilon}dx x^{-n}\varphi(x)\right.$$
$$\left.+\sum_{\mu=0}^{n-2}[\varphi^{(\mu)}(0)/\mu!]\frac{\epsilon^{\mu+1-n}}{\mu+1-n}+\frac{\varphi^{(n-1)}(0)}{(n-1)!}\log\epsilon\right\}$$
$$+\sum_{\mu=1}^{n-1}(1/\mu)\delta^{(n-1)}(\varphi), \quad (3.10)$$

which will be proved in Appendix III. Hence

$$D^{n+1}[f_\pm(\varphi)]=(-1)^n n!\ \mathrm{Pf}[(x^{-n-1})_\pm(\varphi)]$$
$$\mp\sum_{\mu=1}^{n}(1/\mu)\delta^{(n)}(\varphi). \quad (3.11)$$

But, from (2.4) and (3.8, 10), we get

$$D^{n+1}[f_\pm(\varphi)]=D\{D^n[f_\pm(\varphi)]\}=(-1)^{n-1}(n-1)!$$
$$\times D\{\mathrm{Pf}(x^{-n})_\pm(\varphi)\}\mp\sum_{\mu=1}^{n-1}(1/\mu)\delta^{(n)}(\varphi). \quad (3.12)$$

By equating (3.11) and (3.12), the important result

$$D\{\mathrm{Pf}[(x^{-n})_\pm(\varphi)]\}$$
$$=-n\ \mathrm{Pf}[(x^{-n-1})_\pm(\varphi)]\pm[(-1)^n/n!]\delta^{(n)}(\varphi) \quad (3.13)$$

is obtained. This rule holds if n is an integer $\geqslant 0$; if $n=0$, the Pf symbol is superfluous. The appearance of $\delta^{(n)}$ on the right side of (3.13), resulting from the rigorous definition of $(x^{-n})_\pm$ for $x=0$ by the Pf symbol, is very reasonable. Omitting for convenience the symbol φ in the following, we conclude from (3.13) since $\mathrm{Pf}(x^{-n})=\mathrm{Pf}(x^{-n})_+ + \mathrm{Pf}(x^{-n})_-$ that

$$D\{\mathrm{Pf}[(x^{-n})(\varphi)]\}=-n\ \mathrm{Pf}[(x^{-n-1})(\varphi)]. \quad (3.14)$$

Further, we obtain from (3.13) since

$$\mathrm{Pf}(x^{-n})_+-\mathrm{Pf}(x^{-n})_-=\epsilon(x)\ \mathrm{Pf}(x^{-n}),$$

$$D\{\epsilon(x)\ \mathrm{Pf}(x^{-1})(\varphi)\}$$
$$=-[\mathrm{Pf}(x^{-2})_+-\mathrm{Pf}(x^{-2})_-](\varphi)-2\delta'(\varphi)$$
$$=-\epsilon(x)\ \mathrm{Pf}(x^{-2})(\varphi)-2\delta'(\varphi). \quad (3.15)$$

Generally the following relation holds:

$$D^m[\mathrm{Pf}(x^{-n})_\pm]=(-1)^m\prod_{r=0}^{m-1}(n+r)\ \mathrm{Pf}(x^{-(m+n)})_\pm$$
$$\pm\frac{(-1)^n}{(n-1)!}\sum_{r=0}^{m-1}(n+r)^{-1}\delta^{(m+n-1)}(x), \quad (3.16)$$

which will be proved in Appendix IV. Hence we get

$$D^m[\epsilon(x)\ \mathrm{Pf}x^{-n}]=(-1)^m\prod_{r=0}^{m-1}(n+r)\epsilon(x)\ \mathrm{Pf}x^{-(m+n)}$$
$$+\frac{2(-1)^n}{(n-1)!}\sum_{r=0}^{m-1}(n+r)^{-1}\delta^{(m+n-1)}(x). \quad (3.17)$$

Now we are prepared for a criticism of the formula (1.3), which is used extensively in field theory. By investigating the solutions of the Laplace equation.[11] Schwartz has shown that the following formula holds (C being Euler's constant):

$$\bar{F}[\epsilon(z)\ \mathrm{Pf}z^{-1}](\varphi(x))$$
$$\equiv\mathrm{Pf}\left[\int_{-\infty}^{+\infty}dz\epsilon(z)z^{-1}\exp(izx)\right](\varphi)$$
$$=-2[\log|x|+C+\log(2\pi)](\varphi), \quad (3.18)$$

or, reciprocally written,

$$F(\log|x|)\equiv(1/2\pi)\int_{-\infty}^{+\infty}dx\log|x|\ \exp(-izx)$$
$$=-\tfrac{1}{2}\epsilon(z)\cdot\mathrm{Pf}(z^{-1})-[C+\log(2\pi)]\delta(z).$$

However, the integral in (3.18) is not invariant with respect to the transformation $z\to\lambda z$, i.e., it shows a lack of dilatation invariance. The correct formulas are

$$\left[\mathrm{Pf}\int_{-\infty}^{+\infty}dz\epsilon(z)z^{-1}\exp(izx)\right](\varphi)$$
$$=-2[\log|x|+C+\log(2\pi\lambda)](\varphi), \quad (3.19)$$

$$F(\log|x|)(\varphi)=[-\tfrac{1}{2}\epsilon(z)\cdot\mathrm{Pf}(z^{-1})$$
$$-\{C+\log(2\pi\lambda)\}\delta(z)](\varphi), \quad (3.20)$$

where λ is an arbitrary finite constant connected with the dilatation transformation named above. This constant may be called a "normalization constant." In the sense of classical analysis, the integral on the left-hand side of (3.19) is a divergent one, but it is convergent in the sense of distribution analysis as a result of a strict definition of $\epsilon(z)\ \mathrm{Pf}(z^{-1})$ for $z=0$. As stated by Schwartz, the pseudofunction

$$\mathrm{Pf}\int_0^a dx\varphi(x)x^{-n}$$

can be interpreted as the analytical continuation $F(0)$ of an ordinary integral

$$F(z)=\int_0^a dx\varphi(x)x^{z-n}$$

if n is not an integer, or of $F(z)-1/z$ if n is an integer. $F(0)$ is invariant with respect to variable transformations if $n\neq 1$, but if $n=1$ we have $F(0)\to F(0)-\varphi(0)\log\lambda$ by the dilatation transformation $x\to\lambda x$. This lack of dilatation invariance originates from the compactness of the support of the φ's, and seems to be characteristic for particles with a finite nonvanishing rest mass [see Eqs. (4.5, 6)]. This problem may be investigated on the basis of the theory of differential forms of distributions; the latter lies beyond the object of this paper.

By differentiating (3.20) with respect to x taking account of $F(DU(x))=izF(U(x))$, one can deduce the relations (n being an integer ≥ 1)

$$\mathrm{Pf}x^{-n}(\varphi)=(1/2i^n(n-1)!)$$
$$\times\int_{-\infty}^{+\infty}dz\epsilon(z)z^{n-1}\exp(izx)(\varphi), \quad (3.21)$$
$$\mathrm{Pf}\int_{-\infty}^{+\infty}dxx^{-n}\exp(-izx)(\varphi)$$
$$=(\pi z^{n-1}\epsilon(z)/i^n(n-1)!)(\varphi).$$

Further, we find, using (3.17, 20), that

$$F(x(\log|x|-1))=(Fx)*(F(\log|x|-1))$$
$$=i\delta'(z)*F(\log|x|-1)=id[F(\log|x|-1)]/dz$$
$$=\tfrac{1}{2}i\epsilon(z)\ \mathrm{Pf}(z^{-2})-i[C+\log(2\pi\lambda')]\delta'(z).$$

Hence (λ' being a normalization constant),

$$\mathrm{Pf}\int_{-\infty}^{+\infty}dz\epsilon(z)z^{-2}\exp(izx)$$
$$=-2ix[\log|x|-1+C+\log(2\pi\lambda')]. \quad (3.22)$$

Finally, it can be shown by investigating Fresnel's integrals that the formula

$$\mathrm{Pf}\int_{-\infty}^{+\infty}d^4k\exp(izk^2)(\varphi)=i\pi^2\epsilon(z)\ \mathrm{Pf}(z^{-2})(\varphi) \quad (3.23)$$

holds. By differentiating (3.23) with respect to z according to (3.17) [noting that the result of differentiation of the left-hand side of (3.23) reads effectively

$$\mathrm{Pf}\int_{-\infty}^{+\infty}d^4k(ik^2)^n\exp(izk^2)(\varphi)$$

according to (2.20)], we easily obtain the important relation

$$\mathrm{Pf}\int_{-\infty}^{+\infty}d^4k(k^2)^n\exp(izk^2)$$
$$=\pi^2i^{n+1}(n+1)!\epsilon(z)\ \mathrm{Pf}(z^{-n-2})$$
$$+2\pi^2i^{1-n}\sum_{\mu=2}^{n+1}(1/\mu)\delta^{(n+1)}(z). \quad (3.24)$$

[11] L. Schwartz, reference 3, distributions II, p. 114.

From this the formula (1.3) is shown to be incorrect, except for $n=1$.

Now we can compute the S-matrix element M_n [Eq. (1.1)] correctly. Neglecting temporarily the arbitrary distributions resulting from (3.5), the performance of the k-integration according to (3.24) yields the term

$$h(z)=2\pi^2 i^{1-n}\Big[\sum_{\mu=2}^{n+1}(1/\mu)\Big]\delta^{(n+1)}(z),$$

which must be added to the integrand of the z-integral of (1.4), say $\epsilon(z)z^{n-j-2}\to\epsilon(z)z^{n-j-2}+h(z)$. From this it follows that some matrix elements, for instance the transition element of the decay of a scalar τ-meson into two pseudoscalar π-mesons, will be modified [see Eq. (4.10)]. Such additive quantities appear only for elements with $j=n_0$ and $n\leqslant 3$. By the substitution of the Fourier representations of the $\bar{S}$-functions a distribution-analytical division problem is induced, i.e., by $\mathrm{Pf}(k^2+m^2)^{-1}$, which is apparently eliminated by the integral representation of $\mathrm{Pf}(k^2+m^2)^{-1}$ by (1.2). This division problem appears again in the form of negative powers of z in performing the k-integration according to (3.24) by which, as we have demonstrated in the preceding section, a distribution of the form

$$\sum_{j=0}^{N} c_j^{(n)}\delta^{(j)}(z),$$

($N=1, 0, 0$ for $n=1, 2, 3$, respectively, $c_j^{(n)}=0$ if $n\geqslant 4$, $c_j^{(n)}=$arbitrary constants), with the origin as support is produced in the integrand of the z-integral. There is no counterpart of this division problem in classical analysis. This result may also be proved explicitly by verifying carefully each step of the calculation [as with Eqs. (3.1–4)]. After some calculations we find, instead of (1.4), for M_n:

$$\begin{aligned}M_n(x)=(G/4(2\pi)^{4n+2})\sum_{j=0}^{n_0}\prod_{k=1}^{n}\Big(\int_{-\infty}^{+\infty}d^4p_k\bar{U}_k(p_k)\\ \times\int_{-1}^{+1}da_k\Big)A_j\alpha_n i^{n+j+1}(j+1)!\exp(-ixp_0)\\ \times\mathrm{Pf}\int_{-\infty}^{+\infty}dz\exp\Big[iz\Big(m^2+\sum_{k=0}^{n}\beta_k\lambda_k{}^2\Big)\Big]\\ \times\{z^{n-j-2}\epsilon(z)+c_0{}^{(1)}\delta_{n,1}\delta(z)+\delta_{j,n_0}[R(-1)^{n_0}\\ \times[(n_0+2-n)/(n_0-1)!]+c_j^{(n)}]\\ \times\delta^{(n_0-n+1)}(z),\quad(3.25)\end{aligned}$$

from which it follows that

$$\begin{aligned}M_1(x)=(G/4(2\pi)^{10})\int_{-1}^{+1}da_1\{2A_1[m^2-(1-a_1{}^2)\Box/4]\\ \times[\log|m^2-(1-a_1{}^2)\Box/4|+C+\log(2\pi\lambda')\\ -2+c_0{}^{(1)}/2]-A_0[\log|m^2-(1-a_1{}^2)\Box/4|\\ +C+\log(2\pi\lambda)+c_1{}^{(1)}]\}U_1(x),\quad(3.26)\end{aligned}$$

and for $n\geqslant 2$,

$$\begin{aligned}M_n(x)=((-1)^nG/2(2\pi)^{4n+2})\\ \times\prod_{j=1}^{n}\Big(\int_{-\infty}^{+\infty}d^4p_j\bar{U}_j(p_j)\int_{-1}^{+1}da_j\Big)\alpha_n\\ \times\exp(-ixp_0)\Big\{\sum_{k=0}^{n_0}A_k(k+1)!(n-k-2)!\\ \times\Big(m^2+\sum_{0}^{n}\beta_i\lambda_i{}^2\Big)^{k+1-n}-A_{n-1}n!\\ \times B\Big[\log|m^2+\sum_{0}^{n}\beta_i\lambda_i{}^2|+C+D\\ +\log(2\pi\lambda)-c_{n-1}{}^{(n)}/2\Big]\Big\}.\quad(3.27)\end{aligned}$$

Here $B=1$ if $n=2, 3$; $B=0$ for $n>3$; $D=\frac{1}{2}$ if $n=2$, $D=-\frac{5}{6}$ if $n=3$, $D=0$ for $n>3$, and A are given as in (1.4). These matrix elements, however, are seen to be convergent, and contain arbitrary division constants $c_1{}^{(1)}$, $c_{n-1}{}^{(n)}$ and normalization constants λ, λ' if $n\leqslant 3$.

IV. TWO- AND THREE-FIELD PROBLEMS

In this section the formalism explained above will be applied to special interaction problems. First we study the self-energy of the photon. The current δj_μ induced in the vacuum is obtained from M_1 and $U_1=A_\nu{}^{\mathrm{ext}}$, $\Gamma_0=\gamma_\nu$, $\Gamma_1=\gamma_\mu$, as

$$\delta j_\mu(x)=M_1(x)=-4e^2\int_{-\infty}^{+\infty}d^4x_1K_{\mu\nu}(x-x_1)A_\nu{}^{\mathrm{ext}}(x_1),$$

where $K_{\mu\nu}$ is given by

$$K_{\mu\nu}(x_0-x_1)=\mathrm{Sp}\sum S^{(1)}(0,1)\gamma_\mu\bar{S}(1,0)\gamma_\nu.\quad(4.1)$$

Introducing a new normalization constant λ'' by $\log\lambda'=\log\lambda+\frac{1}{2}\log\lambda''$, and using (3.26), the Fourier transform $K_{\mu\nu}(p)$ of $K_{\mu\nu}(x)$ is found to be

$$\begin{aligned}K_{\mu\nu}(p)=\Big[\tfrac{1}{16}(2\pi)^2\Big]\int_{-1}^{+1}da\{(1-a^2)(p_\mu p_\nu-\delta_{\mu\nu}p^2)\\ \times[\log|(1-a^2)(p^2/4)+m^2|+C+\log(2\pi\lambda)+c_1]\\ +\delta_{\mu\nu}[(1-a^2)(p^2/4)+m^2](1-\log\lambda''+c_2)\},\quad(4.2)\end{aligned}$$

where c_1 and c_2 are arbitrary division constants. This expression, i.e., δj_μ, is not gauge-invariant. The gauge-invariant result,

$$\begin{aligned}K_{\mu\nu}(p)=(p^2\delta_{\mu\nu}-p_\mu p_\nu)\Big[\tfrac{1}{8}(2\pi)^2\Big]\int_{-1}^{+1}da((1-a^2)/4)\\ \times\Big\{\mathrm{Pf}\int_{-\infty}^{+\infty}dz\epsilon(z)z^{-1}\exp iz[(1-a^2)(p^2/4)+m^2]+c\Big\},\\ (4.3)\end{aligned}$$

$(c=-c_1/2)$, is obtained either by suitable choice of c_2 (e.g., neglecting the lack of dilatation invariance by using Eq. (3.18), i.e., $\lambda=\lambda'=\lambda''=1$, the choice $c_2=-1$ is sufficient) or, letting c_2 be zero, by the choice $\log\lambda''=1$. This conclusion is shown to be unique [provided that arbitrary distributions (3.5) are neglected], for expanding the left hand of $p_\mu K_{\mu\nu}(p)=0$ in powers of m, expressions of the form $\alpha\delta(z)+\beta\delta'(z)$ must vanish [see Eq. (4.7a)] yielding $\alpha=\beta=0$ (see Sec. II). Therefore, the vanishing of the self-energy of interacting photons is guaranteed exactly, but, according to the arbitrary normalization constant λ and the division constant c we cannot conclude that the unobservable (finite) mass of the bare photon is definite. With

$$K_{\mu\nu}(p)=(p_\mu p_\nu-\delta_{\mu\nu}p^2)K(p^2),$$

$$\log|m^2+(1-a^2)(p^2/4)|$$

$$=\log m^2-\sum_{n=1}^{\infty}[(a^2-1)/4m^2]^n(p^2)^n/n!,$$

we find from (4.3), making use of (3.19), that

$$K(p^2)=(1/48\pi^2)\log(m^2\lambda^*)+(m/4\pi)^2\sum_{n=1}^{\infty}K_n\cdot(p^2)^n, \tag{4.4}$$

where

$$K_n=(1/n!)\int_{-1}^{+1}da[(a^2-1)/4m^2]^{n+1}, \tag{4.4a}$$

$$\log\lambda^*=C+\log(2\pi\lambda)-c/2.$$

The observable quantities are in agreement with those of Schwinger.[5] The renormalization of charge reads

$$\delta e=4e^2K(0)=(\alpha/3\pi)\log(m^2\lambda^*),\ \alpha=e^2/4\pi=1/137, \tag{4.5}$$

which is convergent but indeterminate in the normalization and division constants.

Generally it is seen from (3.25–27) that, according to their common origin, the normalization constants appear simultaneously with the division constants. Since both constants are arbitrary, one of them may be omitted in the results. Thus it can be concluded from the distribution-analytical formulation of field theory that an arbitrary constant corresponds to each quantity which is divergent in the conventional theory [see, for instance, Eq. (4.5)]. Some consequences of this fact will be drawn in what follows.

To analyze the problem of a finite nonvanishing self-energy of the photon we consider for simplicity Eqs. (43) and (44) of the paper of Pauli-Villars.[1] Here the integral

$$\int_{-\infty}^{+\infty}dz\epsilon(z)d[\exp(izx)\ \mathrm{Pf}(z^{-1})]/dz$$

has to be evaluated. This integral is not equal to

$$-2\int_{-\infty}^{+\infty}dz\delta(z)\ \mathrm{Pf}(z^{-1})\exp(izx)$$

obtained by ordinary integration by parts, as usually stated, corresponding to the quadratic divergence of the photon self-energy if—as it is done in the ordinary formalism—the Pf symbol is omitted. Instead of this we find, by differentiating $\epsilon(z)\exp(izx)\ \mathrm{Pf}(z^{-1})$ according to (3.17),

$$\epsilon(z)d[\exp(izx)\ \mathrm{Pf}(z^{-1})]/dz$$
$$=d[\epsilon(z)\exp(izx)\ \mathrm{Pf}(z^{-1})]/dz+2\delta'(z)\exp(izx).$$

The first term on the right-hand side of this equation vanishes when integrated over z. From the second expression a finite self-energy is obtained. But we have

$$2\delta'(z)\exp(izx)=[-2\delta(z)\ \mathrm{Pf}(z^{-1})+c\delta(z)]\exp(izx)$$

[since from $z\delta(z)=0$, $\delta(z)+z\delta'(z)=0$ it follows that $\delta'(z)=\delta(z)\ \mathrm{Pf}(z^{-1})+c\delta(z)$ according to (2.28, 29)] where the first term in the bracket corresponds to the quadratic divergence if the Pf symbol is omitted, i.e., if no use is made of distribution analysis. This explains the discrepancies between the classical quadratic divergence of the photon self-energy, the finite result of Wentzel,[4] and the vanishing observable mass.

The connection of the normalization constant λ with Feynman's cut-off factor may be exhibited as follows: By going over from $\delta(x_\nu^2)$ to $f(x_\nu^2)$ in Feynman's formalism, a convergence factor

$$C(k^2)=(\mu^2-\lambda_0^2)/(k^2-\lambda_0^2)$$

is introduced into the integrand of integrals over the momentum k of virtual particles, like

$$\int_{-\infty}^{+\infty}d^4k(k^2-\mu^2)^{-1}\to\int_{-\infty}^{+\infty}d^4k(k^2-\mu^2)^{-1}C(k^2)$$
$$=-\int_{-\infty}^{+\infty}d^4k\int_{\mu^2}^{\lambda_0^2}dL(k^2-L)^{-2},$$

$\lambda_0\to\infty$, which yields a term $\log(\lambda_0^2\mu^{-2})$. On the other hand, $(k^2-\mu^2)^{-1}$ is shown to be equivalent to $-\delta'(k^2-\mu^2)$ when integrated on k. But by distribution analysis we obtain

$$-\int_{-\infty}^{+\infty}d^4k\delta'(k^2-\mu^2)\sim\mathrm{Pf}\int_{-\infty}^{+\infty}dz\epsilon(z)z^{-1}$$
$$\times\exp(iz\mu^2)\sim\log(\lambda\mu^{-2}),$$

with the normalization constant λ, by omitting a division constant. So we can conclude that the normalization constant (and the division constants) ap-

pearing by application of distribution analysis may be interpreted as a cut-off factor, although its mathematical meaning is quite different from an actual cutoff. We see again that the division constant is equivalent to the normalization constant.

Distribution-analytically, the efficacy of the regulator of Pauli-Villars appears in a new light. As can be shown by considering (3.25) for various processes, the ambiguous terms to be eliminated from the S-matrix generally have the form $[C_1\delta(z)+C_2\delta'(z)]\exp(izm^2)$ in the integrand of the z-integral of (3.25). By introducing the regulator $R(z)=\int d\kappa\rho(\kappa)\exp(iz\kappa)$ into the field-theoretical formalism we get, therefore,

$$[C_1\delta(z)+C_2\delta'(z)]R(z)=[C_1R(0)-C_2R'(0)]\delta(z)+C_2R(0)\delta'(z),$$

which yields the regularization conditions $R(0)=R'(0)=0$. On the other hand, by the distribution calculus there appears an expression $[c_1\delta(z)+c_2\delta'(z)]\exp(izm^2)$ in (3.25) which is able to eliminate the ambiguous terms by the choice of $c_i=-C_i$. From that we conclude that only such terms have to be subjected to the regulator whose the "m-factors" are induced by $\exp(izm^2)$ coming from $\mathrm{Pf}(k^2+m^2)^{-1}$ in $\bar{S}$, without any consideration of the powers of m contained in the traces. This explains the various regularization alternatives,[12] but such doubtful limiting methods are not necessary in the new formalism which is mathematically correct as well as more powerful, even in nonrenormalizable theories.

The discrepancies contained in the relations between S_F-functions and $\bar{S}$- and $S^{(1)}$-functions are removed in the same way. For instance, by calculating the self-energy of the electron in Dyson's formalism, the real part of the one-electron-zero-photon term of the second-order S-matrix, which is not equal to zero in the ordinary formalism, disappears in distribution calculus by suitable choice of division constants (provided arbitrary distributions are put to be identical zero).

Further, an evaluation of $\Delta^{(1)}(x)$ by a distribution-analytical modification of Schwinger's computation[6] shows that

$$\partial\Delta^{(1)}(x)/\partial x_\nu=-x_\nu[\pi^{-2}\,\mathrm{Pf}\zeta^{-2}+(m/2\pi)^2\,\mathrm{Pf}\zeta^{-1}+\text{reg. in }(\zeta=-x_\nu^2)]$$

vanishes identically on the light cone—as a consequence of the Pf symbol—yielding correctly in this manner the continuity relation $\partial K_{\mu\nu}(x)/\partial x_\mu=0$. A strict definition of $\mathrm{Pf}(k^2+m^2)^{-1}$ will not be given here. Some difficulties appear with regard to the properties of symmetry and reality of $\bar{S}$ and $S^{(1)}$, leading to a lack of invariance with respect to reflection in the origin of the light cone, corresponding to the dipole properties of the latter.

To compute the self-energies of the electron and nucleon the same method can be used as for the self-energy of the photon. The essential part of the self-energy of an electron reads:

$$\int_{-1}^{+1}da[i\gamma p(1-a)/2+2m]\,\mathrm{Pf}\int_{-\infty}^{+\infty}dz[\epsilon(z)z^{-1}+c\delta(z)]\times\exp[izp^2(1+a)^2/4].$$

Joining the division constant c with the normalization constant [see Eq. (3.19)]—which is always possible—to get a new constant λ_0 (for instance, neglecting the normalization constant, i.e., putting $\lambda=1$, and using c alone), we find, according to (3.19),

$$\delta m=(3m\alpha/2\pi)[\log(\lambda_0/m)+\tfrac{5}{6}]. \tag{4.6}$$

Examining the calculations of Géhéniau-Villars,[13] the values of the anomalous magnetic moments of the electron and nucleon are shown to remain unchanged provided arbitrary distributions, which appear here as in (3.5), are neglected. But it should be pointed out that there is in general no reason for neglecting such arbitrary quantities, especially in the case of the nucleon moment. By the same methods the self-stress of the electron is found to be

$$\langle\bar{T}_{11}\rangle_0=[e^2m/8(2\pi)^2]\int_{-1}^{+1}da(3-a)(4-c)/2.$$

This is equal to zero, as demanded by the theory of relativity, if we choose $c=4$. Therefore, to obtain a vanishing self-stress no admixture of vector fields is necessary.[14]

Some meson processes may now be discussed. The decay of a boson into a fermion and the processes $\pi\to\mu+\nu$, $\pi\to e+\nu$ via the nucleon field are described by M_1. The divergence theorem, including gauge-invariance, is shown to be fulfilled formally by the types of coupling $(\Gamma_0,\Gamma_1)=(v,v)$, (l,l), (v,pl) and the equivalence theorem by $M_{ps}=(pv,ps)$, $M_{pv}=(pv,pv)$. Evaluating the traces we find from (3.26), including $c_0^{(1)}$ and $c_1^{(1)}$ into λ, λ' temporarily, with $\log\lambda'=\log\lambda+\frac{1}{2}$, that

$$\begin{aligned}K(p)=-(4\pi)^{-2}\int_{-1}^{+1}da\,\mathrm{Sp}\{&((1-a^2)/4)\\&\times[p_\alpha p_\beta+\tfrac{1}{2}\delta_{\alpha\beta}p^2](\gamma_\alpha\Gamma_1\gamma_\beta\Gamma_0)\\&+\tfrac{1}{2}m^2(\gamma_i\Gamma_1\gamma_i\Gamma_0+2\Gamma_1\Gamma_0)\\&-\tfrac{1}{2}imp_\alpha([\gamma_\alpha,\Gamma_1]_-\Gamma_0)\\&\times[\log|m^2+\{(1-a^2)/4\}p^2|\\&+C+\log(2\pi\lambda)]\},\end{aligned} \tag{4.7}$$

[12] S. Tomonaga *et al.*, Prog. Theoret. Phys. **4**, 477 (1949); S. Ozaki *et al.*, Prog. Theoret. Phys. **4**, 524 (1949); **5**, 25, 165 (1950); P. T. Matthews, reference 1; J. Steinberger, reference 1.

[13] J. Géhéniau and F. Villars, Helv. Phys. Acta **23**, 178 (1950).

[14] F. Rohrlich, Phys. Rev. **77**, 357 (1950); F. Villars, Phys. Rev. **79**, 122 (1950).

where

$$K(x)=F[K(p)]=\mathrm{Sp}\sum S^{(1)}(0,1)\Gamma_1\bar{S}(1,0)\Gamma_0,$$

$$x=x_0-x_1,\quad M_1(x_0)=G\int_{-\infty}^{+\infty}d^4x_1U_1(x_1)K(x).$$

From this convergent formula, for instance, the equivalent elements M_{ps} and M_{pv} are calculated, and it is shown that the specified relation $\log\lambda'=\log\lambda+\frac{1}{2}$ between λ and λ' is the necessary and sufficient one for all processes which are subjected to the postulates of gauge invariance, equivalence, and to the divergence theorem. When there are no general prescriptions of this kind, it is not possible to get results which are free of arbitrary constants. In addition, even in the case where there are general rules, no assertion is made about the meaning of the arbitrary distributions (3.5) to be added to M_n. We have seen that the normalization constant is contained only in quantities which are not observable [see (4.5, 6)], i.e., in renormalization factors. Therefore we can say that a distribution-analytical treatment of field theory leads directly to a renormalization. On the other hand, the normalization constant was shown to appear at the same place as the cut-off factor of the conventional theory. Therefore, we no longer have in principle any distinction between renormalizable and nonrenormalizable formalisms. Having "normalized" the matrix elements by λ and c so as to satisfy the general rules, those quantities which are not dilatation invariant, i.e., which contain a normalization constant and therefore do not correspond to observable effects, may be neglected in the results; they may be included in observable masses and coupling constants.

The efficacy of the division constants—which are closely connected with the normalization constants—in eliminating unphysical terms may be demonstrated for M_{ps} and M_{pv}. Computing these elements from (3.25), both expressions can be split up into two parts, $M_{ps}{}^a+M_{ps}{}^b$ and $M_{pv}{}^a+M_{pv}{}^b$, respectively, in such a way that only $M_{ps}{}^b$ and $M_{pv}{}^b$ contain arbitrary constants, say c_1, c_2 and c_1', c_2', respectively. The equivalence theorem is then shown to be valid for $M_{ps}{}^a$ and $M_{pv}{}^a$, so that the relation $ipM_{pv}{}^b+2mM_{ps}{}^b=0$ has to be demanded. Effectively this implies that

$$p_\mu[c_1'\delta(z)+(c_2'-1)\delta'(z)]+2m[c_1\delta(z)+c_2\delta'(z)]=0, \tag{4.7a}$$

yielding $c_1=c_2=c_1'=0$, $c_2'=1$ according to Sec. II. This leads to $M_{ps}{}^b=M_{pv}{}^b=0$, giving the equivalent elements $M_{ps}{}^a$ and $M_{pv}{}^a$ in a unique way.

The calculation of the transitions[15] $\pi\to\mu+\nu$, $\pi\to e+\nu$ via the nucleon field is easily performed by means of M_1 with $\Gamma_0=\Gamma_1=1$. Both elements are finite—in contrast to those obtained by the ordinary formalism—containing arbitrary normalization and division constants, a suitable choice of which may give well $\tau_{\pi\to\mu+\nu}\sim10^{-8}$ sec in agreement with experiments. The ratio $\tau_{\pi\to\mu+\nu}/\tau_{\pi\to e+\nu}$, however, is found to be in accordance with experiment ($<10^{-2}$) only if one assumes a dependence of the ratio of masses of the decay products on the arbitrary constants (e.g., λ).

In the frame of interaction of three fields described by M_2, we discuss in particular the decay of a τ-meson into two π-mesons and the decay of neutral π-mesons into two photons.[16] General theorems, although formally fulfilled in coordinate space—even by using distribution analysis—are mostly destroyed by calculating the matrix elements in momentum space according to the ordinary formalism. Distribution-analytically from (3.27) with $n=2$ the characteristic form K of

$$M_2(x_0)=G\int_{-\infty}^{+\infty}\int d^4x d^4x_2U_1(x_1)U_2(x_2)K(x_0,x_1,x_2)$$

reads

$$K=(1/2^{15}\pi^{10})\int_{-1}^{+1}\int da_1da_2(1-a_1)\int_{-\infty}^{+\infty}\int d^4p_1d^4p_2$$

$$\times\{2A(m^2+\sum_0^2\beta_i\lambda_i{}^2)+2B-ic$$

$$-4D[\log|m^2+\sum_0^2\beta_i\lambda_i{}^2|-\tfrac{1}{2}+C+\log(2\pi\lambda)]\}$$

$$\times\exp[i\sum_{j=1}^{2}p_j(x_0-x_j)], \tag{4.8}$$

where A, B, and D are products of spur terms with momentum variables whose explicit form will not be given here; c is a division constant, and λ the normalization constant. Considering the decay $\pi\to2\gamma$ ($\Gamma_0=1$, $\Gamma_1=\gamma_\mu$, $\Gamma_2=\gamma_\nu$) of a scalar π-meson with scalar coupling, the term $B=-4m\delta_{\mu\nu}$ represents a nongauge invariant term which will be eliminated in a unique manner by choosing $c=-2iB$, with the result $M_2=(G/2m\pi^2)F_{\mu\nu}{}^2(F_{\mu\nu}=\partial_\nu A_\mu-\partial_\mu A_\nu)$; this result was obtained by Steinberger and Fukuda-Miyamoto[16] by the

[15] L. I. Schiff, Phys. Rev. **76**, 303, 1266 (1949); J. Steinberger, reference 1.

[16] Leighton, Wanlass, and Alford, Phys. Rev. **83**, 843 (1951); J. Steinberger, reference 1; H. Fukuda *et al.*, reference 1; S. Ozaki *et al.*, reference 1; A. G. Carlson *et al.*, Phil. Mag. **41**, 701 (1950).

use of regulators. The decay of a scalar τ-meson with scalar coupling into a vector π-meson and a scalar π-meson with vector coupling, which is a nonrenormalizable problem and is described by the element analogous to $\pi\to 2\gamma$, is subjected to the divergence theorem, yielding the same relation between c and B as above in order to fulfill the theorem in a unique way. As an example of equivalence, we studied the process $\pi\to 2\gamma$ of a pseudoscalar π-meson and the decay of a pseudoscalar τ-meson into two vector π-mesons with vector coupling, using the same methods as described under two-field processes. For instance, the transition $\tau\to 2\pi$ is represented by

$$M_{ps}(x)\sim(-G/48\pi^2m^3)(\mu_\tau{}^2+\mu_1{}^2+\mu_2{}^2)\times(\partial_\alpha U_\mu)(\partial_\beta U_\nu)\epsilon_{\mu\nu\alpha\beta}, \quad (4.9)$$

(μ_τ mass of τ, μ_i mass of π_i) and this holds for $(-1/2m)\partial_\mu M_{ps}$ which is nonrenormalizable. Finally, we find for the decay of a scalar τ-meson with scalar coupling into two pseudoscalar π-mesons with pseudoscalar coupling (with $\Gamma_0=1$, $\Gamma_1=\gamma_5$, $\Gamma_2=\gamma_6$, $\mu_1=\mu_2=\mu_\pi$)

$$M\sim-(G/(2\pi)^2)\{m^{-1}[\mu_\tau{}^2+\tfrac{2}{3}\mu_\pi{}^2]-(m/4)[32\{\log(m^2 2\pi\lambda)+C+\tfrac{1}{8}\}+c-16]\}U_1U_2. \quad (4.10)$$

This transition element is divergent in the conventional formalism. According to the theory of distributions it contains arbitrary constants (c, λ). The term -16 in the second bracket comes from Eq. (3.24); it cannot be obtained by the conventional incorrect formula (1.3).

However, the meaning of the arbitrary distributions which were neglected above throughout, is by no means clarified. An evaluation of the respective terms shows that the additive quantities resulting from (3.5) are distinguished from the elements written in the text only by extending the boundaries of the a_i-integrals to $\pm\infty$ and replacing dz by $dzf(z, a_i)$ in the z-integral, $f(z, a_i)$ being an arbitrary distribution.

Numerous examples can be added to show how to treat other questions in field theory by means of distribution analysis in an unambiguous and self-consistent manner. For example, the calculation of radiative corrections can be made by these methods. It is believed that a careful investigation by means of the theory of distributions leads to consistent results in many cases where the conventional methods fail. It is no longer necessary to adopt such doubtful prescriptions as to attach the value zero to certain divergent integrals, as is done, for instance, in the calculation of radiative corrections to the stress tensor of the electron.[17] We are not obliged to go outside the framework of current field theory by introducing unrealistic auxiliary fields so as to compensate undesirable effects. But it should be pointed out that it is not legitimate to consider only the last steps of a calculation by distribution methods. The distribution analysis has to be performed from the beginning, verifying carefully each step of the computation.

A very important question is the degree of uncertainty of the results obtained only from the distribution calculus without new physical assumptions. The situation arising from the appearance of arbitrary constants and functions in the result is quite analogous to that of the theory of linear and partial differential equations. In both cases the arbitrary parameters serve for the adaptation of the result to initial and boundary conditions. Since there are many processes for which no general rules, such as gauge invariance, are known in order to determinate the arbitrary constants, we have to conclude that the fundamental physical assumptions of the field theory are incomplete. In order to determine these arbitrary parameters, especially in meson theory, additive quantities in the interaction Hamiltonian seem to be necessary.

Corresponding to the arbitrary constants, it is not possible to attribute definite values to the parameters of bare particles. The determination of normalization constants by the general rules, for instance by the gauge invariance of a theory with interaction, will exclude the possibility of the simultaneous existence of a theory which is gauge invariant without interaction. The uncertainty of some effects induced by the arbitrariness of normalization constants seems to be a consequence of the idealized localizability of field quantities in space-time, that is, of the finiteness of the masses of particles, which is manifested by a lack of dilatation invariance.

The main problems to be investigated in the future may concern the local and causal structure of invariant propagation functions, which now have to be considered as distributions under the aspect of the Pf symbol. Then the field operators must be replaced by distributions in order to conserve the sense of the commutation relations as distribution equations.

In conclusion, the author should like to express his hearty thanks to Professor Molière (now in Rio de Janeiro) for his kind advice and encouragement throughout this work. He is also indebted to Professor L. Schwartz (Nancy) for his stimulating discussions.

APPENDIX

I. In order to get the definition (2.3) let us consider a displacement operator $\tau_{\pm h}$ acting on $\varphi(x)$ according to $\tau_{\pm h}\varphi(x)=\varphi(x\mp h)$, and define $\tau_{\pm h}T(\varphi)=T(\tau_{\mp h}\varphi)$. Then it is natural to define

$$D[T(\varphi)] \text{ by } \lim_{h\to 0}[\tau_{-h}T(\varphi)-T(\varphi)]/h.$$

[17] S. Borowitz and W. Kohn, Phys. Rev. **86**, 985 (1952).

Since distributions are linear and continuous, we have

$$D[T(\varphi)]=\lim_{h\to 0}[\tau_{-h}T(\varphi)-T(\varphi)]/h$$

$$=\lim_{h\to 0}[T(\tau_h\varphi)-T(\varphi)]/h=\lim_{h\to 0}T(\tau_h\varphi-\varphi)/h$$

$$=T[\lim_{h\to 0}(\tau_h\varphi-\varphi)/h]=T(-\varphi'(x))=-T(\varphi'),$$

in accordance with (2.3).

II. Let us consider in the frame of classical analysis the divergent integral

$$\int_0^\infty dx(1/x^{\alpha+1})g(x),$$

$0<\alpha<1$, with a continuous function $g(x)$ whose function-derivative is continuous. As is known from the theory of partial differential equations, especially from Cauchy's problem, Hadamard[18] has introduced the notion "finite part of a divergent integral" as follows: Choose a constant c in such a way that the quantity

$$\lim_{\varepsilon\to 0}\left\{\int_\varepsilon^\infty dx(1/x^{\alpha+1})g(x)+c/\alpha\varepsilon^\alpha\right\}$$

exists. This expression can be written in the form

$$\lim_{\varepsilon\to 0}\left\{\int_\varepsilon^\infty dx[(g(x)-g(0))/x^{\alpha+1}]\right.$$

$$\left.+g(0)\int_\varepsilon^\infty dx/x^{\alpha+1}+c/\alpha\varepsilon^\alpha\right\}$$

$$=\lim_{\varepsilon\to 0}\left\{\int_\varepsilon^\infty dx[(g(x)-g(0))/x^{\alpha+1}]+(g(0)+c)/\alpha\varepsilon^\alpha\right\}.$$

Since the function-derivative $[g'(x)]$ is continuous, i.e., $|g(x)-g(0)|\leqslant M|x|$, the integral in the latter expression is convergent. Therefore, if c is chosen as $c=-g(0)$, the quantity $\lim_{\varepsilon\to 0}\{\cdots\}$ is a convergent one, and will be explained as the finite part (f.p.) of the divergent integral

$$\int_0^\infty dx(1/x^{\alpha+1})g(x):$$

$$\text{f.p.}\int_0^\infty dx(1/x^{\alpha+1})g(x)$$

$$=\lim_{\varepsilon\to 0}\left\{\int_\varepsilon^\infty dx(1/x^{\alpha+1})g(x)-g(0)/\alpha\varepsilon^\alpha\right\}.$$

[18] J. Hadamard, *Lectures on Cauchy's Problem in Linear Partial Differntial Equations* (Yale University Press, New Haven, 1923).

This definition is a very artificial one, but is useful for Cauchy's problem, especially for the study of the connection of the solutions of the Poisson and wave equations. By choosing $g(x)=\varphi(x)$ we see immediately that the distribution-derivative $Df_+(\varphi)$ of $f_+(\varphi)$ coincides with the finite part of the divergent integral

$$\text{p.f.}\int_{-\infty}^{+\infty} dx[f_+'(x)]\cdot\varphi(x).$$

But this coincidence is quite an accidental one.

III. In order to prove Eq. (3.10) we note that it is true for $n=2$ since, by integration by parts,

$$D^2(f_-(\varphi))=f_-(\varphi'')=\lim_{\epsilon\to 0}\left(\int_{-\infty}^{-\epsilon} dx\log|x|\,\varphi''(x)\right),$$

$$=-\lim_{\epsilon\to 0}\left\{\int_{-\infty}^{-\epsilon} dx(\varphi(x)/x^2)\right.$$

$$\left.-[\varphi(x)/\epsilon+\varphi'(x)\log\epsilon]_{x=-\epsilon}\right\},$$

$$=\lim_{\epsilon\to 0}\left\{\int_{-\infty}^{-\epsilon} dx(\varphi(x)/x^2)-\varphi(0)/\epsilon\right.$$

$$\left.-\varphi'(0)\log\epsilon\right\}-\varphi'(0),$$

$$\equiv-\text{Pf}[(x^{-2})_-(\varphi)]-\varphi'(0)$$

$$=-\text{Pf}[(x^{-2})_-(\varphi)]+\delta'(\varphi).$$

We suppose that (3.10) is true for some fixed n, say $n=k>2$. Then we have, according to (2.4),

$$D^{k+1}[f_-(\varphi)]$$

$$=-D^k[f_-(\varphi')]$$

$$=(-1)^k(k-1)!\,\text{Pf}[(x^{-k})_-(\varphi')]\sum_{\mu=1}^{k-1}(1/\mu)\delta^{(k-1)}(\varphi')$$

$$=(-1)^k(k-1)!\lim_{\epsilon\to 0}\left\{\int_{-\infty}^{-\epsilon} dx[\varphi'(x)/x^k]\right.$$

$$\left.+\sum_{\mu=0}^{k-2}(-1)^{k+\mu}\frac{\varphi^{(\mu+1)}(0)\epsilon^{\mu+1-k}}{\mu!(\mu+1-k)}-\frac{\varphi^{(k)}(0)}{(k-1)!}\log\epsilon\right\}$$

$$-\sum_{\mu=1}^{k-1}(1/\mu)\delta^{(k-1)}(\varphi'),$$

$$=(-1)^k k!\lim_{\epsilon\to 0}\left\{\int_{-\infty}^{-\epsilon} dx[\varphi(x)/x^{k+1}]+(-1)^k\varphi(-\epsilon)/k\epsilon^k+(1/k)\sum_{\mu=1}^{k-1}(-1)^{k+\mu-1}\frac{\varphi^{(\mu)}(0)\epsilon^{\mu-k}}{(\mu-1)!(\mu-k)}-\frac{\varphi^{(k)}(0)}{k!}\log\epsilon\right\}+\sum_{\mu=1}^{k-1}(1/\mu)\delta^{(k)}(\varphi),$$

$$=(-1)^k k!\lim_{\epsilon\to 0}\left\{\int_{-\infty}^{-\epsilon} dx[\varphi(x)/x^{k+1}]+\frac{(-1)^k}{k\epsilon^k}\varphi(0)-\frac{\varphi^{(k)}(0)}{k!}\log\epsilon+(1/k)\sum_{\mu=1}^{k-1}\left[\frac{(-1)^k\epsilon^{\mu-k}}{\mu!}+\frac{(-1)^{k+\mu-1}\epsilon^{\mu-k}}{(\mu-1)!(\mu-k)}\right]\varphi^{(\mu)}(0)\right\}+\frac{(-1)^k}{k}\varphi^{(k)}(0)+\sum_{\mu=1}^{k-1}(1/\mu)\delta^{(k)}(\varphi),$$

$$=-(-1)^{k+1}k!\,\mathrm{Pf}[(x^{-k-1})(\varphi)]+\sum_{\mu=1}^{k}(1/\mu)\delta^{(k)}(\varphi);$$

i.e., (3.10) is true for every n, q.e.d. Eq. (3.8) can be proved in the same manner.

IV. Equation (3.16) is true for $m=1$, n arbitrary, according to (3.13). Assuming (3.16) to be true for $m=k>1$ we have

$$D^{k+1}\,\mathrm{Pf}[(x^{-n})_{\pm}(\varphi)]=D[D^k\,\mathrm{Pf}(x^{-n})_{\pm}(\varphi)]$$

$$=(-1)^k\prod_{\nu=0}^{k-1}(n+\nu)D[\mathrm{Pf}(x^{-k-n})_{\pm}(\varphi)]\pm[(-1)^n/(n-1)!]\sum_{\nu=0}^{k-1}(1/n+\nu)\delta^{(k+n)}(\varphi)$$

$$=(-1)^{k+1}\prod_{\nu=0}^{k}(n+\nu)\,\mathrm{Pf}[(x^{-n-k-1})_{\pm}(\varphi)]\pm(-1)^n\left[(1/(k+n)!)\prod_{\nu=0}^{k-1}(n+\nu)+(1/(n-1)!)\sum_{\nu=0}^{k-1}(1/n+\nu)\right]\delta^{(k+n)}(\varphi)$$

$$=(-1)^{k+1}\prod_{\nu=0}^{k}(n+\nu)\,\mathrm{Pf}[(x^{-n-k-1})_{\pm}(\varphi)]\pm[(-1)^n/(n-1)!]\sum_{\nu=0}^{k}(1/n+\nu)\delta^{(k+n)}(\varphi);$$

i.e., (3.16) is true for all n, m.

PHYSICAL REVIEW VOLUME 89, NUMBER 5 MARCH 1, 1953

The Range Correction for Electron Pick-Up

WALTER H. BARKAS
Radiation Laboratory, Department of Physics, University of California, Berkeley, California
(Received October 15, 1952)

The extension of positive particle ranges caused by pick-up of electrons at low velocities has been studied in Ilford C2 emulsion. Ranges of Li^8 and B^8 nuclei were measured in emulsion and compared with tracks of helium and hydrogen isotopes of the same velocity. The empirical range-energy relation adduced for light nuclei is: $Z^2R/M=F(T/M)+0.12Z^3$, for $\beta>1.04Z/137$.

I. INTRODUCTION

IT has recently[1] been found possible to collect and analyze physically the products formed when the high energy beam of the 184-inch cyclotron is employed to disintegrate atomic nuclei. A reliable analysis of the products of atomic number greater than two was, however, difficult because the range-energy relations in nuclear track emulsion for multiply charged fragments were uncertain. In the preliminary work in which protons bombarded carbon, no "hammer" tracks indicative of the presence of Li^8 and B^8 were found. With further searching on these plates, a few such tracks have now been found, and hammer tracks are also seen in fair abundance on plates exposed to the disintegration products of various light elements bombarded with alpha-particles or deuterons. In the present experiment about one splinter in two hundred was Li^8, and about one in 5000 was B^8.

The unmistakable appearance of the tracks which they produce make Li^8 and B^8 extremely useful isotopes to employ in studying the range-energy relations for multiply charged ions. At low velocities a positive particle tends to be neutralized by electrons, thus reducing its rate of energy loss. It is the purpose of this experiment to utilize the tracks of Li^8 and B^8 to evaluate the range correction arising from this effect.

II. IDENTIFICATION AND MEASUREMENT OF TRACKS

Tracks are identified by plotting the range, R, *versus* the radius of curvature, ρ, for each track. The tracks of

[1] Walter H. Barkas and J. Kent Bowker, Phys. Rev. **87**, 207 (1952).

TABLE I. Calculation of normalization factors. T is the kinetic energy in Mev calculated from the momentum of the particle. M is the atomic weight of the ion, R is the measured range in microns, and $(4R/M)_W$ is taken from Wilkins' tables for the value of T/M listed.

	Isotope	T/M	$(4R/M)$	$(4R/M)_W$	Ratio
Plate I	He^4	1.264	21.8±0.3	21.27	1.025
	He^4	1.334	23.6±0.3	22.94	1.031
	He^3	2.221	49.6±0.3	48.30	1.027
	Adopted factor 1.027±0.002				
Plate II	He^4	2.236	50.0±0.3	48.80	1.025
	He^3	3.936	121.9±0.6	118.50	1.029
	Adopted factor 1.027±0.002				
Plate III	He^4	4.700	160.5±0.6	158.00	1.016
	He^3	8.187	401.7±1.2	396.00	1.015
	Adopted factor 1.0155±0.0005				

a particular nuclear species will then fall on a characteristic locus. For the present measurements a beryllium ribbon was bombarded by the internal alpha-particle beam of the cyclotron. The disintegration products were observed in three intervals of radius of curvature simultaneously by placing Ilford C2 200 micron plates in accurately known positions. Particles leaving the target reached the plates after being bent 180° in the magnetic field. The particles entered the emulsion making a small angle of dip with the surface. The position of the track and its entrance angles were sufficient data from which to calculate the momentum. The radial distribution of the magnetic field in the cyclotron is accurately known. Definite identification of hammer tracks as B^8 as well as Li^8 was made by a study of the ρ *vs* R curves. Loci assignable to B^8 bent in the magnetic field while carrying 5, 4, and 3 units of charge were found as well as loci of Li^8 carrying 3, 2, and 1 units of charge. Additional short unresolved hammer tracks were seen which were attributed to B^8 carrying one or two units of charge. We designate by Z' the actual number of charges carried by an ion of atomic number Z while it is deflected in the magnetic field. Its momentum then is $Z'(e/c)H\rho$.

The range is taken to be the length of the path along the trajectory in the emulsion between the extremities of the first and last grain. Badly scattered tracks were not measured. The grain density was so high, particularly for tracks of He, Li, and B, that no appreciable error could have been introduced by failure to see all of the track. No correction for such effects was made.

In the plates the tracks of many nuclear species coming from the target are found, including isotopes of hydrogen and helium. These tracks are important to the experiment as their ranges provide an over-all calibration of the geometry, magnetic field intensity, and emulsion stopping power.

III. THE RANGE EXTENSION

As a basis for the analysis of range data, I have assumed that a particle of charge Ze loses energy at the rate[2]

$$dT/dR = Z^2 f(\beta), \tag{1}$$

where T is the kinetic energy in Mev of the ion, R is its residual range in microns, and βc its velocity. Since T/M is a function solely of the velocity, M being the ionic atomic weight, Eq. (1) can be written:

$$g(\beta)d\beta = (Z^2/M)dR, \tag{2}$$

with $g(\beta)$ a function of the velocity alone. When the nucleus is moving with a sufficiently high velocity, one assumes that it is completely stripped so that the charge is not a function of the velocity. In a range interval where this condition holds, one may integrate (2) and obtain:

$$\int_{\beta_0}^{\beta} g(\beta)d\beta = G(\beta) - G(\beta_0) = Z^2R/M - Z^2R_0/M. \tag{3}$$

In this expression $\beta_0 c$ is some lower velocity still sufficiently high that the nucleus remains stripped, and R_0 is the corresponding range. Thus for $\beta > \beta_0$ one can write:

$$Z^2R/M = G(\beta) + B_Z. \tag{4}$$

In so far as the above assumptions are valid, the range of an arbitrary particle is derivable from the universal function $G(\beta)$ and the constant B_Z, which is characteristic of the element, and is a measure of the range extension caused by electron pick-up. If Z^2R/M is plotted against β, a separate locus may be anticipated for each element, but at high velocities the curves will be expected merely to be displaced by a constant amount from each other, corresponding to the differences in the values of the B_Z. In particular, if the range of an alpha-particle or other helium isotope is measured at the same velocity as that of an ion of atomic number Z, then

$$Z^2R/M - 4(R/M)_{He} = B_Z - B_2 \tag{5}$$

is obtained by subtraction, and the effect relative to helium can be obtained.

IV. NORMALIZATION OF RANGES

The range increments being evaluated are generally small and are obtained from the differences of two large numbers. Errors are easily introduced under these conditions and a method of analysis should be used which minimizes insofar as possible the systematic errors. In this article a calibration procedure for each plate was employed which eliminates many of the potential sources of difficulty. A careful study of the range-energy relations for Ilford C2 emulsions was made by Wilkins,[3] who based his results primarily on

[2] M. S. Livingston and H. A. Bethe, Revs. Modern Phys. **9**, 245 (1937).

[3] J. J. Wilkins, Atomic Energy Research Establishment (Harwell) Report G/R 664 (1951) (unpublished).

alpha-particle points. In the present experiment, the plates were subjected to normal (~50 percent) humidity before being placed in the cyclotron vacuum where they remained about fifteen minutes before bombardment. It is well known that a period of many hours is required for the water content of emulsions to stabilize so that it is hardly to be expected that the stopping power of the plates employed in this experiment was identical to that used by Wilkins in his calculations. Such a difference, if it exists, would cause all ranges to deviate systematically by roughly the same percentage from those of Wilkins. Since the range is approximately proportional to a power of the momentum, a small percentage error in the momentum also can be corrected by a percentage adjustment in the range. I have, therefore, normalized Wilkins' data to the existing conditions by adjusting his ranges to match the measured ranges of helium tracks in the plates. To good approximation, this procedure eliminates from the data small errors in geometry, magnetic field intensity, and stopping power. I rely on Wilkins' results chiefly in assuming that the shape of his curve is correct over a limited interval.

In Table I, measured values of Z^2R/M are tabulated for groups of helium tracks from each of the plates used in this study. The values predicted by Wilkins are listed in a parallel column. The measured range has been divided by Wilkins' range, and the ratio listed in the last column. Wilkins' ranges have been multiplied by the ratio appropriate to the plate being studied in obtaining the normalized quantity $(4R/M)_N$ of Table II.

The normalization factors for plates I and II check and are sufficiently near unity that they are fully explainable in view of the possible difference in stopping powers mentioned above, or possibly as an effect traceable to the uncertainty in the absolute value of the magnetic field intensity. On the other hand, there appears to be a significant change in the ratio for the third plate. Since the relative momenta are known with high accuracy, this effect can most simply be interpreted as a one percent inconsistency in Wilkins' ranges for alpha-particles of ≈ 20 Mev when compared with those in the region of 5–10 Mev.

V. RESULTS

In Table II are listed the ranges of groups of particles which were identified and measured in this study. The helium isotopes were employed in finding the normalization factors shown in Table I and are not listed again in Table II. The energies calculated from the momenta are entered in Table II as well. The hydrogen isotopes listed were measured in order to make the data complete, but to evaluate B_1-B_2 accurately lower energy particles should be used. Actually the individual determinations of B_1-B_2 appear more consistent than one might have expected. The standard deviations given are statistical and do not include systematic errors arising from possible incorrect normalization factors. For long ranges the determination of B_1-B_2 depends very sensitively on the normalization. The present measurement of B_1-B_2 is somewhat lower in absolute value than the figure of -1.38 microns adopted by Wilkins.[3] The quantities B_Z are much larger for lithium and boron than for hydrogen, and, therefore, are not so sensitive to normalization errors. Whereas for the other isotopes points were determined using 25 to 100 individual tracks, the B^8 tracks were so rare and the pick-up effect so large that each point was determined using five tracks, all of which, however, lay within two percent of the average momentum for the group.

VI. EVALUATION OF B_Z

If Z^* is the effective charge carried by a slowly moving nucleus, then:

$$B_Z=\int_0^{\beta_0}[\langle Z^2/Z^{*2}\rangle_{Av}-1]g(\beta)d\beta. \tag{6}$$

TABLE II. Observed ranges and derived range corrections.

Ion	T_{Mev}	R_{micron}	Z^2R/M	$(4R/M)_N$	$Z^2R/M-(4R/M)_N$
H^3	2.890	42.6±0.4	14.1 ±0.13	15.01	−0.91±0.13
H^3	2.508	41.1±0.2	20.4 ±0.1	21.39	−0.99±0.10
H^3	6.217	129.7±0.4	42.99±0.13	43.81	−0.82±0.13
H^3	9.265	312.6±1.5	154.1 ±0.75	154.90	−0.8 ±0.75
H^1	5.006	177.8±0.7	176.4 ±0.7	177.60	−1.20±0.7
		Adopted (B_1-B_2) · · · · · · · · ·			−0.9
Li^8	4.325	9.1 ±0.12	10.21±0.15	7.50	2.71±0.15
Li^8	5.793	11.6 ±0.1	13.01±0.13	10.50	2.51±0.13
Li^8	9.138	19.46±0.2	21.64±0.25	18.72	2.92±0.25
Li^8	10.69	22.97±0.2	25.76±0.25	23.51	2.25±0.25
Li^8	22.41	64.9 ±0.22	72.80±0.26	69.72	3.08±0.26
		Adopted (B_3-B_2) · · · · · · · · ·			2.7
B^8	18.47	20.99±0.4	65.4±1.3	52.40	13.0±1.3
B^8	26.83	34.78±0.4	108.4±1.3	93.80	14.6±1.3
B^8	60.09	115.6 ±1.0	360.2±3.0	350.00	10.2±3.0
		Adopted (B_5-B_2) · · · · · · · · ·			13.5

The cross section for electron capture by a stripped nucleus first becomes comparable to the cross section for electron loss when β falls to $\approx Z/137$, and the capture cross section rises very rapidly for lower velocities. Knipp and Teller[4] collected experimental data obtained by workers with slow alpha-particles which showed that the root-mean-square charge carried by the alpha-particle varies with β to $\beta\approx 2/137$, and approaches the value 2 asymptotically above $\beta=2/137$. For a nucleus of atomic number Z this behavior will be approximated by putting $\langle 1/Z^{*2}\rangle_{Av}=\lambda^2/137^2\beta^2$ for $\beta<\lambda Z/137$, and $Z^*=Z$ for $\beta>\lambda Z/137$, with λ a number near unity.

$g(\beta)$, which for fast particles is an odd function of β, contains as a divisor the fraction of the emulsion electrons which is effective in stopping. When the velocity

[4] J. Knipp and E. Teller, Phys. Rev. **59**, 659 (1941).

of the moving particle is small, the more tightly bound electrons do not contribute to the energy loss. Those whose velocity exceeds that of the moving particle, in first approximation, interact with it in an adiabatic manner. The number of effective electrons is estimated by Bohr[5] to vary with β over a considerable range when $\beta < Z_2 1/137$, where Z_2 is the atomic number of the stopping material. $g(\beta)$ should then be an even function of β in this region. Empirically the range data[3] for protons between 0.1 and 1.0 Mev are found to fit the formula $g(\beta)=4.08\times10^5\beta^2$ very well. In principle, $g(\beta)$ for lower velocities can be obtained directly from the range-energy relation for negative particles such as mesons. Since meson ranges for the velocities of interest here would be the order of 0.1 micron, it is not, therefore, practical to obtain $g(\beta)$ in this way. From other information it nevertheless appears probable that the number of emulsion electrons with velocities less than βc may continue to fall off roughly with β to a point somewhat below $\beta=1/137$. For example, the data of Wilcox[6] imply that $d\beta/dR$ is quite a good constant for alpha-particles penetrating gold, when β is in the range 6×10^{-3} to 1.5×10^{-2}. These considerations carry one down to residual ranges of less than a micron, so that no large range error can be introduced by assuming $g(\beta)=4.08\times10^5\beta^2$ to arbitrarily low velocities.

One may now evaluate the integral of Eq. 6,

$$B_Z \approx 4.08\times10^5 \int_0^{\lambda Z/137} \left[\left(\frac{\lambda Z}{137\beta}\right)^2 - 1\right]\beta^2 d\beta = 0.106\lambda^3 Z^3.$$

By using the present experimental data, one can obtain the coefficient, a, assuming $B_Z=aZ^3$. From B_1-B_2, $a=0.129$; from B_3-B_2, $a=0.142$; and from B_5-B_2, $a=0.115$. The last value presumably contains the smallest error so it should be weighted most. An adopted value of 0.12 appears most reasonable, and when equated to $0.106\lambda^3$, implies $\lambda=1.04$.

The purpose of this analytical study of B_Z is primarily to seek a *form* in which to express the empirical data. For this the Z^3 law has the great advantages of simplicity and uniform applicability to all light nuclei. As a test of its validity for a higher value of Z, one may compare the value of B_6-B_2 calculated from $B_Z=0.12Z^3$ with B_6-B_2 determined by Miller.[7] The calculated value is 25.0 microns and his measurement is 23.9 $\pm$0.75 microns.

Because of the simplifications introduced in its derivation, some further remarks on the evaluation of B_Z are, however, merited: For β above $Z/137$ the effective charge[8] approaches Z only asymptotically, and in this respect the assumed behavior is an idealization. The effect of discrete electron shells is also smoothed out in this approximation. The introduction of the parameter λ serves to make a suitable adjustment for these effects, and in the integrated result the error should be minimized. For calculating ranges with β less than $Z/137$, however, the present assumptions are less valid.

Regarding the meaning of $\langle Z^2/Z^{*2}\rangle_{Av}$: (a) $\langle Z^{*2}\rangle_{Av}$ is the mean square charge effective for energy loss. Although $\langle 1/Z^{*2}\rangle_{Av}$ should behave generally like the reciprocal of the mean square charge carried by the ion, these quantities probably should not be identified with each other for mathematical reasons, and because the ionization produced by a partially shielded nucleus may not be reduced in virtue of the attached electrons to the full extent of the reduction of the square of the net charge. (b) Even for bare nuclei the strict Z^2 dependence of the rate of energy loss implies by Eq. (1) may fail at low velocities because the time of interaction for a given energy transfer to an electron increases with Z. Such an effect, however, is not evident in the empirical[3] energy loss data for protons and alpha-particles in emulsion.

VII. NEGLECTED EFFECTS

Equation (1) should include a small term corresponding to loss of energy to nuclei. This function contains the particle mass explicitly. The rate of energy loss by nuclear collisions becomes relatively more important as the velocity decreases, and it increases with the mass of the moving particle. However, on examining the range data for the hydrogen and helium isotopes in Tables I and II it is difficult to conclude that an observable isotope effect is present. Theoretically one would not expect to detect the effect until the stopping by electrons virtually ceases ($\beta<1/137$). In any case the electron pick-up effect predominates in the region of importance here. It should be noted that the additional energy loss to nuclei tends to cause a reduction rather than an extension of the range.

In the present analysis certain small experimental effects have also been neglected. The range is somewhat poorly defined since it depends slightly on the sensitivity of the emulsion grains, and also to some extent on their size and closeness of packing.

Finally, the theoretical ideas employed in finding the form of B_Z are idealizations. In particular, it has not been proved that λ, although never deviating much from unity, is independent of Z, and the behavior of $g(\beta)$ for the lowest velocities remains questionable.

Miss Esther Jacobson made many of the range measurements and carried out the numerical reduction of a large part of the data for this study. Dr. Helge Tyren also measured many of the ranges and participated actively in the exposure of the plates. I am indebted to Dr. S. Tamor for a useful discussion of the complex problems of energy loss at low velocities.

[5] Niels Bohr, Kgl. Danske Videnskab. Selskab, Mat.-fys. Medd. **18**, No. 8 (1948), p. 102.
[6] Howard A. Wilcox, Phys. Rev. **74**, 1743 (1948).
[7] James F. Miller, University of California Radiation Laboratory Report 1902, unpublished.
[8] See, e.g., Theodore Hall, Phys. Rev. **79**, 504 (1950).

Momentum Transfer and Angle of Divergence of Pairs Produced by Photons*

A. BORSELLINO†
Laboratory of Nuclear Studies, Cornell University, Ithaca, New York
(Received October 3, 1952)

The distribution of the momentum transferred to the pairs in pair production by photons has been derived from the Bethe-Heitler cross section. The effect of screening is evaluated using a shielded Coulomb potential for the nucleus. In the last part of the article the distribution of the angle of divergence of the pair is obtained, and the most probable angle of divergence is given by $\phi(E_+/k)\cdot 4mc^2/k$, where k and E_+ are the energies of the photon and the positron and $\phi(E_+/k)\sim 1$ for $0.2<E_+/k<0.5$.

SOME of the results of recent experiments[1] on the recoil momentum q of the nucleus in pair production by photons seem to be in disagreement with theoretical prediction.[2] Probably this disagreement is only due to experimental difficulties. Anyway, further research is needed to clarify the question.

In this paper a formula is given for the distribution of the total momentum $P=|\mathbf{p}_+ + \mathbf{p}_-|$ transferred to the electron pair. This formula, in comparison with the distribution-function of the recoil momentum,[2] has some advantages: (a) it is simpler; (b) it allows us to take screening into account in a simple way; (c) it gives information on the angle between the electron and the positron.

From the experimental point of view, the determination of the total momentum P has the advantage of being independent of the knowledge of the direction of the incident photon. Thus it is possible to avoid collimation errors and use all the available volume of the detector. For the same reason it is possible to study the distribution of the momentum transfer in the case of pairs produced by cosmic-ray photons, for which there is no collimation at all. The angle ω between the electron and the positron in pairs produced by cosmic-ray photons has been used[3] to guess at the energy of the pair and the energy k of the generating photon. In the last part of this paper we obtain the distribution of the angle ω and derive from it a correlation between ω and the photon energy.

1. DISTRIBUTION OF THE TRANSFERRED MOMENTUM

From the Bethe-Heitler[4] differential cross section (Born approximation), we obtain the cross section for the distribution of the vector recoil momentum $\mathbf{q}$ of the nucleus (units $\hbar=c=1$), as follows:

$$d\sigma=\sigma_0\frac{2m^2}{\pi k}\frac{g(\mathbf{q})}{q^4}d^3\mathbf{q}, \tag{1}$$

where $\sigma_0=Z^2r_0^2/137$ is the unit cross section of Heitler, k is the energy of the photon, m the electron mass, and $g(\mathbf{q})$ the expression:

$$\begin{aligned}g(\mathbf{q})=&[1+2(m^2-q^2)x+q^2(q^2-k^2-m^2)x^2\\&+2k^2q^2(2q^2-m^2)x^3+k^2q^4(m^2-2q^2)x^4]\cdot\Delta\\&-[2+2(2m^2-q^2)x+(q^4-2k^2q^2-2m^2q^2-4m^4)x^2\\&+2k^2q^2(q^2-2m^2)x^3\\&+k^2q^2(4m^4+6m^2q^2-q^4)x^4]\cdot L,\end{aligned} \tag{2}$$

where

$$\begin{aligned}x^{-1}=(\mathbf{k}\cdot\mathbf{q})=kq\cos\theta_n,\quad \Delta=(1-4m^2/Q^2)^{\frac{1}{2}},\\ L=\cosh^{-1}(Q/2m),\qquad Q=(k^2-P^2)^{\frac{1}{2}};\end{aligned} \tag{3}$$

θ_n is the angle between the directions of the recoil momentum and the incident photon.

The integration of (1) over the angle θ_n gives the distribution of the recoil momentum q as obtained by Jost *et al.*[2] The result agrees with a more general distribution previously derived by us,[5] in which also the energy transfer is taken into account.[6]

To obtain the distribution of the total momentum $P=|\mathbf{p}_+ + \mathbf{p}_-|$ of the pair, we replace in (1) $d^3\mathbf{q}$ by $d^3\mathbf{P}=P^2dP\sin\theta d\theta d\psi$ and integrate over the angles. Assuming that θ is the angle between $\mathbf{P}$ and $\mathbf{k}$, we have $q^2=k^2+P^2-2kP\cos\theta$, $x^{-1}=k^2-kP\cos\theta$; here q varies with θ, but in (2), when we perform the integration over the angles, Δ and L remain constant. For this reason the result is expressible with only elementary functions and gives

$$d\sigma=4\sigma_0\frac{F}{(k^2-P^2)^2}PdP, \tag{4}$$

where $2m=1$ and

$$F=\left[F_1+\frac{Q^2}{2k^2}(F_1-\Delta)\right]\operatorname{sech}^{-1}\frac{Q}{k}-\left(F_2+\frac{Q^2}{6k^2}F_3\right)\frac{P}{k}, \tag{5}$$

with F_1, F_2, F_3 functions of Q only:

$$\begin{aligned}F_1&=(2+2/Q^2-1/Q^4)L-(1+1/Q^2)\Delta,\\ F_2&=\tfrac{1}{6}(16+21/Q^2-17/Q^4)L-\tfrac{1}{12}(28+17/Q^2)\Delta,\\ F_3&=\tfrac{1}{2}(4-1/Q^2)L-\tfrac{1}{2}(2+1/Q^4)\Delta.\end{aligned} \tag{6}$$

* This work has been supported in part by the U. S. Office of Naval Research.
† On leave from the University of Genoa, Italy.

[1] G. E. Modesitt and H. W. Koch, Phys. Rev. **77**, 175 (1950).
[2] Jost, Luttinger, and Slotnick, Phys. Rev. **80**, 189 (1950).
[3] Bradt, Kaplon, and Peters, Helv. Phys. Acta **23**, 24 (1950).
[4] H. Bethe and W. Heitler, Proc. Roy. Soc. (London) **A146**, 83 (1934).
[5] A. Borsellino, Nuovo cimento **4**, 112 (1947), Eq. (42).
[6] We take the opportunity to correct a misprint in the paper of Jost *et al.*, reference 2; the numerator of the last term in the first line of Eq. (43) ought to be $4Q^4-1$.

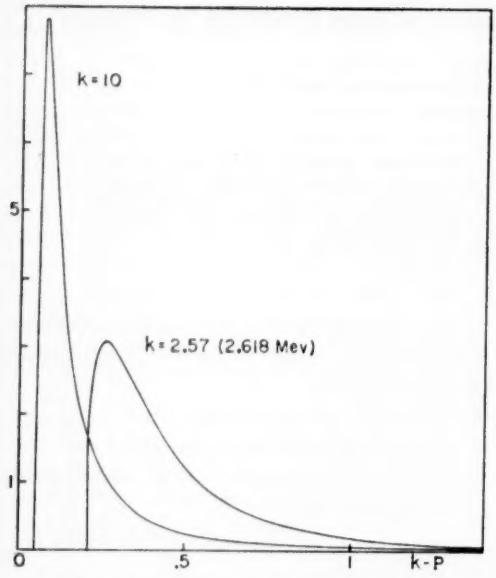

FIG. 1. Distribution of the transferred momentum P for photons of energy $k=2.57$ and $k=10$ (units $2mc^2$). In the abscissa: differences $k-P$ in units $2mc$; the distributions are both normalized to 1, dividing the cross section $d\sigma/dP$ by the total cross section.

As it must be, F is equal to zero at the extreme values, 0 and $(k^2-1)^{\frac{1}{2}}$, that P can reach. For small P, we have $F\sim P/k$, and the cross section is very small and increases as P^2/k^5. The most probable value of P is reached near the maximum value P_M of P, where the cross section for high energy ($k\gg1$) varies as

$$k^{\frac{1}{2}}\cdot\ln(2k)\cdot(P_M-P)^{\frac{1}{2}}.$$

The distribution of transferred momentum P is represented in Fig. 1 for two photon energies: $k=2.57$ (2.618 Mev) and $k=10$. On the abscissa is plotted the difference $k-P$ (in units of $2mc$) and on the ordinate the value of $d\sigma/dP$ given by (4) and (5), divided by the total cross section, to make the area under each curve equal to one. We see that, with increasing energy, the distribution becomes strongly peaked near $P\sim k$, i.e., when the pair receives nearly all the available momentum.

Instead of the P-distribution, it is easier to study the equivalent distribution of Q, which is given by:

$$d\sigma=4\sigma_0(F/Q^3)dQ, \tag{7}$$

where Q varies now between 1 and k.

This quantity Q has a simple invariant meaning: it is the energy of the pair in the center-of-mass system of the electron and the positron.

The most probable values of Q are now close to 1 and, since F increases as slowly as $\ln Q$, the distribution, after the maximum, drops down as $1/Q^3$. Therefore, if the energy is large enough, we are interested essentially in values for which $Q\ll k$. In this case, formula (5) gets simplified as follows:

$$F=F_1\ln(2k)-F_2^*, \tag{8}$$

with

$$F_2^*=F_2+F_1\ln Q. \tag{9}$$

From (8) one sees that the distribution of Q is not very sensitive to the energy of the photon. In Fig. 2 the distribution of Q is given for the same energies as in Fig. 1 and for $k=25$.

2. EFFECT OF SCREENING

Until now, we have not taken into account the screening of the field of the nucleus due to the atomic electrons. To evaluate this effect, we use a shielded Coulomb potential $V(r)=Zer^{-1}\exp(-a_0r)$ to represent the potential of the atom, and we choose[7] the parameter $a_0=mcZ^{\frac{1}{3}}(108\hbar)^{-1}$, in such a way that the total cross section for very high energies agrees with the values deducible from the Fermi-Thomas atom.

With this potential we must only replace in (1) the denominator q^4 by $(q^2+q_0^2)^2$, where $q_0=\hbar a_0$. The calculations are elementary as before. The screening is effective for $k\gg1$, therefore we need consider only the case $Q\ll k$. The distribution of the Q values is again given by (7), where F is now

$$F=F_1\ln\frac{2k}{(1+4k^2q_0^2/Q^4)^{\frac{1}{2}}}-F_2^*, \tag{10}$$

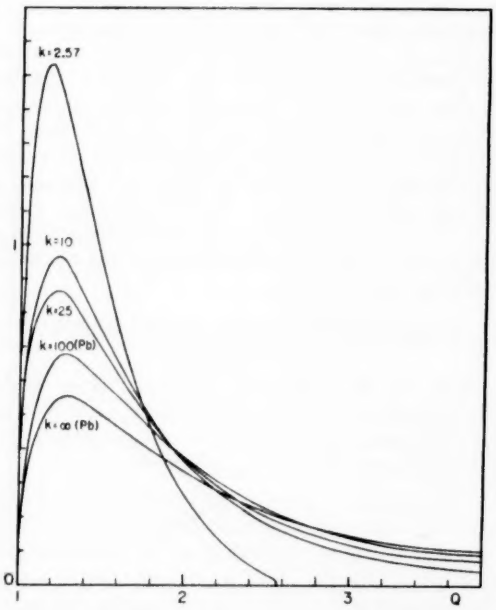

FIG. 2. Q distributions for the same photon energies k as in Fig. 1 and for $k=25$ (no screening); the curves (Pb) are calculated for lead and photon energies $k=100$ (partial screening) and $k=\infty$ (complete screening). All the distributions are normalized to 1.

[7] H. A. Bethe, Proc. Cambridge Phil. Soc. **30**, 524 (1934).

which, for $2kq_0 \ll 1$ (no screening), coincides with (8). In the opposite case of complete screening, we obtain a distribution independent of energy:

$$F = F_1 \ln(216Q^2Z^{-\frac{4}{3}}) - F_2^*. \quad (11)$$

The differential cross section (7), with F given by (10), also yields, when integrated, correct values of the total cross section at intermediate energies (partial screening); therefore it is probable that (10) gives correct Q distributions at these energies. In Fig. 2, the distribution of Q for lead is given, at $k=100$ and for complete screening ($k=\infty$).

3. DISTRIBUTION OF THE ANGLE OF DIVERGENCE ω

The quantity Q depends on the angle ω between the electron and the positron, and on the ratio in which the energy of the photon is divided between the two electrons.

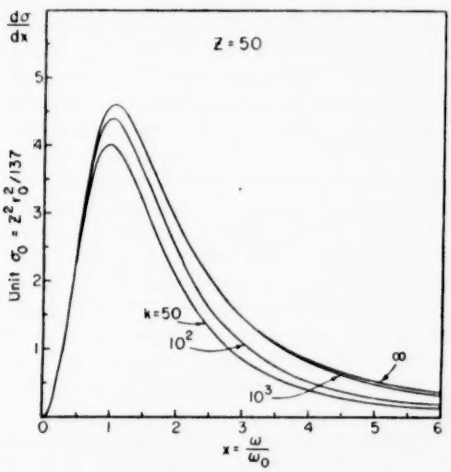

FIG. 3. Distribution of the angle of divergence ω between the two members of a pair for photon energies $k=50$ (51 Mev); 10^2; 10^3; ∞ (complete screening) and atomic number $Z=50$. On the abscissa: ratio ω/ω_0, where $\omega_0=kmc^2/(E_+E_-)$; on the ordinate: cross section $d\sigma/dx$ in unit $\sigma_0=Z^2r_0^2/137$. The curves are given for equipartition ($a=E_+/k=\frac{1}{2}$); otherwise the ordinates must be multiplied by $4a(1-a)$.

If the energy is large enough (E_+, $E_- \gg mc^2$), we may write for Q:

$$Q^2 = E_+E_-(\omega_0^2+\omega^2) = [4a(1-a)]^{-1}(1+\omega^2/\omega_0^2), \quad (12)$$

where a is the ratio E_+/k, and ω_0 is the characteristic angle:

$$\omega_0 = kmc^2/(E_+E_-). \quad (13)$$

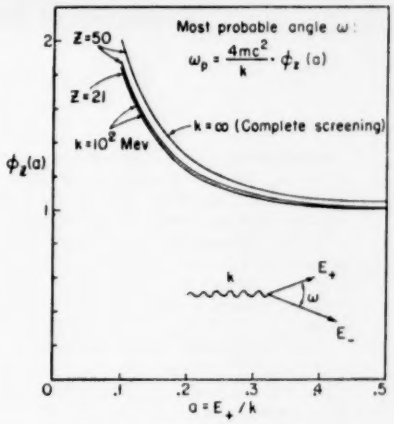

FIG. 4. $\phi_Z(a)$ *versus* $a=E_+/k$.

If one puts $x=\omega/\omega_0$, one obtains for the cross section (7)

$$d\sigma = 16\sigma_0 a(1-a)Fxdx/(1+x^2)^2, \quad (14)$$

which for a fixed value of a gives the distribution of the angle ω. In the region where the factor $x/(1+x^2)^2$ has a maximum ($x=1/\sqrt{3}$), the function F is still rapidly increasing and this shifts the value at which the maximum of the distribution lies towards greater values of x.

Figure 3 represents the distribution of the angle ω, according to (14), for different photon energies and atomic number $Z=50$, in the case of equipartition ($a=\frac{1}{2}$).

The angle ω_p at which the angular distribution has its maximum can be written in the form:

$$\omega_p = (4mc^2/k)\cdot\phi_Z(a), \quad (15)$$

where $\phi_Z(a)$ is a function of a and also depends on the energy k and the atomic number Z. In Fig. 4 the values of $\phi_Z(a)$ for $k=100$ Mev and $k=\infty$ (complete screening) for two different values of Z are given. It is evident from this that the dependence on k and Z is very small. For complete screening the curve for $Z=21$ practically coincides with that for $Z=50$. For equipartition, we have $\phi_Z \sim 1$.

Formula (15) may be of use in guessing at the energy of the pair from the observed value of the angle ω. Bradt *et al.*[3] equated ω to twice the rms angle between the electron and the incident photon, as calculated by Stearns.[8] As a result of the contributions of the angles beyond the maximum of the distribution, this rms angle is greater by a factor of $\ln(k/mc^2)$ than the most probable value given by (15).

Thus it seems more reasonable to the author to equate ω to ω_p. Following the other method, the deduced photon energy turns out to be smaller by a factor of $\ln(k/mc^2)$ than the value obtained using the method proposed here.

[8] M. Stearns, Phys. Rev. **76**, 836 (1949).

Properties of Thermally Treated Germanium

LEO ESAKI
Kobe Kogyo Corporation, Hyogo-ku, Kobe, Japan
(Received July 28, 1952)

Upon heating a piece of germanium in a vacuum of 10^{-6} mm Hg, the following results have been obtained. (1) Below 350°C, the rectification characteristic is improved. Heating the specimen at a temperature between 400°C and 600°C destroys the rectification, which is not recovered completely when it is heated in vacuum. However, heating in an oxygen atmosphere leads to a slight recovery of the rectification.

(2) Treatment above 550°C makes the formation of acceptor levels detectable. With continued heating at 500°C for about 48 hours, the specimen returns again to n type similar to the original state. The formation and disappearance of acceptor levels were followed when the specimen was quenched from a fixed temperature to room temperature. The equilibrium concentration at the heating temperature was determined to be $A=2.5\times10^{21}\exp(-27\,000/RT)$ cm^{-3}.

(3) On the assumption that the acceptor levels produced on the surface diffuse into the interior, the data could be fairly well represented with an estimated diffusion coefficient: $D=300\exp(-37\,000/RT)$ cm^2 sec^{-1}.

(4) The resistivity and Hall coefficient from room temperature to about 200°C have been measured for several specimens.

I. INTRODUCTION

RECENTLY several investigators have suggested that quenching[1] or high energy nucleon bombardment[2] produce lattice defects which are effective for forming acceptor levels in germanium. Theuerer and Scaff especially studied phenomenologically the thermal effect upon the resistivity.

In the present paper, it will be described how the properties of pure n type single crystalline germanium, whose concentration of conduction electrons[3] is 1.88×10^{14} cm^{-3}, is affected by thermal treatment. A small Ge specimen was quenched or annealed arbitrarily by adjusting the heater current of a tiny vacuum furnace; and the rectification characteristic, the resistivity, and Hall coefficient of the specimen were measured at any desired temperature.

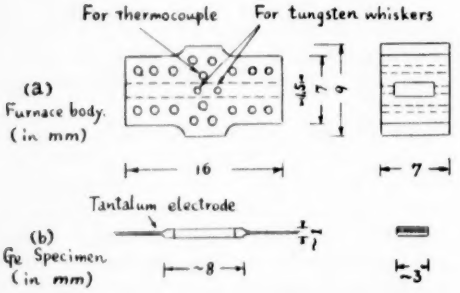

FIG. 1. Sketch of the furnace and the specimen.

[1] K. Lark-Horovitz, NDRC Report, unpublished; H. C. Theuerer and J. H. Scaff, J. Metals **189**, 59 (1951).

[2] Lark-Horovitz, Bleuler, Davis, and Tendam, Phys. Rev. **73**, 1256 (1948); Davis, Johnson, Lark-Horovitz, and Siegel, Phys. Rev. **74**, 1255 (1948); N. H. Brattain and G. L. Pearson, Phys. Rev. **80**, 846 (1950); Cleland, Crawford, Lark-Horovitz, Pigg, and Young, Phys. Rev. **83**, 312 (1951); **84**, 861 (1951).

[3] That used by Cleland, Crawford, Lark-Horovitz, Pigg, and Young is 4×10^{14} cm^{-3}.

2. EXPERIMENTAL APPARATUS

For the thermal treatment, a steatite furnace of small heat capacity of $7\times7\times16$ mm^3 was constructed. A schematic diagram is shown in Fig. 1(a). Along its central axis a rectangular hole of 1.5×4 mm^2 was drilled, into which a germanium specimen of $0.76\times2.65\times8$ mm^3, illustrated in Fig. 1(b), was inserted. On both sides of the specimen four tungsten whiskers, for measuring the rectification and other electrical properties, were pressed against the specimen through small holes marked in Fig. 1(a). Previously the germanium surface was lapped with 500 mesh carborundum and etched with a mixture of HF and HNO_3 for several seconds. Then tantalum ribbons of 1×0.05 mm^2 were tightly wound around both ends of the specimen as nonrectifying electrodes. Both tungsten and tantalum were chemically inert with germanium over the entire experimental temperature range. A tantalum heater wire of 0.2 mm diameter was coiled through many holes of the furnace body and a thermocouple of Pt−PtRh was also put into one of those holes.

The assembled furnace was mounted on a stem and sealed in a tube. A getter chamber was connected to the main experimental tube. The whole system was sealed off after evacuating carefully and flashing a batalum getter. The pressure remained less than 10^{-6} mm Hg throughout the experiment.

The cooling speed of the furnace could be represented by the experimental formula, $dT/dt=-T_0/(1+t)^2$, when the heater current was cut off. T and t are the temperature in °C and time in minutes, respectively, and T_0 the initial temperature. The change of the furnace temperature with time is given in Fig. 2. "Quenching" in the present paper usually means such cooling.

3. PRELIMINARY EXPERIMENTS

Prior to each thermal treatment, the dc rectification characteristic at room temperature, the specific resis-

tivity, and the Hall coefficient up to 200°C were measured by the four whiskers, using the conventional method. Typical changes in the resistivity and Hall coefficient of the specimen, subjected to the treatment given in Table I and quenching, are presented in Fig. 3.

When the specimen was heated at a relatively low temperature, the rectification characteristic underwent a large change, which is illustrated in Fig. 4. The initial characteristic is curve No. 1, but it was improved to

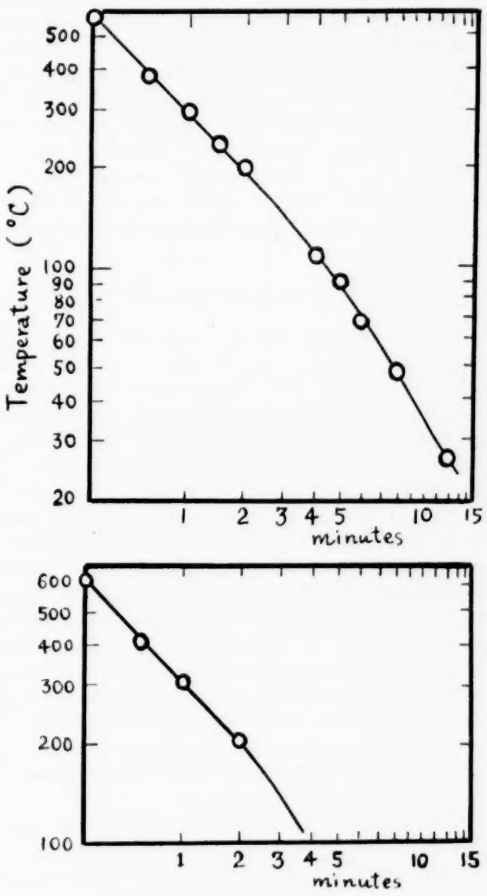

FIG. 2. Cooling of the furnace after cutting off the heater, i.e., the quenching process. Log$T$ is plotted against log $(1+t)$.

curve No. 2 by heating at 300°C for 30 minutes. On continuing to heat further, the rectification characteristic became worse at higher temperatures as indicated by Nos. 3, 4, and 11 in Fig. 4(c). The lost rectification did not recover to the original sharp characteristic by any heat treatment in vacuum; this suggests that the rectification is not always dependent upon the formation of acceptor levels. The experiment on the recovery of rectification is described in more detail in the next section.

TABLE I. Conditions for thermal treatment.

Treatment conditions	Identification No. after treatment	Treatment conditions	Identification No. after treatment
——	1	550°C, 12 min	
300°C, 30 min	2	535°C, 15 min	
400°C, 30 min	3	515°C, 15 min	
460°C, 30 min	4	495°C, 15 min	
525°C, 20 min	5	480°C, 15 min	
545°C, 25 min	6	460°C, 15 min	
570°C, 20 min	7	440°C, 15 min	
585°C, 20 min	8	425°C, 15 min	16
180°C, 30 min;		580°C, 12 min	
15°C, several		550°C, 15 min	
days	9	540°C, 30 min	
595°C, 20 min	10	530°C, 30 min	
625°C, 20 min	11	520°C, 30 min	
355°C, 20 min	12	505°C, 30 min	
535°C, 15 min	13	490°C, 30 min	
520°C, 60 min	14	475°C, 30 min	
550°C, 20 min	15	450°C, 30 min	17
		18±5°C, 3000 hr	18
		500°C, 48 hr	19

This essential feature is quite similar to the result found in the vacuum heat treatment of a silicon point contact rectifier.[4] The temperature above which rectification is completely lost was 1250°C for silicon, while that for germanium is only about 550°C. The tentative discussion for silicon may also be applied to the present case.

Moreover, it is interesting that the above-described damage of rectification has the same behavior as that due to neutron irradiation on the germanium rectifier.[5]

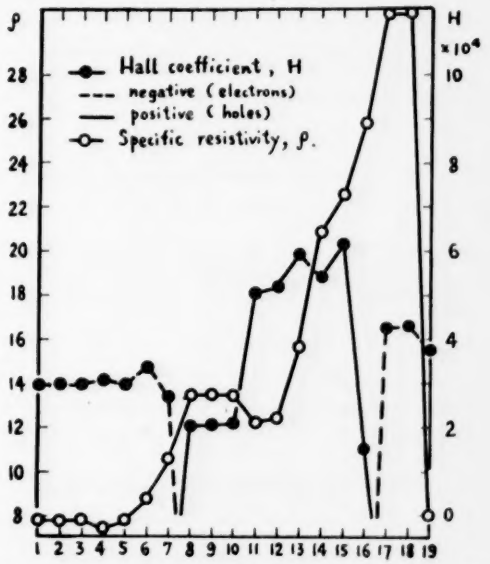

FIG. 3. The effect of miscellaneous treatments on the resistivity and Hall coefficient. The conditions for treatment are listed in Table I.

[4] L. Esaki, Phys. Rev. **89**, 398 (1953).
[5] W. E. Johnson and K. Lark-Horovitz (private communication).

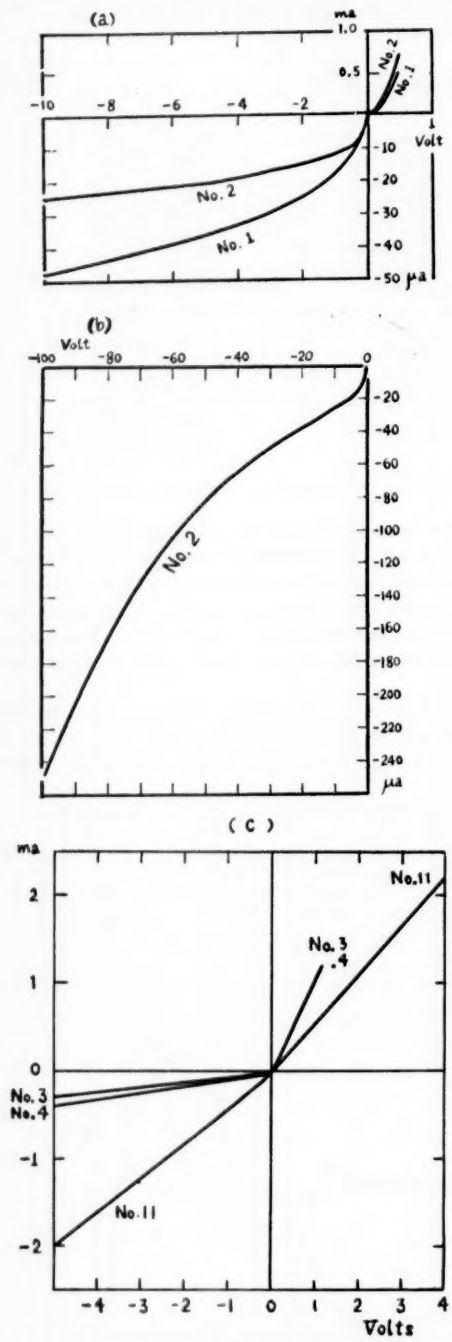

FIG. 4. The change of rectification characteristics.

After heating the specimen at about 600°C, the specific resistivity at room temperature increased gradually at first and then began to decrease, with an accompanying reversal in the sign of Hall coefficient. On subsequent heat treatment below 550°C, the specific resistivity increased to a maximum and then began to decrease. At the same time the sign of the Hall coefficient again became negative. While No. 17 was kept at room temperature for about 3000 hours, the properties remained unchanged. Finally, the specimen recovered the same properties as in the original state, except for the rectification characteristic.

The changes in the specific resistivity and Hall coefficient from room temperature up to 200°C are plotted in Fig. 5. The experimental values were satisfactorily reversible, indicating that no detectable annealing occurs in the measured temperature range. The concentration and mobility of carriers for Nos. 1 and 11 are listed in Table II together with several other quantities. The critical temperature at which the p type specimen converts to n type decreases with progressive heating at a temperature between 500°C and 600°C as seen in Table III, suggesting the gradual disappearance of acceptor levels.

4. RESULTS AND DISCUSSION

To study the behavior of thermally produced acceptors more exactly, the changes of resistivity and Hall coefficient at room temperature were observed successively for the specimen subjected to heating at a fixed temperature from 690°C to 500°C. The results are shown in Fig. 6 (1a), (2a), (3a), (4a), (5a), (6a), and (7a). In Fig. 6 (1a), (2a), (3a), and (5a), after the initial rapid increase or decrease, the resistivity finally approaches a steady value, which becomes smaller at higher temperature. The Hall coefficient indicates that the specimen is p type over the entire range. On the other hand, in Fig. 6 (4a), (6a), and (7a), the resistivity increases initially to a maximum and then decreases gradually to a constant value in the same way that was observed in the preliminary experiment. The Hall coefficient shows that p-n conversion occurs near the maximum resistivity and that the steady state is n type below 540°C. In general, at lower temperatures the changes are much slower.

From the observed values of the specific resistivity, ρ, or conductivity, σ, and the Hall coefficient, H, the concentration of electrons, n, and holes, p, are determined by[6]

$$\rho=\frac{1}{\sigma}=\frac{1}{e\mu_p(nb+p)}, \tag{1}$$

$$H=-\frac{3\pi}{8}\frac{nb^2-p}{e(nb+p)^2}, \tag{2}$$

where μ_p is the hole mobility and b the ratio of electron mobility to hole mobility. The mobilities of electrons and holes will be assumed to be nearly independent of the acceptor concentration thermally produced. The

[6] See W. Shockley, *Electrons and Holes in Semiconductors* (D. Van Nostrand Company, Inc., New York, 1950).

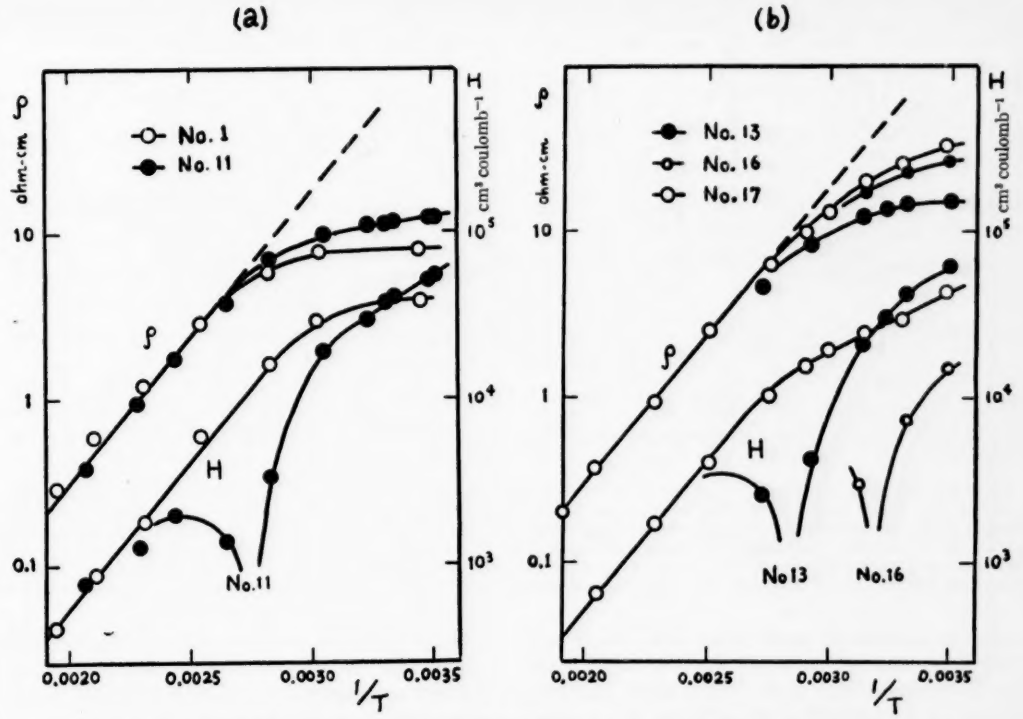

FIG. 5. Specific resistivity ρ and Hall coefficient H (logarithmic scale) *vs* reciprocal of absolute temperature.

hole mobility is determined to be 3600 ± 100 cm² volt^{-1} sec^{-1} for the various specimens in which p is much larger than n, as shown in the last column of Table IV. Therefore the ratio b is about 1.2, using the electron mobility 4340 cm² volt^{-1} sec^{-1} in the original specimen. The calculated p, n, and their product were plotted in Fig. 6 (1b), (2b), (3b), (4b), (5b), and (6b). The concentrations of holes and electrons decrease or increase, and tend to certain values corresponding to each heating temperature. By using the values of p and n, the concentration of acceptors is approximately evaluated as follows: The net charge density is given by

$$e(D-A)-e(n-p-p_a)=0, \tag{3}$$

where D and A are the concentrations of donors and acceptors, p_a that of holes bound to acceptors. The ionization energy required to excite an electron from a donor to the conduction band is so small that excess electrons bound to donors are neglected. The equation governing the relation among holes p, ionized acceptors $A-p_a$, and neutral acceptors p_a may be written

holes+ionized acceptors$\leftrightarrow$neutral acceptors.

Therefore, the equilibrium concentrations satisfy

$$p(A-p_a)=Kp_a.$$

By using Eq. 3, this is modified to

$$p(D+p-n)=Kp_a, \tag{4}$$

where D, p, and n in the left term have already been numerically determined. ($D=1.88\times10^{14}$ cm^{-3}). The equilibrium constant K is statistically given by

$$K=2h^{-3}(2\pi m_p kT)^{\frac{3}{2}}\exp\{-(E_A-E_v)/kT\},$$

where E_A and E_v are the energies of the acceptor level and the valence band, and m_p is the effective mass of a hole. The value of E_A-E_v is not yet known exactly,

TABLE II. Specific resistivity, Hall coefficient, and concentration and mobility of carriers for specimens, No. 1 and No. 11.

Specimen number	Type	Specific resist. (ohm-cm)	Hall coefficient (cm³ coulomb⁻¹)	Concentration (cm⁻³)	Mobility (cm² volt⁻¹ sec⁻¹)
1	*N*	7.7	3.93×10^{14}	1.88×10^{14}	4340
11	*P*	12.2	5.05×10^{14}	1.41×10^{14}	3600

TABLE III. *P-N* transition temperature for specimens from No. 11 to No. 16.

Specimen No.	*P-N* transition temperature
11	93°C
13	81°C
14	63°C
15	63°C
16	39°C

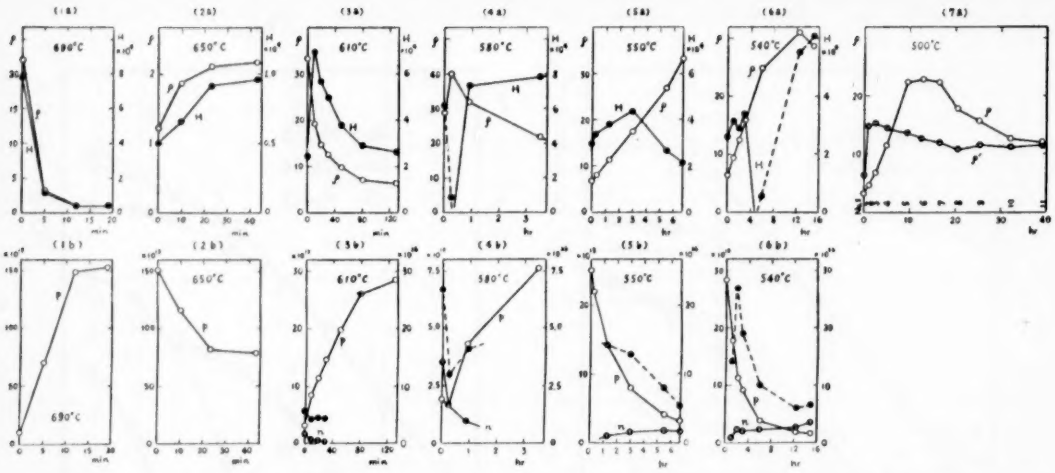

FIG. 6. (a) The changes of the specific resistivity ρ and the Hall coefficient H with heating time. Open and solid circles indicate ρ in ohm-cm on the left ordinate and H in cm² volt^{-1} sec^{-1} on the right ordinate, respectively. The full and dotted lines connecting the solid circles represent the positive and negative signs, respectively, in the Hall coefficient. The black circles with white centers, in (7a) give the resistivity calculated from the spreading resistance at the point contact. (b) The changes of the concentrations of electrons n and holes p and the product $p\times n$ with heating time. Open, black with white centers, and solid circles are p, n, and $p\times n$, respectively. The left and right ordinates represent the concentration in cm^{-3} and the product in cm^{-6}, respectively.

but may be assumed to be the order of 0.2 ev or less, so that K is evaluated to be 10^{16} cm^{-3} or more, if the temperature dependency of E_A-E_v is taken into consideration.[7] Comparing both terms in Eq. (4), p_a must be much smaller than p, suggesting the full ionization of acceptors. Therefore, from Eq. (3),

$$A=D+p-n. \tag{5}$$

The plots of $\log_{10}|A-A_f|$ *vs* t at various temperatures in Fig. 7 are almost straight, where A_f is the final concentration at the corresponding temperature. Experimentally, the relationship between A and t is expressed by

$$A=A_f+(A_i-A_f)\exp(-kt), \tag{6}$$

TABLE IV. Acceptor concentration and diffusion coefficient as several temperatures between 500°C and 690°C, and hole mobility at room temperature.

Temp. °C	A_f cm^{-3}	D cm² sec^{-1}	μ_p cm² volt^{-1} sec^{-1}
690	180×10^{13}	152×10^{-8}	3500
650	95	82	3750
645	—	—	3540
610	50	25	3540
600	40	—	3660
580	27	12	—
550	19	7.1	—
540	17	5.5	—
500	7	1	—
A_0 or D_0*	2.5×10^{21}	3×10^{2}	Mean value
Q_A or Q_D*	27 kcal/g atom =1.2 ev	37 kcal/g-atom =1.6 ev	of μ_p 3600±100

* $A_f=A_0\exp(-Q_A/RT)$; $D=D_0\exp(-Q_D/RT)$.

[7] V. A. Johnson and H. Y. Fan Phys. Rev. **79**, 899 (1950).

A_i being the initial concentration and k a function of temperature. This is the familiar first-order built-up equation, analogous to that derived in the study of neutron bombardment of germanium.[8]

During heating at 500°C, the rectification characteristic at room temperature changed gradually, as illustrated in Fig. 8. The number designated on each curve in Fig. 8 corresponds to the number given in the lower side of Fig. 6 (7a). The spreading resistance R evaluated from the slope of the current-voltage curve in the forward direction provided that the rectification is weak, is given by[4]

$$R=\rho'/2d \text{ ohms},$$

where d is the diameter at the point contact and ρ' the specific resistivity near the surface. Only when the specimen is uniform, is ρ' equal to ρ. For instance, the curve No. 0 in Fig. 8 for the specimen of $\rho=\rho'=3.5$ ohm-cm which was attained by prolonged heating at 645°C, gives $R=500$ ohm, resulting in $d=3.5\times10^{-3}$ cm. The same value of d was also derived for the specimen heated for a long time at any temperature. In curve No. 1, ρ' is not equal to ρ; this indicates that the specimen was unfortunately not homogeneous at the start of the treatment at 500°C. At the beginning of the treatment ρ' usually differs markedly from ρ, and finally both ρ' and ρ approach the same value, as in Fig. 6 (7a). These curves suggest that the spreading resistance changes faster in approaching the steady value than the bulk resistivity. In other words, the

[8] Cleland, Crawford, Lark-Horovitz, Pigg, and Young, Phys. Rev. **83**, 312 (1951).

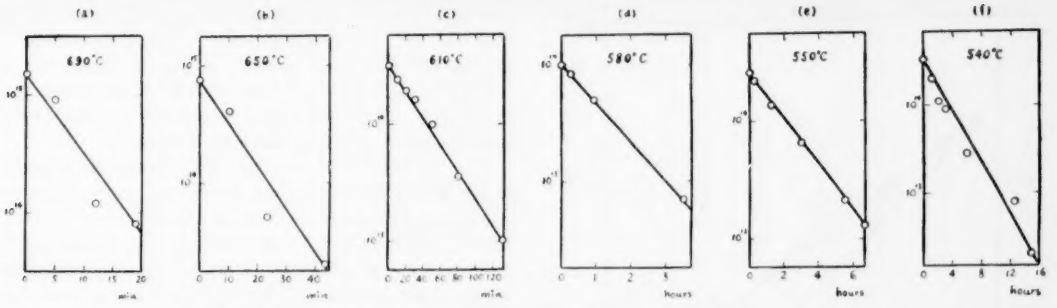

FIG. 7. $\mathrm{Log}_{10}|A-A_f|$ *vs* heating time, where A and A_f are the acceptor concentrations at a given time and at the equilibrium state, respectively.

surface concentration of acceptors becomes constant instantly and they diffuse gradually into the interior.

As previously mentioned, the rectification is destroyed with treatment at a comparatively low temperature and is lost completely if the concentration of acceptors exceeds 3×10^{14} cm^{-3}. In p type no rectification was observed, but the lost rectification is slightly recovered as n becomes richer than p (Fig. 8). Curve No. 11 did not change even by heating at 415°C, 320°C, and 230°C, for each 8 hours. However, it was improved to curve No. 12 and curve No. 13 when the specimen was exposed to atmosphere at room temperature for several hours and when it was heated at 380°C for ten minutes in oxygen of pressure from 2×10^{-2} to 10^{-1} mm Hg, respectively.

The fact that the product of the electron and hole concentrations is not constant near the beginning of the heating in Fig. 6 (3b), (4b), (5b), and (6b), leads to an inhomogeneous distribution of donors and acceptors. According to statistical theory, in the homogeneous specimen the product is independent of impurity concentration at any temperature, having the relation:[6]

$$np=4h^{-6}(2\pi m^{*}kT)^{3}\exp\{-(E_c-E_v)/kT\}, \qquad (7)$$

where m^{*} is the geometric mean of the effective masses of the carriers, and E_c and E_v are the energies of the conduction band and valence band. Johnson and Fan estimated this product to be 9×10^{26} cm^{-6} at 22°C.[7] In the present experiment it ranges from 3×10^{26} cm^{-6} to 3×10^{27} cm^{-6}. The wide distribution in the product will be ascribed to the inhomogeneity in the specimen. Moreover, in Fig. 6 (5b) and (6b) the product tends to 6×10^{26} cm^{-6}, indicating that the specimen becomes homogeneous with prolonged heating in agreement with the conclusion from the spreading resistance.

It seems quite reasonable that acceptor levels, produced on the surface, diffuse into the interior according to Fick's law, which, if the concentration of acceptors be A, is written

$$\partial A/\partial t=D\partial^{2}A/\partial x^{2},$$

in which x is the distance and D the diffusion coefficient of acceptors. The solution, when the boundary condition is $A=A_f$ at $x=0$ and $x=l$, and $A=A_i$ at $t=0$, is given by

$$A=A_f+(A_i-A_f)\frac{4}{\pi}\sum_{n=0}^{\infty}\frac{1}{(2n+1)}\times\exp\left\{-\frac{(2n+1)^2}{l^2}\pi^2Dt\right\}\sin\left\{\frac{(2n+1)}{l}\pi x\right\}, \qquad (8)$$

where the notations A_i and A_f are the same as in Eq. (6) and l is the thickness of the specimen. On integrating, we obtain

$$\int_0^l A\,dx=A_f l+(A_i-A_f)\frac{8l}{\pi^2}\sum_{n=0}^{\infty}\frac{1}{(2n+1)^2}\times\exp\left\{-\frac{(2n+1)^2}{l^2}\pi^2Dt\right\}.$$

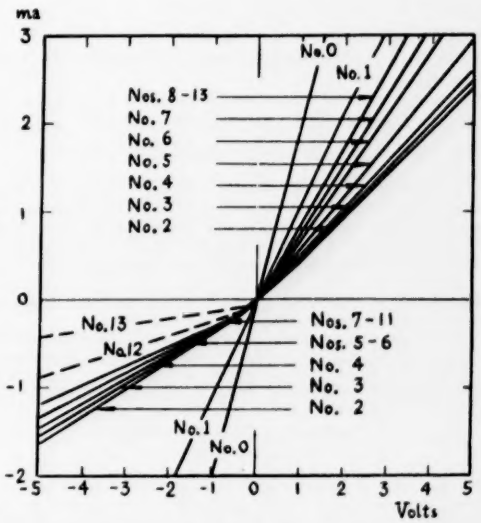

FIG. 8. Changes of the rectification characteristics.

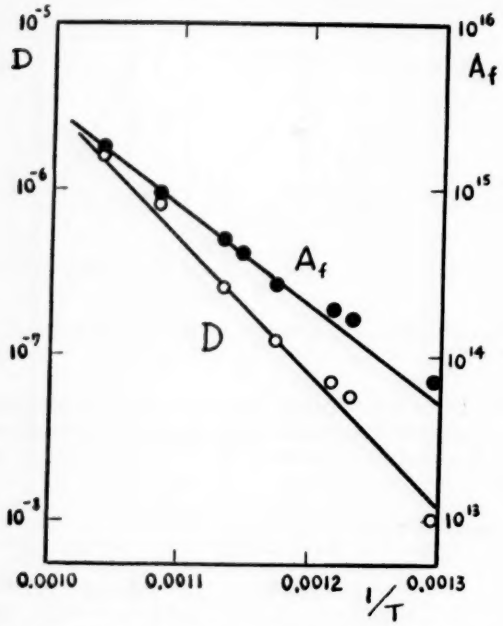

FIG. 9. The diffusion coefficient D in cm^2 sec^{-1} and the equilibrium concentration A_f in cm^{-3}, plotted *vs* reciprocal absolute temperature.

Therefore, the first approximation is given by[9]

$$\int_0^l A\frac{dx}{l}=A_f+(A_i-A_f)\frac{8}{\pi^2}\exp\left(-\frac{\pi^2}{l^2}Dt\right). \quad (9)$$

This equation is similar to the experimental equation (6); k in Eq. (6) is equal to $(\pi^2/l^2)D$ in Eq. (9). The numerical values D obtained at various temperatures are listed in Table IV together with the values A_f and the hole mobilities μ_p. In Fig. 9, D and A_f are plotted against reciprocal absolute temperature, and they are represented by[10]

$$D=300\exp(-37\,000/RT)\ cm^2\ sec^{-1},$$
$$A_f=2.5\times10^{21}\exp(-27\,000/RT)\ cm^{-3},$$

corresponding to activation energies of about 1.6 ev and 1.2 ev, respectively. The activation energy in germanium (37 kcal/g-atom) is higher than that for self diffusion in lead (28 kcal/g-atom),[11] but lower than those for silver (50 kcal/g-atom),[12] copper (45–61 kcal/g-atom), and gold (63 kcal/g-atom).

The final state of each treatment may be expected to be nearly homogeneous. Therefore, on plotting the acceptor concentration A at the last points of 500°C, 540°C, 550°C, 580°C, and 610°C in Fig. 6 against the conductivity σ, we obtain Fig. 10, in which a dotted curve represents the following equation derived from Eqs. (1), (5), and (7):

$$\sigma=\tfrac{1}{2}e[\{(D-A)+[(D-A)^2-4c^2]^{\frac{1}{2}}\}\mu_n + \{(A-D)+[(A-D)^2-4c^2]^{\frac{1}{2}}\}\mu_p], \quad (10)$$

where D, μ_n and μ_p were defined previously and are numerically known, and

$$c=np\doteqdot6\times10^{26}\ cm^{-6}.$$

During the treatment, however, the concentrations n and p vary not only with time but also with distance from the surface, so that the basic Eqs. (1) and (2) for a homogeneous specimen should be reconsidered. If the transverse dimensions of the specimen of germanium plates are given by l and w, where w is equal to the distance between probes for the Hall voltage measurement and is much larger than l, the mean values of $n(x)$, $p(x)$, and $\sigma(x)$ may be written:

$$\int_0^l n(x)dx=\bar{n}l, \quad \int_0^l p(x)dx=\bar{p}l,$$

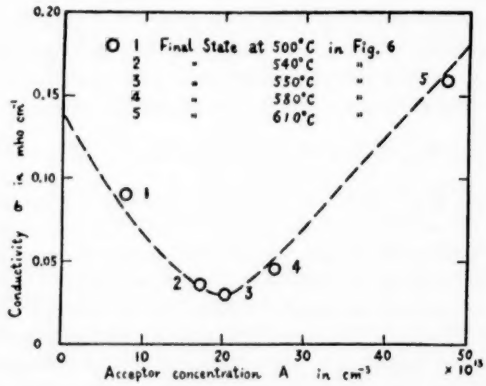

FIG. 10. Acceptor concentration *versus* conductivity. The circles designated by 1, 2, 3, 4, and 5 represent the final states at 500°C, 540°C, 550°C, 580°C, and 610°C. The dotted curve indicates $\sigma=\frac{1}{2}e[\{(D-A)+[(D-A)^2-4c^2]^{\frac{1}{2}}\}\mu_n+\{(A-D)+[(A-D)^2-4c^2]^{\frac{1}{2}}\}\mu_p]$.

[9] In the main part of the present treatment, $(\pi^2/l^2)Dt$ is larger than 0.3. For instance, when $l=2.0$, 3.6, 11.8, 24.5, 41.3, and 53.5 minutes at 690°C, 650°C, 610°C, 580°C, and 540°C, respectively, $(\pi^2/l^2)Dt$ becomes 0.3. In this case, the approximation employed is good because the second term is only one hundredth of the first one.

The author is grateful to Dr. C. S. Fuller and Dr. van Roosbroeck for an interesting discussion on this point.

[10] While the present study was in progress, there appeared a Letter to the Editor by Fuller, Theuerer, and van Roosbroeck, Phys. Rev. **85**, 678 (1952), which has a close connection with the author's study. The values of D and A determined by Fuller *et al.* are

$$D=0.02\exp(-12\,000/RT)\ cm^2\ sec^{-1},$$
$$A=2.1\times10^{21}\exp(-27\,000/RT)\ cm^{-3}.$$

While the value of A is in a fairly good agreement with that of the author, the value of D differs significantly even though possible experimental errors are taken into consideration. These two values coincide at 1300°K. This deviation may probably be ascribed to the differences in both material and temperatures used. Fuller *et al.* used mainly polycrystalline germanium and obtained their results at high temperatures.

[11] See, for example, W. Seith, *Diffusion in Metallen* (J. Springer, Berlin, 1939).

[12] R. E. Hoffman and D. Turnbull, J. Appl. Phys. **22**, 634 (1951).

and

$$\int_0^l \sigma(x)dx = \int_0^l e(n\mu_n + p\mu_p)dx$$
$$= e(\bar{n}\mu_n + \bar{p}\mu_p)l$$
$$= \bar{\sigma}l.$$

Therefore, we get

$$\int_0^l \Delta n dx = 0, \quad \int_0^l \Delta p dx = 0, \quad \text{and} \quad \int_0^l \Delta\sigma dx = 0, \quad (11)$$

where $n(x)-\bar{n}=\Delta n$; $p(x)-\bar{p}=\Delta p$, and $\sigma(x)-\bar{\sigma}=\Delta\sigma$. Although the formation of space charge by diffusion and recombination of electrons and holes and other effects would not be negligible, the Hall voltage V_0 induced between the probes by an uniform magnetic field B, could be tentatively expressed by

$$V_0 = \frac{w}{l}\int_0^l BI(x)H(x)dx,$$

where $I(x)$ and $H(x)$ are current density and Hall coefficient at x, respectively. Using the relations

$$I(x) = E\sigma(x) = Ee(n\mu_n + p\mu_p),$$

and

$$H(x) = \frac{3\pi}{8}\frac{-n\mu_n^2 + p\mu_p^2}{e(n\mu_n + p\mu_p)^2},$$

we have

$$V_0 = \frac{3\pi}{8}\frac{w}{l}BE\int_0^l \frac{-n\mu_n^2 + p\mu_p^2}{n\mu_n + p\mu_p}dx, \quad (12)$$

where E is the applied electric field. The total current I_0 through the specimen may be represented by

$$I_0 = w\int_0^l I(x)dx$$
$$= wE\int_0^l \sigma(x)dx \quad (13)$$
$$= wE\bar{\sigma}l$$
$$= wlEe(\bar{n}\mu_n + \bar{p}\mu_p).$$

Now, let us derive the Hall coefficient H_0, which is equal to V_0l/BI_0, observed for the inhomogeneous specimen in the following cases: Case 1. If $n \gg p$ or $n \ll p$, V_0 and I_0 can be simply written

$$V_0 \doteqdot -\frac{3\pi}{8}wBE\mu_n \quad \text{or} \quad \frac{3\pi}{8}wBE\mu_p,$$

and

$$I_0 \doteqdot wlEe\bar{n}\mu_n \quad \text{or} \quad wlEe\bar{p}\mu_p.$$

TABLE V. The maximum and minimum values of the conductivity σ calculated from Eqs. (8) and (10) during the thermal treatments at 580°C, 550°C, and 540°C. The unit is mho cm^{-1}.

Time of treatment, hours	580°C σ_{max}	580°C σ_{min}	550°C σ_{max}	550°C σ_{min}	540°C σ_{max}	540°C σ_{min}
1	0.055	0.032	——	——	——	——
2	0.055	0.042	——	——	——	——
3	0.055	0.048	0.059	0.031	——	——
4	——	——	0.044	0.031	0.055	0.031
6	——	——	0.033	0.031	0.035	0.031

Therefore, we have

$$H_0 \doteqdot -\frac{3\pi}{8}\frac{1}{e\bar{n}} \quad \text{or} \quad \frac{3\pi}{8}\frac{1}{e\bar{p}}.$$

Case 2. If $|\Delta\sigma|/\bar{\sigma}$ is small throughout the specimen, Eq. (12) for V_0 becomes

$$V_0 = \frac{3\pi}{8}\frac{w}{l}BE\frac{e}{\bar{\sigma}}\int_0^l (-\bar{n}\mu_n - \Delta n\mu_n^2 + \bar{p}\mu_p^2 + \Delta p\mu_p^2) \times\left(1 - \frac{\Delta\sigma}{\bar{\sigma}} + \left(\frac{\Delta\sigma}{\bar{\sigma}}\right)^2 - \cdots\right)dx.$$

Neglecting terms of order $(\Delta\sigma/\bar{\sigma})^2$, $\Delta n(\Delta\sigma/\bar{\sigma})$, $\Delta p(\Delta\sigma/\bar{\sigma})$, and of higher order, and using Eq. (11), we get

$$V_0 \doteqdot \frac{3\pi}{8}wBE\left(\frac{-\bar{n}\mu_n^2 + \bar{p}\mu_p^2}{\bar{n}\mu_n + \bar{p}\mu_p}\right).$$

This leads to

$$H_0 \doteqdot \frac{3\pi}{8}\frac{-\bar{n}\mu_n^2 + \bar{p}\mu_p^2}{e(\bar{n}\mu_n + \bar{p}\mu_p)^2} \quad \text{or} \quad \frac{3\pi}{8}\frac{-\bar{n}b^2 + \bar{p}}{e(\bar{n}b + \bar{p})^2}.$$

The condition for Case 1 may be fulfilled both in the main ranges of treatment at 690°C, 650°C, and 610°C, and in the beginning of those at 550°C and 540°C, as seen from Fig. 6(a). By using Eqs. (8) and (10), the maximum and minimum values of σ are obtained as written in Table V. In such a state as listed, the mean value of $(\Delta\sigma/\bar{\sigma})^2$ relative to x is less than 0.02. Therefore, it is found that Case 2 may be applicable both to the main range of treatment at 580°C, and to those at 550°C and 540°C except for the initial few hours. Thus, the values of n and p determined in the present study from Eqs. (1) and (2) may indicate approximately ordinary mean values, so that the results may be fairly understandable.

It is difficult in the present study to determine the type of lattice defects forming acceptor levels. However, it is noteworthy that nearly all of the effect of lattice defects which were produced by neutron bombardment could be removed merely by heating up to 400°C, and also some of them could be considerably annealed even at room temperature,[8] in contrast to the behavior of lattice defects produced thermally. Therefore, these

two kinds of defect may be considered to be different in type;[18] it may be that the defect produced by bombardment is Frenkel type, while the thermally produced defect is Schottky type.

5. SUMMARY

The changes in some properties of germanium, subjected to heating, are explained quite well by assuming that acceptor levels are formed by the lattice defects produced on the surface and diffusing into interior. When germanium is quenched from a high temperature in a vacuum furnace at a rate given by $dT/dt \fallingdotseq -T_0/(1+t)^2$ °C min^{-1}, it contains a fairly large number of lattice defects "fronzen in." These defects are not easily annealed up to 200°C.

On heating in vacuum, the rectification characteristic is improved at comparatively low temperatures, but is destroyed at higher temperatures, perhaps not only because lattice defects are produced but also because the surface becomes free from adsorbed gas. No theory satisfactorily explains all the phenomena of rectification.

The author wishes to express his particular thanks to Mr. H. Nelson of the Radio Corporation of America for preparing the germanium specimen and also acknowledges his gratitude to Dr. T. Arizumi of the Kobe Kogyo Corporation for his discussion and encouragement.

Note added in proof:—(1) Lately Fuller and Struthers (Phys. Rev. **87**, 526 (1952)) have reported that copper may be an impurity responsible for thermal acceptors in germanium. The diffusion constant at 825°C obtained by them, 1.3×10 cm^2 sec^{-1}, is in a very good agreement with the value, 1.36×10 cm^2 sec^{-1}, calculated from the above-derived equation, $D=300\ \exp(-37\,000/RT)$. (2) The recent results published by Goldberg [Phys. Rev. **88**, 920 (1952)] have several points of agreement with the present study.

[18] See N. F. Mott and R. W. Gurney, *Electronic Processes in Ionic Crystal* (Oxford University Press, London, 1940), p. 36.

PHYSICAL REVIEW VOLUME 89, NUMBER 5 MARCH 1, 1953

Vapor-Liquid Equilibria in He^3-He^4 Solutions

J. C. Morrow
Department of Chemistry, University of North Carolina, Chapel Hill, North Carolina
(Received July 9, 1952)

Recent measurements of the vapor pressures of He^3-He^4 liquid solutions by Daunt and Heer and by Sommers are used to evaluate the solution non-ideality, for the calculation of which the large deviations of the vapor from ideality are taken into account. Estimation of the standard chemical potential of normal He^4 at temperatures below the lambda-point is discussed. Agreement of excess chemical potentials of He^4 above the lambda-point and the values obtained from the simple theory demonstrates the usefulness of the theory in discussions of effect of nonideality on the shift of the lambda-point with He^3 concentration.

I. INTRODUCTION

MEASUREMENTS of vapor-liquid equilibria can be used successfully to study thermodynamic properties of He^3-He^4 solutions, particularly the deviations from solution ideality, as has been pointed out previously.[1] These results are especially valuable since they can be used above the lambda-point, for which condition speculations about superfluid and its influence are not limitations. Recently some measurements of solution vapor pressures both above and below the lambda-point have been made by Daunt and Heer[2] and by Sommers.[3] The results above the lambda-point can be used to give direct information about the magnitude of solution nonideality and about the relative likeness of a simple solution model[1] and the real solution. From these equilibrium measurements one can calculate the model nonideality parameter a, which, for a binary mixture of nonelectrolytes, gives the excess chemical potential of component j as $V_j a f_i^2$, where ${}_jV$ is the molar volume of pure j and f_i is the volume fraction of i. One of the features of such experimentally evaluated parameters which one would immediately subject to scrutiny is concentration dependence, since the model parameter is independent of concentration. The results of Sommers must be used in such an instance since the measurements by Daunt and Heer refer to a single liquid concentration.

[1] J. C. Morrow, Phys. Rev. **84**, 502 (1951).
[2] J. G. Daunt and C. V. Heer, Phys. Rev. **86**, 205 (1952).
[3] H. S. Sommers, Jr., Phys. Rev. **88**, 113 (1952).

II. EQUILIBRIUM ABOVE THE LAMBDA-POINT

Following Sec. III of reference 1, one has for the chemical potential of component i in the binary liquid mixture

$$\mu_{il}{}^0(P_i{}^0, T)+\bar{V}_{il}(P-P_i{}^0)+RT\ln x_i+\mu_i{}^E,$$

where the first term is the standard chemical potential of the pure component at temperature T and pressure equal to the vapor pressure of the pure component at T; $\bar{V}_{il}$ is the partial molal volume of liquid i; P is the

total pressure; x_i is the mole fraction of i in the liquid phase; the last term is the nonideality term or excess chemical potential, which, for the simple model, has the form described above. The chemical potential of component i in the binary gas mixture is

$$\mu_{ig}{}^0(P_i{}^0, T)+RT\ln(Py_i/P_i{}^0)+B_i(P-P_i{}^0) +(2B_{ij}-B_i-B_j)(1-y_i)^2P,$$

where the first term is the standard chemical potential of the pure gaseous component i at $P_i{}^0$ and T; y_i is the mole fraction of i in the gas; B_i is the second virial coefficient of pure gaseous i; B_{ij} is the mixture coefficient. To get the equilibrium equations one equates individual liquid and vapor potentials and obtains two results,

$$Py_j=P_j{}^0x_j\exp\{[(V_j-B_j)(P-P_j{}^0) -(2B_{ij}-B_i-B_j)(1-y_j)^2P+\mu_j{}^E]/RT\}, \quad (1)$$

where j and i can be either 3 and 4 or 4 and 3, respectively. These equations can be used to obtain the value of the excess potentials if all other quantities are known. If one assumes $\bar{V}_j$ is nearly the same as the molar volume of j, then all items except the total pressure, temperature, and compositions are at hand (see reference 1 for complete listing of sources).

TABLE I. Compositions and nonideality parameters.

T°K	y_3/x_3	a cal/cc	a cal/cc Eq. (3)
2.60	4.3– 6.6	0.1013–0.0489	0.1476
2.59	5.3– 8.2	0.1311–0.0770	0.1461
2.49	5.3– 8.1	0.1166–0.0627	0.1364
2.33	6.0– 9.2	0.1134–0.0618	0.1391
2.31	6.2– 9.6	0.1164–0.0655	0.1382
2.30	5.1– 7.8	0.0864–0.0365	0.1387
2.27	6.4– 9.9	0.1137–0.0627	0.1369
2.19	7.5–11.7	0.1234–0.0702	0.1375
2.18	6.0– 9.3	0.0926–0.0433	0.1360

Daunt and Heer[2] have measured the total pressure and the temperature and have found fair limits for the liquid composition. Their values of the vapor composition, however, are calculated from the simple equation

$$y_3=(P-P_4{}^0)/P. \quad (2)$$

It is easily seen that the identity $y_3+y_4=1$ can be used with the two forms of Eq. (1) to eliminate the vapor compositions entirely and to give an excess potential in terms of P, T, and the x's. As soon as one has obtained the excess potentials, he can use them in Eq. (1) to calculate the vapor compositions. For the very small x_3 employed by Daunt and Heer, the liquid solution model should be a good approximation, and the excess potentials should be well represented in terms of a single unknown parameter a. The resulting vapor compositions should be reasonably reliable; perhaps most important of all is the fact that the values of the compositions are based upon results which include the very large gaseous nonideality terms.

TABLE II. Nonideality terms for $T>T_\lambda$; γ is the mole fraction activity coefficient.

X_3	T	γ_3	γ_4	$\mu_3{}^E/V_3f_3{}^2$ cal/cc	$\mu_4{}^E/V_4f_3{}^2$	a cal/cc Eq. (3)
0.0058	2.172	1.439	1.004	0.04091	10.20	0.1365
0.0198	2.177	1.452	1.004	0.04372	0.7969	0.1361
	2.176	1.478	1.002	0.04581	0.1805	0.1361
	2.146	1.547	1.001	0.05063	0.1817	0.1392
0.0521	2.176	1.317	1.009	0.03543	0.2577	0.1361
	2.112	1.433	1.013	0.04520	0.3178	0.1406
0.0949	2.183	1.324	1.014	0.04111	0.1276	0.1360
	2.098	1.395	1.017	0.04715	0.1563	0.1406
	2.004	1.679	1.017	0.04943	0.1517	0.1409
	1.953	1.616	1.015	0.06288	0.1396	0.1420
0.130	2.175	1.303	1.010	0.04308	0.0530	0.1361
	2.070	1.303	1.031	0.04122	0.1505	0.1407
	1.961	1.578	1.027	0.05749	0.1266	0.1419
	1.850	1.655	1.012	0.07049	0.0532	0.1439

In a practical treatment of the data of Daunt and Heer, the simplest method is that of successive approximations applied to the total pressure equation which one obtains by adding Py_3 and Py_4. This equation is suited for the data because the vapor compositions appear only in small correction terms. One uses an approximate y_3 and evaluates an a. The calculated excess potential produces, upon substitution, a new y_3. Since convergence is very rapid, the values of a and y_3 are easily obtained; the results appear in Table I. Two sets of values for y_3/x_3 and for a are presented since Daunt and Heer have given x_3 only within the limits 0.01 and 0.0165. The higher ratios and a values correspond to the lower x_3. The higher ratio of y_3 to x_3 is about 0.5 and the lower one about 0.3 above those calculated by Daunt and Heer using Eq. (2).

Sommers[3] has measured not only total pressures and temperatures but also liquid and vapor compositions at equilibrium. That the vapor compositions are known makes it possible to obtain individual excess potentials directly from Eq. (1) without assumption that they have any particular analytic form. From each of Sommers' determinations above the lambda-point, the excess chemical potentials of isotope three and isotope four, the corresponding mole fraction activity coefficients, and the quantities $\mu_i{}^E/V_if_j{}^2$, have been calculated. The results appear in Table II.

Nonideality parameters can be estimated by the scheme used in reference 1, according to which a is $2a_{34}-a_{33}-a_{44}$ and a_{34} is the geometric mean of a_{33} and a_{44}; a_{jj} is taken as the heat required to vaporize one cm³ of liquid j minus the corresponding external work

$$a_{jj}=d_j\Delta H-p(d_j/D_j-1), \quad (3)$$

where d_j is the liquid density of j, D_j is the vapor density, ΔH is the heat of vaporization per gram, and p is the constant external pressure. Uncertainty in the values of a estimated from the data of Daunt and Heer is necessarily rather large, but the a's are smaller than those calculated from Eq. (3). The values of $\mu_i{}^E/V_if_j{}^2$ obtained from the data of Sommers are smaller than

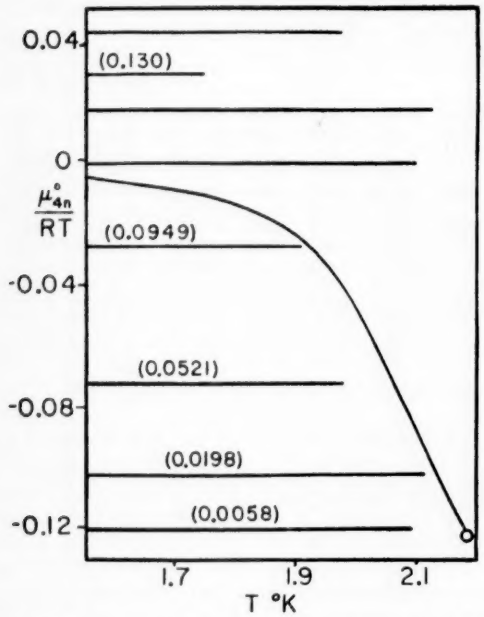

FIG. 1. Extreme values of μ_{4n}^{0}/RT. Lower limits are identified by the He^3 mole fraction in parentheses.

the calculated values for $i=3$ and about the same as the calculated ones for $i=4$. At least over the range $0 \leqslant x_3 \leqslant 0.13$ the excess potential of isotope four is given fairly well by the simple theory.

The fact remains that a single parameter a in the term $V_i a f_j^2$ does not suffice to describe both observed excess potentials. Further, if one examines data for a single temperature, he sees a change in $\mu_i^E/V_i f_j^2$ with concentration, especially for $i=4$. This fact suggests that the excess free energy may be somewhat more complicated than supposed, and that one use a slightly more elaborate expression for it. For instance, the excess free energy may be written $x_3 f_4(B+Cf_4)$, whereupon the excess potentials become $V_4 f_3^2(B+2Cf_4)/V_3$ and $V_3 f_4^2[B+C(f_4-f_3)]/V_3$. The results at 2.176°K give values of the order of 11.2 cal/M for C and -8.82 cal/M for B with $0 \leqslant x_3 \leqslant 0.13$. Prediction,[1] based on molar volumes of the two pure liquids, that use of Flory-Huggins type terms $RT \ln f_i$ and $RT(1-V_i/V_j)f_j$ does not lead in this case to appreciable improvement is borne out by actual calculations with the observed potentials.

III. EQUILIBRIUM BELOW THE LAMBDA POINT

Vapor-liquid equilibrium for temperatures below the lambda-point can be treated just as for those above if one takes into account the chemical potential modifications caused by the presence of superfluid. Using the results of Rice and Engel for the chemical potentials in an ideal solution[4] and including interaction terms, one has for the liquid potentials

$$\mu_{4n}=\mu_{4n}^{0}+RT\ln x_{4n}/(x_{4n}+x_3) +[x_{4s}+\ln(x_{4n}+x_3)]TS_\lambda/(r+1)+\mu_{4n}^{E}, \quad (4)$$

$$\mu_{4s}=-(x_3+x_{4n})TS_\lambda/(r+1), \quad (5)$$

$$\mu_3=\mu_3^{0}(P_3^{0}, T)+RT\ln x_3/(x_{4n}+x_3)+V_3(P-P_3^{0}) +\mu_3^{E}+[x_{4s}+\ln(x_{4n}+x_3)]TS_\lambda/(r+1). \quad (6)$$

In order to employ these equations to calculate excess potentials below the lambda-point, one must obtain, in addition to the information used above the lambda-point, the superfluid mole fraction x_{4s} (or else x_{4n}).

Rice and Engel have pointed out[4] that the equilibrium which exists between normal fluid and superfluid (i.e., equality of their liquid potentials) gives a condition on the system and provides an equation which can be used to find the superfluid mole fraction; equating the appropriate potentials gives

$$0=\mu_{4n}^{0}+RT\ln x_{4n}/(x_{4n}+x_3) +\mu_{4n}^{E}+TS_\lambda(r+1)^{-1}[1+\ln(x_{4n}+x_3)]. \quad (7)$$

The most convenient way to solve is to eliminate μ_{4n}^{E} in Eq. (7) by substitution from the result of equating He^4 gas and liquid potentials. One obtains

$$0=\mu_{4n}^{0}+RT\ln Py_4/P_4^{0}+(P_4^{0}-P)(V_4-B_4) +(2B_{34}-B_3-B_4)(1-y_4)^2P +TS_\lambda(x_{4n}+x_3)/(r+1). \quad (8)$$

The standard potential at a given temperature is to be calculated from the known value at 2.19°K and the heat capacity of normal He^4. Equation (8) is then solved for x_{4n}. The data of Sommers plus equality of liquid and gas potentials can then be used to obtain numerical values of the excess potentials:

$$\mu_3^{E}/RT=\ln Py_3/P_3^{0}+\ln(x_3+x_{4n})/x_3 +[(P_3^{0}-P)(V_3-B_3)+u_{34}(1-y_3)^2P]/RT -[x_{4s}+\ln(x_{4n}+x_3)]S_\lambda/R(r+1), \quad (9)$$

$$\mu_{4n}^{E}/RT=\ln Py_4/P_4^{0}+\ln(x_3+x_{4n})/x_{4n} +[(P_4^{0}-P)(V_4-B_4)+u_{34}(1-y_4)^2P]/RT -[x_{4s}+\ln(x_{4n}+x_3)]S_\lambda/R(r+1). \quad (10)$$

All the simple heat capacity expressions which have been employed in previous discussions of the properties of normal He^4 below the lambda-point lead to an unacceptable temperature dependence of x_{4n}. The appear-

TABLE III. Limits of μ_{4n}^{0}/RT for various concentrations.

X_3	μ_{4n}^{0}/RT
0.0058	−0.1206 to −0.00025
0.0198	−0.1024 to +0.01644
0.0521	−0.07278 to +0.04212
0.0949	−0.02742 to +0.08230
0.130	+0.02888 to +0.1343

[4] O. K. Rice and O. G. Engel, Phys. Rev. **78**, 183 (1950).

ance of the value zero for x_{4n} indicates that all normal He^4 has been converted into superfluid. Vapor pressure data for $x_3=0.0058$ plus the modified cubic heat capacity of Rice and Engel produce a vanishing x_{4n} at about 1.8°K. Investigation showed that no C_p decreasing monotonically to zero from 2.2 cal/deg/M at 2.19°K and giving an entropy reasonably close to 1.59 cal/deg/M at 2.19°K would at the same time produce a positive, nonzero x_{4n} for an appreciable temperature range below the lambda-point. In determination of the source of difficulty with Eq. (8), values of the standard potential obtained without use of an assumed C_p obviously would be of great help; indeed C_p could be found from the temperature dependence of the potential. Since the standard potentials are not known, one must rely on a range of values which, fortunately, can be established without assumption of a particular heat capacity. In order to obtain limits on the standard potential, one uses the fact that $0\leqslant x_{4n}\leqslant 1-x_3$ in all situations. In many particular cases, a smaller range may safely be set. From the pressures, compositions and the above general extremes of x_{4n}, the extremes of $\mu_{4n}{}^0$ have been determined for various values of x_3 and T. The results are presented in Table III; extremes of $\mu_{4n}{}^0/T$ are nearly constant for changing temperature and nearly linear in x_3. It was expected that the various ranges would overlap and narrow the limits on the standard potential to the point where a good estimate of its magnitude could be obtained. The ranges for $x_3=0.0058$, 0.0198, 0.0521, and 0.0949 overlap quite satisfactorily; limits for $x_3=0.13$, however, fall completely outside those for the lowest concentration and overlap the others but little. It is quite apparent that a unique standard potential used in Eq. (8) will give a negative x_{4n} for some one of the He^3 concentrations. A reasonable estimate of the standard potential is obtained by examination of Fig. 1, in which μ^0/RT is plotted as a function of temperature. Since the results for $x_3=0.13$ cannot be reconciled with the others, they are not considered. The range of values common to the four ranges is quite narrow; a smooth curve starting from the known value at 2.19°K and passing through the common range has been used to estimate the values of the standard potential at different temperatures. Calculation of all excess potentials for T less than the lambda-temperature is based on this estimate.

Of the potentials calculated from the extensive measurements of Sommers, only a few* are listed in Table IV; these are typical, however, and show the variation with respect to changes in x_3 and temperature. In the study of temperature dependence of activity coefficients, it should be remembered that, in addition to the lowering of T, there is to be considered conversion of normal fluid to superfluid; this effect, among other things, increases the proportion of isotope three in the normal mixture for a fixed total mole fraction of isotope three. Corresponding to each $\mu_{4n}{}^E$ there is an excess potential* for isotope three obtained in a manner like that for isotope four. For example, with $x_3=0.0058$ and $T=2.066$°K, $\mu_3{}^E/RT=-0.1176$ and $\gamma_3=0.889$. At $T=1.658$ the quantities are -1.1365 and 0.321. In contrast to the behavior of normal isotope four, the activity coefficients are seen to decrease with temperature.

TABLE IV. Nonideality terms for $T<T_\lambda$.

X_3	T°K	X_{4n}	$\mu_{4n}{}^E/RT$	γ_{4n}
0.0058	2.066	0.5237	0.03487	1.036
	1.957	0.2350	0.1117	1.118
	1.847	0.1415	0.1689	1.184
	1.658	0.1056	0.2062	1.229
0.0198	2.082	0.7424	0.01154	1.012
0.0521	1.978	0.6857	0.02989	1.030
0.0949	1.866	0.8372	0.01369	1.014

The thermodynamic relation $\partial(\mu_i/T)/\partial(1/T)=\bar{H}_i$ makes possible the calculation* of partial molal enthalpies from the temperature coefficient of the excess potential. Differentiation with respect to T produces the heat capacity. The fact that one obtains values which seem much too large is directly related to the temperature coefficient of the standard potential used in Eq. (8). It would seem that the standard potential should be understood somewhat better before significance is attached to the values of these enthalpies and heat capacities.

IV. CONCLUSION

Examination of the results of the previous sections makes it seem doubtful that vapor pressure measurements alone will serve to characterize uniquely nonideality for temperatures below the lambda-point; for T greater than the lambda-temperature, with no complications from superfluid, the measurements yield directly excess potentials and activity coefficients. Agreement of the results and the calculations of the simple theory above the lambda-point is especially significant because the excess potential for this temperature condition is used in discussion of the lambda-point shift with changing x_3. Agreement over the tested range is, of course, no absolute assurance that the simple theory can predict as accurately for very high concentrations, but it points out the desirability of using all available information in an effort to understand the solution behavior. Real test of the simple theory for high concentrations of He^3 must await measurements above the lambda-point at these concentrations.

* Results not included in tables or text will gladly be furnished by the author upon application of interested individuals.

The Entropy of Liquid He^3†

TIEN CHI CHEN AND F. LONDON
Department of Chemistry, Duke University, Durham, North Carolina
(Received November 5, 1952)

The vapor pressure of liquid He^3, as measured by Abraham, Osborne, and Weinstock, is found to fit the following equation:

$$\log_{10}(P_{mm}/T^{5/2}) = 2.3126 - 1.1561/T - 0.25254T - 0.00667T^2 + 0.05266T^3 - 0.01210T^4,$$

up to 2.5°K. The entropy curve of the liquid derived from this equation goes smoothly to zero at 0°K, and in fact lies very close to the theoretical curve for a Fermi-Dirac smoothed potential liquid below 1°K. Hence the vapor pressure data furnish no evidence for the existence of a transition below 1°K.

IN a recent paper,[1] Abraham, Osborne, and Weinstock reported very accurate measurements of the vapor pressure of pure liquid He^3 down to 1.025°K on the Kistemaker scale. They represent their data by the following equation, valid up to the critical point,

$$\log_{10}p_{mm} = -0.97796/T + 2.5\log_{10}T + 0.000302T^3 + 1.91594. \quad (1)$$

Equation (1), when extrapolated down to the absolute zero, leads to a residual entropy of $0.21R$ with the nuclear spin contribution of $R\ln 2$ neglected, or $0.91R$ with the spin. This led Abraham *et al.* to suggest that there exists a phase transition or specific heat anomaly in liquid He^3 below 1°K, which removes the residual entropy. Similar views were expressed by Singwi,[2] who suggested that near 1°K the Fermi-Dirac nature of the liquid entropy is replaced by a Debye T^3-law with $\theta_D \sim 4$°K, in "a sort of λ-transition."

It shall be shown that it is possible to represent the vapor pressure data of Abraham *et al.* by a smooth function which has the right vapor pressure constant *including the nuclear spin*, fits the data about as well as (1) from 1 to 2.5°K and leads to a vanishing entropy at 0°K.

The Gibbs potential for a nonideal gas is, up to the second power of the second virial coefficient with higher virial coefficients neglected,

$$G_{\text{nonideal}}(T, p) = G_{\text{ideal}}(T, p) + Bp - (Bp)^2/2RT,$$

where, for a gas of molecular weight 3.0162 and spin ½,

$$G_{\text{ideal}}(T, p) = RT[\ln p_{mm}/T^{5/2} - \tfrac{3}{2}\ln 3.0162 - \ln 2 - 2.976] = RT[2.3026\log_{10}p_{mm}/T^{5/2} - 5.325].$$

Hence,

$$G_{\text{nonideal}}(T, p) = RT[2.3026\log_{10}p_{mm}/T^{5/2} - 5.325] + Bp - (Bp)^2/2RT, \quad (2)$$

which along the vapor pressure curve is equal to the Gibbs potential of the liquid

$$G_{\text{liq}}(T) = G_{\text{nonideal}}[T, p(T)]. \quad (3)$$

The liquid entropy is expressed by

$$S_{\text{liq}}(T) = -(\partial G/\partial T)_p = -dG_{\text{liq}}/dT + V_{\text{liq}}dp/dT, \quad (4)$$

where V_{liq} is the molar volume of the liquid. At the absolute zero S_{liq} should, by Nernst's theorem, be equal to zero. Since near the absolute zero the terms $(d/dT)[Bp - (Bp)^2/2RT]$ and $V_{\text{liq}}dp/dT$ converge rapidly to zero (possibly even with a horizontal tangent), we have, for sufficiently small temperatures,

$$S_{\text{liq}}(T \to 0) = -(dG_{\text{liq}}/dT)_{T\to 0} = 0,$$

which means simply that the expression

$$[2.3026\log_{10}(p_{mm}/T^{5/2}) - 5.325],$$

written in the form of a power series in T, should not contain a constant term nor terms involving lower powers than T^{-1}.

The expression,

$$\log_{10}(p_{mm}/T^{5/2}) = 2.3126 - 1.1561/T - 0.25254T - 0.00667T^2 + 0.05266T^3 - 0.01210T^4, \quad (5)$$

has been found to satisfy the above requirement and to fit the experimental vapor pressure data very well for the range up to 2.5°K. Table I gives a comparison of (1), (5) and the experimental data. Above 2.5°K higher powers are necessary. However, there, deviations resulting from the higher virial coefficients would have to be considered because of the nearness of the critical point (3.35°K).

Substituting (5) in (2) and (4), we have

$$S_{\text{liq}} = R[1.1630T + 0.04608T^2 - 0.4850T^3 + 0.1393T^4] - d/dT[Bp - (Bp)^2/2RT] + V_{\text{liq}}dp/dT, \quad (6)$$

whereas (1) would lead to[3]

$$S_{\text{liq}}{}^{\text{AOW}} = R[0.9134 - 0.002782T^3] - d/dT[Bp - (Bp)^2/2RT] + V_{\text{liq}}dp/dT. \quad (7)$$

A comparison of (6) and (7) is given in Fig. 1. For V_{liq} the measurements of Grilly, Hammel, and Sydoriak[4]

† Supported by the U. S. Office of Naval Research.
[1] Abraham, Osborne, and Weinstock, Phys. Rev. **80**, 366 (1950).
[2] K. S. Singwi, Phys. Rev. **87**, 540 (1952).
[3] Actually the entropy values computed by Abraham *et al.* deviates above 1°K from our values recalculated on the above basis by a small but not identifiable correction. This, however, does not essentially change their general results.
[4] Grilly, Hammel, and Sydoriak, Phys. Rev. **75**, 1103 (1949).

have been used, and for B the computed values of deBoer, Kranendonk, and Compaan.[5]

The entropy of an ideal Fermi-Dirac gas with spin $\frac{1}{2}$, molecular weight 3.0162 and molar volume 38 cm^3 is included in Fig. 1 as $S^{F.D.}$. It can be seen that for low temperatures S_{liq} is linear with temperature with slope $1.17R$. This is very close to the value $S^{F.D.}(T\to 0) = 1.01RT$. This strongly suggests that liquid He^3 can roughly be considered as a degenerate Fermi-Dirac gas confined in the molar volume V_{liq} (this is equivalent to representing the liquid by the smoothed potential model), with other excitations (Debye waves as well as other interactions) entering at higher temperatures. Lifshitz[6] by a similar argument obtained $S_{liq}=0.76RT - 0.068RT^3$ as a crude estimate.

TABLE I. The vapor pressure of liquid He^3 between 1.025 and 2.517°K. p: experimental data of Abraham, Osborne, and Weinstock. p_1: vapor pressure from Eq. (5) proposed here; p_2: vapor pressure from Eq. (1), proposed by Abraham, Osborne, and Weinstock. Up to and including 2.382°K the difference between the two interpolation formulas is nowhere greater than 0.4 percent.

T(°K)[a]	p(mm)	p_1(mm)	p_2(mm)	$p-p_1$(mm)	$p-p_2$(mm)
1.025	9.71	9.75	9.75	−0.04	−0.04
1.026	9.81	9.80	9.79	+0.01	+0.02
1.038	10.41	10.35	10.34	+0.06	+0.07
1.042	10.46	10.54	10.53	−0.08	−0.07
1.058	11.29	11.32	11.30	−0.03	−0.01
1.121	14.74	14.75	14.72	−0.01	+0.02
1.182	18.79	18.69	18.65	+0.10	+0.14
1.183	18.68	18.76	18.72	−0.08	−0.04
1.298	28.00	27.98	27.95	+0.02	+0.05
1.363	34.16	34.33	34.31	−0.17	−0.15
1.513	52.59	52.45	52.51	+0.14	+0.08
1.644	72.78	72.70	72.81	+0.08	−0.03
1.785	99.65	99.69	99.74	−0.04	−0.09
1.935	135.0	134.92	134.72	+0.1	+0.3
2.046	165.1	165.65	165.12	−0.6	±0.0
2.162	201.1	202.13	201.74	−1.0	−0.6
2.257	234.2	234.34	234.39	−1.1	−0.2
2.382	282.7	283.39	283.02	−0.7	−0.3
2.517	342.4	340.14	343.32	+2.3	−0.9

[a] On Kistemaker's scale.

It is clear from Fig. 1 that, in order that liquid He^3 conform to Nernst's theorem, it is *not* necessary to assume a discontinuity at low temperatures in either the entropy curve or the specific heat curve, but that the entropy of liquid He^3 may be perfectly smooth and continuous. The deviation from the $S^{F.D.}$ curve is probably not only due to the Debye specific heat contribution but also to inadequacies of the present interpretation which by necessity could not take proper account of the contributions of the higher virial coefficients of the vapor in the calculation of G_{liq} along the vapor pressure curve.

The change in curvature of S_{liq} might indicate that there is a flat minimum in the specific heat curve $C_p=T(\partial S/\partial T)_p=T[dS/dT+(\partial V/\partial T)_p(dp/dT)]$,

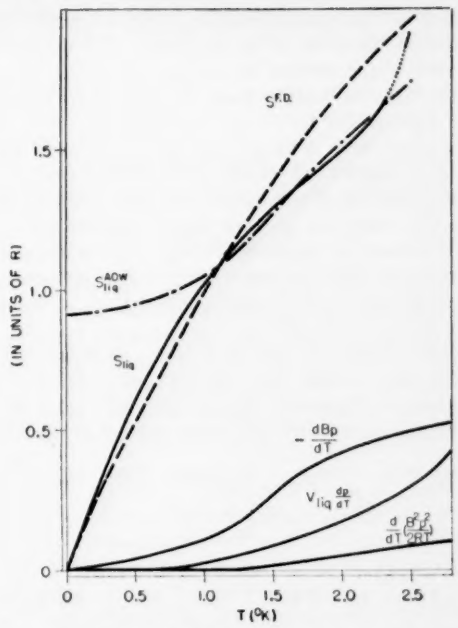

FIG. 1. Entropy of liquid He^3. The solid line (S_{liq}) represents Eq. (6), derived from the vapor pressure equation proposed here. S_{liq}^{AOW} represents Eq. (7), derived from the formula of Abraham *et al.* $S^{F.D.}$ is the entropy of a Fermi-Dirac smoothed potential model liquid included for comparison. The various correction terms employed in Eqs. (6) and (7) are plotted in the lower part of the drawing.

since $(\partial V/\partial T)_p$ is negligible up to 1.5°K. Such a defect was first discussed by Simon in connection with Miller's interpretation[7] of the crude vapor pressure measurements by Sydoriak, Grilly, and Hammel.[8] From S_{liq} as given in Fig. 1 one would estimate the trough to be near 1.5°K. However, its existence can in no way be considered as ascertained, since its magnitude is within the estimated error. It is perhaps worth mentioning that a similar change of curvature at a somewhat higher temperature (~2°K) is obtained for $S^{F.D.}$, if the variation in the molar volume[4] with rising temperatures is being taken into account.

The above discussion does of course not exclude the possibility of a transition in liquid He^3, but it shows that the present vapor pressure data do not give any support for the assumption of such a transition. Direct measurements of the specific heat of liquid He^3 and of the vapor pressure just below 1°K would be most significant.

Pomeranchuk[9] argued that the melting pressure curve for solid He^3 must have a negative slope if there is appreciable nuclear spin alignment in the liquid but not in the solid, that is, if $S_{solid}>S_{liq}$, since he expects

[5] deBoer, van Kranendonk, and Compaan, Physica **16**, 545 (1950).
[6] E. M. Lifshitz, J. Exptl. Theor. Phys. (U.S.S.R.) **21**, 659 (1951).
[7] A. R. Miller, Nature **163**, 283 (1949).
[8] Sydoriak, Grilly, and Hammel, Phys. Rev. **75**, 303 (1949).
[9] I. Pomeranchuk, J. Exptl. Theor. Phys. U.S.S.R. **20**, 919 (1950).

ordering of the spins resulting from magnetic spin interaction alone to occur at about 10^{-7} degree K. However measurements by Weinstock, Abraham, and Osborne[10] give a positive slope of the melting pressure curve down to 0.5°K.

The structure or density of solid He^3 is not yet known. It is quite possible that solid He^3 is different from other solids regarding the alignment of the nuclear spin. Solid He^3 might be so very loosely packed that, for similar reasons as in the liquid state, a spin alignment occurs in the solid state at a much higher temperature than assumed by Pomeranchuk, and that, at a finite temperature, $S_{\text{solid}}<R\ln 2$.

Another possibility would be that, as liquid He^3 is compressed towards the solidification line, it may gradually or discontinuously be squeezed into a structure almost as localized as in the solid state, and lose the characteristics of a smoothed potential liquid. In this case the spins would become disorganized under compression *before* solidification. This would mean that the thermal expansion coefficient of the liquid under sufficient pressure would become negative, since $(\partial V/\partial T)_p=-(\partial S/\partial p)_T$.

Weinstock, Abraham, and Osborne[11] proposed to extrapolate the vapor pressure data in such a way as to give $S_{\text{liq}}>R\ln 2$, $T\gtrsim 0.5$°K. In view of our interpretation ($S_{\text{liq}}\to 0$ when $T\to 0$), this possibility is in no way demanded by the experimental data and appears to us less likely than either of the two alternatives mentioned above.

An experiment to decide directly the degree of nuclear spin alignment in liquid as well as in solid He^3 by measuring the intensity of the nuclear resonance adsorption is being conducted at this University.

[10] Weinstock, Abraham, and Osborne, Phys. Rev. **85**, 158 (1952).

[11] Weinstock, Abraham, and Osborne, Phys. Rev. **89**, 787 (1953).

PHYSICAL REVIEW VOLUME 89, NUMBER 5 MARCH 1, 1953

Bohm's Interpretation of the Quantum Theory in Terms of "Hidden" Variables

JOSEPH B. KELLER
Institute for Mathematics and Mechanics, New York University, New York, New York
(Received May 14, 1952)

An analysis of Bohm's theory, emphasizing the role of probability in it, is presented.

IN two recent articles[1] David Bohm has suggested a "deterministic" interpretation of quantum mechanics based on the introduction of "hidden" variables. It is the purpose of this note to analyze his interpretation and especially the role of probability in it, by examining the complete mathematical formulation of the theory. We are led to the conclusion that if Eq. (10) below must be postulated, then the suggested interpetation is not an ordinary statistical mechanics of a deterministic theory, which is the kind of interpretation many physicists have hoped for and which some have thought this to be. On the other hand, if Eq. (10) can be deduced from the other postulates of the theory, as Bohm attempts to prove in his latest[1] paper, then the theory is essentially an ordinary statistical mechanics of a deterministic theory.

I. DETERMINISTIC MECHANICS OF A SINGLE PARTICLE

In order to present our analysis, we shall first give a precise formulation of Bohm's theory for a single particle in an external potential $V(x)$. Bohm postulates that the particle of mass m has a position $x(t)$ at time t, and thus also a velocity $\dot{x}(t)$. These quantities $x(t)$ and $\dot{x}(t)$ are the so-called "hidden" variables. In addition to $x(t)$ and $\dot{x}(t)$, there is a "quantum mechanical field" $P(x,t)$. The quantities $P(x,t)$ and $x(t)$ satisfy the following equations:

$$\dot{P}+\nabla\cdot(m^{-1}P\nabla S)=0, \tag{1}$$

$$\dot{S}+\frac{1}{2m}(\nabla S)^2+V(x)-\frac{\hbar^2}{2m}\frac{\nabla^2 P^{\frac{1}{2}}}{P^{\frac{1}{2}}}=0, \tag{2}$$

$$\dot{x}=\nabla S/m. \tag{3}$$

In these equations $S(x,t)$ is a modified Hamilton-Jacobi function which is not assigned a physical interpretation,[2] and $\hbar$ is Planck's constant.

The above equations must be supplemented by the following initial conditions in order to determine a unique solution:[3]

$$P(x,0)=P_0(x), \tag{4}$$

$$S(x,0)=S_0(x), \tag{5}$$

$$x(0)=x_0. \tag{6}$$

[1] David Bohm, Phys. Rev. **85**, 166, 180 (1952); **89**, 458 (1953).

[2] An alternative formulation, not employing S, is possible but does not alter the main discussion to be given below.

[3] It is interesting to notice that the function $S_0(x)$ must be given for all x in order to determine a single trajectory. In contradistinction to this, in classical mechanics a trajectory is uniquely

From Eqs. (3) and (5) we notice that $\dot{x}(0)$ is not arbitrary but is given by

$$\dot{x}(0)=\nabla S_0(x_0)/m. \tag{7}$$

Therefore if $\dot{x}(0)$ is given, $S_0(x)$ must be so chosen as to satisfy Eq. (7).

Equations (1)–(6) constitute the formulation of the deterministic theory and determine the trajectory $x(t)$, the velocity $\dot{x}(t)$ and the field $P(x, t)$ uniquely.

II. STATISTICAL MECHANICS OF A SINGLE PARTICLE[4]

Probability is supposed to enter the theory through incomplete knowledge of initial data, just as in classical statistical mechanics. Bohm implies, but does not state explicitly, that $P_0(x)$ and $S_0(x)$ are known exactly, but that x_0 is not. Instead an initial probability distribution $\phi_0(x)$ of x is known, and it is desired to determine the subsequent probability distribution $\phi(x, t)$ of x at time t.[5] By applying the law of conservation of probability we conclude that $\phi(x, t)$ satisfies

$$\dot{\phi}+\nabla\cdot[\phi(x, t)\nabla S/m]=0, \tag{8}$$

$$\phi(x, 0)=\phi_0(x). \tag{9}$$

In Eq. (8), $\nabla S(x, t)/m$ represents the velocity field obtained by solving Eqs. (1) and (2) subject to the initial conditions, Eqs. (4) and (5).

Equations (8) and (9) determine the probability distribution $\phi(x, t)$ corresponding to given $\phi_0(x)$, $P_0(x)$ and $S_0(x)$. The function ϕ characterizes the statistical mechanics of a single particle, the deterministic mechanics of which is given by Eqs. (1)–(6). Although none of the quantities $\phi(x, t)$, $\phi_0(x)$, $P_0(x)$ or $S_0(x)$ was mentioned by Bohm, it appears that they are essential for an understanding of the theory.

III. RELATION OF $P(x, t)$ AND $\phi(x, t)$

By comparing Eqs. (1) and (8) we notice that P and ϕ satisfy the same equation, but nevertheless they are not equal, since they satisfy the independent initial conditions, Eqs. (4) and (9), respectively. The initial function $P_0(x)$ is supposed to represent the initial values of the real quantum-mechanical field present in a particular experiment. The function $\phi_0(x)$ is supposed to represent the initial probability distribution of x, characteristic of some ensemble of experiments. In the statistical treatment of a deterministic theory the initial probability $\phi_0(x)$ is arbitrary, and therefore, it will not generally equal $P_0(x)$. Therefore, in general, $P(x, t)$ will differ from $\phi(x, t)$.

The only instance in which $P(x, t)=\phi(x, t)$ is that in which the initial data are accidentally equal, that is if

$$P_0(x)=\phi_0(x). \tag{10}$$

Only in this case can $P(x, t)$ be given the dual interpretation of a probability distribution characterizing an ensemble of experiments, and a real field present in a single experiment. Thus it is only in this case that the probabilities deduced from the statistical mechanics of Bohm's deterministic theory will coincide with those given by quantum mechanics [with $\psi(x, 0)=P_0^{\frac{1}{2}}(x)\times e^{iS_0(x)/\hbar}$].

In order to assure agreement between these two theories in all cases, it is necessary to add to Bohm's theory the postulate that Eq. (10) always holds. This is a physical postulate which is inherently probabilistic. Therefore, if it is accepted, the resulting theory is no longer an ordinary statistical mechanics of a deterministic theory. Probability enters the theory not only through incomplete knowledge of initial data but also in a deeper way—it affects the initial P field. In other words, if an ensemble of experiments is prepared, the initial P field in each is determined by the nature of the ensemble, and all experiments in the ensemble will have the same initial P field. This surprising hypothesis somewhat strains the notion of a "real" P field. However, if Eq. (10) can be deduced from the other postulates of the theory, as Bohm contends in his latest paper, then probability enters the theory just as in any statistical mechanics.

There is another remarkable difference between Bohm's theory and an ordinary statistical mechanics of a deterministic theory. In an ordinary statistical mechanics the underlying deterministic theory is also a special case of the statistical theory. It is obtained from the latter by assuming that the initial probability distribution is a delta-function. In Bohm's theory, however, only that particular case of the deterministic theory in which $P_0(x)$ is a delta-function can be obtained by specializing the statistical theory. This follows from Eq. (10), since to obtain the deterministic theory $\phi_0(x)$ must be a delta-function, and therefore $P_0(x)$ is also.

The conclusion is that Bohm's interesting interpretation of quantum mechanics, based on the introduction of "hidden" variables, is not an ordinary statistical mechanics of a deterministic theory, unless Eq. (10) can be shown to follow from the other postulates. If not, the theory involves probability in an additional and deeper manner, expressed by Eq. (10).

determined by giving merely $\nabla S_0(x)$ at $x=x_0$, the initial point on the trajectory. This difference is related to the structure of Eqs. (1)–(3), and implies that $S(x, t)$ should also be given a physical interpretation, since its initial values must be determined in order to formulate a problem correctly.

[4] Statistical mechanics, as used here, does not refer to equilibrium theory, but merely to the introduction of probability into a deterministic theory through incomplete knowledge of initial data.

[5] It is significant that Bohm does not seek the joint probability distribution of x and $\dot{x}$. This is not sought because $\dot{x}$ is uniquely related to x and t by $\dot{x}=\nabla S(x, t)/m$ [see explanation after Eq. (9)]. This is related to the fact that quantum mechanics does not yield joint probability distributions of conjugate variables.

Photofission and Photoneutron Emission in Uranium*

ROBERT B. DUFFIELD, *University of Illinois, Urbana, Illinois*

AND

JOHN R. HUIZENGA, *Argonne National Laboratory, Lemont, Illinois*

(Received November 24, 1952)

The yields of the two reactions $U^{238}(\gamma,n)U^{237}$ and $U^{238}(\gamma, \text{fission})$ produced by bremsstrahlung have been measured as a function of the maximum energy of the x-ray spectrum. The ratio of the number of fissions to the number of U^{237} atoms produced decreased from 0.390 at 8 Mev to 0.275 at 12 Mev and then increased to 0.465 at 22 Mev. These data are interpreted to show that for maximum x-ray energies in excess of 12 Mev, a fraction of the U^{237} atoms formed by the (γ,n) reaction are left with sufficient excitation energy that fission or secondary neutron emission can occur. The cross sections for the reactions as a function of gamma-ray energy have been calculated from the yield data.

I. INTRODUCTION

MEASUREMENTS have been made by Price and Kerst[1] of the total photoneutron intensity from various elements excited by 18, 22, and 320 Mev bremsstrahlung. Measurements have also been made at 330 Mev by Terwilliger, Jones, and Jarmie.[2] Price and Kerst found the number of neutrons per mole per roentgen to vary smoothly (approximately as Z^2) for all the elements except that thorium and uranium gave too many neutrons by factors of 1.36 and 1.76 at 22 Mev. The additional neutrons were attributed to photofission and it was calculated that if the number of neutrons emitted per fission was 2.5, an excited uranium nucleus underwent fission with a probability of approximately 0.5 under their irradiation conditions.

A result at variance with this has been reported by Goward *et al.*[3] Using 23-Mev bremsstrahlung, they found that one milligram of uranium gave 24.2±2 fissions per r and 255±25 neutrons per r, indicating a much lower fission branching ratio. The fission yield was determined by particle counting; the neutron yield by measuring the activity induced in a manganese sulfate solution as compared with that produced by a standard Ra–Be source.

The photofission cross section of uranium for the 17-Mev Li(p,n) gamma-rays was measured by Charbonnier, Scherrer, and Wäffler.[4] They counted the number of fission tracks produced in irradiated uranium-loaded nuclear track emulsions. They obtained a result of 0.046±0.015 barn.

We have measured the yields of the two reactions $U^{238}(\gamma,n)U^{237}$ and $U^{238}(\gamma, \text{fission})$ produced by bremsstrahlung from a betatron at energies from 8 to 22 Mev. The yield of the first reaction has been determined by isolating and counting the U^{237} formed and the yield of the second by isolating and counting radioactive fission products. The absolute yields of the two reactions measured in this way depend on an accurate calibration of the counters used. For U^{237}, this calibration was done by measuring the amount of alpha-emitting Np^{237} formed by decay of the U^{237}. For the fission products it was done by measuring the activity of fission products resulting from a known number of neutron-produced fissions. We believe that the absolute values so obtained are correct to a few percent.

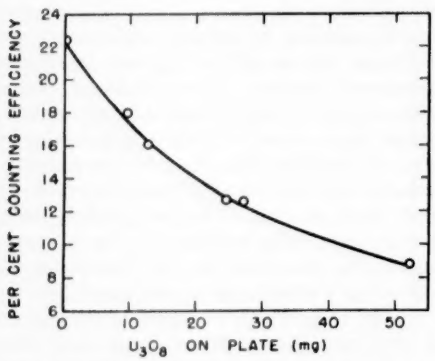

FIG. 1. The counting efficiency for U^{237} in the counter used *vs* sample thickness.

II. EXPERIMENTAL

The uranium samples used were depleted of U^{235} and were in the form of U_3O_8. Each sample consisting of approximately 0.325 g of U_3O_8, was irradiated in the external x-ray beam from the University of Illinois 22-Mev betatron. After irradiation, this material was divided, part being used for the U^{237} determination and part for the fission product analysis. The beam was monitored using a standard Victoreen thimble inside an aluminum block of wall thickness 4 cm.

* This work was supported by the joint program of the U. S. Atomic Energy Commission and the U. S. Office of Naval Research.

[1] G. A. Price and D. W. Kerst, Phys. Rev. **77**, 806 (1950); **79**, 725 (1950).

[2] Terwilliger, Jones, and Jarmie, Phys. Rev. **82**, 820 (1951).

[3] Goward, Jones, Watson, and Lees, Proc. Phys. Soc. (London) **A64**, 95 (1951).

[4] Charbonnier, Scherrer, and Wäffler, Helv. Phys. Acta **22**, 385 (1949).

1. U^{237} Determination

The uranium was separated from fission products and counted by the procedure previously described.[5] This involved ether extractions, deposition as a thin film, and counting on a thin window Geiger counter. This counter was standardized for absolute beta-counting of U^{237} in the following way. A sample of uranium containing 95 percent U^{236} was irradiated in the thimble of the Argonne heavy water reactor to produce U^{237}. After bombardment the uranium was purified of neptunium and fission products. A known portion of the total purified uranium was then used to prepare several thin plates for beta-counting. The U^{237} in these was diluted with various known weights of normal uranium so that the counting efficiency could be obtained as a function of film thickness.

The remainder of the purified uranium was allowed to decay for about five U^{237} half-lives. The Np^{237} formed by this decay was then extracted and purified (*cf.* Appendix) and its amount determined by alpha-counting in a counter of known geometry. Alpha-pulse analysis[6] indicated that more than 99 percent of the alphas were in the energy range of Np^{237}. Good purification from uranium is essential in this step since the U^{234} and Np^{237} alpha-energies are very nearly the same. However, no correction for U^{234} was necessary since U^{236} was not detected in the alpha-pulse analysis (this uranium sample had a U^{236}/U^{234} alpha-activity ratio greater than ten).

Using 6.75 days as the half-life[7] of U^{237} and 2.2×10^6 years as the half-life[8] of Np^{237}, the counting efficiency of U^{237} was found as a function of sample thickness and the results are given in Fig. 1. These data were used to calculate the number of U^{237} atoms formed in the betatron irradiations.

TABLE I. Number of fissions and U^{237} atoms from U^{238} as a function of betatron energy.

Betatron energy	Roentgens	Total number of fissions per mole of U^{238}	Total number of U^{237} atoms per mole of U^{238}	Fissions per mole of U^{238} per 100 r	U^{237} atoms per mole of U^{238} per 100 r	Fissions per atom of U^{237}
8	···	6.69×10^9	1.72×10^{10}	···	···	0.390
10	5746	9.16×10^9	2.31×10^{10}	1.59×10^8	4.02×10^8	0.396
12	9433	3.03×10^{10}	1.10×10^{11}	3.22×10^8	1.17×10^9	0.275
12	···	1.08×10^{11}	3.91×10^{11}	···	···	0.276
14	8793	5.14×10^{10}	1.49×10^{11}	5.85×10^8	1.69×10^9	0.345
16	10 553	7.81×10^{10}	2.05×10^{11}	7.40×10^8	1.94×10^9	0.381
18	···	6.91×10^{10}	1.74×10^{11}	···	···	0.397
20	9808	8.91×10^{10}	2.00×10^{11}	9.08×10^8	2.04×10^9	0.446
20	···	5.45×10^{11}	1.15×10^{12}	···	···	0.474
20	···	3.62×10^{12}	8.13×10^{12}	···	···	0.444
22	···	7.81×10^{10}	1.68×10^{11}	···	···	0.465

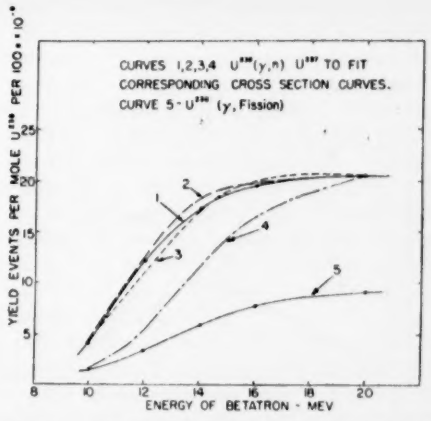
CURVES 1,2,3,4 U²³⁸(γ,n) U²³⁷ TO FIT CORRESPONDING CROSS SECTION CURVES.
CURVE 5 - U²³⁸ (γ, Fission)
YIELD EVENTS PER MOLE U²³⁸ PER 100 r PER 10⁹
ENERGY OF BETATRON - MEV

FIG. 2. The yields of the reactions $U^{238}(\gamma,n)U^{237}$ and $U^{238}(\gamma,\text{fission})$ *vs* betatron energy. 1 and 5 are the experimental yield curves for the reactions $U^{238}(\gamma,n)U^{237}$ and $U^{238}(\gamma,\text{fission})$, respectively. Curves 2, 3, and 4 are hypothetical $U^{238}(\gamma,n)U^{237}$ yields resulting from the corresponding assumed cross-section curves of Fig. 5.

2. Fission Determination

The number of fissions occurring in each irradiated sample was determined by measuring the number of atoms of Ba^{139}, Mo^{99}, and Ba^{140} which were made during the irradiation. These fission products were separated chemically from the uranium using well-known procedures[9] and the amounts determined by counting the activity.

The standardization of the Geiger counter used was done in cooperation with R. W. Spence of the Los Alamos Scientific Laboratory. The procedure consisted in measuring the number of counts of a given fission product in a sample of U^{235} in which a known number of slow neutron-produced fissions had occurred. The latter

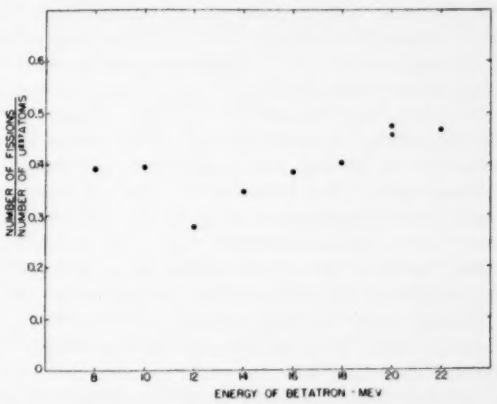

FIG. 3. The ratio, the number of fissions occurring to the number of U^{237} atoms formed by bremsstrahlung *vs* betatron energy.

[5] Huizenga, Magnusson, Fields, Studier, and Duffield, Phys. Rev. **82**, 561 (1951).

[6] The pulse analysis was carried out by J. Mech of the Argonne National Laboratory.

[7] J. R. Huizenga and K. Flynn (unpublished data).

[8] L. B. Magnusson and T. J. LaChapelle, J. Am. Chem. Soc. **70**, 3534 (1948).

[9] *Radiochemical Studies: The Fission Products* (McGraw-Hill Book Company, Inc., New York, 1951), National Nuclear Energy Series, Plutonium Project Record, Vol. 9, Div. IV.

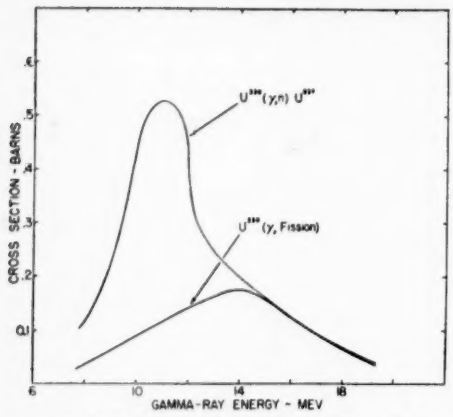

FIG. 4. The cross sections for the reactions $U^{238}(\gamma,n)U^{237}$ and $U^{238}(\gamma,$ fission) *vs* the energy of the gamma-ray.

number of fissions was determined by particle counting in an ionization chamber.

This standardization was checked at Argonne National Laboratory by an independent measurement of the number of fissions occurring in one of the 20-Mev runs. The two numbers differed by 2.5 percent.

III. RESULTS

The data are summarized in Table I and shown graphically in Figs. 2 and 3. For each sample irradiated we have measured the total number of fissions which occurred and the total number of U^{237} atoms formed. These are tabulated in the third and fourth columns of Table I as the number of the corresponding events per mole of uranium. For those runs for which we have an accurate measure of the x-ray exposure we have also tabulated the number of events per mole of uranium per 100 r of x-rays. A number of the runs were made with the sample 25 cm from the betratron target (the usual distance was 55 cm) and for these, an accurate determination of the x-ray exposure was not made. This close distance was used in order to get more intensity.

In calculating the number of photofissions which occurred during the betatron runs, it was assumed that the yield of barium and molybdenum photofission products was 0.9 that from slow neutron fission of U^{235}. There are no experimental data on this point, but the above figure seems reasonable since it is known that fission becomes more nearly symmetric as the energy of excitation is increased. All the absolute fission yields which appear in this paper depend on this assumption of course and if it is incorrect, the fission yields will be incorrect accordingly.

In Fig. 2 are shown the yields (events per mole of U^{238} per 100 r of x-rays) as a function of the betatron energy, the two solid curves representing the experimental data. The U^{237} yield curve has quite a different shape as well as absolute value from the fission yield curve. The other curves in this figure are discussed below.

In Fig. 3 the ratio of the number of fissions to the number of U^{237} atoms formed is plotted as a function of betatron energy. As can be seen, this number is very roughly constant at 0.4 except for a valley in the neighborhood of 12 Mev. This last feature is discussed below.

These yield curves have been analyzed by what are now standard procedures[10,11] to give cross sections as functions of discrete gamma-ray energy. In this procedure the bremsstrahlung spectrum is taken to be that calculated by Schiff.[12] The cross sections so calculated, particularly at the higher energies, are very sensitive to the experimental fluctuations so that the detailed shapes of the cross sections should not be taken too literally.

The cross-section curves calculated from the experimental data are shown in Fig. 4. The cross section for the reaction $U^{238}(\gamma,n)U^{237}$ appears to have a strong maximum at the low energy of 11 Mev, decreasing sharply above this. The reaction $U^{238}(\gamma,$ fission) has a broad maximum at approximately 14 Mev. The latter result is in agreement with previously reported measurements of the U^{238} photofission cross-section shape.[13,14]

The range of uncertainty in these cross sections is indicated in Fig. 5. The solid line is the cross section deduced for the reaction $U^{238}(\gamma,n)U^{237}$ from the experimental data. The broken lines represent other arbitrarily chosen curves which resemble in some features the solid curve. We have used these cross-section curves and the Schiff bremsstrahlung spectrum to calculate back to the hypothetical yield curve to which each of these would

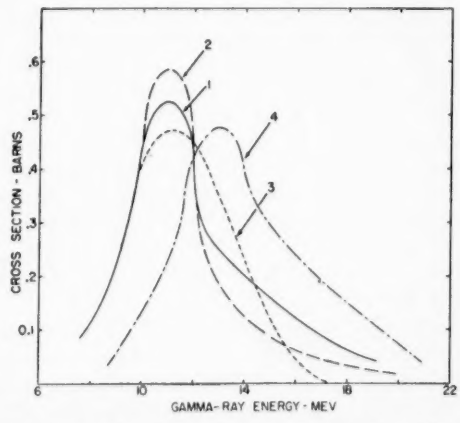

FIG. 5. Cross section for the reaction $U^{238}(\gamma,n)U^{237}$ *vs* gamma-ray energy. Curve 1 is the experimental one. Curves 2, 3, and 4 are arbitrarily chosen to resemble Curve 1 in some features; they give the yield curves numbered correspondingly in Fig. 2.

[10] B. C. Diven and G. M. Almy, Phys. Rev. **80**, 407 (1950).
[11] L. Katz and A. G. W. Cameron, Can. J. Phys. **29**, 518 (1951).
[12] For a discussion, see G. D. Adams, Phys. Rev. **74**, 1707 (1948).
[13] W. E. Ogle and J. McElhinney, Phys. Rev. **81**, 344 (1951).
[14] R. E. Anderson and R. B. Duffield, Phys. Rev. **85**, 728 (1952).

correspond.[15] These yield curves appear in Fig. 2 with numbers indicating the cross-section curve to which they correspond.

It is evident from curves 2 and 3 of Fig. 2 that changing the heights or detailed shape, particularly on the high energy side, of the cross-section curve makes only a small difference in the yield curve. However, curve 4 shows that shifting the position of the maximum by 2 Mev makes a great difference in the yield curve. We conclude from these that the cross section has a maximum near 11 Mev but that its exact shape is uncertain.

The value of the integrated photonuclear cross section up to 20 Mev for the reaction $U^{238}(\gamma,n)U^{237}$ from the above data comes out to be 2.6 Mev-barns and for the reaction $U^{238}(\gamma,\text{fission})$ the corresponding value is 1.2 Mev-barns.

IV. DISCUSSION

Our experiments are in general accord with the results one might expect on the basis of the statistical compound nucleus model. Complete predictions from the model have not been made because of the difficulty of treating the fission process. The questions of the total integrated photodisintegration cross section and the multiplicity of neutron emission have been discussed by Levinger and Bethe[16,17] and by Eyges.[18]

Previous measurements have shown that the threshold for photofission of U^{238} is approximately 5.3 Mev[19,14] and that the threshold for the reaction $U^{238}(\gamma,n)U^{237}$ is 5.97 Mev.[5] The photofission threshold predicted by the liquid drop model calculations for U^{237} is 7 Mev[20] but the indications from other data are that all photofission thresholds for heavy elements are considerably lower, perhaps 5.3 Mev.[19,21] The neutron binding energy in U^{237} is probably about 5.2 Mev.[22] These numbers indicate that a U^{238} nucleus with excitation energy between 6 Mev and approximately 11.3 Mev can either undergo fission or neutron emission. If we let σ_f represent the cross section for the reaction $U^{238}(\gamma,\text{fission})$ and σ_n the cross section for the reaction $U^{238}(\gamma,n)U^{237}$, our experimental results show that the ratio $\sigma_f/(\sigma_f+\sigma_n)$ decreases somewhat between 8 and 11 Mev but has the average value 0.20 to 0.25.

For excitation energies in excess of 11.3 Mev, the U^{237} nucleus left after single neutron emission may either emit a second neutron or may undergo fission. Either process will serve to increase the experimentally observed ratio of the number of fissions to the number of residual U^{237} atoms as a function of betatron energy. This effect is apparent in the data of Fig. 3, and accounts for the rise above a betatron energy of 12 Mev. The cross section for the reaction $U^{238}(\gamma,n)U^{237}$ definitely appears to decrease sharply beyond a gamma-ray energy of 11 to 12 Mev, though as shown by the curves, the exact dependence on energy is rather uncertain.

The product of the $(\gamma,2n)$ reaction, U^{236}, was not measured in these experiments, To do so is very difficult experimentally because of its long half-life. As pointed out above, it should have a threshold of about 11.3 Mev and the cross section may be appreciable in the energy range 15 to 20 Mev.

Levinger and Bethe have shown that a value of 0.23 (independent of excitation energy) for the relative probability of fission of a uranium nucleus would reconcile the neutron yield data at 320 Mev with the value of the integrated photodisintegration cross section predicted by the sum rule formula and neutron yield data for lower Z elements. This formula is

$$\int_0^\infty \sigma dW = 0.06(NZ/A)(1+0.8x),$$

where N, Z, and A are the neutron number, proton number, and mass number of the nucleus in question, and x is the fraction of the neutron-proton force that has an exchange character. These authors show that the 320-Mev data for Cu, I, Ta, and Bi are in accord with this formula written as

$$\int_0^\infty \sigma dW = 0.14NZ/A.$$

This formula predicts an integrated cross section for uranium of 7.9 Mev-barns. This agrees with the observed neutron yield at 320 Mev if the probability of photofission is as given above and if the neutron multiplicity is proportional to the excitation energy.

The coefficient of NZ/A in the above formula required to fit the 320-Mev neutron yield data is higher than expected even for $x=1$. Eyges[18] has shown that the lower energy data for Zn^{64}, Sb and Ta^{181} indicate a smaller value of this coefficient, and he attributes the difference to mesonic interaction at the higher energies. His evaluation indicates an integrated cross section to 20 Mev, for uranium, of 4.7 Mev-barns.

Our data gave integrated cross sections to 20 Mev of 1.2 Mev-barns for photofission and 2.6 Mev-barns for $U^{238}(\gamma,n)U^{237}$. They indicate a total integrated photodisintegration cross section to 20 Mev of at least 3.8 Mev-barns but give no measure of the cross sections for $(\gamma,2n)$ and $(\gamma,3n)$. A value of 1 Mev-barn for the $(\gamma,2n)$ cross section seems not unreasonable and is consistent with the other cross-section data if one assumes that the relative probability of fission as compared to neutron emission is independent of the excitation energy and has the value of about 0.25.

[15] The yield curves were calculated by means of a synchro-operated differential analyzer designed by Arnold T. Nordsieck of the University of Illinois.
[16] J. S. Levinger and H. A. Bethe, Phys. Rev. **78**, 115 (1951).
[17] J. S. Levinger and H. A. Bethe, Phys. Rev. **85**, 577 (1952).
[18] L. Eyges, Phys. Rev. **86**, 325 (1952).
[19] Koch, McElhinney, and Gasteiger, Phys. Rev. **77**, 329 (1950).
[20] S. M. Frankel and N. Metropolis, Phys. Rev. **72**, 914 (1947).
[21] J. R. Huizenga and R. B. Duffield, Phys. Rev. **88**, 959 (1952).
[22] Unpublished calculations independently made by K. Way and J. R. Huizenga.

Finally, our experimental cross-section curve for photofission shows a value of 0.1 barn at 17.5 Mev. Charbonnier, Wäffler, and Sherrer reported a value of 0.046±0.015 barn at this energy. This probably constitutes agreement within the large errors of cross-section determination for the bremsstrahlung spectrum.

We are indebted to R. W. Spence of the Los Alamos Laboratory for the calibration of our fission product counter, to A. T. Nordsieck of the University of Illinois for assistance in the operation of the differential analyzer, and to Kevin Flynn of Argonne National Laboratory for the fission product analysis.

APPENDIX

Procedure for separation of neptunium from uranium.

1. A known amount of Np^{239} tracer was added so that the chemical yield could be determined.
2. Potassium permanganate added to oxidize both Np^{237} and Np^{239} to +6 valence state.
3. The neptunium was reduced with sodium nitrite.
4. Neptunium fluoride was precipitated using lanthanum fluoride as carrier.
5. The fluorides were metathesized with sodium hydroxide and dissolved in acid.
6. Steps 2 through 5 were repeated.
7. The neptunium was extracted into an organic solvent as the thenoyltrifluoracetone complex.

PHYSICAL REVIEW VOLUME 89, NUMBER 5 MARCH 1, 1953

Relativity Precession of the Asteroid Icarus

J. J. GILVARRY
Rand Corporation, Santa Monica, California
(Received July 28, 1952)

The relativity precession of the asteroid Icarus is computed to be 10.05″ per century. This value is about one-quarter that of Mercury and exceeds that of any major planet excluding Mercury. Consideration of a figure of merit, which determines the possible precision in measurement of the perihelion advance, indicates that the motion of Icarus can yield a further test of the precessional formula of general relativity.

THE observational evidence[1,2] for the relativity precession of planetary orbits depends primarily on the rate of advance of the perihelion of Mercury. This note considers the possibility of obtaining a further unequivocal check of the precessional formula from the motion of the asteroid Icarus.

Icarus was discovered by Baade in 1949.[3] It is the minor planet of smallest known mean distance from the sun (its perihelion is within the orbit of Mercury) and is one of the highest in eccentricity. The predicted value of the angular advance v per century of the perihelion of Icarus is listed in Table I. For comparison purposes, the corresponding quantities for Mercury, Venus, the earth, and Mars[2] are likewise tabulated. The quantity α of the third column of Table I is a weighted figure of merit of the possible precision in measurement of the corresponding perihelion motion. For the major planets, the parameter α is essentially *kev* as used by Clemence;[2] for an asteroid, the definition of the over-all figure of merit requires modifications which will be explained in a fuller account of this work (to be published elsewhere).

TABLE I. Predicted relativity precessions.

Asteroid or planet	Advance per century, v	Observational figure of merit, α
Icarus	10.05″	>4.4″
Mercury	43.03	3.01
Venus	8.63	0.03
Earth	3.84	0.06
Mars	1.35	0.38

For Icarus, Table I indicates that the predicted relativity precession per century is about a quarter that of Mercury. However, the advance per century of Icarus exceeds that of any major planet excluding Mercury. The observational figure of merit α for Icarus[4] exceeds that of Mercury, and it exceeds by a factor of at least ten that of any major planet excluding Mercury. One notes from the table that only for Icarus and Mercury are the advance v and figure of merit α both relatively high. Thus, these figures indicate clearly that the motion of Icarus can yield a definite observational check of the precessional formula of general relativity, in the course of time, although decades of astronomical observation may be necessary to measure the perihelion advance with sufficient precision. The relativity precessions of other favorable asteroids amount to only one or two seconds of arc per century.

The author acknowledges helpful discussions of this problem with Professor Samuel Herrick of the University of California, Los Angeles (who computed the orbit elements of Icarus employed).

[1] G. M. Clemence, Revs. Modern Phys. **19**, 361 (1947).
[2] G. M. Clemence, Proc. Am. Phil. Soc. **93**, 532 (1949).
[3] R. S. Richardson, Publ. Astron. Soc. Pacific **61**, 162 (1949).

[4] *Note added in proof:*—Further study indicates that, for Icarus, $\alpha \gtrsim 14$″ (this revision is more favorable to the argument of the text).

Atomic Number Dependence of Neutral Meson Yield from Proton Bombardment*†

R. W. HALES‡ AND B. J. MOYER
Radiation Laboratory, Department of Physics, University of California, Berkeley, California
(Received November 17, 1952)

The relative yield of neutral mesons from various elements in the reaction (p, π^0) has been determined. Single photons from neutral meson decay were observed at 135° to the proton beam in the laboratory system. Detection was by means of a pair scattering detector composed of a converter and two anthracene crystal telescopes in juxtaposition.

The yield in the range of elements from hydrogen to sodium is essentially proportional to the number of neutrons; in the elements aluminum to lead it is proportional to $(N/A)A^{\frac{1}{3}}$.

I. INTRODUCTION

IN a letter[1] work was presented which had been done on the yield of neutral mesons from the light elements. Since that report, additional data have been obtained on many of these elements, and several more elements have been studied, to give yields throughout the periodic series. The purpose of this paper is to present the atomic number dependence of the neutral meson yield.

The photoproduction of mesons[2–4] indicates that the yield *versus* A for charged and neutral mesons, for all energies studied thus far (>42 Mev), is proportional to $A^{\frac{1}{3}}$, i.e., proportional to the nuclear surface. This is taken to indicate that these mesons are rather strongly reabsorbed by the nucleus in which they are produced.

Neutral pions produced from protons are presumed to be the same as those produced by photons and by proton capture of negative pions. Due to experimental difficulties coincident decay gamma-rays have not been observed from proton-produced π^0's; however, the photon energy spectrum from these π^0's shows quite definitely that they are the same as those produced by the other reactions. It was of interest to see how the yield of π^0's from various targets compared with other work done as given above. Specifically, the question arose as to how absorption effects in the nucleus, if any, manifest themselves in terms of cross sections.

The work done on the light nuclei[1] indicated a yield from only the neutrons in the nucleus. The reason for this can be seen by considering the reaction

$$P+p\rightarrow P+p+\pi^0,$$

where the π^0 is assumed to be a pseudoscalar meson. Evidence to date indicates that mesons from nucleon-nucleon collisions are created into P states. The available energies are such that the resulting nucleons should be left in S states. There is no initial state for the two protons, in this case, which will allow this final combination of meson and proton angular momenta. It is possible for the meson to come off in an S state, but this requires either the incoming protons or the resulting protons to be in a triplet P state. Whitehead and Richman[5] set an upper limit of 9 percent for the ratio of meson yield in the S state to that in the P state in the reaction

$$p+p\rightarrow\pi^+ +d.$$

If this same ratio is applicable to the π^0 production reactions, one would assume the π^0 yield from protons in the nucleus to be down by a factor of approximately ten compared with the yield from neutrons where production of the mesons in the P state *is* allowed. Such a favoring of production from neutrons was seen to hold true in the nuclei Be^9, B^{10}, B^{11}, and C^{12}. The yield from hydrogen is further reduced because it is a free nucleon and has no internal nuclear momentum to add to the momentum of the bombarding proton to raise the available energy.

It was hoped that further work might show whether or not this effect continues in the heavier elements. Because the production process is so energy dependent, there were indications that the effect of the internal momenta of the nucleons—especially in the lightest nuclei—might manifest itself in the comparison of cross sections.

II. PROCEDURES AND QUALIFICATIONS

Targets were bombarded in the external proton beam of the 184-inch synchrocyclotron by protons of approximately 340 Mev (Fig. 1) whose current was measured by an ionization chamber. A lead wall fourteen inches thick with a three-inch diameter hole served to attenuate neutrons and other particles coming from reactions in the cyclotron itself and in the collimating system, and targets were placed approximately eight inches downstream from this lead wall.

At an angle of 135° from the beam direction a photon counter viewed the target. The counter consisted of four anthracene crystal—1P11 photomultiplier tube units (Fig. 2). The outputs of pairs of the phototubes were

* Based on a dissertation submitted by one of the authors (RWH) to the University of California in partial fulfillment of the requirements for the degree of Doctor of Philosophy.

† This work was performed under the auspices of the U. S. Atomic Energy Commission.

‡ Now at Brigham Young University, Provo, Utah.

[1] Hales, Hildebrand, Knable, and Moyer, Phys. Rev. **85**, 373 (1952).

[2] R. F. Moxley, Phys. Rev. **80**, 493 (1950).

[3] R. M. Littauer and D. Walker, Phys. Rev. **82**, 746 (1951).

[4] Panofsky, Steinberger, and Steller, Phys. Rev. **86**, 180 (1952).

[5] M. N. Whitehead and C. Richman, Phys. Rev. **83**, 855 (1951).

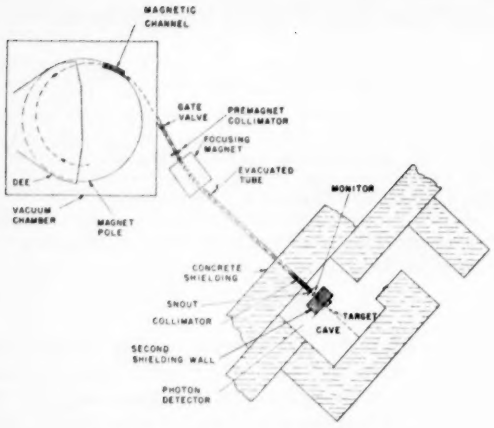

FIG. 1. General layout of the experiment.

mixed in fast double coincidence in the cave; and the coincidence pulses from each pair were mixed in slower double coincidence in the counting area after amplification and pulse shaping. Thus, time coincident pulses from each of the four units in a counter were required to register an event; namely, the detection of a single photon, through conversion and the separation of its pair electrons by scattering in the converter.

The counter was placed at the single angle of 135° for all the different target elements. Thus, the validity of the comparison depends on the angular distribution of photons from neutral meson decay being independent of the target used.

For targets other than hydrogen this is surely a good assumption, as may be easily inferred from a few calculations involving the following facts. The decay photons are emitted isotopically in the rest frame of a neutral pion, so that photon observation at any angle includes contributions from pions moving in all directions (though of course with efficiencies which depend upon direction). Any precise detail in the pion angular distribution in the center-of-mass frame of a proton-nucleon collision is considerably smeared by the nucleon momentum distributions in target nuclei. Consequently, the photon angular distribution is a very insensitive function of the target nucleus for complex nuclei.

This conclusion is sustained by the work of Crowe, Panofsky, Phillips, and Walker[6] who have shown that the energy spectrum of the π^0 decay photons is the same from wolfram and from carbon targets. Nuclear differences which would affect the laboratory angular distribution of the photons should also affect their energy spectrum as observed at a given laboratory angle.

The problem of comparing the yield from hydrogen with that from complex nuclei requires further consideration. If, in the production from hydrogen, it be assumed that the two residual protons interact with sufficient strength so as to recoil from the π^0 emission essentially as a di-proton, the two-body character of the problem then prescribes a unique pion energy in the c.m. reference frame. In this case there is a definite and calculable relationship between the pion angular distribution and the photon angular distribution.

A calculation of the relative photon yields at 135° in the laboratory system for two different pion angular distributions in the c.m. frame, namely, spherical symmetry and $\cos^2\theta$, showed that the latter gave a yield per steradian about 15 percent larger than the former at this laboratory angle. Since these distributions should represent the extremes in any disparity which may exist between the angular distributions arising from hydrogen and from complex nuclei, the 15 percent probably represents the maximum error which could arise from this source. Statistical errors in the H measurement are at present much larger than this. There remains, of course, the need to make some correction for the effects of nuclear momentum in comparing H with complex nuclei; but since this involves knowledge of the energy dependence of the H yield, no such correction has been attempted in the present data.

A corroboratory run on certain relative π^0 yields was performed using the pair spectrometer arrangement of Crandall and Moyer.[7] This was a check by another system of detection at another angle, thus subjecting the assumptions of the results being independent of the angle of observation to a limited experimental check. The arrangement of the components in the Crandall-Moyer experiment is shown in Fig. 3. A target was bombarded at the rear of the cave. Photons emitted at 90° passed through a collimated hole in the cave wall, through a second collimation placed in a magnetic field, and then to the pair spectrometer magnet. A 41.4-mil tantalum radiator was used to convert the photons into electron pairs, which in turn were detected after magnetic bending by double chamber proportional tubes filled with CO_2 and argon.

The pair spectrometer was placed at the intersection of the high energy neutron beam line (this line is tangent to the 81-inch radius) and the line making a 90° angle at the cave target. By having the pair spectrometer look at an internal target at the 81-inch radius,

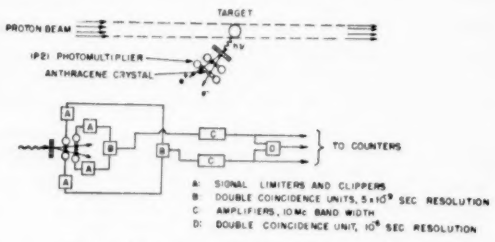

FIG. 2. Apparatus and circuit for detection of high energy photons.

[6] Crowe, Panofsky, Phillips, and Walker, Phys. Rev. **83**, 893 (1951).

[7] Part of a π^0 spectrum study to be published by W. E. Crandall and B. J. Moyer.

proportional counter plateaus could be determined with high counting rates. The pair spectrometer was then turned to look at the cave target. Comparison of yields from C, Al, and Pb by this method were in satisfactory agreement with those observed by the technique of the present article, though estimated evaluation of target conversion of photons makes the Pb yield somewhat in doubt for this method.

III. DETAILS OF THE EXPERIMENT

A. Targets

In designing targets for this experiment, it was necessary to consider the loss of energy of the incoming protons in passing through the target matter, conversion of the neutral meson decay gamma-rays into electron pairs in the target, production of background particles, and the limitation imposed by available sizes and shapes of some elements in their pure form. The targets were not specifically designed to keep a single factor constant. Instead the targets in a given comparison group were made with approximately the same g/cm² thickness. This meant that in the same region of the periodic table the energy degradation would be nearly the same and the background events would be similar. The thickest targets were five g/cm² thick. This corresponds to a maximum energy degradation (for lithium) of 14 Mev. Thicknesses of this order of magnitude and less, combined with small lateral extent, kept corrections for pair conversion in the target to ten percent or less except for carbon tetrachloride and calcium.

The diversity of physical states and geometrical shapes available necessitated the use of the following six series of targets. Yields were compared to carbon as a reference.

Series 1. H_2O, D_2O, C, O_2

The use of liquid oxygen necessitated use of a Dewar vessel. This was constructed of aluminum with a four-mil inner wall, 14-mil outer wall, and two inch diameter liquid chamber. The liquids were all bombarded in this container; the carbon was machined in the shape of a cylinder of comparable size and shape.

Series 2. H_2O, D_2O, C, (*Graphite*), CH_2 (*Polyethylene*), *and* CCl_4

These materials were contained in brass cylinders $3\frac{1}{2}$ inches outside diamer, $3\frac{1}{4}$ inches inside diameter (considerably larger than the beam diameter) with axes parallel to the beam. Aluminum foil of 0.003-inch thickness, cemented over the faces of the cylinder with araldite, closed the beam entrance and exit faces. Because of the different thermal coefficients of expansion of the brass cylinder and aluminum foils, the foils were stretched taut during the process of baking the araldite and subsequent cooling.

The H yield was obtained by CH_2, C subtraction; the D yield by D_2O, H_2O subtraction (where the H_2 yield was a small correction); the Cl yield by CCl_4, C subtraction; and the O yield was taken to be equal to that of H_2O because of the small hydrogen cross section. It is alternatively obtained from the liquid oxygen target of series (1).

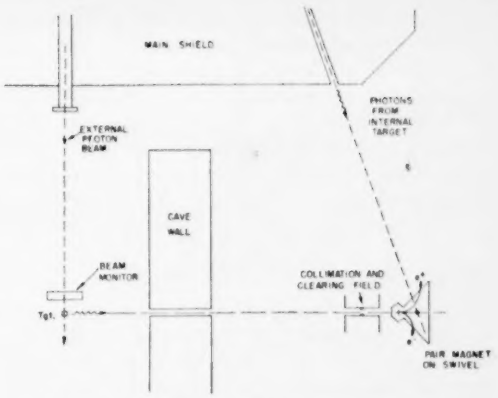

FIG. 3. Arrangement for pair spectrometer run.

Series 3. C, Ca

Calcium was available in elemental form large enough to permit a target 0.928 inch diameter $\times 1\frac{3}{16}$ inches and of a mass 20.44 g to be machined. A graphite target of similar dimensions and mass 21.42 g was also made.

Series 4. Li, Be, B^{10}, B (*natural*), C, Na, K

The lithium target was machined under a light mineral oil and stored in the oil to prevent oxidation. The beryllium target was prepared by the Radiation Laboratory machine shop in a specially ventilated room. The two boron isotopes were each available as one inch diameter $\times\frac{1}{4}$ inch compressed powder cylinders of less than one percent oxygen impurity. There were four disks of each isotope making a one-inch thickness for the targets. Carbon was obtained in one-inch diameter stock.

Sodium and potassium could not be machined because of their softness and great chemical activity. Instead, they were melted and cast (in a light mineral oil bath) in thin walled glass centrifuge tubes of the proper diameter. The tubes were then broken and removed to give the pure metal targets.

Series 5. C, Al, Cu, Pb

These four of the "usual" elements were designed with pair conversion in the target being the major consideration. The mean free paths for pair conversion of 100-Mev photons in these elements are 22, 6.7, 1.02, and 0.342 inches, respectively (as calculated from curves given by Heitler[8]). It was experimentally determined that the photon yield from lead was roughly propor-

[8] W. Heitler, *Quantum Theory of Radiation* (Oxford University Press, London, 1944).

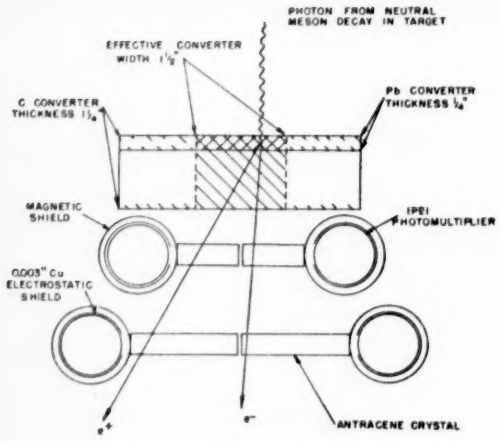

FIG. 4. Photon counter detail.

tional to the target thickness for thicknesses up to $\frac{1}{4}\lambda$. The lead target was chosen to be $\frac{1}{10}\lambda$ thick to be well within the region of calculable correction. The other targets were then chosen to have approximately the same number of g/cm².

Series 6. D_2, He_2

These gases were bombarded in a stainless steel pressure chamber designed by White.[9] The strength of the stainless steel target at 77°K allowed pressures of 2200 psi to be maintained. The densities of deuterium and helium under these conditions are, 0.0883[10] and 0.0745,[11] respectively.

Series 7. C, Al, Pb

This series of targets was viewed by a pair spectrometer (Fig. 3) rather than the crystals. Because of the small solid angle subtended by the tantalum converter in the pair spectrometer, as seen from the target, and because of the large proton beam size ($3\frac{1}{2}$ inches diameter), it was necessary to have relatively large targets in order to obtain a reasonable counting rate. These targets were large both in terms of energy degradation of the proton beam and pair production in the target by the neutral meson gamma-rays. The targets were designed to have the same total energy loss for protons. In a comparison, then, of relative cross sections the different targets would each see the same proton energy spectrum. This eliminated the need for a correction owing to the dependence of the meson production cross section on proton energy. A large correction was required for the pair conversion in the target.

[9] R. S. White, University of California Radiation Laboratory Report, UCRL-1319 (unpublished).
[10] Johnson, Bezman, Rubin, Swanson, Corak, and Rifkin, Atomic Energy Commission Report, MDDC-850, unpublished.
[11] S. W. Akin, Trans. Am. Soc. Mech. Engrs. **72**, 751 (1950).

B. Counters

The general counter scheme used has been reported previously,[12] but for completeness will be briefly described.

Each photon detector consists of a $\frac{1}{4}$-inch thick lead converter followed by four anthracene crystals, each viewed by a 1P21 photomultiplier tube (Fig. 4). These were arranged in two adjacent telescopes with the crystals side by side. The crystals were $\frac{3}{8}$ inch in thickness, the front crystals being one inch by two inches in area, the rear ones $1\frac{3}{4}\times 2\frac{1}{2}$ inches. These crystal sizes were chosen to reduce background without decreasing photon detection efficiency. The effective width of the converter was approximately $1\frac{1}{2}$ inches. The coincidence counts from this strip were limited in solid angle by the size of the rear crystals. By choosing the front crystals to subtend approximately the same solid angle as the rear ones it was possible to cut down their volume and consequently the number of counts due to background and spurious particles coming from the target.

The thickness of these crystals is such that an electron of three Mev will just get through the first crystal. Assuming the pair is produced in the rear layer of the converter, is not scattered in the first crystal, and counts upon just reaching the second, it would require a six-Mev photon to produce a coincidence in the telescope. But at this absolute threshold the efficiency is zero, and for several Mev above it the efficiency slowly increases as greater converter thicknesses and a broader spread in the energy partition between the pair particles become available. The data in reference 12, and the comparisons mentioned there of this counter with the pair spectrometer indicate that its efficiency is quite uniform from 60 Mev upward in photon energy. All experience, as well as rough calculations, indicate that counter response in the region of nuclear gamma-radiation is negligible. Either lead or carbon sheets, or "converters," of $\frac{1}{4}$ and $1\frac{1}{4}$ inches respective thickness were placed between the target and counters, with the target side of the converter being two inches from the front crystals. These converters served two purposes: firstly, they caused the high energy photons to form electron pairs which were then typically separated by scattering; and secondly, they attenuated the flux of of charged particles coming from the target. The thicknesses were chosen for equal stopping power for charged particles. The number of pairs from lead as compared to carbon for these thicknesses should, except for electron losses due to radiative collisions in the lead, be ten to one. Thus, by subtracting the number of counts with a carbon converter from the number with lead converter, the background is essentially subtracted out and one has a relative measure of pairs produced and, consequently, an indication of the relative number of photons coming from the target. The transition curve for lead showed a peak at approximately $\frac{1}{4}$ inch which

[12] Hildebrand, Knable, and Leith, Rev. Sci. Instr. **23**, 243 (1952).

is to be expected of photons of the order of 100 Mev, whereas a corresponding curve for carbon showed a drop from zero converter thickness to 1¼ inches, then a gradual rise, which is compatible with the stoppage of charged particles and small pair cross section in carbon.

C. Electronics

Pulses from the 1P21 phototube were clipped and shaped in a tube base unit of electronic design due principally to Madey. Clipping to 5×10^{-9} second was done with 1½ inches of RG 65/U shorted delay line cable. The pulses were limited in pulse height by cutting off a 6AH6 pentode.

Fast coincidences were made, as shown in Fig. 2, in crystal diode bridge coincidence units with time resolution of 5×10^{-9} second. By careful balancing of circuit elements it was consistently possible to obtain coincident (two inputs) to feed through (single input) pulse-height ratios of 16 to 1.

Total linear amplification was such that pulses up to 80 volts were delivered from each fast coincidence unit to gate shaping circuits. These two gates (0.5×10^{-6} second width) were then joined in a Rossi type coincidence circuit. A coincidence count from this unit signified the detection of a photon.

The pulses passed by the bridge coincidence units were a mixture of coincidences from electron pairs formed by a single photon and accidental coincidences formed by all counts in the phototubes. These counts are caused not only by the charged particles going through the crystals (electrons, mesons, and protons), but also by contributions from the noise inherent in the tube under the conditions of operation. The electrons are of minimum ionization energy so their pulse heights do not extend as high as those of protons and mesons, but do extend down into the noise region. As a consequence, there were no set of operating conditions under which all counts that would give rise to accidentals could be discriminated against. Instead, the beam intensity had to be set at such a level that the counting rate of extraneous counts was low enough that accidentals were a small fraction of the coincidence counts from electron pairs. Thus, there was no plateau region of operation, and trustworthiness of results depended upon satisfactory stability of the conditions.

Operational conditions were picked by setting the photomultiplier voltage at 1.4 to 1.5 kilovolts and the linear amplifier gains at such a level (amplification of 300–400 times) that five-volt maximum output pulses were given by the linear amplifier for feed-through pulses (single input to the bridge coincidence). The discrimination levels of the gating units were then set at 10 volts, or double this value.

With this operational adjustment it was next necessary to choose a beam intensity such that the accidental coincidences were a small fraction of the total. The accidental coincidence count per unit charge in the proton beam is linear with the beam intensity (or of higher order if the accidental coincidence is between more than two particles), whereas the electron pair counts are constant per unit beam charge. Thus, by lowering the beam intensity to a suitable value the ratio of accidentals to nonaccidentals could be reduced to an arbitrarily small value. In these experiments beam currents of $0.8\text{–}3.2\times10^{-11}$ ampere were used, depending on the target thickness.

IV. RESULTS

The relative cross sections and relative cross sections per neutron in the nucleus are tabulated in Table I. The comparisons, in each case, are made to carbon which in one column has an arbitrary value of 6.00 assigned for the cross section (this is to allow comparison with neutron number), and in the next column a value of 1.00. The relative values of σ/N are normalized to 1.00 for carbon. The best value for the absolute carbon cross section is given by Crandall and Moyer[7] at 1.7±0.4 mb.

The relative cross sections for elements up to aluminum are plotted in Fig. 5. It can be seen from this that the yield continues to be nearly proportional to the number of neutrons up to aluminum. For the heavier elements this ceases to hold true as shown in Fig. 6. In this case comparison is made to the number of neutrons on the nuclear surface, which is proportional to $(N/A)A^{\frac{1}{3}}$. This seems to be a good fit to the data; however, an $A^{\frac{1}{3}}$ dependence from sodium or aluminum through lead cannot be excluded by the statistics of the data.

These features of the π^0 yield, namely, 1. production from neutrons, 2. production from all neutrons at low

TABLE I. Neutral meson yields relative to the yield from carbon.

Elem	A	N	Relative σ (C = 6.00)	Relative σ (C = 1.00)	Relative σ/N (C = 1.00)
H	1	0	0.072±0.060	0.012±0.010	——
H^2	2	1	0.856±0.020	0.143±0.034	0.856±0.020
He	4	2	2.22 ±0.25	0.369±0.041	1.106±0.123
Li	6.92	3.92	3.42 ±0.13	0.569±0.021	0.871±0.032
Be	9	5	4.98 ±0.13	0.830±0.022	0.996±0.027
B^{10}	10	5	4.86 ±0.13	0.810±0.022	0.973±0.027
B^{11}	11	6	5.93±0.19	0.988±0.032	0.988±0.032
C	12	6	6.000	1.000	1.000
O	16	8	7.51 ±0.31	1.252±0.051	0.940±0.038
Na	23	12	11.96 ±0.40	1.991±0.067	0.996±0.047
Al	27	14	12.78 ±0.70	2.13 ±0.12	0.914±0.050
Cl	35.5	18.5	13.72 ±0.62	2.29 ±0.10	0.782±0.044
K	39	20	16.61 ±0.60	2.77 ±0.10	0.830±0.042
Ca	40	20	15.79 ±0.96	2.63 ±0.16	0.788±0.046
Cu	63.5	34.5	25.1 ±1.9	4.18 ±0.32	0.727±0.057
Pb	207.2	125.2	58.7 ±3.2	9.79 ±0.53	0.469±0.026
Pair spectrometer					
C	12	6	6.000	1.000	1.000
Al	27	14	13.32 ±1.02	2.22 ±0.17	0.952±0.072
Pb	207.2	125.2	48.2 ±3.8	8.04 ±0.62	0.384±0.029

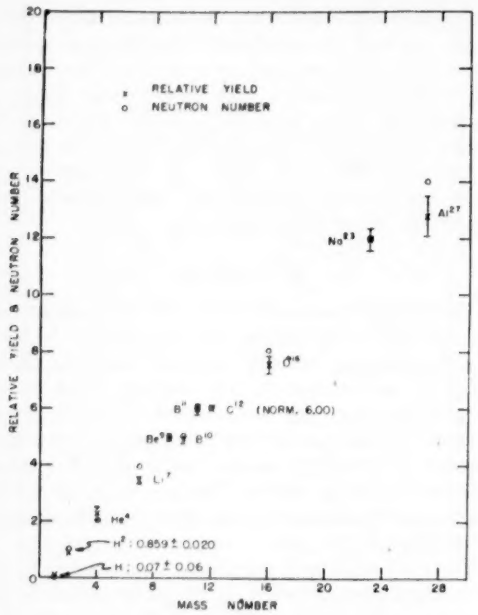

FIG. 5. Relative yield of high energy photons (π^0's) from 340-Mev proton bombardement of nuclei.

Z and shielding of the interior neutrons at high Z, show up quite clearly in a plot of σ/N as a function of A, as seen in Fig. 7. The surface effect, represented by $A^{-\frac{1}{3}}$, now becomes a straight line on the logarithmic plot.

The possibility of seeing other events due to the low energy threshold of the crystal counters is discounted by a comparison with the data obtained using the pair spectrometer at 90°. These results are also given in Table I. The aluminum results from the two methods overlap, whereas the lead yield from the pair spectrometer is approximately 20 percent lower than from

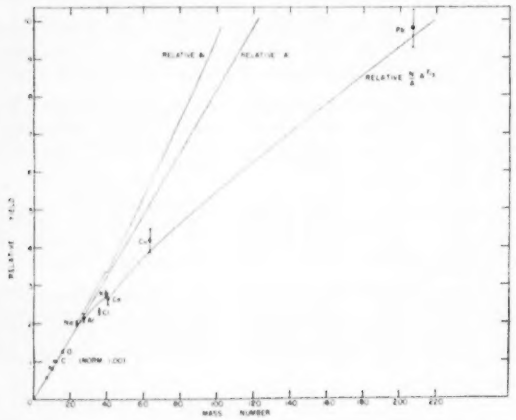

FIG. 6. Relative yield of high energy photons (π^0's) from 340-Mev proton bombardment of nuclei.

crystals. The errors listed are the standard deviations owing to random counts and do not include any estimate of system errors. The grossness of the corrections made in the case of the pair spectrometer targets and the number of different measurements and assumptions that went into the calculations for these corrections do not permit one to say the lead yields from the two methods of measurement are significantly different.

V. CONCLUSIONS

As discussed in our letter,[1] the yield from hydrogen is suppressed. This is in keeping with the assumption that the neutral pion is a pseudoscaler meson created into a P state in nucleon-nucleon collisions. The yield from hydrogen has recently been independently confirmed with 340-Mev protons by Mather[13] who employed a Čerenkov counter detection system and a 90°

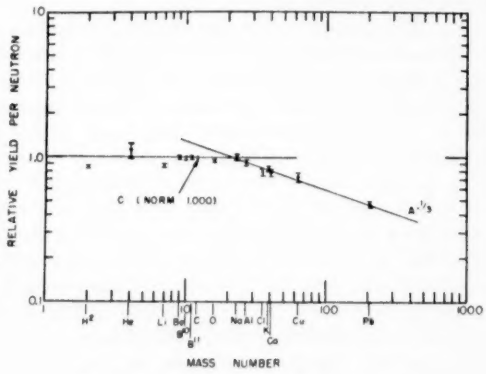

FIG. 7. Relative photon yield per neutron.

angle of view. With 450-Mev protons Marshall *et al.*[14] have measured the hydrogen yield and the beryllium yield of π^0's, and find at this energy a yield ratio H/Be five or six times that at 340 Mev. This is understandable in terms of the selection rule argument which depresses the H yield at low energies.

The suppression of the yield in the high Z region can be accounted for, within the limits of the experimental errors involved, by the fact that for larger nuclei the mean free path for the incoming protons in nuclear matter is smaller than nuclear diameters, so that a portion of the nucleons will be shielded from the high-energy protons. The proportion of shielded nucleons increases with atomic number.

Recent work by Kirschbaum[15] on the inelastic collision cross sections presented by nuclei to 340-Mev protons shows a similar shielding effect.

A constant yield per neutron in the lighter elements,

[13] J. W. Mather, private communication.
[14] Marshall, Marshall, Nedzel, and Warshaw, Phys. Rev. **87**, 220 (1952).
[15] A. J. Kirschbaum, private communication.

coupled with a behavior following the proton absorption in the heavier elements, seems to give no reason to believe that meson re-absorption within the nucleus is playing any strong role in affecting the yields. This is apparently different from the neutral photomeson production as observed by Panofsky *et al.*,[4] in which there is apparently evidence for strong reabsorption, beginning even among the light elements. However, it is to be noted that the meson energy distribution created by the bremsstrahlung spectrum of the 340-Mev synchrotron lies generally at higher energies than that produced by the 340-Mev proton beam; and in the experiments of reference 4 the correlation angle between π^0 decay photons was such as to detect only π^0-mesons of energies over 70 Mev. If nucleon interaction with the mesons were strongly energy dependent, increasing with meson energy, the possible difference in the yield characteristics between proton-produced and photoproduced π^0's in these two experiments may be explicable upon this basis alone.

Essentially nothing can yet be said of the possible effects of internal momentum or shell structure. Among the light elements, deuterium and lithium yields are low and helium has a yield per neutron which is comparable to carbon, but the helium point is not as accurately fixed as the others because of the small amount of helium which could be put in the proton beam.

We wish to express our thanks to Dr. R. H. Hildebrand and Dr. N. Knable for their participation in the early part of the experiment. Thanks are due Dr. R. S. White for the use of his high pressure gas target and to Mr. R. A. Byrns of the engineering group for the construction and assembling of the gas pumping system. To the cyclotron crew under Mr. James Vale and Mr. Lloyd Houser go our thanks for cooperation on the bombardments.

PHYSICAL REVIEW VOLUME 89, NUMBER 5 MARCH 1, 1953

Rotational Intensity Distributions of OH and OD in an Electrodeless Discharge through Water Vapor*

H. P. Broida and W. R. Kane
National Bureau of Standards, Washington, D. C.
(Received October 3, 1952)

The distributions of intensities of the rotational lines of the $^2\Sigma^+ - {}^2\Pi$ transition of OH and OD in a high frequency electrodeless discharge through water vapor have been measured. Effects of water vapor pressures from 0.025 to 3.2 mm Hg and added argon, helium, nitrogen, and oxygen to 10 mm Hg have been studied. Two intensity maxima are found at the same energies in both OH and OD, corresponding to total energies in the excited state of 32 950 and 37 400 cm^{-1}. The position of the higher energy maximum is unaffected by pressure or added gas. This is interpreted as indicating that a lower limit of 150 collisions may be set for the collision lifetime for the transfer of rotational energy of the hydroxyl radical. The intensity of the lower energy maximum, which is probably of thermal origin, increases relative to the higher energy maxima with increasing water pressure and with added gas. Argon has the effect of increasing the intensity of the (0, 0) band by more than a factor of ten.

A predissociation phenomenon previously found in OH is also observed in OD.

1. INTRODUCTION

THE ultraviolet emission bands of $OH(^2\Sigma^+ \rightarrow {}^2\Pi)$ exhibit abnormal rotation when excited in an electric discharge through water vapor. Normally, in molecular bands excited by thermal processes, or bands in which the rotational levels of the initial state remain in thermal equilibrium, the populations of rotational states correspond to a Maxwell-Boltzmann distribution of rotational energies in the initial vibrational state at the temperature of the gas. A plot of intensities as a function of the rotational quantum number will rise to a maximum and then decrease to zero with increasing rotational energy. In contrast, the bands of OH in an electric discharge through water vapor are characterized by the appearance of intense lines at high rotational quantum numbers and, over a wide range of conditions, of a second maximum in the intensity distribution in addition to the thermal maximum at low rotational energies.

The excitation mechanism for these bands was proposed by Bonhoeffer and Pearson[1] to be the simultaneous dissociation of H_2O and excitation of OH by electron impact:

$$H_2O + e \rightarrow H + OH(^2\Sigma^+) + e,$$
$$OH(^2\Sigma^+) \rightarrow OH(^2\Pi) + h\nu.$$

A second excitation mechanism, the production of excited OH by the recombination of atomic oxygen and hydrogen, is indicated by an experiment of Lavin and Stewart[2] in which the bands of OH were observed as

* Supported in part by the U. S. Office of Naval Research.

[1] K. F. Bonhoeffer and T. G. Pearson, Z. physik. chem. **14**, 1 (1931).
[2] G. I. Lavin and F. B. Stewart, Proc. Natl. Acad. Sci. **15**, 829 (1929).

an afterglow downstream from a discharge through water vapor. This was substantiated by other experiments performed by Bonhoeffer and Pearson.[1]

Oldenberg[3] proposed that the observed abnormal rotation of OH might have as its origin the production of excited OH in the dissociation of H_2O. Since the H_2O molecule is nonlinear, with a bond angle of 105°, in the dissociation process the recoiling hydrogen atom might be expected to impart angular momentum to the excited OH radical, leaving it with a high rotational energy. Experimentally he observed that the addition of 20 cm Hg of helium to the discharge caused a disappearance of the high rotational levels, and attributed this to the effectiveness of the light helium atom in removing momentum from the excited OH radical in collisions during the radiative life time of the latter.

The absorption spectrum of OH was obtained by Oldenberg[4] in an electric discharge through water vapor and by Oldenberg and Rieke[5] in a furnace filled with water vapor and oxygen. The rotational distribution in the ground state of the radical was found to be normal. Frost and Oldenberg[6] studied the kinetics of OH produced in a discharge through H_2O_2. Here the rotational distribution of excited OH extended to higher rotational energy levels than in discharges through H_2O.

Lyman[7] conducted detailed photometric studies of the spectrum of OH excited under various conditions by measuring the "rotational temperature" as given by lines in the excited state with rotational energies less than 3000 cm^{-1}. This "temperature" was found to increase with the partial pressure of H_2O present. No attempt was made to use lines in the region of the second maximum. Contrary to the results of Oldenberg, little difference was found among the rotational distributions produced in discharges through pure water vapor and in mixtures of helium and argon with water vapor. Attempts to reproduce the results of Oldenberg, in which as much as 50 cm Hg of helium were introduced into the discharge, produced no appreciable difference in the rotational "temperature," except at very low current densities where a weakening of higher levels was observed. In no case was the distribution of rotational levels thermal, but rather, there always existed an excess of radicals in the higher rotational levels.

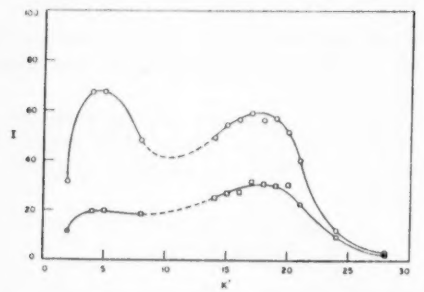

FIG. 1. Intensity distributions of the R_2 branch in the (0, 0) band ($^2\Sigma^+ \rightarrow {}^2\Pi$) of OH in an electrodeless discharge through water vapor.

This apparent difference in the results of Oldenberg and Lyman is probably caused by the difference in the methods of observing the abnormality. The work reported in this paper shows that the addition of rare gases to the water vapor discharge radically changes the appearance of the bands, with the intensity of the lines from the lower rotational levels much increased compared to lines from higher levels. However, the intensities of lines from higher levels still remain relatively greater than in a thermal distribution.

Hayakawa[8] has investigated the dependence of the intensities of the bands of OH and of the Balmer lines of hydrogen upon electron energy in a triode at low pressures. The OH intensity rises rapidly to a maximum at approximately 20 ev, then decreases, while the Balmer lines reach a broad maximum at 100 ev. Appearance potentials for the excited states are approximately 17 and 25 ev, respectively. These results are in good agreement with transition probabilities calculated by Niira[9,10] for the excitation of OH by the dissociation of H_2O in an excited electronic state. Niira has also predicted on theoretical grounds the dissociation of H_2O in such a manner as to impart high angular momentum to the OH radical.

Recently, abnormal rotational distributions have been found in OH emission spectra obtained in hydrocarbon flames at atmospheric pressure diluted with inert gases.[11,12] These results are significant in that for abnormal rotation to appear at atmospheric pressure the excited OH radical with a radiative lifetime of 3.8×10^{-6} sec,[5] must suffer of the order of 10^4 collisions without reaching thermal equilibrium among its rotational degrees of freedom. Such a conclusion is difficult to reconcile with theoretical considerations which indicate that molecular rotation will be easily deactivated by collision.[13]

The present studies consist of detailed observations of rotational and vibrational intensity distributions of OH and OD and of the Balmer lines of atomic hydrogen and deuterium in an electrodeless discharge through water vapor. The purpose was to obtain quantitative data on populations in various rotational and vibrational states which would aid in interpreting the excitation mechanism, to examine in detail the effects of added foreign gases where disagreement exists between

[3] O. Oldenberg, Phys. Rev. **46**, 210 (1934).
[4] O. Oldenberg, J. Chem. Phys. **3**, 267 (1935).
[5] O. Oldenberg and F. F. Rieke, J. Chem. Phys. **6**, 439 (1938).
[6] A. A. Frost and O. Oldenberg, J. Chem. Phys. **4**, 781 (1936).
[7] E. R. Lyman, Phys. Rev. **53**, 379 (1938).
[8] G. Hayakawa, Proc. Phys.-Math. Soc. Japan **26**, 78 (1944).
[9] K. Niira, J. Phys. Soc. Japan **4**, 230 (1949).
[10] K. Niira, J. Phys. Soc. Japan **7**, 193 (1952).
[11] H. P. Broida, J. Chem. Phys. **19**, 1383 (1951).
[12] W. R. Kane and H. P. Broida (to be published).
[13] R. S. Massey and E. H. Burhop, *Electronic and Ionic Impact Phenomena* (Oxford University Press, London, 1952), p. 456.

the results of Oldenberg and Lyman, and, if possible, to obtain information on the transfer of rotational energy in collisions. The behavior with pressure and in the presence of added foreign gases of the group of excited OH and OD radicals with rotational energies greatly in excess of thermal energies was studied with the latter objective. Rotational energies in the region of the "second peak" are so high, and the separation of rotational levels there so great that in collisions only downward transitions to nearby levels will occur with appreciable probability. Thus, the loss of rotational energy by excited OH in collisions should manifest itself by a shift of the "second peak" to lower levels with increasing pressure. While the excitation mechanism might also be influenced by the pressure so that a shift of rotational energies might occur from either cause, a cancelling of the two effects over the entire range of pressures would be unlikely. Furthermore, since, for the same K, the spacing of rotational levels of OD is approximately half that for OH (seven-tenths for the same energy), a given transition results in the exchange of a smaller amount of energy, and the density of final states is greater so that the cross section for transfer of rotational energy in collisions might be expected to be larger for OD. This would cause OD to exhibit a more pronounced change in its rotational distribution with pressure than OH. Such an effect is observed in the rotational dispersion of ultrasonic frequencies by H_2 and D_2,[14] where the frequency for maximum absorption occurs at 10 Mc/atmos for H_2 and that for D_2 at 20 Mc/atmos, indicating a shorter rotational relaxation time for D_2. However, no shift of the higher energy maximum to lower energy was observed in the present studies.

2. EXPERIMENTAL

The electrical discharge was maintained in a cylindrical, water-cooled, fused silica tube, 0.8-cm inner diameter and 30 cm in length with Pyrex extensions to 50 cm. The discharge was viewed from the side; i.e., through 0.8-cm thickness. The discharge length varied from 5 cm at high pressure to over 40 cm at low pressure. Water vapor flowed continuously from above a liquid sample through a controlled leak, through the discharge, into a cold trap and to a diffusion pump. When mixtures of water vapor and various gases were used, the gases were first allowed to stand over water at atmospheric pressure and at 24.5°C in a constant pressure vessel floating in mercury and then admitted slowly to the flow system. The pressure of the water vapor, therefore, was 0.03 of the total pressure. It also was possible to admit separately water vapor and foreign gases at individually controlled pressures. Commercial tank gases were used throughout.

Both a McLeod gauge and an ionization pressure gauge with a radioactive source were used to measure the pressure. Pressures were measured both before and after the discharge tube. Values at these two points differed considerably, which is to be expected from dissociation in the discharge and the pressure drop through the tube owing to the flow. The pressure before the discharge has been chosen as best representing conditions in the discharge. Spectra were obtained in the range of pressures from 0.025 mm to 3.2 mm Hg in water vapor alone and to 10 mm in mixtures of water and argon.

[14] J. L. Stewart and E. S. Stewart, Phys. Rev. **76**, 464 (1949).

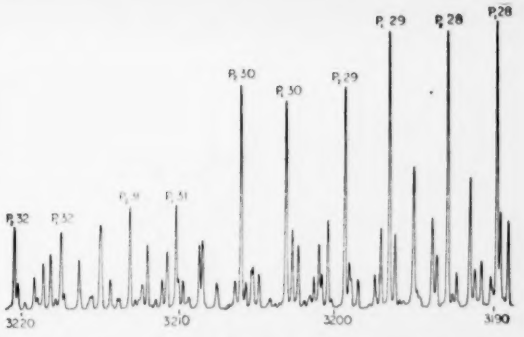

FIG. 2. Spectrum of OD in the region of 3200A showing sharp drop in the intensity of the P lines of the (0, 0) band.

Excitation was provided by a 150-megacycle oscillator, coupled to the tube by a quarter-wave line and semicircular, external electrodes. This high frequency electrodeless discharge in conjunction with the continuous gas flow provided a very stable source.

Spectra were recorded by a high resolution, photoelectric, grating monochromator, with a resolving power, $\lambda/\Delta\lambda$, of 55 000.[15]

3. RESULTS

3.1 Rotational and Vibrational Distributions

Two typical rotational intensity distributions for the (0, 0) band of OH at different pressures of water vapor are presented in Fig. 1 in which the intensity is plotted as a function of the rotational quantum numbers K of the excited state. The prominent features of these distributions are a maximum at low K' numbers such as would appear in an ordinary thermal distribution, a second maximum at high K followed by a sharp drop in intensity, and finally a rather slow "tailing off" in intensity. The positions of the two maxima correspond, for temperature equilibrium, to temperatures of the order of 800°K and 15 000°K. The lower temperature is a reasonable value for this discharge. The sharp drop in intensity is shown by the spectrum in Fig. 2 for the P_1 branch of OD, occurring between $P_1 30(K' = 29)$ and $P_1 31(K' = 30)$. The distributions for OD are similar to those in OH, with corresponding features

[15] This instrument was constructed by the Research Department, Leeds and Northrup Company and loaned to the Heat and Power Division at the National Bureau of Standards on a field trial basis.

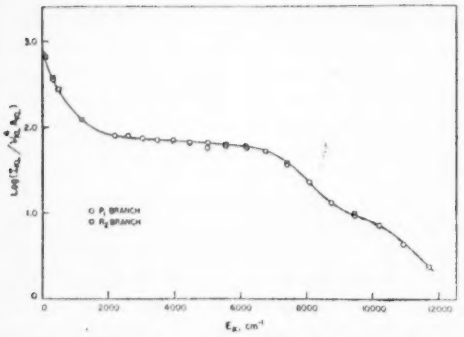

FIG. 3. Logarithmic plot of rotational intensity distributions of OH in a discharge through water vapor at a pressure of 0.4 mm.

occurring at higher values of K but at approximately the same energy of the excited state.

In both OH and OD the position of the second maximum is independent of the pressure or of other experimental conditions. The thermal maximum appears more strongly at higher pressures, however. For OH the ratio of the intensity of the second maximum to that of the first decreases from 1.5 at a pressure of 0.04 mm to 0.35 at 1.7 mm. Ratios for OD are slightly lower at corresponding pressures but follow a similar trend. The position of the lower K maximum increases to slightly higher energy with increasing pressure due to the increase of temperature at the center of the discharge. Likewise, this maximum occurs at lower energy at the edges of the discharge.

There is a choice of two parameters to describe the position of the second peak: the rotational quantum number K, which corresponds closely to a given rotational and total energy, and the total angular momentum quantum number J. Since there are two spin states, J can take the values $K+\frac{1}{2}$ or $K-\frac{1}{2}$. Their difference is so small, however, that a comparison of different branches arising from the two states does not determine whether J or K is the better parameter to use in describing the observed features of the spectra. In view of this, the rotational quantum number K has been chosen.

The abnormal distribution also is indicated by the usual plot of the logarithm of the observed intensity I divided by the transition probability A and the fourth power of the frequency ν *versus* the rotational energy E_K. For a thermal distribution this plot is a straight line, so that lack of equilibrium will be shown by curvature in this plot. Figure 3 shows such a logarithmic plot for the (0, 0) band of OH in a discharge through water vapor at a pressure of 0.4 mm. Experimental points of well-resolved lines of the R_2 and P_1 branches are shown. This curve is characteristic of both OH and OD obtained under most of the discharge conditions. At lower pressures the plateau between 2000 and 6000 cm^{-1} was somewhat flatter and at higher pressures and with added diluents the plateau was less evident. All such plots of the discharge observed showed that there was not a thermal distribution of rotational intensities in the discharge through water vapor. The fact that the measured points of the more intense P_1 lines fall upon the same curve as the R_2 lines shows that there is no falsification of the data by self-absorption.

Distributions in the higher vibrational bands of OH show no second peak. They do, however, show a sudden sharp drop in intensity. In OD there exists a second peak in the (1, 1) band but not in the (2, 2) band. A direct quantitative comparison of populations in the various vibrational levels is impossible because only occasional lines in the higher vibrational bands are well resolved. However, comparison of intensities of corresponding rotational lines of low K gives a ratio of intensities of ten to twenty percent between $v'=1$ and $v'=0$, and one to two percent between $v'=2$ and $v'=0$. For thermal equilibrium, these intensity ratios would correspond to temperatures in excess of 2500°K. These ratios increase with decreasing pressure. Of course, population ratios would be several times smaller than these figures because there are fewer strong rotational lines in the higher vibrational bands.

Discharges through mixtures of H_2O and D_2O show an apparent shift in the position of the second peak of OD from $K'=23\pm1$ in pure D_2O to $K'=25\pm1$ in the mixture. For OH the peak remains at $K'=17$. The presence of blended lines in spectra of the mixtures makes these values somewhat more uncertain than in the pure samples. The shift, however, appears in four different branches in which the lines in the region of interest are fairly well resolved, so that blending seems to be an unlikely cause for this effect. H_2O:D_2O mixtures of 5:1, 1:1, and 1:5 were observed.

The rotational quantum numbers K', rotational energies E_K', and total energies E in cm^{-1} of the molecule corresponding to prominent features of the distributions are presented in Table I. Energy levels for OH were obtained from the data of Dieke and Crosswhite;[16] those for OD were obtained from Ishaq[17] and Sastry.[18]

TABLE I. Prominent features of intensity distributions of OH and OD in the discharges.

Source	Band	Second peak K'	Second peak E_K'	Second peak E	Sharp drop in intensity K'	Sharp drop in intensity E_K'	Sharp drop in intensity E
H_2O	OH(0, 0)	17±1	5001	37 442	23	8755	41 196
	OH(1, 1)	—	—	—	18	5281	40 710
D_2O	OD(0, 0)	23±1	4815	37 343	29	7430	39 958
	OD(1, 1)	17	2616	37 359	26	5848	40 591
	OD(2, 2)	—	—	—	17	2524	39 379
H_2O	OH(0, 0)	17±1	5001	37 442			
D_2O	OD(0, 0)	25±1	5634	38 162			

[16] G. H. Dieke and H. M. Crosswhite, "The ultra-violet bands of OH," Bumblebee Series Report No. 87, unpublished (Bur. Ord., USN) (1948).
[17] M. Ishaq, Proc. Natl. Inst. Sci. India **3**, 389 (1937).
[18] M. G. Sastry, Indian J. Phys. **15**, 455 (1941).

These data show that with the exception of OD in mixtures of H_2O and D_2O prominent features of the spectra occur for the same total energy of the molecule, the position of the second intensity maximum occurring at approximately 37 400 cm^{-1} and the sharp drop in intensity at approximately 40 000 cm^{-1}. The absence of second maxima in the OH(1, 1) and OD(2, 2) bands is seen to be due to the fact that for these higher vibrational bands the lines corresponding to energies of 37 400 cm^{-1} lie in the lower, thermal maxima.

3.2 Relative Concentrations of Emitting Radicals

In addition to the bands of OH and OD, the intensities of the Balmer lines of hydrogen and deuterium were measured. Previous work[19] has indicated that the ratios of the Balmer lines of the two atomic isotopes are very closely proportional to the ratios of the amounts of the isotopes present in the discharge through hydrogen gases. The present studies show similarly that in discharges through water vapor the ratio of atomic intensities is proportional to the concentrations in the water mixture.

The intensities of the lines of OD were found, in pure samples, to be slightly higher at the same pressure than the lines of OH. Since there are more lines of OD in a given wavelength range, owing to the smaller separation of the rotational levels, the total radiation emitted in the bands of OD, and the population of excited radicals, is considerably higher.

At the top of the visible region of the discharge, where presumably water vapor entered into the discharge, the intensities of the OH and OD lines were greatly increased relative to the intensities of the Balmer lines. For example, with a water pressure of 1.4 mm Hg, observations from the center to the top of the discharge showed that the OH line intensities decreased by a factor of 2.5 while the H_β line decreased by a factor of 80. Such an effect was not observed near the bottom of the discharge.

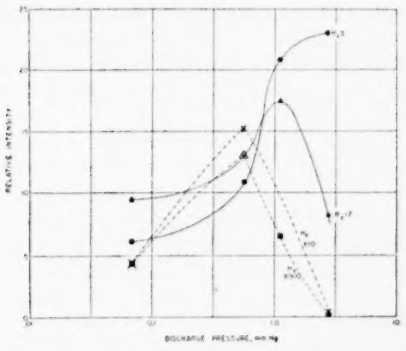

FIG. 4. Pressure dependence of intensities of OH maxima and of the first two lines in the Balmer series of hydrogen.

[19] H. P. Broida and J. W. Moyer, J. Opt. Soc. Am. **42**, 37 (1952).

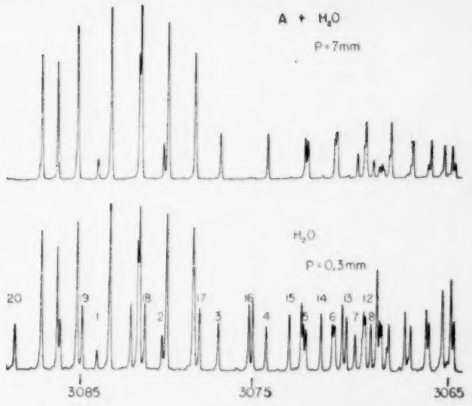

FIG. 5. Effect on the (0, 0) band of OH of the addition of argon to the discharge through water vapor. The R_2 branch is marked.

Intensities were also measured in mixtures in which the ratios of H_2O and D_2O were 5:1, 1:1, and 1:5. In these cases the ratios of intensities of OD lines to corresponding lines of OH were nearly twice the ratios of the abundances of the atomic hydrogen isotopes, for example, in the 1:1 mixture individual lines of OD were nearly twice as intense as those of OH. This effect appeared to be of the same magnitude for both the lines in the low, thermal peak and those in the higher, second peak. There did exist a slight dependence upon position in the discharge. At the top of the discharge, where water vapor entered, this ratio was slightly higher than in the middle or lower regions. This dependence upon position was more pronounced for lines in the second peak than for those in the thermal peak.

The dependence upon pressure of the intensities of the two peaks of OH, and of the first two lines in the Balmer series of hydrogen is shown in Fig. 4. The intensity of the thermal peak is seen to increase with pressure, while that of the second peak attains a maximum and then decreases rapidly.

3.3 The Effects of Diluents

Helium, argon, oxygen, and nitrogen were added to the discharge. These caused a radical change in the rotational intensity distribution. This is illustrated in Fig. 5, in which the R_2 branch of OH is reproduced for discharges in pure H_2O (bottom), and H_2O with added argon (top). The partial pressure of water is approximately the same in the two cases. High-lying rotational lines are seen to be intense in the H_2O spectrum and to be extremely weak or missing in the argon spectrum. Similar effects are seen in Fig. 6, in which spectra are reproduced from H_2O at a low pressure (C), H_2O at a high pressure (B), and H_2O with argon (A). The increased relative intensity of the high K lines relative to lower K lines at low pressures also is evident.

Helium, nitrogen, and oxygen produced distributions similar to argon but with progressively less in-

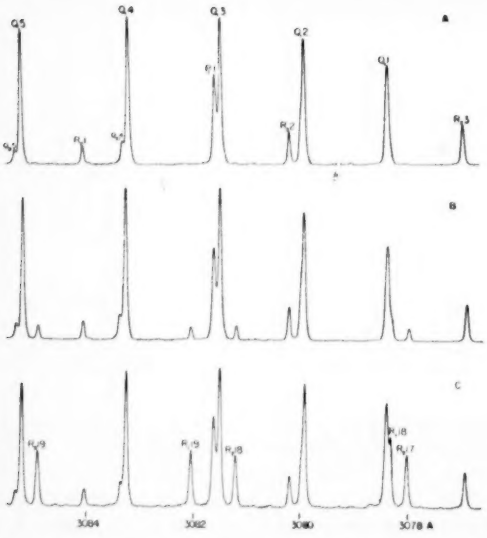

FIG. 6. Effect on relative intensities in the OH spectrum of the change of water pressure in discharge and of the addition of argon. (A) Argon plus water vapor at a total pressure of 8 mm Hg, (B) Water vapor at 1.6 mm, and (C) Water vapor of 0.04 mm.

tensity. With helium and nitrogen there still remained vestiges of the second peak. Logarithmic intensity plots showed in all cases an absence of thermal equilibrium.

While these spectra show a profound change with the addition of gaseous diluents, it is found that this change is due primarily to an enhancement of low-lying lines, rather than to a weakening of higher rotational lines. For example, comparison of a discharge through pure water vapor at a pressure of 1 mm with one through a mixture of 10 mm of argon with a partial pressure of water of 1 mm showed that lines in the thermal maximum were 18 times stronger in the argon mixture than in pure H_2O, while lines in the second maximum were approximately half as strong.

With the added diluents the effect of increased pressure was, as with pure water vapor, to decrease the ratio of high rotational lines to low ones. At a given pressure this ratio depended upon position in the discharge, the low-lying lines being most intense in the center, where the excitation was strongest, while high rotational lines became relatively stronger at the edges of the discharge.

3.4 Predissociation

The effect attributed to a weak predissociation by Gaydon and Wolfhard[20] and observed in flames at low pressures is found in the present studies in both OH and OD. It occurs more strongly in one of the two spin states, the F_1 level ($J=K+\frac{1}{2}$). This effect is characterized by a sudden drop in intensity (see Fig. 2 and Table I) as well as by the relative difference in intensity of the two spin levels. The relative decrease of the spectral emission lines from the F_1 levels as compared to those from the F_2 levels for the P_1 branches of OH and OD is illustrated in Fig. 7. In the (0,0) band of OH the separation sets in at approximately $K'=24$ (41 904 cm^{-1}) and in OD at $K'=33$ (41 946 cm^{-1}). In the (1,1) band of OH it occurs at $K'=17$ (40 177 cm^{-1}) and in OD is not observed out as far as $K'=24$ (41 688 cm^{-1}). The predissociation becomes more pronounced with decreasing pressure.

[20] A. G. Gaydon and H. G. Wolfhard, Proc. Roy. Soc. (London) **A208**, 63 (1951).

4. DISCUSSION

In discharges through pure H_2O and D_2O, the prominent features in the spectra of OH and OD, the second intensity maxima and the sharp drop in intensity, occur at the same total excitation energy in all vibrational levels. In mixtures of H_2O and D_2O, however, a small increase in the rotational energy of the maximum is observed for OD, while the position of the maximum remains unchanged for OH. The molecule HDO is a major constituent of these mixtures. Thus, if the mechanism for the production of excited hydroxyl radicals with high rotational energy is the dissociation of water vapor, the dissociation of HDO should produce excited OD with slightly lower rotational energy than does the dissociation of D_2O. In this mechanism the total energy available for excitation and kinetic energy of the dissociation products should be very nearly the same for all combinations of isotopic species, since the potential surfaces of a molecule are, to a high degree of approximation, independent of the nuclear masses, and the Franck-Condon principle applies to the excitation by electron impact. One cannot predict, however, from the observed rotational energies in H_2O and D_2O, those to be obtained from HDO, since while the division of the available kinetic energy between the hydroxyl radical and hydrogen atom is determined by the conservation of linear momentum, the resultant angular momentum imparted to the hydroxyl radical depends upon the kinematics of the dissociation process, and cannot be predicted without a knowledge of the potential surfaces of the dissociating molecule. Nevertheless, the observed increase of the higher K maximum of OD by 700 cm^{-1} in mixtures of H_2O and D_2O would not be expected.

The absence, both in OH and in OD, of a shift of the second maximum to lower rotational energies with increasing water vapor pressure and with added helium and nitrogen is evidence that the probability for transfer of rotational energy through collisions during the radiative lifetime is small. To verify this, a plot was made of the rotational distribution which would have been obtained had the probability for collisional transfer of rotational energy been equal to the radiative transition probability. The distribution observed at the lowest pressures obtained, corresponding on the average to less than one collision during the radiative lifetime,

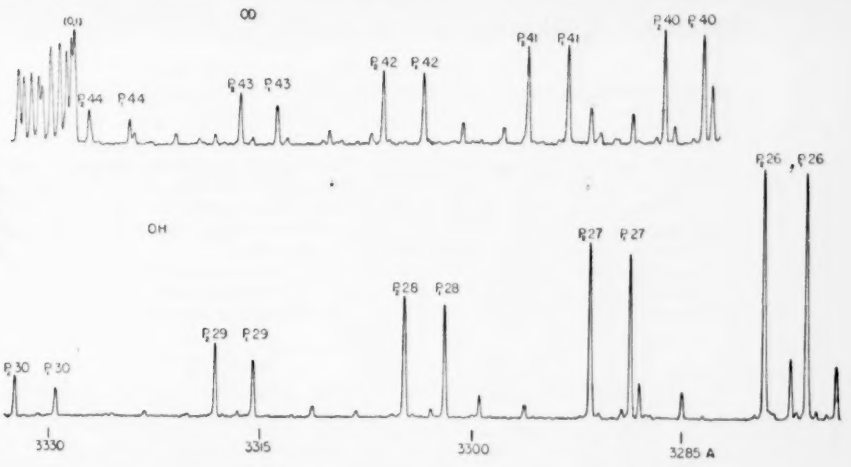

FIG. 7. Spectra of OH and of OD in the region of 3300A showing the stronger predissociation effect on the F_1 levels.

was taken as the initial distribution, and only transitions in collisions of the type $K \rightarrow K-1$ were assumed to have appreciable probability. The resulting plot showed a decrease in the position of the second intensity maximum from $K'=18$ to $K'=16$. The fact that no such shift was observed, up to the highest pressures attained, 3 mm Hg of water, indicates that a lower limit for the collision lifetime for transfer of rotational energy of the hydroxyl radical may be set at 150 collisions. In the experiments of Lyman[7] some 50 cm Hg of helium did not remove the nonthermal distribution. This would indicate that some 10 000 collisions are ineffective in totally removing abnormal rotation. This result is consistent with the experimental work in flames at atmospheric pressure.[11,12]

It is not clear whether the approximately twofold difference in intensities of OH and OD in mixtures of H_2O and D_2O represents a greater equilibrium concentration of OD ($^2\Pi$), or whether there is a preferential dissociation of HDO by electron impact into H+OD ($^2\Sigma^+$) rather than D+OH($^2\Sigma^+$). It is significant that this ratio of intensities between the isotopic species persists for low rotational levels as well as for the high ones, since presumably other mechanisms in addition to the dissociation of water vapor produce excited OH in low rotational levels.

The conclusions from the present experiment correspond more closely to those of Oldenberg[3] than to those of Lyman[7] in that a radical change is produced in the spectrum by the introduction of foreign gases. However, the observation of Lyman, that the rotational levels of the excited state are not in thermal equilibrium, is confirmed. It should be noted that conditions in the experiments by various workers may have been quite different. In Lyman's studies the discharge was maintained in a tube with metal electrodes, with a static concentration of water vapor supplied by water in a side tube. In the present experiment a continuous flow of water vapor was supplied and excitation furnished by an electrodeless discharge.

Niira[10] has suggested that the two maxima occurring in electrical discharges through water vapor are caused by the dissociation of two excited states of H_2O, a singlet state giving a maximum near $J=5$ and a triplet giving a second maximum near $J=20$. The conditions of the present experiments were such that the lower maximum shifted with the temperature of the discharge and apparently is not the result of dissociation of H_2O.

The authors take pleasure in expressing their appreciation to Dr. W. S. Benedict and Professor W. P. Allis for several stimulating discussions.

Interaction of Manganese Activator Ions in Zinc-Orthosilicate Phosphors

SIMON LARACH AND JOHN TURKEVICH
Radio Corporation of America, RCA Laboratories Division and Princeton University, Princeton, New Jersey
(Received November 19, 1952)

A study was made of specially prepared rhombohedral Zn_2SiO_4:Mn phosphors, utilizing magnetic, chemical, and luminescence techniques. From measurements of Weiss constants, it is shown that magnetic interaction occurs between manganese activator ions. The magnetic interaction increases with increasing proportion of manganese in the range where the following related luminescence characteristics decrease: (1) efficiency, (2) temperature break-point, and (3) decay time.

An analysis of the magnetic data shows that isolated noninteracting manganese activator ions have five unpaired electrons, corresponding to Mn^{2+}, and $\bar{\mu}=5.90$ Bohr magnetons (5.92 theoretical).

The molar diamagnetic susceptibility of zinc-orthosilicate was determined as being $(-64.6\pm0.7)\times10^{-6}$.

I. INTRODUCTION

URBAIN,[1] in 1908, first proposed the so-called "law of the optimum" in luminescence, that an optimum activator concentration exists for maximum luminescence emission intensity. Perrin[2] proposed that the decrease in luminescence emission intensity at higher activator concentrations was due to "overlapping fields" of pairs of activators in close proximity, and that such proximity caused coupling, with a concomitant decrease in the ability of the centers to be excited.

The interaction of activator ions has been assumed by several investigators[3–5] for various phosphor systems. Recently, Johnson and Williams have attempted to interpret the dependence of luminescence on activator concentration.[6]

The problem of interaction of manganese activator ions in zinc-orthosilicate and their relation to luminescence was attacked by a combination of magnetic, luminescence, and chemical procedures. Little work has been reported on the magnetic properties of oxygen-dominated phosphors. Johnson and Williams[7] have reported a small decrease in paramagnetic susceptibility on exciting zinc-orthosilicate:Mn, and Spencer *et al.*[8] have investigated the paramagnetic resonance line width of zinc-orthosilicate:Mn.

II. EXPERIMENTAL METHODS

Magnetic

The Gouy method of determining magnetic susceptibility was used.[9] The electromagnet current was supplied by a motor-generator, and the current was varied by adjusting a series of variable resistors. A Christian Becker analytical balance, with a sensitivity of 0.1 milligram, was used, the analytical weights having been checked by the National Bureau of Standards.

The low temperature unit, as shown in Fig. 1, was constructed from a solid block of magnesium-aluminum alloy. The diameter of the widest portion was $1\frac{5}{8}$ in. A channel, $\frac{9}{16}$-in. in diameter, was machined through the center of the block for the sample-tube suspension. A $\frac{1}{8}$-in. channel, $\frac{7}{8}$-in. deep, in the solid portion of the block, accommodated the thermocouple. In order to provide for an inert atmosphere, a groove extending from top to bottom of the main channel was cut, and a cylindrical aluminum sleeve was force-fitted into the channel. A copper tube, through a threaded connection, made contact with the groove, and was used for the gas inlet, while the outlet was the main channel. To provide for temperature variation, several turns of Nichrome wire were wound about the neck of the unit, using asbestos tape as insulation. The temperature of the unit was measured with a calibrated copper-constantan thermocouple, in conjunction with a dc millivoltmeter, which could be read to 0.05 millivolt. A special Dewar flask with completely silvered inner surface was constructed of Pyrex glass, and was shaped to fit between the pole pieces of the magnet.

The sample tubes were made from very thin-walled Pyrex glass, the cross-sectional areas being obtained by calibration with boiled distilled water. A Nylon thread was used for the suspension of the sample, and in order to avoid errors due to air currents, the thread was enclosed in a Bakelite tube. Errors in powder packing were minimized by gravimetrically determining the apparent density for each case.

The electromagnet field strength as a function of current was calibrated with (1) Mohr's salt, $FeSO_4$-$(NH_4)_2SO_4\cdot6H_2O$,[10] as the ground powder;[11] (2) manga-

[1] G. Urbain, Compt. rend. **147**, 1472 (1908).
[2] J. Perrin, Ann. phys. **11**, 5 (1919).
[3] F. A. Kroeger, dissertation, J. Van Campen, Amsterdam, 1940.
[4] T. Muto, Sci. Papers Inst. Phys. Chem. Research (Tokyo) **28**, 171 (1935).
[5] Z. A. Trapezinkova, Doklady Akad. Nauk S.S.S.R. **74**, 465 (1950).
[6] P. D. Johnson and F. E. Williams, J. Chem. Phys. **18**, 1477 (1950); Phys. Rev. **81**, 146 (1951).
[7] P. D. Johnson and F. E. Williams, J. Chem. Phys. **17**, 435 (1949).
[8] Spencer, Garstens, Klick, and Schulman, J. Chem. Phys. **20**, 1177 (1952).
[9] See, for example, P. W. Selwood, *Magnetochemistry* (Interscience Publishers, Inc., New York, 1943).
[10] L. C. Jackson, Trans. Roy. Soc. (London) **A224**, 1 (1923).
[11] It was first established that no ferromagnetic impurities were present, and that grinding did not affect the magnetic susceptibility.

nese sulfate, $MnSO_4 \cdot 4H_2O$;[12] (3) triple-distilled water, boiled free of dissolved air.[13]

Readings were taken at intervals from liquid-nitrogen temperature to room temperature, the gas flow being stopped for each reading. By substituting the appropriate values in the Gouy equation,[9] the specific susceptibility at each temperature is obtained, and this is converted to molar susceptibility.

Chemical

Synthesis of Phosphors

The ingredients used in synthesizing the phosphors consisted of a selected lot of J. T. Baker's analytical-grade zinc oxide, and an "ultrapure" silicic acid (obtained from the Mallinckrodt Chemical Company) which contained 11.9 percent water. The absence of appreciable amounts of metallic impurities in the ingredients was determined in two ways: (1) spectrographic analyses, and (2) luminescence analyses. The latter were performed by conversion of the zinc oxide to an unactivated zinc sulfide phosphor. The intense blue luminescence emission showed the absence of "poison" ions, such as iron, cobalt, nickel in appreciable amounts. Similarly, the silicic acid, when fired, showed the characteristic blue emission of pure fired silica.

Weighed amounts of the ingredients, to yield the orthosilicate,[14] were dry-ball-milled for 24 hours, to insure homogeneity. Manganese, as a solution of the nitrate, was added to give desired concentrations, additional silica having originally been added for reaction with the manganese.

The materials were slurried with triple-distilled water, and dried at 125°C. The mixes were then transferred to platinum crucibles, and the series was fired in air at 1280°C, for four hours, in a Globar-type, temperature-controlled furnace. Only the cores of the phosphor cakes were used, and no grinding was done.

Analytical

In determining the susceptibility of the phosphors, it is essential that the final manganese proportion be known. For example, Rupp[15] found a 20 percent loss of manganese after firing zinc sulfide:Mn. Weighed portions of zinc-orthosilicate:Mn phosphors were dissolved in concentrated hydrofluoric acid, and the bismuthate method[16] was used, manganese being determined colorimetrically as permanganate.

[12] L. F. Bates, *Modern Magnetism* (Cambridge University Press, London, 1948), second edition, p. 130.
[13] S. Seely, Phys. Rev. **49**, 812 (1936).
[14] Zinc-orthosilicate, Zn_2SiO_4, is the only true compound in the system ZnO-SiO_2, as shown by the phase studies of E. N. Bunting, J. Research Natl. Bur. Standards **4**, 131 (1930).
[15] E. Rupp, Ann. Physik **78**, 505 (1925). The loss of manganese reported by Rupp has been traced to volatilization of manganese chloride at the crystallization temperature for hexagonal zinc sulfide.
[16] Described in, for example, I. M. Kolthoff and E. B. Sandell, *Textbook of Quantitative Inorganic Chemistry* (Macmillan Company, New York, 1948), revised edition, p. 755.

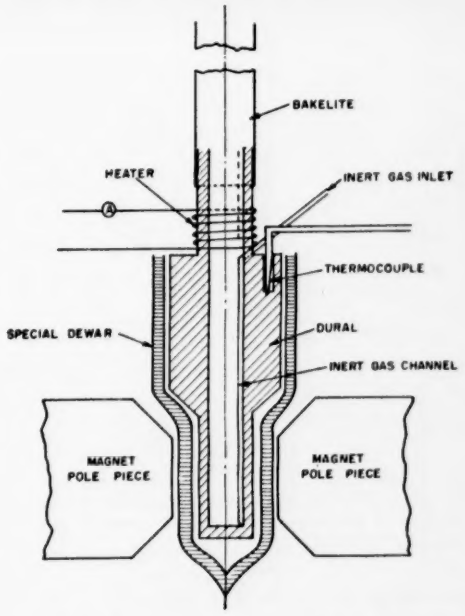

FIG. 1. Low temperature susceptibility unit.

To determine the amount of manganese in higher oxidation states, the iodometric method of Gossner and Bruckl[17] was modified and used. The reagents were standardized and a "blank" of zinc-orthosilicate with no added manganese was used.

Luminescence

Spectral Distribution

Curves of spectral distribution were obtained with a recording spectroradiometer,[18] the phosphor being prepared as a thick patch.[19] Excitation of the phosphor in a demountable cathode-ray tube was by 10-kilovolt electrons, as a dc spot, with a current density of 13 microamperes/cm^2.

Emission Intensity and Decay

Relative integrated luminescence emission intensities were obtained, using a demountable cathode-ray tube, and a 1P21 phototube. The phosphors were excited by an electron beam, and both low (1 μa/cm^2) and high (100 μa/cm^2) current densities were used.

Decay curves, after excitation by cathode rays, were obtained with a dc oscillograph-phosphoroscope.

III. EXPERIMENTAL RESULTS

Test for Ferromagnetic Impurities

The zinc-orthosilicate:Mn phosphors were shown magnetically to be free of contamination by traces of

[17] G. Gossner and K. Bruckl, Zentr. Mineral. T. I 316 (1928).
[18] V. K. Zworykin, J. Opt. Soc. Am. **29**, 84 (1939).
[19] Measurements were made by R. H. Bube and R. E. Shrader.

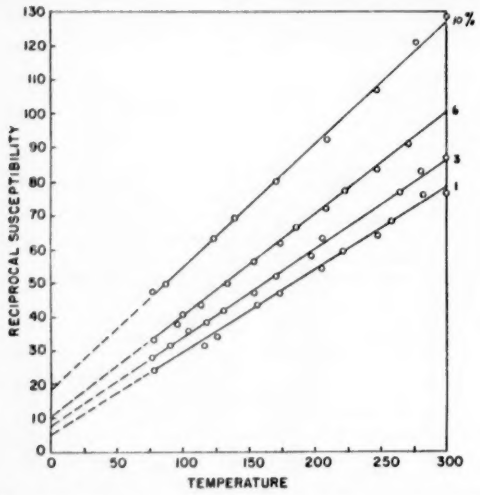

FIG. 2. Reciprocal paramagnetic susceptibility as a function of temperature of zinc-orthosilicate: Mn phosphors, with indicated proportions of manganese.

ferromagnetic impurities, by measuring the weight change as a function of magnetic field strength, H. The change in weight, Δw, was found to vary linearly with H^2, as predicted by the Gouy relation,

$$g\Delta w = \tfrac{1}{2}kAH^2, \tag{1}$$

g, k, and A being constants.

Diamagnetic Susceptibility of Unactivated Zinc-Orthosilicate

The luminescent materials under investigation consist of diamagnetic zinc-orthosilicates, in which small amounts of paramagnetic manganese ions have been incorporated. The problem of susceptibility determinations in such cases has been discussed by Haller and Selwood[20] for the case of trivalent cerium in lanthanum oxide.

The diamagnetic susceptibility of unactivated zinc-orthosilicate was determined from the loss in weight. The value obtained for the specific susceptibility was $-(0.289\pm0.003)\times10^{-6}$, corrected for the slight contribution of the Pyrex container. The susceptibility was found to be independent of temperature in the range 77°–300°K.

No previous determination of the susceptibility of zinc-orthosilicate has been found in the literature. It is interesting, however, to compare the above value with those reported by various investigators for other oxygen-dominated, zinc-containing materials: thus, for zinc oxide, -0.26×10^{-6} and -0.33×10^{-6} have been reported, and for zinc sulfate, -0.27×10^{-6} and -0.53×10^{-6} have been reported.[21]

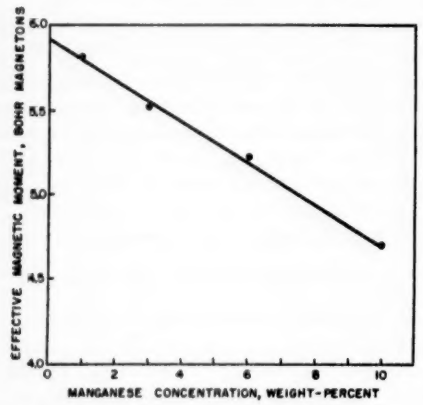

FIG. 3. Effective magnetic moment as a function of the proportion of manganese in zinc-orthosilicate phosphors.

IV. MAGNETIC PROPERTIES AS A FUNCTION OF MANGANESE CONTENT

It was found, for zinc-orthosilicate phosphors, with manganese in the range from one to ten percent by weight, that the Curie-Weiss law was followed:

$$\chi = C/(T+\Delta) \tag{2}$$

TABLE I. Curie and Weiss constants as a function of manganese proportion.

% Mn	C	Δ
1	4.16	16
3	3.84	27
6	3.45	38
10	2.78	57

where χ is the molar susceptibility, C is the Curie constant, T is the absolute temperature, and Δ is the Weiss constant.

The reciprocal susceptibility as a function of temperature is shown in Fig. 2, from which it is seen that both the slope and intercept vary with manganese concentration. Table I illustrates the dependence of the Curie and Weiss constants on the manganese proportion. It is found that the Curie constant decreases with increasing manganese proportion whereas the Weiss constant increases.

Effective Magnetic Moments

The effective magnetic moments, μ_{eff}, in Bohr magnetons were calculated from the relationship:

$$\mu_{eff} = 2.84[\chi(T+\Delta)]^{\frac{1}{2}}. \tag{3}$$

It was found that μ_{eff} decreases monotonically with increasing manganese content, as is shown in Fig. 3. Extrapolation to the region of infinite magnetic dilution

[20] R. B. Haller and P. W. Selwood, J. Am. Chem. Soc. **61**, 85 (1939).

[21] Landolt-Börnstein, *Physikalisch-Chemische Tabellen* (Springer, Berlin, 1923), p. 1245.

yields the value of 5.90 Bohr magnetons, as against the theoretical "spin-only" value of 5.92 Bohr magnetons for Mn^{2+}. Other investigators have reported values of 5.2 to 5.96 Bohr magnetons for manganous salts.[22]

V. LUMINESCENCE OF ZINC-ORTHOSILICATE:Mn PHOSPHORS

Spectral Distribution

Spectral distribution curves for zinc-orthosilicate with one percent manganese and with ten percent manganese are shown in Fig. 4, and are similar to those previously reported.[23] The phosphor with one percent manganese (Curve 1) has an emission whose peak wavelength occurs at 5250A. The effects of increasing the manganese to ten percent (Curve 2) are: (1) the short-wavelength limit of the spectral-distribution curve shifts to 4900A, whereas it occurs at 4750A for the sample with one percent manganese; (2) the peak wavelength is at 5350A; (3) the long-wavelength limit occurs at 6300A.

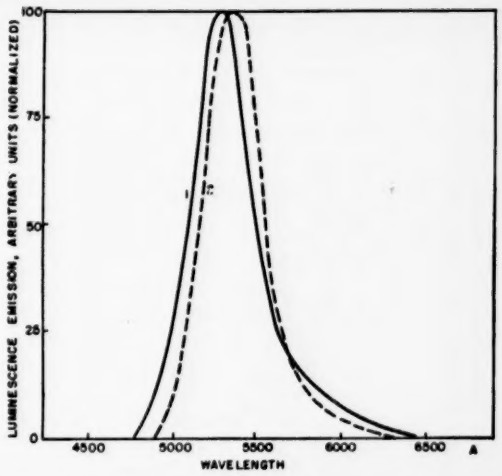

FIG. 4. Cathodoluminescence spectral distribution curves for zinc-orthosilicate phosphors with 1 and 10 percent manganese.

Luminescence Emission Intensity and Decay

Figure 5 shows the relative emission intensities as a function of manganese proportion. For the low current density, the maximum emission intensity occurs at 0.1 percent manganese, while with the higher current density, the optimum occurred at one percent manganese.

TABLE II. Decay characteristics of zinc-orthosilicate:Mn phosphors, with low and high current density excitation.

% Mn	τ (millisec) Low c.d.	High c.d.
0.01	13.3	12.8
0.1	13.3	11.2
1.0	9.1	7.4
10	1.1	3.9

Decay characteristics after excitation by cathode rays are summarized in Table II, for manganese concentrations ranging from 0.01 to 10 percent.

There is apparently no effect on τ, for low current density, until at least 0.1 percent manganese, after which there is a sharp decrease in τ with increasing manganese. With high current density excitation, τ decreases with increasing manganese content from 0.01 percent manganese.

VI. CHEMICAL AND X-RAY ANALYSES

In contrast to the report of Rupp,[15] concerning the loss of manganese on firing zinc-sulfide:Mn, it was found on chemical analysis that the manganese remaining in zinc-orthosilicate, after the crystallization firing, in no case deviated by more than 0.5 percent from the amount used in the synthesis. The calculations of susceptibility are based on the actual amounts of manganese found to be present in the phosphors.

Determination of the amount of manganese in higher oxidation states gave the following results: (1) no manganese existing in a higher oxidation state was found in the sample with 0.1 percent manganese; (2) the phosphors with 1, 3, 6, and 10 percent manganese showed higher valence manganese present only in the amount of 0.03 percent of the manganese in the one percent sample, to 1.02 percent of the manganese in the ten percent sample.

The phosphors became increasingly brown to daylight with increasing amounts of manganese. This has been previously observed with zinc-beryllium-silicate:Mn phosphors by Froelich,[24] who attributed the effect to a brown oxide, probably Mn_2O_3, formed at the surface.

X-ray powder diffraction patterns of the phosphors[25] indicated a high degree of crystallinity, as well as solid

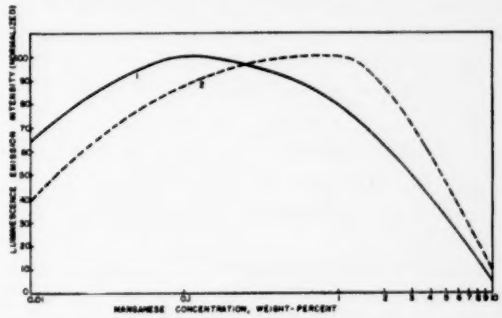

FIG. 5. Relative cathodoluminescence emission intensity of zinc-orthosilicate:Mn, at high (2) and low (1) current densities, as a function of manganese proportion.

[22] See reference 9, p. 99.
[23] H. W. Leverenz, *Introduction to Luminescence of Solids* (John Wiley and Sons, Inc., New York, 1950), p. 225.
[24] H. C. Froelich, Trans. Electrochem. Soc. 87, 429 (1945).
[25] Taken by I. J. Hegyi.

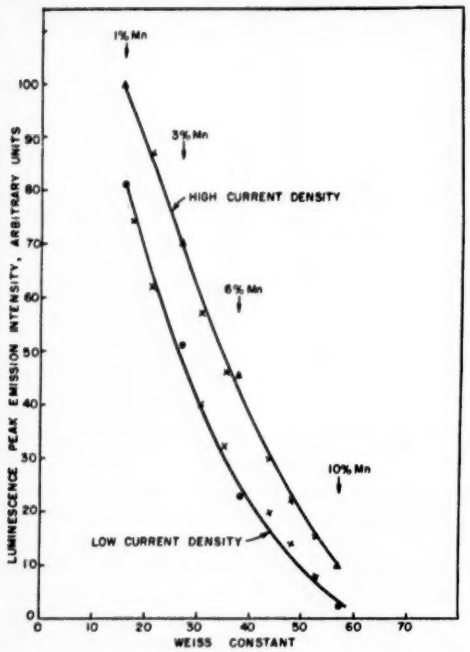

FIG. 6. Cathodoluminescence emission intensity of zinc-orthosilicate: Mn phosphors as a function of the Weiss constant.

solution of the zinc and manganese silicates, in agreement with the work of Kröger.[3]

VII. DISCUSSION

Diamagnetism of Zinc-Orthosilicate

Various attempts have been made to calculate ionic diamagnetic susceptibilities from quantum-mechanical considerations. Pauling[26] has derived the following expression for diamagnetic susceptibility:

$$\chi = 2.010\times10^{-6}\sum \frac{n^4}{(Z-S)^2}\left\{\frac{1-3l(l+1)-1}{5n^2}\right\}, \quad (4)$$

where Z is the nuclear charge, S is a screening constant, and n and l are quantum numbers. Slater[27] obtains for the diamagnetic susceptibility of each electron in a group

$$\chi = -0.807\times10^{-6}(n^*)^2(n^*+\tfrac{1}{2})(n^*+1)/(Z-S)^2. \quad (5)$$

Angus[28] has modified the Slater method, so as to separate s and p electrons having the same quantum number.

Calculated ionic diamagnetic susceptibilities for oxygen, zinc and silicon ions using the methods of Pauling (L.P.), Slater (J.C.S.) and Angus (W.R.A.) are given in Table III.[29]

[26] L. Pauling, Proc. Roy. Soc. (London) **A114**, 181 (1927).
[27] J. C. Slater, Phys. Rev. **36**, 57 (1930).
[28] W. R. Angus, Proc. Roy. Soc. (London) **A136**, 569 (1932).
[29] Values from Angus, reference 28.

Assuming additivity, the diamagnetic susceptibility of zinc-orthosilicate, Zn_2SiO_4, can be calculated. The values obtained, using the various methods, are listed in Table III.

Agreement between calculated and experimental values is good, considering the complexity of the compound involved. The method of Pauling is closest to the experimental value, and it is also indicated that when s and p electrons of the same quantum number are considered separately (Angus), the resulting calculated susceptibility is closer to the actual experimental value.[30]

The Ionization State of Manganese in Zinc-Orthosilicate

The evidence heretofore for the ionization state of manganese in zinc-orthosilicate has been rather indirect in nature, and has been summarized by Kroeger.[31]

The present investigation corroborates the chemical findings, in that only inappreciable amounts of higher-valency manganese were found. In addition the magnetic findings indicate the presence of manganese ions with five unpaired electrons, since at infinite magnetic dilution, a moment of 5.90 Bohr magnetons was obtained, as compared to the theoretical "spin-only" moment of 5.92 Bohr magnetons for a doubly ionized manganese ion.

Magnetic Interaction of Manganese Activator Ions

That magnetic interaction occurs among the manganese activator ions in zinc-orthosilicate has been shown by (1) the decrease in the Weiss constant with decreasing amounts of manganese, and (2) the decrease in the effective magnetic moment with increasing manganese proportion.

Calculated magnetic moments, based on probability considerations of having only isolated manganese ions

TABLE III. Comparison of calculated and experimental values of diamagnetic susceptibility of zinc-orthosilicate ($-\chi\times10^6$).

	L.P.	J.C.S.	W.R.A.	Exptl.
$O^=$	12.6	13.15	11.25	
Zn^{++}	11	15.57	15.45	
Si^{++++}	2.1	2.03	1.87	
Zn_2SiO_4	74.5	85.77	77.77	64.6

[30] The empirical method of P. Pascal, Ann. chim. phys. **19**, 5 (1910), useful for organic compounds, gives a calculated value (probably fortuitous) close to the experimental value. If the Pascal constants for zinc (-13.5×10^{-6}), silicon (-20×10^{-6}), and carboxylic oxygen (-3.36×10^{-6}) are applied to zinc-orthosilicate, taking the constitutive correction as zero, the resulting calculated molar diamagnetic susceptibility is -60×10^{-6}. The value for carboxylic oxygen is used, as it is felt that this approximates most closely the resonance between silicon and oxygen in the orthosilicate radical.
[31] F. A. Kroeger, Trans. Electrochem. Soc. **95**, 356 (1949).

in zinc-orthosilicate[32] contributing to the moment, are lower than the experimentally determined values. These discrepancies can be accounted for by assuming (1) incomplete spin-pairing of pairs and clusters of manganese ions, with resultant contributions to the magnetic moment, or (2) that the distribution of manganese activator ions in zinc-orthosilicate is not of a random nature.

Interaction and Luminescence

If the decrease in luminescence emission intensity with increasing manganese proportion were due only to a decrease in the effective number of emitting centers, then neither the temperature break-point nor the lifetime of the excited state should be affected. However, the fact that both break-point and lifetime are functions of the manganese proportion can be explained by activator interactions which cause an increase in the probability of radiationless transitions. Figure 6 shows the relationship between emission intensity and the Weiss constant, under electron excitation, with high and low current density, for manganese proportions from 1 to 10 percent. It is seen that the decrease in emission intensity occurs for the same range of Mn proportion as the increase in the Weiss constant.

The effectiveness of the magnetic method for determining the ionization state and degree of interaction of small amounts of paramagnetic impurities should prove of value in studies of other systems, as well as in trapping, and the effect of luminescence poisons.

The authors wish to express their appreciation to H. W. Leverenz of the RCA Laboratories for his interest and encouragement, and to Dr. R. H. Bube for valuable discussions.

[32] By *isolated* is meant having no manganese ion in next-adjacent available site; see H. W. Leverenz, reference 23, pp. 477–480. P. D. Johnson and F. E. Williams, J. Chem. Phys. **18**, 323 (1950), assumed for ZnF_2:Mn phosphors that only those manganese ions which do not have other manganese ions at nearest cation sites are capable of luminescing. See also H. W. Leverenz and D. O. North, Phys. Rev. **85**, 930 (1952).

PHYSICAL REVIEW VOLUME 89, NUMBER 5 MARCH 1, 1953

The Evaluation of the Energy Matrix of the Tensor Forces

IGAL TALMI*
Hebrew University, Jerusalem, Israel
(Received November 5, 1952)

It is shown how the use of tensor operators enables a simple calculation of the tensor forces in nuclear configurations by the usual spectroscopic methods. The number of independent parameters necessary to define the energy in the nuclear configuration l^n (or j^n) is found to be $2l$ (or $2j$), whereas it is shown to be only $[4l/3]$ (or $[2j+2/3]$) in the l^n (or j^n) configuration of equivalent nucleons. The energy matrix is given by means of a closed formula for the case of d^n and $(d_{5/2})^n$ configurations (of equivalent nucleons). It is found that in the latter configuration the order of levels for a short-range potential (of the tensor forces) is the same as for short-range central forces.

I. INTRODUCTION

IN a recent paper[1] it has been shown that the tensor forces possess the pairing property, i.e., this interaction is diagonal with respect to the seniority v and the term values of the configuration l^n (or j^n) of equivalent nucleons differ from the corresponding states of the l^v (or j^v) configuration only by the term $\frac{1}{2}(n-v)E_0$. E_0 is the energy of $l^2\,{}^1S$, which vanishes for tensor forces (or j^2, $J=0$). The proof of this fact is based on an expansion of the tensor force interaction between two nucleons into a sum of products of double tensors $\mathbf{s}_1\mathbf{C}_1^{(k)}$ and $\mathbf{s}_2\mathbf{C}_2^{(k)}$ of the two nucleons, where $\mathbf{s}_i$ is the spin vector of the ith nucleon and $\mathbf{C}_{iq}^{(k)}$ differ only by a constant factor from the spherical harmonics of order k which depend on the coordinates of the ith nucleon. This expansion will be used throughout this paper in order to obtain further results on the tensor forces.

The matrix elements of the tensor force interaction were calculated in the case of d^2 and p^2 by Marvin,[2] who took for the potential the special case of $1/r^3$ (which appears in the electromagnetic spin-spin interaction). The results of his long and complicated calculations are very simple, they contain only two independent parameters in the case of d^2 (and only one for p^2). Also, these parameters can be easily expressed by the ordinary Slater coefficients of the potential $1/r^3$. The decomposition described above enables a simpler calculation of the matrix elements of the tensor forces. We shall use a general potential and see to what cause the simplification which occurs in Marvin's results is due. The method used offers a natural definition of the radial parameters for the tensor forces, with the help of which

* Now at the Palmer Physical Laboratory, Princeton University, Princeton, New Jersey.
[1] G. Racah and I. Talmi, Physica (to be published).
[2] H. H. Marvin, Phys. Rev. **71**, 102 (1947).

the number of the independent parameters in the l^n (or j^n) configuration will be found.

By means of the parameters defined, we give the procedure for the calculation of the energy matrix in a nuclear configuration. This will enable us to write down the results of Trees,[3] who used Marvin's results to calculate the terms of the d^n configuration by means of a closed formula.

Using the method of harmonic oscillator wave functions,[4] we will give a method to calculate the radial parameters in terms of simple integrals. By considering these integrals, a discussion of the effect of tensor forces on the levels of the $(d_{\frac{1}{2}})^n$ configuration is given. It is found that for short-range potentials the tensor forces behave in a similar manner to that of short-range central interactions.

II. DECOMPOSITION OF THE INTERACTION

It is well known that the tensor force interaction between two nucleons is the scalar product of two tensors of the second degree, one of which is a function of the spins of the two nucleons and the other is a function of their spatial coordinates. In order to express this interaction by means of operators which operate on the (spin and space) coordinates of a single nucleon, we shall write it down as a sum of tensor products[5] of the double tensors $\mathbf{s}_1\mathbf{C}_1^{(k)}$ and $\mathbf{s}_2\mathbf{C}_2^{(k')}$. The k and k' of tensors whose matrix elements diagonal with respect to l_1 and l_2 do not vanish must be even and satisfy $0\leqslant k\leqslant 2l_1$, $0\leqslant k'\leqslant 2l_2$.

The interaction of the tensor forces between nucleons 1 and 2,

$$S_{12}V(r_{12})=\left[\frac{(\mathbf{s}_1\cdot\mathbf{r}_{12})(\mathbf{s}_2\cdot\mathbf{r}_{12})}{r_{12}^2}-\tfrac{1}{3}(\mathbf{s}_1\cdot\mathbf{s}_2)\right]V(r_{12})$$

$$=\left\{r_1^2\left[\left(\mathbf{s}_1\cdot\frac{\mathbf{r}_1}{r_1}\right)\left(\mathbf{s}_2\cdot\frac{\mathbf{r}_1}{r_1}\right)-\tfrac{1}{3}(\mathbf{s}_1\cdot\mathbf{s}_2)\right]\right.$$

$$+r_2^2\left[\left(\mathbf{s}_1\cdot\frac{\mathbf{r}_2}{r_2}\right)\left(\mathbf{s}_2\cdot\frac{\mathbf{r}_2}{r_2}\right)-\tfrac{1}{3}(\mathbf{s}_1\cdot\mathbf{s}_2)\right]$$

$$-r_1r_2\left[\left(\mathbf{s}_1\cdot\frac{\mathbf{r}_1}{r_1}\right)\left(\mathbf{s}_2\cdot\frac{\mathbf{r}_2}{r_2}\right)+\left(\mathbf{s}_1\cdot\frac{\mathbf{r}_2}{r_2}\right)\right.$$

$$\left.\left.\times\left(\mathbf{s}_2\cdot\frac{\mathbf{r}_1}{r_1}\right)-\tfrac{2}{3}(\mathbf{s}_1\cdot\mathbf{s}_2)\right]\right\}\frac{V(r_{12})}{r_{12}^2},\quad(1)$$

can be written as follows, after introducing the tensors[6] $\mathbf{C}_i^{(k)}=(4\pi/2k+1)^{\frac{1}{2}}\mathbf{Y}_i^{(k)}$ (where $Y_{im}^{(k)}$ are the spherical harmonics of order k which are functions of the coordinates of the ith nucleon):

$$\left[\sum_{\rho\rho'}(-1)^{-\rho+\rho'}s_{1-\rho}s_{2\rho'}(2/3)^{\frac{1}{2}}(1-\rho1\rho'|112,-\rho+\rho')\right.$$

$$\times(r_1^2C_{1\rho-\rho'}^{(2)}+r_2^2C_{2\rho-\rho'}^{(2)})-\sum_{\rho\rho'qq'}(-1)^{q-q'}s_{1-\rho}s_{2\rho'}$$

$$\times5r_1r_2V(112;q,-q',-q+q')V(112;-\rho,\rho',q-q')$$

$$\left.\times(C_{1q}^{(1)}C_{2-q'}^{(1)}+C_{2q}^{(1)}C_{1-q'}^{(1)})\right]\frac{V(r_{12})}{r_{12}^2}.\quad(2)$$

Expansion of $V(r_{12})/r_{12}^2$ in the usual way, namely,

$$\frac{V(r_{12})}{r_{12}^2}=\sum_{k=0}^{\infty}f_k(r_1,r_2)P_k(\cos\omega_{12})$$

$$=\sum_{k=0}^{\infty}f_k(r_1,r_2)\sum_{m=-k}^{+k}(-1)^mC_{1-m}^{(k)}C_{2m}^{(k)},$$

gives after expressing products of spherical harmonics as linear combinations of these functions:

$$\sum_{krm\rho\rho'}(-1)^{-\rho+\rho'+m}f_k(r_1,r_2)s_{1-\rho}s_{2\rho'}\frac{(2/3)^{\frac{1}{2}}(2r+1)}{[5(2k+1)]^{\frac{1}{2}}}$$

$$\times c^r(2,-\rho+\rho',k,m)(1-\rho1\rho'|112,-\rho+\rho')$$

$$\times(r_1^2C_{1\rho-\rho'-m}^{(r)}C_{2m}^{(k)}+r_2^2C_{2\rho-\rho'-m}^{(r)}C_{1m}^{(k)})$$

$$-\sum_{krsm\rho\rho'qq'}10r_1r_2f_k(r_1,r_2)(-1)^{q-q'}s_{1-\rho}s_{2\rho'}$$

$$\times C_{1q-m}^{(r)}C_{2m-q'}^{(s)}\frac{(2r+1)(2s+1)}{3(2k+1)}c^r(1qkm)$$

$$\times c^s(km1q')V(112;q,-q',-q+q')$$

$$\times V(112;-\rho,\rho',q-q').\quad(3)$$

With the help of II (52) this can be written as

$$\sum_{krm\rho\rho'}(-1)^{1+(r+k)/2}f_k(r_1,r_2)(2/15)^{\frac{1}{2}}(2r+1)$$

$$\times(\tfrac{1}{2}C_{2rk})^{\frac{1}{2}}(-1)^{\rho-\rho'}s_{1-\rho}s_{2\rho'}(r_1^2C_{1\rho-\rho'-m}^{(r)}C_{2m}^{(k)}$$

$$+r_2^2C_{2\rho-\rho'-m}^{(r)}C_{1m}^{(k)})(1-\rho1\rho'|112,-\rho+\rho')$$

$$\times(r,\rho-\rho'-m,k,m|rk2,\rho-\rho')$$

$$-\sum_{krsm\rho\rho'qq'}(-1)^{k+1+(r+s)/2}10r_1r_2f_k(r_1,r_2)$$

$$\times(\tfrac{1}{4}C_{1rk}C_{1sk})^{\frac{1}{2}}(2r+1)(2s+1)(-1)^{m-q'}s_{1-\rho}s_{2\rho'}$$

$$\times C_{1q-m}^{(r)}C_{2m-q'}^{(s)}V(112;-\rho,\rho',q-q')$$

$$\times V(112;q,-q',-q+q')V(1rk;-q,q-m,m)$$

$$\times V(1sk;q',m-q',-m).\quad(4)$$

The first sum has already the desired form of a tensor product of $\mathbf{s}_1\mathbf{C}_1^{(r)}$ and $\mathbf{s}_2\mathbf{C}_2^{(k)}$; in order to bring the second sum also to this form we transform the product $V(1rk;-q,q-m,m)V(1sk;q',m-q',-m)$ by means

[3] R. E. Trees, Phys. Rev. **82**, 683 (1951).
[4] I. Talmi, Helv. Phys. Acta **XXV**, 185 (1952).
[5] G. Racah, *Group Theory and Spectroscopy*, Lecture notes, Princeton, 1951 (unpublished).
[6] G. Racah, Phys. Rev. **62**, 438 (1942), which will be referred to as II; the notation defined in it will be used throughout this paper.

of the W function according to the formula

$$\sum_\varphi(-1)^{f+\varphi}V(acf;\alpha-\gamma-\varphi)V(bdf;\beta-\delta\varphi)$$
$$=\sum_{e\epsilon}(-1)^{a+d-f+\epsilon}(2e+1)W(abcd;ef)$$
$$\times V(abe;\alpha\beta-\epsilon)V(cde;-\gamma-\delta\epsilon). \quad (5)$$

We then sum the product of $V(11e;q,-q',-q+q')$, thus obtained, and $V(112;q,-q',-q+q')$ over q, q', and m for fixed $q-m$ and $m-q'$, which yields $\delta(2,e)/(2e+1)$, so that we finally obtain

$$S_{12}V(r_{12})=\sum_{kr}(-1)^{1+(r+k)/2}f_k(r_1,r_2)(2/15)^{\frac{1}{2}}$$
$$\times(2r+1)(\tfrac{1}{2}C_{2rk})^{\frac{1}{2}}\{r_1^2([\mathbf{s}_1\times\mathbf{s}_2]^{(2)}\cdot[\mathbf{C}_1^{(r)}\times\mathbf{C}_2^{(k)}]^{(2)})$$
$$+r_2^2([\mathbf{s}_1\times\mathbf{s}_2]^{(2)}\cdot[\mathbf{C}_2^{(r)}\times\mathbf{C}_1^{(k)}]^{(2)})\}$$
$$-\sum_{krs}(-1)^{k+(r-s)/2}r_1r_2f_k(r_1,r_2)(2r+1)(2s+1)$$
$$\times(\tfrac{1}{4}C_{1rk}C_{1sk})^{\frac{1}{2}}W(11rs;2k)([\mathbf{s}_1\times\mathbf{s}_2]^{(2)}$$
$$\cdot\{[\mathbf{C}_1^{(r)}\times\mathbf{C}_2^{(s)}]^{(2)}+[\mathbf{C}_2^{(r)}\times\mathbf{C}_1^{(s)}]^{(2)}\}). \quad (6)$$

In this expression of the interaction, the angular and spin-dependent parts appear in a form which shows their tensorial properties. For a definite configuration, after the integration over r_1 and r_2, the elements of the energy matrix are sums of matrix elements of definite products of tensors which can be found in every case by the formulas of the tensor algebra and the usual methods of spectroscopy.

In particular, the matrix elements for the case of two nucleons with orbital angular momenta l_1 and l_2 in LS coupling (the case of jj coupling will be treated below) are given by the general formula[3]

$$(\alpha SLJM|S_{12}V(r_{12})|\alpha'S'L'JM)$$
$$=(-1)^{S+L'-J}(\alpha SL\|S_{12}V(r_{12})\|\alpha'S'L')W(SLS'L';J2), \quad (7)$$

and by

$$(SL\|[\mathbf{s}_1\mathbf{C}_1^{(r)}\times\mathbf{s}_2\mathbf{C}_2^{(s)}]^{(22)}\|S'L')$$
$$=5\sum_{S''L''}(SL\|s_1C_1^{(r)}\|S''L'')(S''L''\|s_2C_2^{(s)}\|S'L')$$
$$\times W(S1S'1;S''2)W(LrL's;L''2), \quad (8)$$

in addition to II (44) and Sec. 5 of II.

III. THE l^n CONFIGURATION

We shall now calculate the interaction matrix of the tensor forces in the l^n configuration. We introduce the unit tensor operators by means of II (51):

$$(l\|C_i^{(k)}\|l)=(-1)^{k/2}(2l+1)(\tfrac{1}{2}C_{kll})^{\frac{1}{2}}(l\|u_i^{(k)}\|l), \quad (9)$$

and the double tensor $\mathbf{V}^{(1k)}=\sum_{i=1}^n\mathbf{s}_i\mathbf{u}_i^{(k)}$ which operate on the coordinates of the whole group of the l nucleons. The values of the radial integrals over r_1^2 are equal in this case to those over r_2^2; as a result we obtain, by summing over all the nucleon pairs ij,

$$(l^n\alpha SL\|\sum_{i<j}S_{ij}V(r_{ij})\|l^n\alpha'S'L')$$
$$=-\sum_{kr}\int\int R_l^2(r_1)R_l^2(r_2)\tfrac{1}{2}(r_1^2+r_2^2)f_k(r_1,r_2)dr_1dr_2$$
$$\times(2/15)^{\frac{1}{2}}(2r+1)^2(2l+1)^2(\tfrac{1}{2}C_{2rk})^{\frac{1}{2}}(\tfrac{1}{4}C_{kll}C_{rll})^{\frac{1}{2}}$$
$$\times(l^n\alpha SL\|[\mathbf{V}^{(1k)}\times\mathbf{V}^{(1r)}]^{(22)}\|l^n\alpha'S'L')$$
$$+\sum_{krs}\int\int R_l^2(r_1)R_l^2(r_2)r_1r_2f_k(r_1,r_2)dr_1dr_2$$
$$\times(2r+1)(2s+1)(2l+1)^2(\tfrac{1}{4}C_{1rk}C_{1sk})^{\frac{1}{2}}$$
$$\times(\tfrac{1}{4}C_{rll}C_{sll})^{\frac{1}{2}}W(11rs;2k)$$
$$\times(l^n\alpha SL\|[\mathbf{V}^{(1r)}\times\mathbf{V}^{(1s)}]^{(22)}\|l^n\alpha'S'L'). \quad (10)$$

In the transition from (6) to (10), a term of the form

$$\sum_{i=1}^n(l^n\alpha SL\|[\mathbf{s}_i\mathbf{C}_i^{(r)}\times\mathbf{s}_i\mathbf{C}_i^{(s)}]^{(22)}\|l^n\alpha'S'L')$$

was dropped out since the tensor $[\mathbf{s}_1\times\mathbf{s}_2]^{(2)}$ vanishes because of the triangular conditions (such a term would be linear in n).

Considering the equation analogous to (8),

$$(\alpha SL\|[\mathbf{V}^{(1r)}\times\mathbf{V}^{(1s)}]^{(22)}\|\alpha'S'L')$$
$$=5\sum_{\alpha''S''L''}(\alpha SL\|V^{(1r)}\|\alpha''S''L'')(\alpha''S''L''\|V^{(1s)}\|\alpha'S'L')$$
$$\times W(1S1S';S''2)W(rLsL';L''2), \quad (11)$$

we see that the energy matrix is given if the matrix elements $(l^n\alpha SL\|V^{(1k)}\|l^n\alpha'S'L')$ are calculated. To evaluate them is a problem which is encountered in the calculation of the energy of central interactions. In the special case $n=2$ they are simply

$$(l^2SL\|V^{(1k)}\|l^2S'L')$$
$$=-\tfrac{1}{2}[(-1)^{S+L}+(-1)^{S'+L'}](6)^{\frac{1}{2}}$$
$$\times[(2S+1)(2S'+1)(2L+1)(2L'+1)]^{\frac{1}{2}}$$
$$\times W(\tfrac{1}{2}S\tfrac{1}{2}S';\tfrac{1}{2}1)W(lLlL';lk). \quad (12)$$

For higher n one should use the methods developed by Racah[5–8] and others.[9,10] The calculation may be facilitated by the fact that the tensors $V^{(1k)}$ which should be calculated have all $1+k$ odd. It follows from the triangular conditions and from the fact that the symmetry of a wave function of two nucleons is $(-1)^{S+L}$ that, for odd $1+k$,[7]

$$(l^2SL\|V^{(1k)}\|l^2\,{}^1S)=(l^2\,{}^1S\|V^{(1k)}\|l^2SL)=0 \quad (13)$$

for every S and L. The group theoretical meaning of this fact is that such tensors are representations of the infinitesimal elements of the group which leaves in-

[7] G. Racah, Phys. Rev. **63**, 367 (1943).
[8] G. Racah, Phys. Rev. **76**, 1352 (1949).
[9] H. A. Jahn, Proc. Roy. Soc. (London) **201**, 516 (1950).
[10] B. H. Flowers, Proc. Roy. Soc. (London) **212**, 248 (1952).

variant the antisymmetric form—the wave function of $l^2\,{}^1S$—i.e., the symplectic group in $2(2l+1)$ dimensions $\mathrm{Sp}(4l+2)$. Therefore, the tensors $\mathbf{V}^{(1k)}$ with odd $1+k$ are diagonal with respect to the quantum numbers which characterize these representations. In the special case of equivalent nucleons (the l^n configuration of protons or neutrons only) the double tensors $\mathbf{V}^{(1k)}$ with $1+k$ odd are diagonal with respect to the seniority and independent of n[7]. For this case, it follows from (10) that in LS coupling also the energy is diagonal with respect to the seniority and independent of n, as was found empirically by Trees[3] in the case of d^n.

It is natural to define the sum of radial integrals which multiplies a definite matrix

$$(l^n\alpha SL\|[\mathbf{V}^{(1r)}\times\mathbf{V}^{(1s)}]^{(22)}\|l^n\alpha'S'L'), \qquad (14)$$

which depends only on the angular and spin-dependent parts of the wave functions, as the parameters by means of which the energy can be expressed. These parameters are the analogs for the case of tensor forces of the Slater coefficients in the case of central forces. As r and s must be even and satisfy together with 2 the triangular conditions, it follows that in the l^n configuration there are $2l$ possible matrices (14). In the general case the $2l$ matrices (14) are independent and the number of independent parameters necessary to define the energy is $2l$. In the case of equivalent nucleons, however, the $2l$ matrices (14) are not independent. The proof of this fact and the number of independent parameters in this case can be found by the following group-theoretical reasoning. The operator $\mathbf{V}^{(1k)}$ with even k has the tensorial properties of the wave function of l^2 with $L=k$. Such a state belongs to the representation (20) or (00) of the rotation group in $2l+1$ dimensions $R(2l+1)$. The operator $[\mathbf{V}^{(1r)}\times\mathbf{V}^{(1s)}]^{(22)}$ corresponds in the above manner to a D state (of l^4) which belongs to a representation of $R(2l+1)$ contained in the products $(20)\times(00)$ and $(20)\times(20)$. The first product [which is in fact (20)], contains only one such state. The other product can be decomposed into $(00)+(20)+(22)+(40)$ of which to (00) belongs only an S state; there is only one state $(20)D$ (which is the state already mentioned) and the other D states are $(22)D$ and $(40)D$. But we have to take into consideration only states which have nonvanishing matrix elements between the states of odd L, which are the only triplet states of the configuration l^2 of equivalent nucleons (as the tensor forces vanish in this case either between two singlet states or between a singlet and a triplet state). The states of odd L (for l^2) belong to the representation (11); therefore, the relevant D states belong to a representation of $R(2l+1)$ which is contained in the product $(11)\times(11)$; this is either (20) or (22) but not (40). Therefore, the number of independent matrices (14) is equal to the number of states $(20)D$ and $(22)D$. This number is exactly the number of D states (of l^4) which belong to the representation [22] of the unitary group in $2l+1$ dimensions $U(2l+1)$, as this representation breaks upon restriction to $R(2l+1)$ as follows: $[22]\to(22)+(20)+(00)$ (and to (00) belong S states only). This latter number is given in a recent paper of Gamba and Verde.[11] Putting $j=l$, $J=2$ in their formula for $n=4$ we obtain $[4l/3]$ (the largest integer smaller than $4l/3$). This is the number of independent parameters necessary to define the energy in the l^n configuration of equivalent nucleons.

It is therefore possible in this case to express the $2l$ matrices (14) in terms of $[4l/3]$ of them; these might be chosen for the sake of convenience to have the lowest possible r and s. A given matrix (14) which is equal in the case of l^2 to a certain linear combination of the $[4l/3]$ matrices is equal to the same combination also in the case of l^n. In fact, in the case of l^2 the following relation exists:

$$[\mathbf{V}^{(1r)}\times\mathbf{V}^{(1s)}]^{(22)}=[\mathbf{s}_1\mathbf{u}_1{}^{(r)}\times\mathbf{s}_2\mathbf{u}_2{}^{(s)}]^{(22)}+[\mathbf{s}_2\mathbf{u}_2{}^{(r)}\times\mathbf{s}_1\mathbf{u}_1{}^{(s)}]^{(22)} \qquad (15)$$

(as $[\mathbf{s}_i\mathbf{u}_i{}^{(r)}\times\mathbf{s}_i\mathbf{u}_i{}^{(s)}]^{(22)}$ vanishes). In the case of l^n the analogous expression is

$$[\mathbf{V}^{(1r)}\times\mathbf{V}^{(1s)}]^{(22)}=\sum_{i\neq j}[\mathbf{s}_i\mathbf{u}_i{}^{(r)}\times\mathbf{s}_j\mathbf{u}_j{}^{(s)}]^{(22)}. \qquad (16)$$

Therefore, if the expression of

$$[\mathbf{s}_i\mathbf{u}_i{}^{(r)}\times\mathbf{s}_j\mathbf{u}_j{}^{(s)}]^{(22)}+[\mathbf{s}_j\mathbf{u}_j{}^{(r)}\times\mathbf{s}_i\mathbf{u}_i{}^{(s)}]^{(22)}$$

as a definite linear combination is valid for any pair ij, it is valid also for their sum (16). These facts facilitate essentially the calculation as it is rather easy to construct (14) for l^2 by means of (11) and (12), and then express all the matrices (14) in terms of $[4l/3]$ of them. As a result, one has to calculate in the case of l^n only $[4l/3]$ matrices (14) (with lowest possible r and s).

IV. THE ENERGY MATRIX OF THE CONFIGURATION d^n

In order to see an example how the procedure described above is carried out, we give in detail the case of d^n of equivalent nucleons. The matrices (14) which enter the calculation are $[\mathbf{V}^{(12)}\times\mathbf{V}^{(10)}]^{(22)}$, $[\mathbf{V}^{(12)}\times\mathbf{V}^{(12)}]^{(22)}$, $[\mathbf{V}^{(14)}\times\mathbf{V}^{(12)}]^{(22)}$, and $[\mathbf{V}^{(14)}\times\mathbf{V}^{(14)}]^{(22)}$. All of them can be expressed in terms of $[8/3]=2$ of them, say, $[\mathbf{V}^{(12)}\times\mathbf{V}^{(10)}]^{(22)}$ and $[\mathbf{V}^{(12)}\times\mathbf{V}^{(12)}]^{(22)}$. After the calculation of these four matrices for d^2, we find the relations

$$\begin{aligned}[\mathbf{V}^{(14)}\times\mathbf{V}^{(12)}]^{(22)}&=-\frac{1}{9}[\mathbf{V}^{(12)}\times\mathbf{V}^{(10)}]^{(22)}\\&\quad-\frac{5}{9}[\mathbf{V}^{(12)}\times\mathbf{V}^{(12)}]^{(22)},\\[\mathbf{V}^{(14)}\times\mathbf{V}^{(14)}]^{(22)}&=-\frac{5\sqrt{22}}{54}[\mathbf{V}^{(12)}\times\mathbf{V}^{(10)}]^{(22)}\\&\quad+\frac{5\sqrt{22}}{54}[\mathbf{V}^{(12)}\times^{(12)}]^{(22)}.\end{aligned} \qquad (17)$$

[11] A. Gamba and M. Verde, Nuovo cimento **IX**, 544 (1952).

Introducing these relations into (10) and inserting there the proper values of the k, r, and s, we can express the energy matrix of the d^n configuration (of equivalent nucleons) by means of the closed formula

$$\begin{aligned}(d^n\upsilon SL\|\sum_{i<j}S_{ij}V(r_{ij})\|d^n\upsilon S'L')&\\ =A(d^n\upsilon SL\|[\mathbf{V}^{(12)}\times\mathbf{V}^{(10)}]^{(22)}\|d^n\upsilon S'L')&\\ +B(d^n\upsilon SL\|[\mathbf{V}^{(12)}\times\mathbf{V}^{(12)}]^{(22)}\|d^n\upsilon S'L')&\\ =A(S\|S\|S)W(1S1S';S2)(d^n\upsilon SL\|V^{(12)}\|d^n\upsilon S'L')&\\ +B5\sum_{S''L''}(d^n\upsilon SL\|V^{(12)}\|d^n\upsilon S''L'')&\\ \times(d^n\upsilon S''L''\|V^{(12)}\|d^n\upsilon S'L')&\\ \times W(1S1S';S''2)W(2L2L';L''2).&\quad(18)\end{aligned}$$

In this formula A and B are the radial integrals

$$\begin{aligned}A=\frac{5}{\sqrt{21}}\int\int\Big[&-(r_1^2+r_2^2)f_0(r_1,r_2)\\ &-\frac{1}{7}(r_1^2+r_2^2)f_2(r_1,r_2)+\frac{4}{21}(r_1^2+r_2^2)f_4(r_1,r_2)\\ &+\frac{2}{3}2r_1r_2f_1(r_1,r_2)-\frac{91}{441}2r_1r_2f_3(r_1,r_2)\\ &-\frac{5}{99}2r_1r_2f_5(r_1,r_2)\Big]R_2^2(r_1)R_2^2(r_2)dr_1dr_2,\quad(19a)\end{aligned}$$

$$\begin{aligned}B=\frac{5}{\sqrt{21}}\int\int\Big[&\tfrac{1}{3}2r_1r_2f_1(r_1,r_2)-\frac{2}{9}2r_1r_2f_3(r_1,r_2)\\ &+\frac{5}{99}2r_1r_2f_5(r_1,r_2)\Big]R_2^2(r_1)R_2^2(r_2)dr_1dr_2.\quad(19b)\end{aligned}$$

These are the general expressions in which no reference to a special form of the potential or of the wave functions was done. In general, there exist between the $\varphi_k(r_1,r_2)$ defined by $V(r_{12})=\sum_{k=0}^{\infty}\varphi_k(r_1,r_2)P_k(\cos\omega_{12})$ and the $f_k(r_1,r_2)$, defined above, the relations

$$\begin{aligned}\varphi_k(r_1,r_2)=&(r_1^2+r_2^2)f_k(r_1,r_2)\\ &-\frac{k}{2k-1}2r_1r_2f_{k-1}(r_1,r_2)-\frac{k+1}{2k+3}2r_1r_2f_{k+1}(r_1,r_2).\quad(20)\end{aligned}$$

There are special cases, however, in which it is possible to express $(r_1^2+r_2^2)f_k(r_1,r_2)$ and $2r_1r_2f_k(r_1,r_2)$ in terms of the $\varphi_k(r_1,r_2)$. For the potential $V(r_{12})=1/r_{12}^3$ it is easily found that

$$\begin{aligned}(r_1^2+r_2^2)f_k(r_1,r_2)&\\ =\tfrac{1}{3}(2k+3)\varphi_k(r_1,r_2)+\tfrac{2}{3}(2k+1)&\\ \times[\varphi_{k+2}(r_1,r_2)+\varphi_{k+4}(r_1,r_2)+\cdots],&\quad(21a)\end{aligned}$$

$$\begin{aligned}2r_1r_2f_k(r_1,r_2)=&\tfrac{2}{3}(2k+1)\\ &\times[\varphi_{k+1}(r_1,r_2)+\varphi_{k+3}(r_1,r_2)+\cdots].\quad(21b)\end{aligned}$$

Therefore, the integrations in A and B are over

$$\begin{aligned}-\frac{5}{\sqrt{21}}\big[&(\varphi_0(r_1,r_2)-\tfrac{1}{5}\varphi_2(r_1,r_2))\\ &-\tfrac{2}{3}(\tfrac{1}{5}\varphi_2(r_1,r_2)-\tfrac{1}{9}\varphi_4(r_1,r_2))\big]\end{aligned}$$

and

$$\frac{50}{3\sqrt{21}}(\tfrac{1}{5}\varphi_2(r_1,r_2)-\tfrac{1}{9}\varphi_4(r_1,r_2)),$$

respectively. The M^0 and M^2 of Marvin's paper[3] are given in our notation by

$$\begin{aligned}M^0=-\frac{1}{24}\int\int&[\varphi_0(r_1,r_2)-\tfrac{1}{5}\varphi_2(r_1,r_2)]\\ &\times R_2^2(r_1)R_2^2(r_2)dr_1dr_2,\\ M^2=-\frac{1}{24}\int\int&[\tfrac{1}{5}\varphi_2(r_1,r_2)-\tfrac{1}{9}\varphi_4(r_1,r_2)]\\ &\times R_2^2(r_1)R_2^2(r_2)dr_1dr_2.\end{aligned}\quad(22)$$

Therefore, we obtain in this case,

$$\begin{aligned}A=\frac{120}{\sqrt{21}}(M^0-\tfrac{2}{3}M^2)=40\sqrt{21}\left(M_0-\frac{14}{3}M_2\right),&\\ B=-\frac{400}{\sqrt{21}}M^2=-\frac{19600}{\sqrt{21}}M_2.&\end{aligned}\quad(23)$$

Putting these values in (18), one obtains the results of Trees.[3]

If the wave functions of the harmonic oscillator are used, it is always possible to express the radial parameters defined above (in this case the A and B) as linear combinations of the integrals[4] I_l of the function $V(r_{12})$. The easiest way to do it is to express the $2r_1r_2f_k(r_1,r_2)$ with the help of (20) as (linear) functions of $\varphi_k(r_1,r_2)$ and $(r_1^2+r_2^2)f_k(r_1,r_2)$. These latter functions are the coefficients of $P_k(\cos\omega_{12})$ in the expansion

$$\begin{aligned}(r_1^2+r_2^2)\frac{V(r)}{r^2}=&\frac{1}{2}\frac{4R^2+r^2}{r^2}V(r)=\frac{1}{2}V(r)+\frac{2R^2}{r^2}V(r)\\ &=\sum_{k=0}^{\infty}(r_1^2+r_2^2)f_k(r_1,r_2)P_k(\cos\omega_{12}).\quad(24)\end{aligned}$$

The radial integrals over these coefficients can be evaluated by the method of Sec. 5 of reference 4; the only difference is the appearance of the function $\frac{1}{2}(4R^2+r^2)V(r)/r^2$ instead of $V(r)$. The integral I_0 of $V(r)/r^2$ as well as I_0 of $V(r)$, which appear in the course of the calculation must disappear in the results. For the case of d^n the results are

$$\begin{aligned}A=&-(5/12\sqrt{21})(7I_1-20I_2+21I_3),\\ B=&\tfrac{1}{6}\sqrt{(7/3)}(7I_1-5I_2).\end{aligned}\quad(25)$$

V. TRANSITION TO *jj* COUPLING

In the jj coupling scheme it is not convenient to work with the double tensors $\mathbf{s}_i\mathbf{u}_i^{(k)}$ as these are no more irreducible. We shall decompose such double tensors into a sum of tensors $\mathbf{t}_i^{(1k)K}$ of degree K, irreducible with respect to $\mathbf{j}_i$. This decomposition is given by

$$t_{iQ}^{(1k)K}=[\mathbf{s}_i\times\mathbf{u}_i^{(k)}]_Q^{(K)}=\sum_{\rho q}s_{i\rho}u_{iq}^{(k)}(1\rho kq|\,1kKQ). \tag{26}$$

It can be shown that from this definition it follows that $\mathbf{t}_i^{(1k)K}$ has nonvanishing matrix elements between states with the same j_i only if $(-1)^K=(-1)^{1+k}$; this restricts the values of K, appearing in the calculation of a given configuration, to $k+1$ and $k-1$. Using the relation

$$\begin{aligned}&([\mathbf{T}_1^{(\kappa_1)}\times\mathbf{T}_2^{(\kappa_2)}]^{(\kappa)}\cdot[\mathbf{U}_1^{(k_1)}\times\mathbf{U}_2^{(k_2)}]^{(\kappa)})\\&=\sum_k(-1)^{\kappa_1+k_2}(2\kappa+1)W(\kappa k_1\kappa_2k_2;k\kappa)\\&\quad\times([\mathbf{T}_1^{(\kappa_1)}\times\mathbf{U}_1^{(k_1)}]^{(k)}\cdot[\mathbf{T}_2^{(\kappa_2)}\times\mathbf{U}_2^{(k_2)}]^{(k)}),\end{aligned} \tag{27}$$

we find for the interaction (6) between two nucleons the expression

$$V_{12}=\sum_{kk'K}A_{kk'}(\mathbf{t}_1^{(1k)K}\cdot\mathbf{t}_2^{(1k')K}). \tag{28}$$

Here the coefficients $A_{kk'}$ are sums of definite radial integrals, easily determined from (6) by means of (27).

From this expression the energy of a state with a definite J (the energy matrix is diagonal with respect to the total angular momentum J) can be found by use of the formulas of tensor algebra and the usual methods of spectroscopy.

The equation which should be used is II (33):

$$\begin{aligned}(\alpha JM|\,(\mathbf{T}_a^K\cdot\mathbf{T}_b^K)\,|\alpha'JM)&=\frac{1}{2J+1}\sum_{\alpha''J''}(-1)^{J-J''}\\&\quad\times(\alpha J\|T_a^K\|\alpha''J'')(\alpha''J''\|T_b^K\|\alpha'J).\end{aligned} \tag{29}$$

In order to calculate the energy levels in the case of two nucleons with l_1j_1 and l_2j_2, respectively, we have to use II (44) and[12]

$$\begin{aligned}(\tfrac{1}{2}lj\|t_i^{(1k)K}\|\tfrac{1}{2}lj)&=(3/2)^{\frac{1}{2}}(2j+1)(2K+1)^{\frac{1}{2}}\\&\times[(2l+2)W(l\tfrac{1}{2}j1;l+\tfrac{1}{2},\tfrac{1}{2})W(\tfrac{1}{2}ljk;l+\tfrac{1}{2},l)\\&\times W(1jkj;l+\tfrac{1}{2},K)+2lW(l\tfrac{1}{2}j1;l-\tfrac{1}{2},\tfrac{1}{2})\\&\quad\times W(\tfrac{1}{2}ljk;l-\tfrac{1}{2},l)W(1jkj;l-\tfrac{1}{2},K)].\end{aligned} \tag{30}$$

In the case of the j^n configuration we introduce the tensors $\mathbf{T}^{(1k)K}=\sum_{i=1}^n\mathbf{t}_i^{(1k)K}$ which operate on the coordinates of the whole group of the j nucleons. With the help of these tensors, the interaction (28), summed over all pairs ij of interacting nucleons, can be brought into the form

$$\begin{aligned}\sum_{i<j}V_{ij}&=\sum_{kk'K}A_{kk'}\sum_{i<j}(\mathbf{t}_i^{(1k)K}\cdot\mathbf{t}_j^{(1k')K})\\&=\tfrac{1}{2}\sum_{kk'K}A_{kk'}[(\mathbf{T}^{(1k)K}\cdot\mathbf{T}^{(1k')K})-\sum_{i=1}^n(\mathbf{t}_i^{(1k)K}\cdot\mathbf{t}_i^{(1k')K})]\\&=\tfrac{1}{2}\sum_{kk'K}A_{kk'}(\mathbf{T}^{(1k)K}\cdot\mathbf{T}^{(1k')K})\\&\quad-\frac{n}{2}\sum_{kk'K}A_{kk'}(\mathbf{t}_1^{(1k)K}\cdot\mathbf{t}_1^{(1k')K}).\end{aligned} \tag{31}$$

On the calculation of $(j^n\alpha J\|T^{(1k)K}\|j^n\alpha'J')$ it should be said what was said before on $(l^n\alpha SL\|V^{(1k)}\|l^n\alpha'S'L')$. Only if $n=2$ we have a simple expression

$$\begin{aligned}&(j^2J\|T^{(1k)K}\|j^2J')=(-1)^K[(-1)^J+(-1)^{J'}]\\&\times[(2J+1)(2J'+1)]^{\frac{1}{2}}W(jJjJ';jK)(j\|t_1^{(1k)K}\|j),\end{aligned} \tag{32}$$

in which $(j\|t_1^{(1k)K}\|j)$ is given by Eq. (30).

In the j^n configuration, tensors $\mathbf{T}^K$ with K odd [as are the tensors which appear in (31)] are representations of the infinitesimal operators of the group of transformations which leave invariant the wave function of j^2, $J=0$; this group is the symplectic group in $2j+1$ dimensions $-\mathrm{Sp}(2j+1)$. The tensors considered are therefore diagonal with respect to the quantum numbers which characterize these representations. In particular, in the case of the j^n configuration of equivalent nucleons tensors $\mathbf{T}^K$ with K odd are diagonal with respect to the seniority[1,10] and independent of n. The energy in this case, however, has also a term linear in n, which is equal to $\frac{1}{2}(n-v)E_0$, where E_0 is the energy of the state j^2, $J=0$.

The $A_{kk'}$ introduced in (28) can be defined as the radial parameters in the jj coupling scheme. In the nuclear configuration j^n the number of independent parameters is equal to the number of matrices $(\mathbf{T}^{(1k)K}\cdot\mathbf{T}^{(1k')K})$ with different K, which is $2j$. In the j^n configuration of equivalent nucleons, these matrices are not independent and the actual number of parameters in this case is the number of independent matrices $(\mathbf{T}^{(1k)K}\cdot\mathbf{T}^{(1k')K})$ (matrices $\mathbf{T}^{(1k)K}$ with the same K but different k are proportional). This number is obtained from an analogous argument to that adapted in the l^n configuration. The tensors $\mathbf{T}^K$ with odd K are now to be considered, instead of $\mathbf{V}^{(1k)}$ with even k, but the representation of $\mathrm{Sp}(2j+1)$ to which these tensors (regarded as states of j^2) belong is (20). Similarly, the antisymmetric wave functions of j^2 have even J (instead of the odd L values we had to consider before), but these belong now to the representation (11) of $\mathrm{Sp}(2j+1)$. We have to look for states with $J=0$ (instead of the D states) which belong to a representation, contained in (20)×(20) as well as in (11)×(11); this can be either (00) or (22) (to (20) does not belong a $J=0$ state). The representation [22] of $U(2j+1)$ (for j^4) breaks upon restriction to $\mathrm{Sp}(2j+1)$ into (00)+(11)+(22) of which

[12] This formula in a more general form as well as all the important formulas of the tensor algebra is presented in a paper which will be published by U. Fano and G. Racah.

TABLE I. Energies of the $(d_{5/2})^2$ and $(d_{5/2})^3$ configurations.

State	$(d_{5/2})^2$ Energy	State	$(d_{5/2})^3$ Energy
$J=4$	$\frac{1}{5}I_1 \quad -I_3$	$J=9/2$	$\frac{3}{5}I_1-\frac{18}{35}I_2+\frac{3}{25}I_3$
$J=2$	$\frac{1}{5}I_1-\frac{4}{5}I_2+\frac{23}{25}I_3$	$J=5/2$	$\frac{7}{5}I_1-2I_2+\frac{7}{5}I_3$
$J=0$	$\frac{7}{5}I_1-2I_2+\frac{7}{5}I_3$	$J=3/2$	$\frac{3}{5}I_1-\frac{12}{7}I_2+\frac{9}{5}I_3$

to (11) does not belong any term with $J=0$. As a result we obtain the required number by use of the formula given in reference 11 in the case $n=4$, $J=0$; this number is found to be $[(2j+2)/3]$.

It is therefore possible to express the $2j$ matrices $(\mathbf{T}^K\cdot\mathbf{T}^K)$ in terms of $[(2j+2)/3]$ of them. Also in this case we can find these expressions in the case of j^2 and these hold also in the case of j^n, although the reason given for this fact in the case of l^n is no more valid. Instead of it we have the situation that if

$$(j^2|(\mathbf{T}^K\cdot\mathbf{T}^K)|j^2)=\sum_{K'}a_{K'}(j^2|(\mathbf{T}^{K'}\cdot\mathbf{T}^{K'})|j^2), \quad (33)$$

in the case of j^n there exists the relation

$$(j^n|(\mathbf{T}^K\cdot\mathbf{T}^K)|j^n)=\sum_{K'}a_{K'}(j^n|(\mathbf{T}^{K'}\cdot\mathbf{T}^{K'})|j^n) +n(n-2)[\sum_{K'}a_{K'}(j^n|(\mathbf{t}_1{}^{K'}\cdot\mathbf{t}_1{}^{K'})|j^n) -(j^n|(\mathbf{t}_1{}^K\cdot\mathbf{t}_1{}^K)|j^n)]. \quad (34)$$

The second term on the right-hand side must vanish as it is the same for all the states and vanishes for $v=0$ (for which the products $(\mathbf{T}^K\cdot\mathbf{T}^K)$ with odd K vanish), which proves the statement. It may be noted that because of (15) we can apply the transformation (27) directly on (10) in which the matrices (14) are expressed by means of $[4l/3]$ of them, a fact which facilitates the calculation.

VI. THE LEVELS OF THE $(d_{5/2})^n$ CONFIGURATION

We can now write immediately down the energy matrix of the $(d_{5/2})^n$ configuration. In this case $[4\cdot 2/3]=2$, and also $[(2\cdot 5/2+2)/3]=2$, so that there are 2 independent parameters and starting from (18) no further reduction is necessary. Transformation of (18) with the help of (27) yields the final formula:

$$((d_{\frac{1}{2}})^nJM|\sum_{i<j}V_{ij}|(d_{\frac{1}{2}})^nJM) =-\frac{5}{2J+1}\Big[\frac{A}{\sqrt{15}}((d_{\frac{1}{2}})^nJ\|(\mathbf{T}^{(10)1}\cdot\mathbf{T}^{(12)1})\|(d_{\frac{1}{2}})^nJ) +B\frac{7}{10}\sqrt{\frac{7}{3}}((d_{\frac{1}{2}})^nJ\|(\mathbf{T}^{(12)1}\cdot\mathbf{T}^{(12)1})\|(d_{\frac{1}{2}})^nJ) +\frac{B}{35}\sqrt{\frac{7}{3}}((d_{\frac{1}{2}})^nJ\|(\mathbf{T}^{(12)3}\cdot\mathbf{T}^{(12)3})\|(d_{\frac{1}{2}})^nJ)\Big] +n\Big[-A\frac{6}{25}\sqrt{\frac{7}{3}}+B\frac{6}{35}\sqrt{\frac{7}{3}}\Big]. \quad (35)$$

As there are at most 6 equivalent nucleons in a $d_{5/2}$ state, the relevant configurations are $(d_{5/2})^2$ [which is equivalent to $(d_{5/2})^4$] and $(d_{5/2})^3$. We obtain the energies of these configurations by inserting in (35) the values of A and B from (25), and we write them down multiplied by 12 [in accordance with the usual definition $S_{12}=3(\boldsymbol{\sigma}_1\cdot\mathbf{r}_{12})(\boldsymbol{\sigma}_2\cdot\mathbf{r}_{12})/r_{12}{}^2-(\boldsymbol{\sigma}_1\cdot\boldsymbol{\sigma}_2)$]; the results are given in Table I.

In the short-range approximation,[4] I_2 and I_3 can be neglected in comparison to I_1 (it has no sense to use here the limit of a δ-function as then also I_1 vanishes). On the other hand, in the long-range limit, $I_1=I_2=I_3$. We can now see what are the energy values of the tensor forces in the $(d_{5/2})^2$ and $(d_{5/2})^3$ configurations. If the potential $V(r_{12})$ is negative (or positive and multiplied by P_x, which gives the same results in this case) the order of levels resulting from the tensor forces is $J=0$ (ground level), $J=2$, $J=4$ in $(d_{5/2})^2$ in the short-range approximation and up to the long-range limit (for reasonable form of the potential); in $(d_{5/2})^3$ the order will be $J=5/2$ (ground level), $J=3/2$, $J=9/2$. We see that the results for tensor forces are essentially those for short-range (attractive) ordinary forces, in spite of their very different appearance.

The author would like to express his sincere thanks to Professor G. Racah for many suggestions and discussions.

S-Matrix and Causality Condition. I. Maxwell Field

N. G. VAN KAMPEN
Institute for Advanced Study, Princeton, New Jersey
(Received October 22, 1952)

The general aim is to obtain maximum information about the S-matrix with a minimum of assumptions concerning the interaction. This program is carried through for the scattering of the electromagnetic field by a fixed center. The center is assumed spherically symmetric and of finite size, so that the causality condition can be applied. From this condition it follows rigorously that the S-matrix has a one-valued analytic continuation, whose only singularities are poles in the lower half-plane, and whose behavior at infinity can be specified. Particular consequences are: (i) the analytic properties of Wigner's function R; (ii) the integral relation connecting real and imaginary parts of S; (iii) relations connecting the sum of the oscillator strengths with the scattering cross section.

I. INTRODUCTION

THE S-matrix was introduced by Heisenberg[1] as a device to describe scattering processes without any specific assumptions about the interaction. To compute the S-matrix in a particular case, of course, a certain interaction has to be assumed. But some general properties (e.g., unitarity) could be formulated in terms sufficiently general to raise the hope that they were of more universal character. For their derivation, however, a more or less specific model had to be used.[1,2] This is justifiable from a heuristic point of view, but an attempt to treat the S-matrix without reference to any particular kind of interaction seems none the less desirable. The problem is then no longer: what mathematical properties of S can be derived from the various physical properties of the interaction?—but rather: how are the mathematical properties of S related to actual observations?

Since this question cannot be answered here in its full generality, we shall restrict our investigations in three respects. In the first place, only the scattering of an electromagnetic field by a fixed center is treated. The field is classical, which is equivalent to saying that only the one-photon part is taken into account.[3] Secondly, the scattering center (which for brevity will be called the "core") is assumed to be spherically symmetric, and also invariant with respect to space reflection. In terms of observations, this amounts to assuming that not only multipole waves of different order l, but also the electric and the magnetic multipoles are scattered independently. Thirdly, it is supposed that in all experiments the energy and the frequency (energy per photon) are conserved, and that the "causality condition" is satisfied. These properties are not held to be self-evident, but without these restrictions the analysis would be very cumbersome.

The causality condition states that no scattered wave can be observed until the incident wave packet has reached the core. Obviously it can only be applied when the core has a finite size, which will therefore be postulated throughout this work. This condition turns out to be a powerful aid, because it entails the analytic character of the S-matrix (as a function of the frequency). On the basis of a similar condition, Toll and Wheeler[4] derived the Kramers-Kronig dispersion formula[5,6] for the propagation of light in a medium. It has also been used in electric circuit theory,[7] and its application to the S-matrix was suggested by Kronig.[8]

Schützer and Tiomno[9] considered the scattering of a Schrödinger particle by a core of finite size. In that case, however, the Fourier decomposition of any solution of the Schrödinger equation contains only components with positive E, so that it is impossible to construct a wave packet that is rigorously zero up to a certain time. Hence, the causality condition has to be formulated by means of wave packets that are arbitrarily small in the past, which would make the mathematical treatment more involved. Complications of the same kind arise for relativistic particles, because the values of E between $-m$ and $+m$ are lacking in the Fourier decomposition. This is the reason why we here treat the electromagnetic field only.

Many of the resulting formulas have been found previously starting from more or less special models,[10–12] usually for the scattering of nonrelativistic particles by nuclei. A rather more general approach was attempted by Heisenberg[13] and by Hu,[14] based on the complete-

[1] W. Heisenberg, Z. Physik **120**, 513, 673 (1943).
[2] C. Møller, Kgl. Danske Videnskab. Selskab, Mat.-fys. Medd. **23**, No. 1 (1945); **22**, No. 19 (1946).
[3] H. A. Kramers, "Quantentheorie des Elektrons und der Strahlung," *Hand- und. Jahrbuch der Chem. Physik* (Akademische Verlagsgesellschaft, Leipzig, 1938), p. 439.
[4] J. S. Toll and J. A. Wheeler, unpublished; J. S. Toll, thesis, Princeton, 1952.
[5] H. A. Kramers, Atti cong. intern. fisici, Como, 1927, Vol. 2, p. 545.
[6] R. de L. Kronig, J. Opt. Soc. Am. **12**, 547 (1926).
[7] B. Gross, Phys. Rev. **59**, 748 (1941); R. Kronig, Nederland. Tijdschr. Natuurk. **9**, 402 (1942).
[8] R. Kronig, Physica **12**. 543 (1946).
[9] W. Schützer and J. Tiomno, Phys. Rev. **83**, 249 (1951).
[10] G. Breit and E. Wigner, Phys. Rev. **49**, 519 (1936); P. L. Kapur and R. Peierls, Proc. Roy. Soc. (London) **A166**, 277 (1938); A. J. F. Siegert, Phys. Rev. **56**, 750 (1939); E. P. Wigner and L. Eisenbud, Phys. Rev. **72**, 29 (1947); M. Moshinski, Phys. Rev. **81**, 347 and **84**, 525 (1951); J. Humblet, Mém. Soc. Roy. Scient. Liège **12**, fasc. 4 (1952).
[11] H. A. Bethe and G. Placzek, Phys. Rev. **51**, 450 (1937).
[12] Feshbach, Peaslee, and Weisskopf, Phys. Rev. **71**, 145 (1947).
[13] W. Heisenberg, Z. Naturforsch. **1**, 608 (1946).
[14] N. Hu, Phys. Rev. **74**, 131 (1948).

ness of the solutions of the wave equation (which is related to the causality condition). However, since they used the asymptotic expression instead of the wave function itself, this may lead to incorrect results, as exemplified by the existence of redundant zeros.[15]

II. DEFINITION OF THE S-MATRIX

The S-matrix is defined, in general terms, as the matrix that transforms the wave function describing the ingoing field into the wave function of the outgoing field. For a more specific definition the free-field equations have to be used, and a particular set of field quantities has to be chosen in which to express the transformation. In the present section this is briefly done for the Maxwell field, and the well-known properties (9) of S are derived.

The electromagnetic field outside the scattering center may be described by the complex vector field $\mathbf{F}=\mathbf{E}+i\mathbf{H}$, obeying the equations (we put throughout $c=1$)

$$\partial\mathbf{F}/\partial t=-i\,\mathrm{curl}\mathbf{F},\quad \mathrm{div}\mathbf{F}=0.$$

The solutions are conveniently expressed in terms of a complex Debye potential[16,17] $u(\mathbf{r},t)$:

$$\mathbf{F}(\mathbf{r},t)=(\mathrm{curl}+i\partial_t)\,\mathrm{curl}\,\mathbf{r}u(\mathbf{r},t), \tag{1}$$

$$(\Delta-\partial_t^2)u=0. \tag{2}$$

On introducing polar coordinates $\mathbf{r}=(r,\theta,\phi)=(r,\Omega)$ the asymptotic part of any solution of (2) is a superposition of multipole waves

$$u(r,\Omega,t)\simeq\sum_{l,m}\frac{2Y_{lm}(\Omega)}{[2l(l+1)]^{\frac{1}{2}}}\int_{-\infty}^{+\infty}\left\{B_{lm}(k)\frac{e^{ikr}}{ikr}-(-1)^lA_{lm}(k)\frac{e^{-ikr}}{ikr}\right\}e^{-ikt}dk. \tag{3}$$

The first term consists of outgoing waves, the second of ingoing waves. The sign in front of $A_{lm}(k)$ has been chosen such that absence of scattering is characterized by $A_{lm}(k)=B_{lm}(k)$. The asymptotic expression of the field $\mathbf{F}$ can be derived from (3) by means of (1); one finds $F_r=0$, and

$$\begin{aligned}F_\theta+iF_\varphi&=-\frac{4}{r}\sum_{lm}\left(\frac{\partial}{\partial\theta}+\frac{i}{\sin\theta}\frac{\partial}{\partial\varphi}\right)\times\frac{(-1)^lY_{lm}(\Omega)}{[2l(l+1)]^{\frac{1}{2}}}\int_{-\infty}^{+\infty}A_{lm}(k)e^{-ik(r+t)}dk,\\ F_\theta-iF_\varphi&=-\frac{4}{r}\sum_{lm}\left(\frac{\partial}{\partial\theta}-\frac{i}{\sin\theta}\frac{\partial}{\partial\varphi}\right)\times\frac{Y_{lm}(\Omega)}{[2l(l+1)]^{\frac{1}{2}}}\int_{-\infty}^{+\infty}B_{lm}(k)e^{ik(r-t)}dk.\end{aligned} \tag{4}$$

From this there follows for the total energy entering a sphere with large radius r

$$\int_{-\infty}^{+\infty}dt\oint r^2d\Omega\frac{1}{16\pi}|F_\theta+iF_\varphi|^2=\sum_{lm}\int_{-\infty}^{+\infty}|A_{lm}(k)|^2dk; \tag{5}$$

and a similar expression with $B_{lm}(k)$ for the outgoing energy.

Let it be supposed that these energy amounts are finite. It then follows from the square integrability of $F_\theta+iF_\varphi$ and $F_\theta-iF_\varphi$ that a Fourier expansion (4) is possible. On the other hand, there is no physical justification for imposing square integrability on u; the expansion (3) should therefore be considered as a formal abbreviation for the corresponding expansion (4) of $\mathbf{F}$. Hence we shall only deal with incident wave packets of finite energy; they correspond to square integrable $A_{lm}(k)$. The square integrability of $B_{lm}(k)$ then follows from the conservation of energy.

The coefficients $A_{lm}(k)$ and $B_{lm}(k)$ are connected by a relation expressing the scattering properties of the core. The following properties will be postulated throughout.

(a) *Superposition*

The connection is linear in the following restricted sense: to an ingoing wave $A_{lm}(k)=A_{lm}^{(1)}(k)+A_{lm}^{(2)}(k)$ corresponds the outgoing wave $B_{lm}(k)=B_{lm}^{(1)}(k)+B_{lm}^{(2)}(k)$; and to $cA_{lm}(k)$ corresponds $cB_{lm}(k)$ if c is a *real* constant. From this it follows that

$$B_{lm}(k)=\sum_{l'm'}\int_{-\infty}^{+\infty}\{S'(k;l,m|k';l',m')A_{l'm'}(k')+S''(k;l,m|k';l',m')A_{l'm'}{}^*(k')\}dk,$$

where S' and S'' are integral kernels that are not more singular than $\delta(k-k')$.

(b) *Spherical Symmetry*

On a rotation about the origin, $A_{lm}(k)$ and $A_{l,-m}{}^*(k)$ transform like $Y_{lm}{}^*$, i.e., diagonal in l and irreducible in m. Hence

$$\begin{aligned}S'(k;l,m|k';l',m')&=\delta_{ll'}\delta_{mm'}S_l'(k|k'),\\ S''(k;l,m|k';l',m')&=\delta_{ll'}\delta_{m,-m'}S_l''(k|k').\end{aligned}$$

(c) *Conservation of Frequency*

The frequency of the outgoing wave is equal to that of the ingoing wave:

$$\begin{aligned}S_l'(k|k')&=\tfrac{1}{2}\delta(k-k')S_l^{(1)}(k)+\tfrac{1}{2}\delta(k+k')S_l^{(2)}(k),\\ S_l''(k|k')&=\tfrac{1}{2}\delta(k-k')S_l^{(3)}(k)+\tfrac{1}{2}\delta(k+k')S_l^{(4)}(k).\end{aligned}$$

(d) *Invariance for Space Reflection*

This implies that if $\mathbf{F}(\mathbf{r},t)$ is a possible scattering state, so is

$$\bar{\mathbf{F}}(\mathbf{r},t)\equiv\mathbf{F}^*(-\mathbf{r},t).$$

[15] S. T. Ma, Phys. Rev. **71**, 195 (1947); J. Meixner, Z. Naturforsch. **3a**, 75 (1948).
[16] P. Debye, Ann. Physik **30**, 57 (1909).
[17] J. Meixner, Z. Naturforsch **3a**, 507 (1948).

By substituting in (4) one finds

$$\bar{A}_{lm}(k)=(-1)^l A_{l,-m}{}^*(-k),\ \bar{B}_{lm}(k)=(-1)^l B_{l,-m}{}^*(-k).$$

In order that $\bar{A}$ and $\bar{B}$ satisfy the same relation as A and B, it is necessary that

$$S_l{}^{(j)}(-k)=S_l{}^{(j)*}(k) \quad \text{for} \quad j=1,2,3,4.$$

The relation between A and B is now determined by four complex functions $S_l{}^{(j)}(k)$ of $k>0$ for each $l\geqslant 1$. For our purpose to find more information about these functions, it is sufficient to consider one particular l and to take $m=0$. One may then drop these subscripts and write this relation in the form of a square matrix for each positive value of k

$$\begin{pmatrix} B(k) \\ B(-k) \\ B^*(k) \\ B^*(-k) \end{pmatrix} = \tfrac{1}{2} \begin{pmatrix} S^{(1)} & S^{(2)} & S^{(3)} & S^{(4)} \\ S^{(2)*} & S^{(1)*} & S^{(4)*} & S^{(3)*} \\ S^{(3)*} & S^{(4)*} & S^{(1)*} & S^{(2)*} \\ S^{(4)} & S^{(3)} & S^{(2)} & S^{(1)} \end{pmatrix} \begin{pmatrix} A(k) \\ A(-k) \\ A^*(k) \\ A^*(-k) \end{pmatrix}. \tag{6}$$

This matrix can be reduced by splitting up the four-component vectors A and B according to

$$\begin{aligned}(A(k), A(-k), A^*(k), A^*(-k)) &= (A^{\mathrm{e}}(k), A^{\mathrm{e}*}(k), A^{\mathrm{e}*}(k), A^{\mathrm{e}}(k)) \\ &\quad + (A^{\mathrm{m}}(k), -A^{\mathrm{m}*}(k), A^{\mathrm{m}*}(k), -A^{\mathrm{m}}(k)).\end{aligned}$$

The wave packets with superscript $^{\mathrm{e}}$ are characterized by $A(-k)=A^*(k)$, so that the corresponding u is real. Hence, they represent superpositions of electric 2^l-pole waves, while A^{m} and B^{m} are magnetic 2^l-pole waves. Substitution in (6) yields

$$B^{\mathrm{e}}(k)=\tfrac{1}{2}(S^{(1)}+S^{(4)})A^{\mathrm{e}}(k)+\tfrac{1}{2}(S^{(2)}+S^{(3)})A^{\mathrm{e}*}(k), \tag{7a}$$

$$B^{\mathrm{m}}(k)=\tfrac{1}{2}(S^{(1)}-S^{(4)})A^{\mathrm{m}}(k)+\tfrac{1}{2}(S^{(2)}-S^{(3)})A^{\mathrm{m}*}(k), \tag{7b}$$

where k ranges from $-\infty$ to $+\infty$.

(e) *Conservation of Energy*

Finally, we postulate that no energy is exchanged between the radiation and the core, which according to (5) is expressed by

$$\sum_{lm}\int_{-\infty}^{+\infty}|B_{lm}(k)|^2dk=\sum_{lm}\int_{-\infty}^{+\infty}|A_{lm}(k)|^2dk.$$

In general this means that the relation between A and B is unitary, from which for the specific relation (7a) it can be inferred that either $S^{(1)}+S^{(4)}$ or $S^{(2)}+S^{(3)}$ must vanish. In the latter case

$$B^{\mathrm{e}}(k)=S^{\mathrm{e}}(k)A^{\mathrm{e}}(k), \quad |S^{\mathrm{e}}(k)|=\tfrac{1}{2}|S^{(1)}+S^{(4)}|=1.$$

One is inclined to reject the other case for the reason that there is no continuous transition to the case of no scattering possible. A better reason, however, will be given in the next section: it does not satisfy the causality condition.

The same argument applies to (7b), so that one may write for each particular electric or magnetic multipole wave

$$B(k)=S(k)A(k), \quad (-\infty<k<+\infty) \tag{8}$$

$$S(-k)=S^*(k), \quad S(k)S^*(k)=1. \tag{9}$$

It is sufficient to treat the scattering of electric multipole waves only. For the incident wave packet $A(k)$ may then be chosen any square integrable function that satisfies

$$A(-k)=A^*(k). \tag{10}$$

III. THE CAUSALITY CONDITION

For the following it is essential to assume that the core has a finite size; in other words, that there is a sphere of radius a $(0\leqslant a<\infty)$ outside of which the free-field equations are valid. Let there be an incident wave packet that is known to be rigorously zero at some large distance r_1 for all time $t<t_1$. Outgoing waves cannot be produced until this packet has reached the core; that is, not until $t=t_1+(r_1-a)$. Hence, the outgoing field at the large distance r_2 must be zero until $t=t_1+(r_1-a)+(r_2-a)$. This imposes a restriction on the S-matrix, which will be called the "causality condition" (see reference 9). It is based only on the assumptions that free wave packets do not propagate faster than light, and that they can be decomposed into ingoing and outgoing waves whose interaction is localized in the core. We proceed to investigate to what property of S it corresponds.

To avoid irrelevant complications, it is convenient to take first a point-core, so that a can be taken zero. Then the causality condition states that, if the ingoing wave packet vanishes for $t<-r$, the outgoing wave packet must vanish for $t<+r$. According to (3) or (4), the vanishing of the ingoing wave for $r+t<0$ is tantamount to $A(k)$ being the Fourier transform of a function that is zero for negative values of its argument. From this it can be concluded that $A(k)$ can be continued as a regular analytic function in the upper half of the complex k-plane, as is more precisely stated in the following mathematical theorem.[18,19]

Necessary and sufficient for a square integrable function $A(k)$ $(-\infty<k<+\infty)$ to be the Fourier transform of a function that vanishes for negative values is the existence of an analytic function $A(k+i\gamma)$ of $k+i\gamma=\lambda$ for $\gamma>0$, such that (i) $A(k+i\gamma)\to A(k)$ if $\gamma\to 0$, for almost all values of k; (ii) $A(\lambda)$ is regular for $\gamma>0$; (iii) $\int_{-\infty}^{+\infty}|A(k+i\gamma)|^2dk<M$ for $\gamma\geqslant 0$, M independent of γ. This theorem plays a central role in the present work. When we say in the following proof that a function of k is regular in the upper half-plane, we mean that it has the property described in the theorem. The abbreviations I_+, I_-, I_0 will be used to denote the upper half-plane, the lower half-plane, and the real axis.

[18] R. E. A. C. Paley and N. Wiener, *Fourier Transforms in the Complex Domain* (American Mathematical Society, New York, 1934), p. 8.

[19] E. C. Titchmarsh, *Introduction to the Theory of Fourier Integrals* (Clarendon Press, Oxford, 1937), Chapter V.

The requirement of the causality condition that the outgoing wave must vanish for $t<r$ is tantamount to $B(k)$ being the Fourier transform of a function that is zero for negative values of its argument, according to (4). Since $B(k)$ is square integrable, it can be concluded that $B(k)$ must be regular in I_+. Hence, the causality condition entails the following property of S: whenever $A(k)$ is square integrable and regular in I_+, and satisfies (10), the same is true for $S(k)A(k)$. This enables us to extend the definition of S to I_+ by putting

$$B(\lambda)=S(\lambda)A(\lambda). \quad (\lambda=k+i\gamma, \gamma>0) \tag{11}$$

Since $A(\lambda)$ and $B(\lambda)$ are analytic and regular in I_+, so is $S(\lambda)$; it cannot have poles at the zeros of $A(\lambda)$, because (11) must hold true for any $A(\lambda)$ regular in I_+. When γ goes to zero, then $A(\lambda)\to A(k)$, $B(\lambda)\to B(k)$ for almost all k, and consequently $S(\lambda)\to S(k)$ because of (8).

The definition of S can be extended to I_- by putting

$$S(k+i\gamma)=[S(k-i\gamma)]^{*-1}. \quad (\gamma<0)$$

This is a one-valued analytic function with no other singularities than poles corresponding to the zeros in I_+. For $\gamma\to 0$ it tends to $S(k)$, owing to (9). Thus, $S(\lambda)$ is defined in I_+ and in I_- and has the boundary value $S(k)$ on I_0; it then follows from the Schwarz reflection principle[20] that $S(\lambda)$ is analytic in the whole plane but for the poles in I_-.

It may be possible to prove directly that $S(\lambda)$ is bounded in I_+ by applying condition (iii) of the theorem to $B(\lambda)$. However, it is simpler to use an additional theorem,[19] which states that any function $A(\lambda)$ with the properties (i), (ii), (iii) satisfies

$$A(\lambda)=\frac{1}{2\pi i}\int_{-\infty}^{+\infty}\frac{A(k')}{k'-\lambda}dk'. \quad (\lambda \text{ in } I_+) \tag{12}$$

Choosing $A(k)=i(k+i\beta)^{-1}$ with $\beta>0$, and writing this equation (12) for the corresponding $B(\lambda)=iS(\lambda)(\lambda+i\beta)^{-1}$, one finds

$$\frac{S(\lambda)}{\lambda+i\beta}=\frac{1}{2\pi i}\int_{-\infty}^{+\infty}\frac{S(k')dk'}{(k'-\lambda)(k'+i\beta)}. \quad (\gamma,\beta>0) \tag{13}$$

Since the right-hand side is bounded for $|\lambda|\to\infty$, S cannot become infinite more strongly than $|\lambda|$. It then follows from Phragmén-Lindelöf's theorem[20] that actually S must be bounded, and even

$$|S(\lambda)|<1 \text{ for } \lambda \text{ in } I_+.$$

Incidentally, it can now be shown why the alternative possibility mentioned in Sec. II under (*e*) does not comply with the causality condition. Suppose it did; then the wave packet $A(k)=i(k+i\beta)^{-1}$ would correspond to an outgoing wave packet

$$B(k)=S(k)A(-k)=iS(k)(i\beta-k)^{-1},$$

which would be regular in I_+. Consequently, $S(\lambda)$ would be regular in I_+ with a zero at $i\beta$. This cannot be true for all $\beta>0$.

The properties of the function S may be summarized as follows. $S(\lambda)$ *is a meromorphic function, which maps the real axis onto the unit circle, the upper half-plane into the interior and the lower half-plane into the exterior; the imaginary axis is mapped onto the real axis.* We now proceed to derive from these properties a product expansion for $S(\lambda)$.

Let the zero's of $S(\lambda)$ be denoted by $\Lambda_\nu=K_\nu+i\Gamma_\nu$, $(\Gamma_\nu>0)$, so that the poles are Λ_ν^*. If the following product over all zeros,

$$\prod_\nu\frac{\lambda-\Lambda_\nu}{\lambda-\Lambda_\nu^*}, \tag{14}$$

is convergent, it is easily seen to share all the properties mentioned above for $S(\lambda)$. Dividing $S(\lambda)$ by (14) we are left with another function with the same properties, which moreover has neither zeros nor poles. It must have the form $\pm e^{-2i\alpha\lambda}$ with $\alpha\leqslant 0$ (see below), so that

$$S(\lambda)=\pm e^{-2i\alpha\lambda}\prod_\nu\frac{\lambda-\Lambda_\nu}{\lambda-\Lambda_\nu^*}. \tag{15}$$

Because of (9) the zeros Λ_ν must be symmetrical with respect to the imaginary axis. If Λ_n denotes a zero in the first quadrant ($K_n>0$, $\Gamma_n>0$), then $-\Lambda_n^*$ is a zero in the second quadrant, and Λ_n^* and $-\Lambda_n$ are poles. In addition there may be unpaired zeros on the imaginary axis; they will be denoted by $iL_m(L_m>0)$, with corresponding poles $-iL_m$. Then (15) may be written

$$S(\lambda)=\pm e^{-2i\alpha\lambda}\prod_n\frac{(\lambda-\Lambda_n)(\lambda+\Lambda_n^*)}{(\lambda-\Lambda_n^*)(\lambda+\Lambda_n)}\prod_m\frac{iL_m-\lambda}{iL_m+\lambda}. \tag{16}$$

The case of an extended core can be treated in a similar way. One finds the same properties for $S(\lambda)$, except the boundedness in I_+. If the core can be enclosed in a sphere with radius a, it is found that now $e^{2i\alpha\lambda}S(\lambda)$ must be bounded in I_+. This leads to the same expression (16), but with the weaker restriction for α

$$\alpha\leqslant a. \tag{17}$$

The constant a is only defined as an upper limit for the radius of the core and has to be guessed from some rough model. The constant α is uniquely defined, but can only be determined by actual calculation based on a specific model, or else by experiment. It plays the part of an effective radius, because on a large sphere of radius r no scattered waves are observed until a time $t=2(r-\alpha)$ after the incident wave front entered the sphere. However, it is impossible to conclude from the causality condition that negative α cannot occur.

In order to justify (16) with (17) it has to be shown that both infinite products are convergent, and that the remaining factor is necessarily of the form $\pm e^{-2i\alpha\lambda}$ with

[20] E. C. Titchmarsh, *The Theory of Functions* (Clarendon Press, Oxford, 1939), second edition.

$\alpha \leqslant a$. The criterion for the first product to be (absolutely) convergent is the convergence of the sum

$$\sum \left| \frac{(\lambda-\Lambda_n)(\lambda+\Lambda_n^*)}{(\lambda-\Lambda_n^*)(\lambda+\Lambda_n)} - 1 \right| = 4|\lambda| \sum \frac{\Gamma_n}{|(\lambda-\Lambda_n^*)(\lambda+\Lambda_n)|}.$$

Since $|\Lambda_n| \to \infty$ (the zeros cannot have an accumulation point), this depends on the convergence of $\sum \Gamma_n/|\Lambda_n|^2$. Now, by Carleman's theorem,[20] the convergence of

$$\sum \frac{\Gamma_\nu}{|\Lambda_\nu|^2} = \sum \frac{\Gamma_n}{|\Lambda_n|^2} + \sum \frac{1}{L_m} \tag{18}$$

follows from the fact that $e^{2i\alpha\lambda}S(\lambda)$ is regular and bounded in I_+. Hence, the first product in (16) is convergent, uniformly in any finite closed region not containing a pole, so that it is a meromorphic function with poles Λ_n^* and $-\Lambda_n$. Similarly from the convergence of the last term in (18) it follows that the second product in (16) is convergent and represents a meromorphic function with poles $-iL_m$.

Now consider the function $f_N(\lambda)$, defined by

$$f_N(\lambda) = e^{2i\alpha\lambda}S(\lambda) \Big/ \prod_{n=1}^{N} \frac{(\lambda-\Lambda_n)(\lambda+\Lambda_n^*)}{(\lambda-\Lambda_n^*)(\lambda+\Lambda_n)} \prod_{m=1}^{N} \frac{iL_m-\lambda}{iL_m+\lambda}.$$

This function is again regular and bounded in I_+ and has modulus 1 on I_0; hence, by Phragmen-Lindelöf's theorem $|f_N(\lambda)| \leqslant 1$ in I_+. As the products are convergent for $N \to \infty$, the limit $f(\lambda) = \lim f_N(\lambda)$ exists, and it can easily be seen that it has the same properties. Moreover, it has no zeros or poles, and can therefore be written $f = e^{u+iv}$, where $u+iv$ is an entire function. Its real part u is negative in I_+ and positive in I_-, so that on I_0

$$0 \geqslant \partial u/\partial\gamma = -\partial v/\partial k. \quad (\gamma = 0)$$

Hence $v(k)$ increases monotonely with k and assumes any real value not more than once. Consequently, $u+iv$ assumes each purely imaginary value at most once, and must therefore be a linear function:

$$u+iv = 2i\alpha_1\lambda + \alpha_2;$$

and obviously $\alpha_1 \geqslant 0$, $\alpha_2 = 0$ or π. This completes the proof that $S(\lambda)$ has the form (16) (with $\alpha = a - \alpha_1$).

It should be noted that only the absolute convergence of the products in (16) could be proved, while the convergence of (14) may depend on the order in which the Λ_ν are numbered. (When in the following we use, nevertheless, (15), it is only meant to be a short writing for (16). Also it is not possible to conclude anything about the order of $S(\lambda)$ as a meromorphic function. The reason is that there is no other information about the density of the zeros and poles than the convergence of the Carleman sum (18), which does not prevent them from clustering about the real axis. It is remarkable that this sum is also physically important: it is the sum of the oscillator strengths, as will be shown in the next section. At this point its relation with scattering data may be established by taking the logarithmic derivative of $S(\lambda)$ at $\lambda = 0$:

$$S'(0)/S(0) = 2i\{-\alpha + \sum \Gamma_\nu/|\Lambda_\nu|^2\}. \tag{19}$$

IV. PHYSICAL INTERPRETATION

The cross section for scattering can be derived from (16) by means of [21]

$$\sigma(k) = (\pi/2k^2)(2l+1)|1-S(k)|^2.$$

It may be expected that each zero Λ_n with the corresponding pole Λ_n^* will produce a resonance level. This is easily verified under the following conditions: (i) the distances Γ_n from the real axis are small compared to the mutual distances of the zero's; (ii) $\alpha K_n \ll 2\pi$ for the zero considered, i.e., the resonance wavelength is much larger than the effective radius; (iii) in (16) the $+$ sign has to be taken, i.e., $S(0) = 1$. One may then write in the neighborhood of K_n

$$S(k) = \frac{k-\Lambda_n}{k-\Lambda_n^*} = \frac{k-K_n-i\Gamma_n}{k-K_n+i\Gamma_n}, \tag{20}$$

which leads to the ordinary one-level formula,

$$\sigma(k) = \frac{2\pi}{k^2}(2l+1)\frac{\Gamma_n^2}{(k-K_n)^2+\Gamma_n^2}. \tag{21}$$

When the condition (i) is not satisfied, the maximum of σ is shifted away from K_n, and the line is distorted, so that the width is no longer precisely defined. This can readily be demonstrated in the case of two overlapping lines, Λ_1 and Λ_2 say, if the other factors in (16) may again be omitted. One finds

$$\sigma(k) = \frac{2\pi}{k^2}(2l+1)\frac{\{\Gamma_1(k-K_2)-\Gamma_2(k-K_1)\}^2}{\{(k-K_1)^2+\Gamma_1^2\}\{(k-K_2)^2+\Gamma_2^2\}}. \tag{22}$$

This cross section reaches its maximum value $2\pi(2l+1)/k^2$ at the two points

$$k = \tfrac{1}{2}(K_1+K_2) \pm \tfrac{1}{2}\{(K_1^2-K_2^2)+4\Gamma_1\Gamma_2\}^{\frac{1}{2}},$$

and vanishes at $k = (\Gamma_1K_2+\Gamma_2K_1)/(K_1+K_2)$. Hence, it has two peaks, whose mutual distance is never less than $\{4\Gamma_1\Gamma_2\}^{\frac{1}{2}}$. This is even true if the frequencies coincide, in which case

$$\sigma(k) = \frac{2\pi}{k^2}(2l+1)\frac{\Gamma_1+\Gamma_2}{\Gamma_1-\Gamma_2}\left\{\frac{\Gamma_1^2}{(k-K_1)^2+\Gamma_1^2} - \frac{\Gamma_2^2}{(k-K_2)^2+\Gamma_2^2}\right\}.$$

[21] $\sigma(k)$ is the total outgoing energy current in the electric (or magnetic) 2^l-pole wave, when an incident plane wave of frequency k and unit intensity is scattered. The additional factor $\frac{1}{2}$ [as compared with N. F. Mott and H. S. W. Massey, *Theory of Atomic Collisions* (Clarendon Press, Oxford, 1933), p. 24] is related to the twofold polarization of the electromagnetic field [see N. G. van Kampen, Kgl. Danske Videnskab. Selskab, Mat.-fys. Medd. **26**, No. 15 (1951), Appendix B].

Thus, the total scattering owing to both coinciding levels shows up as a broad line, from which a sharper line is *subtracted* in the middle. (For the special case of equal widths ($\Gamma_1=\Gamma_2$), a slightly different expression for σ follows from (22); but physically the multiple zeros of $S(\lambda)$ may be treated as limiting cases of nearly coinciding levels.)

A similar effect is caused by any zero-pole pair sufficiently remote from the real axis. Such a pair gives rise to a broad resonance line, which forms a background for the narrow lines in the same region. The line form of both together is (22); it follows from this formula that the narrow line causes a sharp minimum and an adjoining sharp maximum in the slowly varying background.[12] The effect of the zeros iL_m can be described in the same way.

The exponential factor does not affect the scattering as long as $2\alpha k$ is sufficiently small, or near to a multiple of 2π. For lines for which $2\alpha K_n$ is not near to a multiple of 2π, but for which $2\alpha\Gamma_n$ is small, it will again act as a background, with which the resonance scattering interferes. This factor is responsible for what Bethe and Placzek[11] called "potential scattering in the narrower sense" (while potential scattering in the more general sense includes all scattering that is not due to the resonance lines in the region under consideration). An example that the exponential factor may actually occur in the electromagnetic case is furnished by Debye's calculation of the scattering by a dielectric sphere;[16] here $S(\lambda)$ is asymptotically in I_+

$$S_l(\lambda)\backsimeq(-1)^l\frac{\sqrt{\mu}-\sqrt{\epsilon}}{\sqrt{\mu}+\sqrt{\epsilon}}e^{-2ia\lambda}$$

(ϵ=dielectric constant, μ=permeability, a=radius of the sphere). However, it is due to the macroscopic treatment, and it is a fair guess that no exponential factor occurs in the scattering by a finite number of elementary particles.

The alternative minus sign in (16) cannot be ruled out on the basis of our conditions for S. It would mean that $k=0$ happens to be the center of a resonance line, for example when there is just one zero iL_1 on the real axis.

In order to describe *emission*, we choose the special wave packet

$$\begin{aligned}A(k)&=[(k-\Lambda_n^*)(k+\Lambda_n)S(k)e^{i\alpha k}]^{-1},\\ B(k)&=[(k-\Lambda_n^*)(k+\Lambda_n)e^{i\alpha k}]^{-1}.\end{aligned}\qquad(23)$$

Clearly $A(k)$ is square integrable, regular in the *lower* half-plane, and is of the type $e^{i\alpha k}$ at infinity; consequently the ingoing field vanishes for $t>-r+\alpha$. The outgoing field vanishes for $t<r-\alpha$, so that on a large sphere with radius r the total field vanishes for $-r+\alpha<t<r-\alpha$. It follows that at $t=0$ there cannot be any field in this sphere, except for the region inside the core. Hence, (23) determines a superposition of stationary scattering states that contains no radiation at $t=0$, and only outgoing radiation at $t>0$: that is an emission state. The ingoing field at $t<0$ serves to produce the desired situation at $t=0$.

The radiation field for $t>r-\alpha$ can be computed by inserting (23) in (4) and doing the integration in the complex plane:

$$F_\theta-iF_\varphi=-\frac{2}{K_n r}\left\{\frac{2\pi(2l+1)}{l(l+1)}\right\}^{\frac{1}{2}}P_l^1(\cos\theta)\times e^{\Gamma_n(r-t-\alpha)}\sin K_n(r-t-\alpha).\qquad(24)$$

This is the familiar expression for a damped wave, but it should be noted that no approximations have been used in the calculation. Thus, the real parts of the zeros of $S(\lambda)$ are the exact emission frequencies, and the imaginary parts are the corresponding line widths, even when the lines overlap.

The connection of Γ_n with the usual oscillator strengths f_n can be established by comparing (24) with the result of perturbation theory. Omitting fourth and higher orders of e, one finds for the transition probability of the nth excited state of the core to the ground state, $2\Gamma_n=(2e^2K_n^2/3m)f_n$. Hence,

$$(e^2/3m)\sum f_n=\sum\Gamma_n/K_n^2,$$

which to this approximation is indeed the sum occurring in (18). Hence, an analog of the well-known sum rule exists for any scattering center complying with our general conditions; its actual value cannot be predicted, but it follows from the causality condition that it must be finite.

If Λ_n is a zero of $S(\lambda)$ with multiplicity m, it is possible to construct m different emission states by putting

$$A_{(\mu)}(k)=[(k-\Lambda_n^*)^\mu(k+\Lambda_n)^\mu S(k)e^{i\alpha k}]^{-1}.\qquad(\mu=1,2,\cdots,m)$$

The corresponding emission fields have the form (24) with additional factors $(r-t-\alpha)$. In actual physical situations it is, of course, not possible to obtain each of these line shapes separately. However, one may choose mutually orthogonal combinations of these m emission fields. They will be emitted independently, provided the excitation of the core is due to a random perturbation.[22] The energy distribution over the frequencies is then the sum of the energy distributions in the chosen orthogonal combinations—which is independent of the particular choice.

To summarize: *the S-matrix is a product of factors, each referring to one level. In emission the levels show up separately, but in the formula for the scattering cross section they all interfere in a complicated way, unless the levels are far apart.*

[22] V. Weisskopf, Z. Physik **85**, 451 (1933).

V. RELATED FUNCTIONS

The fact that $S(\lambda)$ has modulus 1 on the real axis suggests the use of a phase shift $\eta(\lambda)$, defined by

$$S(\lambda)=e^{2i\eta(\lambda)}.$$

The analytic function $\eta(\lambda)$, however, is not one-valued, but has logarithmic branch points at Λ_ν and Λ_ν^*. The imaginary part of $\eta(\lambda)$ vanishes on I_0, and if $\alpha=0$, it is positive in I_+ and negative in I_-. Hence, the derivative $\eta'(k)$ on I_0 is positive. This property makes a unique determination of η from the relation

$$\sigma(k)=(2\pi/k^2)(2l+1)\sin^2\eta(k)$$

possible, when $\sigma(k)$ is known in a certain frequency range. In the case of an extended core this is still possible, unless a is too big.

Another property of $\eta(k)$, well known for nonrelativistic particles,[23] has to be mentioned. Suppose that $\alpha=0$ and that the number of zeros and poles is finite, so that $2\eta(\lambda)$ tends to a multiple of π for $|\lambda|\to\infty$. Let there be N zeros Λ_n and M zeros iL_m. Consider the closed contour consisting of I_0 and an infinite semicircle in I_+. Since η does not vary along this semicircle and $\eta(-k)=-\eta(k)$, one has

$$\eta(\infty)-\eta(0)=\pi(2N+M). \tag{25}$$

The following generalization of (25) for the case of an infinite number of zeros can be proved: If $\eta(k)$ tends to infinity as k^ρ, then ρ is the order of the meromorphic function $S(\lambda)$; if $\eta(k)$ is bounded, the order of $S(\lambda)$ is zero.

Wigner[24] studied the mathematical properties of a matrix R, which is related to the S-matrix by

$$ikR=\frac{e^{2iak}S(k)-1}{e^{2iak}S(k)+1}=i\tan[\eta(k)+ak].$$

Actually he was concerned with the case of nonrelativistic particles and regarded R as a function of $E=k^2$. It then followed from the theory of the compound nucleus that $R(E)$ is a meromorphic function with poles only on the real axis, and maps both I_+ and I_- into themselves. We shall show that these properties follow from the causality condition, even though in the present case E has no physical meaning.

In the first place $R_1(\lambda)\equiv\lambda R(\lambda^2)$ shares all the properties of Wigner's "R-functions". Indeed, it is one-valued analytic, with poles where $e^{2ia\lambda}S(\lambda)=-1$; this equation can only be satisfied on I_0, because the left-hand side is in absolute value less than 1 in I_+, greater than 1 in I_-. Further, on drawing the vectors $e^{2ia\lambda}S(\lambda)\pm1$ in the complex plane, it is seen that the argument of $R_1(\lambda)$ is between 0 and π for $|e^{2ia\lambda}S(\lambda)|<1$, and between $-\pi$ and 0 for $|e^{2ia\lambda}S(\lambda)|>1$; which shows that $R_1(\lambda)$ maps both half-planes into themselves.

It is curious that from this fact it follows that $R(E)$—as a function of $E=\lambda^2$—is also an "R-function". Since $R_1(\lambda)$ is an R-function, it can be expanded in a Mittag-Leffler series,[24]

$$R_1(\lambda)=p\lambda+q+\sum\left(\frac{r_n}{Z_n-\lambda}-\frac{r_n}{Z_n}\right). \quad (p, r_n>0)$$

From this one finds a similar series for $R(E)$

$$R(E)=\frac{R_1(\lambda)-R_1(-\lambda)}{2\lambda}=p+\sum\frac{r_n}{Z^2-E},$$

which proves that it is an R-function.

Finally we mention the Mittag-Leffler series for $S(\lambda)$ itself:

$$S(\lambda)=e^{-2ia\lambda}\{c_0+\sum c_\nu/(\Lambda_\nu^*-\lambda)\}, \tag{26}$$

because it leads to the usual expression for the cross section

$$\sigma(k)=\frac{\pi(2l+1)}{2k^2}\left|\sum\frac{c_\nu}{k-K_\nu+i\Gamma_\nu}+e^{2iak}-c_0\right|^2.$$

The last two terms represent the potential scattering, but the rather arbitrary constant a is here replaced by the well-defined, though unknown, α. If the lines are far apart, then the K_n are resonance frequencies, and the widths are given by $c_n=2i\Gamma_n$. If the lines overlap, however, the connection of the quantities describing scattering with those describing emission is more involved. For a finite number of zeros and poles (26) is certainly valid (with $c_0=1$), but for an infinite number it may be divergent.

VI. INTEGRAL RELATIONS

So far the conclusions from the causality condition have been stated in terms of analytic functions, but they can be translated into relations between functions of real k only. That will give us integral equations connecting the various physical quantities. Such relations are treated in the theory of Hilbert transforms;[19] they have been used in dispersion theory[4,5] and in the theory of electric circuits.[7]

Let $\beta>\alpha$; then $e^{2i\beta\lambda}S(\lambda)\to0$ for $|\lambda|\to\infty$, $0<\arg\lambda<\pi$. Applying Cauchy's integral to a closed curve, consisting of the real axis and a semi-circle with infinite radius, one finds

$$e^{2i\beta\lambda}S(\lambda)=\frac{1}{2\pi i}\int_{-\infty}^{+\infty}\frac{e^{2i\beta k'}S(k')dk'}{k'-\lambda}. \quad (\beta>\alpha) \tag{27}$$

It should be noted that this formula expresses $S(\lambda)$—for complex λ—explicitly in $S(k)$, and therefore allows us in principle to compute the actual values of $S(\lambda)$ from experimental data. It has been remarked before[25]

[23] N. Levinson, Kgl. Danske Videnskab. Selskab, Mat.-fys. Medd. **25**, No. 9 (1949). There is a difference in sign, because Levinson deals with bound states of the scattered particle, rather than with resonance levels.

[24] E. P. Wigner, Ann. Math. **53**, 36 (1951).

[25] N. G. van Kampen, Phil. Mag. **42**, 851 (1951).

that this should be required when using the analytic continuation. It can only be fulfilled if there is a certain *a priori* information about the regularity and the behavior at infinity, such as supplied by the causality condition.

Let in (27) the imaginary part of $\lambda=k+i\gamma$ tend to zero. The zero of the denominator approaches the real axis and contributes a half residue; the formula becomes

$$e^{2i\beta k}S(k)=\frac{1}{\pi i}\int_{-\infty}^{+\infty}\frac{e^{2i\beta k'}S(k')}{k'-k}dk', \tag{28}$$

where it is understood that the principal value has to be taken at $k'=k$. The validity of this equation for all $\beta>\alpha$ is not only a necessary, but also a sufficient condition for the scattering to be causal outside of a sphere with radius α.

For a point-core the exponential factor in (28) cannot be dispensed with, but there is an alternative formula in which it does not occur. Since $S(\lambda)$ is bounded in I_+, one may apply Cauchy's integral to $S(\lambda)/\lambda$, provided the pole at $\lambda=0$ is taken into account

$$\frac{S(\lambda)}{\lambda}=\frac{1}{2\pi i}\int_{-\infty}^{+\infty}\frac{S(k')dk'}{k'(k'-\lambda)}+\frac{S(0)}{2\lambda} \tag{29}$$

(principal value at $k'=0$). This is an alternative for (27); by taking λ real one finds in place of (28):

$$S(k)-S(0)=\frac{k}{\pi i}\int_{-\infty}^{+\infty}\frac{S(k')}{k'(k'-k)}dk'$$

(principal value at $k'=0$ and at $k'=k$). Separating real and imaginary parts

$$\begin{aligned}\mathfrak{J}S(k)&=-\frac{1}{\pi}\int_{-\infty}^{+\infty}\frac{\mathfrak{R}S(k')}{k'(k'-k)}dk'=-\frac{2k}{\pi}\int_0^{\infty}\frac{\mathfrak{R}S(k')}{k'^2-k^2}dk'\\ \mathfrak{R}S(k)&=S(0)+\frac{2k^2}{\pi}\int_0^{\infty}\frac{\mathfrak{J}S(k')}{k'(k'^2-k^2)}dk'.\end{aligned} \tag{30}$$

These relations have been mentioned in a paper by Jost, Luttinger, and Slotnick[26] and have been used by Rohrlich and Gluckstern[27] for the calculation of forward Delbrück scattering. To justify its application, however, the causality condition has to be postulated.

[26] Jost, Luttinger, and Slotnick, Phys. Rev. **80**, 189 (1950).

[27] F. Rohrlich and R. L. Gluckstern, Phys. Rev. **86**, 1 (1952). Actually they deal with inelastic scattering, which we hope to treat in another paper.

The above relations can be used to write the sum rule (19) in a new form. One finds first from (19)

$$\begin{aligned}\sigma(0)&=\tfrac{1}{2}\pi(2l+1)|S'(0)|^2\\ &=2\pi(2l+1)\{-\alpha+\textstyle\sum\Gamma_\nu/|\Lambda_\nu|^2\}^2,\end{aligned}$$

provided $S(0)=1$. It then follows from (30) for the case of a point-core ($\alpha\leqslant 0$) that

$$\begin{aligned}\int_0^{\infty}\sigma(k)dk&=\pi^{\frac{1}{2}}[(l+\tfrac{1}{2})\sigma(0)]^{\frac{1}{2}}\\ &=\pi^2(2l+1)\{-\alpha+\textstyle\sum\Gamma_\nu/|\Lambda_\nu|^2\}.\end{aligned} \tag{31}$$

Without restriction to a point-core one finds

$$\sum\Gamma_\nu/|\Lambda_\nu|^2=\frac{2}{\pi}\int_0^{\infty}\sin^2(\eta+\alpha k)\frac{dk}{k^2}.$$

A new sum rule can be derived by integrating

$$\int\{1-S(\lambda)e^{2i\alpha\lambda}\}d\lambda$$

along the same closed contour. There is no pole, but the contribution of the large semi-circle is no longer zero. If the number of zero's is finite, then for $|\lambda|\to\infty$

$$e^{2i\alpha\lambda}S(\lambda)=\prod(1-\Lambda_\nu/\lambda)(1-\Lambda_\nu^*/\lambda)^{-1}\simeq 1-(2i/\lambda)\sum\Gamma_\nu,$$

and the integration yields

$$2\pi\sum\Gamma_\nu=\int_0^{\infty}|1-e^{2i\alpha k}S(k)|^2dk,$$

which for $\alpha=0$ takes the simple form

$$\int_0^{\infty}k^2\sigma(k)dk=\pi^2(2l+1)\sum\Gamma_\nu. \tag{32}$$

For non-overlapping lines this equation is a trivial consequence of (21). If there are infinitely many lines, (32) may become meaningless, in contrast to (31). Both (31) and (32) lead to the same average cross section over a region large enough to contain many lines, but small compared to the frequency, viz.,

$$\bar{\sigma}(k)=(\pi/k)^2(2l+1)\bar{\Gamma}(k).$$

I would like to express my gratitude to the Institute for Advanced Study for a grant-in-aid, and to its director, Professor Robert Oppenheimer, for hospitality extended to me at the Institute.

Angular Distribution of Protons from Vanadium 52†

J. S. KING AND W. C. PARKINSON
H. M. Randall Laboratory of Physics, University of Michigan, Ann Arbor, Michigan
(Received October 29, 1952)

Angular distributions have been obtained for the protons from the ground and first excited states for the reaction $V^{51}(d,p)V^{52}$. The results indicate that the captured neutron carries in mainly one unit of orbital angular momentum for both states. The 29th neutron is thus presumed to be a $p_{\frac{1}{2}}$ nucleon.

IN two previous letters[1] the angular distributions of protons from the reactions $P^{31}(d,p)P^{32}$ and $Cl^{37}(d,p)Cl^{38}$ were reported. The results were in good agreement with the predictions of the shell model.[2] As a continuation of this study, angular distributions of the protons from the reaction $V^{51}(d,p)V^{52}$ have been obtained for the ground and first excited states of V^{52}. The data are plotted in Figs. 1 and 2 along with the calculated Butler curves for the ground state and first excited state, respectively. The measured Q values were 5.0 and 4.2 Mev, respectively, in close agreement with the values 5.02 and 4.23 Mev reported by Harvey.[3] The theoretical curves were computed for $l_n=1$ and 3 using a value of $r_0=6.3\times10^{-13}$ cm for both states. The mid-foil incident deuteron energy was 7.05 Mev in the c.m. system. The target consisted of a foil of pure vanadium 0.375 mil thick. The vertical lines through the experimental points represent only the uncertainty due to the total number of counts.

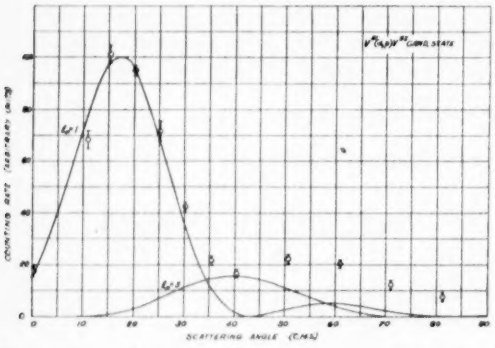

FIG. 1. The angular distribution of the protons associated with the ground state in the reaction $V^{51}(d,p)V^{52}$. The solid curves are calculated from the Butler theory using $r_0=6.3\times10^{-13}$ cm.

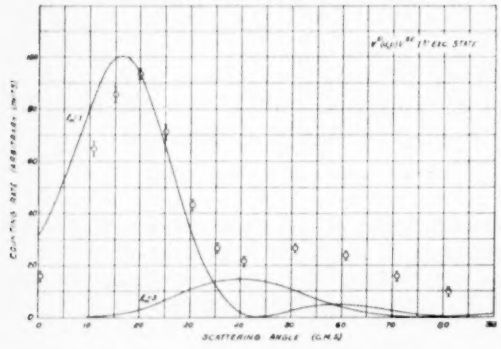

FIG. 2. The angular distribution of the protons associated with the first excited state of V^{52}. The solid curves are calculated from the Butler theory using the same r_0 as for the ground state.

At small angles the data for the ground state of V^{52} fit reasonably well the calculated curve for $l_n=1$. From this one might conclude that the captured neutron carries in one unit of orbital angular momentum and that the 29th neutron in V^{52} is a $p_{\frac{1}{2}}$ nucleon. However, since the relative amplitude of the $l_n=3$ peak is about one-seventh that for $l_n=1$, one cannot rule out the possibility of considerable admixture. It is difficult to make a reliable estimate of the admixture in view of the uncertain "background" rising from other competing processes. In addition most experimental data on angular distributions at these energies are characterized by the fact that the cross sections do not go to zero at the first minimum as might be expected from Butler's calculation. While it is quite possible that further refinements of the theory will bring about better agreement[4] with experiment, on the basis of the present data it would appear that 25 percent of $l_n=3$ would represent an upper limit. Any additional admixture removes the minimum occurring at 40°.

As pointed out by Bethe and Butler,[2] the levels for the shell starting with the 29th nucleon are closely spaced, hence one might expect the 29th neutron to be either a $p_{\frac{1}{2}}$ or an $f_{\frac{1}{2}}$ particle. The selection rules allow $\Delta l=1$, 3, 5 and possibly 7. Although one cannot, on the basis of the data here presented, eliminate a sizable percentage of $l_n=3$ it is probable that it is a $p_{\frac{1}{2}}$ nucleon.

The neutron accepted into the first excited state also appears to carry in mainly one unit of orbital angular momentum (Fig. 2). Although the data appear to be shifted toward larger angles, it clearly does not fit an $l_n=2$ curve. A slightly different value of r_0 results in better agreement. A third level ($Q=3.4$ Mev), presumably the second excited state of V^{52}, also corresponds to the capture of an $l_n=1$ neutron.

† This work was supported in part by the U. S. Atomic Energy Commission and the Michigan Memorial Phoenix Project.

[1] Parkinson, Beach, and King, Phys. Rev. **87**, 387 (1952); J. S. King and W. C. Parkinson, Phys. Rev. **88**, 141 (1952).

[2] H. A. Bethe and S. T. Butler, Phys. Rev. **85**, 1045 (1952).

[3] J. A. Harvey, Phys. Rev. **81**, 353 (1951).

[4] See, for example, P. B. Daitch and J. B. French, Phys. Rev. **87**, 900 (1952); and Bhatia, Huang, Huby, and Newns, Phil. Mag. **43**, 485 (1952).

Direction and Polarization Correlations of Successive Gamma-Rays*

J. J. KRAUSHAAR† AND M. GOLDHABER
Brookhaven National Laboratory, Upton, New York

(Received November 10, 1952)

Experimental arrangements for the measurement of directional and direction-polarization correlations of successive gamma-rays have been set up and considerations given to instrumental corrections and procedures for the analysis of the data. Directional measurements have been made with Co^{60}, Rh^{106}, Sb^{124}, As^{76}, and Ir^{194}, and direction-polarization measurements with Co^{60}, Rh^{106} and ThC″. The results are discussed in the light of present information on the systematics of the spins of the excited states of even-even nuclei. The occurrence of mixtures of magnetic dipole and electric quadrupole radiation in directional correlation experiments is summarized.

I. INTRODUCTION

As part of a general program for the study of the radiations and the excited states of radioactive nuclei, measurements of directional and polarization correlations of successively emitted gamma-rays have been undertaken.

The theory of direction and direction-polarization correlations was initially investigated by Hamilton[1,2] for dipole and quadrupole radiation, and that for polarization-polarization correlations by Falkoff.[3] It was first demonstrated by Brady and Deutsch[4] and Metzger and Deutsch[5] that such measurements can be of practical aid in the determination of the character of gamma-rays and the spins and parities of nuclear levels. Further work along both experimental and theoretical lines has been rapid and extensive in recent years. A summary of developments can be found in the recent review articles of Deutsch[6] and Frauenfelder.[7]

Because of the nature of the decay process, angular correlation measurements have been particularly well suited to obtaining information on the excited states of even-even nuclei. Much of the data recently used in the establishment of systematics in the spins and parities of the excited states of such nuclei[8–11] has been derived from correlation experiments. In the work reported here, some emphasis has been given to neutron induced activities that have a relatively short half-life.

In general, angular correlation studies are complicated by the presence of four disturbing factors, in addition to instrumental effects, any of which may make a unique assignment of spins, and parities of levels, and the character of the gamma-rays difficult.

(1) Gamma-rays in cascade, other than those being studied, are often present, and unless some form of selection is employed, a composite correlation may be observed. In this investigation integral pulse-height discrimination with scintillation counters served to partially select one cascade in the presence of others.

(2) In some cases there are ambiguities in the interpretation of the measured correlation even if only pure radiation is considered.

(3) Atomic perturbations have been shown to be present in the directional correlation of Cd^{111},[12] and are suspected of influencing the correlation in other cases (Rh^{106}, Co^{60}).[13] Theoretical considerations of this effect have been carried out by Goertzel[14] and Alder.[15] Aside from their intrinsic interest and the possibility they offer for the determination of the magnetic moment of the intermediate nuclear state, such perturbations can make the interpretation of the measured directional correlation difficult. Even if the intermediate nuclear state has no measurable lifetime, the excited atom may have a magnetic moment large enough to perturb the correlation.[16]

(4) It appears that the transition probabilities for $M1$ and $E2$ radiation may be comparable. Thus, when one pair of adjacent levels being studied have spins which differ by 1 or 0 units of angular momentum and have the same parity, a directional correlation may be observed that represents a mixture, with interference, of those two kinds of radiation. Correlations involving such mixtures have been observed in a number of cases. Ling and Falkoff[17] and Lloyd[18] have computed the coefficients to be expected for mixtures of various radiations, and Zinnes[19] has computed the effect of mixtures in direction-polarization correlations.

* Research carried out under contract with the U. S. Atomic Energy Commission.

† Part of the work reported here was presented in partial fulfillment of the requirements for the degree of Ph.D. in physics at Syracuse University.

[1] D. R. Hamilton, Phys. Rev. **58**, 122 (1940).
[2] D. R. Hamilton, Phys. Rev. **74**, 782 (1948).
[3] D. L. Falkoff, Phys. Rev. **73**, 518 (1948).
[4] E. L. Brady and M. Deutsch, Phys. Rev. **78**, 558 (1950).
[5] F. Metzger and M. Deutsch, Phys. Rev. **78**, 551 (1950).
[6] M. Deutsch, Rep. Phys. Soc. Progr. Phys. **14**, 196 (1951).
[7] H. Frauenfelder, to be published in *The Annual Review of Nuclear Science*, Vol. II.
[8] M. Goldhaber and A. W. Sunyar, Phys. Rev. **83**, 906 (1951).
[9] Horie, Umezawa, Yamaguchi, and Yoshida, Prog. Theor. Phys. **6**, 254 (1951).
[10] P. Staehelin and P. Preiswerk, Helv. Phys. Acta **24**, 623 (1951).
[11] G. Scharff-Goldhaber, Phys. Rev. **87**, 218 (1952).
[12] Aeppli, Bishop, Frauenfelder, Walter, and Zunti, Phys. Rev. **82**, 550 (1951).
[13] Aeppli, Frauenfelder, Heer, and Ruetschi, Phys. Rev. **87**, 379 (1952).
[14] G. Goertzel, Phys. Rev. **70**, 897 (1946).
[15] K. Alder, Phys. Rev. **84**, 369 (1951); **83**, 1266 (1951).
[16] H. Frauenfelder, Phys. Rev. **82**, 549 (1951).
[17] D. S. Ling and D. L. Falkoff, Phys. Rev. **76**, 1639 (1949).
[18] S. P. Lloyd, Phys. Rev. **83**, 716 (1951).
[19] I. Zinnes, Phys. Rev. **80**, 386 (1951).

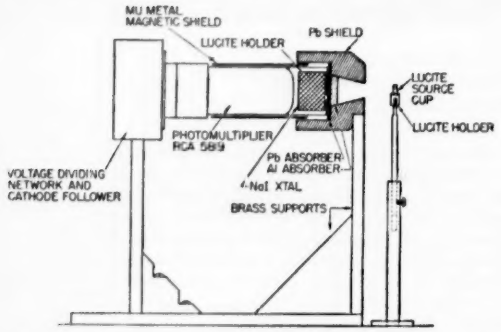

FIG. 1. The arrangement of the absorbers and the shields around the scintillation counter used in the measurement of directional correlations.

II. DIRECTIONAL CORRELATIONS

The determination of a directional correlation pattern involves the measurement of the coincidence counting rate as a function of the angle subtended at the source by two detectors. The general arrangement used in this investigation, is shown in Fig. 1. The Pb absorbers used in front of the scintillation counters to attenuate backscattered radiation were $\frac{1}{16}$ in. thick. The Al beta-absorbers were $\frac{1}{2}$ in. thick, and were used in addition to the Pb to prevent the counting of the energetic beta-rays that appear in some of the radioactive nuclei studied.

The electronic circuits involved were conventional and consisted of a cathode follower at the photomultiplier base, followed by a linear amplifier (5×10^{-8} sec rise time), pulse-height discriminator, and a blocking oscillator which generated a 1×10^{-7} sec pulse. One output of the blocking oscillator went to a univibrator which gave a pulse about 3×10^{-6} sec wide for operation of a scaler to record single events. Another output of the blocking oscillator went to a coincidence circuit employing a 6AS6 as a mixing tube. The coincidence resolving time was measured frequently in the course of the determination of a directional correlation. The counting rates used for the resolving time measurement were made the same as the ones involved with the source under investigation. The resolving time was about 1.2×10^{-7} sec.

The integral discriminator levels were kept sufficiently high so that the counters were insensitive to the Pb x-rays produced in the adjacent shields and absorbers. The "no bias" setting then was actually such that the discriminator levels were at about 0.1 Mev.

For the determination of the correlation function, measurements of the single and coincidence counts were made for fifteen minute periods at the variable angle θ, 90°, 270°, and $360°-\theta$. The sum of θ and $360°-\theta$ together with the sum of 90° and 270° were used in the calculation of $\epsilon(\theta)$.[20] An inverted order of taking data, i.e., 90°, θ, $360°-\theta$, 270°, was then followed. The coincidence counts were normalized by dividing by the product of the single counts. The method of normalization over-corrects for the decay of the source. However, due to the systematic method of taking data, as described above, this effect cancels to the first order and for the shortest activity studied (19 hours) was found to be negligible. The "fixed" counter was periodically rotated to a new position to insure that there was no scattering from adjacent room walls and equipment.

A function of the form $\epsilon(\theta)=a_2\cos^2\theta+a_4\cos^4\theta$ was fitted by a least squares procedure[21] to the experimental points. In a manner described in a previous publication[22] these coefficients were then adjusted for the finite detector resolution. The half-width at half-maximum δ_0 of the angular resolution curve was 12.0° in all cases except for Co^{60} where it was 10.5°, and for part of the work on Rh^{106}, where it was 6.6°. Values of $4\pi Bn/(2n+1)$ were determined by numerical integration and were, for example, in the 12.0° geometry: 1.0000, 0.9050, and 0.7653 for n equal to 0, 2, and 4.

In order to test the apparatus for the presence of effects, such as scattering which would artificially provide an anisotropy, the coincidence counting rate was measured as a function of θ using a source emitting a single gamma-ray. For this purpose a source of Be^7 known to be free of contaminants was used. The use of Cs^{137} and Fe^{59} was avoided inasmuch as these have been shown[23] to possess a small, but measurable, number of coincidence gamma-rays. With no bias and with $\frac{1}{16}$ in. of Pb in front of both counters, the coincidence counting rates at 90°, 130°, and 180° were found to be the same within the statistical accuracy. If

[20] In the notation of Brady and Deutsch (reference 4),
$\epsilon(\theta)=[N(\theta)-N(\pi/2)/N(\pi/2)]\times10^3$.

[21] Least squares values for a_2 and a_4 may be obtained through the use of the following expressions: assuming each point weighted equally

$$a_2=\frac{[8]\Sigma_i\,\epsilon(\theta_i)\cos^2\theta_i-[6]\Sigma_i\,\epsilon(\theta_i)\cos^4\theta_i}{\Delta}\times10^{-3},$$

$$a_4=\frac{[4]\Sigma_i\,\epsilon(\theta_i)\cos^4\theta_i-[6]\Sigma_i\,\epsilon(\theta_i)\cos^2\theta_i}{\Delta}\times10^{-3},$$

where $[N]\equiv\Sigma_i\cos^N\theta_i$ and $\Delta\equiv[4][8]-[6]^2$.

The rms errors of these coefficients are given by:

$$\delta a_2=([8]/\Delta)^{\frac{1}{2}}\delta\epsilon\times10^{-3},$$

and

$$\delta a_4=([4]/\Delta)^{\frac{1}{2}}\delta\epsilon\times10^{-3}$$

where $\delta\epsilon$ is the rms error of each of the experimental points.

Often the error is desired on the quantity a_2+a_4 to facilitate comparison of the coefficients with the value of $\epsilon(180°)$. This error can be shown to be:

$$\delta(a_2+a_4)=\left(\frac{[4]+[8]-2[6]}{\Delta}\right)^{\frac{1}{2}}\delta\epsilon\times10^{-3}.$$

In the event that only a_2 is being considered, i.e., a_4 is taken as 0, the expressions for the least squares value and the error become

$$a_2=\frac{\Sigma_i\,\epsilon(\theta_i)\cos^2\theta_i}{[4]}\times10^{-3},$$

$$\delta a_2=(1/[4])^{\frac{1}{2}}\delta\epsilon\times10^{-3}.$$

[22] E. L. Church and J. J. Kraushaar, Phys. Rev. **88**, 419 (1952).
[23] F. R. Metzger, Phys. Rev. **85**, 727 (1952).

the upper limit of the experimental error were applied as a correction to the measured correlations, it would, for example, amount to a decrease of 2 percent in $\epsilon(180°)$ for As^{76}, where the effect was the largest. That is, the original value of 6.40 would be reduced to 6.27, which is still well within the indicated error.

As a further test of the experimental techniques, the directional correlation of the cascade gamma-rays of Co^{60} was measured. This correlation had been previously measured by Brady and Deutsch[1] and others and essentially agrees with that to be expected for a 4–2–0 (Q–Q) cascade. In the work here the anisotropy was measured at 120°, 140°, 160°, and 180°. By a least squares fit to the data and by adjustment for the finite detector size, values of 0.120 ± 0.052 and 0.043 ± 0.059 were obtained for a_2 and a_4, respectively. These are to be compared with the theoretical values of 0.1250 and 0.0417 for a cascade of the above type. The corresponding value of $\epsilon(180°)$ from the data is 0.163 ± 0.012, while the theoretical value is 0.1667. This experimental value cannot be said, however, to be incompatible with the value recently obtained by Aeppli *et al.*[12] of 0.148 ± 0.002. These authors indicate that the difference between their experimental value and the theoretical value may be attributable to a perturbation of the correlation by the electron shell. The directional correlation of Pr^{144} has also been measured by using the described apparatus and techniques and has been reported elsewhere.[24]

Rh^{106}

In Fig. 2, curve (a), is shown the measured directional correlation of the successive gamma-rays of Rh^{106}, using a ruthenium chloride source in solution and with no bias on the counters. Values of 2.245 ± 0.041 and 2.953 ± 0.047 were obtained for a_2 and a_4 by taking a weighted average of the corrected least squares values listed previously[22] for δ_0 equal 6.6° and 12.0°. The corresponding value of a_2+a_4 is 0.708 ± 0.011. Also shown in Fig. 2 are the experimental points, with their associated rms statistical errors, obtained in the 6.6° geometry.

To estimate the contribution from gamma-rays known to be present[25] other than those involved in the main cascade, 0.51–0.62 Mev, the gamma-ray spectrum was studied with a scintillation spectrometer. Lines at 0.51, 0.62, 0.87, 1.04, and 1.55 Mev were identified and their relative intensities determined to be 1.00, 0.53 ± 0.05, 0.02 ± 0.01, 0.07 ± 0.01, and 0.01 ± 0.01, respectively. These data are in essential agreement with those of Alburger.[25] Thus, if all the gamma-rays are considered to be counted in proportion to their intensity as well as to the efficiency for detection with a 3-cm NaI crystal, 84 percent of the coincidences will be due to the 0.51–0.62 Mev cascade.

The use of integral discrimination permitted the energy dependence of the directional correlation to be studied. By sufficiently raising the bias on one of the counters in two steps the value of $\epsilon(180°)$ was reduced by 16 percent and 34 percent, respectively, and the value of $\epsilon(130°)$ was reduced by 33 percent and 76 percent, respectively, from those measured with no bias on the counters. Through estimating the attenuation of the various cascade processes at the two higher bias settings and with a knowledge of the intensities and the counting efficiencies, small positive values were indicated for the anisotropy of the background coincidences.

The above work indicates that the background coincidences may be assumed to have approximately an isotropic angular distribution without introducing an appreciable error. If the coefficients of the main cascade are adjusted for this 16 percent isotropic background, new values of 2.673 and 3.515 are obtained for a_2 and a_4. Curve (b) in Fig. 2 shows this distribution.

Comparison of curve (b) and the theoretical 0–2–0 correlation function shows about a 12 percent difference. Both curves (a) and (b) indicate a larger anisotropy than those originally measured by Brady and Deutsch[4] and later by Steffen.[26] The recent measurements of Arfken *et al.*[27] are somewhat higher in the region of 150° to 180° than is shown in curve (b).

The 12 percent discrepancy between curve (b) and the theoretical distribution (c) may be due, as has already been suggested,[4,11,28,29] to a perturbation of the correlation by the electron shell. However, if such a perturbation is present, it could not be significantly

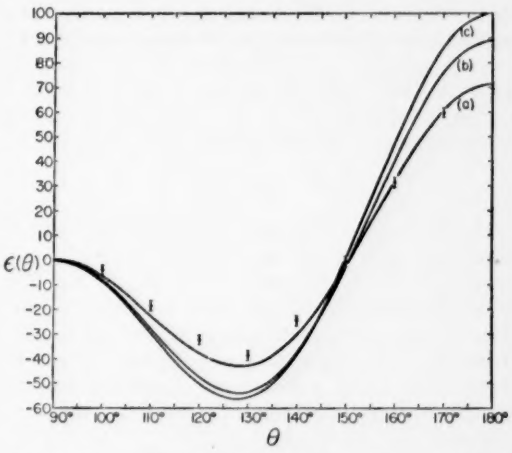

FIG. 2. The experimental points shown are those taken in the 6.6° geometry. Curve (a) represents the weighted averaged values of the 6.6° and 12.0° data corrected for the finite detector size. Curve (b) is curve (a) corrected for the estimated 16 percent isotropic background. The theoretical correlation function for a 0–2–0 (Q–Q) transition is shown in curve (c).

[24] D. E. Alburger and J. J. Kraushaar, Phys. Rev. **87**, 448 (1952).
[25] D. E. Alburger, Phys. Rev. **85**, 734 (1952) and Phys. Rev. **88**, 339 (1952).
[26] R. M. Steffen, Phys. Rev. **80**, 115 (1950).
[27] Arfken, Klema, and McGowan, Phys. Rev. **86**, 413 (1952).
[28] J. J. Kraushaar, Phys. Rev. **85**, 727 (1952).
[29] R. M. Steffen, Phys. Rev. **86**, 632 (1952).

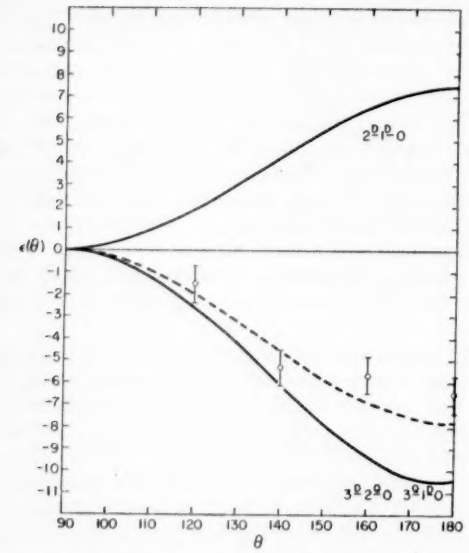

FIG. 3. The directional correlation of Sb^{124}. The dashed curve represents a least squares fit, corrected for the finite detector size, to the experimental points shown. The solid line curves are the theoretical distributions for pure dipole and quadrupole radiation that are nearest in agreement with the experimental curve.

altered by imbedding the sources in different media.[29] It may be that when the intermediate state has a short lifetime ($<5\times10^{-9}$ seconds[30] for Rh^{106}) it is more difficult to change the perturbation. It has been pointed out by Alder[15] and Frauenfelder[7] that if the electron shell is disturbing the correlation, the attenuation of the coefficients of the terms in an expansion in a Legendre series will be greater the higher the term. For a 0–2–0 transition, A_4/A_2 is 3.201; while for curve (b), A_4/A_2 is 3.546. This then provides additional evidence against the explanation of the discrepancy in terms of the influence of extra-nuclear fields.

Sb^{124}

The decay of 60-day antimony involves a complex beta- and gamma-ray spectrum. By far the most prominent gamma-ray cascade consists of the 1.70–0.603-Mev radiation. By the use of integral discrimination, the directional correlation of this cascade has been studied. It has been found previously by workers concerned with the β–γ directional correlation that the composite γ–γ coincidences showed no significant anisotropy.[31]‡

Sources of about 0.1 millicurie of Sb^{124} were prepared by neutron bombardment of metallic antimony in the Brookhaven reactor. The discriminator level of one of the counters was set so that the counter responded only to radiation appreciably above 0.7 Mev. The other counter was biased at about 0.1 Mev. The presence of adequate beta-ray absorbers precluded any contribution from the known β–γ correlation to the measured γ–γ anisotropy. The results of the measured γ–γ correlation are shown in Fig. 3. The dashed curve is a least squares fit of the points adjusted for the finite geometry of the apparatus. The value of a_2 thus obtained is -0.078 ± 0.009. Also indicated are the closest approaching computed curves, considering only pure dipole and quadrupole radiation and assuming that the ground state of Te^{124} has spin zero. The consideration of pure octupole radiation also provides no agreement with experiment.

The mixtures of dipole and quadrupole radiation in one of the transitions, which agree with the results, are shown in Table I. Recently Metzger[32] measured the internal conversion coefficient of the 0.603-Mev gamma-ray and found that it agreed with the theoretical value for electric quadrupole radiation. With the usual assumption concerning the spin and parity of the ground state of even-even nuclei, the first excited state, then, must have spin 2 and even parity. The fact that there is no parity change in that transition is also in agreement with Stump's[33] measurement of the β–γ direction-polarization correlation. Of the mixture possibilities listed, then, only 3–2–0 (D, Q–Q) is consistent with the above results.

TABLE I. Mixtures of dipole and quadrupole radiation in the first transition that are consistent with the directional correlation data for Sb^{124}.

Spins	α/β	Phase difference
$3\overset{D,Q}{\text{——}}2\overset{Q}{\text{——}}0$	36	0°
$1\overset{D,Q}{\text{——}}1\overset{D}{\text{——}}0$	7.8 or 0.115	180°
$2\overset{D,Q}{\text{——}}1\overset{D}{\text{——}}0$	5.6 or 4.8	0°

On the basis of the present experiments, the possibility that the correlation is being perturbed by the electron shell or perhaps by other causes cannot be dismissed. Inasmuch as the effect of such perturbations is to attenuate the coefficients, it is apparent that the original correlation must be negative and that a_2 must be equal to or greater than 0.078. Other than 3–2–0, only a 1–2–0 assignment would meet this requirement and still be consistent with present information. Of course the very weak intensity of the probable cross-over transition ($\sim$0.02 percent)[34] very much favors the 3–2–0 assignment.

[30] M. Deutsch and W. E. Wright, Phys. Rev. **77**, 139 (1950).
[31] S. L. Ridgeway, Phys. Rev. **78**, 821 (1950); J. R. Beyster and M. L. Wiedenbeck, Phys. Rev. **79**, 169 (1950); D. T. Stevenson and M. Deutsch, Phys. Rev. **83**, 1202 (1951).
‡ *Note added in proof:*—The γ–γ directional and polarization correlations of Sb^{124} have recently been measured by Kloepper, Lennox, and Wiedenbeck (Phys. Rev. **88**, 695 (1952)). Without using energy discrimination they found no anisotropy for the directional correlation.

[32] F. R. Metzger, Phys. Rev. **86**, 435 (1952).
[33] R. Stump, Phys. Rev. **86**, 249 (1952).
[34] V. Meyers and A. Wattenberg, Phys. Rev. **75**, 992 (1949).

If a mixture is present, there would be a strong argument in favor of having the parity of the 2.30-Mev level even. In principle, however, mixtures of electric dipole and magnetic quadrupole radiation could take place.

It is interesting to note that the directional correlation of Y^{88}, measured by Brady and Deutsch,[4] is similar to that shown in Fig. 1. One must assume, then, that the mixtures listed in Table I are also approximately applicable to that gamma-ray cascade process. In addition to the 2–1–0 (D, Q–D) assignment hitherto considered,[4,17] the other possibilities should also be viewed in the light of present information on the decay of Rb^{88} and Y^{88}. There does not appear at present to be any strong evidence favoring the 2–1–0 assignment over the 3–2–0. The importance of this assignment lies mainly in the fact that it may be one of the few remaining exceptions to the observation that the spin and parity of the first excited states of even-even nuclei

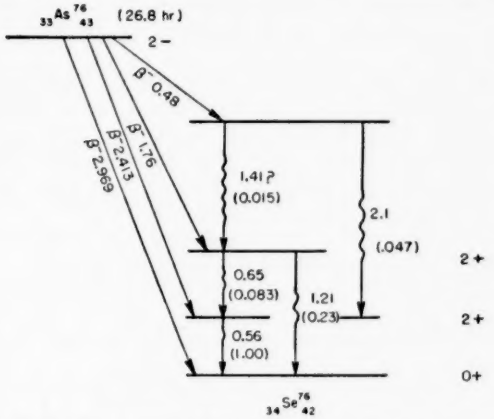

FIG. 4. The decay scheme of As^{76}. The quantities in parentheses are the relative gamma-ray intensities as indicated by Hubert.

are 2, even.[8,9] Further experiments on this nuclide are in preparation.

As^{76}

The decay of As^{76} (27 hours) involves several cascade gamma-rays from the excited states of Se^{76}. In addition to the information summarized in *Nuclear Data*,[35] there has been some recent work on the beta-[36] and gamma-ray[37,38] spectra. Because of the discrepancy between the decay scheme consistent with the data of Tomlinson and Ridgway[37] and Hubert[38] and the suggested scheme of the earlier workers, the gamma-ray spectrum was analyzed[39] in both singles and coincidences.

The singles spectrum clearly showed γ-rays at 0.56, 0.65, 1.21 Mev and a weaker high energy line of about 2.1 Mev. The coincidence spectrum showed strong lines at 0.56 and 0.65 Mev, and a weak and perhaps composite peak at 1.2 Mev. The ratio of the peak height of the singles to the coincidences for the 0.65-Mev line indicated that this gamma-ray was in direct cascade with the 0.56-Mev line. The ratio of singles to coincidences for the 1.2-Mev line was much greater than that to be expected were it in direct cascade with the prominent gamma-rays. The above results are in agreement with the data of Hubert except that a 1.41-Mev gamma-ray was not resolved.

The decay scheme that summarizes the data of Hubert, Tomlinson, and Ridgway, and the present work, is shown in Fig. 4.

In order to determine the spins of the excited states of Se^{76} the directional correlation of the successive gamma-rays has been measured. Sources were prepared by irradiating 10 mg of metallic As powder with slow neutrons for 6 minutes in the Brookhaven reactor. The results of the correlation measurements, taken with no bias on the counters, is shown in Fig. 5. The values of a_2 and a_4, corrected for the finite detector size, are -0.611 ± 0.030 and 0.700 ± 0.034, respectively. There is no assignment of spins, considering pure dipole, quadrupole, and octupole radiation that will present such a distribution, assuming a spin of 0 for the ground state of Se^{76}. Of the possibilities involving mixtures of dipole and quadrupole radiation in one of the transitions only 2–2–0 (D, Q–Q) with $\alpha/\beta=0.5$ to 1.5 has coefficients at all compatible with the measured values.

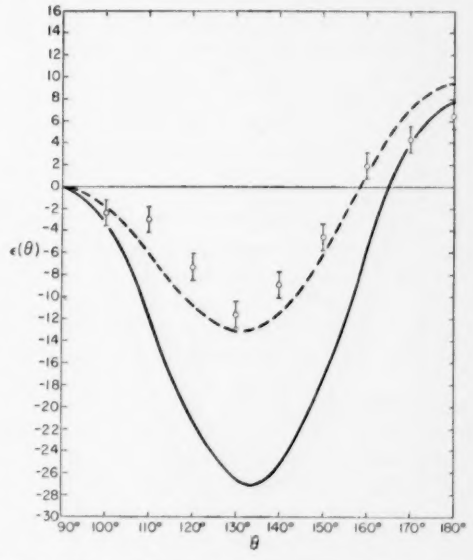

FIG. 5. The dashed curve is the least squares fit, corrected for the finite geometry, to the indicated experimental points obtained with As^{76}. The solid curve is the theoretical distribution for a 2–2–0 (Q–Q) transition.

[35] *Nuclear Data*, National Bureau of Standards, Circular No. 499 (1950).
[36] E. P. Tomlinson and S. L. Ridgway, Phys. Rev. **88**, 170 (1952), and private communication.
[37] J. K. Bair and F. Maienschein, Atomic Energy Commission Report NEPA 1620, unpublished.
[38] P. Hubert, J. phys. et radium **12**, 823 (1951).
[39] This work was done in cooperation with A. W. Sunyar of this laboratory, to whom our thanks are due.

On the basis of the intensity measurements of Hubert and considering the crystal efficiencies, 67 percent of the coincidences counted would be due to the 0.56–0.65 Mev cascade. Preliminary work using differential discrimination on one of the counters showed that the exclusion of a large portion of the higher energy cascades did not significantly change the anisotropy at 180°. This would not be inconsistent with the fact that the spin of the highest level might logically be taken as 3, from intensity considerations. The largest contribution to the coincidence background would then be from a cascade (2.1–0.56 Mev) which would offer little anisotropy.

It would appear that by taking into account the contribution from the other coincidence γ-rays, agreement could be obtained between the 0.56–0.65 correlation and that to be expected for a 2–2–0 spin assignment with $\alpha/\beta=0.5$ to 1.5 (20–66 percent D, 80–34 percent Q). In fact, simply the knowledge that a_2 is negative and a_4 is positive uniquely requires a 2–2–0 spin assignment for the 1.21-, 0.56-, and 0.0-Mev levels, if the possibility of a 0–2–0 assignment is disregarded because of the observed cross over. The phase difference is not determinable from our data.

Based on the directional correlation measurements, spins have been assigned to the excited levels of Se^{76} as shown in Fig. 4. The assignment of a spin of 2 to the first excited state is in agreement with the measurement of Tomlinson and Ridgway of the conversion coefficient of the 0.56-Mev gamma-ray, and the beta-gamma directional correlation measurements of Ridgway and Pipkin.[40] The assignment of an even parity to the second excited level is based on the fact that the mixture is probably between $M1$ and $E2$ radiations, both of which require no change of parity.

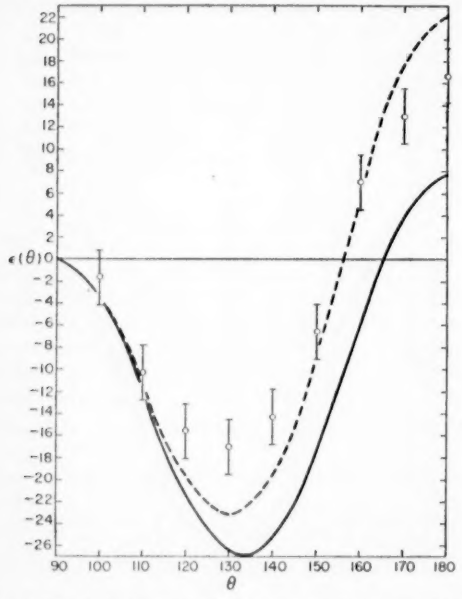

FIG. 6. The dashed curve is the least squares fit, corrected for the finite geometry, to the experimental points obtained with Ir^{194}. The solid curve is the theoretical distribution for a 2–2–0 (Q–Q) transition.

Ir^{194}

The decay of 19-hour Ir^{194} is known[35] to involve cascade gamma-rays of energies 0.33 and 1.48 Mev. However, due to uncertainties in some of the available information on this nuclide, a study of the gamma-radiation was undertaken as a preliminary to the directional correlation measurements.

Sources were prepared by neutron bombardment of a few mg of pure metallic iridium powder in the Brookhaven reactor. The decay of one source, irradiated for 5 minutes, was followed for a period of days, after letting the 1.5-minute activity of Ir^{192} decay. Two activities of 18.5 hours and 70 days were found. The 70-day activity of Ir^{192} accounted for about 21 percent of the gamma-rays at the beginning of the measurements.

Inasmuch as the data of Wilson[41] and Wattenberg[42,34] were in disagreement on the presence of Be photoneutrons from Ir^{194}, an experiment to detect such photoneutrons was carried out. In agreement with Wilson, photoneutrons were detected from Be, which decayed with a 19-hour half-life. The intensity of the responsible gamma-rays was estimated to be about 1 percent of the intensity of the two prominent lines.

The gamma-rays were also studied with a scintillation spectrometer. The two prominent lines of 0.33 and 1.48 Mev were observed and found to have about equal intensity. Weak, higher energy gamma-rays of 1.8 and 2.1 Mev were also in evidence. It would seem reasonable to assume that the 1.8-Mev gamma-ray is the cross-over transition. The 2.1-Mev gamma-ray could be the direct transition to the ground state that appears in the decay of Au^{194}.[43]

Inasmuch as the 70-day activity of Ir^{192} was also present in the sources used, precautions were necessary in order to insure that the measured directional correlation was only that due to the 1.48- and 0.33-Mev gamma-rays of Ir^{194}. The most intense gamma-rays of Ir^{192} are known to have energies of 0.3 and 0.47 Mev. One of the discriminator levels was therefore raised until annihilation radiation coincidences were no longer counted. The coincidences counted with the Ir source under these conditions decayed with a 19-hour half-life.

The measured directional correlation is shown in Fig. 6. The values of a_2 and a_4, obtained by a least squares procedure and corrected for the finite geometry, were -1.118 ± 0.061 and 1.340 ± 0.070, respectively. The situation is similar to As^{76}, and again only a 2–2–0 (D, Q–Q) assignment is compatible with the data, with

[40] S. L. Ridgway and F. M. Pipkin, Phys. Rev. **87**, 202 (1952).
[41] R. Wilson, Phys. Rev. **79**, 1004 (1950).
[42] A. Wattenberg, Phys. Rev. **71**, 497 (1947).
[43] Steffen, Huber, and Humbel, Helv. Phys. Acta **22**, 167 (1949).

$\alpha/\beta=0.13$ (98 percent Q, 2 percent D) and a phase difference of 180°. The agreement with this assignment is just outside the indicated errors.

It is interesting to note that a similar directional correlation has been observed[44] for the gamma-rays from the excited states of the neighboring even-even nucleus Pt^{196}. Further, the cross-over transition here is known also to be very weak (<1 percent). This, of course, as in Pt^{194}, is hard to reconcile with the 2–2–0 (Q–Q) assignment.

Measurements of the directional correlation of the gamma-rays of Pt^{194} have recently been reported by Whittle and Jastram.[45] While one of the alternative assignments 2–2–0 indicated by their data agrees with the assignment purported here, the measured directional correlation is apparently different.

There is no direct evidence on the energy of the first excited state. However, it seems most reasonable on the basis of systematics[11] of even-even nuclei of adjacent atomic number to take its energy as 0.328 Mev. Such an energy is also preferred over 1.48 on the basis of the low intensity of the cross-over transition. The K/L ratio of the 0.328-Mev gamma-ray has been determined[46] to be 2. This information, taken together with life-time considerations, would favor an $E2$ assignment for the transition. Such an assignment would be consistent with the directional correlation data and would add another member to the family of first excited states of even-even nuclei that have spin 2, even parity.

The decay of Au^{194} has been studied rather extensively by Steffen *et al.*[43] With the possible exception of the measured internal electron conversion coefficient for the 0.328-Mev gamma-ray, the information thus obtained on the excited states of Pt^{194} is in good agreement with that from Ir^{194}.

III. DIRECTION-POLARIZATION CORRELATIONS

The two counters used in the directional correlation work were placed so that they each subtended an angle of 90° at the source with a polarimeter. The value of θ was thus 90° and remained so. For such an arrangement, considering dipole and quadrupole radiation, the expressions of Hamilton[4] for J_θ/J_φ are reduced to $(1+a_2+a_4)/(1-a_2-a_4)$ or its reciprocal for yes-yes or no-no parity changes, respectively. For mixed parity changes, assuming equal coincidence counting efficiencies, J_θ/J_φ should be unity.

The polarimeter, based on Compton scattering, was similar to that employed by Metzger and Deutsch.[5] Its essential features are shown in Fig. 7. Another brass bearing to the rear of the chassis permitted rotation of the entire assembly through 360°. The lead shield was approximately symmetrical about the axis of rotation. The angular resolution in θ was about equal to that of the individual counters, i.e., 12.0°.

[44] B. M. Steffen and D. M. Roberts, Phys. Rev. **83**, 222 (1951).
[45] C. E. Whittle and P. S. Jastram, Phys. Rev. **87**, 203 (1952).
[46] J. W. Mihelich (unpublished data).

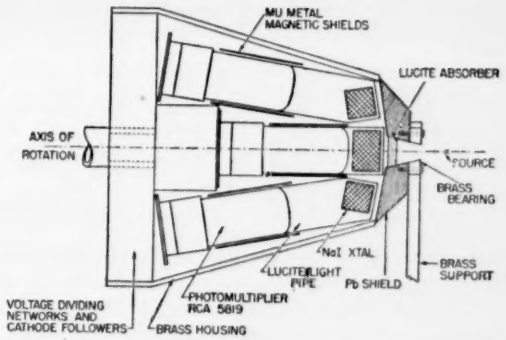

FIG. 7. The experimental arrangement for the measurement of the polarization of gamma-rays. A line joining the two single counters (not shown) would pass through the source perpendicular to the page.

The two individual counters were coupled together, as were the two side counters of the polarimeter. After amplification, the pulses from the three sets of counters went to integral pulse-height discriminators and blocking oscillators identical to the ones used in the directional correlation work. Three coincidence circuits monitored all double coincidence events so that the chance coincidences could be computed. The resolving time of the three circuits was 1.2×10^{-7} second. A slow resolving time coincidence circuit then registered double coincidences common to the center-side counter circuit and the center-individual counter circuit.

Data were taken by measuring the triple coincidence rate for half-hour periods for the four values of φ: 0°, 90°, 180°, and 270°. One determination of $N_{\parallel}/N_{\perp}$ consisted then of $(N_{0^\circ}+N_{180^\circ})/(N_{90^\circ}+N_{270^\circ})$, corrected for random coincidences.

The value of the angle δ (notation of Metzger and Deutsch[5]) was made 80°. Instead of attempting to evaluate the asymmetry ratio in terms of the spreads in δ and φ and correcting for scattering from the side to the center counter, an effective asymmetry ratio as a function of energy was determined in the following way. The collimated beam of gamma-rays from Co^{60} was scattered through 90° by a Cu plate. The value of $N_{\parallel}/N_{\perp}$ was measured for three thicknesses of the scatterer. The extrapolated value for zero thickness for $N_{\parallel}/N_{\perp}$ was thus determined to be 1.48 ± 0.05. From the Klein-Nishina formula, the value of J_θ/J_φ for the scattered beam is 2.19. The asymmetry ratio at 0.36 Mev is then 3.14 ± 0.1.

A more realistic determination of the effective asymmetry ratio was made using Co^{60} and Rh^{106} in a direction-polarization experiment. Inasmuch as the character of the prominent gamma-rays is known, a measurement of both the direction and polarization correlations should afford a determination of the effective asymmetry ratio at the energies involved. For Rh^{106}, the value of a_2+a_4 measured using the apparatus previously described was $+0.57\pm0.03$ for the 12.0° geometry. This is uncorrected

TABLE II. Values of $N_{\parallel}/N_{\perp}$ to be expected for the most probable spin and gamma-ray character assignments for the excited states of Pb^{208}.

Assignment	$N_{\parallel}/N_{\perp}$	Assignment	$N_{\parallel}/N_{\perp}$
3–1–0 ($E2$–$M1$)	1.02	4–2–0 ($E2$–$E2$)	0.97
3–2–0 ($E2$–$E2$)	1.06	4–2–0 ($E2$–$M2$)	1.00
3–1–0 ($E2$–$E1$)	1.00	4–2–0 ($M2$–$E2$)	1.00
3–2–0 ($M1$–$E2$)	1.02		

for detector size as the direction-polarization apparatus has approximately the same angular resolution. $N_{\parallel}/N_{\perp}$ was measured and a value of 0.62 ± 0.03 obtained. The asymmetry ratio at the average energy of 0.57 Mev is then 2.39 ± 0.20.

Likewise the experimental value of a_2+a_4 for Co^{60} was 0.1517 ± 0.0126, and $N_{\parallel}/N_{\perp}$ was measured to be 0.959 ± 0.02. The asymmetry ratio at the average energy of 1.22 Mev is then 1.31 ± 0.03.

ThC″

Recently, Petch and Johns[47] made a careful determination of the directional correlation of ThC″. Although other gamma-rays are present, the 0.58–2.62 Mev gamma-ray cascade will be observed about 65 percent of the time. Their measured correlation agreed well with that expected from a 4–2–0 (Q–Q) transition. The conversion coefficients have been measured by Martin and Richardson.[48] Their work indicated that the 0.58-Mev gamma-ray is $E2$. The measured coefficient for the 2.62-Mev gamma-ray (1.8×10^{-3}) falls between the values to be expected for $E2(1.0\times10^{-3})$ and $M1(2.1\times10^{-3})$ radiation. The authors preferred the closer $M1$ assignment.

Because of this discrepancy in the assignment of spins to the 3.20- and 2.62-Mev states of Pb^{208}, a direction-polarization correlation was undertaken. Such a measurement will act as a check on the spins as determined by the directional correlation measurements and will serve to indicate the relative parities of the three levels involved.

Deposits of 10.6-hour ThB on Al foil were used as sources of about 0.1-mC strength. There was no appreciable bias on any of the counters; the value of $N_{\parallel}/N_{\perp}$ obtained was 0.958 ± 0.03.

In view of the results of the measurements of the asymmetry ratio as a function of energy previously described, the asymmetry ratio for the gamma-ray cascade in Pb^{208} has been estimated as 1.2. Using this, the value of $N_{\parallel}/N_{\perp}$ to be expected for the most probable gamma-ray and spin assignments have been calculated and are shown in Table II.

The 4–2–0 ($E2$–$E2$) assignment is in more satisfactory agreement with our experimental value than the 3–1–0 ($E2$–$M1$) assignment given by Martin and Richardson. With this result, then, the parities of the first and second excited states are the same as the ground state, i.e., even, and the spins are in agreement with the result of the directional correlation measurements. The spin and parity of the first excited state lends support to the generalization[8–11] discussed previously.

Recently, the internal pair production coefficient of the 2.62-Mev gamma-ray has been measured by Slätis and Siegbahn.[49] The value obtained, agrees with that to be expected for an $E2$ transition.

IV. SUMMARY AND DISCUSSION

The occurrence of mixtures of radiation and the presence of extra-nuclear fields in directional correlation measurements has made necessary more accurate evaluations of the data and more care in correcting for instrumental effects. It is evident, also, that the further application of the techniques of directional correlations to the determination of spins and gamma-ray characteristics in the more complex decay schemes will be dependent on the energy selectivity of the detectors.

In the work reported here it has been demonstrated that the major contribution to the discrepancy between the earlier measured directional correlation of Rh^{106} and that expected for a 0–2–0 transition probably lay in the geometrical correction. The discrepancy that still exists after accounting for the effects of the detector size and the other gamma-rays is still a matter for speculation. The directional correlation of the 1.70–0.65 Mev gamma-ray cascade of Sb^{124} has been measured and indicates spins of 3, 2, and 0 for the three levels involved with a small admixture of quadrupole with the dipole radiation in the first transition.

The directional correlations of As^{76} and Ir^{194} are similar, and spin assignments of 2–2–0 (D, Q–Q) have been made. It is rather surprising to find such large ratios of quadrupole to dipole radiation in the mixed transitions and such weak intensities for the cross-over gamma-ray. This may support the contention[50] that the ground state of an even-even nucleus has a relatively purer wave function than the excited states.

The direction-polarization measurements with ThC″ substantiated the assignment of spins 4, 2, and 0, as determined by the directional correlation measurements, and determined the character of both gamma-rays to be $E2$.

It is interesting to note that the majority of the directional correlation measurements made recently require mixtures of dipole and quadrupole radiation in one of the transitions in order to interpret the data. Considering even-even nuclei and assuming that the first excited state has spin 2, even parity, mixtures can occur with spins of 1, 2, or 3 for the second excited state. Table III shows the results of directional corre-

[47] H. E. Petch and M. W. Johns, Phys. Rev. **80**, 478 (1950).
[48] D. G. E. Martin and H. O. W. Richardson, Proc. Phys. Soc. (London) **A63**, 223 (1950).
[49] H. Slätis and K. Siegbahn, *M. Siegbahn Commemorative Volume* (Uppsala, Sweden, 1951), p. 153.
[50] A. de-Shalit and M. Goldhaber (unpublished).

TABLE III. The occurrence of mixtures of radiation from Lipher excited states of even-even nuclei.*

Parent nuclide	Assigned spins	Percent dipole radiation in the first transition	Phase difference	Energy of first transition in Mev	Cross-over transition energy (Mev)	Cross-over transition percentage branching	Reference
Pr^{144}	1–2–0	94–100	0°	1.48	2.185	73	a
In^{114}	2–2–0	95.6	0°	0.548	1.26	3–6	b, c, d, e
Sb^{122}	2–2–0	20		0.68	1.24		f
As^{76}	2–2–0	20–66	180°	0.65	1.21	72	present paper
Au^{196}	2–2–0	{5	180°	0.33	0.69	<1	g, m
		{6	180°				e
Ir^{194}	2–2–0	2	180°	1.48	1.81	1	present paper
Rh^{106}	2–2–0	10–20	180°	1.045	1.55	24	h
Sb^{124}	3–2–0	99.9	0°	1.70	2.3	0.02	present paper
Cl^{38}	3–2–0	0		1.60	3.8	<0.02	i
Y^{88}*	3–2–0	99.9	0°	0.908	2.76	~1	j, k, l

* A spin and parity of 2+ has been assumed for the first excited state of Sr^{88}, however, as discussed before, 1+ cannot be excluded. The recent internal conversion measurements of Metzger and Amacher indicate that if there is a mixture of radiation in the first transition it must be of $E1$ and $M2$ radiation

[a] D. E. Alburger and J. J. Kraushaar, Phys. Rev. **87**, 448 (1952).
[b] Johns, Cox, and McMullen, Phys. Rev. **86**, 632 (1952).
[c] R. M. Steffen and W. Zoebel, Phys. Rev. **88**, 170 (1952).
[d] E. D. Klema and F. K. McGowan, Phys. Rev. **87**, 524 (1952).
[e] H. Heer and collaborators, reported at the Amsterdam Conference on beta- and gamma-rays.
[f] M. J. Glaubman and F. R. Metzger, Phys. Rev. **87**, 203 (1952).
[g] R. M. Steffen and D. M. Roberts, Phys. Rev. **83**, 222 (1951).
[h] Arfken, Klema, and McGowan, Phys. Rev. **86**, 413 (1952).
[i] R. M. Steffen, Phys. Rev. **80**, 115 (1950).
[j] E. L. Brady and M. Deutsch, Phys. Rev. **78**, 558 (1950).
[k] D. S. Ling and D. L. Falkoff, Phys. Rev. **76**, 1639 (1949).
[l] F. R. Metzger and H. C. Amacher, Phys. Rev. **88**, 147 (1952).
[m] R. M. Steffen, Bull. Am. Phys. Soc. **27**, No. 5, 18 (1952) and Phys. Rev. (to be published).

Note added in proof:—A private communication from Dr. H. Frauenfelder has informed us of the results of D. Schiff and F. Metzger for the directional correlation of the γ-rays of Hg^{198}. These are in the order given in the table: 2–2–0, 30–50 percent dipole, 0°, 0.68 Mev, cross-over 1.091 Mev, 20 percent. We wish to thank Dr. Frauenfelder for this information and for other valuable remarks.

lation measurements that have been interpreted as having either of these three spins for that excited state. The striking feature of the compilation is the sporadic behavior of the relative amounts of dipole radiation that are involved in 2–2 transitions.

Thanks are due E. L. Church for valuable contributions to the procedure for analyzing the data, to H. Finston who performed some chemical changes on the Rh^{106} sources, and to P. Prentkey who designed the amplifiers used.

Neutral Meson Production in n-p Collisions*

ROGER H. HILDEBRAND
Department of Physics and Institute for Nuclear Studies, University of Chicago, Chicago, Illinois
(Received November 17, 1952)

The angular distribution of neutral pions formed by 400-Mev neutrons in the process $n+p\rightarrow d+\pi^0$ has been measured using an experimental arrangement in which both of the π^0 decay gamma-rays are detected in coincidence with the deuteron. The results can be described in the center-of-mass system by the function $\cos^2\theta+0.2$. The agreement between this distribution and the π^+ distribution of the process $p+p\rightarrow d+\pi^+$, which has been measured by Whitehead and Richman and by Durbin, Loar, and Steinberger, gives evidence in support of the hypothesis of charge independence in meson-nucleon interactions.

I. INTRODUCTION

YANG has observed that a comparison of the reactions

$$n+p\rightarrow d+\pi^0, \tag{1}$$

and

$$p+p\rightarrow d+\pi^+ \tag{2}$$

should provide a severe test for the hypothesis of charge independence in meson-nucleon interactions.[1-8]

If we do not assume charge independence then we have no reason to expect any similarity between the angular distributions of the pions produced in these two reactions nor have we reason to expect any simple relationship between the cross sections. But if we do assume conservation of isotopic spin, in accordance with the charge independence hypothesis, and if we assume that the π^0 and π^+ both have isotopic spin one, then the pion angular distributions should be identical and the cross sections should be in the ratio 1:2 for reactions (1) and (2), respectively.

These simple relationships arise because under the assumptions just made the states of the end products of the two reactions must be regarded as identical except for the value of the charge variable. Similarly the initial p-p state is identical with that part of the n-p state which can contribute to the reaction, again except for the value of the charge. The angular distributions must, then, be the same since in the charge independence hypothesis we assume that meson-nucleon interactions are invariant under rotations in isotopic spin space. The 1:2 ratio of the cross sections results from the fact that the $n+p$ system is in a mixed state containing two equal parts with isotopic spins 0 and 1, only the latter part of which has the required isotopic spin, whereas the $p+p$ system is in a pure state of isotopic spin 1, all of which can contribute.

A strong angular dependence of the π^+ distribution has been observed by Whitehead and Richman[9] and by Durbin, Loar, and Steinberger[10] in their extensive experiments on reaction (2) and its inverse. The form of the distribution, which is nearly independent of energy, is well described by the function $\cos^2\theta+0.2$. The striking nature of this distribution makes the comparison of the π^0 and π^+ angular distributions a particularly severe test of charge independence.

In order to make this comparison the author is now investigating reaction (1) at a neutron energy of 400 Mev. By doing the experiment at this energy it is possible to compare the results directly with the highest energy measurements of Durbin, Loar, and Steinberger, since in each case the pion energy in the center-of-mass system is 53 Mev.

II. EXPERIMENTAL ARRANGEMENT

The important feature of the experiment is that the deuteron and both of the π^0 decay gamma-rays are detected in coincidence. This system makes it possible to distinguish between bound deuterons and free protons in the final system and it allows the selection of events caused by neutrons in a narrow energy range.

The experiment is only possible because of the large flux of neutrons well above the reaction threshold which is available at the University of Chicago synchro-cyclotron. The flux density of the collimated beam in the experimental area is about 5×10^5 neutrons cm^{-2} sec^{-1}. The spectrum extends from about 300 to 450 Mev with a peak a little below 400 Mev.

The neutral mesons are detected by means of their two decay gamma-rays in a manner similar to that used by Panofsky, Steinberger, and Steller[11] in studying π^0 production by photons. Each photon detector consists of a 0.63-cm thick lead plate to convert the γ-rays to electron pairs followed by a thin scintillator and a Čerenkov counter to count the electrons. The Čerenkov

* Research supported by the joint program of the U. S. Office of Naval Research and the U. S. Atomic Energy Commission.

[1] This test, originally suggested by C. N. Yang, unpublished, is a special case of a relationship given by Brueckner and Watson [Phys. Rev. 83, 1 (1951)]. This, and further tests, are discussed in references 2 to 8.

[2] R. L. Garwin, Phys. Rev. 85, 1045 (1952).

[3] A. M. L. Messiah, Phys. Rev. 86, 430 (1952).

[4] M. Ruderman, Phys. Rev. 87, 383 (1952).

[5] J. M. Luttinger, Phys. Rev. 86, 571 (1952).

[6] Van Hove, Marshak, and Pais, Phys. Rev. 88, 1211 (1952).

[7] W. Heitler, Proc. Roy. Irish Acad. 51, 33 (1946).

[8] K. M. Watson, Phys. Rev. 85, 852 (1952).

[9] M. N. Whitehead and C. Richman, Phys. Rev. 83, 855 (1951).

[10] Durbin, Loar, and Steinberger, Phys. Rev. 84, 581 (1951).

[11] Panofsky, Steinberger, and Steller, Phys. Rev. 86, 180 (1952).

counter,[12] which is filled with water, has the advantage of excluding the large background of heavy charged particles. The thin scintillator prevents counts due to photons which are converted in the relatively thick Čerenkov counter. Using this arrangement the ratio of the coincidence rates with and without the lead converters is about 100 to 1. Since good voltage plateaus are obtained, it is likely that the efficiency is nearly constant throughout the energy range of the experiment. The solid angle subtended by the photon detector is limited by the scintillation counter which is 5 cm in diameter and is placed 14 cm from the target.

The deuterons are detected by two scintillation counters which are separated a few centimeters to allow insertion of absorbers for range measurements. The deuteron detector is placed in the plane which contains the neutron beam and the bisector of the angle between the photon detectors which is approximately the direction of the π^0. The deuteron, neutron, and the pion must, therefore, move in the same plane in order for a sixfold coincidence[13] to occur between the two counters of the deuteron detector and the four counters of the

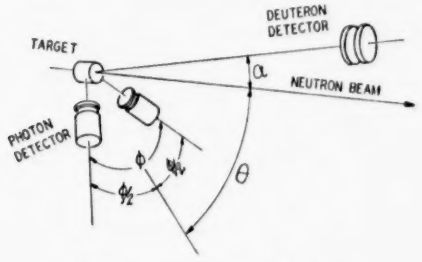

FIG. 1. Arrangement of detectors.

photon detectors. The requirement of coplanarity greatly reduces the chance of detecting pions formed within the carbon nuclei of the polyethylene and graphite targets because of the lateral component of momentum of the bound carbon nucleons. Accordingly the sixfold coincidence rate drops to $\frac{1}{3}$ of its former value when the polyethylene target is replaced by a graphite target of the same carbon content whereas the fourfold coincidence rate between the two photon detectors alone drops only to $\frac{2}{3}$. Thus, besides providing for a more positive identification of the reaction, the inclusion of the deuteron detector greatly reduces the error in determining the net count due to collisions with free protons.

Counting rates are obtained in terms of a BF_3 monitor. The ratio of coincidence to monitor counts remains constant as the beam intensity is varied and

[12] The Čerenkov counter construction is described by the author in a laboratory and shop note submitted to *The Review of Scientific Instruments*.

[13] The high speed, multi-channel coincidence analyzer which was used was designed by R. L. Garwin. A description by Garwin will appear in *The Review of Scientific Instruments*.

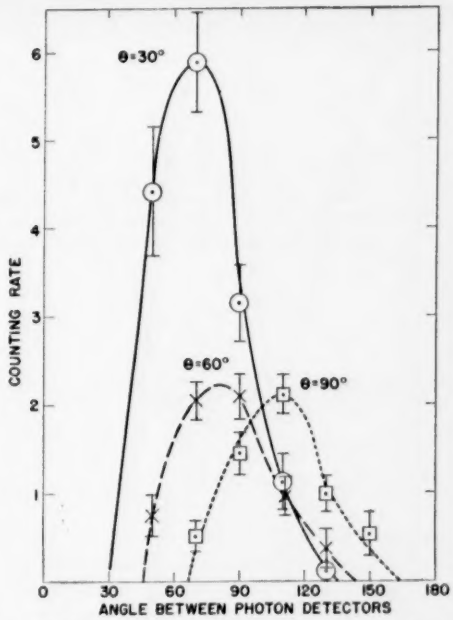

FIG. 2. Relative counting rates as a function of the photon correlation angle ϕ for three values of the angle θ. Arbitrary curves are drawn to aid in distinguishing the three sets of points.

measurements can be successfully repeated. Hence the monitor is believed to be reliable.

III. ANGULAR CORRELATIONS

If we assume, as is shown below, that the pion is formed in a two body $(d+\pi^0)$ system and not in a three body $(n+p+\pi^0)$ system then we expect a unique relationship between θ and α (the directions of the π^0 and deuteron) for a given neutron energy (see Fig. 1). The angle ϕ between the photons in the laboratory system depends not only on the velocity of the pion but also on the angle between the photon pair and the direction of motion of the pion measured in the π^0 frame. However, the distribution in ϕ, which has been given by Panofsky *et al.*,[11] favors the minimum laboratory angle $\phi_c=2\sin^{-1}\gamma^{-1}$, $(\gamma=E/E_0)$ so strongly that ϕ is also almost uniquely determined by θ and the neutron energy.

IV. PRELIMINARY EXPERIMENTS

As the angle between the photon counters is varied, counting rates are obtained corresponding to different parts of the neutron energy spectrum. Figure 2 shows the variation in counting rate as a function of ϕ for three different values of the pion angle θ. It will be seen that the peaks of these curves shift to the right as the angle θ is increased. This is to be expected since the meson energy decreases as θ increases. The locations and widths of the peaks agree well with predictions based on the known neutron energy distribution and the assumption of a two-body system. A three-body system should

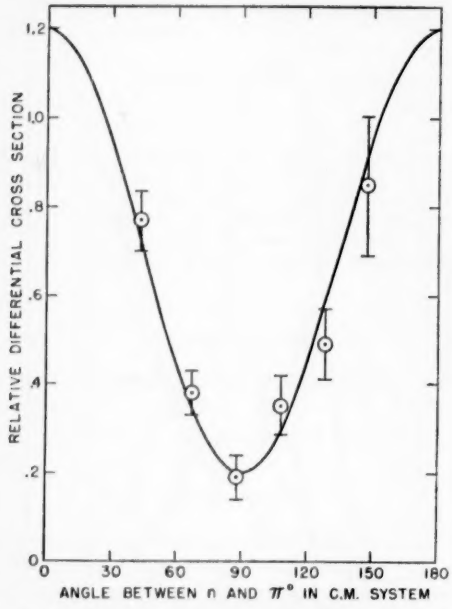

FIG. 3. Angular distribution of neutral mesons formed in n-p collisions. The function $\cos^2\theta+0.2$ corresponding to π^+ production in p-p collisions is drawn for comparison.

give a lower and more diffuse π^0 spectrum. By integration of these curves with appropriate geometrical corrections, one can obtain the relative flux of pions at the various angles θ due to the whole neutron beam. This has been done and the results agree with those given below: however, the transformation to the center-of-mass system is not unique if the whole neutron spectrum is included. The principal value of the curves in Fig. 2 is not to give the pion angular distribution but to confirm the assumption we have made that the pion is usually formed in a two-body $(d+\pi^0)$ system.

The assumption that the neutron and proton of the final system are usually bound is also confirmed by range measurements. Since, at this neutron energy, the velocity of either a deuteron or an unbound proton will be primarily due to the motion of the center of mass, the deuteron will have about twice the momentum of the proton and the two charged particles can easily be distinguished by their range. Still further evidence for the two-body system is the disappearance of coincidence counts when the deuteron detector is displaced from the plane of the π^0 and neutron beam. A measurement of the fraction of unbound protons is in progress.

V. MEASUREMENT OF π^0 DISTRIBUTION

The π^0 angular distribution has been measured by choosing values of ϕ and α at each of six angles θ to correspond to events caused by neutrons near the peak of the neutron distribution. The value of ϕ which was used was the median angle ϕ_m which is a few degrees larger than the minimum angle ϕ_c. The energy resolution, which is determined by the range in ϕ covered by the photon detectors, is good enough to establish a neutron energy of 400 ± 20 Mev. The corresponding energy of the pion in the center-of-mass system is 53 ± 8 Mev. The range of neutron energy ΔK which is accepted depends, somewhat, on the value of ϕ. Hence a factor $d\phi/dK$ must be included in calculating relative cross sections from the counting rates. This is easily calculated from the kinematics of the reaction if we assume that ϕ is uniquely related to the meson velocity by the expression for the median angle $\phi_m=2\sin^{-1}[2/(3\gamma^2+1)^{\frac{1}{2}}]$. (Nearly the same result is obtained if we use the relationship for the minimum angle $\phi_c=2\sin^{-1}\gamma^{-1}$.) The probability that the two photons shall be in a plane which contains the two photon detectors also depends on ϕ. This introduces a factor $\sin\phi$ in calculating the cross sections. Of course, a solid angle transformation is also included in order to express the results in the center-of-mass system. These factors are shown in Table I

TABLE I. Results.[a]

Angular settings θ_{lab}	α	ϕ	Counting rate	Correction factors $d\phi_m/dk$[b]	$\sin\phi_m$	$d\Omega_{lab}/d\Omega_{c.m.}$	Relative differential cross-sections	$\theta_{c.m.}$
25°	5.3°	74°	4.46±0.42	0.485	0.961	0.369	7.7±0.7	43°
40°	7.4°	81°	1.77±0.24	0.500	0.988	0.432	3.8±0.5	67°
55°	8.5°	90°	0.67±0.16	0.520	1.000	0.552	1.9±0.5	88°
70°	8.4°	101°	0.85±0.16	0.540	0.982	0.767	3.5±0.7	108°
90°	7.5°	115°	0.78±0.12	0.575	0.906	1.214	4.9±0.8	128°
115°	5.4°	129°	0.79±0.15	0.625	0.777	2.210	8.5±1.6	147°

[a] Neutron energy = 400 Mev.
[b] Degrees in ϕ per Mev neutron energy.

with the results. In Fig. 3 the angular distribution measurements are shown together with the function $\cos^2\theta+0.2$.

VI. CONCLUSIONS

The experiments on the reaction $n+p\rightarrow d+\pi^0$ may be summarized by the following observations:

(a) The reaction does occur and its cross section is of the same order of magnitude as that of the reaction $p+p\rightarrow d+\pi^+$.

(b) The measurements of the π^0 angular distribution can be fit by the function $\cos^2\theta+0.2$.

(c) The agreement between this distribution and the π^+ distribution of the reaction $p+p\rightarrow d+\pi^+$ gives evidence in support of the hypothesis of charge independence.

The fine cooperation of the cyclotron crew has been a great help in this experiment. The interest and encouragement of many members of the Institute and the Department of Physics are gratefully acknowledged.

Excitation Cross Section for Helium Atoms. II*

SAUL ALTSHULER
Department of Physics, Iowa State College, Ames, Iowa
(Received November 17, 1952)

The excitation scattering of electrons from helium atoms is investigated for the case of transition to the first excited singlet metastable level in order to examine quantitatively the error introduced by the fact that the description of the helium target is only approximately known. The cross section is calculated in Born approximation using formally equivalent matrix elements which weight the wave functions differently in space. The shape of the total cross section-energy curve is the same although absolute values differ while the angular distributions are considerably different.

IN a recent paper[1] (referred to as Paper I) the excitation scattering of electrons from helium atoms was investigated in order to examine the uncertainty introduced by the fact that the wave functions of the helium target are necessarily inaccurate. In Paper I, the investigation was confined to transitions to P-states. The present work follows the analysis in Paper I but pertains to the transition to the first excited metastable state of the helium atom. That is, two formally equivalent expressions for the differential cross section in Born approximation are employed, and these expressions do not lead to the same results in actual calculations because of the approximate nature of the helium atomic wave functions. As in Paper I, Method I will refer to the standard matrix element for the excitation differential cross section while Method II refers to results derived from the alternative expression obtained by the transformation

$$\psi_q^*\psi_p=\frac{\psi_q^*(\nabla_1^2+\nabla_2^2)\psi_p-\psi_p(\nabla_1^2+\nabla_2^2)\psi_q^*}{2(E_q-E_p)}. \quad (1)$$

Here ψ_q and ψ_p refer to exact wave functions for the final and initial helium states, respectively. Hartree units are employed everywhere.

The wave function for the $(1s\,2s)^1S$ level was originally suggested by Vinti[2] and already employed by Massey and Mohr[3] and is given by

$$\psi_q=B(\varphi_2-\gamma\psi_p), \quad \gamma=\int\psi_p^*\phi_2 d\tau_1 d\tau_2,$$

where ψ_p is the ground state of helium taken to be

$$\psi_p=\psi_{100}(N/r_1)\psi_{100}(N/r_2), \quad (N=1.687),$$

while

$$\phi_2=\frac{\psi_{100}(\alpha/r_1)\psi_{200}(\beta/r_2)+\psi_{100}(\alpha/r_2)\psi_{200}(\beta/r_1)}{\{2(1+b^2)\}^{\frac{1}{2}}},$$

with

$$b^2=(2x)^3(x-1)^2/(x+\tfrac{1}{2})^8; \quad x=\alpha/\beta; \quad B=(1-\gamma^2)^{-\frac{1}{2}}.$$

$\psi_{nlm}(Z/r)$ is the wave function of a single electron in the nlm state moving in a field of charge Z. The values of the screening parameters α and β were found[3] by the Ritz condition of minimum energy to be

$$\alpha=1.98, \quad \beta=1.20.$$

It is clear that ψ_q is properly normalized and orthogonal to the ground state.

The differential cross section for a momentum change of magnitude dK for excitation transition $1^1S\rightarrow 2^1S$ is then calculated by Method I and is given by

$$I(K)dK=\frac{8\pi dK}{k_p^2K^3}\left|\frac{36.879}{(13.447+K^2)^2}+\frac{(11.457)(2.547+2.887K^2)}{(5.2304+K^2)^3}-\frac{52.863}{(11.384+K^2)^2}\right|^2 \quad \text{(by Method I)}.$$

The matrix element for the excitation differential cross section by Method I is transformed by using Eq. (1), with the result (see appendix):

$$\sum_{i=1}^{2}\int e^{-iKz_i}\psi_p\psi_q^*d\tau_1d\tau_2=\frac{1}{(1-\gamma^2)^{\frac{1}{2}}\Delta E}\left[K^2\int\varphi_2e^{-iKz_1}\psi_pd\tau_1d\tau_2+2iK\int\varphi_2e^{-iKz_1}\frac{\partial}{\partial z_1}\psi_pd\tau_1d\tau_2\right], \quad (2)$$

in which $\Delta E=E_q-E_p$, the transition energy change, equals 0.75584. The final result of the cross section for

* The research reported in this paper has been sponsored by the Geophysical Research Directorate of the Air Force Cambridge Research Center, Air Research and Development Command under Contract AF19(122)-469. This material comprises part of a dissertation presented to the University of Southern California Graduate School in partial fulfillment of the requirements for the degree of Doctor of Philosophy in the department of Physics.

[1] S. Altshuler, Phys. Rev. **87**, 992 (1952).
[2] J. P. Vinti, Phys. Rev. **37**, 449 (1931).
[3] H. S. W. Massey and C. B. O. Mohr, Proc. Roy. Soc. (London) **A140**, 613 (1933).

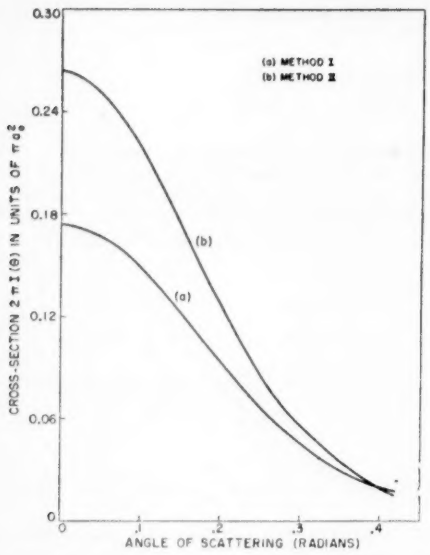

FIG. 1. Angular distributions for excitation scattering of electrons by helium atoms (1^1S to 2^1S transition) at an incident energy of 200 ev.

momentum change is given by

$$I(K)dK=\frac{8\pi dK}{k_p^2K^3}\left|3.7372\times10^2K^2\left[\frac{5.2159\times10^{-3}}{(13.4469+K^2)^2}+\frac{6.9338\times10^{-2}-9.876\times10^{-3}K^2}{(5.2304+K^2)^3}\right]\right|^2 \quad \text{(by Method II)}.$$

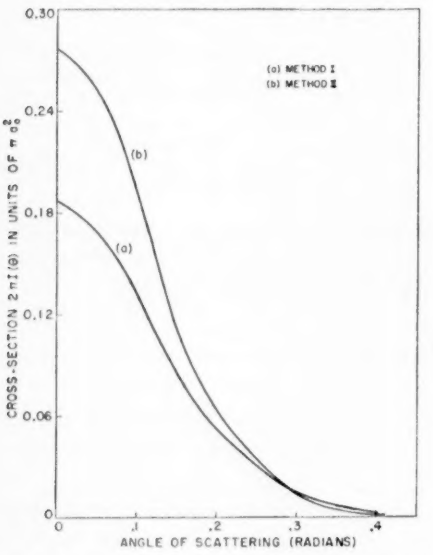

FIG. 2. Angular distributions for excitation scattering of electrons by helium atoms (1^1S to 2^1S transition) at an incident energy of 400 ev.

Comparative angular distributions of the differential cross section per unit solid angle, $I(\theta)$, in units of πa_0^2 (a_0=first Bohr radius) are portrayed in Figs. 1 and 2 for incident energies of 200 and 400 electron-volts, respectively. The total cross sections for both Methods I and II were obtained by numerical integration, and the results appear in Fig. 3.

DISCUSSION

Just as in the case of transitions to P-states (Paper I) we observe that the total cross section for either of the two methods may be normalized to measured values. However, such is not the case for the angular distributions in the case of the transition to the first excited metastable state. The disagreement in the shape of the angular distribution indicates that the Vinti function does not describe the metastable state as well as the Eckhart functions for the P-states (Paper I).

In order to discriminate between the results of either method it would be necessary to have accurate experimental data. Nevertheless, an argument may be advanced which favors the results of Method II. If we expand the exponential in Eq. (2) and exploit the symmetry of the wave functions, the matrix element may be rewritten

$$\sum_{i=1}^{2}\int e^{-iKz_i}\psi_p\psi_q^*d\tau_1d\tau_2 = 2\int\psi_q^*\left\{-iKz_1+\left(\frac{-iKz_1}{2!}\right)^2+\cdots\right\}\psi_pd\tau_1d\tau_2. \quad (3)$$

It is then apparent that considerable contribution to the integral is made from regions of configuration space other than those which contribute most to the energy integral. The space weighting of the wave functions using Method II places more emphasis on the region closer to the origin since it involves derivatives of the wave functions, and thus more accurate results should be expected when employing Method II. Verification of this argument has been demonstrated in one pertinent case in photoabsorption calculations.[4] This work dealt with the calculation of the continuous absorption coefficient of the H^- ion, where it was shown that the matrix element of the momentum operator gives more reliable results than that of the dipole. In the case of small angle scattering the leading term in Eq. (3) (for transition to P-states) is precisely the dipole element, while the matrix element of the momentum operator corresponds to Method II.

APPENDIX

The alternative matrix element which is the basis of Method II, as given in Eq. (2), is established as follows:

[4] S. Chandrasekhar, Astrophys. J. 102, 223 (1945).

In the case of the transition considered in this note, $\psi_p\psi_q^*$ is symmetric. Therefore,

$$J\equiv\sum_{i=1}^{2}\int e^{-iKz_i}\psi_p(\bar{r}_1,\bar{r}_2)\psi_q^*(\bar{r}_1,\bar{r}_2)d\tau_1d\tau_2$$
$$=2\int e^{-iKz_1}\psi_p\psi_q^*d\tau_1d\tau_2,$$

and, substituting from Eq. (1), we have

$$J=\frac{1}{\Delta E}\int e^{-iKz_1}\{\psi_q^*(\nabla_1^2+\nabla_2^2)\psi_p$$
$$-\psi_p(\nabla_1^2+\nabla_2^2)\psi_q^*\}d\tau_1d\tau_2$$
$$=\frac{1}{\Delta E}\Big[\int e^{-iKz_1}\{\psi_q^*\nabla_1^2\psi_p-\psi_p\nabla_1^2\psi_q^*\}d\tau_1d\tau_2$$
$$+\int e^{-iKz_1}\{\psi_q^*\nabla_2^2\psi_p-\psi_p\nabla_2^2\psi_q^*\}d\tau_1d\tau_2\Big].$$

The second term on the right vanishes identically because of the Hermitian property of ∇_2^2.

Consequently (since the 2^1S state is real),

$$J=\frac{1}{\Delta E}\int e^{-iKz_1}\{\psi_q\nabla_1^2\psi_p-\psi_p\nabla_1^2\psi_q\}d\tau_1d\tau_2.$$

Introducing

$$\psi_q=B(\varphi_2-\gamma\psi_p),$$

we have

$$J=\frac{B}{\Delta E}\Big[\int e^{-iKz_1}(\varphi_2-\gamma\psi_p)\nabla_1^2\psi_pd\tau_1d\tau_2$$
$$-\int e^{-iKz_1}\psi_p\nabla_1^2(\varphi_2-\gamma\psi_p)d\tau_1d\tau_2\Big]$$
$$=\frac{B}{\Delta E}\Big[\int e^{-iKz_1}(\varphi_2\nabla_1^2\psi_p-\psi_p\nabla_1^2\varphi_2)d\tau_1d\tau_2\Big].$$

We now employ the identity:

$$\int e^{-iKz_1}\psi_p\nabla_1^2\varphi_2d\tau_1d\tau_2=\int\varphi_2\nabla_1^2(\psi_pe^{-iKz_1})d\tau_1d\tau_2$$
$$=\int\varphi_2\{\psi_p\nabla_1^2e^{-iKz_1}+e^{-iKz_1}\nabla_1^2\psi_p$$
$$+2\nabla\psi_p\cdot\nabla e^{-iKz_1}\}d\tau_1d\tau_2.$$

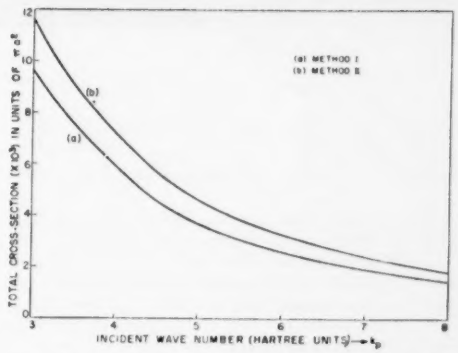

FIG. 3. Total excitation cross section for electron impact with helium atoms as a function of incident energy (1^1S to 2^1S transition).

Substituting, the expression for J becomes

$$J=\frac{B}{\Delta E}\Big[\int\{-\varphi_2\psi_p\nabla_1^2e^{-iKz_1}$$
$$-2\varphi_2\nabla_1\psi_p\cdot\nabla_1e^{-iKz_1}\}d\tau_1d\tau_2\Big]$$
$$=\frac{B}{\Delta E}\Big[K^2\int\varphi_2e^{-iKz_1}\psi_pd\tau_1d\tau_2$$
$$+2iK\int\varphi_2e^{-iKz_1}\frac{\partial}{\partial z_1}\psi_pd\tau_1d\tau_2\Big].$$

Note added in proof:—Errata in reference 1 are corrected as follows. The absolute value symbol in Eq. (3) should appear squared. The plus sign separating the two terms on the right in Eq. (7) should be changed to minus.

Equations (10) and (11) pertaining to the $^1S\rightarrow3^1P$ transition should read

$$Q_I(k_p)=\frac{1.507}{k_p^2}\Big[\frac{1}{X^7}\{-7.699\times10^2-\text{etc.}\cdots\}\Big]_{k_p-k_q}^{k_p+k_q}, \quad (10)$$

$$Q_{II}(k_p)=1.3515Q_I(k_p)-\frac{0.5245}{k_p^2}$$
$$\times\Big[\frac{1}{X^7}\{8.570K^6-1.241\times10^2K^4-7.342\times10^2K^2$$
$$-9.380\times10^2\}\Big]_{k_p-k_q}^{k_p+k_q}. \quad (11)$$

The shape of Fig. 4 is not changed but the magnitudes are altered slightly. The following is a table of corrected values (units are the same as in reference 1).

k_p	3	4	5	6	7	8
$Q_I\times10^3$	28.3	20.7	15.6	12.2	9.76	8.02
$Q_{II}\times10^3$	35.6	26.4	20.1	15.7	12.7	10.4

Relativistic Statistical Thermodynamics*

A. E. SCHEIDEGGER
Imperial Oil Limited, Calgary, Canada
AND
R. V. KROTKOV
Princeton University, Princeton, New Jersey

(Received March 6, 1952; revised manuscript received September 25, 1952)

Bergmann has generalized Gibbs' classical statistical mechanics so as to make it applicable to both relativistic and quantum-mechanical systems. His method, however, involves some complicated differential geometry, and the resulting formulas are not easily manageable. A different method for obtaining a relativistic and quantized statistical thermodynamics is proposed which avoids the differential geometry and gives simpler final formulas. The end results agree with the usual phenomenological relativistic thermodynamics, in which the entropy is a relativistic invariant, while heat and inverse temperature are generalized to be quadrivectors.

The new method is essentially to replace the Hamiltonian operator appearing in ordinary quantum statistics by a quadrivector, the energy-momentum operator $\mathfrak{P}$. The relativistic canonical ensemble is then defined by the density operator $\mathfrak{U}=\text{const}\exp(-\mathbf{\Theta}\mathfrak{P})$, which is Lorentz invariant, for the inner product $\mathbf{\Theta}\mathfrak{P}$ is. Then $k\mathbf{\Theta}$ (k = Boltzmann's constant) is a quadrivector of inverse temperature, while the entropy S, defined as $S=\text{const.}\ \text{trace}(\mathfrak{U}\log\mathfrak{U})$, is clearly invariant, since $\mathfrak{U}$ is. Heat may also be defined, in a way closely analogous to that used in the classical case, as a quadrivector $\delta\mathbf{Q}$ satisfying the relativistic second law $k\mathbf{\Theta}\delta\mathbf{Q}=dS$.

I. INTRODUCTION

IN view of the success of the statistical method in thermodynamics,[1] it seems a natural thing to try to generalize the latter so as to make it applicable to quantum-mechanical and to relativistic systems. This problem has been investigated before.[2] The procedure used was as follows: first, the classical, nonrelativistic and nonquantized, statistical mechanics of Gibbs was extended so as to describe relativistic systems. The new theory was, of course, to agree with the phenomenological relativistic thermodynamics developed by authors such as Planck,[3] Einstein,[4] Van Dantzig,[5] Tolman,[6] and Costa de Beauregard.[7] Finally, to obtain relativistic quantum statistics, the relativistic but nonquantized, statistical thermodynamics had to be generalized once more to describe quantum mechanical systems.

In Bergmann's paper,[2] the transition from Gibbs' classical theory to the relativistic statistical mechanics involved some rather complicated differential geometry and led to calculations which are not easily manageable. Accordingly, not much progress could be made beyond a general indication as to how the thermodynamic functions were to be obtained.

Therefore, it occurred to us that a different approach might be more successful. Generally, one might argue that one's interest lies, finally, only in the relativistic *quantum* statistics anyway. From this point of view the introduction of a nonquantized relativistic statistics appears as an intermediate step along the path to the final formalism. If one could by-pass this intermediate step, perhaps one could avoid the complicated differential geometry.

We were thus led to the following scheme: Gibbs' classical methods are *first* adapted to the quantum theory and only then is the generalization to relativity made. Thus, in the present paper we shall attempt to set up a generalization of the quantum statistical formalism of Neumann[8] and Klein[9] which will yield, in the end, the phenomenological, relativistic thermodynamic theory of Costa de Beauregard.[7] We shall show that it is quite easy to write down the required generalization of the canonical ensemble and to give the form of the phenomenological thermodynamic functions explicitly in terms of the partition function for that ensemble.

II. NOTATION

For the convenience of the reader we shall summarize briefly the notation and the principal facts of relativistic thermodynamics and of nonrelativistic quantum statistics.

Starting with the former, we note that we shall have to deal with vectors, operators, eigenvalues, etc. Throughout this paper, we shall denote vectors by boldface type, their components by corresponding italic lightface type. Operators will be denoted by upper case German type, their classical analogs by the corresponding italic type and their quantum eigenvalues by the corresponding lower case italic type.

Following the definitions of Costa de Beauregard,[7]

* This work was done while the authors were at Queen's University, Kingston, Canada.

[1] E. Schrödinger, *Statistical Thermodynamics* (Cambridge University Press, Cambridge, 1946).
[2] P. G. Bergmann, Phys. Rev. **84**, 1026 (1951).
[3] M. Planck, Ann. Physik **26**, 1 (1907).
[4] A. Einstein, Jahrb. Radioakt. u. Elektronik **4**, 441 (1907).
[5] D. Van Dantzig, Physica **6**, 673 (1939).
[6] R. C. Tolman, *Relativity, Thermodynamics, and Cosmology* (Oxford University Press, London, 1934).
[7] O. Costa de Beauregard, *La Théorie de la Relativité Restreinte* (Masson et Cie, Paris, 1949).
[8] J. von Neumann, Nachr. Ges. Wiss. Göttingen. mat.-physik. Klasse **3**, 273 (1927).
[9] O. Klein, Z. Physik **72**, 767 (1931).

we consider a body traveling relative to some Galilean frame of reference with uniform speed in a straight line. The quadrivelocity V^μ of the body is defined by the relation

$$V^\mu = dx^\mu/d\tau, \quad \mu = 1 \cdots 4, \tag{2.1}$$

where the x^μ are the position coordinates ($x^4 = ict$) and τ is its proper time. If m_0 is the rest mass of the body, its energy-momentum vector P^μ is given by

$$P^\mu = m_0 V^\mu. \tag{2.2}$$

Imagine now that the body is being heated. As a result of this process, the energy-momentum vector changes by the amount ΔP^μ. The "heat" transferred is defined as a quadrivector δQ^μ satisfying the equation

$$\Delta P^\mu = J \delta Q^\mu, \tag{2.3}$$

where J is Joule's constant (4.18 joules/calorie).

If T_0 is the absolute, proper temperature of the body, one can define an inverse temperature vector, θ^μ, by the relation

$$\theta^\mu = \theta_0 V^\mu, \tag{2.4}$$

where θ_0 is $1/T_0$. The change dS in the entropy of the body is then given by

$$dS = -\theta^\mu \delta Q^\mu, \tag{2.5}$$

where the summation convention is applied. Since dS is the inner product of two vectors one immediately sees that it is a relativistic invariant.

Turning now to the nonrelativistic quantum statistics of Neumann[8] and Klein,[9] the situation is as follows: an ensemble is represented by a density operator $\mathfrak{U}$ such that the expectation value $E(R)$ of an observable R over the ensemble is given by

$$E(R) = \text{trace}(\mathfrak{U}\mathfrak{R}). \tag{2.6}$$

The operator $\mathfrak{U}$ is Hermitian, non-negative definite, and has unit trace:

$$\text{trace}\mathfrak{U} = 1. \tag{2.7}$$

If it has a pure point spectrum, $\mathfrak{U}$ may be given the following simple interpretation: an ensemble represented by $\mathfrak{U}$ consists of systems which are in states corresponding to the eigenvectors of $\mathfrak{U}$, weighted with the corresponding eigenvalues.

With an ensemble of N systems there is associated an entropy S given by

$$S = -Nk \,\text{trace}(\mathfrak{U} \log \mathfrak{U}), \tag{2.8}$$

where k is Boltzmann's constant. To see that this expression behaves in the same way entropy should, we imagine two ensembles, 1 and 2, with density operators $\mathfrak{U}_1$, $\mathfrak{U}_2$, and weights α_1, α_2, respectively ($\alpha_1 > 0$, $\alpha_2 > 0$, $\alpha_1 + \alpha_2 = 1$). If we let these ensembles be combined to form a composite ensemble, the new, composite ensemble will have a density operator $\alpha_1\mathfrak{U}_1 + \alpha_2\mathfrak{U}_2$. It is then a mathematical theorem that

$$-\text{trace}[(\alpha_1\mathfrak{U}_1 + \alpha_2\mathfrak{U}_2)\log(\alpha_1\mathfrak{U}_1 + \alpha_2\mathfrak{U}_2)] \geq -\alpha_1 \,\text{trace}(\mathfrak{U}_1 \log \mathfrak{U}_1) - \alpha_2 \,\text{trace}(\mathfrak{U}_2 \log \mathfrak{U}_2), \tag{2.9}$$

the equal sign holding only for $\mathfrak{U}_1 = \mathfrak{U}_2$. This inequality states that when two ensembles are mixed, the total entropy cannot decrease, which of course is the desired property.

Canonical ensembles are characterized by having the maximum entropy of all possible ensembles, subject to the condition that the mean energy $E(H)$ is a constant. For such ensembles, the density operator $\mathfrak{U}$ is given by

$$\mathfrak{U} = a \exp(-\theta\mathfrak{H}), \tag{2.10}$$

where $\mathfrak{H}$ is the Hamiltonian operator of the system under consideration, and a, θ are constants to be determined by the auxiliary conditions (2.7) and

$$\text{trace}(\mathfrak{U}\mathfrak{H}) = E(H). \tag{2.11}$$

The Hamiltonian $\mathfrak{H}$ is here considered to be a constant of the motion.

The thermodynamic functions, now, are described by a partition function, $Z(\theta)$, which in the case of a canonical ensemble is defined by the equation

$$Z(\theta) = \text{trace}\exp(-\theta\mathfrak{H}). \tag{2.12}$$

Then we have, T being the temperature of the ensemble

$$\mathfrak{U} = [1/Z(\theta)]\exp(-\theta\mathfrak{H}), \tag{2.13}$$

$$S = Nk[\theta E(H) + \log Z(\theta)], \tag{2.14}$$

$$E(H) = -(\partial/\partial\theta)\log Z(\theta), \tag{2.15}$$

$$\theta = 1/kT. \tag{2.16}$$

III. THE RELATIVISTIC PARTITION FUNCTION

We now generalize the above scheme so as to make it relativistically covariant. Consider an ensemble of N independent relativistic systems, each of which is represented by a state vector. Then, as before, we can introduce a Hermitian, definite, operator $\mathfrak{U}$ such that the expectation value, $E(R)$, of any observable R taken over the ensemble will be

$$E(R) = \text{trace}(\mathfrak{U}\mathfrak{R}). \tag{3.1}$$

As before, the relation

$$\text{trace}\mathfrak{U} = 1 \tag{3.2}$$

holds. With this ensemble we associate the entropy

$$S = -Nk \,\text{trace}(\mathfrak{U} \log \mathfrak{U}),$$

which of course, in this case also, obeys Eq. (2.9).

To obtain the density operator which represents an equilibrium (canonical) ensemble, the expression $-Nk \,\text{trace}(\mathfrak{U} \log \mathfrak{U})$ is to be maximized, subject to certain conditions. The condition (2.7) used in the nonrelativistic case has, of course, to be carried over into the relativistic one, but Eq. (2.11) must be modi-

fied, for as it stands it is manifestly not covariant. This may be remedied by replacing it with the four conditions

$$\text{trace}(\mathfrak{U}\mathfrak{P}^\mu)=E(P^\mu)=\text{const.},\quad \mu=1\cdots 4, \tag{3.3}$$

where the $\mathfrak{P}^\mu$ are components of the energy momentum vector, now converted into an operator, introduced in (2.2). Each $\mathfrak{P}^\mu$ is assumed to be a constant of the motion which means all the $\mathfrak{P}^\mu$ commute with each other. This will be the case if the Lagrangian of the system in question is relativistically invariant. The problem we now wish to solve, is to minimize the expression $\text{trace}(\mathfrak{U}\log\mathfrak{U})$ subject to the conditions (2.7) and (3.3).

The solution is easily found if we reformulate the problem in terms of the eigenvalues u_n of $\mathfrak{U}$, which we assume to have a pure point spectrum. Since the u_n can be interpreted as statistical weights attached to each system of the ensemble, we require that the u_n be Lorentz invariant. One would also require this on the alternative grounds that the entropy,

$$S=-Nk\,\text{trace}(\mathfrak{U}\log\mathfrak{U}),$$

and hence $\mathfrak{U}$ itself together with its eigenvalues are to be relativistically invariant. In the new formulation, the problem becomes that of minimizing the sum

$$\sum_n u_n\log u_n \tag{3.4}$$

under the restrictions that

$$\sum_n u_n=1 \tag{3.5}$$

and that

$$\sum_n u_n p_n{}^\mu=E(P^\mu). \tag{3.6}$$

Here we have written $p_n{}^\mu$ for the nth eigenvalues of the operator $\mathfrak{P}^\mu$. It should be noted that in writing (3.6) we assume that $\mathfrak{U}$ commutes with all of the $\mathfrak{P}^\mu$ (which in turn commute with each other). This simply means that the systems comprising our ensemble are each in an eigenstate of the vector operator $\mathfrak{P}^\mu$, i.e., the weight attached to the system, and its energy momentum vector can be known simultaneously.

The method of Lagrange's multipliers gives the solution

$$u_n=a\exp(-\theta_\mu p_n{}^\mu), \tag{3.7}$$

where the summation convention is observed and the five numbers a, θ_μ are to be determined by the auxiliary conditions (3.5) and (3.6). Writing $\theta_\mu p_n{}^\mu$ as the inner product $\boldsymbol{\theta}\mathbf{p}_n$ of two vectors $\boldsymbol{\theta}$ and $\mathbf{p}_n$ with components θ_μ and $p_n{}^\mu$, respectively, the relativistic partition function $Z(\boldsymbol{\theta})$ is defined as

$$Z(\boldsymbol{\theta})=\sum_n\exp(-\boldsymbol{\theta}\mathbf{p}_n)=\text{trace}\exp(-\boldsymbol{\theta}\mathfrak{P}). \tag{3.9}$$

The density operator $\mathfrak{U}$ of a canonical ensemble can then be written in the following way:

$$\begin{aligned}\mathfrak{U}&=\sum_n u_n\mathfrak{Z}_n=\sum_n a\exp(-\boldsymbol{\theta}\mathbf{p}_n)\mathfrak{Z}_n\\&=[1/Z(\boldsymbol{\theta})]\exp(-\boldsymbol{\theta}\mathfrak{P}).\end{aligned} \tag{3.10}$$

Here the $\mathfrak{Z}_n$ are projection operators projecting on the eigenvectors of $\mathfrak{U}$. The general properties of Hermitian operators then justify the first step. To understand the last step one should note that the relation

$$a=1/Z(\boldsymbol{\theta}) \tag{3.11}$$

is a consequence of (3.5) and (3.9) and that the operator $\exp(-\boldsymbol{\theta}\mathfrak{P})$ is *defined* by the equation

$$\exp(-\boldsymbol{\theta}\mathfrak{P})=\sum_n\exp(-\boldsymbol{\theta}\mathbf{p}_n)\mathfrak{Z}_n.$$

The four conditions (3.6) may now be rewritten to read

$$\begin{aligned}E(P^\mu)&=\sum_n u_n p_n{}^\mu=(1/Z)\sum_n\exp(-\boldsymbol{\theta}\mathbf{p}_n)p_n{}^\mu\\&=-\frac{1}{Z}\frac{\partial}{\partial\theta_\mu}Z(\boldsymbol{\theta})=-\frac{\partial}{\partial\theta_\mu}\log Z(\boldsymbol{\theta}).\end{aligned} \tag{3.12}$$

These four relations can conveniently be combined into one

$$E(\mathbf{P})=-\nabla\,\log Z(\boldsymbol{\theta}), \tag{3.13}$$

where ∇ denotes the gradient with respect to $\boldsymbol{\theta}$.

The expression for the entropy can also be put into the following form

$$\begin{aligned}S&=-Nk\,\text{trace}(\mathfrak{U}\log\mathfrak{U})\\&=-Nk\,\text{trace}\left[\frac{\exp(-\boldsymbol{\theta}\mathfrak{P})}{Z}\log\frac{\exp(-\boldsymbol{\theta}\mathfrak{P})}{Z}\right]\\&=-(Nk/Z)\,\text{trace}[\exp(-\boldsymbol{\theta}\mathfrak{P})(-\boldsymbol{\theta}\mathfrak{P}-\log Z)]\\&=Nk[\boldsymbol{\theta}E(\mathbf{P})+\log Z(\boldsymbol{\theta})].\end{aligned} \tag{3.14}$$

From this equation it is at once clear that the entropy S is relativistically invariant, as it should be according to the discussion in Sec. II. The four relativistic Eqs. (3.9), (3.10), (3.13), and (3.14) are completely analogous to the nonrelativistic Eqs. (2.12), (2.13), (2.14), and (2.15). We have thus succeeded in generalizing the canonical ensemble relativistically.

However, there is one flaw in the preceding theory. This is that for many systems of interest (e.g., quantized fields) the operators $\mathfrak{P}^\mu$ have continuous spectra. Hence $Z(\boldsymbol{\theta})$, as defined by Eq. (3.9), and with it the thermodynamic functions $E(\mathbf{P})$ and S, will be infinite (for the trace of an operator with a continuous spectrum is infinite). This is natural, for one would expect, of course, that the entropy, for example, of a field filling all space would be infinite. Indeed, the same difficulty arose in the nonrelativistic theory [Scheidegger and McKay[10]].

In the paper by Scheidegger and McKay referred to, finite answers were obtained by enclosing the system of interest in a box, thus forcing the Hamiltonian $\mathfrak{H}$ to have a discrete spectrum, and the partition function Z to be finite. Upon letting the volume of the box go to infinity, finite expressions for the density (per unit

[10] A. E. Scheidegger and C. D. McKay, Phys. Rev. **83**, 125 (1951).

volume) of the thermodynamic functions for the field were obtained.

The same sort of procedure may be adopted in the present relativistic theory. The system of interest may be enclosed in a box. There are two possibilities to confine the system in a box: either the system is confined by walls which are not part of the system (case A), or there are no walls separate from the dynamical system (case B).

In case A, the walls provide a preferred coordinate system and discussion of Lorentz covariance becomes pointless. In case B, however, there is no state of thermodynamic equilibrium of the system. Mathematically, the latter difficulty will show up in the fact that the $\mathfrak{U}$ for equilibrium has a continuous spectrum, such that the above theory cannot be directly applied.

There is, however, a rational way out of this dilemma. One must stay in case B because one must have no preferred reference frame. Now there are two ways in which the system can fail to have an equilibrium state, and both of these must be taken care of. The system may just tend to fly apart and also the system may fly away bodily. In order to keep the system from flying apart one may introduce gravitational forces, and this may help for sufficiently heavy systems at sufficiently low temperatures, but leads one out of special into general relativity. If one does not want to introduce such gravitational forces, one must enclose the system into a flexible sack which is strong enough so that it will not tear, is impervious to its contents, and has zero vapor pressure at all temperatures. This may seem somewhat artificial but it is perfectly legitimate as the dynamical variables of the sack will be counted as dynamical variables of the system and the P's will include them.

There remains the difficulty that the whole system, intact, may fly away bodily. This is reflected in the fact that trace $\mathfrak{U}$ is proportional to the volume of space accessible to the sack and its contents, and if the sack is as postulated above, this is the only factor of trace $\mathfrak{U}$ which is infinite. But this factor is a constant and may be divided out. In other words, one can replace $\mathfrak{U}$ by a density matrix per unit volume of space which will then have a finite trace.

With these modifications to take care of an infinite partition function, the formalism here described may be used to calculate the thermodynamic functions of relativistic systems.

IV. RELATIVISTIC TEMPERATURE AND HEAT

In the nonrelativistic quantum statistics the parameter θ was, up to a constant, the inverse of the absolute temperature. We can easily show that in the relativistic case, the quadrivector $\boldsymbol{\theta}$ also has the usual properties associated with an inverse temperature.

In the first place, it is an immediate consequence of the relation (2.9) that if, with respect to a given Lorentz frame, two canonical ensembles with the same value of the parameter $\boldsymbol{\theta}$ are joined together to form a composite ensemble, this composite ensemble will also be canonical. In other words, systems with the same $\boldsymbol{\theta}$ (relative to the same Lorentz frame) are in equilibrium, as is to be expected if $\boldsymbol{\theta}$ is considered as, essentially, an inverse temperature.

As a second justification for associating $\boldsymbol{\theta}$ with an inverse temperature, one can show that $\boldsymbol{\theta}$ is an integrating factor for a suitably defined heat as follows: The procedure we adopt is analogous to that described by Schrödinger,[1] page 11, and by Khinchin,[11] page 135. The operator $\mathfrak{P}$ appearing in Eq. (3.3) depends generally on a set of external parameters, $\lambda_1\lambda_2\cdots\lambda_n$. For instance, one of the λ's could be the volume of the system considered, or perhaps some mass appearing in the explicit expression for $\mathfrak{P}$. With the introduction of the λ's, the thermodynamic functions become functions not of just $\boldsymbol{\theta}$ but of $\boldsymbol{\theta}$ and the λ's.

The λ's can, in general, transform in any way under Lorentz transformations. Let us, however, restrict ourselves to the case where the λ's are components of a tensor $\lambda_{\gamma\delta\cdots}^{\alpha\beta\cdots}$. This may be expected to include all physically interesting situations. Then the tensor-operator

$$\mathfrak{F}_{\alpha\beta\cdots}^{\mu\gamma\delta\cdots}=\partial\mathfrak{P}^{\mu}/\partial\lambda_{\gamma\delta\cdots}^{\alpha\beta\cdots}$$

may, by analogy with the classical case, be considered as a "force" acting in the "direction" of $\lambda_{\gamma\delta\cdots}^{\alpha\beta\cdots}$. The expectation value, $E(F_{\alpha\beta\cdots}^{\mu\gamma\delta\cdots})$, of this force over an ensemble with density operator $\mathfrak{U}$ is then given by Eq. (3.1) to be the tensor

$$E(F)_{\alpha\beta\cdots}^{\mu\gamma\delta\cdots}=\operatorname{trace}\left(\mathfrak{U}\frac{\partial\mathfrak{P}^{\mu}}{\partial\lambda_{\gamma\delta\cdots}^{\alpha\beta\cdots}}\right). \tag{4.1}$$

(Remember that $\mathfrak{U}$ is Lorentz invariant.)

For the special case, of a canonical ensemble, $\mathfrak{U}$ according to Eq. (3.10) is

$$\mathfrak{U}=\frac{1}{Z(\boldsymbol{\theta})}\exp(-\boldsymbol{\theta}\mathfrak{P}).$$

By inserting this last expression into (4.1), one obtains the relation

$$E(F)_{\alpha\beta\cdots}^{\mu\gamma\delta\cdots}=\operatorname{trace}\left(\frac{1}{Z}\exp(-\theta_{\mu}\mathfrak{P}^{\mu})\frac{\partial\mathfrak{P}^{\mu}}{\partial\lambda_{\gamma\delta\cdots}^{\alpha\beta\cdots}}\right)$$

$$=\sum_{n}\frac{\exp(-\theta_{\mu}p_{n}^{\mu})}{Z}\frac{\partial p_{n}^{\mu}}{\partial\lambda_{\gamma\delta\cdots}^{\alpha\beta\cdots}}, \tag{4.2}$$

where the p_n^{μ} are defined as in Eq. (3.9). The last equation (4.2) may be rewritten as

$$\theta_{\mu}E(F)_{\alpha\beta\cdots}^{\mu\gamma\delta\cdots}=-\frac{\partial}{\partial\lambda_{\gamma\delta\cdots}^{\alpha\beta\cdots}}\log Z(\boldsymbol{\theta}). \tag{4.3}$$

[11] A. I. Khinchin, *Mathematical Foundations of Statistical Mechanics* (Dover Publications, New York, 1949).

Now, let each $\lambda_{\gamma\delta\ldots}{}^{\alpha\beta\cdots}$ be changed by a small amount $\delta\lambda_{\gamma\delta\ldots}{}^{\alpha\beta\cdots}$, and $\boldsymbol{\theta}$ by $d\boldsymbol{\theta}$. This will change our canonical ensemble into another, neighboring, but still canonical one, with slightly different entropy and mean energy momentum vector. The "work," $E(\delta A)^\mu$, done in making the change may be defined, again in close analogy with the classical case, by the expression

$$E(\delta A)^\mu = NE(F)_{\alpha\beta\ldots}{}^{\mu\gamma\delta\cdots}\delta\lambda_{\gamma\delta\ldots}{}^{\alpha\beta\cdots}, \tag{4.4}$$

where N is the number of systems in the ensemble. Combining Eq. (4.4), (4.3), and (3.13), and remembering that $Z(\boldsymbol{\theta})$ now depends on both $\boldsymbol{\theta}$ and the λ's, we have

$$\begin{aligned}\theta_\mu E(\delta A)^\mu &= N\theta_\mu E(F)_{\alpha\beta\ldots}{}^{\mu\gamma\delta\cdots}\delta\lambda_{\gamma\delta\ldots}{}^{\alpha\beta\cdots}\\ &= -N\frac{\partial}{\partial\lambda_{\gamma\delta\ldots}{}^{\alpha\beta\cdots}}\log Z(\boldsymbol{\theta})\delta\lambda_{\gamma\delta\ldots}{}^{\alpha\beta\cdots}\\ &= -N[d\log Z(\boldsymbol{\theta}) - \nabla\log Z(\boldsymbol{\theta})\cdot d\boldsymbol{\theta}]\\ &= -N[d(\log Z(\boldsymbol{\theta})) + E(\mathbf{P})d\boldsymbol{\theta}]. \end{aligned}\tag{4.5}$$

The last relation (4.5) in conjunction with (3.14) may now be used to evaluate the change dS in entropy, associated with the changes in the λ's and $\boldsymbol{\theta}$

$$\begin{aligned}k\boldsymbol{\theta}(NdE(\mathbf{P}) - NE(\delta\mathbf{A})) &= Nk[\boldsymbol{\theta}dE(\mathbf{P}) + d\boldsymbol{\theta}E(\mathbf{P}) + d\log Z]\\ &= d[Nk(\boldsymbol{\theta}E(\mathbf{P})) + \log Z(\boldsymbol{\theta})] = dS. \end{aligned}\tag{4.6}$$

Thus, once more in close analogy with the classical case, we can define the quantity

$$\delta Q^\mu = N[dE(P)^\mu - E(\delta A)^\mu] \tag{4.7}$$

to be the "heat" transferred to the ensemble during the change considered. Thus, we see from Eq. (4.6), which may be written in the equivalent form,

$$k\theta_\mu\delta Q^\mu = dS, \tag{4.8}$$

that $k\boldsymbol{\theta}$ is an "integrating factor" for the heat vector $\delta\mathbf{Q}$. This result, very similar to the corresponding one holding in the classical theory, is a second justification for associating $\boldsymbol{\theta}$ or, more exactly, $k\boldsymbol{\theta}$, with an inverse temperature.

Thus, we see that, as in the phenomenological theory of Costa de Beauregard, heat and temperature are quadrivectors.

V. CONCLUSION

By the treatment above, we have succeeded in developing a relativistic quantum statistics by generalizing the quantized but nonrelativistic formalism of Neumann[8] and Klein.[9]

The canonical ensemble is generalized relativistically by substituting for the Hamiltonian $\mathfrak{H}$, the energy momentum operator $\mathfrak{P}$ (a quadrivector), which is assumed to be a constant of the motion. The relativistic partition function, $Z(\boldsymbol{\theta})$, then may be written as

$$Z(\boldsymbol{\theta}) = \text{trace}\exp(-\boldsymbol{\theta}\mathfrak{P}),$$

where $k\boldsymbol{\theta}$ (k is Boltzmann's constant) is the inverse temperature quadrivector. The thermodynamic functions S (the entropy), and $E(\mathbf{P})$ (the expectation value of $\mathfrak{P}$ over the ensemble) then become

$$S = Nk(\boldsymbol{\theta}E(\mathbf{P}) + \log Z(\boldsymbol{\theta}))$$

and

$$E(\mathbf{P}) = -\nabla\log Z(\boldsymbol{\theta})$$

where ∇ denotes the gradient with respect to $\boldsymbol{\theta}$, and N is the number of systems in the ensemble.

When a small change is made in the condition of a canonical ensemble, a suitably defined heat vector $\delta\mathbf{Q}$ satisfies the relation

$$k\boldsymbol{\theta}\,\delta\mathbf{Q} = dS.$$

The above scheme is in agreement with the usual phenomenological relativistic thermodynamics in that heat and (inverse) temperature are quadrivectors, while the entropy is a scalar. It should be further noted that the formulas above are closely analogous to the corresponding ones in the nonrelativistic quantum statistics.

Microwave Absorption Spectrum of ND_3

R. G. NUCKOLLS, L. J. RUEGER, AND HAROLD LYONS
National Bureau of Standards, Washington, D. C.

(Received October 10, 1952)

The main $J=K$ sequence of inversion lines of the ND_3 absorption spectrum were observed and measured between 1589 and 2540 Mc. Quantum numbers up to $J,K=18,18$ were assigned by the use of an approximate empirical formula.

THE investigation of the microwave absorption spectra of the deutero ammonias previously reported[1,2] has been extended. The isotopic analysis of 24 of the lines between 2 and 17 kMc showed[2] that the principal ground state ND_3 lines were to be expected below the 2080-Mc cut-off frequency of the *S*-band absorption cell[3] used previously. Accordingly a coaxial type Stark cell of novel design[4] was constructed to permit measurements as low as 900 Mc, currently the lowest frequency gas spectrometer reported. Table I lists both the frequencies of the main $K=J$ series of lines as measured to a precision of approximately 0.05 Mc, and the corresponding frequencies calculated according to the empirically determined approximate equation:

$$\nu=1595.69-7.155J(J+1)+10.03K^2, \quad (1)$$

based on the NH_3 type theoretical formula:

$$\nu=\nu_0-BJ(J+1)+AK^2. \quad (2)$$

Additional terms in higher powers of J and K are required to calculate the series of lines at high J,K numbers to the measurement precision. The table was discontinued at $J,K=12,12$ where these higher order terms begin to dominate the calculation. A number of additional lines were observed incidentally, but are not given in this preliminary Table, which have been discussed previously.[5] The identification of the proper peaks for the 1,1 and 2,2 lines is made uncertain by a combination of effects—the overlapping of the 1,1 and 2,2 quadrupole patterns, the recently reported[6] K doubling of the 1,1 line (and its quadrupole components), and an unfortunate waveguide resonance between 1580 and 1600 Mc. It is hoped to resolve this uncertainty with a modification of the apparatus and technique. Computation of both the molecular constants and higher order terms in the empirical formula awaits this investigation.

TABLE I. Frequencies of ND_3 inversion lines (Mc).

J,K	Measured	Calculated	J,K	Measured	Calculated
1,1	1589.10	1591.41	10,10	1815.37	1812
2,2	1591.72	1592.88	11,11	1872.43	1865
3,3	1599.53	1600.10	12,12	1937.31	1924
4,4	1612.99	1613.1	13,13	2010.57	
5,5	1631.82	1631.8	14,14	2092.32	
6,6	1656.18	1656.3	15,15	2183	
7,7	1686.46	1686.5	16,16	2285	
8,8	1722.85	1722.4	17,17	2403	
9,9	1765.80	1764.2	18,18	2540	

Previous theoretical predictions of ν_0 have varied from 1200[7] to 2000[8] Mc. A semi-empirical calculation of the constants in Eq. (1) is discussed elsewhere,[9] and confirms the experimental assignments listed in the table.

Other features of the spectra, such as the splitting of the 3,3 and 6,6 lines[10] have also been observed.

It is a pleasure to acknowledge the helpful discussions with Professor Charles H. Townes of Columbia University, consultant to the Microwave Standards Section of the National Bureau of Standards.

[1] Harold Lyons, Phys. Rev. **76**, 161 (1949); Harold Lyons, J. Appl. Phys. **21**, 59 (1950).
[2] Lyons, Kessler, Rueger, and Nuckolls, Phys. Rev. **81**, 297 (1951); Lyons, Rueger, Nuckolls, and Kessler, Phys. Rev. **81**, 630 (1951).
[3] Rueger, Lyons, and Nuckolls, Rev. Sci. Instr. **22**, 428 (1951).
[4] L. J. Rueger and R. G. Nuckolls, Rev. Sci. Instr. **23**, 635 (1952).
[5] Rueger, Nuckolls, and Lyons, Symposium on Molecular Structure and Spectroscopy, American Physical Society (June 13, 1951); Nuckolls, Rueger, and Lyons, Phys. Rev. **83**, 880 (1951).
[6] Good, Coles, Gunther-Mohr, Schawlow, and Townes, Phys. Rev. **83**, 880 (1951); J. H. Van Vleck, Phys. Rev. **83**, 880 (1951).
[7] C. H. Townes, private communication. This estimate was later raised to 1600 on the basis of inversion absorption in the first excited vibrational state.
[8] M. T. Weiss and M. W. P. Strandberg, Phys. Rev. **81**, 286 (1951) and **83**, 567 (1951). The latter article also shows precision measurements for a number of the partially deuterated ammonia lines above 5000 Mc, and, more significantly, their quantum assignments and the molecular constants.
[9] Madigan, Javan, and Lotspeich (to be published).
[10] H. H. Nielson and D. M. Dennison, Phys. Rev. **72**, 1101 (1947).

Nuclear Constitution and the Interpretation of Fission Phenomena

DAVID LAWRENCE HILL*
Vanderbilt University, Nashville, Tennessee, and Los Alamos Scientific Laboratory, Los Alamos, New Mexico

AND

JOHN ARCHIBALD WHEELER†
Princeton University, Princeton, New Jersey, and Los Alamos Scientific Laboratory, Los Alamos, New Mexico

(Received October 14, 1952)

An attempt is made to correlate in a unified picture the features of the empirical evidence on nuclear constitution, some of which appear to require for their explanation the liquid drop model as others require the independent particle picture. As an idealized and exploratory basis for an inclusive description, the extreme saturation assumption has been adopted: potential on a typical nucleon in the nuclear interior nearly independent of the position of the other nucleons, this potential falling off in a small distance at the nuclear surface. In the resulting *collective model* of the nucleus a distinction is made between the nucleonic state of the system—as defined by the states occupied by the individual nucleons—and the state of vibration and rotation of the nucleus as a whole. On quantum-mechanical grounds it is shown how the kinetic energy of this motion receives an explanation in terms of the degrees of freedom of the individual particles. As in the electronic-vibrational-rotational description of molecular constitution, so in the case of the nucleus it is reasonable to think of the sums of the energies of the individual particle states, plus the sum of the interaction energies, as defining a potential energy of deformation as a function of the shape of the system. Different states of the totality of individual particles give rise to different potential energy surfaces. A given sheet touches one of the surfaces immediately above or below it only at certain isolated "funnels" as in the case of polyatomic molecules. For full validity of the collective model it is necessary that nonadiabatic transitions from one surface to another occur infrequently compared to the frequency of rotation and capillary oscillations, so that these collective motions have a well-defined existence. The mathematical consequences of the collective model have not been explored fully enough to tell whether this condition of self-consistency is fulfilled well or very roughly or not at all for any given excitation energy. The vibrational frequencies correspond in general terms to those predicted by the simple liquid drop model, with, however, certain characteristic quantum mechanical differences. Instances of the Franck-Condon principle have to be accepted, analogous to those in the molecular case. Discussed are some consequences of the collective model or of its liquid drop simplification for energy levels, compatibility of strong neutron capture with individual particle effects in binding, quadrupole moments, alpha-decay, fission thresholds, photofission, spontaneous fission, asymmetry in nuclear fission, hydrodynamics of the division process, fission alpha-particles, and fragment excitation.

I. THE LIQUID DROP AND THE INDEPENDENT PARTICLE

FISSION is unusual among nuclear processes. The division of a many-particle system into two equal fragments is beyond explanation in terms of the movement of a single nucleon, or any small number of nucleons. In evidence is the collective behavior of the nucleus as a whole. This behavior has been idealized in the liquid drop model. The nuclear substance is compared with a nearly incompressible fluid, of almost uniform volume density of electrification, with an approximately constant energy of binding per particle, except as modified (1) by the electrostatic energy of interaction of the different portions of the fluid and (2) by the deficit of binding of the incompletely surrounded particles at the surface—a deficit proportional to the extent of the surface, and therefore responsible for the phenomenon of a surface tension, as in ordinary liquids.[1,2] Such a system is susceptible to deformation (Fig. 1[3]). The stabilizing effect of the surface tension overbalances the potentially disruptive influence of the electrostatic repulsions even for heavy nuclei in their normal nearly spherical configurations. Consequently a small disturbance will lead to oscillations about the equilibrium shape. However, a marked dumbell-like distortion will decrease the perimeter available for the action of surface tension proportionately more than it cuts down the electrostatic repulsion of the two halves of the system.[4] Consequently sufficient deformation of a heavy nucleus will cause instability. Then a still greater extension will occur, with electrostatic energy being set free faster than the consumption of energy in the increase of the surface. The movement thus accelerates. Ultimately the nucleus breaks into two or more parts. Thus the act of fission has several stages:[5] (1) raising the nucleus to the given level of excitation by radiation or impact of a material particle; (2) concentration of sufficient of this energy in a capillary oscillation to lead to a critical deformation (Figs. 2 and 3); (3) subsequent automatic growth of this deformation (Fig. 4); (4) scission into distorted fragments; (5) separation of these fragments; (6) de-excitation of the new nuclei.

While fission demonstrates that nucleons can undergo collective modes of motion, evidence has recently been growing[6–9] that nucleons also behave as if they possess individual and nearly independent states of binding—

* Holder for part of this work at Princeton University of a Socony Vacuum Fellowship, which is gratefully acknowledged.
† Holder for part of this work of a John Simon Guggenheim Fellowship, for which hearty appreciation is expressed.

[1] N. Bohr, Nature **137**, 344, 351 (1936).
[2] N. Bohr and F. Kalckar, Kgl. Danske Videnskab. Selskab, Mat.-fys. Medd. **14**, No. 10 (1937).
[3] All figures in this paper, together with related discussions, have been placed in the Appendix.
[4] L. Meitner and O. R. Frisch, Nature **143**, 239 (1939).
[5] N. Bohr and J. A. Wheeler, Phys. Rev. **56**, 426 (1939).
[6] M. G. Mayer, Phys. Rev. **78**, 16, 22 (1950).
[7] Haxel, Jensen, and Suess, Z. Physik **128**, 295 (1950).
[8] L. W. Nordheim, Phys. Rev. **75**, 1894 (1949).
[9] E. Feenberg and K. C. Hammack, Phys. Rev. **75**, 1877 (1949).

evidence from spins and magnetic moments, and from the shell structure in nuclear binding energies. We are forced to conclude that two such apparently dissimilar views as the liquid drop picture and the independent particle model are necessarily incomplete parts of a larger unity. Consequently, it must be possible to see and understand the collective aspects of nuclear behavior starting with what we can reasonably say about the properties of individual nucleons. If we justify in this way hydrostatic-theoretic calculations of the general trend with atomic number and atomic weight of the critical energy required for fission, we must at the same time expect that deviations have to be expected about these average values from nucleus to nucleus because of the individual character of nucleon states.

That neither the liquid drop model nor the model of individual nucleons moving in a field of spherical symmetry are separately adequate shows very clearly in the evidence on nuclear quadrupole moments (Figs. 5, and 29). Both pictures fail to account for asymmetries in the distribution of nuclear electric charge nearly so large as many of the typical observed values.[10,11] However, one must recognize that the pressure of a few individual nucleons against the nuclear surface will deform the collective assemblage of nuclear charge (Fig. 6). In this way one estimates quadrupole moments of the observed order of magnitude, as first pointed out by Rainwater.[12]

The lesson of the quadrupole moments is the strength of interaction of nucleons with each other by way of the surface compared to the strength of their direct interactions with each other. In support of this conclusion is the empirical evidence on nuclear binding energies. The energy of a nucleon which has an adequate complement of neighbors within a distance of order 10^{-13} cm is evidently little affected by the presence or absence of more nucleons outside this distance. Neither does this difference much affect the average spacing of the closer neighbors. How this saturation character of nuclear forces comes about is as little understood as the origin of these interactions.[13,14] Nor is it clear why spins, magnetic moments, and finer details of the nuclear binding energies should be consistent with the picture of individual nucleons travelling nearly independently through an average potential. Nevertheless, the evidence requires us to take seriously and to explore the consequences of the idealization in which each particle moves in a potential well, of depth approximately constant throughout the nuclear interior, abruptly falling off within a distance of the order r_0 near the surface.

Finer details of nuclear shell structure have suggested the hypothesis that the individual nucleons are subject not only to the nuclear potential field but also to a spin-orbit coupling.[6] Without in any way questioning this fruitful proposal, we can legitimately overlook the existence of such a coupling in a first survey of the relation between the independent particle picture and a more nearly unified description of the nucleus.

II. THE COLLECTIVE MODEL

We shall explore the *collective model* of the nucleus, based upon the following assumptions.

Features Regarded as Reasonable in Any Model

(1) Roughly constant density; one particle per volume $(4\pi/3)r_0^3$, with $r_0 \sim 1.4\times10^{-13}$ cm $= e^2/2mc^2$.

(2) Maximum kinetic energy, F, per nucleon consequently nearly independent of mass number; roughly 24 Mev.

(3) Distribution of charge over volume uniform to perhaps 25 percent or better.

(4) Nucleon binding energies generally between 5 and 10 Mev; average potential energy of order of -30 Mev.

(5) Saturation character of nuclear forces.

Special Assumptions

(1) Extreme saturation: forces regarded as giving a potential for a typical nucleon in the nuclear interior nearly independent of the position of the other nucleons, this potential falling off in a small distance at the nuclear surface. Contrast this idealization with the opposite extreme model of an impenetrable liquid drop, with forces conceived as sharply dependent on positions of nearby nucleons, whether the particle in question is in the interior or at the surface. In that picture the direct coupling between the particles is envisaged as so large that individual nucleon states have absolutely no well-defined existence. The observations which suggest the notion of nearly independent particle orbits refer mostly to ground states and low, excited states. There circumstances are at work specially favorable to suppress the consequences of nucleon-nucleon interactions which deviate from the saturation average. There appear to be no strong arguments for or against such over-the-background interactions of quite significant strength. Nevertheless, the essential idealization of the collective model is to *neglect* these direct couplings in comparison with the indirect couplings which take place through the intermediation of the movable potential wall. In this respect the picture is a first approximation whose distance from the truth will only be found by full exploration of its consequences. The theory of the collective model is in too early a stage to make a detailed confrontation with experiment.

(2) The state of the whole system is assumed to be specified in first approximation by the states of motion of the individual nucleons—or, as will be seen, by a

[10] Walter Gordy, Phys. Rev. **76**, 139 (1949).
[11] Townes, Foley, and Low, Phys. Rev. **76**, 1415 (1949).
[12] J. Rainwater, Phys. Rev. **79**, 432 (1950).
[13] L. Rosenfeld, *Nuclear Forces* (Interscience Publishers, Inc., New York, 1948).
[14] V. F. Weisskopf, Helv. Phys. Acta **23**, 187 (1950); Science **113**, 101 (1951).

particular one out of many potential energy curves—and by appropriate quantum numbers for the rotation of the system and its collective vibration on the potential energy curve in question. In actuality exchange of energy will take place with a finite probability between vibration and individual particle excitations, via couplings of both modes of motion with the wall. These exchanges are not accidental side issues of the collective model—they are the vital part of reaction kinetics. But if they are frequent, compared to the oscillation rate, then the division of energy into a collective part and an individual particle part will not be well defined, and the collective model will lose its sense. We must therefore ask, is the model self-consistent? We have not yet been able to carry through a detailed comparison of the energy exchange rate with the vibration frequency. Rough estimates below suggest the possibility of a borderline situation, with the two rates comparable, and the division into general vibrational and proper nucleonic motion smudged out in part. It is too soon to exclude the possibility that the two rates compare more favorably; or that the numbers go the other way, in which case the usefulness of the collective model will be strictly limited. Unaffected would be general conclusions about the influence of quadrupole moments upon alpha decay, about fluctuations from element to element in height of fission barriers, etc., but most of the anticipated quantitative applications of the model would become nearly hopeless. We have hope enough about the approximate self-consistency of assumption B2 to have gone some distance in investigating in this report certain mathematical details of the collective model and its applications.

Nuclei *vs* Atoms and Molecules

The idealization that we now contemplate for the behavior of nucleons in the nucleus recalls in many ways the motion of electrons in an atomic field. There is a similar justification to speak of individual quantum states and transition probabilities. One is invited to consider the same possibilities for calculation of a self-consistent nuclear potential. Yet there is one important difference of principle. In the electronic case the field of force is dominated by the nucleus. Percentage-wise the field on one electron in a many-electron atom changes little as a second electron sweeps through its orbit. Thus the potential is reasonably thought of as static.

In the nuclear case the *value* of the potential *in the interior* may perhaps be idealized as unaffected by the orbit of any individual nucleon, and as constant in space and time; but the *boundaries* of that potential as seen by one particle are very greatly affected by the motion of a small number of the other entities. To this extent the potential field has to be considered as fluctuating or oscillating.

Moreover, there is necessarily a kind of momentary self-perpetuation in such displacements of the local surface from its time average position. New particles coming up are turned back at the same place; in so far as they in turn have an effect on the potential, they keep the effective surface approximately where it already was.

There might be some point to overlooking fluctuations in the position of the nuclear surface if our concern were limited to the ground states of nuclei, where the amplitude of the movements is of the order r_0.[5] However, it is necessary to consider also states of excitation and fission processes where the amplitude of motion is comparable to the nuclear extension itself. How are we then to describe the quantum mechanics of a system of many independent particles with the characteristic new feature of collective modes of motion?

Illuminating is a comparison of the collective model of the nucleus with a typical molecule. In that case the electrons move rapidly in a field of force whose own alterations—by changes in the internuclear separation—go on at a frequency 10 to 100 times slower. Thus each electron adjusts itself for the most part adiabatically to the potential of the moment. The total energy of the electronic system at each instant provides on the other hand a storehouse of potential energy. On this supply internuclear motion can draw for kinetic energy, and into the pool it again returns energy as the molecular oscillation comes to rest at one or other limit of its amplitude. Similarly the characteristic time of radial motion of a nucleon of average kinetic energy, $T=15$ Mev, is

$$\begin{aligned} t_{\text{nucleon}} &\doteq \oint\left[\frac{2T}{M}-\frac{l(l+1)\hbar^2}{M^2r^2}\right]^{-\frac{1}{2}}dr \\ &=\frac{2R}{(2T/M)^{\frac{1}{2}}}\left[1-\frac{l(l+1)\hbar^2}{2MTR^2}\right]^{\frac{1}{2}} \\ &<\frac{2R}{(2T/M)^{\frac{1}{2}}}\equiv\frac{2R}{v}=\frac{2A^{\frac{1}{3}}r_0}{0.18c} \\ &=0.3\times10^{-21}\text{ sec for U}^{236}, \end{aligned} \tag{1}$$

an interval 15 times smaller than the estimated period,

$$\begin{aligned} t_2&=2\pi\hbar/\hbar\omega_2 \\ &\doteq 2\pi\times0.658\times10^{-21}\text{ Mev sec}/0.8\text{ Mev} \\ &=5\times10^{-21}\text{ sec}, \end{aligned} \tag{2}$$

of the lowest mode of capillary oscillation of the same nucleus. Therefore, in the nuclear case also, the states of the particles will be expected to follow the changing configuration of the nuclear boundary with little probability of a nonadiabatic jump from one state to another, provided that the deformation in question is a simple one.

Response of Nucleons to Surface

In the case of a complicated distortion of the surface, the particle will require a longer time to feel out the

whole surface, and the adiabaticity condition will not be so readily satisfied. For a surface deformation of order n, it is reasonable to require that $(n/2)t_{\text{nucleon}}$ exceed the period t_n of nth order disturbances, a condition which plainly cannot be satisfied for disturbances of very high order ($n>\sim 6$). Such disturbances therefore have no well defined significance in the collective model.

A natural limit to the finest irregularities to which the nucleon can respond is clearly the square of the reduced de Broglie wavelength, $\lambda=\lambda/2\pi$, of the particle. The time required to make this response will be of the order (number of encounters to touch all regions of the surface S) (time between encounters) $\sim(S/\lambda^2)(R/v)$ $\sim(V/\lambda^3)(\hbar/E)\sim\hbar/\Delta E$, where V is the accessible volume, E is the kinetic energy of the nucleon, and ΔE is the typical spacing (Fig. 11) between individual particle levels in a region of the given size. Such a spacing is so small, and the corresponding time therefore so long compared to oscillation periods, that the adiabaticity condition will not allow any discussion of very fine grain irregularities. If two particles are involved, and they interact strongly with each other, then the time required by the two-particle system for response to fine grained surface deformations will be increased by the factor V/λ^3, the number of distinguishable positions for the second particle within the nucleon volume V. As the number of strongly interacting particles grows larger, the factor in question goes up: by a term V/λ^3 for distinguishable particles, less rapidly for particles which satisfy the Pauli principle; but the increase is always such that the time in question is $\hbar$ divided by the spacing of levels of the total system. Obviously such times would be far too long to allow any adiabatic response to surface oscillations. In other words, the collective model can be justified only if the individual particles interact with each other in a strongly saturated manner, free of dependence on the location of any one particle in the nuclear interior.

As we are accustomed to the idea of molecular potential energy curves as a function of internuclear separation, so we arrive at the notion of nuclear potential energy curve as a function of surface deformation. As there are in the case of a polyatomic molecule several independent coordinates, so in the nuclear case a number of parameters will be required to specify the shape of the surface (Fig. 1). We deal with a potential energy surface. As the minima of the various surfaces do not coincide in the molecular case, neither will they in the nuclear case. The equilibrium quadrupole moment will differ from state to state, according to the special features of the push exerted on the surface by the nucleons in excess of closed shells. The energy of the system will consist of proper nucleonic energy, plus vibrational energy, plus rotation energy.

Kinetic Energy of Collective Motion

In the molecular case the vibrational kinetic energy comes into evidence in the motion of the nuclei. But in the nuclear case, what mass is it whose motion gives account of the vibrational kinetic energy? The nucleons? Is not their energy of motion already included in the ordinate of the oscillational potential energy curve itself? That vibrational potential energy is defined by adding up the potential and kinetic energies of all the individual nucleon states calculated for the static configuration of a deformed nucleus. However, such a calculation by its very nature overlooks the slow change in the shape of the nucleus. That alteration in form necessarily implies a bulk transport of mass from one place in space to another. With such a current of matter there is inevitably associated a kinetic energy of the nucleonic system over and above the energy reckoned for the individual nucleons in a static potential well. This additional kinetic energy has to be interpreted as the oscillational energy of motion of the system.

In the quantum-mechanical description (Figs. 7 and 8) the fluid motion comes into evidence in the transport of the nodes of the wave function of the bound nucleon from place to place in harmony with the motion of the surface. In the simpler situations the nodal surfaces move like lines of ink bodily carried along with the irrotational flow of an imaginary liquid. The wave function ψ of the nucleon at any moment of the slow wall deformation differs from the value u, which it would have for stationary walls of the same shape by a factor which in this approximate description of the nodal motion may be taken to be $\exp(-iM\phi/\hbar)$, where ϕ is the velocity potential of the liquid movement in question. From this circumstance it follows that the kinetic energy of the nucleon is greater than the value it would have had in the absence of wall motion by an amount proportional to the square of the wall velocity. The coefficient of proportionality is identical with that expected for a classical irrotational fluid subject to the same wall constraints.

Particularly interesting among surface changes is one which leaves the shape of the wall unaltered: a pure rotation of the boundary. In this case the amount of matter transported from place to place is set by the size of the departures from sphericity, not by the total mass content of the figure. The effective moment of inertia of the system is likewise far less than would correspond to the picture of rigid rotations. The corresponding rotational levels lie far higher. All of these consequences of a proper quantum picture of nuclear rotations have been pointed out by A. Bohr,[15,16] who has also shown their importance for the analysis of nuclear spins and magnetic moments.

The lower rotational excitations, though far larger than the few tens of kev values which would follow for a rigid nucleus, are still lower than most of the quanta

[15] A. Bohr, Phys. Rev. **81**, 134 (1950).
[16] A. Bohr, Kgl. Danske Videnskab. Selskab, Mat.-fys. Medd. **26**, No. 14 (1952); A. Bohr and B. R. Mottelson, Phys. Rev. **89**, 316 (1953).

of vibrational energy. For this reason it is appropriate to follow the manner of speaking employed in molecular physics and to employ the term "potential energy surface" for the case where the rotational angular momentum either vanishes or is treated as negligible. Higher angular momenta produce modifications in the potential energy surface of the kind familiar from molecular spectroscopy.[17] These rotation-induced modifications in the potential surface will give rise to a number of complicated and interesting effects. They will be disregarded in this paper, however, in comparison with the vibrational and nucleonic-excitational phenomena.

Under certain circumstances the deformation of the surface will displace the nodal surfaces in a manner which is no longer even approximately described by transport in irrotational fluid flow. Then a vortical motion of the carrier fluid must be envisaged. The effect upon the nucleonic wave function (see Fig. 10) may be considered as the quantum analog of the swirls which can be set up in classical fluids. In so far as such effects show up only in one nucleon state out of many, the kinetic energy of the whole system under deformation will not differ greatly from the value expected on the simple liquid drop picture.

Quantum Description of Collective Motion

Granted that the kinetic energy of the droplet model can be brought into evidence in the collective picture of the nucleus when the wall motion is regarded as given, how is the wall motion itself ever to appear as part of a proper quantum-mechanical description of the N particle system rather than something imposed from outside? Is not the full quota of degrees of freedom already accounted for without the wall motion? How then can the surface oscillation be described by degrees of freedom which are not there? Physically, we answer, the fluctuations in wall position and the collective character they imply for the N particle system are an unavoidable consequence of the strong coupling of particles at the nuclear surface. Mathematically we can describe the situation in the following terms. Were the wall position described by externally fixed parameters of the type of α, then the wave function of the system—apart from unimportant details—would have the character of the determinant:

$$\Psi_{\text{stationary}}=\begin{vmatrix} u(1, x_1; \alpha) & \cdots & u(1, x_N; \alpha) \\ \cdot & & \cdot \\ \cdot & & \cdot \\ \cdot & & \cdot \\ \cdot & & \cdot \\ u(N, x_1; \alpha) & & u(N, x_N; \alpha) \end{vmatrix}, \quad (3)$$

where the $u(n, x_j; \alpha)$ represent the individual particle wave functions in a potential well of the given shape.

[17] G. Herzberg, *Molecular Spectra and Molecular Structure* (D. Van Nostrand Company, Inc., New York, 1950).

With a changing but still externally controlled deformation, α becomes a function of time and the determinant on the right has to be multiplied by the factor,

$$\exp\{-i(M/\hbar)[\phi(x_1)+\cdots+\phi(x_N)]\}, \quad (4)$$

in order to obtain the approximate wave function for the nucleonic system. Here ϕ (expressed in cm²/sec) is the velocity potential of the irrotational motion of the imaginary carrier fluid. Conversely, when the nucleons are regarded as determining the potential energy of deformation for the coordinate α, then the vibrational state of the system—if that could be thought of as having an independent existance—would have the value $h_n(\alpha)$ appropriate to a quasi-harmonic oscillator. To write the wave function of the whole system as the product of determinant, of velocity potential factor, and of harmonic oscillator function, is illegitimate because there would be too many independent variables in the product for an N particle system. However, integration of this product with respect to α yields a wave function

$$\Phi(x_1, \cdots, x_N)=\int \Psi(x_1, \cdots, x_N; \alpha) \times\exp\{-i(M/\hbar)\sum_j \phi(x_j)\}h_n(\alpha)d\alpha, \quad (5)$$

which depends only on the coordinates of the particles themselves.[17a] This function, nevertheless, provides a physically reasonable description of the collective motion in question. (a) It has the proper antisymmetry. (b) It is large in the vicinity of the classical turning points of the oscillation in the sense that presence of one of the particles in a region a little outside the average position of the nuclear surface is associated preferentially with a probability for other particles to be a similar distance outside the average surface; and a similar probability to see one missing at a given distance outside the average surface is associated with an increased likelihood for other nucleons to be absent there; and these correlation probabilities are greatest when the distances in question are comparable with the amplitudes of the corresponding classical surface vibrations. (c) Two of

[17a] The $\dot{\alpha}$-factor in the velocity potential in the exponent (Figs. 7 and 8) is of course to be replaced before integration over α by its operator value, $(\hbar/iM_\alpha)(\partial/\partial\alpha)$. Alternatively, if we use for $h_n(\alpha)$ its J.W.K.B. approximate value, then the exponential operator acting on this oscillator function gives two additive terms. In one of the terms the $\dot{\alpha}$-factor in the exponent is given the value

$$+\{2[E-V(\alpha)]/M_\alpha\}^{\frac{1}{2}},$$

and the exponential function is multiplied into that part of $h_n(\alpha)$ which represents a wave running to the right; similarly for the other term, where $\dot{\alpha}$ is given the opposite sign. Although the wave function of (5) is formulated on the basis of physical reasoning, one can of course alternatively regard $h_n(\alpha)$ as a quite undetermined function, which is to be so chosen as to make Φ the "best possible wave function" in the sense of the Ritz variation principle. How this method of approach can be used to derive from first principles a wave equation for $h_n(\alpha)$ is a problem identical in principle with the formulation of the method of "resonating group structure" [J. A. Wheeler, Phys. Rev. **52**, 1107 (1937)]. In particular, it is not at all necessary that the potential $V(\alpha)$ be quasi-elastic nor that $h_n(\alpha)$ be a harmonic oscillator wave function.

the individual determinants which are combined by integration are very nearly orthogonal to each other (Fig. 9) when the displacements α_1 and α_2 to which they correspond differ in normal surface coordinate by an amount of the order r_0/N, where N is the number of particles of identical character and $4(4\pi r_0^3/3)$ is the volume available to one of these particles. In physical terms there is a very high correlation between the probability distribution of the particles and the values of the "hidden" deformation variable α. This near-orthogonality of the piece-wise functions makes it a reasonable approximation to treat the alpha-variable almost as an independent coordinate.

The deformation coordinate is indeed expressible in terms of the particle variables; the collective model does not contemplate a quite inadmissible increase in the total number of degrees of freedom. How then can we justify a count of the states of the system in which we tally up not only the indices of the individual particle states but also reckon in all the quantum states of the surface oscillators? The system of functions is already complete when the oscillator quantum numbers have specified values. To sum subsequently over vibrational quantum numbers too is to get the same complete set many times over. The solution to this counting paradox is of course that no such extended summations are either intended mathematically or sensible physically. Only the few lowest modes of oscillation have a well-defined physical existence. Moreover, the rate of interchange of energy between vibrational and nucleonic motion depends on the choice of potential energy surface and becomes the greater the higher the degree of excitation of the nucleons in that state. Thus there is a limit of energy beyond which no vibrations of any kind make sense. The problem in the collective model is not that we have too many states but too few. The failure of the description above some tens of Mev has to be accepted physically. A nucleus endowed with sufficient excitation is capable of breaking apart into many individual particles, as evidenced by cosmic-ray stars. The collective model is valid only for not too high excitations.

Conventional expansions of nuclear wave functions in terms of individual particle states in a spherical potential are quite unadapted to describe states of collective oscillation and rotation. Staggering would be the number of kinds of multiple excitations of nucleons required to describe a combination of vibration and nucleonic excitation.

III. THE DEFORMATION POTENTIAL

Definition and Survey Formula

Key to the collective description is the concept of potential energy of deformation: sum of the kinetic and potential energies of the individual nucleons moving inside a nuclear surface of fixed shape. For a first survey of the energy surfaces it is reasonable to make the following simplifications: (a) Neglect spin-orbit coupling. (b) Treat the internuclear force as having such an extreme saturation character that the potential energy of a particle is constant within the nuclear matter and at the surface suffers a sudden and abrupt rise. The actual wave functions will penetrate into the region of negative kinetic energy to a distance of order r_0. In dealing with wave functions for bound nucleons it is often convenient to idealize the potential discontinuity at the wall as infinitely high. Then the calculated nucleonic wave function does not penetrate at all outside the wall. This effect—and its consequences in shifting nodal surfaces inside the potential well and displacing energy proper values—can be corrected in a reasonable approximation by an appropriate slight adjustment in the values adopted for nuclear dimensions. For each particle put down then a contribution to the total energy equal to (i) the appropriate eigenvalue of $\nabla^2\psi_n+(2ME_n/\hbar^2)\psi_n=0$, subject to the boundary condition, diminished by (ii) a standard quantity B_0, of the order of 14 Mev, representing the saturation binding per nucleon. (c) Represent the deficit from saturation binding of the particles at the nuclear surface by a term in the total nucleonic energy of the system which is proportional to the surface area, S. The constant of proportionality we denote by O(potential) —not the total surface tension[18] $O=O_p+O_k\sim 14$ Mev$/4\pi r_0^2$, of the nuclear matter, but that part of this quantity which has to do with specific nuclear forces. The other part, O_k, of the usual surface tension has to do with the total kinetic energy of a system of particles bound in a potential, in so far as that total depends upon the *surface*, as distinct from the *volume*, of the potential well. This kinetic part is already included in (b). Whatever differences there are in the dependence of kinetic energy upon deformation magnitude between statistical analysis as typified in the constant O_k and detailed analysis via summation of eigenvalues E_n, the latter is to be considered the more nearly definitive. As to the dependence of specifically nucleonic *potential* energy upon deformation, it would likewise be more nearly accurate—if it were practicable—(i) to evaluate the expectation value of the interaction energy with respect to a determinantal wave function built up out of individual eigenfunctions ψ_n than (ii) to use for A nucleons the expression $-AB_0+O_pS$ as statistical means to estimate this nucleonic interaction energy. The difference between (i) and (ii) is the less the more nearly the forces between nucleons have the extreme saturation character which is assumed in the idealized collective model. (d) The electric energy of interaction between protons could likewise be evaluated via the determinantal wave function of the system, but again it is a reasonably consistent approximation to represent the Coulomb interactions in terms of the electrical

[18] W. J. Swiatecki, Phys. Rev. **83**, 178 (1951); C. F. von Weizsäcker, Z. Physik **96**, 431 (1935); E. Feenberg, Phys. Rev. **60**, 204 (1941).

energy of a uniformly charged fluid contained within the given boundaries:

$$V_e = \rho_e^2 \int\int d(\text{vol})_1 d(\text{vol})_2 / 2r_{12}.$$

It would be possible to consider—although we do not do so here—a refinement of this analysis, in which (i) slightly different boundaries are ascribed to the regions in which the neutrons and the protons move,[19] (ii) there are two different potential wells inside which the two kinds of particles move, (iii) neither potential well is of constant depth, (iv) the potential gradient is in such a direction to make the number of protons in the outer half of the nucleus, and the number of neutrons in the inner half, slightly greater than would correspond to a uniform proton-neutron ratio,[20] and (v) oscillations of the neutrons en masse relative to the protons become possible, as discussed by Goldhaber and Teller, and Jensen and Steinwedel,[21] especially in reference to the maximum observed in the nuclear photoabsorption cross section between 10 Mev and 20 Mev.

In summary, the collective model envisages a deformational potential energy function, $V(\alpha_2, \alpha_3, \cdots; n_1, \cdots)$, which depends (a) upon the coordinates α_2, α_3, etc., which specify the shape of the nuclear surface, and (b) upon the quantum numbers $n_1, \cdots$ of the occupied nucleonic states. This potential energy is taken to have the form

$$V(\alpha, n) = -AB_0 + O_p S(\alpha) + \sum E_n(\alpha) + V_e(\alpha). \quad (6)$$

Level Density

Interest attaches to the deformation potential both in its dependence upon deformation for a fixed state $n=(n_1, \cdots)$ of the whole nucleonic system, and its variation with quantum state for a specified configuration, α, of the wall. The variation of potential with wall configuration specifies an energy surface in (V, α) space. Upon this potential surface the representative point of the system may be considered to move like a marble. This surface ordinarily possesses at least one minimum—a point of equilibrium for the collective oscillations of the nucleonic system. The location of the minimum specifies the normal equilibrium deformation of the nucleus. A first rough impression of the curvature of the potential surface about the minimum is given by identifying $V(\alpha, n)$—up to an additive constant and a shift in the origin of α-space—with the expression $V_{\text{liquid drop}}(\alpha) = (O_p + O_k) S(\alpha) + V_e(\alpha)$. For a fixed value of the distortion coordinates, α, there are many different values of V, according as the nucleons are placed in one or another set of individual particle states. The spacing of successive potential surfaces therefore goes qualitatively much like the pattern of levels of a spherical A particle nucleus, with the same statistical relationship between the density of proper values of the totalized energy, and the density of individual particle proper values:[22] (a) The lowest level of the whole system is found by filling up the individual particle levels, starting at the bottom, until all A particles are accommodated: kinetic energy of the order of $F \sim 24$ Mev for the highest single particle state; for all particles together, $\sum E_n \sim \frac{3}{5} AF$. (b) The first few excited states of the whole system have spacings of the same order as the average spacings, ΔE_F, of the levels of a single particle at excitation F. (c) For excitations $E_N = \sum E_N$ larger than several times ΔE_F, yet very much smaller than AF, (by which excitation the collective model will already long since have failed) the density of system levels increases roughly exponentially (neglecting power factors) with an exponent $\pi(8E_N/3\Delta E_F)^{\frac{1}{2}}$. Consequently the number of potential energy surfaces of the nucleus, like the corresponding number for the case of a polyatomic molecule, increases more and more rapidly with the excitation, nucleonic in the one case, electronic in the other.

The density, dZ/dE, of states of the collective nuclear model at relevant energies will increase with energy even faster than the density of potential surfaces, dZ_N/dE, because there are many ways in which the total energy $E = E_N + E_{\text{vib}}$ can be partitioned between individual particle excitation and collective oscillation:

$$dZ/dE = \int_0^E \left(\frac{dZ_N}{dE}\right)_{E_N} \left(\frac{dZ_{\text{vib}}}{dE}\right)_{E-E_N} dE_N. \quad (7)$$

The density of capillary oscillational levels increases with energy, as Wergeland[23] has shown, at a rate also dominated by an exponential factor, this factor depending upon energy in roughly the same way as the factor for the density of nucleonic levels. However, instead of *comparing* the two expressions for level density, we *combine* them by the indicated integration. The result is to increase the exponent in the level density by a factor in the neighborhood of $2^{\frac{1}{2}}$ for those

[19] J. H. D. Jensen and P. Jensen, Z. Naturforsch. **5a**, 343 (1950).

[20] E. P. Wigner, *Nuclear Masses and Binding Energies*, p. 27, part IV of University of Pennsylvania Bicentennial Conference Publication, *Nuclear Physics* (University of Pennsylvania Press, Philadelphia, 1941); E. Feenberg, Revs. Modern Phys. **19**, 239 (1947); W. J. Swiatecki, Proc. Phys. Soc. (London) **A64**, 226 (1951).

[21] M. Goldhaber and E. Teller, Phys. Rev. **74**, 1046 (1948); H. Steinwedel and J. H. D. Jensen, Phys. Rev. **79**, 1019 (1950); Z. Naturforsch. **5a**, 413 (1950).

[22] N. Bohr and F. Kalckar, Kgl. Danske Videnskab. Selskab, Mat.-fys. Medd. **14**, 10 (1937); V. F. Weisskopf, Phys. Rev. **52**, 295 (1937); L. Landau, Physik. Z. Sowjetunion **11**, 556 (1937); H. A. Bethe, Phys. Rev. **50**, 332 (1936); J. Bardeen, Phys. Rev. **51**, 799 (1937); J. Bardeen and E. Feenberg, Phys. Rev. **54**, 809 (1938); C. Van Lier, and G. E. Uhlenbeck, Physica **4**, 531 (1937); L. Motz and E. Feenberg, Phys. Rev. **54**, 1055 (1938); K. Husimi, Proc. Phys.-Math. Soc. Japan **20**, 912 (1938); V. F. Weisskopf and D. H. Ewing, Phys. Rev. **57**, 472 and 935 (1940); I. N. Sneddon and B. F. Touschek, Proc. Cambridge Phil. Soc. **44**, 391 (1948); J. M. Blatt and V. F. Weisskopf, *Theoretical Nuclear Physics* (John Wiley and Sons, Inc., New York, 1952), Chap. VIII, Sec. 6.

[23] H. Wergeland, Skrifter Norske Videnskaps-Akad. Oslo, No. 1, (1941); H. Wergeland, Fysik. Verden **3**, 223 (1945); see also H. A. Bethe, Revs. Modern Phys. **9**, 86 (1937).

excitations not so high that the collective model fails. No breakdown of the total level density according to angular momentum has yet been carried out, nor—therefore—any comparison with the experimental data summarized by Blatt and Weisskopf.[22]

Crossover and "Slippage"

The connectivity of the many-sheeted potential energy surface is a matter of interest and importance for the collective model. There are two contradictory tendencies at work: (a) Potential surfaces never cross nor even touch provided that the wall configurations under consideration are devoid of all symmetry, whether of rotation or reflection or inversion. Let the representative point of the system be required to stay away from those lower dimensional regions in α-space which describe shapes with symmetry properties. Also let jumps from one surface to another be ruled out. Then the connectivity of the sheets is such that no path in α-space, however tortuous, can ever carry the representative point from one sheet to another. The surfaces therefore admit a unique serial numbering according to energy, this *canonical classification* $V_1(\alpha)$, $V_2(\alpha),\cdots$, being the same for whatever α it is carried out, provided α does not lie in the forbidden set of "symmetry points." (b) For deformations which *do* possess one or more symmetry properties, crossovers from one energy surface to another *do* take place as one or another deformation parameter is varied. Consequently there exist shapes, α, for which two successive surfaces, $V_k(\alpha)$ and $V_{k+1}(\alpha)$, touch each other. For shapes of appropriate symmetry it is possible for more than two surfaces to meet, the contact point then being of higher order.

When the representative point is allowed freedom to take on all values of α, it can then by appropriate choice of path work its way up mine-shaft-like from surface to surface, sliding smoothly from V_k to V_{k+1} at one point in α-space, and from V_{k+1} to V_{k+2} at another point. We shall use the word "slippage" to describe this fundamental process, which in the theory of polyatomic molecules is known under the name of "radiationless transition,"[24] and the word "funnel" to speak of the potential energy surface near the crossover point.

Qualitative description of the character of the many sheeted potential energy surface requires (a) ascription of a suitable set of index numbers to each crossover point, telling the number of surfaces that meet there and the lowest order in deviations $\delta\alpha$ from the crossover point in which the degeneracy is removed, (b) giving of the lowest nonzero coefficients in the power series development of the energy values about this point, (c) evaluation of the frequency distribution of transition points in α-space for a typical potential surface, (d) order of magnitude estimate of the height or depth—energywise—of funnel vertices relative to the immediately surrounding potential energy surface, (e) order of magnitude estimate of the curvature of a given surface in the large (looking apart from funnels), this quality being described by coefficients of curvature with respect to the several axes in α-space. To discuss these points in detail would require more study than has been given to the subject so far. However, some glances at the matter from various sides (Figs. 10–25) may give an impression of the situation. In most of the idealized cases to be mentioned, attention has been given to the behavior, not of the surface for total oscillational potential energy, $V_k(\alpha)$ [Eq. (6)], but of the individual particle energy, $E_n(\alpha)$. Of course every crossover in $E_n(\alpha)$ implies a crossover in $V_k(\alpha)$, so that the connection between the two kinds of surface is not remote.

Survey of Level Behavior

Figure 10 deals with two energy levels of a particle in a rectangular potential well, a configuration of high symmetry, except that this symmetry is destroyed by a slight irregularity in the wall. This irregularity is sufficient to prevent the two energies from crossing, as they would for the symmetric surface. In that case a given function would have a well-defined number of nodal planes normal to each coordinate surface, a number which does not change during the course of the deformation. The energy of the state decreases or increases according as the principal part of the wave propagation is parallel or perpendicular to the direction of stretch—as is to be expected from the corresponding classical problem. Interesting is the contrast with the one-dimensional case. There an expansion in the one direction lowers *all* energies; two levels never cross. A similar character is given to the three dimensional problem by removal of symmetry.

Figures 11 and 12 connect the discussion of the single-nucleon curves $E_n(\alpha)$ with the total potential curves $V_k(\alpha)$. The curves of Fig. 12 give the closest over-all analogy at this moment available to the potential surfaces for the collective nuclear model. However, it should be noted that Fig. 12 represents a cross section through the energy surfaces along an abnormal line in deformation space; namely, a slice which cuts all surfaces in such a way as to reveal their crossovers. Were an irregular deformation superposed on the distortion shown, then every crossover would be replaced by a curve such as shown in Fig. 10. Noteworthy is the qualitative connection of the irregularly scalloped potential energy curves with the smooth curve predicted by the statistical concept of kinetic surface tension. Zero potential energy contribution to surface tension has been assumed in this simple example, and also zero electrostatic energy. One sees that the statistical concept of a constant surface tension is limited in accuracy.

Frequency of crossing of individual particle energy levels is easily estimated. Stretch of the system in one direction by a fractional amount α raises or depresses levels of energy F by an amount of the order $F\alpha$,

[24] E. Teller, J. Phys. Chem. **41**, 109 (1937); see also J. von Neumann and E. P. Wigner, Physik. Z. **30**, 467 (1929).

according as the propagation vector is primarily perpendicular or parallel to the stretch axis. The average spacing of levels of a particle without spin at the $(A/4)$th level—this level having energy F—is of the order $8F/3A$ (Fig. 11). Consequently an increase in α of the order $1/A$ will on the average suffice to make a given level cross one more of the levels originally below or above it—provided that the symmetry of the surface allows crossings.

Considerable can be said about single particle energy levels within an ellipsoidal wall. Inequality of the three axes (Fig. 13) removes rotational symmetry and leaves the configuration invariant with respect only to inversion and reflection. Figures 14–18 illustrate the level splitting brought about by small ellipsoidal deviations from sphericity. Larger deviations, leading all the way from sphere to fission, are considered in Figs. 19–22—at the price of having to make the wall axially symmetric, and therefore having to deal with the atypical case of many crossovers.

The relation between individual particle levels and system levels is further illuminated by Fig. 23. This diagram shows how the quadrupole-producing force for nearly spherical nuclei rises to a maximum when the number of nucleons is about right to give a half-filled shell. This diagram will not be valid for substantial deviations from symmetry, for then levels change their character, as seen in Fig. 10 and Figs. 19–22. More about splitting of single particle levels and behavior in the large of system levels is seen in Figs. 24–25. The irregularities in the totalized potential energy curve for a system of many particles will not be expected to be greater in order of magnitude than the bumps in the potential energy curve for the highest individual particle state. The rise of a lower one of the filled states to an inverted funnel and the fall of a next higher surface to a mating upright funnel represent perturbations which when added together largely cancel out.

IV. QUADRUPOLE MOMENTS IN THE GROUND STATE

Figure 26 discusses the qualitative dependence to be expected for quadrupole moment as a function of degree of shell-filling so long as the deformations in question are not large enough to carry the system past a funnel. Still sticking to this restrictive condition on the size of distortions, Fig. 27 discusses possible consequences of the existence of two well separated minima in the potential energy surface for the ground state of the system. While passage of a heavy nucleus through a high barrier of this kind might conceivably require a time exceedingly long in comparison with characteristic nuclear times, passage around the barrier can take place with greater facility in the α-γ plane (Fig. 28) through a sequence of ellipsoids with three unequal axes. Knowledge of nuclear deformation potential energy surfaces is far too scanty as yet to allow any well-founded discussion of energies or lifetimes of such deformation-isomeric states.

Figure 29 recalls the empirical evidence on periodicity in nuclear quadrupole moments. Here too it would be inappropriate to carry out any detailed discussion of the correlation between the observational data and the model without a more detailed knowledge of the deformation potential energy surface than is now available (see forthcoming paper by K. W. Ford on this point).

Quadrupole moments of the sizes now already well-attested experimentally will have very substantial consequences for alpha-decay phenomena, as indicated in Figs. 30 and 31. Likewise they must wash out the minima in nuclear diffraction scattering (Fig. 32), an effect which it would appear possible to observe granted a primary beam of sufficiently short wavelength, sufficiently well defined in energy and in direction of incidence. Asymmetries in nuclear shape, far from being isolated phenomena, are seen to connect closely with important questions of principle in nuclear physics. It is evidently important for the development of nuclear physics to learn the quadrupole moments of many more nuclei, particularly among the heavy elements and alpha-emitters. In this connection diffraction scattering, anomalies in alpha-decay half-lives (Fig. 31), in isotope shift,[25] and level splittings in the mumesonic Chang[26] K-radiation offer additional means to increase the experimental evidence.

V. RATE OF EXCHANGE OF ENERGY BETWEEN OSCILLATION AND NUCLEONIC EXCITATION

Cross Section for Slippage

The distinction is not sharp between deformations with complete lack of symmetry and complete ordering of energy levels on the one hand, and on the other hand deformations of high symmetry with energy levels crossing each other. The most relevant illustration is the probability for a jump from the lower potential energy surface to the upper one when the system executes an axially symmetric elongation upon which is superimposed a small amount of an ellipsoidal deformation of each cross section of the figure away from its otherwise circular form. The two energy levels in question would cross were the elliptical deformation absent. The actual coupling splits the levels as shown in Fig. 33. It follows that if the elongation were carried out very slowly the system would remain on the lower potential curve as previously discussed. However, if the time of passage through the critical region is comparable with, or shorter than, the minimum time $h/(E_{\text{up}}-E_{\text{low}})_{\text{minimum}}$ associated by quantum mechanics with the splitting, then the jump from the lower state

[25] L. Wilets, Phys. Rev. **87**, 1018 (1952).
[26] W. Y. Chang, Revs. Modern Phys. **21**, 166 (1949).

to the upper state can occur with appreciable probability (Fig. 34).[27]

The possibilities for a nonradiative transition are seen in more detail in Fig. 35, which is a representation of the two potential surfaces near their conical point of contact. Figure 36 describes one of the limiting cases of leakage from the upper funnel down to the lower one, or the reverse process. The considerations[24] of Fig. 35 lead to a formula,

$$\sigma=(\hbar\dot{\alpha}/s)^{\frac{1}{2}},$$

for the cross section for a collision with the cone with transition from lower to upper surface ("slippage"). Here $\dot{\alpha}$ is the speed of motion of the representative point, regarded classically, while s represents the slope of the cone (energy per unit of deformation), the cone itself being here taken for simplicity to be right circular. The system point continues its motion in the (α,γ) deformation space after this switchover as before. However, a part of the energy which was previously available in the form of vibration has now gone into nucleonic excitation as the system moves on the higher potential surface. Such radiationless switches near points of contact between two potential surfaces give the means for pure nucleonic excitation to go into vibration; for oscillations in turn to be damped and thereby to raise the nucleonic energy; and for all these exchanges of energy to take place in a relatively smooth manner, without discontinuous changes in velocity or deformational potential energy.

We evidently can view the collective model as being internally self-consistent for those energies and states of excitation—if any—for which the probability of slippage out of the given potential surface is substantially less than one during the time of one oscillation. Even if the contrary is true and the characteristic time to make one slippage is *short* compared to the vibration period, the model will still be consistent provided that the *fractional* change during one period in the energy available for oscillation is small compared to this energy itself. In other words the general requirement for consistency is that the coefficient of fractional "damping" per period must be small compared to unity.

"Slippage" evidently constitutes the elementary act in a viscous phenomenon. This primary mechanism is of course reversible, as in the case of all frictional processes. Any irreversibility comes from asymmetry in time of the initial conditions. Consider for example the case where the representative point oscillates rapidly and with large amplitude on the lowest potential energy surface. The partition between nucleonic excitation and oscillational energy is as one sided as it can possibly be. Then the statistical result of slippages sometimes up, sometimes down, will on the average be a degradation of much of the vibration into nucleonic excitation. If the collective model is self-consistent, then this damping must be small enough to be susceptible to a statistical description, with an appropriate kind of macroscopic friction coefficient. In contrast to most familiar physical systems, the present one has a quite restricted number of degrees of freedom. Consequently degradation of the energy cannot continue indefinitely. Statistical fluctuations in the distribution of energy over the degrees of freedom will go on until a given one of these modes of excitation will have accumulated all or a large part of the maximum available amount. When the nucleus has sufficient energy, the accumulation may take place on the lowest mode of capillary oscillation and lead to fission; or the energy may pile up in excitation of one nucleon, followed by neutron emission. In either case, the energy concentration process will have a history which is the reversal in time of the corresponding dissipation process. If there are circumstances when the dissipation is describable by an appropriate friction coefficient, then the reverse concentration of energy will be describable by a coefficient of the same magnitude and opposite sign.

Estimates of Damping

It is too soon to say anything definitive about the magnitude of the dissipation per oscillation cycle, and therefore premature to decide whether the collective model is self-consistent. A first crude estimate may not be amiss, as indicating a few of the many factors that must be taken into account in an ultimate assessment. We shall limit the discussion to collective oscillations in the α-γ plane, i.e., to deformations of order $n=2$ (Fig. 1). In actuality the representative point of the system moves in a multidimensional space. Its chance of slippage from one potential surface to another might therefore seem to depend upon the number of dimensions taken into account. However, consider the effect of some high order deformation coordinate, α_n. The characteristic quantum of energy associated with this mode will be large. Therefore it will be reasonable to assume this part of the system to be always in its lowest quantum state. The amplitude of zero-point oscillation will be small. Moreover, per unit of amplitude of the coordinate α_n the displacement of individual particle levels will be small, because the relevant wave functions do not well feel surface deformations of small wavelength. Consequently the effects of the given high order displacement can be disregarded in a reasonable approximation. In this sense the theory of the slippage rate shows a satisfying invariance with respect to cut-off of the number of dimensions taken into account, provided that this number is large enough. However, it is doubtful that it is sufficient to consider only deformations of order 2, as we shall do. In this case the deformation space is two-dimensional in the dimensionless parameter, α; the probability of slippage on near encounter with a funnel is measured by a cross section, σ, one dimensional in the parameter α; and the damping

[27] C. Zener, Proc. Roy. Soc. (London) **A137**, 696 (1932).

coefficient is of the form

$$\begin{pmatrix}\text{Damping}\\ \text{coefficient}\end{pmatrix}=\frac{\begin{pmatrix}\text{probability per}\\ \text{second of slippage}\end{pmatrix}}{(\text{circular frequency})}\frac{\begin{pmatrix}\text{energy change}\\ \text{on slippage}\end{pmatrix}}{(\text{oscillational energy})}<\sim\frac{\dot{\alpha}\sigma}{\omega}\frac{\begin{pmatrix}\text{number of funnels}\\ \text{accessible to oscillator}\end{pmatrix}}{\begin{pmatrix}\text{area in }\alpha\text{-space}\\ \text{accessible to oscillator}\end{pmatrix}}.$$

To evaluate this expression, we shall assume that the potential surface in question has roughly the same overall curvature that is predicted by the simple liquid drop model. Then we have for the order of magnitude of the excursion in α (Fig. 1) roughly $\delta\alpha\sim(v+\frac{1}{2})^{\frac{1}{2}}/A^{7/12}$, where v is the vibrational quantum number and A is the mass number; and for the circular frequency, $\omega\sim 24$ Mev$/\hbar A^{\frac{1}{3}}$. The slope of a funnel (energy per unit of α) we shall assume to be of the order of the Fermi energy, $F\sim 25$ Mev. The number of funnels accessible to the oscillator is of the order $A\delta\alpha$, provided that we limit attention to a low-lying potential surface. About the size of the accessible area in α-space we have the least information. The simplest assumption is that this area is of the order $(\delta\alpha)^2$, though it is easy to imagine shapes for the potential surface which make this number either much larger or much smaller (see Fig. 28). We obtain as an exceedingly uncertain estimate of the damping coefficient:

$$<\sim(\omega\delta\alpha\sigma/\omega)(A\delta\alpha/(\delta\alpha)^2)=A\sigma$$
$$=A(\hbar\omega\alpha/\text{funnel slope})^{\frac{1}{2}}\sim A(\alpha/A^{\frac{1}{3}})^{\frac{1}{2}}\sim(v+\tfrac{1}{2})^{\frac{1}{2}}A^{11/24}.$$

If we assume instead that the accessible area is of the order constant$\cdot\delta\alpha$ (normal quadrupole moment; ring shaped region accessible in α-space), then we find as order of magnitude for the damping coefficient $\sim(v+\frac{1}{2})^{\frac{1}{2}}A^{-\frac{1}{3}}$. Without knowing the numerical coefficients, we cannot say whether these numbers are less than one or greater.

"Damping" is one way to speak of the exchange of energy between vibration and nucleonic excitation; another is to ask for the eigenvalues of the energy of the combined system after this coupling is taken into account. This manner of speaking can hardly be expected to be very fruitful in the nuclear case. The number of parts of the system is so great, and the number of ways of dividing up energy between them is so enormous, that it seems beyond reason to trace out all the couplings and their consequences. Figure 37 presents a one-dimensional example of the influence of small and large slippage effect upon energy level pattern. When many degrees of freedom are involved, the treatment of the case of strong slippage would be utterly complicated. That of weaker slippage is obviously much simpler. It corresponds to the notions of the idealized collective nuclear model. The partition between nucleonic and vibrational energy is well defined in first approximation. We limit ourselves to the study of the collective model because there is in sight no other mathematically analyzable picture that makes the necessary combination of elementary particle model and liquid drop picture. If it should turn out that the slippage rate is too great to make the collective model a self-consistent scheme, then it would seem necessary to content ourselves with a much vaguer conception of the nucleus, but still one that inescapably unites the individual and droplet characteristics.

Franck-Condon Principle

The molecule-like partition that we envisage between vibrational and nucleonic energy recalls the Franck-Condon principle (Fig. 38) and its many important applications to the field of molecular physics. Analogous consequences for the nucleus will be expected to include vibrational excitation following either nuclear photoabsorption or mu-meson charge exchange reactions or impact of a fast particle that disturbs directly only a single nucleon. Likewise, anomalies in the apparent spacing of nuclear levels will be anticipated from the action of the Franck-Condon principle.

Wall Coupling as Doppler Effect

The collective model makes the wall the coupling between individual particle energies and oscillatory motion. For this reason it is interesting to examine the coupling in its time-dependent aspects. The shift, δE_n, of a particle level due to a wall displacement, $\delta\alpha$, has so far been visualized without reference to the rate at which it occurs: $\delta E_n=(\partial E_n/\partial\alpha)\delta\alpha$. Alternatively, the level change can be considered as due to Doppler effect at a moving wall: a change in energy in one reflection at the wall of the order $\delta_1 E_n\sim$(wall velocity/nucleon velocity) $E_n\sim R_0\dot{\alpha}E_n/v_n$; a number of reflections per unit time of the order v_n/R_0; and a time equal to $\alpha/\dot{\alpha}$; or a total change $\delta E_n\sim E_n\alpha$. Left out of account in this order of magnitude estimate is a numerical coefficient of the order of unity, which will of course be negative if the wave propagation takes place primarily towards a retreating part of the wall, otherwise positive. We are speaking here of a neutron already inside the nucleus being reflected at the wall; but similar considerations apply to a neutron which comes from outside and undergoes a change of wavelength on entry (Fig. 39): then the particle will have less energy than would be expected for a static wall, provided that the wave comes in at a region of expansion of the nuclear surface; conversely at a region of contraction. When the energy of the incident neutron is smaller than the depth of the average potential at the nuclear interior, then the energy change due to the wall motion will

still be of the order $\delta_1 E_n \sim R_0 \alpha E_n / v_n$, where E_n and v_n are energy and velocity inside the barrier. The mechanism to take energy away from an incident particle and give it to collective oscillation—for later redistribution to other nucleons—is obviously of interest in connection with the neutron capture process (Fig. 40).

Nucleus as Quantum Fluid

We have encountered in this discussion some of the properties of an unusual idealized quantum fluid. It is considered to be completely transparent internally with respect to motion of the constituent particles, and to receive disturbances solely by way of surface deformations. Its near incompressibility comes about, not by particle to particle push, as in an ordinary liquid, but by more subtle means. It is capable of collective oscillations, but it is the wall which organizes these disturbances, not nucleon to nucleon interactions. Oscillations experience a damping, but the mechanism of the damping is unlike that encountered in ordinary liquids. The liquid can evaporate a particle, but in a way quite different from evaporation from ordinary liquids. The wave function of the particle to come out is spread over the whole nucleus and has energy pumped into it by Doppler effect; it is not concentrated near a part of the surface before emission. The rotational properties of the quantum fluid are quite different from those of ordinary fluids. Altogether one is dealing with a most interesting new form of matter.

VI. FISSION PROCESSES

Barriers and Thresholds

In the account of fission given earlier,[5] it was noted that energy imparted to the nucleus by radiation or impact of a material particle becomes redistributed over the whole system and later by a chance fluctuation may be concentrated either on a neutron (evaporation process) or on the mode of deformation which leads to fission. For fission then to take place with appreciable probability it is necessary that the available energy exceed the fission threshold (Fig. 3)—the energy required to produce a critical deformation (Fig. 2). This energy was estimated then, and calculated more accurately later by Frankel and Metropolis[28] by way of the simple liquid drop model. According to this model, the same mode of deformation, when endowed with less energy, will oscillate quasi-periodically, with a characteristic quantum energy shown in Fig. 41, but fission will still be able to occur with a very low probability by way of penetration through the barrier. These predictions about barrier height, oscillation frequency, and tunnel probability will be expected to be qualitatively correct in the liquid drop model, but there will be characteristic differences in detail. The same kind of individualities in the potential energy surfaces that cause quadrupole deformations of the order $\alpha \sim 0.03$ in nuclear ground states will cause fluctuations of fission thresholds of the order of ~ 1 Mev with respect to a uniform dependence on Z^2/A (Fig. 42). The experimental results[29,30] summarized in Table I show a similar fluctuation about the liquid drop predictions.

TABLE I. Fission thresholds obtained from neutron impact and photofission experiments, compared with thresholds calculated from simple liquid drop treatment, neglecting corrections for polarizability and compressibility. The irregular deviations between observation and calculation are of the order of magnitude to be expected from the size of typical quadrupole moments (Fig. 29).

Neutron fission thresholds					
Target nucleus	Compound nucleus	Neutron threshold[a] E_n	Neutron binding[c] B_n	Observed barrier $E_n+B_n=F_n$ (obs)	Calculated[d] barrier F_n(calc)
$_{90}Th^{232}$	$_{90}Th^{233}$	1.05 Mev	4.9±0.2	6.0±0.2	6.5
$_{91}Pa^{231}$	$_{91}Pa^{232}$	0.45 Mev	4.9±0.4	5.4±0.4	5.0
$_{92}U^{238}$	$_{92}U^{239}$	0.92 Mev	4.6±0.2	5.5±0.2	5.5
$_{92}U^{234}$	$_{92}U^{235}$	0.28 Mev	4.9±0.4	5.2±0.4	4.5
$_{93}Np^{237}$	$_{93}Np^{238}$	0.25 Mev	5.0±0.4	5.3±0.4	4.2

Photofission thresholds		
Target nucleus (=compound nucleus)	Observed photofission threshold[b]	Calculated threshold
$_{90}Th^{232}$	5.40±0.22	6.21
$_{92}U^{233}$	5.18±0.27	4.19
$_{92}U^{235}$	5.31±0.27	4.53
$_{92}U^{238}$	5.08±0.15	5.24
$_{94}Pu^{239}$	5.31±0.25	3.40

[a] See reference 29.
[b] See reference 30.
[c] The tabulated neutron binding energies are obtained by interpolation and extrapolation among the binding energies derived from (γ, n) and $(d-p)$ reactions, as listed by J. A. Harvey [Phys. Rev. **81**, 353 (1950)], and assuming the systematic deviation due to the 126 neutron shell which these values indicate for the actual binding energies from those predicted by the Weizsacker-Fermi semi-empirical mass formula [E. Fermi, *Nuclear Physics* (University of Chicago Press, Chicago, 1949), notes by Orear, Rosenfeld, and Schluter; E. Feenberg, Revs. Modern Phys. **19**, 239 (1947)]. The calculated fission barriers are taken from the formula of Fig. 3.
[d] The fission barrier formula of Fig. 3 yields the listed values of F_n when the values of $y=1-x$ are inserted. Here the "fissionability parameter" x is defined as in Fig. 2 to be $\frac{1}{2}$ the ratio of Coulomb energy to surface energy of the spherical nucleus,

$$x=\frac{1}{2}\frac{E_c}{E_s}=\frac{1}{2}\frac{\frac{3}{5}(e^2/r_0)}{4\pi r_0^2 O}\frac{Z^2}{A}=(Z^2/A)/(Z^2/A)_{\text{limiting}}.$$

If we set $r_0=\frac{1}{4}e^2/mc^2=e^2/1.022$ Mev, and $4\pi r_0^2 O=14$ Mev [E. Feenberg, Phys. Rev. **55**, 504 (1939); Revs. Modern Phys. **19**, 239 (1947)] we get $(Z^2/A)_{\text{limiting}}=45.7$. Because of the uncertainty in these constants, however, we compute $(Z^2/A)_{\text{limiting}}$ by another method:

With ξ_{max} as given in Fig. 3,

$$F_n=(4\pi r_0^2 O)A^{\frac{1}{3}}\xi_{max};$$

we choose x to reproduce the experimental value of 5.5 Mev for the fission barrier of U^{238}, carrying through the work both for $(4\pi r_0^2 O)=13.0$ Mev, as given by the Weizsacker-Fermi formula, and for $(4\pi r_0^2 O)=14.0$ Mev, as given by Feenberg's estimate. The resulting values of $(Z^2/A)_{\text{limiting}}$ are, respectively, 46.78 and 46.45. We do not here make the small correction (-0.38) following from the fact that the zero-point excitation of the fission mode diminishes from 0.45 Mev for the spherical form to zero for the form at the peak of the barrier curves of Fig. 3. Noting the insensitivity of these results to the choice of surface energy, we arbitrarily fix the value of $(4\pi r_0^2 O)$ at 13.0 Mev to compute the barriers listed in the table.
We see that the calculated and the observed barriers differ by more than the experimental uncertainties, the calculated values showing a steeper change with Z^2/A than the experimental values.

[28] S. Frankel and N. Metropolis, Phys. Rev. **72**, 914 (1947); see also R. D. Present and J. K. Knipp, Phys. Rev. **57**, 751, 1188 (1940); and Present, Reines, and Knipp, Phys. Rev. **70**, 557 (1946).

[29] U. S. Atomic Energy Commission Unclassified Document AECU-2040, 1952 (unpublished), compilation of the Atomic Energy Commission Neutron Cross Section Advisory Group.

[30] Koch, McElhinney, and Gasteiger, Phys. Rev. **77**, 329 (1950).

Cross Sections

The dependence upon energy of the cross section for neutron induced fission (Fig. 43) is characterized first of all by a threshold, below which the cross section begins to fall off in a general way exponentially with energy. Above, it rises to an approximate plateau. Writing the fission cross section in the form

$$\sigma_f = \sigma_{\text{geom}} \Gamma_f / (\Gamma_f + \Gamma_n),$$

where Γ_f and Γ_n represent the probabilities per second for the compound nucleus to dispose of its excitation by fission or by neutron evaporation, we have to conclude from the existence of the plateaus that the ratio of Γ_f to Γ_n does not change much, though both rate constants individually are of course rapidly increasing functions of energy. Still another feature of fission cross sections at neutron energies of the order of 8 Mev is a rise towards a new plateau—a rise associated with the possibility for the nucleus to make a second try at fission, if in the first try it has instead evaporated away one neutron.[31] Aside from these general features, the results collected in Fig. 43 show most interesting irregularities in the lower energy regions in the dependence of fission cross section upon neutron energy. While the shape and density distribution of potential energy curves are irregular, and while these irregularities must react upon the fission cross section, it seems premature to try to trace out the connection any more specifically.

Also the individualities of the potential energy surfaces must have their influence upon the life time for spontaneous fission (Figs. 44 and 45): most important of all in causing fluctuations from nucleus to nucleus in the heights of the fission barrier, upon which the tunneling probability is most dependent; but also important in changing the shape of the barrier as between two nuclei with about the same barrier height. From this point of view one can understand how it is possible for the lifetime[31a] with respect to spontaneous fission of U^{235} to exceed that of U^{238} whereas the smooth dependence upon Z^2/A given by the liquid drop model would attribute to U^{235} the shorter life.

Fission Asymmetry

Energy Release not an Explanation

An outstanding feature of the fission process is the disparity in size of the two fragments (Fig. 46). U^{235} split by thermal neutrons has 600 times less chance to divide into equal parts than to break up into the most frequent 2:3 mass ratio. The energy release is not markedly different between the different pairs of fission fragments, a point upon which beautiful observations have been made by Brunton and Hanna.[32] Moreover, at the critical moment of passage over the fission barrier, the critical form for uranium (Fig. 2) is calculated to have still a diameter, 11×10^{-13} cm, as great as that of the copper nucleus. It is difficult to see how a system so far from the actual act of scission can have any feel for, or be influenced by, the energy or nature of the fragments to which it can potentially give rise.

Shell Effects not an Explanation

Magic number and shell binding effects have been considered as possible causes of fission asymmetry.[33] While we have much to learn about shell structure, the considerations of Sec. II show how greatly the order of levels in a deformed nucleus differs from that familiar from the study of spherical potential wells. Again it is difficult to see how the nucleus in the transition state can feel any potential shell structure in the not yet formed products. And of systematic differences in abundance between fission chains of even charge numbers and odd charge numbers there is yet no trace, much as the energies of even-even and even-odd nuclei differ from each other. There is some suggestion of shell structure in recent more detailed studies of the fission yield curve (Fig. 47), but just this circumstance makes it seem all the more unlikely that the division into two broad mass peaks come from the same cause. Attempts have been made to show[33a] statistically that shell structure determines the most probable division of mass. But any account of fragment abundances would seem unreasonable which overlooks the nature of the transition state, however thoroughly it analyzes the *statistical* weight of the various *final* configurations. A simple counting of statistical factors, with or without an examination of the relative size of the energy release, would for instance suggest that ternary fission should be far more probable than binary division, quite contrary to observation (Table III).

Barrier Penetration not an Explanation

Passage, not over the fission barrier, but through it, is the process considered in quite another explanation of fission asymmetry put forward by Frenkel.[34] Recalling the expression for probability of barrier penetration[5] in spontaneous fission,

$$\exp\left[(-2/\hbar)\int\{2[V(\alpha)-E]\textstyle\sum_i M_i(d\mathbf{r}_i/d\alpha)^2\}^{\frac{1}{2}}d\alpha\right]$$

$$=\exp\left[(-2^{\frac{1}{2}}/\hbar)\int\left\{\begin{pmatrix}\text{potential minus}\\ \text{available energy}\end{pmatrix}\times\begin{pmatrix}\text{effective}\\ \text{mass}\end{pmatrix}\right\}^{\frac{1}{2}}d(\text{distance})\right],$$

[31] N. Bohr, Phys. Rev. **58**, 864 (1940).
[31a] E. Segré, Phys. Rev. **86**, 21 (1952).
[32] D. C. Brunton and G. C. Hanna, Phys. Rev. **75**, 990 (1949).
[33] M. G. Mayer, Phys. Rev. **74**, 235 (1948); G. C. Wick, Phys. Rev. **76**, 181 (1949); K. H. Kingdon, Phys. Rev. **76**, 136 (1949).
[33a] T. D. Newton, Phys. Rev. **87**, 187 (1952); Peter Fong, Phys. Rev. **89**, 332 (1953).
[34] S. Frenkel, J. Phys. (U.S.S.R.) **10**, 533 (1946); also E. Bagge, Z. Naturforsch. **2a**, 565 (1947).

he ascribes the greater probability of unequal masses to the smaller value in this case of the reduced mass of the system. However, such a picture does not seem to be relevant in the case of induced fission. There, the nuclear excitation exceeds the critical energy, and passage over the barrier is far more probable than penetration through it. Were the excitation so low that barrier leakage became critical, then the cross section for fission would have a dependence upon energy quite different from that observed. Also the absolute probability of division would be impossibly low. Specifically, we have between 140–94 division and 117–117 splitting a difference in reduced mass of fragments, 56.2 *vs* 58.5, of one part in 25, or—on the hypothesis in question—a difference in penetration exponent of one part in 50. This difference in exponent is called upon to explain a factor of 10^{-2} in relative probability of symmetrical and unsymmetrical partition. Then the absolute probability of penetration would have to be $(10^{-2})^{50}$, and fission could not occur, contrary to observation.

Indications that Saddle Point Configuration is Symmetric

It has also been proposed as a mechanism giving preference for asymmetric fission[35] that the critical form of unstable equilibrium is itself asymmetric. The potential barrier over which the nucleus must pass is defined, as already illustrated in Fig. 4, by giving the deformation energy in terms of the quantities $\alpha_2, \alpha_3, \cdots$, which specify the shape of the nucleus. For a nucleus which has just barely enough energy to pass over the fission barrier, one would on a classical picture expect the unrolling of the motion to proceed in a unique way, leading to fragments of well-defined mass. If there are several minima in the potential energy ridge which must be surmounted for fission, one would therefore expect several different possibilities for the course of fission, each leading to a specific and distinct mass division. This deterministic classical picture of what happens after passage over the fission barrier is, of course, quite untenable. At most it can be taken to suggest that there might be some correlation between the mass division and the shape of the one or more critical forms of unstable equilibrium, which correspond to the one or more conceivable passes over the potential energy ridge. Passage over various passes would occur with relative probabilities depending on the various critical energies, E_f, and upon the effective temperature, T, as expected from the usual Boltzmann formula. One might in this way, for example, try to understand why symmetric fission is so improbable at low excitation and why the relative probability for equal division increases with energy of bombardment.

No theoretical argument yet shows that the fission barrier should have this suggested asymmetry. Frankel and Metropolis[28] have explored by ENIAC calculations the shape of the fission barrier and find that a well-defined saddle point occurs for a symmetric division. The energy of the potential ridge increases, they find, with asymmetric departures from this symmetric critical form. There is no evidence for any other saddle point, symmetric or unsymmetric. Swiatecki[18] has noted that nuclear polarizability and compressibility will change slightly the simple liquid drop dependence of energy on deformation, and has suggested that this effect will work in such a direction to split the symmetric saddle-point into two asymmetric ones. Even in the absence of this Wigner-Feenberg-Swiatecki phenomenon of slight redistribution of electric charge over the nuclear volume, such a splitting of the saddle point will be expected to occur for sufficiently small fissionability parameter x (proportional to Z^2/A) as indicated in Fig. 48. The redistribution effect will move to higher x the point of first occurence of asymmetric saddle-point forms. However, the amount of the redistribution effect does not off-hand seem great enough to lead to asymmetric critical forms for uranium; and for still heavier nuclei the calculated critical form approaches closer and closer to a sphere (Fig. 49).

Asymmetry Favored by Shape-Dependent Viscosity

It is conceivable that a certain symmetry phenomenon in the collective model of the nucleus may also act to favor an asymmetric deformation of the nucleus. For a completely symmetric deformation, individual particle states can be divided into two classes according as the wave function does not change sign on reflection ("gerade") or does change sign ("ungerade"). For small departures from sphericity both sets of states will be filled approximately to a common energy, F. As the deformation increases, the gerade states will rise more in energy than the ungerade ones because the one kind of wave function feels the pinch of the necking-off process more than the other. Consequently the energy of the deformed system could be lowered, and fission made easier, if the particles were allowed to move from the higher gerade states into ungerade ones. Such slippages cannot occur for a completely symmetrical deformation, but will readily take place if a sizeable asymmetry is present. Consequently a quite appreciable effect is at work to favor an asymmetric configuration for the critical form.

Whatever the shape of the nucleus at the moment it goes over the barrier, there is room for variations in the division ratio between one fission act and another, granted the same nuclear species and the same excitation energy, just a little above the barrier. There will be a quantum-mechanical spread in the possible paths which can be taken in configuration space, from the moment of surmounting the saddle-point, to the moment of actual scission. A simple way to visualize this effect qualitatively is to imagine the trajectory of the representative point in configuration space to be completely definable classically but the direction of this point at the moment of transmigration to have an

[35] R. D. Present and J. K. Knipp, Phys. Rev. **57**, 751 (1940).

uncertainty of the order of that to be expected from the unavoidable zero-point amplitudes of the simplest modes of capillary oscillation.

Asymmetry Favored by Inviscid Hydrodynamic Instability

These unavoidable asymmetries at the moment of passage over the barrier can also lead to large asymmetries if there is any intrinsic hydrodynamical instability at work to magnify the amplitude of the disturbances. Qualitative arguments for the existence of such an instability phenomenon are easily visualized (Fig. 50) and seem to receive some preliminary support from the initial calculations on the subject which have so far been carried out (Figs. 51 and 52). Consequently it seems appropriate to say that there appears nothing paradoxical about the phenomenon of asymmetric fission. On the contrary, the problem that remains is to decide which of the two effects that work in the same direction is the more important quantitatively: gerade-ungerade differences in individual particle wave functions, or hydrodynamic instability.

The more disturbed the nucleus is at the moment of passage over the fission barrier, by reason of more than adequate energy, the more will be the tendency to override the more delicate factors that favor asymmetric fission, and the greater will be the yield of fission fragments of equal mass. Consistent with this view is the experimental evidence on variation of fission yield with excitation of the initially formed compound nucleus (Fig. 53). The ratio of symmetric to asymmetric fission varies qualitatively as one might expect[5] from the usual statistical-mechanical formula exp[-(difference in activation energy)/(temperature)] for the ratio of rates of competing processes, where in the nuclear case the temperature goes roughly as the square root of the excitation. The activation energy difference is reasonably interpreted as the extra cost energy-wise of a disturbance of the nuclear surface which pinches in the critical form of unstable equilibrium around its equatorial symmetry plane. Any attempt to evaluate this critical energy difference from the observational material is of course complicated because at high energies one is dealing with a superposition of fission of newly formed compound nuclei, and fission of residual nuclei subsequently formed by evaporation of one or more neutrons. A preliminary estimate for the activation difference, neglecting these complications of identification, gives a value of the order of a few Mev[36,37] which seems not unreasonable.

In spontaneous fission the distribution of fragment sizes will have as little directly to do with considerations of energy release as in induced fission. Energy factors can be expected to apply only to passage through the critical state. The sequence of events which follow will be expected to go as in induced fission. The final result will therefore depend upon the same kind of mirror symmetry and hydrodynamic instability effects. We should therefore not expect any great differences between the fragment distribution and neutron release in case of spontaneous fission and of induced fission with moderate excitation, in conformity with the observations[38] (see Fig. 46 and caption).

Angular Distribution of Fragments

From the moment of input of energy into the nucleus by radiation or impact of a material particle to the time when that energy is concentrated on the mode of deformation that leads to fission, the simple liquid drop picture envisages a complicated many-stage process of redistribution of energy to go on in the nucleus. Consequently it would be expected on that impenetrable-fluid idealization that correlation should be practically absent between direction of incidence of the energy and direction of emergence of the fission fragments. On the contrary, Halpern and Winhold[39,40] find a correlation in the photofission of thorium between the two directions, separated by an angle θ, of the form $1+b\sin^2\theta$, where in preliminary measurements b is 0.3 ± 0.1 for 16-Mev radiation and about four times that value at 8 Mev. What does the collective model predict? According to the Franck-Condon principle (Fig. 38), starting with the nucleus in its ground state, the act of absorption will lead to an excited potential energy surface, with nuclear wall still in its original configuration—which is ordinarily not at all a shape of equilibrium for the new potential energy surface. Consequently a very sizeable oscillatory motion will ordinarily be set up, making excursions on both sides of the new shape of equilibrium. If the departures from sphericity are great enough in the course of this motion, then the restoring force will weaken, the potential curve will bend over, and one will be dealing, not with a periodic phenomenon, but with passage over a potential barrier leading to fission. On this view the correlation between the act of absorption and the act of fission is much more direct than in the picture of a nearly impenetrable liquid drop. Of course we are discussing an idealized version of the collective model, in which the viscous forces due to slippage phenomena are neglected. How much these frictional effects complicate the picture is not yet clear theoretically; from the experiments themselves one can hope to learn more about this point.

The qualitative nature of the directional correlation in photofission suggests the following very schematic and tentative picture: (1) The gamma-ray is absorbed

[36] Jones, Fowler, and Paehler, Phys. Rev. **87**, 174 (1952).
[37] J. L. Fowler *et al.*, Phys. Rev. **88**, 71 (1952).
[38] Hanna, Harvey, Moss, and Tunnicliffe, Phys. Rev. **81**, 466 (1951).
[39] Winhold, Demos, and Halpern, Phys. Rev. **87**, 1139 (1952).
[40] I. Halpern and E. J. Winhold, Progress Report of the Laboratory of Nuclear Science and Engineering, Massachusetts Institute of Technology (1952) (unpublished). We are indebted to Professor Halpern and Mr. Winhold for interesting discussions of their results.

by photoeffect on a single proton. (2) Among all proton orbits those will absorb radiation the most strongly whose angular momenta are greatest, and whose planes are normal to the direction of the incident beam. (3) The most probable type of absorption is that in which the angular momentum increases by one unit, the direction of the plane of the orbit remaining unchanged. Points (1), (2), (3) are simple consequences of the theory of absorption of light by a single charged particle. (4) The greater centrifugal force exerted by the now faster moving excited particle pushes out parts of the nuclear wall normal to the direction of the photons. (5) The deformational oscillation generated as a consequence of the Franck-Condon principle therefore leads preferentially to fission in the observed direction.

If this description of directional asymmetry in photofission is correct, then a similar effect should be observed in fission induced by neutrons of 1 Mev or more. However, here the fragments should go preferentially parallel to the direction of incidence. The pressure exerted by the neutron against the nuclear wall in the act of capture (Figs. 39 and 40) will be predominantly such as to produce an elongation of the nucleus parallel to the beam. The application of the Franck-Condon principle to this process goes through otherwise as in the case of photofission.‡

How probabilities for the compound nucleus to undergo neutron evaporation or fission depend upon excitation energy and angular momentum, and how fission widths will be expected to vary with passage from the region of tunnel effect to the region of free passage over the fission barrier, and what explanation can be given for irregularities in the dependence of fission cross section upon energy, are interesting questions on which nothing will be said here now from the standpoint of the collective model.

Charge Division

Another feature of the act of division is a certain variation from fission act to fission act in the number of protons which come off in a fragment of given mass number. In connection with these charge fluctuations, it is evidently quite inappropriate to consider the dividing nucleus as a fluid continuum of precisely defined charge to mass ratio. But it would be even more misleading to view the two kinds of nucleons as behaving like gas molecules, with quite independent motions, susceptible to simple statistical considerations. On the contrary, the energy of correlation of the neutrons and protons is quite high; and a separation of the two sorts of entities can be considered to come about at the moment of splitting only as a result of their specific quantum-mechanical zero-point relative motions.

To give a treatment of the zero-point motions sufficient for an accurate analysis of the charge fluctuations would of course be most difficult. However, an approximate estimate may be obtained by considering only that mode of motion which Teller and Goldhaber[21] call the "dipole vibration" of the nucleus, a movement of all of the protons of the nucleus relative to the neutrons. They give reasons for assigning to this vibration the marked maximum in the photofission cross section—and presumably also of the photoneutron cross section—observed for U and Th at about 17 Mev. The frequency and the restoring force associated with this motion are high, but not so high as to exclude some variability in the number of protons which go into a given one of the two fragments. Thus, comparing the actually rather complicated scission form with a sphere, and denoting the displacement of neutrons relative to protons by x, we have for the excess of protons on the left-hand fragment the number

$$\delta Z=[Z/(4\pi R^3/3)]\pi R^2 x,$$

and for the relative probability of a displacement x the usual quantum mechanical expression

$$\exp[-M_N M_Z(M_N+M_Z)^{-1}\omega x^2/2\hbar].$$

Thus, the charge variation at half-maximum probability in the present approximation has the form

$$\begin{aligned}\delta Z_{\frac{1}{2}}&=(3Z/4)(0.693\hbar^2/M_{\text{red}}R^2\hbar\omega)^{\frac{1}{2}}\\&\sim 69(0.693\times 0.010\text{ Mev}/17\text{ Mev})^{\frac{1}{2}}\\&\sim 1.38.\end{aligned}$$

Two corrections have to be applied to this result, in opposite directions. First, higher modes of vibration up to an order $n\sim A^{\frac{1}{3}}=6$ have to be considered, on which account there should be introduced inside the square root above a further factor qualitatively of the form

$$1+\tfrac{1}{2}+\tfrac{1}{3}+\cdots+\tfrac{1}{6}.$$

Second, the quantum energy 17 Mev in the denominator should be substantially increased because a given movement of charge will be more expensive of energy for the deformed nucleus than for the approximately spherical system. That this second correction will outweigh the first, and reduce the expected charge fluctuation to one unit or less in δZ, is the conclusion suggested by examination of the elongated shape of the U nucleus as

‡ *Note added in proof:*—The angular distribution of fragments from neutron-induced fission has been studied, since this paper was written, by W. C. Dickinson and J. E. Brolley, Jr., of the Los Alamos Scientific Laboratory [reported January 24, 1953, at Cambridge Meeting of the American Physical Society]. They have measured the ratio of fission fragments moving parallel to those moving perpendicular to the beam of incident neutrons, both for thermal and for 14-Mev neutrons, with results in agreement with the above expectations:

Target nucleus	$I(0°)/I(90°)$ thermal	14 Mev
$_{92}U^{233}$	1.00±0.08[a]	1.32±0.11[a]
$_{92}U^{235}$	0.99±0.09	1.27±0.17
$_{90}Th^{232}$		1.53±0.21
$_{92}U^{238}$		1.53±0.17
$_{93}Np^{237}$		1.20±0.13

[a] Statistical errors defined to give 0.95 chance of bracketing true values.

TABLE II. The known delayed neutron half-lives, energies, and yields.[a]

Half-life	Energy kev	Yield (percent relative to total neutron emission)	Reference
0.05 sec		0.025	42
0.43	420	0.085	42
1.52	620	0.241	42
4.51	430	0.213	42
22.0	560	0.166	42
55.6	250	0.025	42
3 min		8×10^{-7}	43
12		3×10^{-9}	43
120		1.3×10^{-10}	43
	Total:	0.755 percent	

[a] Delayed neutrons associated with fission to the extent of roughly one per hundred events were interpreted in an earlier discussion (reference 5) as follows: (1) fission occurs; (2) fission fragment is deexcited by radiation; (3) the fragment undergoes beta-decay; (4) in the case of certain fission products the energy release in the beta-decay is greater than the binding of the neutron in the product nucleus; (5) in these cases the product nucleus is occasionally left excited and promptly emits a neutron. The average kinetic energies of some of the delayed neutron groups have in the meantime been measured and found to be consistent with this explanation. Some of the beta-active sources have been identified radiochemically. In these cases the odd-even changes are such as to permit beta-decay processes with more energy release than the neutron binding.

it approaches the point of scission (Fig. 2). A final source of fluctuations has to be considered, due to release of secondary neutrons. Fission chains of mass number A originate partly from fragments of mass $A+n$ which have given off n neutrons, and partly from products of mass $A+n+1$ which have lost $n+1$ secondaries. A difference of mass of ±0.5 in the relevant part of the nuclear table corresponds to a change in charge of about ±0.2. Recalling that one has first to square the magnitudes of independent fluctuations before combining them, we conclude that we can neglect the influence of variability in secondary neutron release in an account of charge fluctuations. Then it appears that we have a reasonable order of magnitude account of the fluctuations in length of given fission chains,

$$\delta Z_{\frac{1}{2}}=1.0,$$

observed by Glendenin, Coryell, and Edwards.[41] It is therefore reasonable to conclude that these variations in charge distribution are indeed directly attributable to the unavoidable quantum zero-point uncertainties in the positions of the nucleons.

Fission Neutrons

Emission of a neutron associated with fission requires an amount of energy for which three sources are available: hydrodynamic disturbances at the moment of scission; excitation of the fragments after division; and re-excitation of stopped fragments following beta-decay. The last effect is well known to give a reasonable account of the phenomenon of delayed emission (Table II)[42,43] responsible for somewhat less than a percent of all the secondary neutrons from the fission of uranium. The other 99^{+} percent of neutrons are observed to come off within less than 10^{-12} sec of the moment of fission and must be attributed to the first two processes of excitation.

Between hydrodynamic disturbances just before scission, and just afterwards, it is difficult to make any simple comparison of importance in exciting a neutron to a level sufficient for escape. The rapid change of wall shape throughout the whole scission process via Doppler effect will raise the energy of neutrons with suitably oriented propagation vector. However, it may well be that the final stages of raising of energy to the emission threshold occur only as the newly formed and quite distorted fission fragments relapse towards a spherical form. On this basis it will be expected that most of the prompt neutrons will be given out after that particular stage of the fission process which we name scission. Moreover, the walls of both fragments being at that time in rapid contraction along the axis of fission, the Doppler effect in internal nucleonic reflections will be in such a direction as to give maximum energy to neutrons with propagation vector parallel to this axis. It thus seems reasonable to expect maximum neutron emission parallel to the axis of fission.

The observed distribution in energy of fission neutrons (Fig. 54) is qualitatively consistent with the picture of isotropic emission from moving fission fragments, with a distribution in energy in the moving frame of reference of the general character to be expected on the evaporation picture, $dN/dE\sim E\times\exp(-E/T)$. It is primarily simplicity that has suggested this form of representation in the past, and there is little doubt that a substantial preference for emission parallel and antiparallel to the line of fragment motion is also compatible with the observed distribution in energy.

The observations on angular distribution fall into two classes. De Benedetti and collaborators[44] have measured the angular correlation of prompt neutrons from the neutron-induced fission of U^{235}. They find that the number of coincidences is fairly constant from 30° to 90°, and increases by a factor about 2 from 90° to 180°. Assuming that neutrons go mainly in the direction of the fragment from which they are emitted, they conclude that fission neutrons are emitted preferentially by opposite fragments, and that there are at least twice as many pairs of neutrons emitted from opposite fragments as from the same fragment.

Fraser[45] has measured the correlation of fast neutrons with collimated fission fragments, finding 4.35 ± 0.15 times as many neutrons parallel to the line of fission as

[41] Glendenin, Coryell, and Edwards, *Radiochemical Studies, The Fission Products* (McGraw-Hill Book Company, Inc., New York, 1951), Paper No. 52, National Nuclear Energy Series, Plutonium Project Record, Vol. 9, Div. IV.

[42] Hughes, Dabbs, Cahn, and Hall, Phys. Rev. **73**, 111 (1948).

[43] Kunstadter, Floyd, Borst, and Weremchuk, Phys. Rev. **83**, 235 (1951).

[44] de Benedetti, Francis, Preston, and Bonner, Phys. Rev. **74**, 1645 (1948).

[45] J. S. Fraser, Phys. Rev. **85**, 726 (1952).

perpendicular to that direction; and finding indication that the light fragment emits about 30 percent more neutrons on the average than does the heavy one. It is premature to try to say from the observations whether there is an indication of preference *in the moving frame of reference* for emission parallel to the line of fission.

Tripartition

Another interesting phenomenon is the occasional observation of alpha-particles (Fig. 55) and other light nuclei in fission (Table III).[46–54] For this effect, a simple explanation offers itself in terms of the liquid drop model of nuclear division. From classical hydrodynamics it is well known that the disintegration of a liquid jet into drops leads to the formation between these fragments of tiny droplets. Likewise in the case of nuclear fission it is not surprising to find some portion of the nuclear substance set free between the fission fragments in the act of scission. It is necessary to distinguish between alpha-particles, protons and neutrons. Of these only the alpha-particles represent nearly saturated nuclear matter, and only they are energetically capable of emerging from the original nucleus already in its unexcited state. But an alpha-particle at the surface of the original nucleus is far below the level of the Coulomb potential, on account of the coupling to its surroundings. In contrast, an alpha-particle in the region of scission lies at the point of maximum Coulomb potential, and yet has less than the normal amount of nuclear matter immediately around it with which to form bonds. This particular alpha-particle has in effect been raised to a point but little lower than the top of the barrier, by means of the changes of nuclear form which took place up to the moment of scission. An alpha-particle in such a position will have a significant probability to pass through the barrier. Thus it is reasonable to connect up the energy of the observed alpha-particles with the value of the electrostatic potential in the small interval between the newly formed fission fragments. On this view the alpha-particle will be expelled in a direction roughly perpendicular to the line of separation with an energy of about 20 Mev. The unequal repulsion by the lighter and heavier fission fragments will be responsible for some deviation from perpendicular emission, as observed.

Similar effects will be expected for other light nuclear fragments, except that here the relevant potential barriers will be higher, and emission probabilities lower.

TABLE III. Modes of ternary fission.[a,b]

Compound nucleus		Mass of third particle in atomic mass units	Range in c.a.e.	Energy in Mev	Binary fissions per event	Reference
U^{235}	+slow neutron	40 to 90		>40	7×10^{6}	46
U^{233}	+slow neutron	13±3	0 to 0.8		75	47
U^{235}	+slow neutron	13±3	0 to 0.8		75	47
Th^{232}	+2.5-Mev neutron	8		20	10^{3} to	48
U^{235}	+23-Mev photon	8		20	10^{4}	49
U^{233}	+slow neutron	4	10 to 50	5 to 25 maximum frequency at 15	400	50
U^{235}	+slow neutron	4	10 to 50	5 to 25 maximum frequency at 15	500	50
Pu^{239}	+slow neutron	4	10 to 50	5 to 25 maximum frequency at 15	450	50
Th^{232}	+2.5-Mev neutron	4		5 to 23	~400	51
U^{238}	+2.5-Mev neutron	4		5 to 21	~400	51
Th^{232}	+23-Mev photon	4			~400	52
U^{238}	+23-Mev photon	4		17		53
U^{235}	+slow neutron	1		up to 2.1	5000	54

[a] The range is given in c.a.e. (cm of air equivalent). One c.a.e. is an absorptive unit equivalent, for range diminution of an alpha-particle or proton, to one cm of air at 15°C and 760 mm Hg pressure.

[b] Following the original work by Alvarez (see reference 54) many modes of fission into more than two charged fragments have been identified. The earliest published measurements [L. L. Green and D. L. Livesey, *Conference on Physics of Fundamental Particles* (Cambridge University Press, 1946); Tsien, Chastel, Ho, and Vigneron, Compt. rend. **223**, 986, 1119 (1946); **224**, 272 (1947); Farwell, Segrè, and Wiegand, Phys. Rev. **71**, 327 (1947)] identified α-particles emitted in coincidence with fission. This work was refined and extended [Tsien, Ho, Chastel, and Vigneron, J. phys. et radium **8**, 165 (1947); **8**, 200 (1947); L. L. Green, and D. L. Livesey, Phil. Trans. **A241**, 323 (1948)] as indicated by the present extensive literature, from which some of the more recent and complete papers are cited for each of the fission modes listed in the table. For the fission alpha-particles it has also proved possible to measure the angular distribution [Wollan, Moak, and Sawyer, Phys. Rev. **72**, 447 (1947); L. Marshall, Phys. Rev. **75**, 1339 (1949)] which turns out to be near-Gaussian about 82° (relative to the light fragment) with a half-width of 25° (Titterton, reference 52). The infrequency of symmetric tripartition serves to emphasize the principle (which is already apparent in binary fission) that the mass division is primarily determined by the dynamics of passage through the transition forms (Fig. 50) rather than by the total energy content of the final nuclei, which is much lower for the fragments of symmetric ternary fission than for the fragments of binary fission.

When C^{12} or He^{4} are emitted, the mass division between the heavy fragments is comparable to that observed in binary fission [Allen, reference 50, and L. Marshall, Phys. Rev. **75**, 1339 (1949)].

Lines 4 and 5 of the table refer to Be^{8} nuclei, which are actually observed as two He^{4} particles in small angular separation. Thus from the description of ternary fission follows a process which might be classified as quaternary fission, occasionally reported elsewhere (Tsien *et al.*) as occurring with similar intensity but with all four fragments of mass number greater than 20. However, in this connection see E. W. Titterton [Nature **170**, 794 (1952)], where strong reasons are given to doubt any evidence so far presented in favor of quadripartition.

Emission of protons will be practically forbidden in comparison with alpha-particle emission, because the binding of the particle to nuclear matter—even near the scission neck—places its energy far below the top of the Coulomb barrier. Those protons which are observed (Fig. 56) have rather to be interpreted as due to processes of impact between fission fragments and the stopping material through which they pass. Their energy distribution is consistent with this view, and quite contrary to what would be expected if they came directly from either the dividing system or the fission fragments.

[46] L. Rosen and A. M. Hudson, Phys. Rev. **78**, 533 (1950).
[47] K. W. Allen and J. T. Dewan, Phys. Rev. **82**, 527 (1951).
[48] E. W. Titterton, Phys. Rev. **83**, 1076 (1951).
[49] Goward, Titterton, and Wilkins, Nature **164**, 661 (1949).
[50] K. W. Allen and J. T. Dewan, Phys. Rev. **80**, 181 (1950).
[51] E. W. Titterton, Phys. Rev. **83**, 673 (1951).
[52] E. W. Titterton, (private communication, March, 1950).
[53] E. W. Titterton and F. K. Goward, Phys. Rev. **76**, 142 (1949).
[54] D. L. Hill, Phys. Rev. **87**, 1049 (1952).

VII. CONCLUSION

This summary of the collective model of the nucleus and some of its connections with fission phenomena, while not comprehensive, may indicate how liquid drop and individual particle models come naturally together in a larger unity, consistent with experiment; and indicate also how important is the nuclear wall in the exchange of energy within the nucleus.

VIII. ACKNOWLEDGMENT

To Professor Niels Bohr we are indebted for many fruitful discussions over the past few years of topics treated in this paper, especially on the unification of the individual particle picture and the liquid drop model, the asymmetry of nuclear fission, and other fission phenomena. Many of these considerations were embodied in an earlier manuscript prepared jointly with Professor Bohr. For Professor Bohr's permission to include these specific parts of the early discussion in the present article, as well as for the hospitality of his Institute on many past occasions, we wish to express our deep appreciation. We also wish to thank the many collaborators we have had in the preparation of figures, performance of calculations, discussion of experimental results, and completion of the manuscript.

APPENDIX. FIGURES AND DISCUSSION

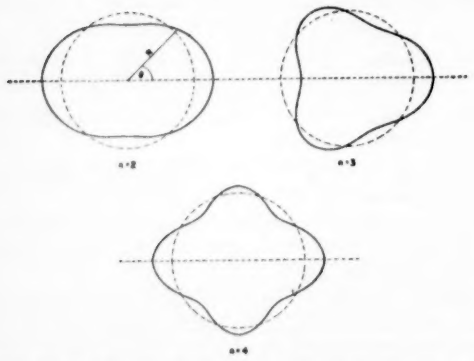

FIG. 1. Independent modes of small oscillation of a liquid droplet.

Illustrated are the first three orthogonal modes of small oscillation for a liquid moving under the constraint of surface tension. Addition of uniform volume electrification, as in the liquid drop model of the atomic nucleus, does not affect the form but does affect the frequency of the orthogonal oscillations, for the decrease in Coulomb energy somewhat offsets the increase in surface energy when the shape deviates from the spherical form of equilibrium.

To evaluate these frequencies of oscillation for, say, the uranium nucleus according to this model, note that a component of orthogonal oscillation is represented by each term (except the term for $i=1$, which gives no oscillation, but only a shift for the center of mass) in the expression

$$R(\mu)=a_0\Big[1+\sum_{i=1}^{N}\alpha_i P_i(\mu)\Big]$$

for the distance from the center of mass to the surface of a cylindrically symmetric nucleus as a funct on of $\mu=\cos\theta$, argument of the Legendre polynomials $P_i(\mu)$. (a_0 is chosen for volume normalization.) Evaluating the coefficients in the quadratic forms for kinetic and potential energies of small oscillations, one finds for the frequency of general order n:

$$\nu_n=A^{-\frac{1}{2}}\left[\frac{O}{3M_p\pi}n(n-1)\frac{(2n+1)(n+2)-20x}{2n+1}\right]^{\frac{1}{2}},$$

where M_p is the proton mass, and the other notation as in Fig. 2. Quantization of the surface oscillations gives, for the zero-point energy, $\langle E_n\rangle_{\text{a.p.}}=\frac{1}{2}h\nu_n$, and for the zero-point value of the mean square relative amplitude:

$$\langle\alpha_n^2\rangle_{\text{a.p.}}=A^{-7/5}\left\{\frac{\hbar^2}{12M_p r_0^3(4\pi r_0^3 O)}\,\frac{n(2n+1)^3}{(n-1)[(2n+1)(n+2)-20x]}\right\}^{\frac{1}{2}}.$$

Evaluating these quantities for the first three modes of oscillation gives:

n	ν_n	$\langle E_n\rangle_{\text{a.p.}}$	$\langle\alpha_n^2\rangle_{\text{a.p.}}^{\frac{1}{2}}$
2	2.15×10^{20}/sec	0.45 Mev	0.064
3	6.21×10^{20}/sec	1.29 Mev	0.054
4	10.78×10^{20}/sec	2.23 Mev	0.053

It should be noted that the rms values of α_n here predicted are smaller by a factor 5 or 6 from the values used in illustrating the orthogonal oscillations, each drawing having been computed from the expression for $R(\mu)$ by assuming $\alpha_n=0.3$ and all other α_i zero.

The infinite sequence of possible oscillations for an ideal liquid drop must be terminated at some value of n between 6 and 10 when applied to the atomic nucleus because of the finite number of constituent nucleons present. If we then estimate the diffuseness of the nuclear surface for the collective model in its ground state, with the help of the quantity

$$\alpha_{\text{effective}}=\Big[\sum_{i=2}^{N}\langle\alpha_n^2\rangle\Big]^{\frac{1}{2}},$$

we find the aggregate indetermination of the surface position to be about 15 percent of the nuclear radius.

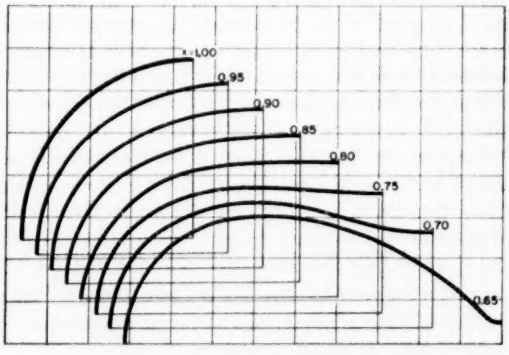

FIG. 2. Critical form of unstable equilibrium.

This critical form depends, in the approximation of the simplest liquid drop model, only upon the ratio of the square of the charge number to the first power of the mass number; or more conveniently, upon the dimensionless parameter:

$$x=\frac{(\text{charge})^2}{10\times\text{volume}\times\text{surface tension}}=\frac{Z^2e^2}{10A(4\pi/3)r_0^3O}=\frac{(Z^2/A)}{(Z^2/A)_{\text{limiting}}},$$

where $(Z^2/A)_{\text{limiting}}=2(4\pi r_0^3O)/(3e^2/5r_0)\cong47.8$. For an imaginary nucleus, "cosmium," sufficiently far beyond the known limits of stability, x will be 1, and the nucleus will already be unstable against fission in its spherical form. For values of x very close to 1 the critical form has been found (reference 5) to be $R=R_0\Sigma a_n P_n(\cos\theta)$, where R_0 is the original radius, $a_0=1$, $a_2=7(1-x)/3$, and all other

coefficients a are negligible. For four values of x the critical form has been calculated by S. Frankel and N. Metropolis [Phys. Rev. **72**, 914 (1947)]. Interpolating between their results and extrapolating beyond them, we find the continuous sequence of shapes illustrated in the diagram. Each form is an equilibrium shape for a different nucleus. It is also possible to view the set of curves as describing the changes in a given nucleus—a nucleus with a fixed x—as it undergoes a conceivable deformation. The curves when used in this sense need not be considered to have anything to do with the question of equilibrium forms. For this reason it is appropriate to distinguish each individual shape by the value of a parameter y, equal to 1 minus the value of x shown on the curve. Thus y describes the *shape*, and x describes the (charge)^2-to-mass ratio of that particular droplet which is calculated to have this critical form; but we can speak of a deformation y for a system with a different x. The curves are calculated from the interpolation and extrapolation formulas:

$$a_0=1-y^2\left[1.06+\frac{9.76\times10^{-4}}{(0.49-y)^4}\right],$$

$$a_2=y\left[2.3+\frac{5.42\times10^{-4}}{(0.49-y)^4}\right],$$

$$a_4=y^2\left\{1.6+y\left[3.0+\frac{2.84\times10^{-3}}{(0.49-y)^4}\right]\right\},$$

$$a_6=\frac{-2.36\times10^{-5}}{(0.49-y)^4},$$

$$a_8=\frac{-4.72\times10^{-5}}{(0.49-y)^4}.$$

Other a's zero.

It is possible that for values of the [(charge)^2/mass] parameter x near 0.65, the symmetric equilibrium form may not represent the lowest saddle point configuration in a multidimensional plot of deformation energy as a function of shape. It may be that two asymmetric forms, mirror images of each other, may lie lower. It is also conceivable that nuclear compressibility and redistribution of neutrons and protons between surface and interior may appreciably modify both the shapes themselves and the value of x, if any, for which the asymmetric saddle point is preferred. These effects have less and less influence the closer x is to unity, provided that y is rewritten as $1-x^*$. Here $x^*=x+z$, where the quantity x is as previously defined, and z is a measure of the compressibility and redistribution effects first considered in this connection by E. Feenberg [Revs. Modern Phys. **19**, 239 (1947)] and W. J. Swiatecki [Proc. Phys. Soc. (London) **A63**, 1208 (1950)] having a value of the rough order of magnitude of 0.04 for nuclei near uranium, and uncertain by a factor of perhaps two. Assumption of a nonzero value for z will require a readjustment in the number which now has the value 47.8, in order to leave the height of the fission barrier unchanged.

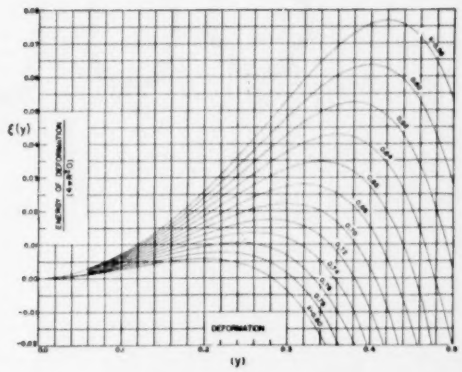

FIG. 3. Energy as a function of deformation en route to fission.

A given curve of the family here drawn describes the deformation energy, relative to the total surface energy of the spherical shape, for the forms described as a function of the shape parameter y of Fig. 2. Different curves represent different nuclei, as described by the parameter x of Fig. 2.

In the general formula,

$$\xi(x,y)=2.178(1-x)y^2-4.09(1-0.645x)y^3+18.64(1-0.894x)y^4-13.33y^5,$$

we note that the value of y corresponding to the maximum value of ξ for a given x represents the critical shape of unstable equilibrium for the nucleus so specified. Hence upon setting $y=1-x$, we obtain the expression for the fission threshold energies for any x value,

$$\xi_{max}=0.728(1-x)^3-0.661(1-x)^4+3.330(1-x)^5.$$

An examination of the deformation potential energy surface (see projection in Fig. 4) indicates that for the sequence of shapes as here defined by y the curve $\xi(x,y)$ is a fair approximation to the minimal path following the valley stream in the potential surface of a given x, and traversing the pass to scission.

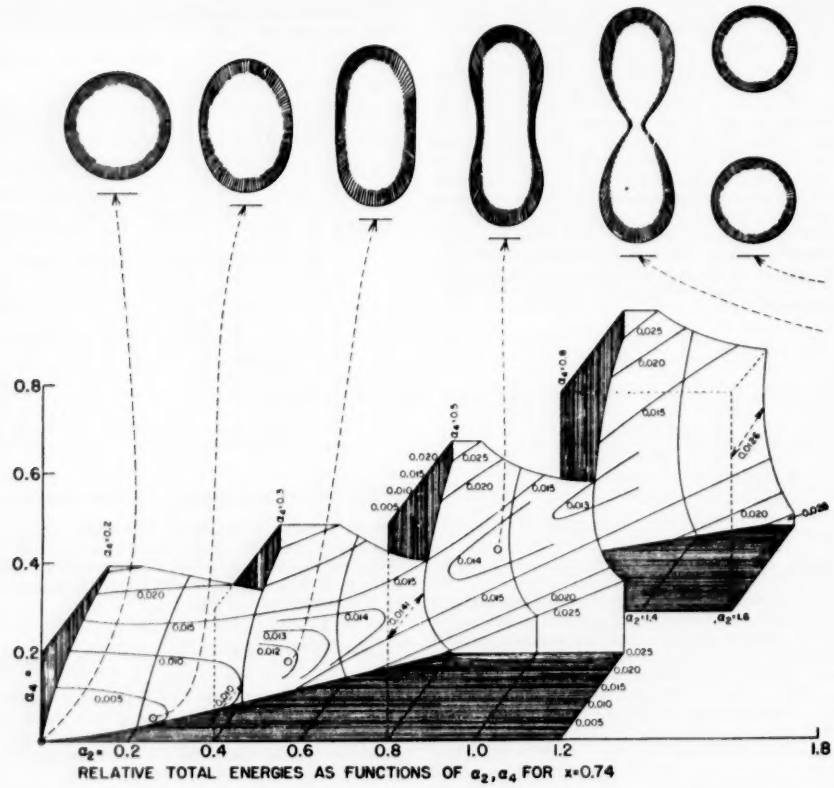

FIG. 4. Sequence of acts in fission.

The sequence of shapes leading from the initial uranium nucleus to the separated fragments is here shown, in correlation with the potential energy surface [taken from S. Frankel and N. Metropolis, Phys. Rev. **72**, 914 (1947)] of deformations described by points in the $\alpha_2-\alpha_4$ plane (see Fig. 1). The events leading to fission may be imagined as follows. The capture of a neutron by a uranium nucleus converts it into an excited compound nucleus, in which the energy of excitation is partly in the internal motion of individual nucleons, and partly in the collective motion of the entire nucleus for which typical components are illustrated in Fig. 1. The collective motion may be represented by the path of a "systen point" on an energy hypersurface of which the surface shown is the projection in the $\alpha_2-\alpha_4$ plane. This representative point will describe a Lissajous pattern with amplitude changing as the energy content of the nucleus passes back and forth between internal and collective modes of excitation.

Consider a case in which the total excitation is only slightly greater than the height of the saddle point in the energy surface, corresponding to the threshold for fission. Such a case results from the capture of thermal neutrons in uranium. Then it must follow that fission cannot occur until (1) essentially all of the excitation is in the collective motion, and (2) the phases and amplitudes of the different modes of collective motion are such as to lead the system point nicely along the valley stream toward the pass in the surface. Clearly the many degrees of freedom in the internal and collective motion of the system will permit many nuclear eons to elapse before the capture of a slow neutron will, on the average, bring about fission. A similar comment applies to the competing processes of neutron and photon emission.

Once the system point passes the saddle, however, the increase in surface energy with further elongation is more than offset by the decrease in Coulomb energy, and the motion is self-accelerating until division occurs. The resulting fragments will contain high excitation, both internal and collective, giving rise to prompt photon and neutron emission.

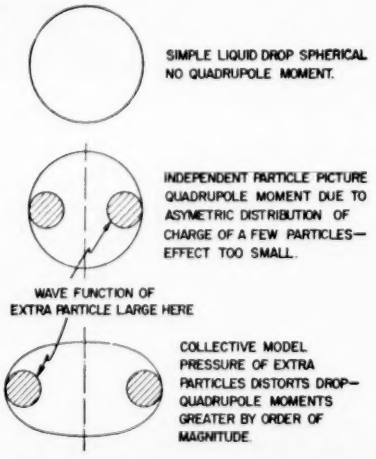

FIG. 5. Quadrupole moments and nuclear models.

Neither the simple liquid drop model nor the independent particle picture individually are capable of accounting for the order of magnitude of the quadrupole moment, or the asymmetry in the distribution of electric charge, of typical nuclei.

A negative quadrupole moment does follow in the liquid drop model if we assume that the entire nucleus with uniform volume electrification is rotating with l units of angular momentum. For a nucleus the size of uranium we find, upon minimizing the sum of deformation energy (see Fig. 3) and rotational energy, that the

reduced quadrupole moment is [K. Way, Phys. Rev. **55**, 964 (1939)]

$$Q/eR^2 = 6\alpha Z/5 = -P \times 2.8ZA^{-7/3}/(1-x).$$

As nuclear spins seldom exceed 4, the size of this moment is sharply at variance with the moments of 1 to 10 units commonly observed. Moreover, no mechanism is apparent by which the liquid drop could assume the prolate form required to produce a positive quadrupole moment.

More instructive is the inability of the independent particle model to predict moments of the proper size. The shaded ring-shaped region is the region of large probability amplitude for the wave function of a single proton in excess of a closed-shell (spherically symmetric) configuration. The quadrupole moment due to it in typical cases is 5 to 15 times too small to agree with observation. From the wave function $\Psi_{ln}(\mathbf{r})$ of a particle in a spherical well, the quadrupole moment may be computed on the assumption that the charge density controlled by the nucleon in question is proportional to $|\Psi_{ln}(\mathbf{r})|^2$. Taking the total charge so described to be one electronic unit, we discover that, even for very large angular momenta, and for any value of the total quantum number n, the largest value of the reduced quadrupole moment attainable is 0.5, and that the values to be commonly expected are less than 0.2 in magnitude. Thus, even the assumption that the effects of four or five nucleons could be simply additive does not allow us to account for observed moments.

However, Rainwater (reference 12) pointed out that the pressure of the nucleon against the surface works against surface tension to produce a sizeable deformation. The resulting bulk displacement of charge gives rise to a quadrupole moment an order of magnitude greater than that directly due to the extra particle. Thus the study of quadrupole moments provided the first convincing proof of the importance of the interaction of nucleons with the wall, a central point in the collective model of the nucleus.

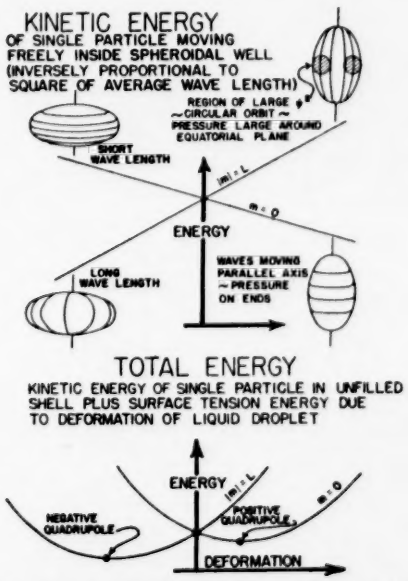
KINETIC ENERGY
OF SINGLE PARTICLE MOVING FREELY INSIDE SPHEROIDAL WELL (INVERSELY PROPORTIONAL TO SQUARE OF AVERAGE WAVE LENGTH)
REGION OF LARGE ψ²
~CIRCULAR ORBIT~ PRESSURE LARGE AROUND EQUATORIAL PLANE
SHORT WAVE LENGTH
|m| = L
m = 0
ENERGY
LONG WAVE LENGTH
WAVES MOVING PARALLEL AXIS ~PRESSURE ON ENDS
TOTAL ENERGY
KINETIC ENERGY OF SINGLE PARTICLE IN UNFILLED SHELL PLUS SURFACE TENSION ENERGY DUE TO DEFORMATION OF LIQUID DROPLET
ENERGY
|m| = L
m = 0
NEGATIVE QUADRUPOLE
POSITIVE QUADRUPOLE
DEFORMATION

FIG. 6. More detailed picture how a single extra nucleon causes a deformation.

The upper diagram shows the energy of the particle itself as a function of the static deformation. When the angular momentum is parallel to the axis, the waves run around azimuthally, and the wavelength is increased by an oblate, pancake-like deformation. The lower diagram shows the sum of energy of the extra particle, plus the energy of the residual closed shell nucleus, this latter parabola being calculated from the simple surface tension idealization, energy = (2/5)(radius)^2(surface tension)(deformation, α)^2. The sign of the resultant quadrupole moment differs according as the projection of the angular momentum along the symmetry axis is small or nearly equal to the total angular momentum.

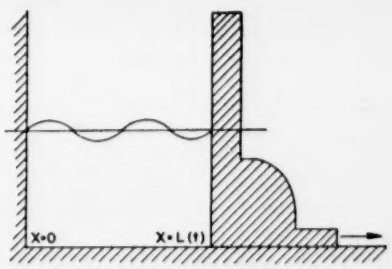

FIG. 7. Effect of wall motion on state of particle in simple one-dimensional case.

For the case of a stationary wall, the wave function $(2/L)^{\frac{1}{2}} \times \sin(n\pi x/L) \exp(-i\int^t E dt/\hbar)$, where $E = n^2\pi^2\hbar^2/2ML^2$ = a constant. For the case of a slowly moving wall, an approximate wave function $\psi(x, t)$ is obtained by inserting in this expression the assumedly known functional dependence of L on t, and multiplying the resulting preliminary wave function by $\exp(-iM\phi(x, t)/\hbar)$. Here $\phi(x, t)$ is the classical velocity potential; its derivative, $v(x, t) = -\partial\phi/\partial x$, gives the velocity with which a classical gas of infinite sound velocity would respond to the motion of the wall. The term in the velocity potential ensures that the wave function satisfies the equation of continuity,

$$\frac{\partial}{\partial x}\left\{\frac{\hbar}{2Mi}\left(\psi^*\frac{\partial\psi}{\partial x} - \psi\frac{\partial\psi^*}{\partial x}\right)\right\} + \frac{\partial}{\partial t}(\psi^*\psi) = 0.$$

It describes a motion of matter to the right as the restraining wall goes in that direction. The resulting wave function *satisfies exactly the* potential-free *wave equation* between the walls when the distance L increases linearly with time. For a more general dependence of L upon time the wave function satisfies the equation,

$$i\hbar\partial\psi/\partial t = -(\hbar^2/2M)(\partial^2\psi/\partial x^2) - (Mx^2\ddot{L}/2L)\psi.$$

Here the extra term on the right will be negligible for the case of a slowly *accelerating* wall. In this approximation the effect of the wall motion on the state of the particle is adequately described by the factor in the classical velocity potential.

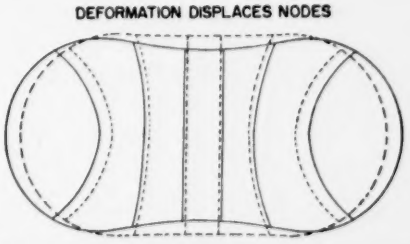

FIG. 8. Effect of wall motion on particle state—three-dimensional.

We shall derive here the result that the expectation value of the energy of a set of identical particles held within a slowly changing boundary of constant volume content is given at any instant approximately by the energy the particles would have were the wall stationary, augmented by a term which represents the classically calculated kinetic energy of an incompressible fluid of the same mass, M, urged into irrotational motion by the same walls. Let the symbol x typify the three space coordinates of one particle, the symbol α specify the configuration of the wall, $f(x, \alpha)$ and $E(\alpha)$ stand for wave function and energy for the case of the static wall, and $\phi(x, \alpha, \dot{\alpha})$ represent the velocity potential of the classical fluid motion: $\partial\phi/\partial t - \frac{1}{2}(\nabla\phi)^2 - p/\rho = 0$; $\nabla^2\phi = 0$; $-\partial\phi/\partial n$ = normal velocity of wall. We represent the wave function of the particle in the approximate form

$$\psi(x, t) = f(x, \alpha(t)) \exp\left[-i\int^t E(\alpha(t))dt/\hbar - iM\phi/\hbar\right].$$

To test this function in the Schrödinger equation, we calculate

$$i\hbar\partial\psi/\partial t = \exp[\quad][i\hbar\dot{\alpha}\partial/\partial\alpha + E + M\partial\phi/\partial t]f.$$

We now argue that in first approximation the nodes and values of f are carried along with the classical fluid velocity, so that

$$\dot{\alpha}\partial f/\partial\alpha \doteq (-1)^2(\nabla\phi)\cdot(\nabla f).$$

Thus

$$i\hbar\partial\psi/\partial t \doteq \exp[\quad][i\hbar(\nabla\phi)\cdot(\nabla f)-(\hbar^2/2M)\nabla^2 f+(Mf/2)(\nabla\phi)^2 +(Mp/\rho)f]=-(\hbar^2/2M)\nabla^2\psi+(Mp/\rho)\psi.$$

We conclude that the wave function in question satisfies approximately Schrödinger's equation, through velocity dependent terms, and neglects essentially only the accelerative terms of the form (pressure/density). For the kinetic energy of the state we now find

$$(\hbar^2/2M)\int(\nabla\psi^*)(\nabla\psi)d(\text{vol})=(\hbar^2/2M)\int(\nabla f^*)(\nabla f)d(\text{vol})$$
$$+(i\hbar/2)\int(f^*\nabla f-f\nabla f^*)\nabla\phi d(\text{vol})+(M/2)\int(\nabla\phi)^2 f^* f d(\text{vol}),$$

a result in which the last term—summed over the occupied states—goes over into the kinetic energy of the classical fluid in the limit of large quantum numbers, as was to be shown. The first term gives energy of the particles in a static potential. The second is important for the interaction between unpaired particles and wall rotation.

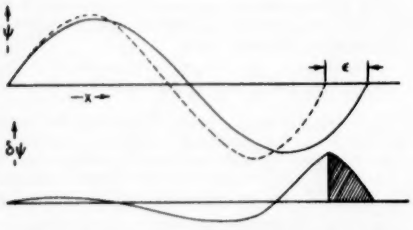

FIG. 9. Approximate orthogonality of the nucleonic wave functions of Eq. (3) for two slightly different values of the deformation parameter, α.

The general principles involved here are illustrated by the example of a one-dimensional potential well, extending from $x=0$ to $x=a=R_0(1+\alpha)$ or to $x=b=R_0(1+\alpha)(1+\epsilon)$, according as we deal with the one or the other value of α. The determinantal wave functions, Φ, of the N particle system are constructed out of individual particle wave functions of the form $u(n,x)=(2/a)^{\frac{1}{2}}\times\sin(n\pi x/a)$. The desired matrix element between the wave functions for the same nucleonic state but slightly different values of α is

$$\sum_{\substack{\text{permutations}\\ 1\,2\cdots N\\ \alpha\,\beta\cdots\nu}}(-1)^P\int u(n_1,x,a)u(n_\alpha,x,b)dx\cdots \times\int u(n_N,x,a)u(n_\nu,x,b)dx,$$

where the sum goes over all permutations, P, of the labels, $n_1,\cdots,n_N$, of the occupied states. When the state labels are the same in one of the individual integrals, the integral has the approximate value

$$1-\epsilon^2[(1/8)+(n^2\pi^2/6)],$$

and, when the labels are different, the approximate value

$$\epsilon(-1)^{n+m}2mn/(m^2-n^2).$$

Combining factors of the form $(1-\epsilon_1)(1-\epsilon_2)\cdots(1-\epsilon_N)$ into exponentials of the type $\exp(-\epsilon_1-\epsilon_2\cdots-\epsilon_N)$, we have for the value of the scalar product $\int\cdots\int\Psi_a\Psi_b\,d(\text{volume})$ the approximate formula

$$\exp[-\epsilon^2\{(N/4)+(41/288)+(12)^{-1}(6N^2+6N+1)\ln 3.562N\}]$$

from which there follows the result quoted in the text. Thus wave functions of the one-dimensional system are nearly orthogonal for a fractional extension $\epsilon\sim N^{-1}(\ln 3.562N)^{-\frac{1}{2}}$ or for a volume change equal to a fraction $(\ln 3.562N)^{-\frac{1}{2}}$ of the cell occupied by the typical particle. Generalizing to three dimensions, we conjecture that the nucleonic system wave functions are practically orthogonal as soon as the volume not common to the two configurations exceeds some small fraction of one cell.

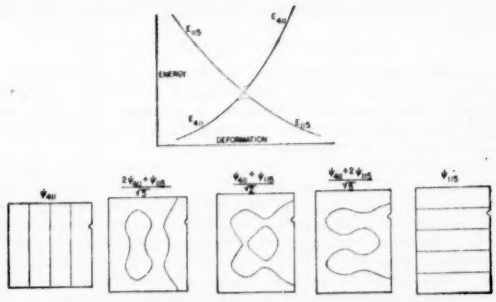

FIG. 10. Effect of a small asymmetry in mixing two otherwise orthogonal states.

We examine here the mixing of two states of a particle in a rectangular box, possessing a small irregularity, as two of the box dimensions are altered in a volume-preserving deformation. Shown are the nodes of the total wave function at successive stages of the deformation. In the absence of the irregularity in the surface, the two levels cross without interaction as the deformation proceeds. The irregularity mixes the two wave functions in comparable proportions only near the point of crossover. The nodes were found by solving the equation $R\sin 4x\sin z+\sin x\sin 5z=0$, where x and z represent the distances from the lower left hand corners of the rectangles expressed in such units that $x=\pi$, $z=\pi$ at the diagonally opposite corners.

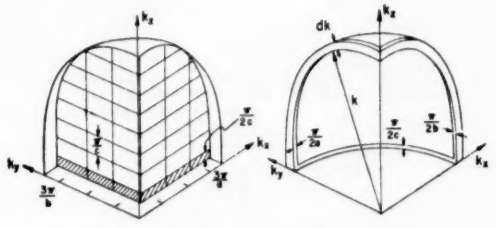

FIG. 11. Asymptotic frequency of proper values.

We shall "derive" here the asymptotic formula for the number of solutions of the equations $\nabla^2\psi+k^2\psi=0$, $\psi_{\text{surface}}=0$, with wave numbers in the interval k to $k+dk$:

$$dN=Vk^2dk/2\pi^2-Skdk/8\pi+\left[\int\kappa dS\right]dk/8\pi^2.$$

Here V is the volume of the region under consideration, S its surface, and κ the local total curvature of the surface. The case actually considered is that of a rectangular parallelepiped, of dimensions a, b, c. Each proper solution, $\sin k_x x\sin k_y y\sin k_z z$, corresponds to a lattice point in k space, $k_x=l\pi/a$, $k_y=m\pi/b$, $k_z=n\pi/c$, with which is associated a characteristic "box" of volume $(\pi/a)(\pi/b)(\pi/c)$. When the states are filled out to a given wave number $k_{\max}$, the boxes occupy an octant of a sphere (left-hand diagram) except for slab-like regions near the coordinate planes. The region thus to be excluded from the volume count is shown in more detail in the right-hand diagram, for the case when the number of states between k and $k+dk$ is desired: relevant volume = shell − correction for ring like strips + recorrection for corners subtracted twice in counting volume of rings

$$=(4\pi/8)k^2dk-(\pi/2)(kdk)[(\pi/2a)+(\pi/2b)+(\pi/2c)] +dk[(\pi/2a)(\pi/2b)+\text{two similar terms}].$$

Division by the volume of one box gives for the number of states:

$$dN\doteq abck^2dk/2\pi^2-(2ab+2bc+2ca)kdk/8\pi+(4a+4b+4c)dk/16\pi.$$

Generalization of this expression to an enclosure whose shape is not too irregular gives the cited formula. Then the number of states with wave number less than k is

$$N\doteq Vk^3/6\pi^2-Sk^2/16\pi+Lk/8\pi^2,$$

and their totalized kinetic energy, E, is given by

$$2ME/\hbar^2 = V k^5/10\pi^2 - Sk^4/32\pi + Lk^3/24\pi^2 = (V/10\pi^2)(6\pi^2 N/V)^{5/3} + (S/32\pi)(6\pi^2 N/V)^{4/3} + (6\pi^2 N/V)(S^2/128V - L/12\pi^2).$$

The proportionality of a part of this energy with the surface implies the existence of a contribution to the surface tension of kinetic origin [C. F. Weiszäcker, *Die Atomkerne* (Akademische Verlagsgesellschaft, Leipzig, 1937); E. Feenberg, Revs. Modern Phys. **19**, 239 (1947)]. For nuclei with approximately equal numbers of neutrons and protons, and a volume per particle of $4\pi r_0^3/3$ the appropriate term in the surface tension is

$$O_{\text{kin}} = 4(\hbar^2/64\pi M)(9\pi/8r_0^3)^{4/3},$$

with

$$4\pi r_0^2 O_{\text{kin}} = 28 \text{ Mev}.$$

This calculated value is twice as great as the empirical figure, 14 Mev, for the *sum* of kinetic and potential surface tension coefficients. However, the calculated value is reduced to a more nearly reasonable magnitude when the height of the potential wall is diminished from infinity to a finite value, according to a kind private communication of Professor Feenberg.

After having completed this manuscript we were kindly shown by Professor Eugene Feenberg the June, 1951 Washington University thesis of K. C. Hammack, "Topics in Nuclear Structure," which discusses the asymptotic density of independent particle levels for potential wells both of infinite and of finite depth, and proposes also the three-term asymptotic formula which appears in this caption.

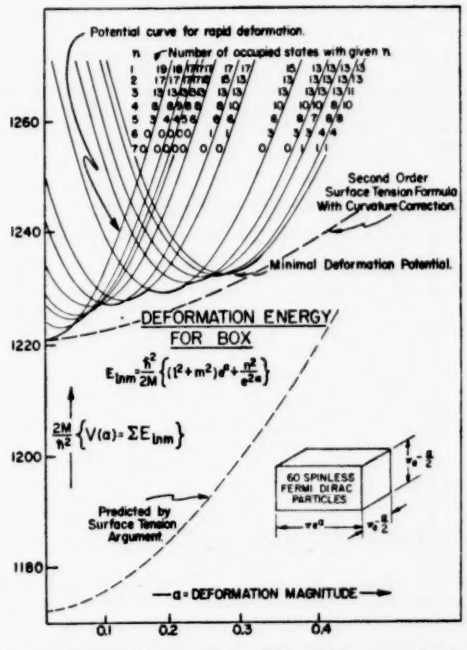

FIG. 12. Potential curves for a deformable rectangular box.

The energy of deformation depends upon the nucleonic state of the system as well as upon the magnitude of the deformation itself. Each potential curve in the diagram is obtained by considering the 60 particles in question to be placed in 60 specified distinct individual particle states, and summing their energies. For the energy of the system to keep to a minimum value, it is necessary that the distribution of particles among states should change during the course of the deformation. The scalloped curve therefore gives a qualitative representation of the type of potential energy curve to be expected for actual nuclei. If the deformation changes so fast that switches from one potential curve to another do not have time to occur with appreciable probability, or if such switches are altogether forbidden because of the high symmetry of the system—as in the case of a box with smooth rectangular walls—then the distribution of particles among states will not change during the course of the deformation. Then the energy required to produce the distortion will be much greater than one would estimate from the notion of surface tension. The dashed curve is predicted by applying the statistical arguments and formula of Fig. 11 to the present idealized problem, putting $N=60$, volume $=\pi^3$, surface $=2\pi^2 e^{-\alpha}+4\pi^2 e^{\alpha/2}$, integrated curvature $=2\pi^2 e^{\alpha}+4\pi^2 e^{-\alpha/2}$,

$$\Sigma 2ME/\hbar^2 = (\pi/10)(360/\pi)^{5/3} + (\pi/16)(360/\pi)^{4/3}(e^{-\alpha}+2e^{\alpha/2}) + (45/4)e^{-2\alpha} + (45-120/\pi)e^{-\alpha/2} + (45-60/\pi)e^{\alpha}.$$

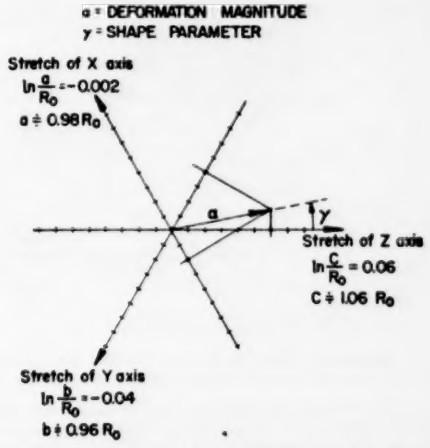

FIG. 13. Coordinates (α, γ) for volume-preserving ellipsoidal deformations.

Volume-preserving ellipsoidal deformations may be described by two polar coordintes in a plane: α=deformation magnitude, γ=shape parameter. These coordinates are defined in terms of the semi-major axes of the ellipsoid,

$$\frac{x^2}{a^2}+\frac{y^2}{b^2}+\frac{z^2}{c^2}=1,$$

by the equations

$$a = R_0 \exp[\alpha \cos(\gamma - 2\pi/3)],$$
$$b = R_0 \exp[\alpha \cos(\gamma + 2\pi/3)],$$
$$c = R_0 \exp[\alpha \cos\gamma],$$

which are required to satisfy the condition of volume constancy,

$$abc = R_0^3.$$

For example, a deformation in which the changes of length of the x, y, and z axes are -1 percent, -2 percent, and $+3$ percent, or any small positive common multiple of these fractions, is described by one or another positive value of the positive "deformation magnitude" α and a value of the "shape parameter," γ, equal to 10.895°.

As another example, let α be given a positive value, say 0.02, and let γ be increased, starting with $\gamma=0$. Then the ellipsoid takes on the following shapes:

γ	a/R_0	b/R_0	c/R_0	Shape	Symmetry axis
0°	0.990	0.990	1.020	prolate spheroid	z
30°	1.000	0.983	1.017	ellipsoid	none
60°	1.010	0.980	1.010	oblate spheroid	y
90°	1.017	0.983	1.000	ellipsoid	none
120°	1.020	0.990	0.990	prolate spheroid	x

With further increase of γ the cycle repeats, except for cyclic interchange of the labels x, y, z; a, b, c.

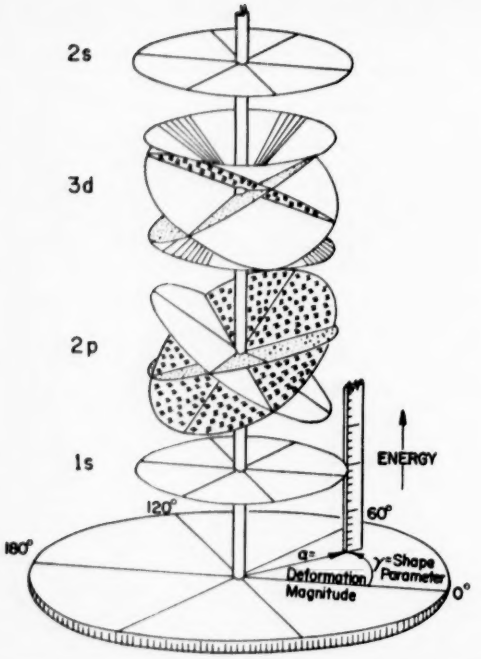

FIG. 14. Qualitative effect of small ellipsoidal deviations from sphericity upon the first few energy levels of a single nucleon.

Spin-orbit coupling is neglected. Consequently this diagram and those in following few figures are to be considered as primarily illustratory. The deformation of the ellipsoid is expressed in terms of the polar variables, α and γ, as indicated in Fig. 13. The simplest case to consider is distortion into a prolate spheroid, rotation-symmetric about the z axis ($\gamma=0$). Then the quantum number m is well defined. The level of orbital angular momentum $l\hbar$ breaks up into components, of which the one with quantum number m is raised by an amount

$$\delta E=2\alpha E\frac{3m^2-l(l+1)}{(2l-1)(2l+3)}$$

with respect to the original energy, E. Levels with $m=+|m|$ and $m=-|m|$ coincide. Points not shown in this diagram: (1) Effect on the energy surfaces of displacements so large that δE is no longer proportional to α. Then terms of order higher than the first have also to be taken into account. The resulting curvature of the energy surfaces is most easily visualized by saying that energy surfaces repel each other except in the neighborhood of exceptional points. At such a point the two surfaces ordinarily meet in a double funnel, as shown in Fig. 35. Many such funnels would be seen in a more extended version of the present diagram. (2) Dependence of energy upon surface deformations of order higher than the second is not shown here, for want of dimensions. In treating the asymmetry of nuclear fission it is important to consider deformations of order $n=3$ as well as the ellipsoidal distortions ($n=2$) envisaged here.

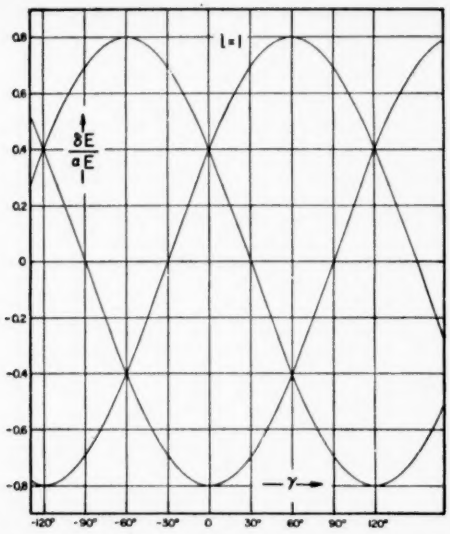

FIG. 15. Splitting of levels of a p particle (orbital angular momentum $l=1$) in a potential well of constant depth, the boundaries of which have received a slight volume-preserving ellipsoidal deformation away from the spherical form.

In the diagram E represents the kinetic energy of the nucleon in the original spherical well, and δE the displacement of the level for a small distortion of magnitude α. This quantity, and the shape parameter γ which is plotted horizontally, are as defined in Fig. 13. Note that a p particle will have the lowest possible energy when it goes into a nucleus shaped like a prolate spheroid.

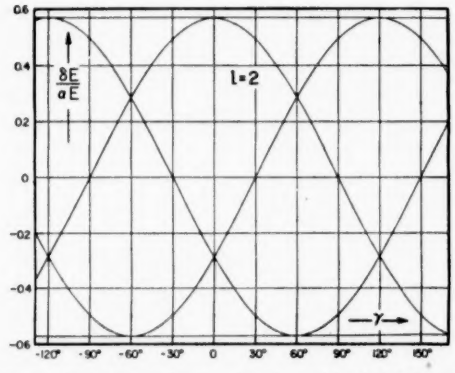

FIG. 16. Splitting of levels of a d particle (orbital angular momentum $l=2$), shown as a function of the shape parameter γ of the ellipsoidal deformation.

The five levels group as three for an axially symmetric deformation ($\gamma=0°$, $\pm60°$, $\pm120°$, etc). The energy of a single d nucleon

which goes into the lowest accessible level in first approximation is independent of the shape parameter γ. The present case, $l=2$, is the neutral point. For $l=1$ a prolate deformation gives the greatest energy lowering, and for $l=3$ or more a prolate deformation is energetically preferred in the case of a single nucleon.

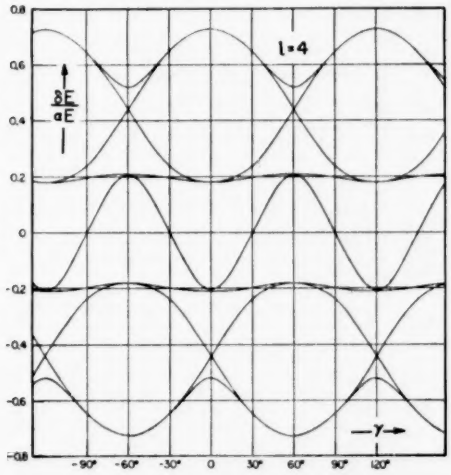

FIG. 17. Removal of the ninefold degeneracy of a g nucleon ($l=4$) by small ellipsoidal deformation.

A single g particle achieves the lowest possible energy when it goes into an oblate ellipsoid ($\gamma=\pm 60°$; 180°). The calculation of first-order energy displacement is made as follows: Let u_1 be the wave function which vanishes at the surface of the sphere and which satisfies $\nabla^2 u_1+k_1^2 u_1=0$ inside; let the very slightly different function u_2 vanish on the surface of the ellipsoid and satisfy $\nabla^2 u_2+k_2^2 u_2=0$ within *that* surface. Then, by Green's method,

$$k_2^2-k_1^2=\int(u_2^*\partial u_1/\partial n-u_1\partial u_2^*/\partial n)dS\Big/\int u_1 u_2^* d(\text{vol}),$$

where the integral in the denominator is taken over the volume common to the two solids, and the integral in the numerator over the surface which encloses that common volume. Let S_1 be innermost at a certain point of S. Then on S_1, $u_1=0$ and in terms of the normal displacement, δn, of S_2 with respect to S_1,

$$u_2\doteq-(\delta n)(\partial u_2/\partial n)\doteq-(\delta n)(\partial u_1/\partial n).$$

A similar result is found when S_1 lies outermost. Consistent with the neglect of terms of order higher than the first, we thus have

$$\delta(k^2)=-\int|\partial u_1/\partial n|^2\delta n dS\Big/\int|u_1|^2 d(\text{vol}),$$

provided that the difference between u_2 and u_1 is indeed small; i.e., provided that we have chosen, or will choose for u_1—as below—the proper linear combination of the wave functions of the originally degenerate levels. Let the corresponding proper linear combination of spherical harmonics be denoted by

$$Y(\theta,\varphi)=\Sigma c_m Y_L^{(m)}.$$

Also let $F_l(\rho)$ denote the regular solution of the radial equation

$$d^2F_l/d\rho^2+[1-l(l+1)/\rho^2]F_l=0,$$

so that

$$\int_0^\rho F_l^2 d\rho=\tfrac{1}{2}\rho[(F_l)^2+(F_l')^2]-\tfrac{1}{2}F_lF_l'-l(l+1)(F_l)^2/2\rho$$
$$=\tfrac{1}{2}\rho(F_l')^2 \text{ when } \rho \text{ is a node.}$$

Then the unperturbed wave function is

$$u_1=r^{-1}F_l(kr)Y(\theta,\varphi),$$

and the first-order perturbation in energy is given by

$$\frac{\delta E}{\alpha E}=\frac{\delta(k^2)}{\alpha k^2}=-\frac{2}{\alpha R_0}\int Y^*(\delta R)Y d\Omega\Big/\int Y^* Y d\Omega.$$

Let I be that indempotent operator which, when applied to any general surface harmonic,

$$U=\sum_{l,m} b_{l,m}Y_{l,m}(\theta,\varphi),$$

annuls all terms except those which belong to the value of l of present interest to us, and leaves these terms unaltered. Then

$$\int Y^*\Lambda Y d\Omega=\int Y^* I\Lambda Y d\Omega,$$

where Λ is an abbreviation for the perturbation

$$\Lambda=-2\delta R(\theta,\varphi)/\alpha R_0.$$

A proper linear combination Y will satisfy the eigenvalue equation

$$I\Lambda(\theta,\varphi)Y(\theta,\varphi)=\lambda Y(\theta,\varphi),$$

where λ is a numerical constant. This is a secular equation for the determination of the coefficients c_m and the energy shift,

$$\delta E=\lambda\alpha E.$$

In the standard equation for the ellipsoid (caption of Fig. 13), we write

$$x=(R_0+\delta R)\sin\theta\cos\varphi,$$
$$y=(R_0+\delta R)\sin\theta\sin\varphi,$$
$$z=(R_0+\delta R)\cos\theta,$$

and insert the expressions for the semi-major axes, a, b, c, in terms of R_0 and the deformation parameters α and γ. To terms of the first order it is found that the alteration, δR, in the length of the radius vector from the origin to the surface is given by the equation

$$\Lambda(\theta,\varphi)=-2\delta R(\theta,\varphi)/\alpha R_0=3^{\frac{1}{2}}\sin^2\theta\cos 2\varphi\sin\gamma-2P_2(\cos\theta)\cos\gamma.$$

Of this quantity the matrix element vanishes between spherical harmonics $Y^{(m)}$ of the same l value (the one of interest) but of different m values, except in the following cases:

(1) Same m values (diagonal elements of matrix).

$$\Lambda_{mm}=\frac{2\cos\gamma[3m^2-l(l+1)]}{(2l-1)(2l+3)}.$$

(2) Values of m which differ by two units:

$$\Lambda_{m\pm1,\,m\mp1}=\frac{+3^{\frac{1}{2}}\sin\gamma[l^2-m^2]^{\frac{1}{2}}[(l+1)^2-m^2]^{\frac{1}{2}}}{(2l-1)(2l+3)}.$$

The solution of the secular equation,

$$\text{determinant}\,|\Lambda_{jk}-\lambda|=0,$$

gave the values for the energy shifts of the present and preceding figures.

The effects of deformations upon energy levels, as calculated here for the case of an infinite well, will be decreased in the case of a finite well by a factor analyzed by Feenberg and Hammack (reference 9).

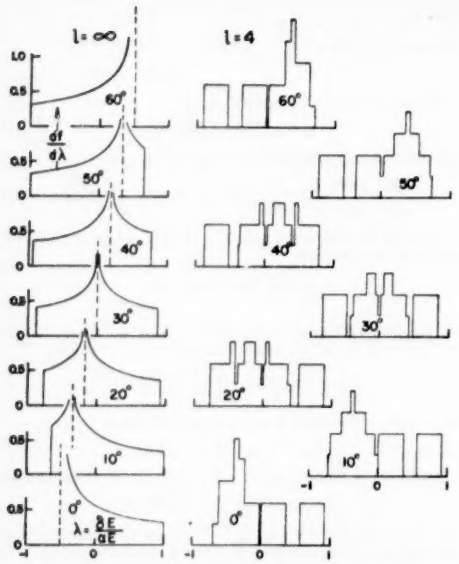

FIG. 18. Splitting of levels for case of small ellipsoidal deformations but very large orbital angular momentum.

The secular equation (preceding figure) has in this case so many roots that it is appropriate to describe their distribution statistically. Plotted horizontally is the value of the root of the secular equation, $\lambda = \delta E/\alpha E$. Plotted vertically is the fraction of the number of such roots, per unit range of λ:

$$\int (df/d\lambda)d\lambda = 1.$$

Whatever be the value of the "shape parameter," γ, the distribution function has a singularity at one value of λ, the dimensionless measure of level shift. In other words, there are many levels for which λ lies in the neighborhood of this singular value, $\lambda_{sing} = \cos(\gamma - 2\pi/3)$ (when γ lies between 0° and 60°). The extremal values of the level shift in the present limit of large l are $\lambda_{min} = \cos(\gamma + 2\pi/3)$; $\lambda_{max} = \cos\gamma$. Plotted at the right for comparison is the distribution of levels found from the secular determinant for the case $l = 4$, except that each level has been spread out to give an approach to a continuous distribution. There is a qualitative but of course not a quantitative correspondence between the cases $l = 4$ and $l = \infty$. As the predictions of quantum mechanics approach those of classical mechanics in the limit of large quantum numbers, the method of calculation was to write

$\lambda = \delta E/\alpha E =$ (average of the perturbation, $\Lambda(\theta, \phi)$
$= -2\delta R(\theta, \phi)/\alpha R_0$, over the unperturbed classical motion).

In the unperturbed classical motion the particle moves in a plane which passes through the center of the sphere. The motion is a series of straight line segments, with abrupt changes of direction each time the particle hits the surface. In all orbits except a set of measure zero, the angular period of the motion will be incommensurable with 2π, and the particle will come arbitrarily close in the course of time to every point on a certain great circle. Let the normal to this great circle have the polar angles θ^* and ϕ^*. Then the average of Λ over this great circle gives

$$\Lambda_{Av} = \lambda = \cos\gamma P_2(\cos\theta^*) + 2^{-1}3^{\frac{1}{2}} \sin\gamma \sin^2\theta^* \cos 2\phi^*.$$

To ask that this quantity should lie in an interval λ to $\lambda + d\lambda$ is to pick out upon the surface of the sphere a band of points, any one of which specifies the direction of the axis of angular momentum of an acceptable orbit. The solid angle, $d\Omega$, subtended by this band tells the fraction of eigenvalues which lie between λ and $\lambda + d\lambda$:

$$\frac{df}{d\lambda} = \frac{1}{4\pi}\frac{d\Omega}{d\lambda} = \pi^{-1}3^{-\frac{1}{4}} (\sin\gamma)^{-\frac{1}{2}} (\cos\gamma - \lambda)^{-\frac{1}{2}} K(\kappa),$$

where K is the complete elliptic integral and

$$\kappa = \left\{ \frac{(\lambda - \cos 120° + \gamma) \sin 120° + \gamma}{(\cos\gamma - \lambda) \sin\gamma} \right\}^{\frac{1}{2}},$$

this expression applying when γ lies between 0° and 60° and when in addition λ lies between λ_{min} and λ_{sing}. When λ lies between λ_{sing} and λ_{max}, the corresponding formula is

$$\pi^{-1}3^{-\frac{1}{4}} (\lambda - \cos 120 + \gamma)^{-\frac{1}{2}} (\sin 120 + \gamma)^{-\frac{1}{2}} K(\kappa^{-1}).$$

These formulas were used in the plotting of the distribution curves $df/d\lambda$.

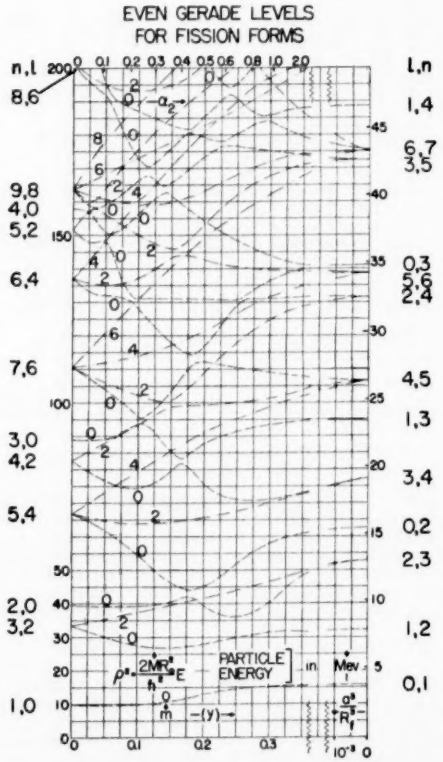

FIG. 19. Effect of deformation leading to fission upon single-particle energy levels of even-gerade symmetry.

The Frankel-Metropolis sequence of forms (Fig. 2) is considered for definiteness. Plotted vertically are the values of the dimensionless measure of energy, $\rho^2 = 2MR_0^2E/\hbar^2$, where R_0 is the radius of the original sphere. The magnitude of the deformation is measured by the parameter $\alpha_2 = (7/3)y = (7/3)(1-x)$, where x and y have the meanings described in Fig. 2. This definition of α_2 agrees with the definitions in Fig. 1 and in Fig. 13 to the first order for small distortions, but all three definitions differ for large disturbances. The right-hand edge of the diagram gives the energy levels when the boundary is deformed into two spheres of half the original volume, connected with each other by a small orifice. Whatever the magnitude of the single deformation parameter here considered, the boundary is invariant with respect to inversion ($x, y, z \to -x, -y, -z$) and with respect to reflection at a plane through the origin normal to the axis, z, of rotational symmetry ($x, y, z \to x, y, -z$). Consequently, the levels fall into four classes:

		Ratio of values of wave function at two points which differ by a reflection $= (-1)^{l+m}$			
		+(gerade)		−(ungerade)	
Ratio of values of wave function at two points which differ by an inversion $= (-1)^l$	+ (even)	l even m even	Fig. 19	l even m odd	Fig. 20
	− (odd)	l odd m odd	Fig. 22	l odd m even	Fig. 21

Among these only even-gerade levels are shown in the present diagram. Of the levels which are plotted in this and the following three figures, only those are shown in full detail which have a quantum number of angular momentum about the symmetry axis equal to $m=0$ or $m=3$. The full line curves in these four figures were calculated in detail as described in the caption of Fig. 21; the dotted curves are only schematic and have *no quantitative basis* other than the initial and final ordinates and slopes, and the use of inflection points here and there to permit level jumps as needed to preserve the proper relation between the number n of nodal surfaces in the initial and final wave functions.

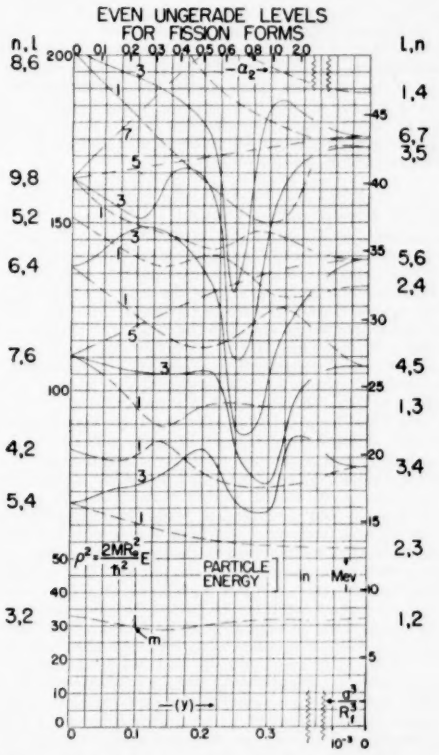

FIG. 20. Energy levels of even-ungerade symmetry inside a boundary of Frankel-Metropolis form.

The energy level diagram is consistent with the usual well known correlation principle: two levels are then and only then incapable of crossing—granted arbitrary deformation magnitude—when they belong at the same time to the same one of the four symmetry classes (here the even-ungerade class) and to the same value of m. This principle applies only so long as the system has axial symmetry. If instead the boundary were an ellipsoid with three unequal axes, then m would not be a good quantum number and *none* of the levels would cross which belong to a particular one of the four symmetry classes. For configurations near the original sphere, the energy levels $E=(\hbar^2/2MR_0^2)\rho^2$ are obtained from the perturbation formula (Fig. 17),

$$\rho^2=\rho_{nl}^2\left[1+2\alpha_2\frac{3m^2-l(l+1)}{(2l-1)(2l+3)}\right].$$

Here the quantity ρ_{nl} is the $(n-l)$th root of the regular solution $F(\rho)$ of the differential equation,

$$d^2F/d\rho^2+[1-l(l+1)/\rho^2]F=0,$$

for the radial part of the wave function,

$$\psi(r,\theta,\phi)=r^{-1}F(kr)P_l^{(m)}(\cos\theta)\exp(im\phi).$$

All values of ρ_n^2 less than 200 [*Tables of Spherical Bessel Functions, Vol. I* (Columbia University Press, New York, New York, 1947)] follow:

l \ $n-l$	1	2	3	4
0	9.870	39.479	88.827	157.914
1	20.191	59.679	118.899	197.858
2	33.218	82.719	151.854	
3	48.831	108.516	187.635	
4	66.955	137.005		
5	87.531	168.130		
6	110.519	201.850		
7	135.886			
8	163.605			
9	193.649			

The number n represents—in the case of spherical and nearly spherical configurations—the total number of nodal surfaces in the wave function, counted as follows: m in the ϕ direction, $l-m$ in the θ coordinate, $n-l$ in the radial direction (counting the boundary itself as a nodal surface). As the magnitude of the deformation is increased, l ceases to be a good quantum number and even the total number, n, of nodal surfaces ceases to remain constant as such surfaces migrate to the outer boundary or coalesce inside. The only firm ordering principle is the requirement that levels of the same m do not cross.

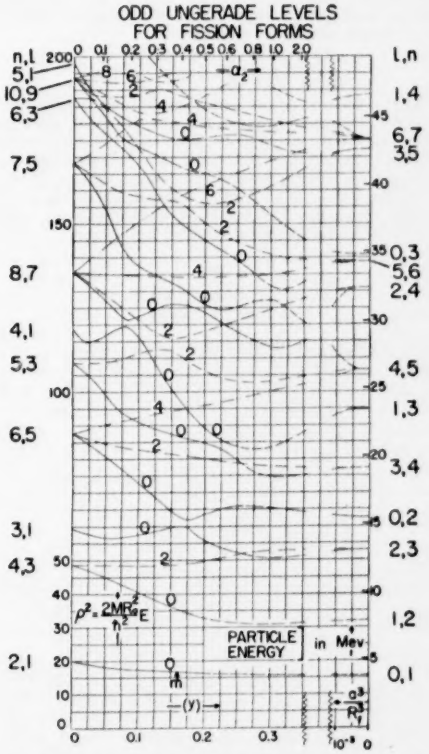

FIG. 21. Odd-ungerade levels in the Frankel-Metropolis sequence of forms.

Only the levels with $m=0$ are here shown in full detail. The wave functions are taken to satisfy the equation $\nabla^2\psi+k^2\psi=0$ in the interior, and on the surface $\psi=0$ (infinite potential wall). W. Elsasser [J. phys. et radium **5**, 625 (1934)] and H. Margenau [Phys. Rev. **46**, 613 (1934)] have in this approximation obtained the level spacings for nucleons in spherical nuclei. This neglect of penetration of the wave function into the region of negative kinetic energy outside the boundary (finite potential wall) can be considered to be compensated approximately by appropriate small readjustment of the dimensions of the figure: normal displacement by the distance $\hbar/[2M(W-E)]^{\frac{1}{2}}$, where W is the height of the potential wall and E is the kinetic energy of the state in question. In detailed calculations (smooth curves) the wave function for odd-gerade levels with angular momentum m about the symmetry axis were written as the product of the factor $\exp(im\phi)$ by

the sum

$$\Sigma C_l j_l(\rho r/R_0) P_l^{(m)}(\cos\theta),$$

where R_0 is the original radius of the sphere and $\rho^2 = 2MR_0^2E/\hbar^2$ is the dimensionless measure of energy plotted in the figure. The sum goes over even values of l for the case of a level of even parity, and over odd l for odd parity. This function automatically satisfies the differential equation. Vanishing of the solution over the boundary, $r/R_0 = f(\cos\theta)$, as specified in Fig. 2, gives a continuous infinity of conditions on the infinitely many coefficients C_l. The approximation was made to use only five terms in the sum, and to require the vanishing of the sum only at the five points on the surface for which $\mu = \cos\theta = \mu_s$, with $\mu_s = 0.19, 0.38, 0.57, 0.76, 0.95$ for ungerade levels, and $\mu_s = 0.105, 0.315, 0.525, 0.735, 0.945$ for gerade levels. The resulting five equations for the five unknown coefficients C_l possess a solution when and only when ρ is such as to annul the determinant,

$$|\, j_l(\rho f_s) P_l^{(m)}(\mu_s) \,|,$$

where $s = 1, 2, \cdots 5$ is the column index and $l = 0, 2, 4, 6, 8$ is the row index, for example, for the case of $m = 0$ and even parity, and for $m = 0$ and odd parity $l = 1, 3, 5, 7, 9$. The functions j and P were generated in an IBM–CPC electronic calculator—the associated Legendre functions [divided by $(1-\mu^2)^{m/2}$] from their terminating power series expressions, the spherical Bessel functions $j(x)$, which satisfy the equation

$$\frac{1}{x^2}\frac{d}{dx}\left(x^2\frac{dj}{dx}\right) + \left[1 - \frac{l(l+1)}{x^2}\right] j = 0,$$

from their standard power series expansions when the ratio $x/(l+\frac{1}{2})^{\frac{1}{2}}$ was less than 5, and for larger values of the argument from the well known expressions $j(x) = (\text{terminating polynomial in } 1/x)\sin x + (\text{terminating polynomial in } 1/x)\cos x$. The roots, ρ, of the determinant were found by a refined scheme of trial and error. We are indebted for help in these calculations to Stewart Schlesinger, Seymour Parter, Max Goldstein, and others in Group T-1 of the Los Alamos Scientific Laboratory.

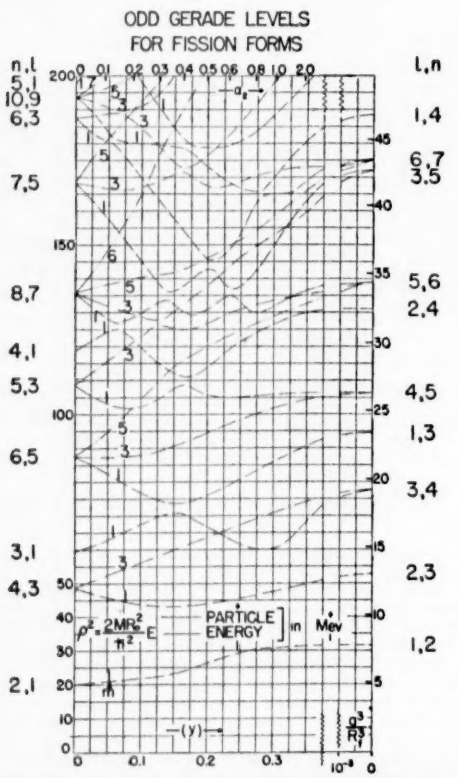

FIG. 22. Odd-gerade levels in the Frankel-Metropolis sequence of forms leading to fission.

Shown at the right in this and the three preceding figures are the levels for two spheres of radius $R_f = R_0/2^{\frac{1}{3}}$, connected by a circular orifice of radius, a, small compared with R_0. When $a = 0$, the levels are those of a sphere, and consequently the appropriate values of the dimensionless energy parameter ρ^2 are $2^{\frac{1}{3}}$ times those listed in the caption of Fig. 20. When the orifice is opened slightly, the wave functions in the two spheres join together, and two cases have to be recognized: gerade case—the wave functions in the two spheres join up so as to have no node at the point of join (mirror symmetry with respect to the plane of the orifice); ungerade case—node in the over-all wave function at the point of join (wave function antisymmetric with respect to mirroring in the orifice plane). A half-volume sphere contains up to a given energy (top of Fermi distribution) only approximately a half as many levels as the full volume sphere, so the doubling of number of states by reason of the two ways of joining at the window gives the right number of individual particle states for the system. The energies of the ungerade states are in first approximation independent of the size of the orifice opening (wave function vanishes at point of perturbation). On the other hand, the energies of the corresponding gerade states *fall* as the orifice is opened, the fractional magnitude of the drop being

$$(1/\rho^2)\delta(\rho^2) \doteq -(2/3\pi)(2l+1)(a^3/R_f^3)$$

for states with $m = 0$, and much smaller (higher power of a/R_0) for higher values of m. To derive this result, compare the gerade wave function ψ_0 for the case of completely closed orifice and ψ_1 for the case of small orifice opening. The two functions look alike except within distances of the order a from the center of the orifice.

There $\psi_0 = r^{-1}F_l(kr)P_l^{(m)}(\cos\theta)\exp(im\phi)$ (in the left-hand sphere; the mirror image of this in the right-hand sphere) behaves for positive m approximately as $\psi_0 = Qz\rho^m \exp(im\phi)$, where z is distance measured normally from the orifice towards the center of the left-hand sphere, ρ is the appropriate cylindrical polar coordinate, and the constant has the value $Q = -R_f^{-1-m}kF_l'(kR_f) \times (l+m)!/2^m m!(l-m)!$. In the case $m = 0$ our approximation for ψ_0 increases linearly with distance from the surface. We have to deal with the wave mechanical analog of a constant electric field. In electrical terms, opening the orifice now allows lines of force to leak out. Superposed on the linearly varying electric potential is another term—a local disturbance—which also satisfies Laplace's equation approximately: the bucklings of this term normal to the orifice and parallel to the plane of the orifice are opposite in sign and both very large compared to the net buckling, k_1^2. This net buckling we therefore neglect in considering the correction, $\delta\psi = \psi_1 - \psi_0$, in the wave function. Hence, we compute this difference by solving Laplace's equation subject to the boundary conditions: (1) $\delta\psi$ falls off relative to ψ_0 for large distances from the orifice; (2) $\partial(\delta\psi)/\partial z$ vanishes over portions of the surface (here treated as flat) not pierced by the orifice; (3) over the orifice the correction term has such a normal derivative as to make ψ_1 itself have zero derivative (condition of mirror symmetry): $\partial(\delta\psi)/\partial z = -Q\rho^m \exp(im\phi)$. General positive m is used in the last equation because nothing about the basic argument is peculiar to $m = 0$. The use of new coordinates, such that $z = auv$, $\rho = a[(1-u^2)(1+v^2)]^{\frac{1}{2}}$, translates Laplace's equation to a form with separable solutions of the type $P_n^{(m)}(u)f(v)\exp(im\phi)$. Here the function f is such as to be annulled by the operator

$$\frac{d}{dv}(1+v^2)\frac{d}{dv} + \frac{m^2}{1+v^2} - n(n+1).$$

The original wave function ψ_0, not too far from the median plane, is of exactly this form, with $n = m+1$, and with $f(v)$ a multiple of $P_{m+1}^{(m)}(iv)$:

$$\psi_0 = Qa^{m+1}u(1-u^2)^{m/2}v(1+v^2)^{m/2}\exp(im\phi).$$

In the corresponding product expression for $\delta\psi$, everything must be the same except the function $f_{m+1}^{(m)}(v)$, which is now to fall off at large positive v:

$$\delta\psi \doteq Qa^{m+1}u(1-u^2)^{m/2}\exp(im\phi)v(1+v^2)^{m/2} \times \int_v^\infty v^{-2}(1+v^2)^{-m-1}dv \Big/ \int_0^\infty v^{-2}[1-(1+v^2)^{-m-1}]dv.$$

Here the definite integral in the denominator normalizes $\delta\psi$ so as to satisfy the required boundary conditions. The change in wave number produced by the perturbation is found to first order by inserting in Green's accurate relation,

$$k_1^2 - k_0^2 = \int \psi_1^*(\partial\psi_0/\partial n)dS \Big/ \int \psi_1^*\psi_0 d(\text{vol}),$$

the expression for $\psi_1 = \psi_0 + \delta\psi$ in terms of ellipsoidal coordinates

in the numerator,

$$\partial\psi_0/\partial n = -Qa^m(1-u^2)^{m/2}\exp(im\phi)$$

$$\psi_1^* = \delta\psi^* = Qa^{m+1}u(1-u^2)^{m/2}\exp(-im\phi)\frac{2\cdot 2\cdot 4\cdot 6\cdots(2m)}{\pi\cdot 3\cdot 5\cdot 7\cdots(2m+1)},$$

and in the denominator replacing ψ_1^* by ψ_0^*,

$$\int \psi_1^*\psi_0 d(\text{vol}) = (R_f/2)[F_l'(kR_f)]^2[4\pi/(2l+1)](l+m)!/(l-m)!.$$

Thus we find for the shift in gerade levels due to a small orifice:

$$\frac{k_1^2-k_0^2}{k_0^2} = -\frac{2(2l+1)}{\pi}\frac{(l+m)!}{(l-m)!} \times\frac{1}{1^2\cdot 3^2\cdot 5^2\cdots(2m+1)^2\cdot(2m+3)^1}\left(\frac{a}{R_f}\right)^{2m+3}.$$

This formula was used in constructing the right-hand portion of the diagrams for gerade levels.

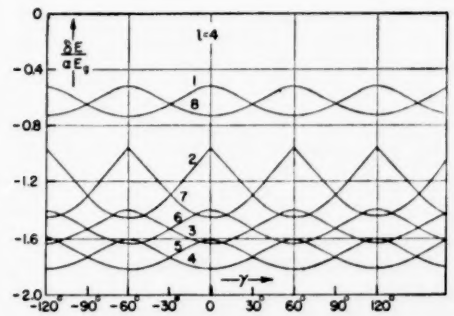

FIG. 23. Total nucleonic energy as a function of γ, for one to nine nucleons in states with $l=4$.

The total nucleonic energy of a many-particle closed shell configuration plus an incompletely filled g shell containing the indicated number of particles, for ellipsoidal deformations of small magnitude, α, in the approximation of the idealized collective model, is $E=E_0+\alpha E_g f(\gamma)+c\alpha^2$, where $f(\gamma)$ is plotted here as a function of the shape parameter, γ, of Fig. 13, and E_0, E_g, and c are constants, E_g being the kinetic energy of one nucleon with four units of angular momentum. The diagram has been drawn for simplicity as if nucleons had no spin and only 9 particles were required to fill the shell. The appropriate correction by a factor two is easily made. The quantity $f(\gamma)$ is obtained by summing over the appropriate number of nucleons the corresponding individual particle coefficients already plotted in Fig. 17, taking in each case the lowest energy—or most negative coefficient—allowed by the Pauli principle. It is seen from the diagram how the quadrupole-producing force, as measured by the coefficient $f(\gamma)$, increases to a maximum for a half-filled shell and then decreases. Oblate deformations are favored at the beginning of the shell and cigar-like ones at the end. Of course, this discussion refers to intrinsic quadrupole moment, not the moment after averaging with respect to precession about the nuclear spin axis.

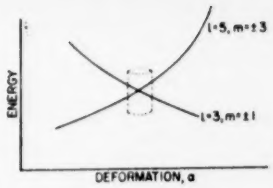

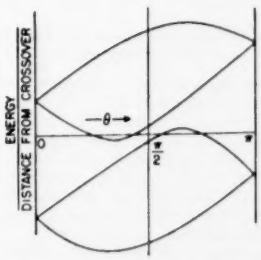

FIG. 24. Splitting of two double levels near a point of crossover.

Levels which cross without interaction for deformations of high symmetry experience a mutual repulsion for deformations of lower symmetry. For axially symmetric deformations the crossing levels are themselves ordinarily doubly degenerate except in the case $m=0$, so that four levels result from introduction of a slight ellipticity in the cross section of the otherwise axially symmetric form. The appropriate deformation coordinate $\eta=\alpha\sin\gamma$ (Fig. 13) is perpendicular to the plane of the upper diagram. The cylinder sketched in perspective there cuts the four sheeted energy level surface in the four lines which are shown as functions of angle in the lower diagram. An example in point would be the crossing of the doubly degenerate level $l=3$, $m=1$ by the level $l=5$, $m=3$. Details: Let $\xi=\alpha\cos\gamma-\alpha_0$ denote the component of departure from the crossing point which is visible in the upper diagram. Then, near the crossing point, the energy matrix of the four level system, omitting unessential complications, has the form

$$H=\begin{Vmatrix} s\xi+t\eta & 0 & f\eta & -g\eta \\ 0 & s\xi-t\eta & g\eta & -f\eta \\ f\eta & g\eta & -s\xi+u\eta & 0 \\ -g\eta & -f\eta & 0 & -s\xi-u\eta \end{Vmatrix},$$

where s, t, u, f, and g are constants, and the diagonal elements represent the level locations in the absence of coupling between the one pair of levels and the other. We write $\xi=r\cos\theta$, $\eta=r\sin\theta$, and (energy)$/r=y$, and find the secular equation for the four plotted roots:

$$y^4-[2s^2\cos^2\theta+(2f^2+2g^2+t^2+u^2)\sin^2\theta]y^2+2s(u^2-t^2)\times\cos\theta\sin^2\theta y+s^4\cos^4\theta+s^2(2f^2+2g^2-t^2-u^2)\sin^2\theta\cos^2\theta+(g^2-f^2+ut)^2\sin^4\theta=0.$$

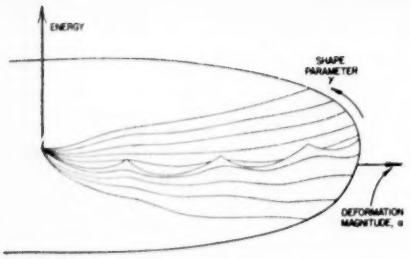

FIG. 25. Qualitative picture of inverted cones in lowest potential energy surface.

Here the lowest sheet of the multi-sheeted system potential energy surface is sketched qualitatively in its dependence on the ellipsoidal deformation parameters of Fig. 13. Only at the inverted funnels, i.e., only for prolate and oblate spheroidal deformations, which have $\gamma=0°$, $60°$, $120°$, etc., does this surface touch the one above it. That surface in turn (not shown) possesses both upright and inverted funnels. Important in affecting the probability of slippage from one surface to the one above or below it is the general curvature of the surface and particularly the size of the region upon this surface which is accessible to the representative point of the system when it has any given amount of total (potential plus oscillational kinetic) energy.

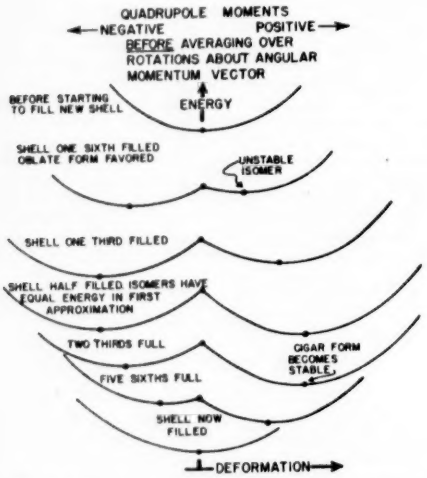

FIG. 26. Deformation potentials and quadrupole moments expected as a function of degree of filling of shells.

This is a qualitative picture of the effect of shell building on the intrinsic quadrupole moments, i.e., on the shape of the nucleus as it affects the motion of particles inside, not as it appears to an atomic electron after averaging over nuclear precession—an averaging which cuts to zero the quadrupole moment observed in atomic spectra when the nuclear spin is $\frac{1}{2}$ or 0 (even-even nuclei). Several particles in a partly filled shell bring about a deformation in the same way that one does (Fig. 6), with these amendments: (a) The particles cooperate. Coupling with the wall makes it energetically preferable for the second particle's orbit to line up in the plane of the first's. In first approximation the deformation thereby produced is twice as great, and the energy lowering (with respect to the spherical configuration) four times as large, as for one particle. (b) With increasing number of particles the quadrupole-producing force (see, for example, Fig. 23) goes through a maximum, showing a certain symmetry between the start of filling (oblate forms energetically preferred) and the near completion of the shell (prolate form lower in energy). (c) In the region extending roughly from $\frac{1}{3}$ filling to $\frac{2}{3}$ completion, both pancake- and cigar-like forms lie at relative minima of the energy curves, suggesting the possibility of configurationally-isomeric forms of the same nucleus. (d) All these considerations assume that the contribution to the deformation potential from all the residual, closed shell, nucleons is a quadratic function of the deformation parameter, α. In actuality a sufficiently large distortion will rearrange the order of levels and even the term "closed shell" will no longer have any simple meaning. On this account the suggested regular variation of quadrupole moment with progress of the filling will no longer necessarily be a reasonable expectation.

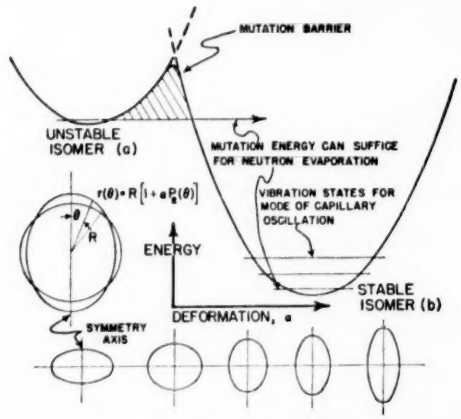

FIG. 27. Nuclear mutation forms.

The phenomenon of nuclear mutation from oblate to prolate form, or conversely, according to direction of energy release, is suggested by the considerations of Fig. 26 as conceivable for nuclei about $\frac{1}{3}$ or $\frac{2}{3}$ the way through the process of filling up a long shell. For deformations as great as those required to give the effect in question, it seems unreasonable to believe that the deformation energy of the closed shells is still proportional to α^2. Consequently this diagram has to be viewed as only an idealized schematization of the actual potential energy surface, and this only for walls of spheriodal character (axial symmetry). The spherical configuration represents a peak in the potential barrier against mutation from the stable to the unstable isomeric form.

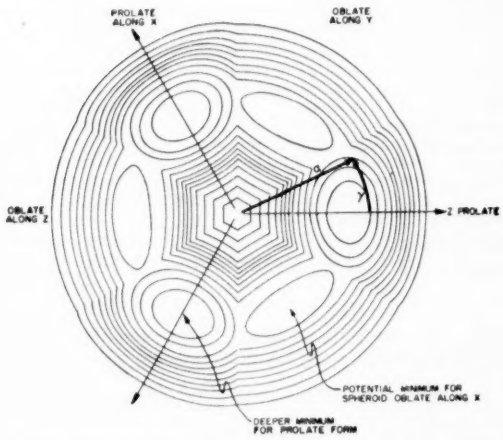

FIG. 28. Contour plot of energy as a function of the deformation variables α and γ of Fig. 13 for the ground state of a heavy nucleus with a shell which is little more than half full.

This energy is idealized as the sum of surface energy and the energies of the single particle states which lie lowest in a potential well of the given shape. The minima of the total energy occur

when the angular momenta of the nucleons lie as nearly parallel-antiparallel to the symmetry axis as possible (oblate form) and when the angular momenta lie as nearly perpendicular as possible to the symmetry axis (prolate form). To pass from prolate to oblate form via the spherical form is very expensive of energy. The easiest route, as pointed out to us by Professor Edward Teller, is passage over the potential ridge in the diagram. On this ridge the system has the form of an ellipsoid with three unequal principal axes.

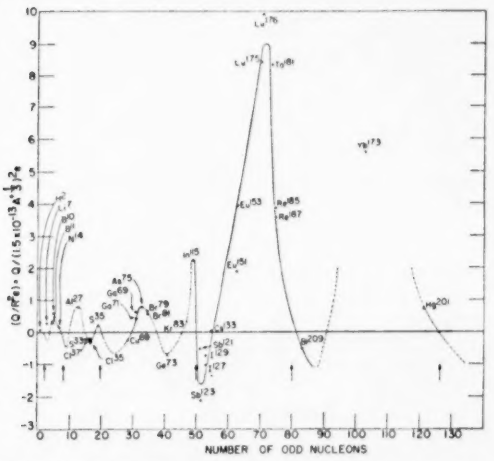

FIG. 29. Effective nuclear quadrupole moments for hyperfine structure divided by the square of the nuclear radius $(1.5\times10^{-13}A^{\frac{1}{3}})^2$.

The known moments of odd-proton nuclei and odd-proton odd-neutron nuclei (excepting Li^6 and Cl^{36}) are plotted as circles against the number of protons, and the moments of odd-neutron nuclei as crosses against the number of neutrons. The arrows indicate closing of major nucleon shells. The solid curve represents regions where quadrupole moment behavior seems established, the dashed curve more doubtful regions. This figure and caption are taken from the report of Townes *et al.* (reference 11). See Fig. 5 for relation between Q and α.

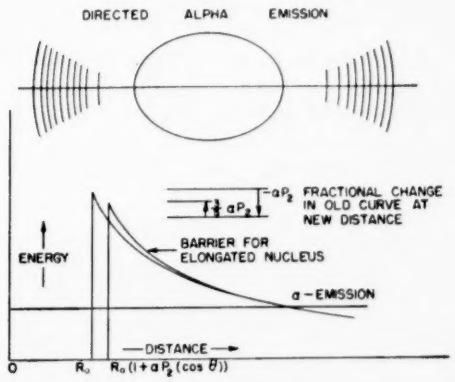

FIG. 30. Directed alpha-decay.

An alpha-active nucleus will ordinarily have a quadrupole moment and will therefore emit preferentially from the outermost parts of its surface, where the peak of the potential energy barrier has been lowered. The reduced wavelength, $\lambda=\lambda/2\pi$, of a 5-Mev alpha-particle is 1×10^{-13} cm, a quantity small compared to a typical nuclear diameter of 18×10^{-13} cm. Consequently the directionality of emission will have a definition relative to the nuclear axes which is ordinarily better specified than the correlation of the nuclear axes themselves relative to a direction fixed in space. In particular a nuclear state of angular momentum zero will be characterized by alpha-emission isotropic in the laboratory frame of reference, however anisotropic the surface emissivity is in the nuclear frame of reference. The maximum observable directionality will be found when at the same time the nuclear spin, I, is large, when the projection, I_s, of I upon a chosen space axis (strong magnetic field, low temperature) is $\pm I$, and when the nucleus in question is on a time average prolate with respect to the nuclear spin axis I. Then emission will take place preferentially parallel and antiparallel to the magnetic field. Under the same conditions observations of maximum probability for directions perpendicular to the magnetic field will indicate an oblate ellipsoid.

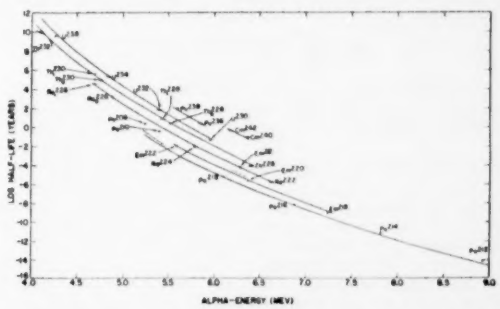

FIG. 31. Alpha-particle half-lives *versus* alpha-energy.

The Geiger-Nuttal relationship between alpha-particle energy and life time with respect to alpha-particle decay is not a one-to-one correspondence, as shown in this recent compilation of results for even-even nuclides taken from Perlman, Ghiorso, and Seaborg [Phys. Rev. **77**, 26 (1950). For other compilations and analyses of alpha-decay data, see the references cited in this paper. including A. Berthelot, J. phys. et radium **3**, 17 (1942); also I. Kaplan, Phys. Rev. **81**, 962 (1951) and J. M. Blatt and V. F. Weisskopf, *Theoretical Nuclear Physics* (John Wiley and Sons, Inc., New York, 1952), Chapter XI.] Perlman *et al.* give similar curves for the other classes of nuclei. Nor should it be. The Gamow treatment of barrier penetration gives a formula [see also Rasmussen, Thompson, and Ghiorso, Phys. Rev. **89**, 33 (1953)]:

$$\begin{pmatrix}\text{probability}\\ \text{per second of}\\ \text{alpha-decay}\end{pmatrix}=\begin{pmatrix}\text{intrinsic alpha}\\ \text{emission prob-}\\ \text{ability}\end{pmatrix}\times\exp\{-2(2Z/137)(2M_\alpha c^2/E_\alpha)^{\frac{1}{2}}f(u)\},$$

in which there enters not only the alpha-particle energy (we look apart from the well-known small corrections for the finite mass and recoil energy of the residual nucleus), but also the charge and radius of the nucleus:

$$u=\frac{E_\alpha}{\text{barrier height}}=\frac{E_\alpha R_0}{2Ze^2}=\frac{E_\alpha A^{\frac{1}{3}}}{4mc^2Z};$$
$$f(u)=\arccos u^{\frac{1}{2}}-u^{\frac{1}{2}}(1-u)^{\frac{1}{2}}.$$

Nevertheless, the fluctuations of the points of such diagrams away from the curve for the appropriate Z appear too great and also too irregular to be laid solely to the Gamowian dependence upon Z and A. Binding anomalies for nuclei near shell limits give irregular variations of E_α from element to element, but such variations in *energy* cannot by themselves account for deviations from the barrier *penetration* formula. However, the existence of quadrupole moments necessarily implies a deviation from the Gamow formula which will be very sensitive to departures from closed-shell structure—or more directly, sensitive to the nuclear deformations called forth by asymmetric pressure against the surface by nucleons in unfilled shells. For a distortion $R=R_0[1+\alpha P_2(\cos\theta)]$ the potential energy of an alpha-particle outside the nucleus is altered in first order to

$$V=(2Ze^2/r)[1+(3R_0^2/5r^2)\alpha P_2(\cos\theta)].$$

Re-evaluating the integral

$$(2/\hbar)\int_{R(\theta)}^{\text{turning point}}[2M_\alpha(V-E_\alpha)]dr,$$

in the exponent of the penetration factor, we find that the factor $f(u)$ is changed by the amount

$$\delta f(u) = -(2/5)\alpha P_2(\cos\theta) u^{\frac{1}{2}}(1-u)^{\frac{1}{2}}(2-u).$$

This consideration neglects the fact that the area of the surface from which significant emission takes place has been cut down from $4\pi R_0^2$ to some smaller amount. This reduction we neglect compared to the improvement in penetration through the thinner barrier. Accordingly we insert for the angle θ the value at the point of maximum emission:

$-\alpha P_2(\cos\theta) = -\alpha$ for prolate ellipsoids;
$-\alpha P_2(\cos\theta) = \alpha/2$ for oblate ellipsoids;
$\delta f(u) =$ a negative number in both cases.

The factor of improvement in decay rate made by the ellipsoidal deformation is

$$\exp -2\left(\frac{2Z}{137}\right)\left(\frac{2Mc^2}{E}\right)^{\frac{1}{2}}\delta f(u),$$

or, for $Z=90$, $A=234$, barrier height of 30 Mev before deformation, decay energy $E=5$ Mev, rest energy of alpha-particle $Mc^2 = 3700$ Mev, with the dimensionless ratio $u=5$ Mev/30 Mev,

$$\exp -101\delta f = \exp -101\times -0.273\alpha P_2 = \begin{cases} \exp 28\alpha \text{ (prolate)} \\ \exp -14\alpha \text{ (oblate)} \end{cases}.$$

Thus a deformation which stretches the axis by the fractional amount $\alpha=0.1$—a value well within the range indicated by observed quadrupole moments—will be expected to increase the decay rate by a factor of roughly $e^{2.8}=16$. Of course, from the observed decay rate associated with a given alpha-emission process one cannot determine *both* the nuclear radius and the quadrupole moment. One gets only some combination of the two, which we have to identify—in the absence of other effects—with the quantity generally known as the effective radius. Between it, the radius R_0 of a sphere of the same volume, and the quadrupole moment exists the relation

$$R_{eff} = (2Ze^2/E_\alpha)u_{eff} = (2Ze^2/E_\alpha)[u+\delta f/(df/du)] = R_0[1+(2/5)(2-u)\alpha P_2],$$

or with sufficient accuracy for most nuclei

$$(R_{eff}-R_0)/R_0 = 0.533\alpha P_2 = \begin{cases} 0.533\alpha \text{ (prolate)} \\ -0.267\alpha \text{ (oblate)} \end{cases}.$$

These considerations have an interesting application to the alpha-activity of samarium. The alpha-energy has been measured as 2.18 Mev by W. P. Jesse and J. Sadauskis [Phys. Rev. **78**, 1 (1950)] and the activity has been assigned to Sm^{147}. [A. J. Dempster, tentative result given in Argonne National Laboratory Report ANL-4355, 1949 (unpublished); Rasmussen, Reynolds, Thompson, and Ghiorso, Phys. Rev. **80**, 475 (1950)]. We are indebted for discussion of this case to Professor I. Perlman, who with a nuclear radius of 7.81×10^{-13} cm, such as would normally be expected, calculates [I. Perlman and T. J. Ypsilantis, Phys. Rev. **79**, 30 (1950)] a half-life 2.9×10^{12} years (private communication) compared to a measured half life 10–20 times shorter. Perlman also concludes that a 80-kev increase in the value of the decay energy, *or* a roughly 10 percent increase in nuclear radius, would resolve the discrepancy. Alternatively we can say that a prolate distortion of 10 percent/0.533 = 19 percent or an oblate deformation of 10 percent/0.267 = 37 percent would account for the situation, assuming that 7.81×10^{-13} cm is indeed an appropriate figure for the radius of a sphere of the same volume. Quadrupole deformations of these general magnitudes are found experimentally for nuclei in the general neighborhood of samarium. P. Brix and H. Kopfermann [Z. Physik **126**, 344 (1949)] mention their reasonable bearing on the alpha-lifetime of this substance. Of course the shortening of life that occurs for Sm^{147} in extreme measure must also occur for most other nuclei in greater or lesser degree. Consequently the nuclear radii which have been found from analysis of alpha-decay must on this account at least be larger on the average than the appropriate volume-equivalent spherical radii. For this reason the nuclear radii reported [Phys. Rev. **77**, 26 (1950)] for polonium isotopes, previously thought of as abnormally low, are perhaps now to be considered as the more nearly normal figures. Obviously direct measurements of the quadrupole moments of alpha-active nuclei—where possible—are most relevant to the further discussion of this topic. Mention should also be made of anomalies in the isotope shifts in atomic spectra, (reference 25), which may be in good measure explained by increase in electron-effective nuclear radius *via* ellipsoidal deformations, according to recent interesting discussions with Dr. Lawrence Wilets of Princeton. From the characteristic or "Chang" radiation given out when mu-mesons drop from $2p$ to $1s$ Bohr orbits it is not impossible that one may be able to develop another experimental tool to study nuclear quadrupole moments—closely related to the study of atomic spectra, but with energy shifts and splittings percentage-wise enormously greater than in the atomic case because of the larger fraction of time spent within the nucleus by the meson. Alpha-lifetimes are affected not only by the Gamow-Gurney-Condon penetration factor, but also by the Franck-Condon principle; not only by the equilibrium deformation in the original nucleus, but also by the *difference* in normal shapes between initial and final nucleonic states. If this difference is large, the residual nucleus will have little chance to be formed in the state of zero-point oscillation. On this account there will be a reduction in alpha-decay rate not taken into account in the above discussion. Transitions to the lowest vibration state will be inhibited relative to transitions to those vibration states favored by the Franck-Condon principle. This circumstance must evidently be taken into account in interpreting the fine structure of typical alpha-spectra.

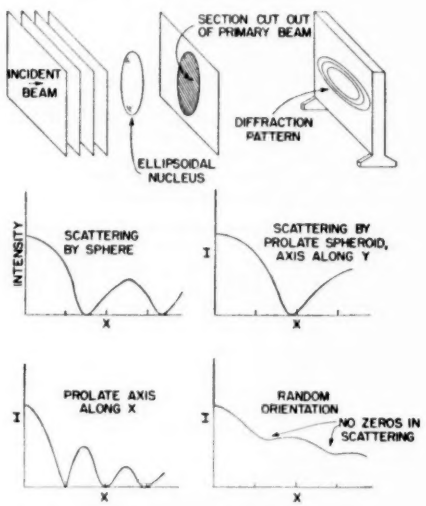

FIG. 32. Diffraction by ellipsoidal nucleus.

Will not diffraction or "shadow" scattering by an ellipsoidal nucleus be sufficiently different from that by a spherical nucleus to allow observation of the difference? This interesting question was raised in discussion with us by Dr. J. B. Cladis of Los Alamos. The qualitative analysis in the figure shows that the ratio of minima to maxima in the diffraction by randomly oriented nuclei of the given species is indeed a sensitive measure of nuclear deformation, being zero (in the diffraction-idealization of scattering) only for spherical scattering centers. A quantitative analysis can be made along the following lines. Let f and g be the principal axes of the ellipsoid as projected in imagination onto the plane of the receptor, and let the X and Y axes be oriented parallel to the f and g axes. The absence of the ellipsoidal piece from the transmitted beam produces the same scattered wave as if this piece alone were present. A portion $dS=d\xi d\eta$ of its area makes a contribution to the scattering amplitude at a distance r_{12} and at not too great an angle θ to the primary beam equal to $(-ik/2\pi r_{12})\times\exp(ikr_{12})dS$, where k is the wave number. The differential scattering cross section is the square of r times the absolute value of the integrated scattering amplitude:

$$d\sigma/d\Omega = \left|(k/2\pi)\int\exp[-ik(x\xi+y\eta)/r]d\xi d\eta\right|^2.$$

Here the direction of the scattering is indicated by the ratios x/r and y/r. We write $\xi = fu\cos\theta$, $\eta = gu\sin\theta$, and integrate first over

θ, then over u from 0 to 1, finding

$$d\sigma/d\Omega=\left\{\frac{kfgJ_1[(k^2f^2x^2/r^2+k^2g^2y^2/r^2)^{\frac{1}{2}}]}{(k^2f^2x^2/r^2+k^2g^2y^2/r^2)^{\frac{1}{2}}}\right\}^2$$

for the scattering for one orientation of the ellipsoid. A superposition of such curves gives the distribution which is to be compared with observation. Richardson, Ball, Leith, and Moyer [Phys. Rev. 86, 29 (1952)] first mentioned the existence of this effect which with present experimental accuracy remains undetected.

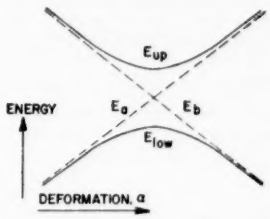

FIG. 33. Behavior of two levels at a point of near cross-over, $\alpha=\alpha_0$.

The levels, as they would be in the vicinity of cross-over in absence of interaction, are

$$E_a=E_0+a(\alpha-\alpha_0);\quad E_b=E_0+b(\alpha-\alpha_0).$$

The coupling which brings about the interaction is $H_{ab}=H_{ba}$; its dependence upon α is neglected in immediate neighborhood of α_0. The actual wave function for a stationary state of the system is

$$\psi=A\psi_a+B\psi_b.$$

The equation for determination of coefficients A and B and energy value E in case of any *fixed* value of the deformation parameter, α, is

$$i\hbar\dot{\psi}=E\psi=H\psi,$$
$$EA=E_aA+H_{ab}B,$$
$$EB=H_{ba}A+E_bB.$$

The two eigenvalues of the energy are shown in the diagram:

$$E_{\rm up}=(\tfrac{1}{2}E_a+\tfrac{1}{2}E_b)+\{(\tfrac{1}{2}E_a-\tfrac{1}{2}E_b)^2+|H_{ab}|^2\}^{\frac{1}{2}},$$
$$E_{\rm low}=(\tfrac{1}{2}E_a+\tfrac{1}{2}E_b)-\{(\tfrac{1}{2}E_a-\tfrac{1}{2}E_b)^2+|H_{ab}|^2\}^{\frac{1}{2}}.$$

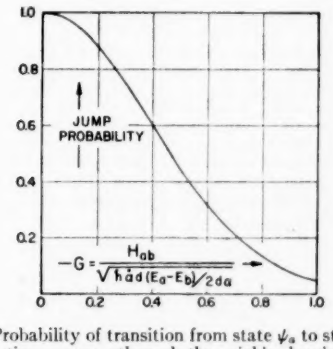

FIG. 34 Probability of transition from state ψ_a to state ψ_b when the deformation α passes through the neighborhood of the cross-over, α_0, (Fig. 33) at the fixed speed $\dot{\alpha}$ (reference 27).

The probability of a jump is very small when the interaction H_{ab} between the levels is very weak, or when the rate of deformation, $\dot{\alpha}$, is very large, or both. Then the system, if originally in the state ψ_a with energy E_a, will have high probability to be in the same state, ψ_a, after deformation has carried the system through the region of cross-over. In other words, there will be a high probability for a jump to take place from the lower level, $E_{\rm low}$, to the upper level, $E_{\rm up}$, as in other familiar cases of nonadiabatic excitation. The opposite will be the case for strong interaction, or slowly varying deformation, or more generally, for large values of the dimensionless "interaction parameter" G, defined by

$$G^2=\frac{|H_{ab}|^2}{\hbar\dot{\alpha}d(E_a-E_b)/2d\alpha}.$$

The detailed dependence of transition probability upon G is found by considering the equation

$$i\hbar\dot{\psi}=H(t)\psi,$$

or

$$i\hbar\dot{A}=E_a(t)A+H_{ab}B,$$
$$i\hbar\dot{B}=H_{ba}A+E_b(t)B.$$

To translate into dimensionless variables, write

$$A(t)=f(t)\exp[-i(E_a+E_b)t/2\hbar],$$
$$B(t)=g(t)\exp[-i(E_a+E_b)t/2\hbar],$$

in order to abstract away from the unimportant general slope of the cone, and

$$t^2=x^2 2\hbar/(a-b)\dot{\alpha},$$

where $a-b$ represents the difference in slope of the two unperturbed potential energy curves, $d(E_a-E_b)/d\alpha$. Also assume H_{ab} is real and positive, since any complex argument present in H_{ab} can always be absorbed into the probability amplitudes, A and B. The origin of time is chosen as the moment when the deformation arrives at the cross-over point, $\alpha=\alpha_0$. The problem is then to find for very large positive times the value of the probabilities $|f|^2$ and $|g|^2$ of being in the states a and b from the differential equations,

$$idf/dx=xf+Gg,$$
$$idg/dx=Gf-xg;$$

or from the equivalent single second-order equation,

$$d^2f/dx^2+(G^2+x^2+i)f=0,$$

subject to the initial condition that at $t=-\infty$, or $x=-\infty$,

$$f\sim\exp[-(ix^2/2)-(iG^2/4)\ln 2x^2],$$
$$g\sim 0.$$

The solution is

$$f=(2\pi)^{-\frac{1}{2}}\int_0^\infty dy\exp[ix^2/2-y^2/2-(iG^2/2)\ln y]$$
$$\times\{\exp[\pi G^2/8-(1-i)xy]+\exp[-3\pi G^2/8+(1-i)xy]\},$$

and behaves asymptotically for large positive time ($x=+\infty$) as

$$\exp[-\pi G^2/2-ix^2/2-(iG^2/4)\ln 2x^2].$$

The probability of a jump having taken place is evidently

$$J(G)=|f_{\rm final}|^2/|f_{\rm initial}|^2=\exp(-\pi G^2).$$

The values of the function are plotted in the figure. It is to be noted that this analysis of the transition probability treats the nucleonic motion in appropriate quantum-mechanical terms: a wave function ψ, or probability amplitudes A and B of being in states ψ_a and ψ_b. However, the progress of the deformation itself is treated as a pure classical motion: $\alpha=\dot{\alpha}t$. This procedure is ordinarily justifiable because the mass of the individual nucleon is so small compared to the mass of the capillary oscillator.

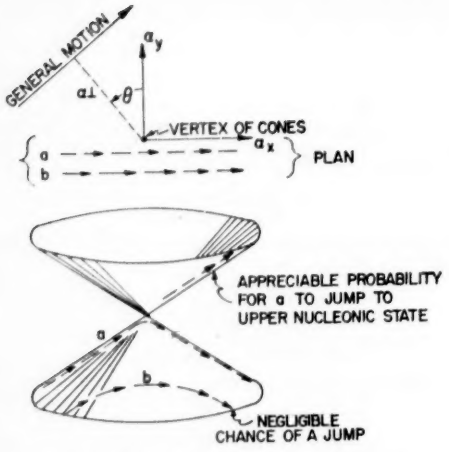

FIG. 35. Transition cross section for energy surfaces in conical contact.

This figure illustrates the concept of effective cross section for the jump from one potential energy surface to another, as first introduced by Teller [reference 24; F. O. Rice and E. Teller, J. Chem. Phys. **6**, 489 (1938)] in connection with the vibrations of polyatomic molecules. Vertically is plotted the energy. In the two horizontal directions go two of the several coordinates which are required to describe a deformation. The two potential energy surfaces meet in a double cone, which in the present example is supposed to be circular in cross section, for sake of simplicity. Represented here in magnified form is only a very small portion of the two potential energy surfaces (see Fig. 25 for other details). The kinetic energy with which the collective oscillation is endowed is considered to be large in comparison with any of the energies seen here. Consequently, the deformation is idealized as proceeding in a direction and at a rate, $\dot{\alpha}$, uninfluenced by this minor local irregularity in the potential energy surface (plan view). When the oscillator coordinates pass close to the vertex of the cone; that is, when the representative point of the system has a small impact parameter, $\alpha_{\min}$, there is an appreciable chance for the nucleonic state of the system to jump from the lower surface to the upper surface (case *a*). When the oscillator coordinates stay far from the critical value, the chance of a jump is negligible (case *b*). When the state of the system executes repeated oscillations, the representative point of the system carries out a Lissajous type of motion (not shown) in plan view. In this case the probability of a jump is best stated in statistical form, in terms of the concept of "cross section" for a jump. In the present case this cross section, σ, has the dimensions of the deformation parameter, α, raised to the first power, for the space of the motion itself is only two dimensional. From dimensional arguments Teller showed that

$$\sigma = \text{const}(\hbar\dot{\alpha}/s)^{\frac{1}{2}},$$

where s is the slope of the circular cone. The value of the cross section also follows directly from the jump probability, $J(G)$, of Fig. 34:

$$\sigma = \int_{-\infty}^{+\infty} J(G)d\alpha_\perp,$$

where $\alpha_\perp$ is the impact parameter or the distance of closest approach. Let the deformation α be measured away from the center of the circular cone as origin, so that (Fig. 34):

$$\begin{aligned} E_a - E_b &= 2s\alpha_x, \\ H_{ab} &= s\alpha_y, \\ E_{\text{up}} = -E_{\text{low}} &= s(\alpha_x^2+\alpha_y^2)^{\frac{1}{2}} = s\alpha, \\ G^2 &= \alpha_y^2 s/\hbar\dot{\alpha}. \end{aligned}$$

Integration gives for Teller's constant in the expression for the cross section the value

$$\text{const} = \int_{-\infty}^{+\infty} J(G)dG = 1.$$

In the more general case where the two potential energy surfaces meet in tilted cones, elliptical rather than circular in cross section, the axes x and y can still be oriented to lie along the principal axes of the ellipse,

$$\begin{aligned} E_{\text{up}} &= c_1\alpha_x + c_2\alpha_y + (s_x^2\alpha_x^2 + s_y^2\alpha_y^2)^{\frac{1}{2}}, \\ E_{\text{low}} &= c_1\alpha_x + c_2\alpha_y - (s_x^2\alpha_x^2 + s_y^2\alpha_y^2)^{\frac{1}{2}}. \end{aligned}$$

Directions of incidence of the representative point of the collective oscillator are now inequivalent and have to be considered separately:

$$\begin{aligned} \alpha_x &= \dot{\alpha}t\cos\theta - \alpha_\perp\sin\theta, \\ \alpha_y &= \dot{\alpha}t\sin\theta + \alpha_\perp\cos\theta. \end{aligned}$$

Then

$$G^2 = \frac{(s_x^2\sin^2\theta + s_y^2\cos^2\theta)\alpha_\perp^2}{\hbar\dot{\alpha}(s_x^2\cos^2\theta + s_y^2\sin^2\theta)^{\frac{1}{2}}},$$

the cross section for incidence in the direction θ is

$$\sigma_\theta = (\hbar\dot{\alpha})^{\frac{1}{2}}(s_x^2\cos^2\theta + s_y^2\sin^2\theta)^{\frac{1}{4}}(s_x^2\sin^2\theta + s_y^2\cos^2\theta)^{-\frac{1}{4}},$$

and the effective cross section is found by averaging this expression over all angles of incidence (Lissajous motion).

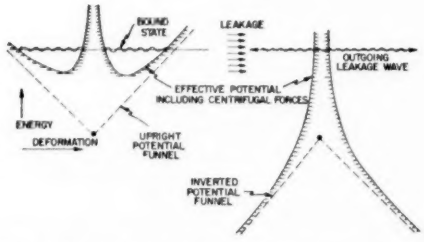

FIG. 36. Probability of a radiationless jump for system bound in cone of intersurface contact.

We consider here the exceptional case where the amount of energy in the collective oscillation is so small, and the potential energy surface is so shaped, that the system oscillates about in the neighborhood of the funnel's mouth with only a few quanta of vibrational energy. In this case both the nucleonic *and* the collective oscillation have to be treated quantum-mechanically. The system behaves in first approximation as if bound in a stable conical potential, with characteristic energy levels. In next approximation it is necessary to allow for a characteristic probability to switch over to an unstable potential energy surface, without change in total energy, but with great increase in kinetic energy. From the results of the quantum-mechanical analysis can be presumably derived, in the case of large quantum numbers, the same formula for the cross section which is derived and discussed in Fig. 35. Details follow for the case of a right circular cone of slope $dE/d\alpha = s$. Here $\psi_a(\alpha_x, \alpha_y)$ represents the probability amplitude for the oscillator coordinates to have the values α_x and α_y *and* for the nucleonic system to be in the state a; similarly for ψ_b. Then the wave equation for a stationary energy state of the whole system is

$$\begin{aligned} E\psi_a &= -\frac{\hbar^2}{2M_\alpha}\left(\frac{\partial^2\psi_a}{\partial\alpha_x^2} + \frac{\partial^2\psi_a}{\partial\alpha_x^2}\right) + s\alpha_x\psi_a + s\alpha_y\psi_b, \\ E\psi_b &= -\frac{\hbar^2}{2M_\alpha}\left(\frac{\partial^2\psi_b}{\partial\alpha_x^2} + \frac{\partial^2\psi_b}{\partial\alpha_x^2}\right) + s\alpha_y\psi_a - s\alpha_x\psi_b, \end{aligned}$$

where M_α is the coefficient in the classical expression, $\frac{1}{2}M_\alpha\dot{\alpha}^2$, for the kinetic energy of the oscillator. We write

$$\begin{aligned} \alpha_x &= (\hbar^2/2M_\alpha E)^{\frac{1}{4}}u\cos\theta, \\ \alpha_y &= (\hbar^2/2M_\alpha E)^{\frac{1}{4}}u\sin\theta, \\ \beta &= \hbar s/(2M_\alpha E^3)^{\frac{1}{4}}, \end{aligned}$$

and use the circular symmetry of the system to separate variables:

$$\begin{aligned} \psi_a &= u^{-\frac{1}{2}}[F(u)\cos\tfrac{1}{2}\theta + G(u)\sin\tfrac{1}{2}\theta]\exp(im\theta), \\ \psi_b &= u^{-\frac{1}{2}}[F(u)\sin\tfrac{1}{2}\theta - G(u)\cos\tfrac{1}{2}\theta]\exp(im\theta), \end{aligned}$$

finding the radial wave equations

$$\begin{aligned} \frac{d^2F}{du^2} + \left[1 - \beta u - \frac{m^2}{u^2}\right]F &= -\frac{im}{u^2}G, \\ \frac{d^2G}{du^2} + \left[1 + \beta u - \frac{m^2}{u^2}\right]G &= \frac{im}{u^2}F. \end{aligned}$$

In absence of the coupling term on the right the first equation describes the motion of a system of the prescribed angular momentum in an upright funnel. The second equation describes the runaway motion of a system of the same energy and angular momentum under the action of the potential of an inverted funnel. The coupling term makes possible transitions from the stable state to the unstable state. The coupling term vanishes for the case $m=0$, contrary to what one might have expected from the classical analysis of Fig. 35, where the probability of a jump is the greater the smaller is the impact parameter. However, this classically founded expectation must be confirmed by detailed calculations of the jump probabilities for values of m greater than 0 from the above coupling terms. Despite the proportionality of these terms with m, the leakage probabilities fall off fast with m. These probabilities can in principle be evaluated by perturbation methods. We calculate F from the first equation neglecting the term in G on the right hand side. The eigenfunction F is then inserted on the right-hand side of the second equation to determine G:

$$G(u)=\left\{\int_0^u G_1(u)G_2(v)+\int_u^\infty G_2(u)G_1(v)\right\}(im/v^2)F(v)dv,$$

where G_1 and G_2 are two independent solutions of the *homogeneous* equation for G, the first behaving as an outgoing plane wave at infinity, but irregular at the origin; and the second regular at the origin. The normalization is chosen so that

$$G_2dG_1/du-G_1dG_2/du=1.$$

For large u these functions have the form

$$G_1\doteq-\left(1+\beta u-\frac{m^2}{u^2}\right)^{-\frac{1}{4}}\exp\left[i\left\{\frac{\pi}{4}+\int_{u_{\min}}^u\left(1+\beta u-\frac{m^2}{u^2}\right)^{\frac{1}{2}}du+\delta\right\}\right],$$

$$G_2\doteq\left(1+\beta u-\frac{m^2}{u^2}\right)^{-\frac{1}{4}}\sin\left\{\frac{\pi}{4}+\int_{u_{\min}}^u\left(1+\beta u-\frac{m^2}{u^2}\right)^{\frac{1}{2}}du+\delta\right\},$$

where δ is the correction to the phase shift of the J.W.K.B. approximation. The probability per second, A, for transition from the upper potential energy surface to the lower one is found by comparing the flux of particles outgoing in G asymptotically at large u with the number of particles bound in state F:

$$A=2\pi[G(u)^2du/dt]_{u=\infty}/2\pi\int F^2(u)du,$$

$$=\frac{2E}{\hbar}\left[\int_0^\infty G_2(v)(m/v^2)F(v)dv\right]^2\Big/\int_0^\infty F^2(u)du.$$

The dependence of transition probability upon the quantum number m of rotatory oscillation is derivable by semiclassical arguments in the case of small m and large energy. Then the transition occurs—if at all—when the representative point in α-space is near its point of closest approach, $\alpha=\alpha_{\min}$. The point is then describing a nearly rectilinear path. Consequently it is appropriate to use the previously derived formula for the probability of a jump in a single pass (Fig. 35):

$$\exp(-\pi G^2)=\exp(-\pi s^2\alpha_{\min}^2/\hbar\dot{\alpha}s).$$

The number of passes per unit time in the periodic orbit of the representative point follows from the classical mechanics of a system with energy E, mass M_α and angular momentum $m\hbar$ moving in a conical potential, $V=s\alpha_r$:

$$\text{Period}=\oint\frac{d\alpha_r}{\dot{\alpha}_r}=\oint\frac{d\alpha_r}{(2/M_\alpha)^{\frac{1}{2}}(E-s\alpha_r-m^2\hbar^2/2M_\alpha\alpha_r^2)^{\frac{1}{2}}}$$

$$\doteq(8M_\alpha E/s^2)^{\frac{1}{2}}.$$

Inserting in the expression for the transition probability the value

$$\alpha_{\min}\doteq m\hbar/(2M_\alpha E)^{\frac{1}{2}},$$

and

$$\dot{\alpha}=(2E/M_\alpha)^{\frac{1}{2}},$$

and dividing by the period, we find for the chance per second of a jump:

$$A=(E/\hbar)(\hbar s/2^{\frac{1}{2}}E^{\frac{1}{2}}M_\alpha^{\frac{1}{2}})\exp(-\pi m^2\hbar s/2^{\frac{1}{2}}E^{\frac{1}{2}}M_\alpha^{\frac{1}{2}}),$$

$$A\doteq(E/\hbar)(\beta/2)\exp(-\pi\beta m^2/2).$$

As an example, consider a slope of the cone equal to 10 Mev per unit in the magnitude, α, of ellipsoidal deformations. The kinetic energy is

$$\tfrac{1}{2}M_\alpha\dot{\alpha}^2=\tfrac{1}{2}\rho(4\pi R_0^3/3)(3R_0^2\dot{\alpha}^2/10),$$

so that for the case of U^{236} the effective "mass" is

$$M_\alpha=236M(3r_0^2/10)(236)^{\frac{1}{3}}.$$

Finally, let the energy E available for oscillation about the vertex of the cone be 4 Mev. Then the dimensionless quantity β—whose reciprocal is related to the number of states bound in the cone with energy less than E—has the value

$$\beta=10\text{ Mev }(\hbar^2/0.6Mr_0^2)^{\frac{1}{2}}/(236)^{5/6}(4\text{ Mev})^{\frac{1}{2}}$$
$$=0.0781.$$

The probability for a radiationless jump from a state bound in the upper cone with $m=1$ to the lower state is

$$A=(4\text{ Mev}/0.66\times10^{-21}\text{ Mev sec})\,0.039\exp(-0.123)$$
$$=2.1\times10^{20}\text{ sec}^{-1},$$

corresponding to a level width $A\hbar$ of 0.14 Mev.

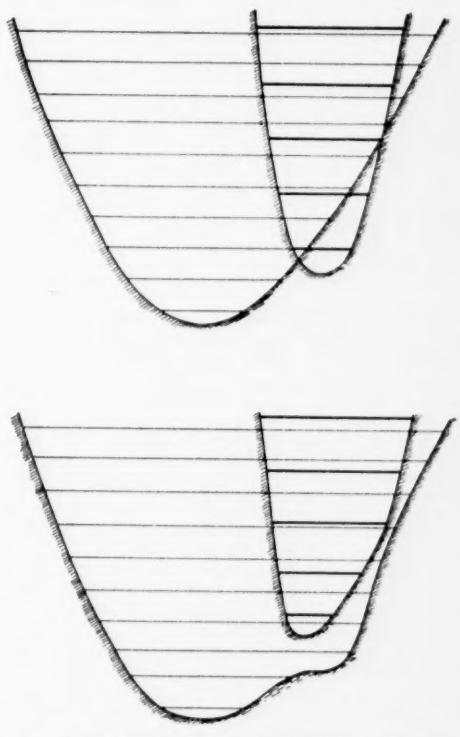

FIG. 37. One-dimensional example of influence of slip-over effect upon energy level pattern.

We shall describe the slippage phenomenon in terms of displacement of stationary energy values rather than in terms of transition probabilities. The latter way of speaking is the more natural in the idealized collective model where these transition probabilities are relatively small. The energy level description is unworkable in practice when the number of ways of dividing the energy between oscillation and nucleonic excitation is very great. In contrast, the figure shows an idealized case—not expected to occur in actual nuclei, but illustrative of the general principles involved—where only two nucleonic states, a and b, come into play. The probability amplitude function has two components, $\psi_a(\alpha)$ and $\psi_b(\alpha)$, whose absolute squares give the probabilities for the system to be in one or the other nucleonic states with a wall deformation, α. We write the Schroedinger equation in the form

$$i\hbar\partial\psi_a/\partial t=-(\hbar^2/2M_\alpha)\partial^2\psi_a/\partial\alpha^2+V_a(\alpha)\psi_a+H_{ab}\psi_b,$$

$$i\hbar\partial\psi_b/\partial t=-(\hbar^2/2M_\alpha)\partial^2\psi_b/\partial\alpha^2+V_b(\alpha)\psi_b+H_{ba}\psi_a.$$

In the extreme case of very small coupling H_{ab}, the problem separates into two eigenvalue equations which will possess characteristic energy values as shown in the upper part of the diagram. In the opposite extreme case of large coupling, the simplest description is obtained when the characteristic level spacings are small

compared to the coupling constant H_{ab}; in other words, when the mass M_a is very large. Then it is reasonable to consider the eigenvalue equations,

$$E\psi_a = V_a\psi_a + H_{ab}\psi_b,$$
$$E\psi_b = V_b\psi_b + H_{ba}\psi_b.$$

The two energy values $E_1(\alpha)$ and $E_2(\alpha)$ obtained from these equations give two new potential energy curves with respect to which the oscillation now takes place—at least in so far as those potential curves can be considered to be felt out by a particle of very large mass. In the case of intermediate coupling the ordering of the energy levels will be very complicated. However, in all three cases the total number of energy levels less than any given large energy E will have the same rate of increase with E.

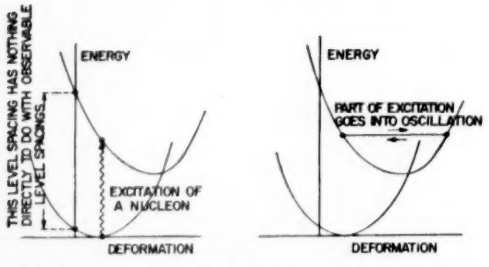

FIG. 38. Franck-Condon principle for nuclear transitions.

In the collective-model idealization of the nucleus as in a molecule, excitation processes (very high energy impact; photoabsorption) which raise a single particle (nucleon; electron) to an excited state can be thought of in first approximation as taking place in such a way that the heavy part of the system (collective oscillator; atomic nuclei) will keep position and velocity coordinates unchanged. The individual particle therefore may be considered to jump from one potential surface to the other at a fixed value of the deformation coordinates. The principle of Franck and Condon indicates that the energy absorbed in the primary act bears a simple relation neither to the energy difference between the minima of the two curves, nor to the separation of the curves for zero deformation, nor to the amount of the absorbed energy which will be available afterwards for vibration (right-hand portion of diagram). In the nuclear case subsequent slippage down from one potential energy surface to another will of course occur after repeated oscillations, and the distribution of energy over the system will finally be randomized, granted time before radiation carries the energy away. From the diagram it is seen that the observed spacing of energy levels may be expected to depend upon the ellipticity of the configuration in which the spacing is measured. It appears reasonable to attribute to this circumstance an appreciable part of the observed anomalies in the spacing of the levels of Pb and Bi [J. A. Harvey, Phys. Rev. **79**, 241 (1950)].

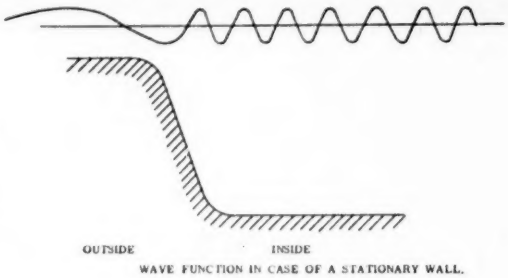

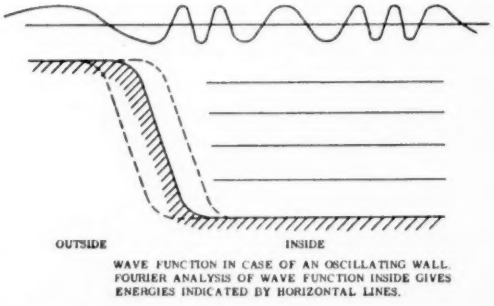
OUTSIDE
INSIDE
WAVE FUNCTION IN CASE OF AN OSCILLATING WALL. FOURIER ANALYSIS OF WAVE FUNCTION INSIDE GIVES ENERGIES INDICATED BY HORIZONTAL LINES.

FIG. 39. Phase modulation of nucleon wave function at nuclear surface.

The Doppler change of wavelength of the nucleonic wave function due to wall motion is the elementary mechanism of exchange of energy between nucleonic excitation and collective oscillation. Of this energy exchange *no such analysis as that illustrated in the diagram is permissible.* To observe the phase modulation of the immigrant wave requires freedom from subsequent reflections at the walls. Only then would space and time enough be available to analyze the frequency spectrum with sufficient precision to show up side bands corresponding to exchange of one or more vibrational quanta with the wall. For this purpose the time would have to exceed several periods of collective oscillation. But in fact the time for one traversal of the nucleus is many times *shorter* than the vibrational period. Quite the opposite of a frequency analysis, the proper way to describe the exchange of energy between particle and wall is as adiabatic readjustment of the proper function of the particle to the configuration of the wall. As the boundary changes, the wave function and energy alter, and the energy change can quite properly be attributed to Doppler effect at a moving wall. The important point is that the particle has no way to remember that the wall motion is *periodic.* Thus follows the inappropriateness of a description in terms of phase modulation.

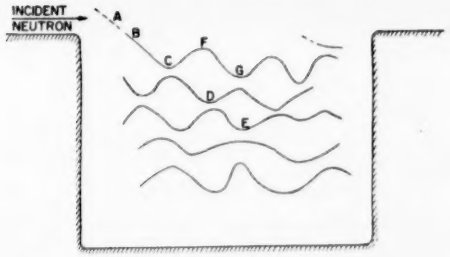

FIG. 40. Schematic representation of neutron capture on the collective model.

The hatched-in potential trough gives an impression of the relative location of the levels of zero kinetic energy inside and outside and has otherwise nothing directly to do with the main part of the diagram: A plot of potential energy surfaces for the compound nucleus as a function of a typical one of the many deformation parameters. The neutron enters and forms a virtual state of the compound nucleus at A. If the oscillational coordinate passes B before the neutron has emerged from the virtual state, then this particle is trapped, at least temporarily. The representative point of the system can then oscillate in principle over the potential energy curve ABCFG, etc. However, the excitation is so high that there can be no well-defined partition of energy between vibration and nucleonic excitation. Otherwise stated, the system jumps from one potential curve to another with a frequency large compared to what would otherwise be the natural oscillation period. Consequently the neutron very rapidly gives up its energy to the rest of the system. The mechanism of transfer is idealized in this discussion as acting entirely through the wall. This wall effect can of course be visualized in terms of Doppler effect, as illustrated in the previous figure.

The neutron is caught, so to speak, because the nodes in its wave function were so oriented relative to the wall motion that the particle lost energy by reflections from the retreating boundaries.

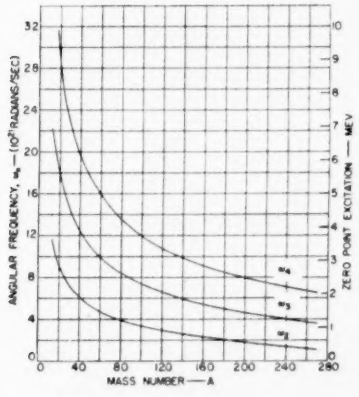

FIG. 41. Nuclear oscillational surface frequencies *versus* mass number.

Plotted as a function of mass number are the nuclear surface oscillational frequencies, $\omega_n = 2\pi\nu_n$, and the associated zero-point excitation values. The values shown follow from the classical analysis of Fig. 1. At small mass numbers the excitation energies rise sharply, but the concept of surface motion loses its validity for low mass numbers. As noted in Fig. 1, the higher the nuclear mass number, the higher the maximum mode of oscillation which may be reasonably defined, but even at mass 240 the highest order acceptable is less than 10.

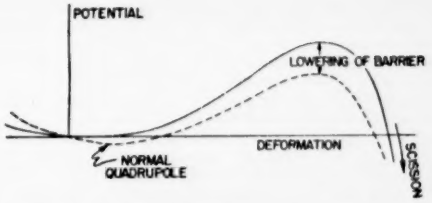

FIG. 42. Fission barrier shift associated with the ground-state quadrupole moment.

This is a schematic representation of the difference in fission threshold between the liquid drop picture and the collective model. The same individualities in potential energy surfaces which are responsible for quadrupole moments also bring about anomalies in fission barrier heights. The order of magnitude of these anomalies can be estimated by comparing the liquid drop potential curve, $V = V(\alpha)$, which near the minimum varies about as 50 Mev α^2, and at the maximum has a height of the order of 5 Mev at a value of α of the order of 0.7, with another potential curve,

$$V^* = V(\alpha) - c\alpha,$$

where the constant c is a crude measure of the quadrupole producing force. The minimum of V^* will lie near $\alpha_0 = c/100$ Mev, and the shift in the height of the maximum will be of the order

$$\delta E_f \sim c\alpha_{\max} \sim 100\ \text{Mev}\,\alpha_0\alpha_{\max} \sim 2\ \text{Mev}$$

for typical quadrupole moments, $\alpha_0 \sim 0.03$. Of course the above description is highly schematized; the actual potential energy surface will run much less smoothly as a function of deformation.

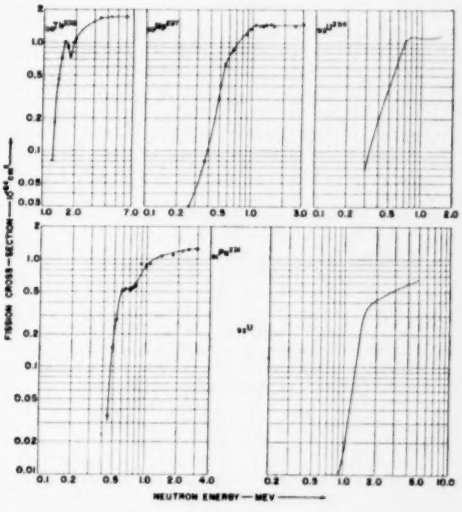

FIG. 43. Neutron fission cross section as a function of neutron energy for five fissile elements. All data are taken from the compilation of reference 29.

The features common to these five cross-sectional curves are in line with the discussion of reference 5. At low energies the probability of fission is inappreciable, until the total excitation of the compound nucleus (neutron binding plus kinetic energy of external neutron motion) approaches the height of the potential barrier to fission, as shown in Figs. 3 and 4. For excitations somewhat less than this value the cross sections show the precipitous rise characteristic of barrier penetration (Fig. 44). Beyond this excitation the cross section increases more slowly, being governed primarily by the competition with neutron emission, as alternative mode for the compound nucleus decay. For excitations several Mev in excess of the barrier height (but less than the binding energy of two

neutrons) the variation of fission cross section with energy is expected to be smooth. The fission cross section may be expected to increase substantially when the excitation becomes sufficiently high for fission still to occur after the compound system emits one or more neutrons [Bohr, reference 31].

A striking example of the possible effect of the internal state of the nucleus upon the fission probability is afforded by the observations of Street, Ghiorso, and Thompson [Phys. Rev. **84**, 135 (1952)] on the formation by neutron capture in Am^{241} of two isomers of Am^{242}, of which one decays into the other with a 16-hr half-life. They find that the ground-state form is susceptible to fission by thermal neutrons with a 6000 barn cross section, while the fission cross section is 2000 barns for the excited form. Whether this difference comes in the probability of neutron capture and emission, of de-excitation by radiation, or in the differing effects of the different internal states on the fission barrier (Figs. 6 and 42) is apparently an open question.

In studies of the photofission of thorium and uranium, G. C. Baldwin and G. S. Klaiber [Phys. Rev. **71**, 3 (1947)] found the cross sections to be peaked at 17 Mev with a 3-Mev half-width at half-maximum. This result is one of a large number of similar results, as noted by v. H. Steinwedel and J. H. D. Jensen [Z. Naturforsch. **5a**, 413 (1950)].

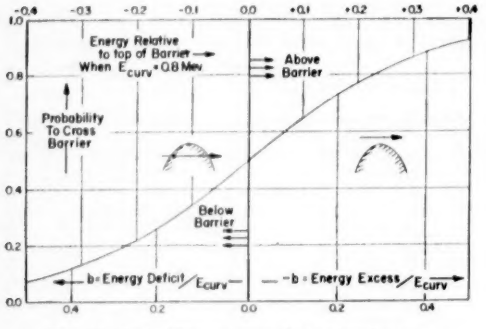

FIG. 44. Probability to cross fission barrier as a function of energy.

The probability to cross the fission barrier as a function of energy, is given by

$$P = 1/(1+e^{2\pi b}).$$

Here b is the energy deficit relative to the top of the barrier, divided by a characteristic quantum energy, E_{curv}, which is fixed by the curvature of the top of the barrier and by the effective mass associated with the fission mode of deformation. To visualize the meaning of E_{curv}, imagine the sign of the potential energy to be reversed, so that the barrier peak becomes a trough. Then the system will behave like a harmonic oscillator in the neighborhood of the critical point, with a natural circular frequency, ω_{imag}, and a characteristic quantum energy, $\hbar\omega_{imag}$. This latter quantity is by definition equal to E_{curv}. In a first approximation it is reasonable to take $\hbar\omega_{imag}$ to be equal to the characteristic quantum energy, $\hbar\omega_2$, of the lowest mode of capillary oscillation of the system about its normal nearly spherical equilibrium form, for the following reason: The potential energy, expressed as a function of deformation, will have for leading terms in its expansion

$$V(\alpha) = A\alpha^2 - B\alpha^3.$$

But this function has at its maximum the same second derivative (except for sign) that it has at its minimum, and therefore the same frequency, $\omega_{imag} = \omega_2$. We conclude that for uranium, where $\hbar\omega_2$ is estimated to be about 0.8 Mev, the characteristic curvature energy of the barrier will also be of the order of 1 Mev, thus leading to the energy scale shown in the diagram. Note that the probability for crossing the barrier is but 0.5 when the available energy first exceeds the critical energy, and only reaches a value close to unity at considerable distance above the barrier. This result is contrary to the predictions of the usual penetration formula, which would have given

$$P = \exp\left[-(2/\hbar)\int[2M_\alpha(E_{top} - \tfrac{1}{2}V''\alpha^2 - E_{available})]^{\frac{1}{2}}d\alpha\right]$$
$$= \exp[-2\pi(E_{top} - E_{available})/\hbar\omega_{imag}]$$
$$= \exp(-2\pi b).$$

The more complete penetration formula is most easily justified by writing the wave equation for the fission mode in dimensionless variables:

$$d^2\psi/dx^2 + (x^2 - 2b)\psi = 0.$$

The solution we desire represents a wave running to the right on the right-hand side of the barrier, and on the left an incident wave and a reflected wave. In terms of the parabolic cylinder function,

$$\psi = D_{-\frac{1}{2}-ib}[(1-i)x]$$
$$= [\Gamma(\tfrac{1}{2}+ib)]^{-1}\int_0^\infty dt\, \exp[ix^2/2 - (1-i)xt - t^2/2 - (\tfrac{1}{2}-ib)\ln t],$$

with the asymptotic behavior for large positive x:

$$\approx 2^{-\frac{1}{4}}x^{-\frac{1}{2}}\exp[ix^2/2 - (ib/2)\ln 2x^2 + i\pi/8 - \pi b/4],$$

and for large negative x:

$$\approx 2^{-\frac{1}{4}}|x|^{-\frac{1}{2}}\exp[ix^2/2 - (ib/2)\ln 2x^2$$
$$-3i\pi/8 + 3\pi b/4] \quad \text{(reflected wave)}$$
$$+ (2\pi)^{\frac{1}{2}}[\Gamma(\tfrac{1}{2}+ib)]^{-1}2^{-\frac{1}{4}}|x|^{-\frac{1}{2}}\exp[-ix^2/2$$
$$+ (ib/2)\ln 2x^2 + i\pi/8 + \pi b/4] \quad \text{(incident wave)}.$$

Comparison of strengths of incident and transmitted waves gives the cited penetration formula. It is valid so long as the relevant portion of the potential curve—when plotted against a dynamically uniformized deformation variable—is close to an inverted harmonic oscillator curve.

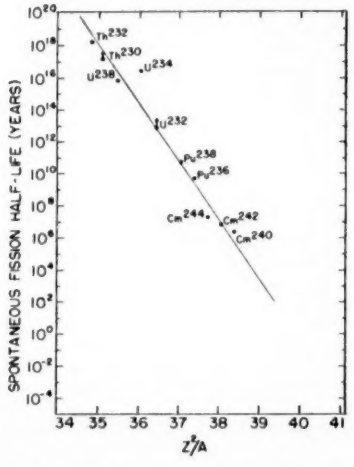

FIG. 45. Relation of spontaneous fission half-life to (Z^2/A).

By this plot of spontaneous fission half-life against (Z^2/A) G. T. Seaborg [Phys. Rev. **85**, 157 (1952)] has demonstrated the neat connection between spontaneous fission rates and the characteristic parameter (Fig. 2, and Table I) to measure fissionability in the liquid drop model. The linear relation shown holds not only for the labeled nuclei but also for the nucleus cosmium (Figs. 2, 51) for which $(Z^2/A) \approx 47$ and which undergoes spontaneous fission in a time of the order of the period of the lowest order vibration for such a nuclide as U^{238} (Fig. 1). Small deviations from the linear relation appear, in line with the expectations (Figs. 6, 26, 42) on the variation of ground-state quadrupole moments, and consequent effects on the fission barrier (Fig. 3). The analogy with the case of alpha-decay (Fig. 30) is evident. Not included on the plot is U^{235}, which undergoes spontaneous fission at a rate lower than that of U^{238}, despite the higher Z^2/A [reference 31a].

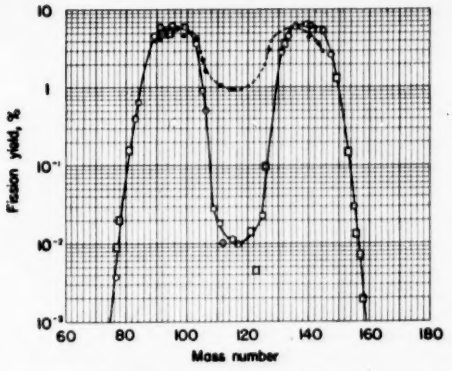

FIG. 46. U^{235} fragment mass distribution for thermal and 14-Mev neutrons.

Shown are the fragment mass distributions for U^{235} bombarded by thermal neutrons [Plutonium Project, Revs. Modern Phys. **18**, 539 (1946)] and (by the solid points) with 14-Mev neutrons [R. W. Spence, Atomic Energy Commission Unclassified Document BNL-C-9, 1949 (unpublished), Brookhaven Chemistry Conference No. 3]. Evidence that the trend toward symmetrical fission with excitation is completed is afforded by the mass distributions of the heavy elements struck by very high energy particles [P. R. O'Connor and G. T. Seaborg, Phys. Rev. **74**, 1259 (1948); R. H. Goeckermann and I. Perlman, Phys. Rev. **73**, 1127 (1948)].

A simple hydrodynamic explanation of the mass asymmetry, and its variation with energy, is proposed in Figs. 50 and 51.

Specially interesting is the observation (reference 38) that in Cm^{242}, with its half-life for spontaneous fission of 7.2×10^6 years, spontaneous fission events are sufficiently frequent to enable a study of the distribution in kinetic energy of the fragments. The pattern obtained indicates the same sort of mass distribution as is found for thermal neutron induced fission.

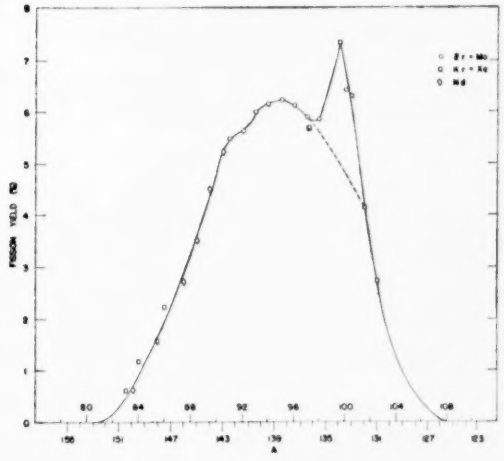

FIG. 47. Fine structure in fission mass yield.

This compilation by Glendenin, Steinberg, Inghram, and Hess [Phys. Rev. **84**, 860 (1951)] of spectrometric measurements on the fission mass yield, plotted with the heavy and light fragment yields folded over one another to produce a common curve, demonstrates a sharp deviation in a limited mass region of the yields from the smooth variation known from earlier work [Plutonium Project, Revs. Modern Phys. **18**, 539 (1946)]. The masses involved in this deviation are consistent with the hypothesis that it follows from the effects of nuclear shells on fission, contrary to the dominant asymmetry of the smooth curve itself.

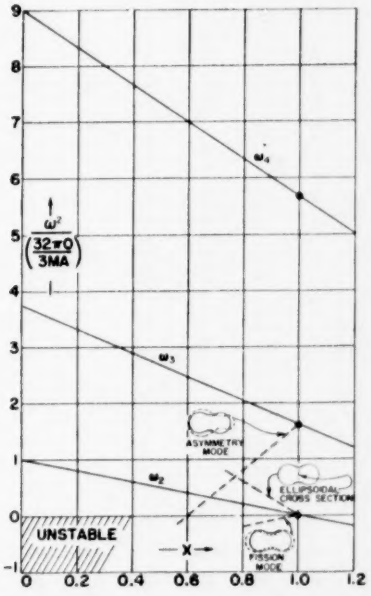

FIG. 48. Characteristic circular frequencies, ω, of the lowest modes of oscillation of an incompressible uniformly charged liquid droplet of mass AM and surface tension O as a function of the fission instability parameter x for the spherical form (smooth lines) and for the symmetrical critical form of unstable equilibrium (dashed lines; estimates obtained by calculating limiting slope in neighborhood of $x=1$; i.e., for nuclei differing from the spherical by only a very slight ellipsoidal deformation).

The five independent degenerate modes of vibration of the sphere of order $n=2$ are describable in terms of radial extensions proportional to the five harmonics $P_2(\cos\theta)$, $P_2^{(1)}(\cos\theta)[\cos\phi$ or $\sin\phi]$, $P_2^{(2)}(\cos\theta)[\cos2\phi$ or $\sin2\phi]$, but these vibrations can also be visualized in terms of revolution of a hump of material over the surface of the sphere (three degrees of freedom) and two types of pure vibration. It is assumed here that the system has no angular momentum, although allowance for rotation would produce a number of complicated and interesting subdivisions of the curves shown here. The two vibration frequencies are distinct for the critical form of unstable equilibrium. The first mode of deviation from the saddle point moves in the direction of decreasing potential energy, either an extension leading to fission or a contraction towards the normal spherical form. The second moves uphill from the saddle point. In it the cross sections of the figure cut normal to the symmetry axis undergo ellipsoidal oscillations about the normal circular form without the length of the dumbbell undergoing change.

Of the subcomponents of the vibration of third order we consider for the forms of unstable equilibrium only that particular one which is of lowest frequency, is axially symmetric, and is the better described by the harmonic $P_3(\cos\theta)$ the more closely x approaches 1. This vibration represents a coursing of fluid to and fro through the neck of the dumbbell—an asymmetry oscillation. Its frequency becomes the less the smaller is x, and vanishes for some value of $x=x_{\text{crit}}$ not yet known, perhaps near $x=0.65$. For lower values of x the symmetric saddle point configuration still exists, but two new and unsymmetric saddle point configurations come into existence which are lower in energy. If x for uranium is significantly greater than x_{crit}, as may well be the case, then the asymmetric saddle points should neither exist nor have anything to do with the observed asymmetry of fission for uranium.

W. J. Swiatecki [Phys. Rev. **83**, 178 (1951)] in a brief note has given reasons for believing that the compressibility and polarizability of nuclear matter will favor the development of the asymmetric saddle points; i.e., depress the lowest component of ω_3, in the present manner of describing the situation. However, it is not clear that this interesting effect is great enough to make the saddle point of uranium asymmetric.

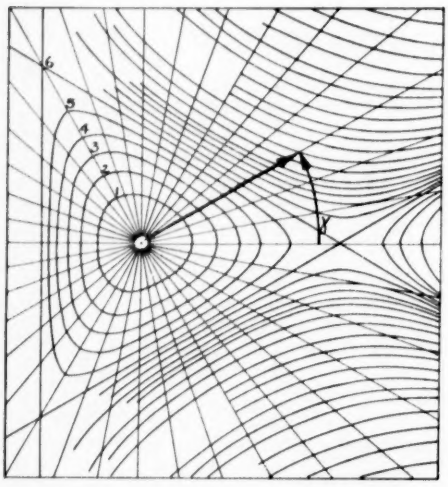

FIG. 49. Contour map of barrier against fission in the idealized limit of a fission criticality parameter close to $x^*=1$.

Only a small deformation is required to carry the system to the saddle point for passage over the barrier. The only deformations considered in the diagram are of ellipsoidal character, as there is no instability in distortions described by spherical harmonics of higher order. The ellipsoidal deformations are measured in terms of polar variables in the diagram: a "deformation magnitude" α (radius) and a "shape parameter" γ (angle), as defined in Fig. 13. There are three saddle points in the diagram because a prolate extension along any one of the three principal axes of the ellipsoid will result in fission. The present idealized picture is based entirely on the simple liquid drop model. No account is taken of any intrinsic quadrupole moment nor of any angular momentum of the nucleus. The deformation energy in the lowest relevant order of approximation is

$$V(\alpha,\gamma)=4\pi R_0^2O\{[2(1-x-z)/5]\alpha^2-[(12x+20z)/105]\alpha^3\cos3\gamma\}$$
$$=B[(u^2/2)-(u^3/18)\cos3\gamma]=Bf(u,\gamma).$$

Here $4\pi R_0^2O=14$ Mev $A^{\frac{2}{3}}$ is the normal surface tension energy and x and z the parameters defined earlier, whose sum, x^*, is the relevant criticality parameter. In the alternative way of writing deformation energy on the second line, B is a constant with the units of energy, in terms of which the height of the top of the barrier is 6. The contour diagram gives the dimensionless quantity $f=V/B$ as a function of γ and the multiple, u, of α:

$$u=(18x+30z)\alpha/7(1-x-z).$$

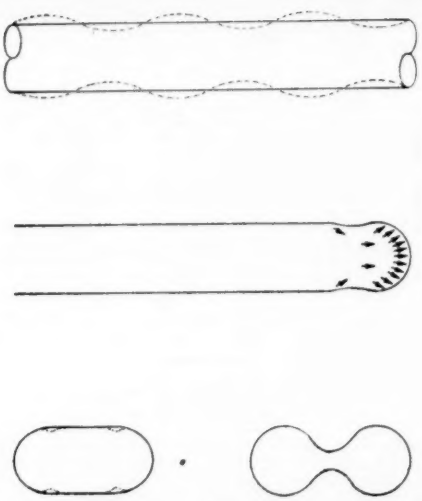

FIG. 50. A qualitative classical hydrodynamical interpretation of the asymmetry of nuclear fission.

The critical form of unstable equilibrium for a nucleus in the vicinity of uranium is so much like an elongated cylinder (Fig. 2) that we are invited to consider the stability of a long jet of incompressible uniformly electrified fluid endowed with a surface tension. Were the charge density zero, the jet would be unstable against small disturbances with wavelength greater than the jet's circumference, as is well known. Such disturbances are the first step in reassembly of the fluid into separated spheres of the same mass but smaller surface. The size of the eventual spheres is the greater the longer the wavelength. The presence of even a small volume electrification makes reassembly of the fluid into very large spheres energetically unfavorable. Consequently, the charge stabilizes the jet against disturbances of long wavelength, just as the surface tension works against deformations of short wavelength. The intermediate zone of wave numbers, k, of instability becomes the narrower the larger the charge density. Total stability occurs when

$$y=\frac{2(\text{charge per unit length})^2}{\pi(\text{radius})(\text{surface tension})}\geq y_{\text{crit}}\doteq 1.125.$$

This condition is satisfied for U^{235} by the critical Metropolis-Frankel forms for the fissionability parameter $x=4\pi R_0^3\rho_e^2/30O=0.74$. The radius R of the cylindrical part of the figure is $0.64R_0$; and

$$y=2\pi R^3\rho_e^2/O=2\pi\times0.74\times(30/4\pi)(R/R_0)^3=2.92.$$

How can a repulsive force produce such stability? Only by virtue of the ends of the cylinder being at infinity. Consider instead a cylinder of finite length. The capillary force will round off the ends, but be unable to withstand the repulsion of the long column of electric charge. A sizeable drop will break off the end—the elementary act of fission, and of a fission which is very asymmetric indeed. How asymmetric? Let L represent the distance from the end at which the cylinder starts to neck in, and let ϵ represent the diminution in radius at this point. Out of the neck into the incipient drop has been squeezed a volume of fluid of the order

$\epsilon 2\pi RL$, thus carrying the drop forward and diminishing the electric energy of the system by an amount $\sim 2\pi^2\epsilon L^2R^2\rho_e^2$, which goes into kinetic energy $\sim\rho_m(\dot{\epsilon}^2L^2/R^2)\pi R^2L$. Consequently, ϵ/R, the fractional necking off, goes in the beginning as $(t/t_{\text{crit}})^2$, where

$$t_{\text{crit}}\sim(L\rho_m/R\rho_e^2)^{\frac{1}{2}}.$$

The shortest growth constant and fastest necking-in is found for a neck length L of the same order as the radius, for the character of the expression for t_{crit} changes for smaller L. We conclude that successive fragments from this machine-gun type of fission will all have roughly the same size.

The following picture suggests itself for the division of a nucleus like U^{236}, when the available excitation is only little in excess of the threshold requirement. On arrival at the fission barrier the system has so little energy of movement that the nucleus remains for an appreciable time in a form not very different from the elongated shape of unstable equilibrium. This configuration resembles that of a cylinder of electrified fluid. In a crude approximation we may say that, in so far as the behavior of one end of the cylinder is concerned, the other end might as well be indefinitely far away. At each end we will expect the machine-gun type of fission to start. At which end necking-in first starts will be an accident. Once started at one end, however, this type of deformation will grow so rapidly that it will ordinarily soon get far ahead of anything that is happening at the other end, and a fragment will come off with length roughly comparable to its diameter ("light fission fragment").

Moreover, the separation of the two ends is really not large. Between them there is a significant interaction. The start of necking-in near one end will increase the curvature and hence the tautness of the surface near the other end. The effect will inhibit the necking-in which would otherwise have started near the other end, but a little later. Thus there comes about a division into a large and a small fragment. This suggested mechanism for the origin of fission asymmetry is a straightforward application of the most elementary notions of surface tension, electrostatics, and hydrodynamics.

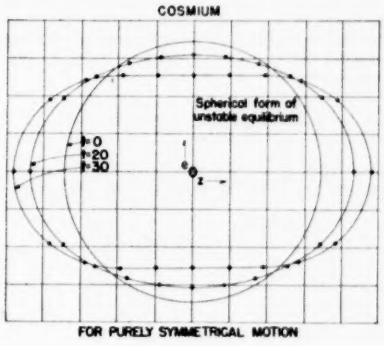

FIG. 51(a)

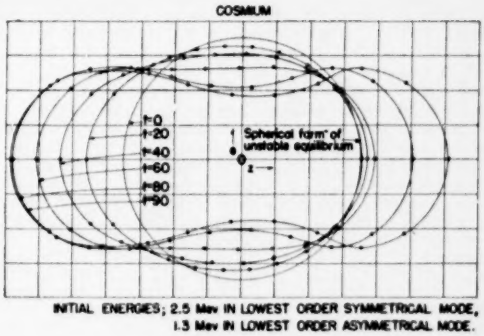

(b)

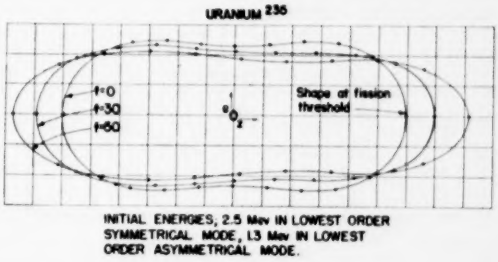

(c)

FIG. 51. Results of dynamical analysis of nuclear fission carried out [D. L. Hill, Phys. Rev. **78**, 330 (1950); **79**, 197 (1950); Ph.D. dissertation, Princeton University, Princeton, New Jersey (unpublished)] on the basis of simple liquid drop model.

These International Business Machine Corporation—endowed electronic computations started with a configuration near the point of unstable equilibrium and followed out the motion by way of the classical hydrodynamic equations for an incompressible fluid with surface tension and uniform volume density of electrification. From the preceding figure the working hypothesis suggests itself that inevitable small asymmetries in the form of the nucleus in the transition state become magnified in the subsequent course of the motion, and lead to a necking-off of the elongated figure near one end or the other in the great majority of the cases. The hydrodynamic phenomena were described by classical mechanics. However, the size and origin of the small initial asymmetries were considered to be connected with the quantal zero-point amplitudes of the various modes of capillary oscillation.

With increasing excitation of the compound nucleus, there will be an increase in the irregularities in the nuclear surface at the moment of passage over the fission barrier, over and above the effect of the zero-point oscillations. These irregularities will increasingly affect the location of the point at which necking-in commences. A sufficiently great displacement of the normal point of necking-in will lead to symmetric fission. The relative probability of symmetric fission will therefore be expected to rise with

increasing excitation energy. Two cases were considered: "cosmium," that unrealizable nucleus for which the fission criticality parameter $x=(Z^2/A)/(Z^2/A)_{crit}=1$; and a droplet for which $x=0.74$, estimated to come close to simulating the case of U^{235}. Axial symmetry was assumed in all the calculations. Cosmium was started off in the first calculation with a very small deformation of the second order, which remained symmetric as it grew ($t=20$ signifies a time of $20\times6.66\times10^{-23}$ sec). In the second calculation on cosmium a deformation of order three was superposed on the symmetric deformation, with such a magnitude as to correspond to the zero-point energy estimated for the asymmetric mode. In this case the small initial asymmetry multiplied itself in the course of time in such a way as to suggest an eventual division into two fragments of rather different size. This growth of asymmetry arises from the dynamics of the fission process. In this case there cannot be any question of asymmetry in the saddle point configuration, for that is the spherical form itself. In the third case, $x=0.74$, a small initial asymmetry superposed on the initial symmetrical Metropolis-Frankel saddle point configuration again multiplies itself in such a way as to appear to favor division into quite unequal parts. The calculations were broken off in all cases well before neck-off because the mesh was not fine enough to treat the narrowing part of the neck accurately. The results cannot be considered to prove, but are at least consistent with, the view that fission asymmetry is a classical hydrodynamic effect.

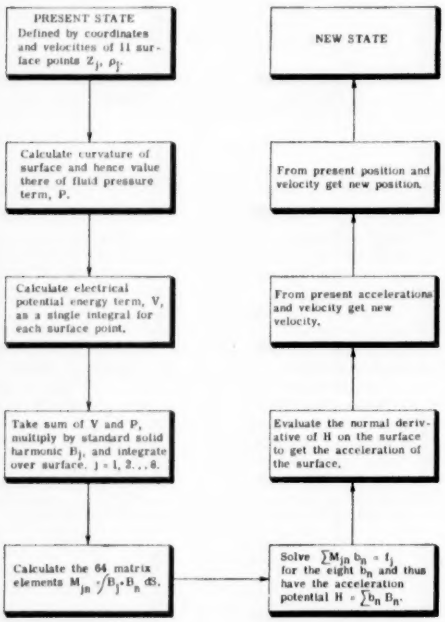
PRESENT STATE
Defined by coordinates and velocities of 11 surface points Z_j, ρ_j.
Calculate curvature of surface and hence value there of fluid pressure term, P.
Calculate electrical potential energy term, V, as a single integral for each surface point.
Take sum of V and P, multiply by standard solid harmonic B_j, and integrate over surface, j = 1, 2 . . . 8.
Calculate the 64 matrix elements $M_{jn}=\int B_j B_n\, dS$.
Solve $\sum M_{jn} b_n = f_j$ for the eight b_n and thus have the acceleration potential $H=\sum b_n B_n$.
NEW STATE
From present position and velocity get new position.
From present accelerations and velocity get new velocity.
Evaluate the normal derivative of H on the surface to get the acceleration of the surface.

FIG. 52. Schematic flow sheet of hydrodynamic calculations illustrated in the preceding figure.

The motion is taken to be irrotational flow of incompressible fluid, so that the velocity can be expressed as $\mathbf{u}=-\text{grad}\phi$, where $\nabla^2\phi=0$, $u_n=-\partial\phi/\partial n$ gives the normal component of the velocity of the fluid surface, and the time rate of change of the velocity potential is

$$\partial\phi/\partial t=\tfrac{1}{2}(\text{grad}\phi)^2+V+P\equiv H.$$

The quantity $H-\frac{1}{2}(\text{grad}\phi)^2$ is the acceleration potential; P is the pressure divided by the density, taking values at the surface determined only by the local curvature κ,

$$P_{surf}=(O\kappa/\rho_m)=(O/\rho_m)\{\rho^{-1}[1+(d\rho/dz)^2]^{-\frac{1}{2}} -(d^2\rho/dz^2)[1+(d\rho/dz)^2]^{-\frac{3}{2}}\},$$

where O is specific surface energy and ρ_m is mass density; and V is the electrical potential energy of a unit mass element, expressible in cylindrical polar coordinates z and ρ as

$$V_1=(\rho_e^2/\rho_m)\int d\tau_2/r_{12}$$
$$=2(\rho_e^2/\rho_m)\int\left\{d z_2\rho_2\frac{[\rho_2+\rho_1+(z_1-z_2)d\rho_2/dz]K-2\rho_1 D}{[(\rho_1+\rho_2)^2+(z_1-z_2)^2]^{\frac{1}{2}}}\right\},$$

where $K(k)$ and $D(k)=[K(k)-E(k)]/k^2$ are defined in terms of complete elliptic integrals of the argument k,

$$k^2=4\rho_1\rho_2/[(\rho_1+\rho_2)^2+(z_1-z_2)^2],$$

and ρ_e is the electrical charge density. The actual system with its infinitude of degrees of freedom is replaced by a system with a limited number of degrees of freedom: the location of eleven tracer points which are considered to define the surface. The locations of the two points at the two poles of the figure are specified by coordinates z_0 and z_{10}. The nine other points have z coordinates, z_j, equally spaced between z_0 and z_{10}. Eleven independent position coordinates z_0, ρ_1, ρ_2, $\cdots$, ρ_9, z_{10}, and eleven corresponding velocity coordinates thus give the state of the system at one time. At the next instant the new positions follow purely kinematically from the old positions and velocities; while the new velocities follow equally simply as soon as the old accelerations have been found from the acceleration potential:

$$d\mathbf{u}/dt=-\text{grad}(H-u^2/2).$$

The quantity H has zero Laplacian in the interior, and on the surface a value which is known from the old state of the system. In the calculations the term $u^2/2$ is neglected, both when it appears in the boundary conditions for H and when it is subsequently subtracted from H, as the 170-Mev kinetic energy of fission is small compared with perhaps 540-Mev surface energy and 780-Mev electrostatic energy of the relevant nuclei. In the computations H was represented as a sum,

$$H(z,\rho,t)=\sum_{n=1}^{8} b_n(t)B_n(z,\rho),$$

of eight solid harmonics, with the b_n chosen at the time interval in question so as to minimize the departure of H from its proper boundary value:

$$\int(H-V-P)_{surface}^2 dS=\text{minimum}.$$

From this requirement follows an 8×8 system of linear equations for the coefficients $b_n(t)$:

$$\Sigma M_{jn}b_n=f_j,$$

where

$$M_{jn}=\int B_j B_n dS \quad\text{and}\quad f_j=\int B_j(V+P)dS$$

can be found from the state of the system at the old times. Thus the whole cycle of calculations is advanced to the new time.

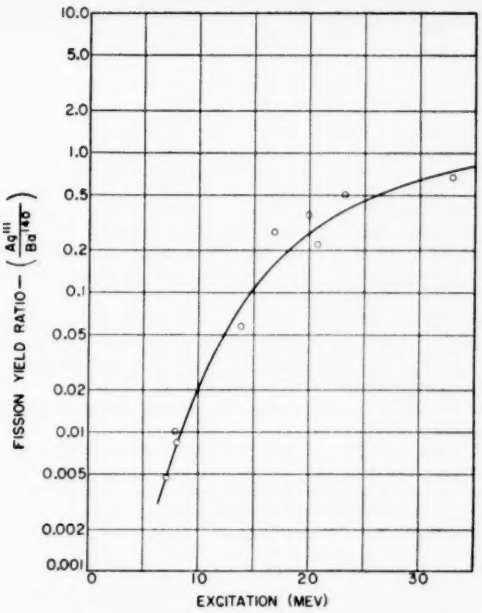

FIG. 53. Fission asymmetry as function of initial excitation.

The fission yield of Ag^{111} relative to the yield of Ba^{140} provides a measure of the asymmetry of the mass division, for experience indicates (Fig. 46) that the entire yield curve varies in an approximately uniform way with excitation energy. The yields here plotted as a function of the excitation in the original nucleus are obtained (references 36 and 37) from the bombardment of several different fissile elements by several different projectiles. Moreover, for the high excitations indicated, the excited compound nucleus will usually emit several neutrons before splitting. Nevertheless, we note that the mass division which finally occurs shows an over-all trend toward increasing symmetry with increasing excitation of the initial nucleus.

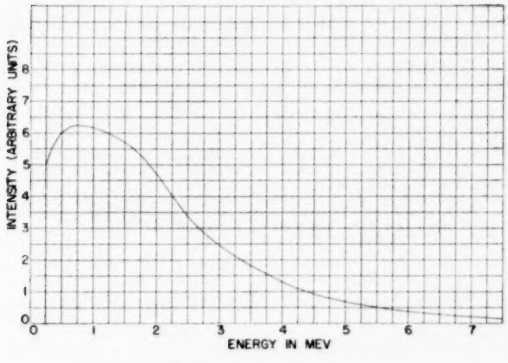

FIG. 54. U^{235} fission neutron spectrum.

Recently published papers [Bonner, Ferrell, and Rinehart, Phys. Rev. **87**, 1032 (1952); D. L. Hill, Phys. Rev. **87**, 1034 (1952); B. E. Watt, Phys. Rev. **87**, 1037 (1952)] dealing with the low, medium, and high energy neutrons emitted in the fission of U^{235}, enable us to draw qualitative conclusions on the manner in which they are released. The three measurements fit nicely together to yield a total distribution-in-energy consistent with the hypothesis that the neutrons are emitted from the excited fragments with distributions-in-energy characteristic of nuclear evaporation [J. M. Blatt and V. F. Weisskopf, *Theoretical Nuclear Physics* (John Wiley and Sons, Inc., New York, 1952), while the fragments are in rapid motion. The broad spread in excitation of the fission fragments gives a further spread in the number and energy of the neutrons emitted in different fission acts. Finally, the neutrons are emitted, in this hypothesis, at a spread of angles relative to the parent fragment motion which we know according to the work of Brunton, Hanna, and Thompson [Can. J. Research **28A**, 190 (1950); **28A**, 498 (1950)] to have a spread of kinetic energies of at least 20 Mev for a typical mass division. The resultant energy spectrum observed in the laboratory is thus averaged many times over different sorts of energy spreading effects.

The curve shown is taken from D. L. Hill [Phys. Rev. **87**, 1034 (1952)], being deduced from the range spectrum of recoil protons detected with an assembly of proportional counters. The maximum near 0.8 Mev is corroborated by Bonner, Ferrell, and Rinehart [Phys. Rev. **87**, 1032 (1952)]; the high energy side of the spectrum falls off exponentially with a 1.6-Mev relaxation energy, in agreement with Watt's result [Phys. Rev. **87**, 1037 (1952)].

The fission neutron intensity observed is compatible with the announced value (U. S. Atomic Energy Commission release) of 2.5 neutrons per thermal neutron induced fission of U^{235}.

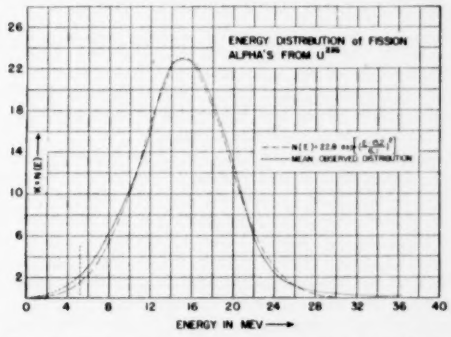

FIG. 55. U^{235} α-particle spectrum, coincident with fission.

Of the many different modes of ternary fission listed in Table III, by far the most intensively studied are the long-range alpha particles coincident with fission. Reproduced here is a measurement (reference 54) of the energy distribution of these particles. The close match of this distribution to a Gaussian curve over the high intensity region is indicated by the dashed line.

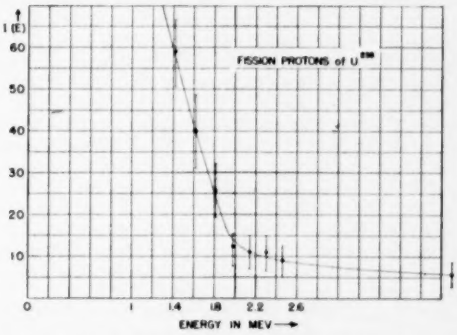

FIG. 56. U^{235} fission proton energy distribution.

This curve shows the energy distribution of the protons listed in Table III as being emitted in a rare mode of ternary fission. Although they are somewhat too numerous to be readily explained as arising by (n, p) or (fragment, p) reactions, the energy distribution indicates that they are not associated with the fission mechanism in a manner similar to the particles of the preceding figure. For particles which have penetrated through a potential barrier, one expects a peak at the right side of the graph rather than a monotonic fall. It is unreasonable to believe that these "fission" protons have anything directly to do with the act of fission.

Letters to the Editor

PUBLICATION of brief reports of important discoveries in physics may be secured by addressing them to this department. The closing date for this department is five weeks prior to the date of issue. No proof will be sent to the authors. The Board of Editors does not hold itself responsible for the opinions expressed by the correspondents. Communications should not exceed 600 words in length and should be submitted in duplicate.

Identification of the Seven-Hour Mo^{93} Isomer

D. E. ALBURGER* AND S. THULIN
Nobel Institute of Physics, Stockholm, Sweden
(Received January 6, 1953)

THE seven-hour isomer of molybdenum is known[1,2] to decay by a 0.3-Mev lifetime determining transition followed by two cascade gamma-rays of 0.7 and 1.5 Mev. From the $K/(L+M)$ ratio of 2.8±0.3 and the energy 256 kev measured[3] by the group at Brookhaven, the isomeric transition was shown[4] by Goldhaber and Sunyar to be an $E4$ type. Ruby and Richardson later obtained[5] an energy of 262 kev and a $K/(L+M)$ ratio of 2.9±0.2 for the 7-hour transition and the values 692±11 kev and 1.51 ±0.035 Mev for the cascade gamma-rays.

Although a mass number 93 has been tentatively assigned[1] to this isomer, it is difficult to understand why the activity cannot be formed by the (d,p) or (n,γ) reactions on Mo^{92} or the (γ,n) reaction on Mo^{94}. Also, this mass number is not consistent with the predictions of shell theory, as pointed out[3] by Goldhaber and Hill. Recently, more evidence in favor of the mass 93 assignment was obtained[6] by Boyd and Charpie who studied the excitation functions for the production of 7-hour Mo and 10-day Nb^{92} formed by proton bombardment of Nb. Their data indicated that the first of these is due to the (p,n) reaction and the second due to the (p,pn) reaction on Nb^{93}. They concluded that the 7-hour isomer probably belongs to Mo^{93}.

We have made a direct mass assignment of this activity in the isotope separator at the Nobel Institute using sources obtained by bombarding Nb metal powder with deuterons. The cyclotron targets were prepared by forcing the powder under very high pressure into the surface of a copper block from which it could be scraped after the bombardment. Irradiations of 80 microampere-hours were made at a beam energy of 25 Mev, after which the active powder was introduced into a perforated lava tube and inserted in the separator ion source. This was arranged so that chlorine gas could pass through the powder and extract the activity in a manner somewhat similar to the technique used[7] by Keim at Oak Ridge. The lava tube was heated indirectly to a few hundred degrees by the ion source filament. It had been shown beforehand that the chlorine method gave strong lines from the stable isotopes of molybdenum when Mo metal powder was used in the ion source. With the bombarded niobium powder samples, stable Nb^{93} was also extracted by the chlorine and could be identified at once on the separator viewing screen by comparing the position of its line with those of the stable krypton isotopes and with three lines resulting from doubly-ionized $W^{182,183,184}$.

Separation of the Mo activity was carried out for 2 hours at a current of 1–3 microamperes on a 2.5 mg/cm² Al collector foil. A blackening of the foil at mass number 93 as a result of stable Nb^{93} was observed. By counting areas of the collector covering 10 successive mass units beginning with 88 and also from a radioautograph of the foil, it was established that the only activity present was at mass number 93.

A 6-mm wide strip at mass number 93 was then cut from the collector foil (adjacent masses in this region are about 9 mm apart) and examined in the double-focusing spectrometer. Figure 1 shows the internal conversion spectrum from this sample measured at a resolution of 0.8 percent. The energy of the transition is

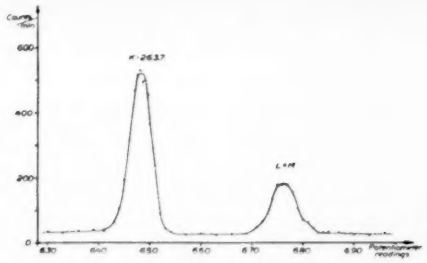

FIG. 1. Internal conversion spectrum of the Mo^{93} separated sample.

263.7±1.0 kev, and the $K/(L+M)$ ratio 2.79±0.15 is in favorable agreement with earlier results. The M line is not quite resolved but from the appearance of the curve probably accounts for 20–30 percent of the $L+M$ component. The half-life of 7 hours used to correct for decay was later checked by measuring the activity on the foil.

The gamma-rays from an unseparated portion of the active Mo were examined in the double-focusing spectrometer by observing the external conversion electrons from a 9-mg/cm² gold foil. Figure 2 shows the photolines and Compton electrons corresponding to the isomeric transition and two gamma-rays of 0.685±0.003 and 1.479±0.005 Mev. The total decay energy based on these measurements is 2.428±0.006 Mev.

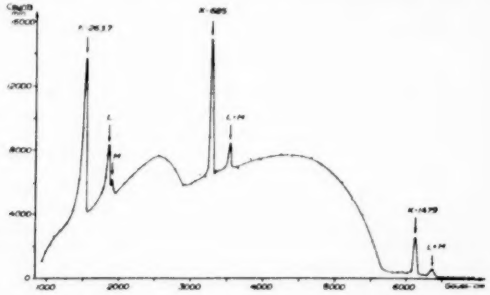

FIG. 2. External conversion of Mo^{93} gamma-rays in a 9-mg/cm² gold foil (unseparated sample).

We are indebted to Dr. H. Atterling for designing the Nb targets and arranging for the cyclotron irradiations.

* National Science Foundation Fellow on leave from Brookhaven National Laboratory.

[1] Kundu, Hult, and Pool, Phys. Rev. **77**, 71 (1950).
[2] M. Goldhaber and R. D. Hill, Revs. Modern Phys. **24**, 179 (1952).
[3] D. Alburger *et al.*, Brookhaven National Laboratory Report BNL 82(S-7), 1950 (unpublished).
[4] M. Goldhaber and A. W. Sunyar, Phys. Rev. **83**, 906 (1951).
[5] L. Ruby and J. R. Richardson, Phys. Rev. **83**, 698 (1951).
[6] G. E. Boyd and R. A. Charpie, Phys. Rev. **88**, 681 (1952).
[7] C. P. Keim, Nucleonics **10**, No. 8, 29 (1952).

"Core Isomerism"—Remarks on Mo^{93m}†

M. GOLDHABER
Brookhaven National Laboratory, Upton, Long Island, New York
(Received January 19, 1953)

IT has been pointed out[1] that the 7-hr Mo isomer behaves in some respects as if it were an even-even nucleus. Now that this activity has been definitely assigned to an odd mass number, both by the study of the $Nb^{93}(p,n)$ excitation function[2] and by a direct mass spectrographic determination,[3] it seems appropriate to discuss the probable mode of excitation of Mo^{93m} further. This isomer lies outside the usual odd A "islands of isomerism," and it appears that we are dealing here with a case of "core isomerism" where the isomerism can be ascribed to an excitation of the

even-even core to a high spin state, probably 8+. This may be obtained by breaking a $g_{9/2}$ pair of protons and putting one of the protons into a $g_{7/2}$ state. The odd neutron probably remains in a $g_{7/2}$ state throughout the three-step isomeric transition while the core goes from $8+\rightarrow 4+\rightarrow 2+\rightarrow 0+$. Thus, the spin of Mo^{93m} may be as high as $(8+)+g_{7/2}=23/2+$, and this is supported by the absence of cross-over transitions.[4]

The total excitation energy of Mo^{93m}, 2.43 Mev,[3] is of the order expected on the assumption that it is due to the breaking of a $g_{9/2}$ proton pair (1–2 Mev) and the flipping of a spin $g_{9/2}\rightarrow g_{7/2}$ (spin orbit coupling energy ~1.5 Mev). The low cross section of the $Nb^{93}(p,n)Mo^{93m}$ reaction[5] and the lack of success of attempts to produce Mo^{93m} by (d,p), (n,γ), and (γ,n) reactions (see reference 1) may be connected with the unusual character of this state. General consideration on even-even nuclei[6] indicate that "core isomerism" should be a rare phenomenon.[7]

My thanks are due Dr. Boyd, Dr. Charpie, Dr. Alburger, and Dr. Thulin for informing me of their results before publication.

† Work performed under the auspices of the U. S. Atomic Energy Commission.

[1] M. Goldhaber and R. D. Hill, Revs. Modern Phys. **24**, 179 (1952).
[2] G. E. Boyd and R. E. Charpie, Phys. Rev. **88**, 681 (1952).
[3] D. E. Alburger and S. Thulin, preceding letter [Phys. Rev. **89**, 1146 (1953)]; R. Bernas and S. Beydon, Compt. rend. **236**, 194 (1953).
[4] A search for cross-over transitions was made by Alburger, der Mateosian, Friedlander, Goldhaber, Scharff-Goldhaber and Sunyar (unpublished) who used scintillation counters as well as (Be, D) photoneutron detectors.
[5] Blaser, Boehm, Marmier, and Preiswerk, Helv. Phys. Acta **24**, 441 (1951).
[6] G. Scharff-Goldhaber, Phys. Rev. **87**, 218 (1952); Physica (to be published); Phys. Rev. (to be published).
[7] The question may be raised: Where are the many excited states expected in this energy range (≤ 2.4 Mev) from the one-particle excitation ($d_{5/2}$, $d_{3/2}$, $h_{11/2}$, $\cdots$) and from coupling of the $g_{7/2}$ neutron to the excited states of the core? They may, indeed, exist without showing up in the γ-ray transitions. If their energy does not differ considerably from the states which are populated in the decay of the isomer, they may be bypassed because transitions of minimum spin change win out. They should, however, be expected to show up under different excitation conditions.

Energy Loss and Čerenkov Radiation of a Relativistic Ionizing Particle

P. Budini
Department of Physics, University of Trieste, Trieste, Italy
(Received December 19, 1952)

In the energy region where the bremsstrahlung is still not effective, the energy lost by a relativistic ionizing particle in traversing a material medium contributes essentially to the following three phenomena: (a) ionization of the atoms of the medium; (b) excitation of the atoms of the medium; (c) emission of the Čerenkov radiation.

At impact parameters larger than $\rho_0\approx 10^{-8}$ cm, the calculation of the energy lost in processes like (a) or (b) leads to the formula:

$$\left.\frac{dW_\sigma}{dx}\right|_{>\rho_0}=\frac{ne^2c}{\pi v^2}\int_0^\infty\frac{\sigma(\omega)}{|\epsilon(\omega)|^2}\left\{\log\frac{4v^2}{\gamma^2\omega^2|1-\epsilon(\omega)\beta^2|\rho_0^2}-\beta^2\,\mathrm{Re}[\epsilon(\omega)]\right\}d\omega, \quad (1)$$

where $\sigma(\omega)$ is the atomic cross section, related to the process considered, for a photon of frequency ω, n is the number of atoms per cm³, and $\epsilon(\omega)$ is the frequency-dependent dielectric constant of the medium. All other symbols have the conventional significance. $\mathrm{Log}\gamma=0.577\cdots$.

The energy lost by direct excitation (that is, neglecting[1] reabsorption of the Čerenkov radiation) can be calculated by substituting in the preceding relation

$$\sigma(\omega)=-\mathrm{Re}[i\omega\epsilon(\omega)/cn]. \quad (2)$$

For the energy lost in processes (c) we have found the formula

$$\frac{dW}{dx}=\frac{e^2}{v^2}\int_{\check{C}erenkov}\left[\beta^2-\frac{\mathrm{Re}[\epsilon(\omega)]}{|\epsilon(\omega)|^2}\right]\omega d\omega, \quad (3)$$

where the integration is to be performed over all frequencies for which

$$\mathrm{Re}[\epsilon(\omega)]>\beta^{-2}\quad(\text{Čerenkov frequencies}). \quad (4)$$

It should be pointed out that, when the emitted radiation is to be observed at the distance ρ, the supplementary condition $\beta^2(\omega/v)\,\mathrm{Im}[\epsilon(\omega)]\rho\ll 1$ should be added.

When the damping constants are not too large, one gets, by adding Eq. (3) to Eq. (1) [and using (2)], the well-known Fermi[2] formula giving the total amount of energy emitted by the ionizing particle to a distance larger than ρ_0. The repartition of this energy between Eq. (3) and Eq. (1) [with (2)] depends critically on the value of the quantity

$$\Theta_i=mg_i\omega_i/4\pi Ne^2f_i, \quad (5)$$

where ω_i, f_i, and g_i are, respectively, the frequency, the oscillator strength, and the damping constants relating to the ith spectral line, and N = number of electrons per cm³. When $\Theta_i\ll 1$ (dense media with narrow lines), the relativistic increase of the energy loss beyond the minimum relative to the ith line is caused by the emission of Čerenkov radiation, while the energy lost in excitation of the corresponding line does not show any increase (as in the case discussed by Schönberg,[3] who puts $g_i=0$). When $\Theta_i\ll 1$ (dense media with wide lines, or rarified gases) Eq. (1) [with (2)] gives

$$\left.\frac{dW_{exc}}{dx}\right|_{>\rho_0}=\frac{2\pi Ne^4}{mv^2}\sum_{i=1}^{r}f_i\left\{\log\frac{4v^2}{\gamma^2\omega_i^2\rho_0^2[(1-\beta+\beta^2D_i)^2+\beta^2\Theta_i^{-2}]^{\frac{1}{2}}}-\beta^2\right\}, \quad (6)$$

where

$$D_i\approx\frac{4\pi Ne^2}{m\omega_i^2}\sum_{j=1}^{i-1}f_j.$$

Hence, it is seen that the Bethe-Bloch formula is valid for energies E satisfying the condition

$$E^2\lesssim\beta^{-2}(D_i^2+\Theta_i^{-2})^{-\frac{1}{2}}, \quad (7)$$

which determines the upper limit of the energy, below which there is no Čerenkov radiation from the corresponding band.

The expected behavior of the ionization may be discussed classically, considering the transition to the continuum as pertaining to wide bands ($\Theta_i\ll 1$) and therefore described by Eq. (6). According to the two following conditions:

$$\text{Case I:}\quad D_i>\Theta_i^{-1},$$
$$\text{Case II:}\quad D_i<\Theta_i^{-1},$$

the saturation of the ionization occurs gradually (I), as expected from the Halpern and Hall[4] formula, or more sharply (II). (See Fig. 1.)

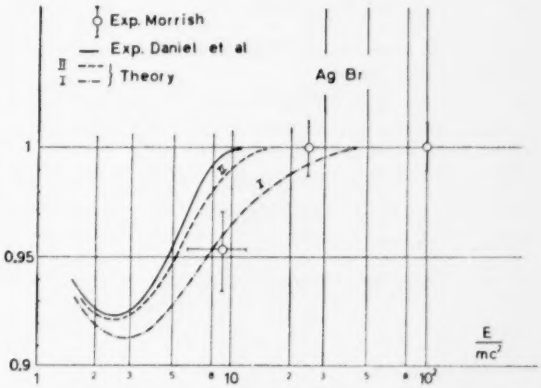

FIG. 1. Total rate of ionization in silver bromide (transfers less than 5 kev). The dashed curve II is computed with Eq. (6) and $D_i<\Theta_i^{-1}$. The dot-dash curve I is computed with Eq. (6) and $D_i>\Theta_i^{-1}$.

Preliminary calculations have been carried out on the basis of Eq. (6) for emulsions. For Ag and Br one should expect to have an intermediate case between I and II, but nearer to II than to I. A more precise definition is difficult since the photoelectric cross sections of Ag and Br as functions of the energy of the incident photon are not very well known. We have carried out calculations in both limiting cases I and II. The results are reported in Fig. 1 together with the experimental data of Morrish[5] and Daniel *et al.*,[6] both experimental and theoretical curves being normalized to 1 for $E\to\infty$.

According to this theory, as the kinetic energy of the ionizing particle becomes larger than its rest energy, a relativistic increase of both the specific ionization and the emitted Čerenkov radiation should be expected in dense media. In gases, there should be an increase of specific ionization and of excitation. In this case the emission of Čerenkov radiation of moderate intensity should become appreciable only at larger energy.

A detailed account of this work will be published in *Il nuovo cimento*.

[1] The absorbed Čerenkov radiation in a grain of emulsion is less than 1/50 of the emitted one, given by Eq. (3): P. Janssens and M. Huybrechts, Bull. Centre Physique Nucleaire l'Université Libre, Bruxelles **29** (1951). Čerenkov
[2] E. Fermi, Phys. Rev. **57**, 485 (1940).
[3] M. Schönberg, Nuovo cimento **8**, 159 (1951).
[4] O. Halpern and H. Hall, Phys. Rev. **73**, 477 (1948).
[5] H. A. Morrish, Phil. Mag. **43**, 533 (1952).
[6] Daniel, Davies, Malvey, and Perkins, Phil. Mag. **43**, 753 (1952).

The Energy Loss of a Fast Charged Particle by Čerenkov Radiation*

R. M. STERNHEIMER
Brookhaven National Laboratory, Upton, New York
(Received January 7, 1953)

IT has been shown[1] that for a medium with no absorption and described by a single type of dispersion oscillator, the relativistic rise of the ionization loss should escape as Čerenkov radiation. This result is in disagreement with the observed rise of the ionization pulse of μ mesons in crystals[2] and with the relativistic rise of the grain count in emulsion.[3] In actual cases, the index of refraction n has contributions from the various absorption limits. Moreover, most of the Čerenkov radiation should occur near the line frequencies where the absorption coefficient is large. It will be shown that when these effects are included the resulting energy escape is small (<0.01 Mev/g cm^{-2}) both for macroscopic crystals and for emulsion.

According to Fermi's theory,[4] the energy escaping to a distance larger than b from the particle is[5]

$$W_b=\frac{2e^2b}{\pi v^2}\,\mathrm{Re}\int_0^\infty\left(\frac{1}{1+\alpha}-\beta^2\right)i\omega k^*K_1(k^*b)K_0(kb)d\omega, \qquad (1)$$

where α is 4π times the polarizability and k is the square root with real part $\geqq 0$ of

$$k^2=(\omega^2/v^2)(1-\beta^2)-(\omega^2\alpha/c^2). \qquad (2)$$

In order to treat the case of emulsion, we take $b=0.13\mu$ ($\sim$grain radius). Since $|k|b$ is generally >1, we may use[6]

$$K_0(kb)\cong(\pi/2kb)^{\frac{1}{2}}\exp(-kb), \qquad (3)$$

$$K_1(k^*b)\cong(\pi/2k^*b)^{\frac{1}{2}}\exp(-k^*b). \qquad (4)$$

Equation (1) becomes

$$W_b=\frac{e^2}{v^2}\,\mathrm{Re}\int_0^\infty\left(\frac{1}{1+\alpha}-\beta^2\right)i\omega\left(\frac{k^*}{k}\right)^{\frac{1}{2}}\exp[-(k+k^*)b]d\omega. \qquad (5)$$

α is given by[7]

$$\alpha=-\frac{4\pi ne^2}{m}\sum_i(f_i/\omega_i^2)\times\frac{\ln[(\omega_i^2-\omega^2-2i\bar\eta_i\omega)/\omega_i^2]+[(\omega^2+2i\bar\eta_i\omega)/\omega_i^2]}{[(\omega^2+2i\bar\eta_i\omega)/\omega_i^2]^2}, \qquad (6)$$

where f_i, ω_i, $2\bar\eta_i$ are the oscillator strength, frequency, and damping constant of the ith absorption limit. Equation (6) is obtained from the Kramers-Kallmann-Mark theory of dispersion and gives good agreement with measurements of n in the x-ray region.[7] Fourteen terms in Eq. (6) were considered corresponding to the K, L, M_I, $M_{II-III}\cdots$ limits of Ag and Br. The ω_i were obtained from the table of Sommerfeld;[8] the widths $2\bar\eta_i$ were taken as[7] 11.2 ev for the K limit of Ag, 4.7 ev for K of Br, 3.2 ev for the L and M limits, and 1 ev for the N limits of both elements. Equation (5) was integrated numerically for $\beta=1$, giving 2.2×10^{-3} Mev/g cm^{-2}. This value is considerably smaller than the rise of the ionization loss (0.12 Mev/g cm^{-2}) for two reasons: (1) Because of the absorption bands on the high frequency side of each absorption limit, the index of refraction does not attain as large values as would be predicted for a single narrow line. In fact, n does not rise much above 1, except for $\hbar\omega<0.47$ ry below the ultraviolet absorption band. Since the condition for Čerenkov radiation is essentially $n>1$, this leads to a sharp reduction of the Čerenkov loss. (2) The effect of absorption is pronounced because the radiation is emitted in the forward direction so that it travels a distance $>b$ before leaving the grains traversed by the particle.

In the visible region, where the absorption is negligible (α=real), Eq. (5) reduces to the Frank and Tamm expression, in agreement with the result of Fermi[4] for a single dispersion oscillator.

In view of the result for emulsion, the Čerenkov loss for a macroscopic crystal is negligible compared to the ionization pulse, since the factor $\exp[-(k+k^*)b]$ decreases rapidly as b is increased. A more detailed account will be published soon.

I would like to thank Dr. Ernest D. Courant for stimulating discussions.

* Work done under the auspices of the U. S. Atomic Energy Commission.
[1] A. Bohr, Kgl. Danske Videnskab. Selskab, Mat.-fys. Medd. **24**, No. 19 (1948); H. Messel and D. Ritson, Phil. Mag. **41**, 1129 (1950); M. Schönberg, Nuovo cimento **8**, 159 (1951).
[2] W. L. Whittemore and J. C. Street, Phys. Rev. **76**, 1786 (1949); F. Bowen and F. X. Roser, Phys. Rev. **85**, 992 (1952).
[3] E. Pickup and L. Voyvodic, Phys. Rev. **80**, 89 (1950); H. A. Morrish, Phil. Mag. **43**, 533 (1952); M. Shapiro and B. Stiller, Phys. Rev. **87**, 682 (1952).
[4] E. Fermi, Phys. Rev. **57**, 485 (1940).
[5] Unless otherwise indicated, the notation is the same as in R. Sternheimer, Phys. Rev. **88**, 851 (1952).
[6] G. N. Watson, *Theory of Bessel Functions* (Cambridge University Press, Cambridge, 1944), second edition, p. 202.
[7] A. H. Compton and S. K. Allison, *X-Rays in Theory and Experiment* (D. Van Nostrand Company, Inc., New York, 1935), second edition, pp. 293, 746.
[8] A. Sommerfeld, *Atomic Structure and Spectral Lines* (Methuen and Company, Ltd., London, 1934), third edition, p. 237.

The Fermi Term in $\beta-\nu$ Correlation*

D. C. PEASLEE
Columbia University, New York, New York
(Received January 19, 1953)

A SURVEY is made to find the β-transitions most suitable for a $\beta-\nu$ (recoil) correlation experiment to determine the Fermi part of the β-decay interaction. The most favorable parent isotope appears to be A^{35}.

The linear combination in β-decay appears[1] to be half Fermi (F) and half Gamow-Teller (G). Absence of $1/W$ terms in allowed spectra[2] shows that F must be pure S or pure V, and G must be pure T or pure A. Measurements[3] of $\beta-\nu$ correlation on He^6 show that $G=T$. One now seeks a suitable case for determining the F component by $\beta-\nu$ correlation.

The G component is excluded only in a $0\to0$ transition; and the only known examples (C^{10} and O^{14}) have energetic gammas following the β-decay, which disturb the recoil and make the experiment almost prohibitively difficult. In allowed transitions where $\Delta I=0$ but $I_i=I_f\neq0$, both F and G components will be present. For mirror image transitions the matrix element of F is unity and of G is σ^2. The $\beta-\nu$ correlation function for this case

is $1+\alpha(v/c)\cos\theta$, where

$$\alpha=(\tfrac{1}{2}\sigma^2\pm 1)/(\sigma^2+1). \quad (1)$$

The sign in Eq. (1) is + for V and − for S. From an experimental point of view it is desirable to have a minimum value for σ^2, in order to maximize the difference between α_+ and α_-.

Table I accordingly lists σ^2 for radioactive gases that undergo mirror image β-decays. The values of σ^2(calc) are computed for the configurations listed, and σ^2(obs) are taken from the ft values fitted to the empirical[1] constant $1+\sigma^2=5.2\times10^3$ sec/ft. For $Ne^{19}-F^{19}$ we adopt the independent suggestions of E. Feenberg and M. Umezawa that the configuration is $(d_{5/2}{}^2d_{3/2})_{1/2}$, which gives the best agreement between σ^2(calc) and σ^2(obs).

TABLE I. Mirror image β-decays.

Gas	Configuration	σ^2(calc)	ft	σ^2(obs)
N^{13}	$p_{1/2}$	0.33	4.7×10^3 sec	0.11
O^{15}	$p_{1/2}{}^{-1}$	0.33	3.8	0.37
F^{17}	$d_{5/2}$	1.4	2.3	1.3
Ne^{19}	$(d_{5/2}{}^2d_{3/2})_{1/2}$	1.6	2.0	1.6
Cl^{33}	$d_{3/2}$	0.60	3.4	0.53
A^{35}	$(d_{3/2}{}^2d_{1/2})_{3/2}$	0.32	3.4	0.53

The average recoil energies of the nuclei, neglecting $\beta-\nu$ correlation, are on the order of 60 ev for N^{13}, 100 ev for O^{15}, F^{17}, Ne^{19}, and 200 ev for Cl^{33}, A^{35}. Simple gaseous molecules containing N, O, or C have exceptionally high binding energies on the order of 10 ev, which might seriously interfere with the recoil ions in at least the case of N^{13}. The situation is much more favorable for Cl^{33}, with a molecular binding energy of order 10^{-2} times the recoil energy. The discrepancy between σ^2(calc) and σ^2(obs) for A^{35} is commensurate with the rather large probable error in the ft value. If both chemical binding and the values of σ^2 are considered, the isotopes of Table I are roughly in order of increasing suitability for a $\beta-\nu$ correlation measurement of the Fermi term.

The author wishes to thank Professor E. Feenberg for helpful comments.

* This work was performed under the research program of the U. S. Atomic Energy Commission.

[1] O. Kofoed-Hansen and A. Winther, Phys. Rev. **86**, 428 (1952); G. L. Trigg, Phys. Rev. **86**, 506 (1952); R. Bouchez and R. Nataf, Compt. rend. **234**, 86 (1952).
[2] M. Fierz, Z. Physik **104**, 553 (1937).
[3] B. M. Rustad and S. L. Ruby, Bull. Am. Phys. Soc. **28**, No. 1, 41 (1953); J. S. Allen and W. K. Jentschke, Bull. Am. Phys. Soc. **27**, No. 5, 17 (1952).

Molybdenum 90

R. M. DIAMOND
Chemistry Department, Harvard University, Cambridge, Massachusetts
(Received January 13, 1953)

IN observing the high energy spallation products of niobium,[1] evidence for the existence of a new isotope of molybdenum was obtained. In order to identify this activity, niobium metal foils were bombarded with 55–60-Mev protons in the Harvard 95-inch synchrocyclotron for periods of an hour, and the molybdenum activities were isolated by ether extraction from 6N hydrochloric acid. Gross decay curves taken with an end-window Geiger counter on aliquots of such fractions showed a 5.5–6.0-hour and a 14.5–15.0-hour activity; neither half-life corresponds to known molybdenum periods. The decay curve of a sample separated quickly after the end of the bombardment exhibited an additional 15–20-minute activity ascribable to Mo^{91} (15.5 minutes[2]).

Since Nb^{90} is reported to have a half-life of 15 hours,[3,4] it was considered likely that the observed activities were due to a new nucleide, Mo^{90}, decaying with a 5.5–6.0-hour period into the longer lived Nb^{90}. To check this, niobium carrier was added and separated at twelve hour intervals from purified molybdenum fractions and then counted. One such series of separations was done by precipitating the niobium away from the molybdenum with ammonia, and two more series were done by repeated ether extractions of the molybdenum away from the niobium in 6N hydrochloric acid. The separated samples were then ignited to the oxide, weighed, and counted. In all three series a plot of the yield of the niobium daughter activity *vs* time showed a slope of 5.7±0.2 hours. One series is shown in Fig. 1. All of the separated samples showed a decay period of 14.7±0.2 hours; some were followed through eight half-lives and showed no sign of turning over.

Comparison of the activity of Mo^{90} and its daughter on an end-window (3.5 mg/cm²) Geiger counter indicated a counting efficiency for the molybdenum activity of 75–80 percent of that of the Nb^{90}. Since the latter is known to have a considerable amount of particulate radiation,[5] then Mo^{90} must also. In fact, aluminum absorption measurements indicate a considerable amount of ~100-kev conversion electrons, some ~240-kev conversion electrons, and either K x-rays or positrons of about 1.4-Mev maximum energy, or both, as is most likely the case. Unfortunately, no beryllium absorbers were available to differentiate these last two types of radiation, but positrons must be

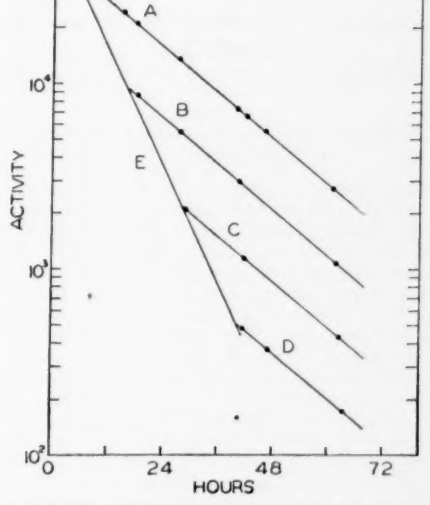

FIG. 1. Yield of Nb^{90} as a function of time of separation from Mo^{90}, curve E. Curves A to D show the decay of the individual Nb^{90} samples.

present to an appreciable extent, as there would be too many K x-rays involved for all of the radiation to be electromagnetic.

The value of the positron energy, 1.4 Mev, is an estimate from the extrapolated range in aluminum, and is certainly not a very reliable figure. However, similar aluminum absorption measurements on a sample of Nb^{90} gave a curve with a comparable section due to K x-rays and positrons, and the extrapolated range of the positrons corresponds to an energy of 1.2 Mev. This agrees with the value of 1.2 Mev reported by Kundu and Pool,[4] but not so well with the value of ~1.7 Mev given by Boyd.[3]

Lead absorption measurements on a sample of Mo^{90} exhibited a 1.1-Mev gamma-ray, and 240–260 kev and 100–125 kev gamma-rays; aluminum absorption data indicate that both of these last two are partially electron converted, the lower energy ray to the greater extent. Positron annihilation radiation was not resolvable in the lead absorption curve, but a small amount would not show up among the other electromagnetic radiation observed.

In summary, it may be said that from this work Mo^{90} appears to have (1) a half-life of 5.7±0.2 hours; (2) a disintegration scheme involving predominantly three gamma-rays, with energies of approximately 1.1, 0.24–0.26, 0.10–0.13 Mev, of which the second gamma-ray is electron converted to a small extent, and the third to a much larger degree; (3) positrons of roughly 1.4-Mev maximum energy (or of an energy slightly greater than the maximum energy of those from Nb^{90}), and a greater amount of electron capture relative to positron emission than is the case with Nb^{90}.

I wish to state my gratitude to Dr. J. Meadows and Mr. R. Wharton of the Harvard Cyclotron Group for their invaluable help with the bombardments, and to Mr. Rodman Sharp of this laboratory for his assistance with counting.

[1] This preliminary work was performed at the University of California Radiation Laboratory, and the author desires to express his thanks for the guidance and interest of Professor G. T. Seaborg.
[2] R. B. Duffield and J. D. Knight, Phys. Rev. **76**, 573 (1949).
[3] G. E. Boyd, Oak Ridge National Laboratory Report ORNL-229, February, 1949 (unpublished) as reported by Hollander, Perlman, and Seaborg, *Table of Isotopes*, University of California Radiation Laboratory Report UCRL-1928, August, 1952 (unpublished).
[4] D. N. Kundu and M. L. Pool, Phys. Rev. **76**, 183 (1949).
[5] L. Jacobson and R. Overstreet, *Radiochemical Studies: The Fission Products* (McGraw-Hill Book Company, Inc., New York, 1951), Paper No. 91, National Nuclear Energy Series, Plutonium Project Record, Vol. 9, Div. IV.

Systematic Calculations of Gamma-Ray Penetration*

HERBERT GOLDSTEIN AND J. ERNEST WILKINS, JR., *Nuclear Development Associates, Inc., White Plains, New York*
AND
L. V. SPENCER, *National Bureau of Standards, Washington, D. C.*
(Received January 19, 1953)

A NUMBER of methods[1] of varying degrees of rigor have been proposed for finding the intensity and spectrum of Compton-scattered photons arising in the penetration of gamma-rays through a medium. Recently, Spencer and Fano[2] have indicated a seminumerical technique of solving the Boltzmann transport equation for an infinite medium, which is well adapted for use with high speed automatic calculators. In essence the procedure reduces the original transport equation to a set of integral equations for the spatial moments of the gamma-ray flux. These equations now involve only one independent variable, the energy, and are so interlinked that any given number of spatial moments can be found by the numerical integration of a *finite* number of the equations, without any need for analytical approximations. The required flux distribution function can be approximated in various ways from a knowledge of a finite number of its moments, one of the most suitable being an expansion in terms of an appropriate system of polynomials.

Study of the rate of convergence in the polynomial expansion and comparison of the results with experiment[3] indicated that the method could provide answers of adequate accuracy for a wide range of problems of interest.[4] Accordingly, with the support and encouragement of the U. S. Atomic Energy Commission, especially the Oak Ridge National Laboratory, an extensive calculational program has been undertaken to exploit the method, making use of the SEAC, the National Bureau of Standards calculating machine. The materials investigated have covered the complete periodic table, including pure Compton-scattering medium, H_2O, Al, Fe, Sn, W, Pb, and U. For most of these substances calculations have been made for both point isotropic and plane monodirectional sources. In addition, for Pb, Fe, and pure Compton scatterer (which are the most important materials in practice), calculations have been made for infinite plane source geometries in which the photons leave the source with angular distributions corresponding to the Legendre polynomials $P_n(\cos\theta)$, $n=1, 2, 3$.[5] It is hoped that any source angular distribution with symmetry about the normal that does not vary too rapidly can be approximated well enough out of the first four Legendre polynomials. The range of initial energies considered, 0.5 to 10 Mev, was chosen so as to cover the problems of interest in the shielding of reactors. The calculations reported here include the range of penetrations from 1 to 20 mean free paths from the source. For deep penetrations, greater than 15–20 mean free paths, it is not practical to calculate enough terms to obtain adequate convergence.[6]

In the computations it has been assumed that the only scattering process is incoherent Compton scattering of unpolarized gamma-rays. For the energies involved coherent scattering is so nearly forward as to be no collision at all, and it has therefore been omitted from both the total cross section and the scattering kernel. The only other processes considered have been pair production and photoelectric effect, both of which have been treated as completely absorptive. All cross-sectional data were taken from the National Bureau of Standards compilation.[7]

At the present time all machine work has been completed, and final computations are now in progress. Full details of the calculations will be issued later this year.[8] Complete tables of build-up factors and differential spectra will be included in the report, along with examples of angular distributions. These results will not exhaust the calculations which can be made with the raw output from the SEAC. To make these more generally available it is intended to place annotated microfilm copies of the output tapes at each of the U. S. Atomic Energy Commission Depositary Libraries.

We should like to acknowledge the assistance of the Mathematics Division of the National Bureau of Standards, which did the actual coding of the problem and operating of the SEAC, and of the Computing Section of Nuclear Development Associates, which is calculating the finished results from the machine computations.

* Work supported by U. S. Atomic Energy Commission contracts.
[1] See, for example, Hirschfelder, Magee, and Hull, Phys. Rev. **73**, 852 (1948); Bethe, Fano, and Karr, Phys. Rev. **76**, 538 (1949); L. L. Foldy, Phys. Rev. **81**, 395 (1951); G. H. Peebles and M. S. Plesset, Phys. Rev. **81**, 430 (1951).
[2] L. V. Spencer and U. Fano, Phys. Rev. **81**, 464 (1951) and J. Research Natl. Bur. Standards **46**, 446 (1951). Also see L. V. Spencer and Fannie Stinson, Phys. Rev. **85**, 662 (1952).
[3] G. R. White, Phys. Rev. **80**, 154 (1950); E. Hayward, Phys. Rev. **86**, 493 (1952); Elliot, Farrar, Myers, and Ravilious, Phys. Rev. **85**, 1048 (1952).
[4] Examples of the results that can be provided by the moments methods will be found in references 2 and 3.
[5] The P_0 case (plane isotropic) can be determined directly from the point isotropic solution.
[6] Semi-asymptotic techniques have been developed which overlap with the moments method and carry the solution out as far as desired. See L. V. Spencer, Phys. Rev. **88**, 793 (1952).
[7] G. R. White, National Bureau of Standards Report No. 1003, 1952 (unpublished).
[8] U. S. Atomic Energy Commission Report, NYO-3075 (to be published).

Heavy Isotopes of Magnesium and Silicon

MANFRED LINDNER
California Research and Development Company, San Francisco, California
(Received January 9, 1953)

IN bombardments of chlorine (as sodium chloride) with 340-Mev protons from the Berkeley 184-inch cyclotron, a magnesium chemical fraction contained a 21-hour activity of high radiochemical purity. The radiations present were beta-particles of about 0.4 Mev and of about 3 Mev, in addition to gamma-rays of less than 100 kev and of about 1.7 Mev. The hard radiations were shown by chemical separation to be due to a 2.3-minute Al^{28} daughter, so that the 21-hour activity must be Mg^{28}.

A silicon fraction was removed from the same target and was found to contain the 160-minute Si^{31} in high abundance. If another activity attributable to the unknown isotope Si^{32} were formed in yield comparable to that of Si^{31}, its half-life would have to be either equal to or less than that of Si^{31}, or greater than several hundred years.

The study of the radiations of Mg^{28} and the search for a silicon isotope attributable to Si^{32} are being continued, and the results will be reported at a later date.

Q Values for the $N^{14}(\alpha,p)O^{17}$ Reaction

ELIS HJALMAR AND HILDING SLÄTIS
Nobel Institute of Physics, Stockholm, Sweden
(Received January 15, 1953)

EMPLOYING our earlier arrangement for exposing nuclear research emulsions with protons from targets bombarded with polonium alpha-particles[1] we have found the Q values -1.16 and -2.02 Mev in close agreement with the values -1.16 and -2.0 Mev obtained by Roy.[2] The target consisted of a thin layer of chromium nitride on a chrome-plated copper sheet. The emulsion was exposed in June, 1950, by use of the same polonium source already employed in our bombardments of boron, aluminum, fluorine, and sodium targets. The energy distribution of the elastically scattered protons originating in (α,p) recoils in the mica window of the polonium source was estimated theoretically. The result is in agreement with the experimentally measured energy distribution, which is used as a zero-effect for the protons from the (α,p) reactions.

A detailed description of the experiments will be published later in *Arkiv für Fysik*.

[1] Slätis, Hjalmar, and Carlsson, Phys. Rev. **81**, 641 (1951); Arkiv Fysik **3**, No. 17 (1951); E. Hjalmar and H. Slätis, Arkiv Fysik **4**, No. 14 (1952).
[2] R. R. Roy, Centre Phys. Nucleaire, Univ. Libre de Bruxelles, No. 21, September, 1950; Phys. Rev. **82**, 227 (1951).

The Angular Distribution of $Be^9(d,t)Be^8$ at Low Energy*

P. CÜER AND J. J. JUNG
Institut de Physique, Université de Strasbourg, Strasbourg, France
(Received December 1, 1952)

IT is well known that the weakly bound neutron in Be^9(~1.6 Mev) favors p,d and d,t reactions. In the study[1] of Be^9+d we found that the distribution of tritons in the forward direction might indicate a pick-up process even at 0.7- and 1-Mev bombarding energies. In view of the significance of this result for a theory of the pick-up near threshold and the conventional analysis of Resnick and Hanna[2] (sixth power of $\cos\theta$) up to 880 kev, we performed experiments with improved geometry, namely, at small angles and with better statistics. Since then, El-Bedewi[3] has given data above 20° at 7.7-Mev bombarding energy, and Butler[4] has discussed and calculated the mechanism at 8 Mev.

At low bombarding energy we have shown[5] that $Be^9(d,t)Be^8$ is not the only Be^9+d reaction producing tritons. At least two other sources are in competition: $Be^9(d,t)Be^{8*}$ (in its broad excited state at ~2.9-Mev), followed by $Be^{8*}\rightarrow 2\alpha$; and $Be^9(d,\alpha)Li^{7*}$ (in its second excited state at ~4.6-Mev), followed by $Li^{7*}\rightarrow\alpha+t$. Figure 1 shows the spectrum obtained at 90° in Ilford E_1 emulsions under good geometrical conditions (±0.5°) when magnetically analyzed 1.3-Mev deuterons were used to bombard 0.5μ Be. A second magnet (~10 000 gauss) beyond the target was used to analyze the disintegration particles in order to eliminate protons of $Be^9(d,p)Be^{10*}$ and $O^{16}(d,p)O^{17*}$ in studying the triton continuum. An accurate range-energy relation was used in this energy region for these emulsions in vacuum.[6]

Residual triton tracks between 3.3 and 3.85 Mev may originate either from a true immediate reaction or more likely from $Li^{7*}\rightarrow\alpha+t$ (Li^{7*} being in its third excited state[7] at ~6.5 Mev). In a more likely "tripartition" case, we have carefully analyzed $B^{10}+d$(1 Mev), where the available energy in the c.m. system of C^{12*}, 25.2 Mev, is higher than the 3α binding energies. The proportion of α possible in a true tripartition continuum, not originating from excited Be^8 states, is quite low. The so-called $Be^9(d,t)2\alpha$ reaction may then lead to confusion, since for the most part two alternative intermediates are operative: Be^8 or Li^7 in different excited states, either the triton or the α being emitted first. We give below the results for the angular distribution of tritons leaving Be^8 in its ground state.

A circular camera was built with a hollow target holder in the middle at an angle of 60° with the incident 3-millimeter collimated deuteron atomic beam. The target was 0.5μ of pure Be evaporated on 10μ gold. From 0° to 150°, at 30° (±1°) intervals, the solid angle was defined in good geometry conditions by two 3-millimeter circular holes bored in two concentric rings 10 cm apart. At each angle a cylindrical box with a separate bottom and a rubber gasket were attached to the camera by a tube. An Ilford E_1 plate tilted at 6° recorded the whole collimated disintegration beam in the box. In some exposures gold windows were needed to reduce ranges in order to record only the reactions $Be^9(d,t)Be^8$, $Be^9(d,p)Be^{10}$, and $C^{12}(d,p)C^{13}$. A second camera was used to register distributions accurately at 0°, 7°, 10°, 15°, 20°, and 30° angles. The correctness of the device for mechanical alignment was tested, after a rough trial with Rutherford scattering, by measuring the α angular distribution of $Li^6(d,\alpha)\alpha$ for $E_d=0.5$ Mev. Results were compared with the findings of Heydenburg and others[8] and the calculations of Inglis.[9] Scanning was performed by three observers with Stiassnie immersion microscopes using standard methods. Tracks were divided according to length into different groups and were counted in equal solid angles of ejected disintegration particles. Results are given in Fig. 2 for $E_d=1.3$ Mev in the c.m. system. At each angle the result is the mean of several exposures giving a great number of tracks, 12 300 measures at 0° and 7120 at 30°. The indicated experimental uncertainties arose mainly from the error in comparing the $Li^6(d,\alpha)\alpha$ distributions and gold scattering differences at various angles. The scattering uncertainty was measured in exposures without windows at angles corresponding to thin backing thickness (namely 90°).

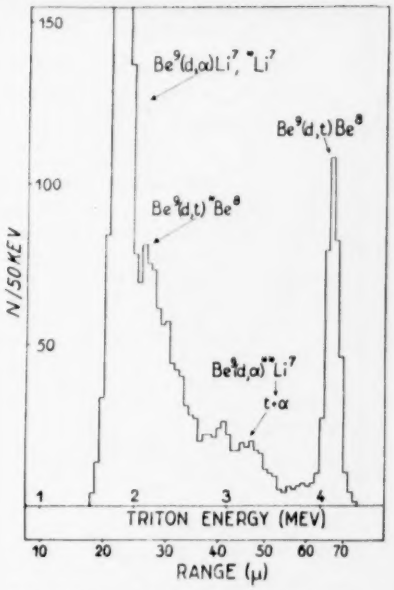

FIG. 1. Part of the magnetically analyzed disintegration spectrum of Be^9+d observed at 90°. $E_d=1.3$ Mev. The ordinates give the number of tracks per 50-kev interval.

The main curve and the small angles curve were normalized using the ratio $N(0°)/N(30°)$. (N = number of tracks.) The angular distribution of protons from $Be^9(d,p)Be^{10}$ is in good agreement with the results of Canavan[10] and may then be interpreted partly as a stripping process[11] even at this low bombarding energy. The protons of $C^{12}(d,p)C^{13}$ are in accord with Phillips'[12] measurements above 60°. Below this angle they differ noticeably; for example, our number is bigger at 0°. Further measurements are in progress in this field in order to clear up this important point concerning a stripping process. Even for a deuteron bom-

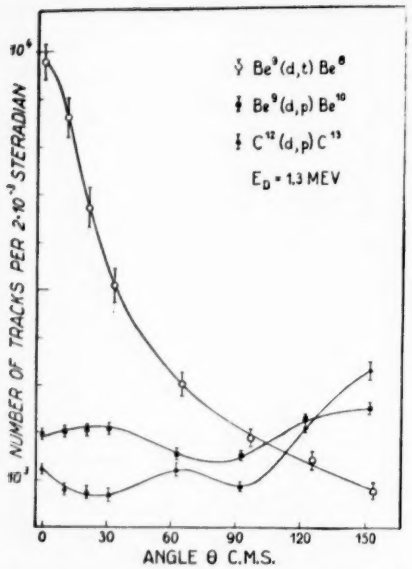

FIG. 2. Angular distributions in the c.m. system. $E_d = 1.3$ Mev. The ordinates give the numbers of measured tracks reported in the c.m. solid angles.

barding energy well below the neutron binding energy, the forward distribution of tritons is striking; it is then possible, taking account of a substantial amount of pick-up, to give a less complex analysis than Resnick and Hanna at low energy. Results at 1 Mev and at more angles, showing still a substantial effect, will be published later. The pick-up process for light elements seems to be more frequent even at low energy that we would expect according to the Bohr model. Its extensive study will certainly give interesting results concerning the possibility of substructures. Similar experiments are in progress with $C^{13}+d$ and are planned with $O^{17}+d$ and Be^9+He^3.

We wish to thank Dr. W. D. Allen and Dr. R. H. V. M. Dawton of Harwell for kindly supplying Li^6, B^{10} and C^{13}, and Professor S. Gorodetzky for facilities granted during the many exposures at the high tension set of Strasbourg. Thanks are due to Mr. Liess for the mechanical device.

* Some consequences of these results relating to substructures for light elements have been presented at the Mainz colloquium, Germany, March, 1952 (unpublished).

[1] Cüer, Magnac-Valette, Jung, and Gorodetzky, J. phys. et radium **2**, 41 (1950).
[2] I. Resnick and S. S. Hanna, Phys. Rev. **82**, 463 (1951).
[3] F. A. El-Bedewi, Proc. Phys. Soc. (London) **A64**, 947 (1951).
[4] S. T. Butler, Proc. Roy. Soc. (London) **A208**, 559 (1951); S. T. Butler and E. E. Salpeter, Phys. Rev. **88**, 133 (1952).
[5] P. Cüer and J. J. Jung, Compt. rend. **234**, 204 (1952).
[6] P. Cüer and J. J. Jung, Science et inds. phot. **22**, 401 (1951).
[7] W. Franzen and J. G. Likely, Phys. Rev. **87**, 667 (1952).
[8] Heydenburg, Hudson, Inglis, and Whitehead, Phys. Rev. **74**, 405 (1948).
[9] R. Resnick and D. R. Inglis, Phys. Rev. **76**, 1318 (1949).
[10] F. L. Canavan, Phys. Rev. **87**, 136 (1952).
[11] W. W. True and L. Diesendruck, Phys. Rev. **87**, 381 (1952).
[12] G. C. Phillips, Phys. Rev. **80**, 164 (1950).

Microwave Observation of the Collision Frequency of Electrons in Germanium

T. S. BENEDICT AND W. SHOCKLEY
Bell Telephone Laboratories, Murray Hill, New Jersey
(Received January 16, 1953)

THE effective mass m^* and relaxation time τ, caused by collisions, for electronic conduction in crystals can be deduced indirectly from such combinations as the drift mobility and the Hall mobility.[1] In germanium, however, at temperatures between 298°K and 160°K the mobility rises from 3800 to 10 000 cm²/volt-sec. At microwave frequencies $\omega\tau$ becomes an appreciable fraction of one radian of phase of the microwaves, and it becomes possible to observe the carrier (electron) contribution to the dielectric constant.[2] A measurement of this contribution then leads in a fairly direct way to the determination of m^* and τ.

Let us assume that germanium can be considered a lossless continuum characterized by a dielectric constant κ_0 to which is added N noninteracting carriers (electrons) per unit volume. These electrons are assumed to have a fixed relaxation time τ and effective mass m^*. The equation of motion for the electrons under the influence of a sinusoidal electric field is given (in MKS units) by

$$\dot{I}+\frac{I}{\tau}=\frac{Ne^2}{m^*}E_0\exp(i\omega t). \tag{1}$$

The electron current is therefore

$$I_0\exp(i\omega t)=\frac{Ne^2\tau}{m^*}\left(\frac{1}{1+i\omega\tau}\right)E_0\exp(i\omega t). \tag{2}$$

The dielectric constant[3] is then given by

$$\kappa=\kappa_0-\frac{Ne^2\tau^2}{\epsilon_0 m^*[1+(\omega\tau)^2]} \tag{3}$$

and the conductivity by

$$\sigma=\frac{Ne^2\tau}{m^*[1+(\omega\tau)^2]}. \tag{4}$$

The dc conductivity is $\sigma_0=Ne\mu=Ne^2\tau/m^*$, where $\mu=e\tau/m^*$ is the mobility of the carriers. The dielectric constant may therefore be written

$$\kappa=\kappa_0-\frac{Ne^2}{\epsilon_0 m^*[(e/m^*\mu)^2+\omega^2]}. \tag{5}$$

It is seen that if the number of carriers and the mobility are known, a measurement of the dielectric constant will yield a value of the effective mass. Over the temperature range 298°K to 160°K the number of carriers for relatively pure germanium remains essentially constant[1] and the mobility[4] varies approximately as $T^{-\frac{3}{2}}$.

The samples were prepared by doping intrinsic germanium with arsenic in order to obtain enough carriers to make the effect observable. Measurements were made of the attenuation and phase shift resulting from a 0.016-inch transverse sample which completely filled the rectangular wave guide of a 1.24-cm microwave bridge. From these measurements the dielectric constant

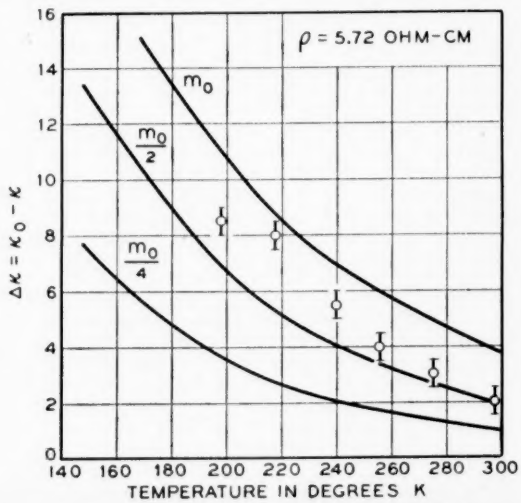

FIG. 1. Plot of $\Delta\kappa=\kappa_0-\kappa$ *vs* absolute temperature for germanium ($\rho=5.72$ ohm cm).

was determined by numerically evaluating the complex transmission coefficient[5] (including multiple reflections in the sample).

For a very pure specimen ($\rho=40$ ohm cm) the contribution of the carriers to κ is negligible at room temperature and for these conditions a value of 16.0 ± 0.5 was obtained. This value was used for κ_0 in Eq. 5 and is in good agreement with infrared data for the index of refraction[6] which leads to $\kappa=16.55$ for $\lambda=2.60$ microns.

The results of the measurements are given in Figs. 1 and 2 where $\Delta\kappa=\kappa_0-\kappa$ is plotted as a function of temperature for samples with room temperature dc resistivities of 5.72 ohm cm

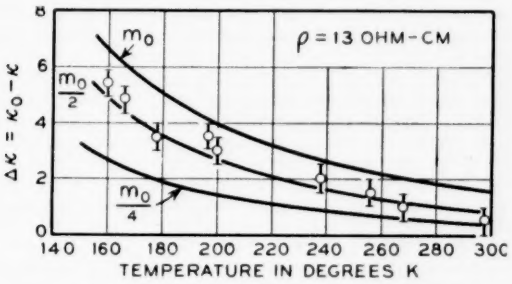

FIG. 2. Plot of $\Delta\kappa=\kappa_0-\kappa$ *vs* absolute temperature for germanium ($\rho=13.0$ ohm cm).

and 13.0 ohm cm. The solid curves are the theoretical curves predicted by Eq. 5 for various effective masses. It is seen that both sets of measurements predict an effective mass of about 0.6 times the free electron mass. It also is seen that the simple theory presented here predicts the proper temperature dependence from which we obtain $\tau=6.6\times10^{-9}T^{-\frac{3}{2}}$ sec for the relaxation time.

The authors wish to thank G. L. Pearson for preparing the samples and M. B. Prince for providing the mobility data prior to publication.

[1] For a recent review and references see E. Conwell, Proc. Inst. Radio Engrs. **40**, 1327 (1952).
[2] The electron contribution to the dielectric constant has recently been used as a correction term for measurements made at room temperature with 10 cm microwaves. [J. M. Goldey and S. C. Brown, Bull. Am. Phys. Soc. **28**, No. 1, 7 (1953)].
[3] This treatment is essentially that of the Drude-Zener theory. See for example, F. Seitz, *Modern Theory of Solids* (McGraw-Hill Book Company, Inc., New York, 1940), Sec. 147.
[4] Drift mobilities of electrons in p type germanium of comparable impurity density have recently been measured by M. B. Prince. These values were used for the theoretical curves.
[5] E. G. Montgomery, *Technique of Microwave Measurements* (McGraw-Hill Book Company, Inc., New York, 1947), pp. 565–584.
[6] H. B. Briggs, Phys. Rev. **77**, 287 (1950).

The Hall Coefficient of Calcium

V. FRANK AND O. GRAM JEPPESEN
Technical University of Denmark, Copenhagen, Denmark
(Received January 9, 1953)

IN the course of other investigations regarding the Hall effect, we have measured the Hall coefficient of calcium which seems not to have been determined before.[1] A sample of calcium was kindly put at our disposal by the Metallurgical Laboratory, Technical University of Denmark. The purity was not specified but was supposed to be high. As it seems rather laborious to analyze calcium for small impurities (e.g., CaO), we have measured the electric resistivity, the density, and the lattice constant in order to give a specification of our calcium.

The resistivity was found by passing a known current through a rod of the material and measuring (with a potentiometer) the potential difference between two probes placed over various lengths of the rod. The density was found by weighing a cylinder of known dimensions. The lattice constant was determined with cobalt K_α radiation in a Debye-Scherrer camera calibrated with copper.

The results were, at room temperature:

Resistivity	$(3.60\pm0.03)\times10^{-6}\Omega$ cm.
Density	1.543 ± 0.004 g cm^{-3}.
Lattice constant	$(5.59\pm0.01)\times10^{-8}$ cm (face-centered cubic).

For comparison we may quote:[2]

Resistivity	$4.3\times10^{-6}\Omega$ cm.
Density	1.542 g cm^{-3}.
Lattice constant	5.57×10^{-8} cm.[3]

The density found corresponds well with the ordinarily accepted values of density and lattice constant, whereas the lattice constant found by us is a little too high. The resistivity found is very low, however, and as one would hardly expect the resistivity to decrease as a consequence of impurities, we think we can be pretty sure that our calcium was of high purity, say at least 99 percent.

For measurement of the Hall coefficient the material was rolled down to a thickness of (0.203 ± 0.002) mm. The rolling was carried out at room temperature and in the atmosphere, but the material was protected by an oil film; one annealing (by heating in a very good vacuum) was necessary. The specimens were cut out in rectangular shape, 48 by 17 mm, and measured in air, still being protected against oxidation by an oil film. Immediately

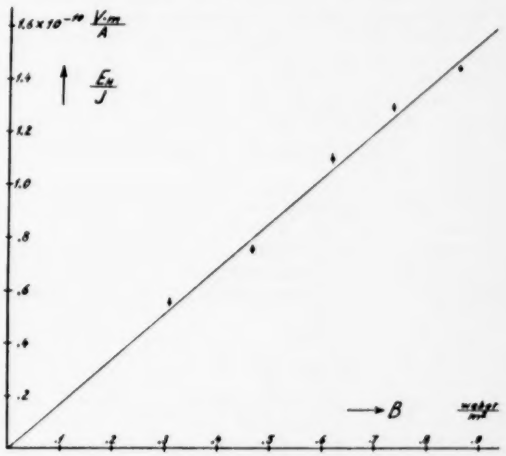

FIG. 1. Ratio E_H/J as a function of magnetic induction B.

before measuring, the surface was scraped clean under oil; no change in the measured Hall potential difference was noticeable for hours afterwards.

The dc was supplied through two circular contacts (2 mm diameter) placed symmetrically at a distance of 40 mm between centers. Reversal of the current direction did not influence the results. Each measurement was performed by measuring the change in Hall potential difference caused by reversal of the magnetic field while the current through the specimen was kept constant.

The two points on the edges of the specimen between which the Hall PD was measured were situated on the same equipotential of the current-field in the absence of the magnetic field. (This was secured in the usual way by connecting one of the leads not to the edge but to a copper wire connected to two points of the edge, and sliding the lead along the copper wire until no change in PD between the two leads appeared on reversal of the current. To minimize thermoelectric forces, this copper wire and all connecting wires were taken from the same piece of wire).

Figure 1 shows the ratio of the measured Hall-field strength E_H to the current density J as a function of the magnetic induction B. Each point is the result of several measurements with different current densities, and the standard deviation ("root mean square error") is indicated. As will be seen, the Hall-coefficient (slope of

the line) is constant for magnetic fields up to about 1 weber/m² (=10 000 gauss). The value of the slope is $(17.0\pm0.5)\times10^{-11}$ m³/coulomb.

In order to obtain the Hall coefficient, this figure has to be increased by 5 percent owing to short-circuiting of the Hall-field by the contacts for the primary current.[4]

The sign was found to be negative (the same sign as for copper, "normal" Hall-effect). The final result is thus

$$R_H=-(17.8\pm0.5)\times10^{-11}\ \text{m}^3/\text{coulomb}.$$

The authors wish to thank Professor H. Højgaard Jensen for much valuable advice and Professor T. Bjerge for his interest in the work.

[1] R. H. Kingston, Phys. Rev. **84**, 944 (1951).
[2] A. E. van Arkel, *Reine Metalle* (J. Springer, Berlin, 1939).
[3] In van Arkel's Fig. 5.56, A refers to the "Siegbahn-angstrom," 1.002 $\times10^{-8}$ cm.
[4] See forthcoming publication by V. Frank.

Mixing of States and Antiferromagnetism*

H. P. Hanson†
Massachusetts Institute of Technology, Cambridge, Massachusetts
(Received January 13, 1953)

THE phenomenon of antiferromagnetism has been discussed by Anderson[1] in terms of Kramers'[2] theory of superexchange. In essence the theory as applied to an antiferromagnetic material such as[3] MnO attributes the magnetic interaction of the Mn^{++} ions to the intermediary O^{--} ions. Anderson points out that simple O^{--} ions could not lead to superexchange, but there is good reason to believe that the wave function included an admixture of other states.

There exists in the literature much direct evidence for this mixing of states, in particular that provided by x-ray absorption spectroscopy. As has been shown in many studies,[4,5] the fine structure within a few tens of volts of the edge is principally due to transitions to low energy states associated with the atom rather than with the crystal as a whole, and thus provides information about the bonding.

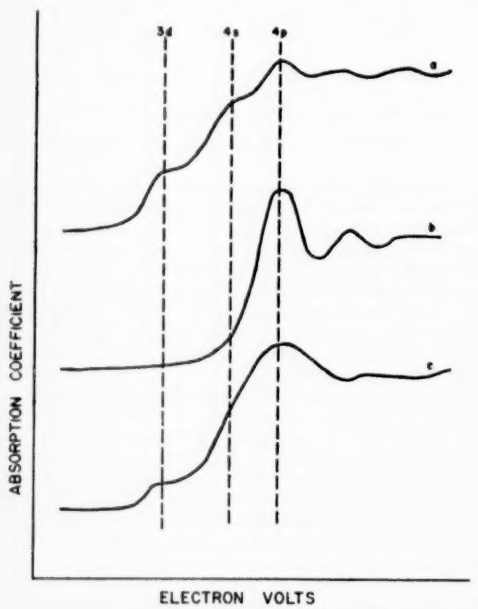

FIG. 1. Typical edge structures for the transition elements and their compounds. (a) *K* edge for the metal; (b) edge for the ion when observed in solution and in ionic compounds such as the chlorides, nitrates, etc., and (c) edge for sulfides and oxides.

Over a period of years, the data have been taken by different experimenters using techniques and spectrometers of varying reliability and resolving power. There are, however, some generalizations that may be safely drawn. In the idealized curves of Fig. 1, we see edge structures which are quite typical for the transition elements and their compounds. Figure 1, curve (a) shows the *K* edge for the metal. The structure has been ascribed to transitions of the 1*s* electron to 3*d*, 4*s*, and 4*p* levels as indicated in the figure. This apparent violation of the free atom selection rules is in keeping with the mixing of states required for metallic behavior. Figure 1, curve (b) shows the edge for the ion when observed in solution and in ionic compounds such as the chlorides, nitrates, etc. Studies on manganese salts show small but observable absorption into the 3*d*–4*s* region, the magnitude of which seems correlated in an inverse fashion to the electronegativity of the anion. The edge for the transition elements combined as the sulfides and the oxides are represented by curve (c). Actually this group shows the greatest variation among the members, and it is difficult to draw a truly typical curve. In each case, however, there is a very significant absorption into the 3*d*–4*s* region. The essential similarity to metallic edge structure has been commented on by Coster and Kiestra[5] and by Yoshida.[6] Qualitatively, for those compounds for which the x-ray and magnetic information exists, it appears that, the greater the mixing of states as indicated by the magnitude of the 3*d*–4*s* absorption, the stronger is the antiferromagnetic effect as revealed by the height of the Curie temperature.

Sincere thanks are due Dr. P. W. Anderson and Professor J. C. Slater for comment and criticism.

* The research in this document was supported jointly by the Army, Navy, and Air Force under contract with the Massachusetts Institute of Technology.
† On leave from the University of Florida, Gainesville, Florida.
[1] P. W. Anderson, Phys. Rev. **79**, 350 (1950).
[2] H. A. Kramers, Physica **1**, 182 (1934).
[3] C. G. Shull and J. S. Smart, Phys. Rev. **76**, 1256 (1949).
[4] W. W. Beeman and J. A. Bearden, Phys. Rev. **61**, 455 (1942).
[5] D. Coster and S. Kiestra, Physica **14**, 184 (1948).
[6] S. Yoshida, Sci. Papers Inst. Phys. Chem. Research (Tokyo) **38**, 272 (1941).

The Calculation of *F* Center Energy Levels*

J. A. Krumhansl and N. Schwartz
Cornell University, Ithaca, New York
(Received December 30, 1952)

ENERGY levels of electrons trapped at vacent negative ion sites in ionic crystals are usually obtained using the model that treats the vacancy as a hole surrounded by a continuous, isotropic dielectric. This model has been used by various investigators,[1] and it has been pointed out that the levels should be evaluated by a self-consistent method, since the equilibrium positions of the ions surrounding the vacancy are determined, in part, by the charge distribution of the trapped electron. Simpson[1] has made self-consistent calculations using a variational method. Pincherle[1] has obtained results substantially in agreement with those found by Simpson. Although Pincherle did not use a self-consistent field, he found it necessary to modify the form of the potential energy, in evaluating the energy of the excited state, in order to obtain agreement with Simpson's calculations.

The main purpose of this note is to question the choice of the depth of the potential well which is used in the calculation of the energy levels of *F* centers. The usual assumption is that the potential well is of the form shown in Fig. 1. The potential energy of the electron when at the center of the vacancy is V_0 with respect to the bottom of the conduction band. At large distances it is $e^2/\kappa_0 r$ where κ_0 is the optical dielectric constant, since in the course of the electron motion the ionic displacements cannot follow. The present comments concern the choice of V_0. The usual argument goes as follows: (a) At the center of the vacancy which the electron is to occupy to form an *F* center, the principal contribution to V_0 is the Madelung potential V_m. From this is subtracted the electron affinity χ. (b) In addition, since there is a vacancy, there exists a potential at its center resulting from

the polarization of the surrounding medium given by[3]

$$\varphi=\frac{e}{R}\left(1-\frac{1}{\kappa_0}\right). \tag{1}$$

(c) Thus, in removing an electron from the center of the vacancy to a point in the crystal far removed from the vacancy and at the bottom of the conduction band the work done is

$$W=eV_m-\chi-e\varphi. \tag{2}$$

The criticism of this reasoning is that including in V_0 the full potential which would exist at the vacancy center in the absence of the electron is tantamount to assuming that the optical polarization of the medium cannot follow the motion of the F-center electron. If this assumption is correct then the usual choice of V_0 is justified. If, on the other hand, the optical polarization follows the electron motion adiabatically, then the medium will not be polarized at all (to a first approximation) when the electron replaces the negative ion right at the vacancy center. Since the characteristic frequencies for fundamental optical absorption are much higher than those of the electron in the F center, it is probable that the polarization can in fact follow the

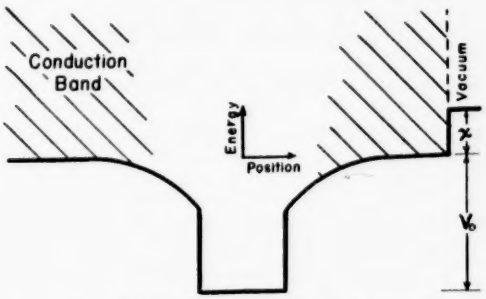

FIG. 1. Potential energy for electron in F center.

electron motion adiabatically. In this case, using the same argument usually applied to calculations of energies of formation of defects in ionic crystals,[3] one must use the average polarization so that instead of (2) one gets

$$W=eV_m-\chi-\tfrac{1}{2}e\varphi. \tag{3}$$

In typical calculations in the alkali halides the polarization potential φ is of the order of 3 electron volts, and the factor of $\frac{1}{2}$ in (3) then makes the well deeper than the conventional estimate by about 1.5 ev. This has a strong effect on the $1s$ level but does not lower the $2s$ and $2p$ so much. The result is to increase the energy separation between the $1s$ and $2p$ levels.

Some further remarks are in order. In the first place the simple potential model used is already an idealization made necessary for simplifying calculations. For this reason the quantitative significance of the present criticism is not very great (at least in so far as the results on the alkali halides are concerned). On the other hand, in the alkaline earth oxides where φ is larger the difference may be significant. In the second place, the use of (3) leads to a higher thermal activation energy than estimates based on (2). This may give greater disagreement between theory and experiment; for instance, see Dutton, Heller, and Maurer,[4] concerning experiments on V_1 centers where very small thermal activation energies are observed compared with what one might expect.

Professor H. Brooks has brought to the authors' attention the similarity between this problem and that of estimating the image potential for Schottky corrections to thermionic emission. Here also it is assumed that the conduction electrons in the metal can follow the motion of an external electron adiabatically. The analogous competing arguments are: (a) If an electron is at a distance x from the metal the electrostatic potential produced by its image is $e/2x=\varphi$ at the electron. If the electron is removed to infinity the work done would be $W=e\varphi$, if it is assumed that the metal electrons (image charge) cannot follow adiabatically. But, (b) if one assumes that the metallic electrons do follow adiabatically, the work done is only $\frac{1}{2}e\varphi=e^2/4x$, in agreement with the usual choice.[5]

We have included these considerations in a calculation of F center levels in representative alkali halides. The levels for NaCl and KCl are tabulated below. The energies are given in ev, and the zero of energy has been taken at the bottom of the conduction band. These results were obtained using (3), and the contribution to the potential energy that depends upon the wave function of the trapped electron was introduced as a perturbation. The perturbation calculation shows that the effect of the latter on the ground state is small, thus accounting for the agreement between the results obtained by Pincherle and those found by Simpson. The effect on the excited state is greater, as expected. Agreement with experiment is as good or better than that obtained by previous calculations.

	$-E_{1s}$	$-E_{2p}$	$(E_{2p}-E_{1s})$ Calc.	Obs.
NaCl	3.85	1.23	2.62	2.7
KCl	3.18	0.82	2.36	2.3

* This work was assisted by the U. S. Office of Naval Research.

[1] S. R. Tibbs, Trans. Faraday Soc. **35**, 1471 (1939); J. H. Simpson, Proc. Roy. Soc. (London) **197**, 269 (1949); L. Pincherle, Proc. Phys. Soc. (London) **64**, 648 (1951).

[2] W. Jost, J. Chem. Phys. **1**, 466 (1933).

[3] N. F. Mott and R. W. Gurney, *Electronic Processes in Ionic Crystals* (Oxford University Press, London, 1948), Chap. II.

[4] Dutton, Heller, and Maurer, Phys. Rev. **84**, 363 (1951).

[5] F. Seitz, *Modern Theory of Solids* (McGraw-Hill Book Company, Inc., New York, 1940), p. 163.

Uranium Photofission Yields*

ROMAN A. SCHMITT† AND NATHAN SUGARMAN
Institute for Nuclear Studies, University of Chicago, Chicago, Illinois

(Received January 9, 1953)

MANY investigations of high energy fission, both with particles and x-rays, have been reported.[1–8] One striking feature of these studies is the decrease in the peak-to-trough yield ratio of the yield-mass curve as the energy of the bombarding particle increases, resulting in the one hump yield-mass curve as the energy of the particle enters the hundred Mev range. This paper reports the results of the radiochemical study of the photofission of natural uranium at the University of Chicago Betatron.[9] The study was made, in the main, at 48 Mev maximum energy, with a beam intensity of 300 roentgens per minute, 1 meter from the target. Measurements were made on the yields of 28 fission-product nuclides. Some experiments at 22 and 100 Mev were performed on the yields of selected peak and trough nuclides. Experiments were performed on the contribution of neutrons to the observed fission rate; it was found that this effect could not have appreciably affected the results.

In the betatron experiments, about 10 g of uranyl nitrate was irradiated within the half-angle of the x-ray beam about 32 cm from the tungsten target for periods of 10 min to 2 days. Radiochemical analyses[10] were employed to isolate the desired nuclides which were counted with a Geiger-Mueller β-counter. Most of the separated samples had counting rates of about 2000 counts per minute. In addition, neutron irradiations were performed in which about 2 g of uranyl nitrate was irradiated in the thermal column of the Argonne heavy-water pile, and the same nuclides were studied as in the betatron irradiations. Some neutron irraditions were also made at the 37-inch cyclotron of the University of Chicago. The photoyield curve was obtained by the comparison method, previously described by Spence[4] and Turkevich and Niday.[11]

The photoyields given in Fig. 1 were calculated from a thermal-neutron fission-yield curve for U^{235} which is a combination of that given by Glendenin *et al.*[12] for yields greater than 2 percent, and of the familiar double-humped curve[13] for yields less than 2 percent. The photocurve of Fig. 1 was constructed by the "folding" process with the fragment mass sum of 234 for masses in the mass range 90 to 103 and 131 to 141. In the mass range 111 to

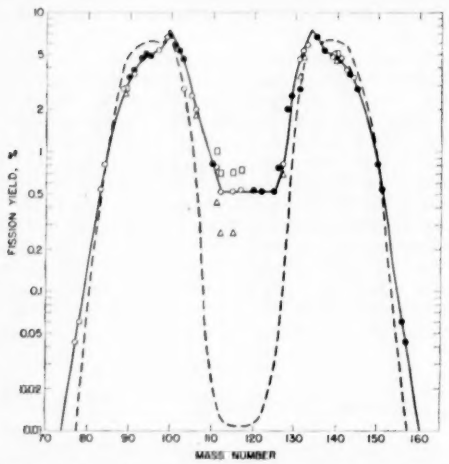

FIG. 1. Photofission yields of uranium at 22 Mev, 48 Mev, and 100 Mev. Dashed curve is that of thermal-neutron fission of U^{235}, solid curve for 48-Mev x-rays. △, 22 Mev; ○, 48 Mev; ●, 48 Mev reflected yields; □, 100 Mev. The yield of Mo^{99} at 22 Mev and 100 Mev is normalized to 6.6 percent.

127 it was noted that more concordant agreement was obtained with a mass sum[14] of 237. The curve is normalized to 200 percent total fission yield.

The peak-to-trough ratio, as determined from the yields at masses 97 and 115, was observed to be dependent upon the maximum energy of the x-ray beam, varying from 7 at 100-Mev maximum energy to 20 at 22-Mev maximum energy. These results, as well as those of other reported experiments, are summarized in Table I. The fact that the peak-to-trough ratio was

TABLE I. Peak-to-trough ratios at various x-ray energies.

Energy of x-rays, Mev	Nuclide irradiated	Peak-to-trough ratio	Reference
2.6, fission neutrons	U^{238}	100	Engelkemeir, Seiler, Steinberg, and Winsberg. See reference 10, Paper 218.
10	U^{238}	126	See reference 6.
16	U^{238}	121	See reference 6.
~20	U^{238}	20	See reference 4.
22	U^{238}	20	This paper.
48	U^{238}	10	This paper.
69	Th^{232}	10	D. M. Hiller and D. S. Martin, Jr., presented before the 122nd Natl. Meeting of the American Chemical Society, Sept. 14–18, 1952.
100	U^{238}	7	This paper.

observed to change from 48 to 100 Mev indicates that absorption of photons is occurring in this energy interval and that the average fission process is of a more symmetric type than that occurring at lower energies. The fission activation curve for uranium given by Baldwin and Klaiber[15]—their cross-section curve has a maximum at 16 Mev with a half-width of about 4 Mev, and approaches zero at about 33 Mev—must then have a high energy tail. If it is assumed that the trough yield at high energy is due to symmetric fission,[11] then the contribution to the total fission rate from photons of 48 to 100 Mev energy amounts to about 3 percent.

Further work on the (γ,f) reaction of uranium is planned at the 330-Mev University of Illinois Betatron. Work is also in progress on independent yields of some shielded nuclides and other selected fission products.

We wish to acknowledge the assistance of Mr. B. C. Cook and the Betatron Group, Mr. M. Fielding and the staff of the 37-inch cyclotron of the University of Chicago, and the personnel of the Argonne National Laboratory responsible for the thermal neutron irradiations. The 22-Mev irradiations at the University of Illinois Betatron were accomplished through the generous cooperation of Professor D. W. Kerst and Mr. T. J. Keegan.

* This research was supported in part by a grant from the U. S. Atomic Energy Commission.

† Presented in partial fulfillment for the Ph.D. degree in the Department of Chemistry, University of Chicago, Chicago, Illinois.

[1] P. R. O'Connor and G. T. Seaborg, Phys. Rev. **74**, 1189 (1948).
[2] A. S. Newton, Phys. Rev. **75**, 17 (1949).
[3] R. H. Goeckermann and I. Perlman, Phys. Rev. **76**, 628 (1949).
[4] R. W. Spence, *Brookhaven Conference Report*, Chemistry Conference No. 3 (Brookhaven National Laboratory, 1949), pp. 43–51 (unpublished).
[5] N. Sugarman, Phys. Rev. **79**, 532 (1950).
[6] H. G. Richter, Ph.D. thesis, Massachusetts Institute of Technology, August 16, 1952 (unpublished).
[7] Fowler, Jones, and Paehler, Phys. Rev. **88**, 71 (1952).
[8] Turkevich, Niday, and Tompkins, Phys. Rev. **89**, 552 (1953).
[9] W. F. Westendorp and E. E. Charlton, J. Appl. Phys. **16**, 581 (1945).
[10] *Radiochemical Studies: The Fission Products* (McGraw-Hill Book Company, Inc., New York, 1951), National Nuclear Energy Series, Plutonium Project Record, Vol. 9, Div. IV, Part VI.
[11] A. Turkevich and J. B. Niday, Phys. Rev. **84**, 52 (1951).
[12] Glendenin, Steinberg, Inghram, and Hess, Phys. Rev. **84**, 860 (1951).
[13] Appendix B of reference 10.
[14] Similar results were obtained in other mass-yield curves by C. D. Coryell of the Massachusetts Institute of Technology and L. E. Glendenin and E. P. Steinberg of the Argonne National Laboratory.
[15] G. C. Baldwin and G. S. Klaiber, Phys. Rev. **71**, 3 (1947).

Assignment of Y^{92} and Y^{94}*

G. L. SCHOTT† AND W. WAYNE MEINKE
Department of Chemistry, University of Michigan, Ann Arbor, Michigan
(Received January 12, 1953)

A SHORT-LIVED isotope of yttrium assigned to Y^{94} has been reported as a fission product from uranium[1] and plutonium[2] and as the result of an (n,p) reaction on zirconium.[3] A recent investigation of the isotope indicates that the half-life is 16.5 ± 1 minute,[4] but the mass assignment of this activity is still listed[5,6] as "probable but not certain." In addition, the assignment of the 3.5-hour yttrium activity to Y^{92} has recently been reclassified[8] as "probable but not certain."

We have checked the mass assignment of these activities by comparing relative bombardment yields of Y^{90}, Y^{92}, and Y^{94} prepared by the (d,α) reaction. Zirconium metal (high purity foil except for two percent hafnium content) was bombarded in the 7.8-Mev deuteron beam of the University of Michigan cyclotron and the yttrium produced was separated chemically. The foil was dissolved in dilute hydrofluoric acid, carriers of niobium and yttrium added, and the yttrium precipitated as the fluoride. This precipitate was metathesized to the hydroxide and then dissolved. The resulting solution was scavenged with zirconium phosphate and niobic acid precipitates to complete the separation. A final precipitate of yttrium fluoride was slurried onto copper plates for counting. The total separation required about 25 minutes. It gave a decontamination from zirconium and niobium of at least 10^4 and a yield of yttrium of about 50 percent.

Decay of the samples was followed for several weeks to determine the relative yields of the yttrium isotopes formed. The gross decay of the yttrium samples was resolved into a 65-hour, a 3.5-hour, and an 18-minute line. No 2.0-hour Y^{88m} was detected in the decay. A small amount of 105-day Y^{88} was undoubtedly formed in the bombardment, but its yield was so low as to be scarcely detectable above background. The energy of the bombardment was low enough that no products of a $(d,\alpha n)$ reaction were observed. The lutecium isotopes arising from a (d,α) reaction on the small amount of hafnium impurity present in the target material were not separated by the chemical procedure but were formed in such low abundance that their effect on the decay curve was negligible.

Absorption curves taken at different times on the above samples indicated that the 18-minute isotope emitted a beta-particle of energy greater than 5 Mev; the 3.5-hour isotope emitted a beta-particle of about 3.5-Mev energy and a gamma-ray of about 0.5 Mev; while the 65-hour activity emitted a beta-particle of 2.35 Mev. These energy data are consistent with the values reported in the literature.[5]

The experimental yields for these three isotopes normalized to

TABLE I. Yields of zirconium isotopes.

Zr mass	Rel. abundance (%)	Relative yields Theoret.	Run I	Run II
92	17.1	1.00	1.00	1.00
94	17.4	1.02	1.06	1.07
96	2.80	0.164	0.186	0.169

the 65-hour Y^{90} activity are presented in Table I, together with the theoretical yields expected from the abundance data.

It can be seen that the results of both bombardments agree very well with the theoretical yields. This agreement lends very strong support to the assignment of the 16.5-minute yttrium activity to Y^{94} and the 3.5-hour activity to Y^{92}. It also substantiates the assignments of the strontium, rubidium, and krypton isobars of mass 92 and 94 whose genetic relationship to the yttrium activities has already been shown. This method of mass assignment has presupposed equal yields for all the (d,α) reaction products from the even-even isotopes of zirconium and has presumed no isomeric states of Y^{90}, Y^{92} and Y^{94} to consume part of the (d,α) reaction yield. Both of these assumptions appear to be good in this case.

It should be pointed out, however, that this method of mass assignment by equal yields has been shown to be valid only for the (d,α) reaction products of even-even isotopes. Other work in progress at this laboratory appears to show considerable difference in (d,α) reaction yields for mixed even-even and even-odd parents.

The cooperation of Professor W. C. Parkinson, Professor P. V. C. Hough, and the crew of the University of Michigan cyclotron is gratefully acknowledged.

* This work was supported in part by the U. S. Atomic Energy Commission.

† Present address, Department of Chemistry, California Institute of Technology, Pasadena, California.

[1] O. Hahn and F. Strassmann, Naturwiss. **31**, 249 (1943).
[2] Katcoff, Miskel, and Stanley, Phys. Rev. **74**, 631 (1948).
[3] W. Seelmann-Eggebert, Naturwiss. **31**, 510 (1943).
[4] L. J. Brown and S. Katcoff, J. Chem. Phys. **17**, 497 (1949).
[5] Hollander, Perlman, and Seaborg, "Table of Isotopes," University of California Radiation Laboratory Report UCRL–1928, revised, December, 1952.
[6] A Chart of the Nuclides, General Electric Research Laboratory, October, 1950.

The Gamma-Radiation from Am^{241}

J. O. NEWTON AND B. ROSE
Atomic Energy Research Establishment, Harwell, Berkshire, England
(Received January 19, 1953)

IN a recent letter[1] we have reported measurements made with a proportional counter on the gamma- and L radiation following the alpha-decay of Am^{241}. Browne,[2] using a crystal spectrometer and thick sources, has also made measurements on this nuclide and has reported gamma-rays of energies 38.0 kev, 33.4 kev, 22.2 kev, and 18.8 kev in addition to those which we found. The first two of these were stated to have intensities of 6 percent and of 28 percent, respectively, relative to that of the 59.7-kev gamma-ray; it would not have been possible for us to resolve the last two from the Np^{237} L radiation with our instruments. The location of these lines together with a further line at 14.4 kev in a decay scheme is discussed briefly by Asaro, Reynolds, and Perlman[3] who state that it is necessary to assume the presence of levels in Np^{237} other than those directly excited by the observed alpha-particle groups.

In view of this apparent anomaly, we have re-examined the spectrum more closely in the energy region 26–41 kev using proportional counters filled with krypton and xenon. A typical spectrum obtained, using a carrier free source of Am^{241} and a krypton filled proportional counter, is shown in Fig. 1. An upper limit of 0.1 percent[4] per 59.7-kev γ-ray can be set to the intensity of gamma-rays at 33.4 and 38.0 kev from the combined measurements.

In Fig. 2 is shown a spectrum, obtained from an Am^{241} source containing lanthanum which is commonly used as a carrier for Am, in which strong lines are present at ~33.1 and 38.0 kev, having a relative intensity (~5:1) similar to that observed by Browne. These are clearly the $K\alpha$ and $K\beta$ radiations of lanthanum excited by the 59.7-kev gamma-ray. The mean energies of the lanthanum $K\alpha$ and $K\beta$ lines are 33.4 and 37.9 kev, to be compared with the values of 33.4 and 38.0 kev reported by Browne for the "γ-rays". We therefore suggest that these lines are not of nuclear origin.

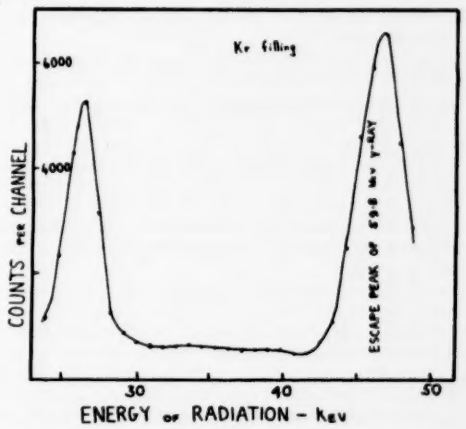

FIG. 1. Spectrum obtained with thin carrier free source of Am^{241}.

Similarly, the energies of the weaker gamma-rays mentioned above, namely, 14.4, 18.8, and 22.2 kev, are to be compared with those of the $L\alpha_1$, $L\beta_1$, and $L\gamma_1$ radiation of Am, namely, 14.6, 18.8, and 22.0 kev. Furthermore, the relative intensities are consistent with the hypothesis that these lines are due to fluorescent excitation of the Am source by the 59.7- and 26.3-kev radiations which are known[1] to accompany the decay process.

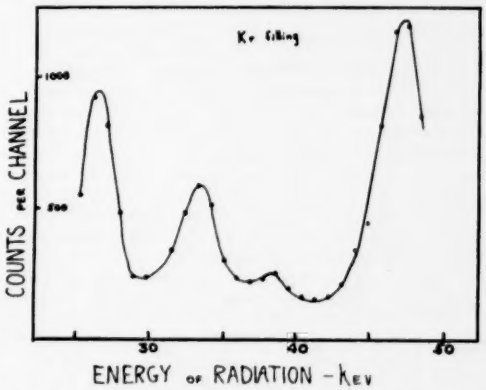

FIG. 2. Spectrum obtained with Am^{241} source containing La carrier, showing presence of lines at 33.1 and 38.0 kev.

It therefore appears to be unnecessary to assume the presence of low-lying levels in Np^{237} other than those excited directly by the observed alpha-particle groups.[5]

We are grateful to the Director, Atomic Energy Research Establishment, for permission to publish this letter.

[1] Beling, Newton, and Rose, Phys. Rev. **86**, 797 (1952).
[2] C. I. Browne, University of California Radiation Laboratory Report UCRL 1764, June 1952 (unpublished).
[3] Asaro, Reynolds, and Perlman, Phys. Rev. **87**, 277 (1952).
[4] In reference 1 an upper limit to the intensity of any γ-ray lines in the range 29–40 kev was incorrectly given as 0.02 percent per 59.7-kev γ-ray. This should have read 0.2 percent per 59.7-kev γ-ray.

Symmetric Pseudoscalar Theory of Nuclear Forces

ABRAHAM KLEIN*
Harvard University, Cambridge, Massachusetts
(Received December 22, 1952)

IN his recent work on the problem of nuclear forces, Lévy[1] has employed a form of three-dimensional perturbation theory to deduce an adiabatic nuclear potential from the symmetric pseudoscalar theory with pseudoscalar coupling. We have re-examined the entire field-theoretic problem and will submit a full account shortly. The purpose of this letter is to report a number of errors in the Lévy potential.

Consider first the leading two-pair terms of the fourth-order potential ($V_4^{(a)}$ of L2). Contrary to reference 13 of L2, one must calculate beyond the zeroth approximation to the energy denominators if one wishes to avoid an error of relative order μ/M compared to the leading term. In the next approximation, the contribution from intermediate states with pairs precisely cancels $V_4^{(b)}$ of L2, whereas the contribution from the intermediate state without pairs yields a force which is velocity-dependent.[2] We have been able to show, however, that the velocity-dependent potential need not be included in application to the low energy two-nucleon problem.[3]

Consider next the one-pair terms. The basic matrix elements are represented in Fig. 2 of L2. It is easy to show that in the adiabatic limit the sets a_1, b_1, c_1, and a_2, b_2, c_2 yield precisely the same contribution except for charge dependence. The sum of the contributions is an ordinary force and just three times the value for the neutral theory.[4] The correct fourth-order adiabatic potential, not including terms of relative order $(\mu/M)^2$ compared to the leading term, has the form

$$V_4(r)=-3\left(\frac{G^2}{4\pi}\right)^2\left(\frac{\mu}{2M}\right)^2\frac{1}{\mu r^2}\left[\frac{2}{\pi}K_1(2\mu r)-\frac{\mu}{M}\left(1+\frac{1}{\mu r}\right)^2e^{-2\mu r}\right]. \quad (1)$$

The no-pair potential of L2, Eq. (20) is also inaccurate. This term should agree precisely with the leading contribution to the fourth-order potential of the pseudoscalar theory with derivative coupling if one multiplies the latter by $(\mu/M)^4$. The agreement fails in two respects. The first term of Eq. (20) cancels to first order in the coupling constant[5] against velocity-dependent corrections to the second-order potential. Secondly, there is a charge-dependent term missing of the form

$$-\left(\frac{G^2}{4\pi}\right)^2\frac{\boldsymbol{\tau}^1\cdot\boldsymbol{\tau}^2}{(2M)^4}\int\frac{d\mathbf{k}_1d\mathbf{k}_2\exp[i(\mathbf{k}_1+\mathbf{k}_2)\cdot\mathbf{r}]}{\omega_1\omega_2(\omega_1+\omega_2)}(\mathbf{k}_1\cdot\mathbf{k}_2)^2\left(\frac{2}{\omega_1^2}+\frac{1}{\omega_1\omega_2}\right). \quad (2)$$

Finally we have re-examined the leading terms of the sixth and eighth-order adiabatic potentials. If we include contributions only of the type represented explicitly in Fig. 3 of L2, we obtain essential agreement with Eqs. (23) and (24) of the latter. However, a large class of matrix elements of the same order of magnitude has been omitted in each case.[5] Moreover, we can delete from the results those parts which "cancel" the leading velocity-dependent contribution of the fourth-order result.[3] The remaining potentials are given by the expressions

$$V_6(r)=\left(\frac{G^2}{4\pi}\right)^3\left(\frac{\mu}{2M}\right)^4\frac{4}{3}\boldsymbol{\tau}^1\cdot\boldsymbol{\tau}^2\{\boldsymbol{\sigma}^1\cdot\boldsymbol{\sigma}^2+S_{12}\}\frac{e^{-3\mu r}}{\mu^2r^3}\left[1+\frac{1}{\mu r}\right]^2, \quad (3)$$

$$V_8(r)=-3\left(\frac{G^2}{2M}\right)^4(2\pi)^{-12}\int\frac{\exp[i(\mathbf{k}_1+\mathbf{k}_2+\mathbf{k}_3+\mathbf{k}_4)\cdot\mathbf{r}]}{\omega_1\omega_2\omega_3\omega_4(\omega_1+\omega_2)}$$
$$\times\left[\frac{3}{(\omega_1+\omega_3)(\omega_2+\omega_4)}+\frac{2}{(\omega_1+\omega_3)(\omega_1+\omega_4)}\right]d\mathbf{k}_1\cdots d\mathbf{k}_4. \quad (4)$$

The result of applying the above potentials to the low energy two-nucleon problem will be included in the full report.

* Junior Fellow, Society of Fellows.
[1] M. M. Lévy, Phys. Rev. **88**, 72, 725 (1952); hereafter referred to as L1 and L2. Our notation follows these papers.
[2] This much has recently been shown by G. Lüders, Institute for Theoretical Physics, Copenhagen, Denmark (unpublished).
[3] By using the variational principle, Eq. (49) of L1, one shows that the kernel consisting of velocity-dependent corrections to the fourth-order potential plus part of the sixth and eighth-order potential leads to no first-order change in the coupling constant.
[4] The result for the neutral theory given in reference 14 of L2 should be multiplied by two.
[5] As an example, there is a considerable class of eighth-order matrix elements which have at most two mesons in all intermediate states in which there are no pairs. These have apparently been omitted.

A Microwave Spectrum of the Free OH Radical*

T. M. SANDERS, JR.,† A. L. SCHAWLOW,‡ G. C. DOUSMANIS, AND C. H. TOWNES
Columbia University, New York, New York
(Received January 5, 1952)

A STRONG microwave absorption spectrum resulting from the free radical $O^{16}H^1$ has been found.

The radicals are produced in a radiofrequency discharge through water vapor. The vapor flows continuously through the discharge and the absorption cell, at a pressure near 0.1 mm of mercury. The intensity of the lines is strongly dependent both on discharge current and on pressure.

The absorption cell is a one-meter length of low loss (Corning type 707) glass tubing approximately three centimeters in diameter and located within a split cylindrical wave guide. A solenoid wound on this assembly produces a magnetic field which is used for detection of lines by Zeeman modulation.

The microwave lines result from transitions between members of Λ-type doublets in the paramagnetic ground state of the molecule.[1] In these transitions none of the angular momenta $\Lambda=1$, $S=\frac{1}{2}$, K, $J=K+\frac{1}{2}$ changes. The energy levels are further split by magnetic hyperfine structure. Corresponding to the two values of F ($\mathbf{F}=\mathbf{J}+\mathbf{I}$) possible for each molecular level, one expects that each line will be split into four components. The transitions with $\Delta F=0$ are expected to be approximately fifty times as intense as the $\Delta F=\pm1$ lines. To date we have observed only the $\Delta F=0$ lines listed in Table I, although our signal-to-noise ratio is in excess of 300:1. The quantum numbers J, K are assigned on the basis of ultraviolet data.[2] The F values are determined from the observed relative intensity of the hyperfine components, which is approximately the ratio of their F values. The Zeeman patterns of these lines are markedly asymmetric even in small fields where $g_J\mu_0H/h\sim0.5$ Mc/sec. This suggests that for one member of the Λ-doublet,

$$|W(F=J+\tfrac{1}{2})-W(F=J-\tfrac{1}{2})|/h=|\Delta\nu|\sim0.5 \text{ Mc/sec},$$

whereas for the other $|\Delta\nu|\sim9$ Mc/sec. Under such circumstances the $\Delta F=\pm1$ lines would lie too near the main lines to be observed.

TABLE I. Observed frequencies of $O^{16}H^1$ absorption lines.

Transition	Frequency in Mc/sec
$K=4,\ J=4\frac{1}{2},\ F=5\rightarrow F=5$	$23\,826.90\pm0.05$
$K=4,\ J=4\frac{1}{2},\ F=4\rightarrow F=4$	$23\,818.16\pm0.05$
$K=5,\ J=5\frac{1}{2},\ F=6\rightarrow F=6$	$36\,994.43\pm0.15$
$K=5,\ J=5\frac{1}{2},\ F=5\rightarrow F=5$	$36\,983.47\pm0.15$

Three separate effects may enter the hyperfine structure. First, the interaction of the proton magnetic moment with electron spin magnetic moments; second, the interaction of the proton moment with the magnetic field arising from orbital motion; and third, the relativistic interaction which gives rise to the hyperfine structure of atomic S states. Of these, we expect only the first to produce different splittings in the two Λ-doubling states.[3] The observed splitting agrees reasonably well with an approximate calculation of the dipole-dipole interaction assuming the coupling to be pure Hund's case (b), and assuming the odd electron to have a probability near one-half of being found in a $2p$ state about the proton.

The Λ-doubling frequencies agree with ultraviolet data[2] to within 1000 Mc/sec, which is about the expected accuracy of the earlier measurements. Using the value $\lambda\equiv A/B=-7.547$ obtained by Dieke and Crosswhite, we arrive at the following tentative values for the two parameters describing the Λ-type doubling:[4]

$$4\Sigma\frac{(-1)^S}{\nu\Pi\Sigma}(\Pi|AL_y+2BL_y|\Sigma)(\Sigma|BL_y|\Pi)=+3592\pm18 \text{ Mc/sec},$$
$$4\Sigma\frac{(-1)^S}{\nu\Pi\Sigma}|(\Pi|BL_y|\Sigma)|^2=-524.4\pm0.8 \text{ Mc/sec}.$$

We are not now able to give an accurate value for the abundance of radicals, since the line intensity is proportional to the square

of the as yet unknown electric dipole moment of the molecule. On the basis of a rough estimate of this quantity, however, we believe the fraction of OH present to be a few tenths of one percent. This figure is in agreement with some earlier values,[5] but does not seem to be consistent with others.[6]

The very substantial intensity of the lines gives hope that one may be able to study by microwave methods OH radicals produced in a variety of chemical reactions, and that other free radicals may prove accessible to microwave techniques.

* Work supported in part by the Signal Corps and the U. S. Office of Naval Research.
† Radio Corporation of America Fellow.
‡ Carbide and Carbon Chemical Corporation Postdoctoral Fellow. Now at Bell Telephone Laboratories, Murray Hill, New Jersey.
[1] For a discussion of this type of spectrum see Hicks, Ossofsky, and Jones, Technical Note No. 130, Ballistics Research Laboratory, Aberdeen Proving Grounds, November, 1949 (unpublished).
[2] G. H. Dieke and H. M. Crosswhite, Bumblebee Report No. 87, The Johns Hopkins University, November, 1948 (unpublished).
[3] The different behavior of the two Λ-doubled states is a consequence of the interaction between a spin on the symmetry axis and off-axis spins. This type of effect has been observed in the inversion spectrum of ammonia, and will be discussed in a future paper by G. R. Gunther-Mohr *et al.*
[4] J. H. Van Vleck, Phys. Rev. **33**, 467 (1929); R. S. Mulliken and A. Christy, Phys. Rev. **38**, 87 (1931).
[5] A. A. Frost and O. Oldenberg, J. Chem. Phys. **4**, 642 (1936); O. Oldenberg and F. F. Rieke, J. Chem. Phys. **7**, 482 (1939).
[6] W. H. Rodebush and M. H. Wahl, J. Chem. Phys. **1**, 696 (1933). See also R. W. Campbell and W. H. Rodebush, J. Chem. Phys. **4**, 293 (1936) and K. H. Geib, J. Chem. Phys. **4**, 391 (1936).

Experimental K to $L+M$ Ratios for Internal Conversion Lines

R. E. Maerker and R. D. Birkhoff
Department of Physics, University of Tennessee, Knoxville, Tennessee
(Received January 12, 1953)

MEASUREMENTS have been made on the K to $L+M$ ratios of seven γ-rays, four of which have not been reported previously. These values were obtained by means of a solenoidal type β-ray spectrometer of the design described by DuMond,[1,2] using a value for the fundamental radius R of 20 cm.

Sources were prepared by deposition and evaporation of solutions onto a polyethelene backing $\sim$0.5 mg/cm² thick. Gold foil $\sim$100 μg/cm² was vacuum evaporated on the backing to render the source conducting. Sources varied in thickness between 1 mg/cm² and 10 mg/cm², yielding resolutions of the order of one percent.

The K conversion line was completely separated from the corresponding $L+M$ line in every case, although neighboring conversion lines of other γ-rays interfered in some measurements. In the case of Cs^{134}, the K line resulting from the 602-kev γ-ray masked the $L+M$ line of the 560-kev γ-ray, so that it was necessary to estimate the size of the latter. In the case of the equilibrium run of $Ba^{140}-La^{140}$, the K line resulting from the 540-kev γ-ray in Ba^{140} partially interfered with the $L+M$ line of the 488-kev γ-ray in La^{140}.

Uncertainties in the ratios were increased by the low intensity of the $L+M$ lines as a result of the relatively low transmission of the instrument. The counting rates at the peaks of the $L+M$ lines in Nb^{95}, Sb^{124}, and Ba^{140} were all less than 10 cpm above background, and in addition, the latter line was superimposed on top of a relatively strong continuous β-background $\sim$400 cpm.

Table I. Values of $K/(L+M)$ obtained.

Isotope	γ-ray energy, kev	$K/(L+M)$
Cs^{137}	663	4.52 ±0.07
Cs^{134}	602	6.6 ±0.2
Cs^{134}	799	7.8 ±0.4
Sb^{124}	607	15.5 ±2
Nb^{95}	774	6.6 ±0.4
Ba^{140}	540	6 ±2
La^{140}	488	3.7 ±0.2

The results obtained for the two Cs^{134} conversion lines compare favorably with those reported recently by LeBlanc *et al.*[3] The value for the 663-kev γ-ray in Cs^{137} also is in good agreement with the results of Kelly.[4]

The experimental values appear in Table I.

[1] J. W. M. DuMond, Rev. Sci. Instr. **20**, 160 (1949).
[2] J. W. M. DuMond, Rev. Sci. Instr. **20**, 616 (1949).
[3] LeBlanc, Nester, Martin, Brice, and Cork, Bull. Am. Phys. Soc. **27**, No. 5, 22 (1952).
[4] W. C. Kelly, Phys. Rev. **85**, 101 (1952).

The Charge Independence of Nuclear Forces*

David Feldman
Department of Physics, University of Rochester, Rochester, New York
(Received January 15, 1953)

IN this note we should like to call attention to some consequences of the charge-independence hypothesis for high-energy neutron-proton and proton-proton scattering. Let us consider the general process of the elastic scattering of a nucleon by a nucleon,

$$N_1+N_2\rightarrow N_3+N_4, \tag{1}$$

where N_i denotes a nucleon of momentum $\mathbf{p}_i$ and spin s_i. If we agree to keep the incident and final momenta and spins fixed throughout our considerations, then, by varying the charge assignments of the individual nucleons, we can obtain a number of physically distinguishable reactions.[1] These include

$$p_1+p_2\rightarrow p_3+p_4, \tag{2a}$$
$$n_1+p_2\rightarrow n_3+p_4, \tag{2b}$$
$$n_1+p_2\rightarrow p_3+n_4, \tag{2c}$$

plus three additional reactions which are directly related to (2a), (2b), and (2c) by charge symmetry. The notations n and p indicate neutron and proton, respectively; the subscripts refer to the preassigned momenta and spins.

It may now be readily shown that, if f and g denote the isotopic triplet and singlet scattering amplitudes, respectively, for the two-nucleon system (where f and g are functions of the initial and final momenta as well as the spins), the scattering amplitudes for the three processes (2a), (2b), (2c) are f, $\frac{1}{2}(f+g)$, $\frac{1}{2}(f-g)$, so that with proper normalization of the wave functions we have for the corresponding differential cross sections

$$\sigma_{pp}=|f|^2, \tag{3a}$$
$$\sigma_{np}=\tfrac{1}{4}|f+g|^2, \tag{3b}$$
$$\sigma_{pn}=\tfrac{1}{4}|f-g|^2. \tag{3c}$$

The three cross sections are here expressed in terms of three unknowns (the magnitudes of the triplet and singlet scattering amplitudes as well as their relative phase) so that one cannot derive *equalities* relating the cross sections, but one can deduce *inequalities*. For example, it can be proved that σ_{pp}, σ_{np}, and σ_{pn} will be compatible with the charge-independence hypothesis if and only if

$$(\sigma_{np})^{\frac{1}{2}}+(\sigma_{pn})^{\frac{1}{2}}\geq(\sigma_{pp})^{\frac{1}{2}}, \tag{4a}$$
$$(\sigma_{pn})^{\frac{1}{2}}+(\sigma_{pp})^{\frac{1}{2}}\geq(\sigma_{np})^{\frac{1}{2}}, \tag{4b}$$
$$(\sigma_{pp})^{\frac{1}{2}}+(\sigma_{np})^{\frac{1}{2}}\geq(\sigma_{pn})^{\frac{1}{2}}. \tag{4c}$$

Now, when the incident nucleons are unpolarized, the corresponding differential scattering cross sections σ_{pp}, σ_{np}, and σ_{pn} (which involve an averaging over the initial and a summation over the final spins) are given by expressions similar to (3a)–(3c), so that the inequalities (4a)–(4c) remain valid. In the center-of-momentum system we have $\sigma_{pn}(\theta)=\sigma_{np}(\pi-\theta)$, whence the restrictive relations become

$$[\sigma_{np}(\theta)]^{\frac{1}{2}}+[\sigma_{np}(\pi-\theta)]^{\frac{1}{2}}\geq[\sigma_{pp}(\theta)]^{\frac{1}{2}}, \tag{5a}$$
$$[\sigma_{np}(\pi-\theta)]^{\frac{1}{2}}+[\sigma_{pp}(\theta)]^{\frac{1}{2}}\geq[\sigma_{np}(\theta)]^{\frac{1}{2}}, \tag{5b}$$
$$[\sigma_{pp}(\theta)]^{\frac{1}{2}}+[\sigma_{np}(\theta)]^{\frac{1}{2}}\geq[\sigma_{np}(\pi-\theta)]^{\frac{1}{2}}. \tag{5c}$$

At high energies the Coulomb interaction in the proton-proton system plays a small role in the scattering except in the region of very small angles. Hence equations (5a)–(5c) may be directly applied as a test of the charge-independence hypothesis. For the neutron-proton scattering cross section one has[2] $\sigma_{np}(\theta)\cong\sigma_{np}(\pi-\theta)$ so that relations (5b) and (5c) are essentially satisfied identically. Furthermore, in view of the known angular dependences of $\sigma_{np}(\theta)$[2,3] and $\sigma_{pp}(\theta)$,[4–6] the most critical test of (5a) will be obtained for $\theta=90°$, whence one is led to the inequality

$$R\leq 4, \tag{6}$$

where $R=\sigma_{pp}(90°)/\sigma_{np}(90°)$.

Equation (6) has already been quoted in the literature[4] as holding in the absence of tensor forces; however, it is clearly subject to no limitations beyond those contained in the assumption of charge independence. From the data which are currently available,[2–6] R is largest for energies of the order of 220–260 Mev. In view of the experimental discrepancies and uncertainties (particularly with respect to σ_{pp}), it is unfortunately impossible at the present time to say whether (6) is or is not violated. The ratio R is 2.8 ± 0.5 or 3.8 ± 0.6 according to whether one uses the Berkeley[4] or the Rochester-Harwell[5,6] determination of σ_{pp}. It is clear that a more precise determination of R, both at the energies already referred to and particularly at higher energies, may serve as a useful check of the charge-independence hypothesis.

The general considerations which we have applied to nucleon-nucleon scattering can also be extended to other cases involving the elastic and inelastic scattering of light nuclei by light nuclei at sufficiently high energies. For example, in the inelastic scattering of nucleons by deuterons, we have three physically distinguishable reactions,

$$p+d\rightarrow n_1+p_2+p_3, \tag{7a}$$

$$p+d\rightarrow p_1+n_2+p_3, \tag{7b}$$

$$p+d\rightarrow p_1+p_2+n_3, \tag{7c}$$

plus the three reactions corresponding to neutron-deuteron scattering. If we denote the differential scattering cross sections for (7a), (7b), and (7c) by σ_{npp}, σ_{pnp}, and σ_{ppn}, respectively, these cross sections will satisfy inequalities of the type given by (4a)–(4c), *viz.*,

$$(\sigma_{npp})^{\frac{1}{2}}+(\sigma_{pnp})^{\frac{1}{2}}\geq(\sigma_{ppn})^{\frac{1}{2}}, \quad \text{etc.}$$

Finally, we should like to note that restrictive inequalities of the sort we have been dealing with always appear when one compares reactions which differ from one another only as to charge assignments, but that these inequalities *may* already be included in whatever restrictive equalities one may have. Thus, in the single-meson production in nucleon-nucleon scattering,[1] there are two equalities which relate the cross sections, one of which is Watson's relation[7] and the other is a phase relationship [see Eqs. (1) and (2) of reference 1]. Actually, the phase relationship already contains implicitly all the restrictive inequalities for this case.[8] On the other hand, in the elastic scattering of mesons by nucleons, there is only one restrictive equality, *viz.*, Heitler's relation,[9]

$$\tfrac{1}{2}\sigma(\pi^-+p\rightarrow\pi^0+n)+\sigma(\pi^0+p\rightarrow\pi^0+p)$$
$$=\tfrac{1}{2}\sigma(\pi^++p\rightarrow\pi^++p)+\tfrac{1}{2}\sigma(\pi^-+p\rightarrow\pi^-+p). \tag{8}$$

The absence of a restrictive equality in the form of a phase relationship means that the experimental meson-nucleon scattering cross sections will be compatible with charge independence when and only when Eq. (8) and the following are satisfied:

$$[\sigma(\pi^++p\rightarrow\pi^++p)]^{\frac{1}{2}}+[\sigma(\pi^-+p\rightarrow\pi^-+p)]^{\frac{1}{2}}$$
$$\geq[2\sigma(\pi^-+p\rightarrow\pi^0+n)]^{\frac{1}{2}}, \tag{9}$$

plus the two additional inequalities which are obtained from (9) by permuting the bracketed quantities. Since $\sigma(\pi^0+p\rightarrow\pi^0+p)$ is not a readily measurable quantity, it is the inequalities (9) which alone have any practical value.

* This research was supported, in part, by the U. S. Atomic Energy Commission.

[1] Van Hove, Marshak, and Pais, Phys. Rev. **88**, 1211 (1952).
[2] Kelly, Leith, Segrè, and Wiegand, Phys. Rev. **79**, 96 (1950).
[3] Guernsey, Mott, and Nelson, Phys. Rev. **88**, 15 (1952).
[4] Chamberlain, Segrè, and Wiegand, Phys. Rev. **83**, 923 (1951).
[5] C. L. Oxley and R. D. Schamberger, Phys. Rev. **85**, 416 (1952); O. A. Towler, Phys. Rev. **85**, 1024 (1952).
[6] Cassels, Pickavance, and Stafford, Proc. Roy. Soc. (London) **A214**, 262 (1952).
[7] K. M. Watson, Phys. Rev. **85**, 852 (1952).
[8] However, it is important to notice that, if the incident nucleons are unpolarized, the phase relationship of Van Hove, Marshak, and Pais is lost. Under these circumstances, the restrictive inequalities do need to be given explicitly.
[9] W. Heitler, Proc. Roy. Irish Acad. **51**, 33 (1946).

Divergence of Perturbation Expansion*

A. PETERMANN
Physics Department, University of Geneva, Geneva, Switzerland
(Received December 29, 1952)

THE difficulties encountered in quantum field theory in the ultraviolet region have been successfully resolved by the renormalization technique. Other difficulties, discussed by many authors[1,2] and resulting from the failure of the Born approximation, can be removed by a procedure developed by Dyson.[3] But the problem of the convergence after renormalization of the power-series expansions encountered in calculating physical quantities has not yet been resolved, although some attempts have been recently made in this direction.[4–6] A direct proof of divergence is the subject of the present letter.

We consider the calculation of a Green's function in electrodynamics. It is first shown that the total number K_{2n} of Feynman graphs belonging to the nth approximation is given by an exact but very complicated formula, the asymptotic form of which is

$$K_{2n}=N_{2n}=(2n-1)N_{2n-2}. \tag{1}$$

As an example, we give the exact number K_{2n} of graphs for the four first approximations:

$$K_4=4; \quad K_6=27; \quad K_8=248; \quad K_{10}=2830. \tag{2}$$

Retaining now only a subset of the K_{2n} graphs belonging to the nth approximation, namely the "pattern" graphs as defined by Neuman,[7] one can show that the number N_{2n}' of these self-energy graphs is

$$N_{2n}'=(2n-3)N_{2n-2}'. \tag{3}$$

These N_{2n}' graphs can be described in the following ways. Starting with the simplest self-energy graph, from the source line we draw a photon line crossing the one already existing and joining the source line again. This diagram contains now three source lines (crossed self-energy graph); from each of them we iterate the preceding operation, and so on $(n-1)$ times.

Limiting ourselves to the simple case of a scalar theory,[8] we can show by intricate calculations, exhibiting the structure of the n fold integrals, that the contribution of the self-energy nth approximation is asymptotically greater than

$$\alpha^n(4c)^{-n}n^{-1}(n/2)!\equiv a_n \tag{4}$$

in the limit $(-p^2)\rightarrow 0$, and the series

$$\sum_n^\infty a_n \tag{5}$$

is consequently divergent.

A generalization of the present method to other field theories must be possible without extensive modifications. A detailed account of the contents of this letter will shortly be published.

We wish to thank Professor L. Rosenfeld and Professor E. C. G. Stueckelberg for valuable discussions on this matter.

* Assisted by the Swiss Atomic Energy Commission (C. S. A.).
[1] R. Jost and A. Pais, Phys. Rev. **82**, 840 (1951).
[2] B. Ferretti, Nuovo cimento **8**, 108 (1951).
[3] F. J. Dyson, Phys. Rev. **83**, 608 (1951).
[4] C. A. Hurst, Proc. Roy. Soc. (London) **A214**, 44 (1952).
[5] Y. Katayama and K. Yamazaki, Prog. Theoret. Phys. **7**, 601 (1952).
[6] F. J. Dyson, Phys. Rev. **85**, 631 (1952).
[7] M. Neuman, Phys. Rev. **85**, 129 (1952).
[8] See C. Hayashi and Y. Munakata, Prog. Theoret. Phys. **7**, 481 (1952).

New Equation in the Affine Field Laws

G. BANDYOPADHYAY
Department of Mathematics, Indian Institute of Technology, Kharagpur, India
(Received November 10, 1952)

IN his recent affine field theory based on nonsymmetric affinities, Schrödinger has deduced his field equations from a variation principle.[1] He has taken as Lagrangian the square root of the determinant (with changed sign) of the Einstein tensor $R_{\mu\nu}$, defined by

$$R_{\mu\nu}=-\frac{\partial\Gamma_{\mu\nu}{}^{\sigma}}{\partial x_{\sigma}}+\frac{\partial\Gamma_{\mu\sigma}{}^{\sigma}}{\partial x_{\nu}}+\Gamma_{\mu\tau}{}^{\rho}\Gamma_{\rho\nu}{}^{\tau}-\Gamma_{\rho\sigma}{}^{\sigma}\Gamma_{\mu\nu}{}^{\rho}. \tag{1}$$

There is no reason why $\bar{R}_{\mu\nu}$, defined by

$$\bar{R}_{\mu\nu}=-\frac{\partial\Gamma_{\mu\nu}{}^{\sigma}}{\partial x_{\sigma}}+\frac{\partial\Gamma_{\sigma\nu}{}^{\sigma}}{\partial x_{\mu}}+\Gamma_{\sigma\nu}{}^{\rho}\Gamma_{\mu\rho}{}^{\sigma}-\Gamma_{\sigma\rho}{}^{\sigma}\Gamma_{\mu\nu}{}^{\rho}, \tag{2}$$

will not play an analogous role in the theory. It is therefore suggested here that the field equations should be obtained from two variation principles instead of one. The Lagrangians in them will be the square roots of the determinants of $R_{\mu\nu}$ and $\bar{R}_{\mu\nu}$. (Use of two variation principles has already been made by Einstein.[2]) Manipulating the equations obtained from the variation principles, it is not difficult to show that

$$R_{\mu\nu;\sigma}\equiv\partial R_{\mu\nu}/\partial x_{\sigma}-R_{\mu s}\Gamma_{\sigma\nu}{}^{s}-R_{s\nu}\Gamma_{\mu\sigma}{}^{s}=0, \tag{3}$$

and

$$\Gamma_{\lambda}\equiv\tfrac{1}{4}(\Gamma_{\lambda s}{}^{s}-\Gamma_{s\lambda}{}^{s})=0. \tag{4}$$

Let us now introduce the nonsymmetric $g_{\mu\nu}$'s. Manipulating in the same way as Schrödinger did to obtain his equations in *para* form from the *genuine* form,[1] we get

$$R_{\mu\nu}=\lambda g_{\mu\nu}, \tag{5}$$

$$g_{\mu\nu;\sigma}=0. \tag{6}$$

Equations (4)–(6) now constitute the complete field equations here suggested. These equations reduce to Einstein's strong field equations (described by him as I) if $\lambda=0$ and have the same position as regards over-determinacy.[3]

It may further be noted that, by virtue of (3) and (4),

$$R_{\mu\nu}=\bar{R}_{\mu\nu}.$$

An interesting, particularly rigorous solution of these field equations has been obtained which (with suitable interpretation of the antisymmetric part of $g_{\mu\nu}$) leads to the conclusion that an isolated magnetic pole cannot exist.[4] In contrast to this the results of a similar solution[5] of Einstein's strong field equations may be mentioned. The remark about it by Schrödinger leads to the possibility of the existence of an isolated magnetic pole, though only in the absence of mass.[6]

[1] E. Schrödinger, Proc. Roy. Irish Acad. **51**, 69 (1946).
[2] A. Einstein, *Meaning of Relativity* (Methuen and Company, Ltd., London, 1951), fifth edition, Appendix II.
[3] It has been called to my attention that the equations arising out of the present method may permit only a too restricted manifold of solutions, just as in the case of Einstein's equations derived from two variation principles (of which this method is an analog).
[4] To be read at the Indian Science Congress in January 1953, after which the details may be published. There the field equations have been taken for granted.
[5] G. Bandyopadhyay, Nature **167**, 648 (1951).
[6] E. Schrödinger, Nature **168**, 40 (1951).

A Focusing Method for Large Accelerators

T. KITAGAKI
Department of Physics, Faculty of Science, Tohoku University, Sendai, Japan
(Received December 29, 1952)

FOR the guiding field of synchrotrons, fields providing continuous focusing, $1>n>0$, have usually been used. Recently, Courant, Livingston, and Snyder[1] showed that fields which consist of periodic focusing and defocusing regions, $n_1=-n_2\gg1$, have strong focusing properties. We have tried another application of the periodic field. The magnet is divided into guiding magnets and focusing magnets, and the latter are placed in the linear portion of the orbit. Quadrupole or solenoid magnets may be used as focusing magnets.

(A) The stability condition formulated by Courant *et al.* now involves the factor ξ, the ratio of the length of the focusing magnet to π/M, where $M=$the number of pairs in 2π. Let $p_1{}^2$ and $p_2{}^2$ be the coefficients of the focusing field in Fig. 1(a). The stability conditionis as follows:

$$|\eta|<1,$$

$$\eta=\cos\frac{\pi}{M}\xi p_1\cos\frac{\pi}{M}\xi p_2+\sin\frac{\pi}{M}\xi p_1\sin\frac{\pi}{M}\xi p_2\left[\left\{\frac{\pi}{M}(1-\xi)\right\}^2 p_1p_2-\frac{p_1{}^2+p_2{}^2}{p_1p_2}\right]\frac{1}{2}-\frac{\pi}{M}(1-\xi)\left\{p_1\sin\frac{\pi}{M}\xi p_1\cos\frac{\pi}{M}\xi p_2+p_2\cos\frac{\pi}{M}\xi p_1\sin\frac{\pi}{M}\xi p_2\right\}. \tag{1}$$

Figure 1(b) shows the first stable region.

The quadrupole field shown in Fig. 2 increases linearly with x near the center. This field provides focusing and defocusing force in the x and z directions, respectively, and the forces are given by the equivalent n_{eq} and $-n_{eq}$, respectively, where,

$$n_{eq}=(H'/H_0)R. \tag{2}$$

$R=$the radius of the orbit in the guiding field, $H_0=$the guiding field strength, and $H'=$the gradient of the quadrupole field.

The central part of this field is used and is placed in the linear part of the orbit, changing the direction of the field alternately, and is excited by ac synchronizing with the guiding field, keeping the p^2 near the maximum value allowed by Eq. (1).

n_{eq} of this field can easily be 2 to 3 times greater than that of Courant, *et al.*, and ξ can be taken small. There seem to be some advantages. This method of focusing may also be applied to linear accelerators.

Some examples of design are as follows: (1) 500-Mev electron synchrotron. If we take the effective radius of the whole orbit $=380$ cm, $M=16$, $n_{eq}\lesssim460$ and $\xi=0.12$, the converging distance will be $\gtrsim150$ cm, the length of a guiding field sector$=56$ cm, and the length of a focusing magnet$=9$ cm. The guiding field index may be $1>n>0$ roughly. (2) 100-Bev proton synchrotron. If we take the radius of the whole orbit$=336$ m, $M=150$, $n_{eq}\lesssim40\,000$, and $\xi=0.12$, the converging distance will be $\gtrsim14$ m, the length of a guiding field sector$=5.6$ m, and the length of a focusing magnet$=0.85$ m. The guiding field index may be 0 roughly.

(B) For a periodic focusing field as shown in Fig. 3(a), the stability condition is

$$|\eta|<1,$$

$$\eta=\cos\frac{\pi}{M}\xi p_1\cos\frac{\pi}{M}(2-\xi)p_2-\frac{p_1{}^2+p_2{}^2}{2p_1p_2}\sin\frac{\pi}{M}\xi p_1\sin\frac{\pi}{M}(2-\xi)p_2, \tag{3}$$

This focusing region is shown in Fig. 3(b). For the limit $p_2\to0$, the condition is

$$|\eta|<1,\ \eta=\cos\frac{\pi}{M}\xi p_1-\frac{\pi}{M}(2-\xi)\frac{p_1}{2}\sin\frac{\pi}{M}\xi p_1,$$

or for the first region, $2(f+g)>\pi/M(2-\xi)$,

$$f=\frac{1}{p_1}\csc\left(\frac{\pi}{M}\xi p_1\right),\quad g=\frac{1}{p_1}\cot\left(\frac{\pi}{M}\xi p_1\right). \tag{4}$$

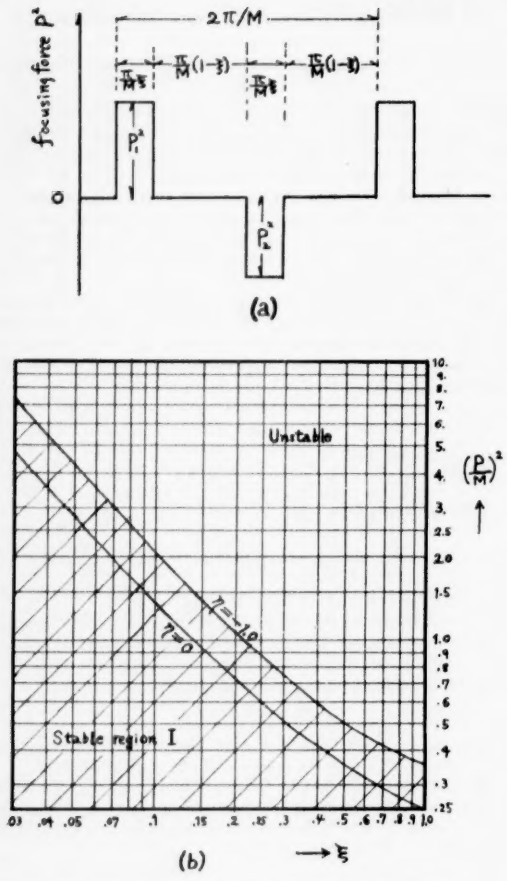

FIG. 1. (a) A periodic focusing field. (b) Stable region I.

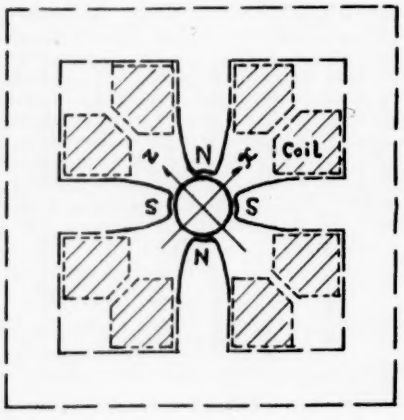

FIG. 2. Quadrupole focusing magnet.

This is the condition that a converging distance should be longer than $2\pi/M$, and has been reported by DePackh[2] for thin solenoid fields.

The focusing index is as follows:

$$n_{eq}=(H_s/2H_0)^2\,, \tag{5}$$

where H_s = solenoid field. It can be used in a way similar to that as in (A) with ac excitation in the linear part of the orbit, though it is not suitable near the maximum beam energy. This may be enough for small accelerators, since the scattering occurs predominantly in the earlier stages of acceleration. For the low energy period, from injection until the synchrotron phase starts, a conventional type of machine with solenoids on the donut may be enough.

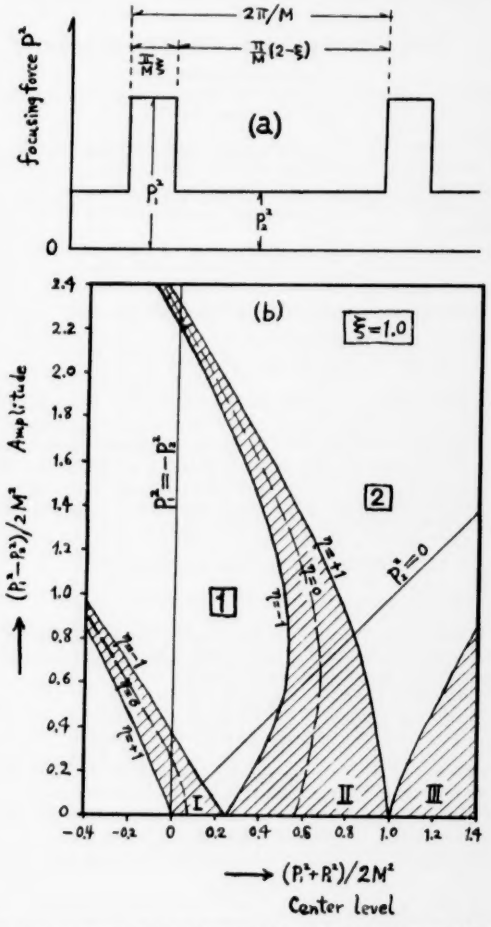

FIG. 3. (a) A general periodic focusing field. (b) Stable regions are shaded.

These focusing principles are now being tested. The author wishes to express his thanks to Professor M. Kimura for his valuable suggestions and encouragement.

[1] Courant, Livingston, and Snyder, Phys. Rev. **88**, 1190 (1952).
[2] D. C. DePackh, Phys. Rev. **86**, 433 (1952).

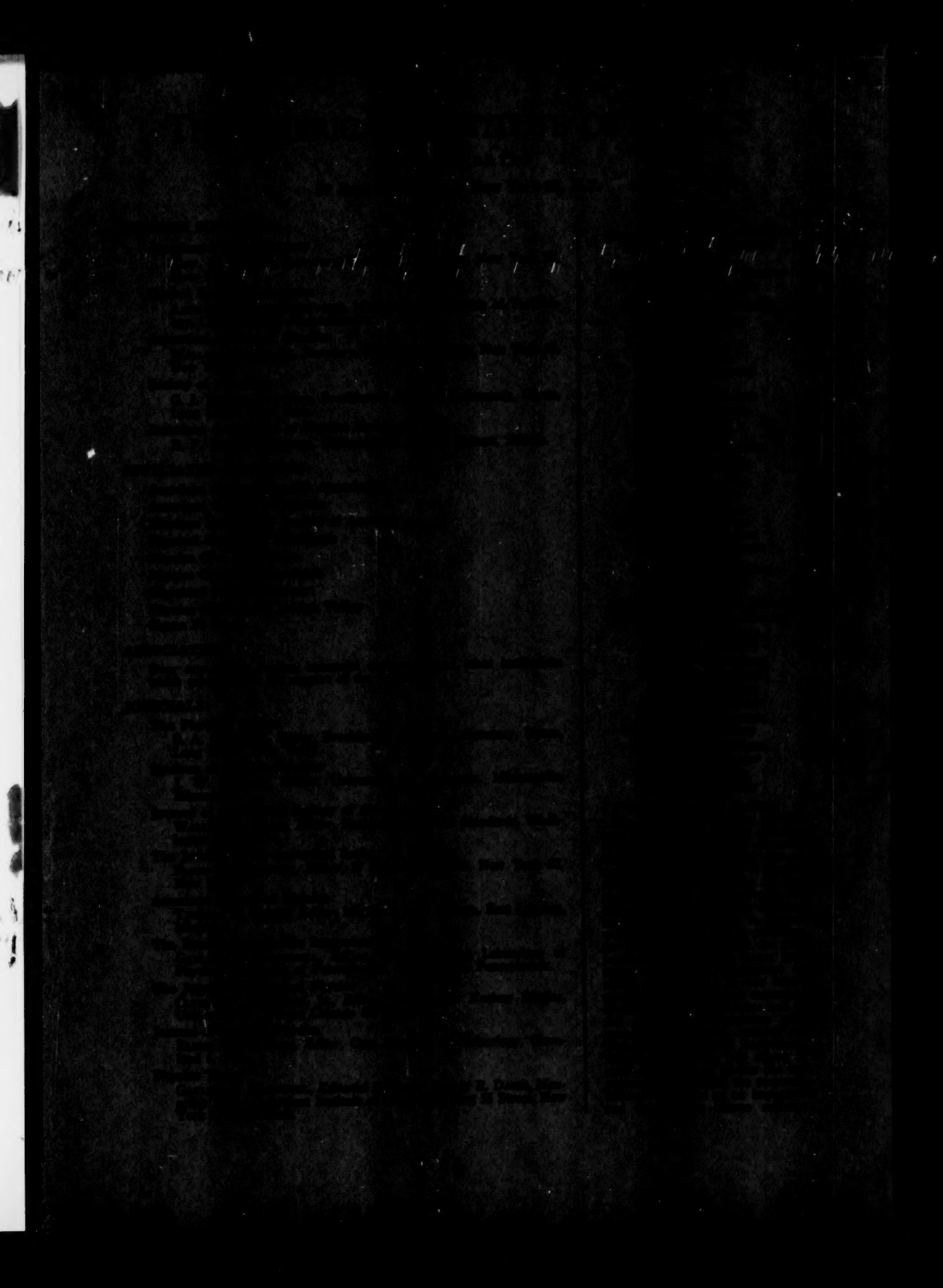

CONTENTS

THE PHYSICAL REVIEW — SECOND SERIES. VOLUME 89, NO. 5 — MARCH 1, 1953

Decay of Resonance Radiation by Spontaneous Radiation . . . . . R. J. Hellwig 949

Magnetic Moments of Sb^{121}, Sb^{123}, Zn^{67}, As^{75}, Sb^{121}, Te^{125}, and Te^{127} . . . . . H. E. Weaver, Jr. 953

Atomic Excitation and Ionization Accompanying Orbital Electron Capture by Nuclei . . . . . E. Pitchford and P. T. Porter 956

Upper Limit for Atomic Orbital Electron Excitation Accompanying K-Capture in Fe^{55} . . . . . P. T. Porter and H. P. Hoyt 962

Theory of the Magnetoresistive Effect in Semiconductors . . . . . V. A. Johnson and W. J. Whitehill 961

Tables for Second Born Approximation Scattering from Various Potential Fields . . . . . Lorant Mezey 967

Electron-Electron Scattering at 6.1 Mev . . . . . W. C. Barber, G. E. Seidel, and E. L. Chu 968

Pair Creation in Intermediate Coupling Theory . . . . . R. G. Moorhouse 969

First-Order Meson Wave Equations . . . . . H. S. Green 969

Seven-Mev Triton Target Reconsidered . . . . . J. W. Meyer, William Mieher, and M. O. Wyckoff 970

Second-Order Acoustic Fields: Relations between Energy and Intensity . . . . . Jordan J. Markham 972

Transport Phenomena in a Completely Ionized Gas . . . . . Lyman Spitzer, Jr., and Richard Härm 977

Enhanced Reactor . . . . . F. R. O'Meara 980

Gamma-Rays from Negative μ-Mesons Captured in Lead . . . . . Gerard G. Sacker and T. J. B. Shanley 980

Acousto-Electric Effect . . . . . R. H. Parmenter 990

Multiple Compton Scattering of Low Energy Gamma-Radiation . . . . . R. C. O'Rourke 990

Quantum Field Theory in the Light of Distribution Analysis . . . . . Werner Gottstein 1004

Range Correction for Electron Pair-Ty . . . . . Walter H. Barkas 1021

Momentum Transfer and Angle of Divergence of Pulse Produced by Photons . . . . . A. Bondelevsky 1023

Properties of Thermally Treated Germanium . . . . . Leo Esaki 1028

Vapor-Liquid Equilibria in He^3–He^4 Solutions . . . . . J. C. Morrow 1036

Entropy of Liquid He^3 . . . . . Tien Chi Chen and F. London 1038

Bohm's Interpretation of the Quantum Theory in Terms of "Hidden" Variables . . . . . Joseph B. Keller 1039

Photofission and Photoneutron Emission in Uranium . . . . . Robert B. Duffield and Jerry B. Hubbard 1042

Relativity Precession of the Asteroid Icarus . . . . . J. J. Gilvarry 1046

Atomic Number Dependence of Neutral Meson Yield from Proton Bombardment . . . . . R. W. Mains and B. J. Moyer 1047

Rotational Intensity Distributions of OH and OD in an Electrodeless Discharge through Water Vapor . . . . . H. P. Broida and W. R. Kane 1052

Interaction of Manganese Activator Ions in Zinc-Orthosilicate Phosphors . . . . . Shozo Larach and John Tuchtenhagen 1060

Evaluation of the Energy Matrix of the Tensor Forces . . . . . Izak Talmi 1065

S-Matrix and Causality Condition. I. Maxwell Field . . . . . N. G. van Kampen 1072

Angular Distribution of Protons from Vanadium 52 . . . . . J. S. Eenc and W. C. Parkinson 1080

Direction and Polarization Correlations of Successive Gamma-Rays . . . . . J. J. Kraushaar and M. Goldhaber 1081

Neutral Meson Production in π-p Collisions . . . . . Roger H. Hildebrand 1090

Radiation Cross Section for Hollow Atoms. II . . . . . Emil Altschuler 1090

Relativistic Statistical Thermodynamics . . . . . A. E. Scheidegger and R. V. Krotkov 1095

Microwave Absorption Spectrum of HD_2 . . . . . R. G. Nuckolls, L. J. Rueger, and Harold Lyons 1101

Nuclear Constitution and the Interpretation of Fission Phenomena . . . . . David Lawrence Hill and John Archibald Wheeler 1102

Letters to the Editor:

Identification of the Seven-Hour Mn^{56} Isomer . . . . . D. E. Alburger and S. Tiffany 1105

"Core Isomerism"—Remarks on Mn^{56} . . . . . M. Goldhaber 1106

Energy Loss and Curvature Radiation of a Relativistic Ionizing Particle . . . . . P. Rumer 1107

Energy Loss of a Fast Charged Particle by Curvature Radiation . . . . . R. M. Sternheimer 1108

Fermi Term in β–ν Correlation . . . . . D. C. Peaslee 1108

Molybdenum 99 . . . . . R. M. Diamond 1109

Systematic Calculations of Gamma-Ray Penetration . . . . . Herbert Goldstein, J. Ernest Wilkins, Jr., and L. V. Spencer 1109

Heavy Isotopes of Magnesium and Silicon . . . . . Manfred Lindner 1110

Q Values for the $N^{14}(\alpha, p)O^{17}$ Reaction . . . . . Elis Hjalmar and Hilding Ryde 1111

Angular Distribution of $Be^9(d, \alpha)Be^8$ at Low Energy . . . . . F. Cern and J. J. Jung 1111

Microwave Observations of the Collision Frequency of Electrons in Germanium . . . . . T. S. Benedict and W. Shockley 1112

Hall Coefficient of Cadmium . . . . . V. Frantz and O. Grace Jonker 1113

Mixing of States and Antiferromagnetism . . . . . H. P. Hanson 1114

Calculation of F-Center Energy Levels . . . . . J. A. Krumhansl and N. Schwartz 1114

Uranium Photofission Yields . . . . . Roman A. Schmitt and Nathan Sugarman 1115

Assignment of Y^{91} and Y^{91} . . . . . G. L. Schott and W. Walter Meinke 1116

Gamma-Radiation from Ag^{111} . . . . . J. O. Newton and B. Rose 1117

Symmetric Pseudoscalar Theory of Nuclear Forces . . . . . Abraham Klein 1118

Microwave Spectrum of the Free OH Radical . . . . . T. M. Sanders, Jr., A. L. Schawlow, C. C. Degnan, and C. H. Townes 1119

Experimental K to $L+M$ Ratios for Internal Conversion Lines . . . . . R. E. Marshak and R. D. Sard 1119

Charge Independence of Nuclear Forces . . . . . David Feldman 1120

Divergence of Perturbation Expansion . . . . . A. Peterman 1120

New Equation in the Affine Field Laws . . . . . G. Rainich-Hlavaty 1121

Pressing Method for Large Accelerators . . . . . T. Kitagaki 1121

LANCASTER PRESS, INC., LANCASTER, PA.